WILEY VCH

Edited by Shinobu Takizawa and
Mohamed S. H. Salem

Atropisomerism in Asymmetric Organic Synthesis

Challenges and Applications

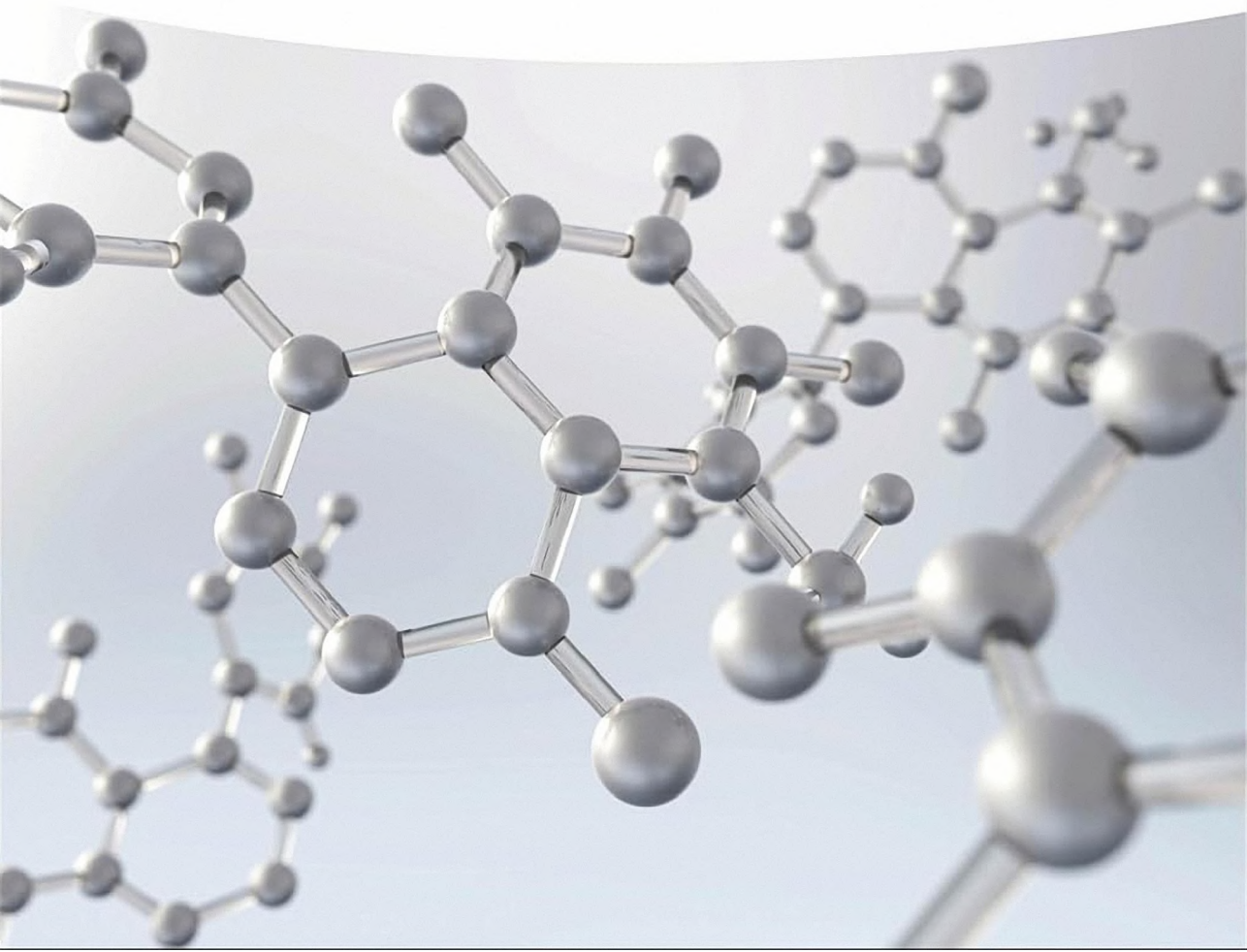

Atropisomerism in Asymmetric Organic Synthesis

Atropisomerism in Asymmetric Organic Synthesis

Challenges and Applications

Edited by Shinobu Takizawa and Mohamed S. H. Salem

WILEY VCH

Editors

Dr. Shinobu Takizawa
Osaka University
Mihogaoka, Ibaraki-shi
Osaka, 567-0047
Japan

Dr. Mohamed S. H. Salem
Osaka University
Mihogaoka, Ibaraki-shi
Osaka, 567-0047
Japan

Cover Image: © Anusorn Nakdee/Shutterstock

Library of Congress Card No.:
applied for

British Library Cataloguing-in-Publication Data
A catalogue record for this book is available from the British Library.

Bibliographic information published by the Deutsche Nationalbibliothek
The Deutsche Nationalbibliothek lists this publication in the Deutsche Nationalbibliografie; detailed bibliographic data are available on the Internet at <http://dnb.d-nb.de>.

Print ISBN: 978-3-527-35283-8
ePDF ISBN: 978-3-527-84423-4
ePub ISBN: 978-3-527-84424-1
oBook ISBN: 978-3-527-84425-8

Typesetting Straive, Chennai, India

“In blessed memory of Naho Takizawa, whose love and light continue to guide us every day.”

Contents

Preface

Atropisomerism, a form of conformational chirality arising from restricted rotation about single bonds, was first identified in 1922 by George Christie and James Kenner in a tetra-substituted biphenyl diacid. This discovery marked a significant milestone in chemistry, laying the groundwork for further exploration into this intriguing phenomenon. Subsequent advancements, particularly in the realm of asymmetric catalysis, have propelled the study of atropisomerism to new heights. Ligands with axial chirality, such as derivatives of BINOLs, BINAPs, and BINAMs, have emerged as powerful tools for controlling asymmetric reactions. The recent surge in literature addressing atropisomerism reflects its growing significance in various scientific disciplines. Naturally occurring molecules exhibiting atropisomerism have become subjects of intense investigation, opening new avenues for innovation in reaction concepts and bridging the gap between chemistry, biology, and physics. In fields such as medicinal chemistry and materials science, atropisomers play pivotal roles due to their diverse biological activities and functions. However, challenges persist, particularly in understanding the varying biological activities of stable atropisomeric compounds, including FDA-approved drugs. The phenomenon of rapidly interconverting atropisomerism adds further complexity to the study of these compounds. Despite being conventionally considered achiral, they exhibit atroposelective binding to protein targets, highlighting the intricate interplay between molecular structure and biological function. Overall, the exploration of atropisomerism continues to inspire new avenues of research and holds promise for future advancements in chemistry and beyond.

Recognizing the need for a comprehensive resource addressing the opportunities and challenges in this field, we present this handbook, focusing on recent advances in atroposelective synthesis and their different applications. The handbook covers a wide range of atroposelective synthetic approaches, including cross-coupling reactions, ring-opening reactions, formation of aromatic rings, and desymmetrization *via* functional group transformation, utilizing various metals and organocatalysts. By exploring these diverse asymmetric methodologies, readers gain insight into the versatility and importance of atropisomerism in modern synthetic chemistry. By showcasing the impact of these advances on asymmetric catalysis, natural product synthesis, material-based applications, and pharmaceutical development, it bridges the gap between theoretical insights and practical implementations, catering to both

academic researchers and industrial practitioners. Moreover, the handbook adeptly navigates through unresolved challenges within the field, thereby stimulating further inquiry and innovation. With its rigorous academic discourse and analysis, this handbook stands as an indispensable resource for scholars, students, and professionals alike, facilitating a deeper understanding of atropisomerism's current landscape and guiding future research endeavors.

The book is structured into two parts: **Part I**, titled "Atroposelective Synthesis," and **Part II**, titled "Challenges and Applications." **Part I** elucidates recent breakthroughs and challenges in atroposelective synthesis through six chapters. The introductory chapter provides a foundational understanding of atropisomerism's significance in contemporary chemistry. Chapters 2–4 explore diverse metal-catalyzed atroposelective coupling strategies, specifically targeting the synthesis of biaryls and heterobiaryls. Chapter 5 delves into the organocatalytic enantioselective formation of atropisomers, while Chapter 6 offers a historical overview of asymmetric ring-opening strategies. In **Part II**, the focus shifts to the versatile applications of atropisomeric scaffolds across various domains. Chapters 7–9 delve into their role in asymmetric catalysis, while Chapter 10 discusses their contribution to the total synthesis of natural compounds. Chapter 11 explores their significance in drug discovery and development. The editors extend their gratitude to the Wiley-VCH editorial team for their invaluable support and guidance throughout the project. They also express deep appreciation for the contributions of all chapter authors, whose expertise has enriched and elevated the content of this indispensable resource.

June 2024

Shinobu Takizawa
Mohamed S. H. Salem
Osaka, Japan

About the Editors

Shinobu Takizawa was born in Yokohama, Japan. He earned his Ph.D. in 2000 from Osaka University under the supervision of Professor Yasuyuki Kita. He was a JSPS research fellow from 1999 to 2000. He joined SANKEN, Osaka University, as an Assistant Professor in 2000, later advancing to an Associate Professor. From 2006 to 2008, he served as a Research Associate with Professor Dale L. Boger at the Scripps Research Institute. Since 2024, he has been a Professor at SANKEN, Osaka University. His current research focuses on developing environmentally friendly organic synthetic processes.

Mohamed S.H. Salem, born in Ismailia, Egypt, earned his master's degree in pharmaceutical chemistry from Suez Canal University, Egypt. He then received the MEXT Scholarship from the Japanese government to pursue his Ph.D. at Osaka University, Japan, under the guidance of Prof. Hiroaki Sasai and Prof. Takayoshi Suzuki. In 2022, he completed his Ph.D., focusing on the electrochemical synthesis of polycyclic heteroaromatics and their optical behavior. From 2022 to 2024, he worked as a postdoctoral researcher, and since 2024, he has been serving as an Assistant Professor in the Takizawa group at SANKEN, Osaka University. His current research focuses on developing green synthetic approaches for the bottom-up synthesis of functionalized small organic molecules.

Part I

Atroposelective Synthesis

1

Introduction

Mohamed S. H. Salem[1,2] and Shinobu Takizawa[1]

[1] Osaka University, SANKEN, 8-1 Mihogaoka, Ibaraki, Osaka 567-0047, Japan
[2] Suez Canal University, Faculty of Pharmacy, Pharmaceutical Organic Chemistry Department, Ismailia, 4.5 KM Ring Road, 41522, Egypt

1.1 Molecular Chirality and Atropisomerism

1.1.1 Molecular Chirality

The exploration of stereochemistry has captivated the chemical community since Pasteur's groundbreaking revelation of molecular chirality in 1848 [1], followed by van 't Hoff and Le Bel's influential introduction of tetrahedral carbon in 1874 [2, 3]. The International Union of Pure and Applied Chemistry (IUPAC) defines **chirality**, derived from the Greek word χείρ (kheir) meaning hand, as *the geometric property of a rigid object (or spatial arrangement of points or atoms) being nonsuperposable on its mirror image. Such an object lacks symmetry elements of the second kind, including a mirror plane, a center of inversion, or a rotation-reflection axis* [4]. Chiral molecules typically possess at least one stereogenic element, giving rise to their chirality. The most prevalent type of stereogenic element is a stereogenic center or **chirality center**, which is *an atom holding a set of ligands in a spatial arrangement which is not superposable on its mirror image* (IUPAC) [5]. A chirality center is thus a generalized extension of the concept of the asymmetric carbon atom to the central atoms of any element, for example, nitrogen N or phosphorus P. There are other types of stereogenic elements that can give rise to chirality, including a stereogenic axis (axial chirality), a stereogenic plane (planar chirality), and a screw axis (helical chirality) (Figure 1.1) [5].

Chirality axis: *An axis around which a set of ligands is held so that it results in a spatial arrangement that is not superposable on its mirror image.*

Chirality plane: *A planar unit connected to an adjacent part of the structure by a bond, which results in restricted torsion so that the plane cannot lie in a symmetry plane.*

Atropisomerism in Asymmetric Organic Synthesis: Challenges and Applications, First Edition.
Edited by Shinobu Takizawa and Mohamed S. H. Salem.

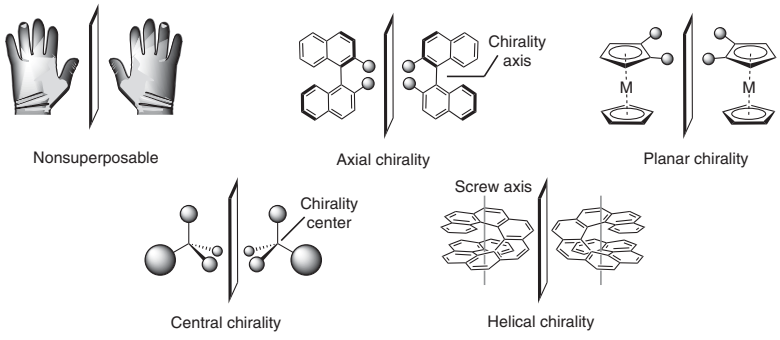

Figure 1.1 Different types of molecular chiralities and stereogenic elements.

Screw axis: *An axis around which the atoms are held in a screw-shaped arrangement that is not superposable on its mirror image. While certain sources categorize helical chirality as a form of axial chirality, IUPAC does not acknowledge helicity as a subtype of axial chirality.*

Chirality is a ubiquitous phenomenon observed in various disciplines, mainly in the realms of biology, pharmaceuticals, organic chemistry, and materials science [6]. Biological homochirality of essential molecules such as L-amino acids in proteins and D-sugars in nucleic acids is vital for the proper functioning of living organisms [7]. The thing is reflected in the drug industry, as often only one enantiomer of a chiral drug exhibits therapeutic efficacy, leading to the development and production of single-enantiomer drugs to enhance their efficacy and minimize associated side effects [8]. Chirality extends its impact to materials science, where certain chiral molecules exhibit unique chiroptical features, such as circularly polarized luminescence (CPL) and circular dichroism (CD), facilitating the design of advanced materials and devices [9–12]. Chiral catalysts in organic chemistry have a key role in asymmetric synthesis, contributing to the selective production of enantioenriched chiral compounds, especially in the synthesis of pharmaceuticals and functionalized materials [13–16].

1.1.2 Axial Chirality and Atropisomerism

Earlier investigations primarily focused on central chirality, with the pioneering works of Pasteur, van't Hoff, and Lebel centered on chiral tetrahedral carbon with four distinct substituents [1–3]. However, a milestone was achieved a century ago in 1922 when George Christie and James Kenner first identified atropisomerism in a tetra-substituted biphenyl diacid **1** [17]. After this groundbreaking discovery, some efforts were exerted to explore this new type of chirality, but a quantum leap transpired with the advent of asymmetric catalysis. Ligands exhibiting axial chirality, such as derivatives of 1,1′-bi-2-naphthols (BINOLs), 2,2′-bis(di-phenylphosphino)-1,1′-binaphthyls (BINAPs), and 2,2′-diamino-1,1′-binaphthalenes (BINAMs) (refer to Chapters 7 and 8 for detailed insights), demonstrated superior efficacy in controlling asymmetric metal-based reactions, as elucidated by Ryoji Nyori [18].

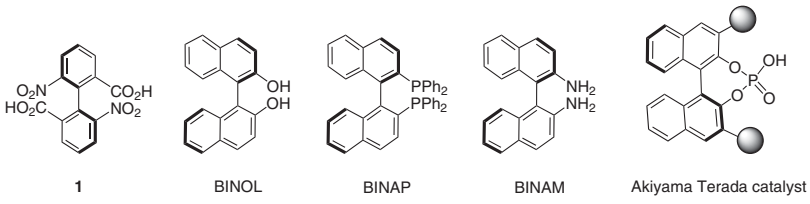

Figure 1.2 Atropisomerism in privileged chiral ligands and organocatalysts.

The prevalence of axial-to-central chirality transfer became evident in the realm of asymmetric catalysis. Over the past two decades, these ligands have additionally proven their superiority in various organocatalysts, such as chiral phosphoric acid catalysts, independently developed by Akiyama and Terada (Figure 1.2). These advancements captivated researchers, prompting them to delve deeper into the study and exploration of axial chirality and atropisomerism [19, 20].

While some may mistakenly conflate axial chirality and atropisomerism concepts considering them synonymous, it is imperative to recognize that axial chirality encompasses broader forms. According to IUPAC, **axial chirality** is precisely defined as a *stereoisomerism resulting from the nonplanar arrangement of four groups in pairs about a chirality axis* [5]. In essence, these frameworks possess a **chiral axis**, imposing restrictions on the rotation of two pairs of groups. As per the IUPAC definition, this concept encompasses diverse families of organic molecules featuring noncoplanar arrangement of two pairs of substituents in the parent backbone. The most prominent class of axially chiral compounds falling under this definition is **atropisomers**, including biaryls, heterobiaryls, aryl alkenes, anilides, and diaryl ethers, whose *axial chirality arises from the restricted rotation about single bonds* [5]. Allenes, spiro compounds, spiranes, and alkylidene-cyclic compounds are other examples of axially chiral compounds, wherein their chirality comes from the perpendicular geometry of two pairs of substituents (Figure 1.3) [21].

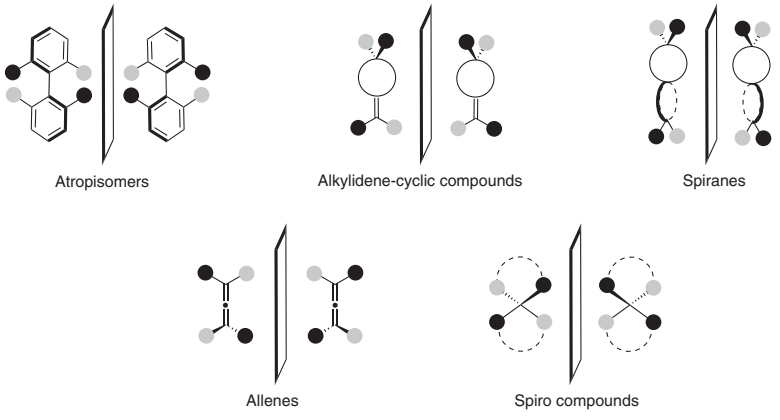

Figure 1.3 The most prominent classes of axially chiral compounds.

The recent surge in literature addressing atropisomerism has significantly impacted the field, capturing attention with its exploration of naturally occurring molecules that exhibit this chirality element [22]. These molecules play a pivotal role in advancing various scientific domains, addressing not only physical organic issues related to structure and stability but also inspiring the development of innovative reaction concepts [23]. The design and synthesis of novel scaffolds showcasing atropisomerism contribute to the ongoing expansion of this interdisciplinary field, which seamlessly integrates chemistry, biology, and physics, finding applications in both medicinal chemistry and materials science [24–28]. Atropisomers, as a fundamental chirality element in nature, exhibit diverse biological activities and functions, rendering them indispensable in asymmetric catalysis. Numerous atropisomers serve as privileged chiral ligands, demonstrating their critical role in catalytic processes [29, 30]. However, despite their immense potential, challenges persist, exemplified by the varying biological activities observed in stable atropisomeric Food and Drug Administration (FDA)-approved drugs and experimental compounds. The phenomenon of rapidly interconverting atropisomerism adds complexity, as these compounds, while conventionally considered achiral, exhibit atroposelective binding to protein targets [31, 32].

Recognizing the need for a comprehensive resource addressing the opportunities and challenges in this field, we present this handbook, focusing on recent advances in atroposelective synthesis and their different applications. This book explores diverse atroposelective synthetic approaches, including cross-coupling reactions, ring-opening reactions, formation of aromatic rings, and desymmetrization *via* functional group transformation, utilizing different metal and organocatalysts [33, 34]. By showcasing the impact of these advances on asymmetric catalysis, the synthesis of natural products, functionalized materials, and drug industry, this book contributes to a deeper understanding of the current state of atropisomerism and highlights unresolved challenges. In alignment with the broader context, this book integrates and complements existing literature, particularly *Axially Chiral Compounds: Asymmetric Synthesis and Applications* by Bin Tan (WILEY-VCH GmbH, **2021**) [35] and *Atropisomerism and Axial Chirality* by José M Lassaletta (World Scientific Publishing Europe Ltd, **2019**) [36]. By collating and discussing recent advances, we aim to provide valuable insights for researchers working in this dynamic field.

1.2 Atropisomerism in Asymmetric Organic Synthesis

The pursuit of atroposelective synthesis of various atropisomers, mainly biaryls [37] and heterobiaryls [38] holds significant relevance due to its applications across various domains, including polymers, ligands, natural products, and pharmaceuticals. One of the most straightforward methods is based on oxidative coupling reactions, a methodology presenting a direct pathway that, while having a restricted substrate scope, obviates the need for prefunctionalization of starting materials (Scheme 1.1) [39]. A second strategy entails the direct establishment of chirality

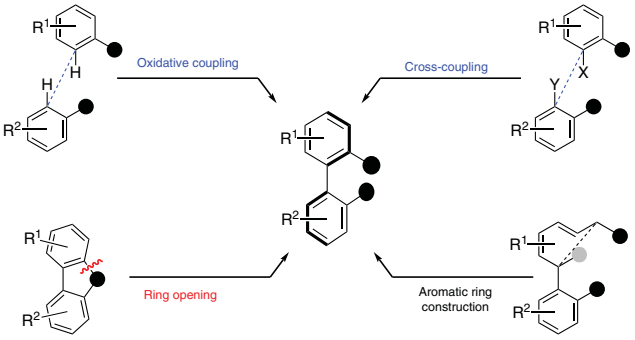

Scheme 1.1 Straightforward strategies for enantioselective synthesis of atropisomers.

axes through C—C bond-forming asymmetric cross-coupling reactions. This approach necessitates highly efficient catalysts capable of imparting the requisite stereocontrol, especially in the context of coupling hindered *ortho*-substituted substrates [40–42]. A third alternative is based on the *de novo* formation of one or more aromatic rings by cycloaddition or cyclization reactions [43]. Additionally, a noteworthy strategy, stemming from the seminal work of Bringmann et al. in 1986 [44], focuses on atroposelective ring opening, incorporating the enantioselective cleavage of diverse bonds [45]. Great advances have been introduced in this domain, especially with the expansion of their applications. A diverse array of metal-based and organocatalysts alongside enzymatic transformations have proven their efficiency in the highly controlled and selective construction of atropisomers [46]. While numerous enduring challenges have been recently addressed, the field still confronts unresolved issues and offers multiple opportunities that can propel it further [47]. The ongoing interplay between challenges and opportunities underscores the dynamic nature of atroposelective synthesis and presents avenues for continued advancement.

Recognizing the need for a comprehensive resource addressing the opportunities and challenges in this field, we present this handbook, focusing on recent advances in atroposelective synthesis. This book is structured into two parts: Part I, titled "Atroposelective Synthesis", and Part II, titled "Challenges and Applications". Part I primarily focuses on recent advancements and challenges in atroposelective synthesis, employing diverse approaches. Chapters 2–4 delve into various metal-catalyzed atroposelective coupling strategies, specifically targeting the construction of biaryls and heterobiaryls, which are prevalent in this context. Chapter 2 concentrates on group 8 transition-metal complexes, mainly iron and ruthenium, as catalysts for atroposelective oxidation of different arenols. Within this chapter, **Prof. Uchida** extensively discusses the key role played by iron and ruthenium complexes in achieving stereoselective oxidative homo- and hetero-coupling reactions of arenols. The author emphasizes recent breakthroughs, showcasing how the design of innovative ligands has overcome long-standing challenges in hetero-coupling methodologies. Notable examples include Pappo's recent work in 2022, illustrating the cross-selective synthesis of NOBIN through the introduction

of a chiral iron disulfonate complex as the catalyst [48]. Additionally, Smith's 2023 findings highlight the efficiency of an iron Pybox complex as a catalyst in the cross-coupling of 3-hydroxynaphthoates with indole derivatives as coupling partners, utilizing bis(*tert*-butyl) peroxide as the oxidant [49]. Uchida's work is also discussed, demonstrating the cross-coupling of arenols with similar structures and electronic natures using (H_2O)Ru-Salen complexes [50].

Chapter 3 delves into recent advancements in the catalytic oxidative coupling of arenols utilizing vanadium complexes, with a particular focus on its application in the preparation of polycyclic heteroaromatics (PHAs). Notably, optically active vanadium complexes, featuring a Schiff base ligand and a tetravalent or pentavalent vanadium metal center, have garnered attention as environmentally benign catalysts facilitating the generation of axially chiral molecules [51]. **Prof. Salem** and **Prof. Takizawa** discuss with many mechanistic insights why these complexes exhibited noteworthy characteristics, serving as active catalysts in diverse regio- and enantioselective C—C bond formation reactions. Importantly, the inherent selectivity and distinctive catalytic activity of vanadium not only mitigate undesirable side reactions and peroxidation but also confer broad functional group tolerances in various organic syntheses [51]. Therefore, the applications of this chemistry extend beyond their catalytic role, finding utility in the atroposelective synthesis of heterocyclic nanographenes endowed with favorable optical properties, such as helicenes and dehydrohelicenes [12, 52]. Furthermore, these vanadium complexes have been instrumental in synthesizing various naturally occurring substrates (also refer to Chapter 10).

In the context of cross-coupling reactions for synthesizing biaryl and heterobiaryls, particular attention is directed toward the Suzuki–Miyaura coupling (SMC) – an indispensable transformation in contemporary synthetic chemistry [53]. This reaction holds paramount significance in the synthesis of functionalized materials, various ligands, natural products, and biologically active molecules [54–56]. Consequently, we dedicated Chapter 4 to explore the atroposelective SMC for the production of axially chiral biaryls. In this comprehensive chapter, **Prof. Korenaga** systematically reviews numerous successful examples of atroposelective SMC toward biaryl synthesis, emphasizing the pivotal role played by directing groups in the enantioinduction. Furthermore, it delves into recent studies that have reconsidered established mechanisms, exemplified by the work of Patel et al. [57]. Their theoretical considerations and density functional theory (DFT) calculations shed light on the importance of weak interactions in the asymmetric induction of aryls lacking directing groups. The chapter also addresses the challenges prevailing in the field and highlights issues such as the necessity for high catalyst loading and the limited substrate scope. It also assesses potential avenues for overcoming these challenges, including the utilization of Buchwald ligands with preliminary efforts by the Korenaga group to implement this approach.

In contrast to the preceding chapters, which discussed the metal-based methodologies for atroposelective synthesis, Chapter 5 delves into the diverse array of

organocatalysts and their pivotal role in the enantioselective synthesis of atropisomers. **Prof. Bencivenni** introduces an array of organocatalytic approaches, encompassing aminocatalysis, base catalysis, phase-transfer catalysis (PTC), and phosphoric acid catalysis (PAC). The inherent adaptability of these catalytic modalities to various synthetic strategies, coupled with the orthogonality of their modes of action, renders them invaluable for the enantioselective construction of a broad spectrum of atropisomers exhibiting diverse scaffolds. The chapter discusses selected examples of structurally diverse atropisomers, including C–C (biaryls and non-biaryls) and C–N as well as C–O, C–B, and N–N atropisomers [33]. The chapter also highlights various recent advancements, including Sparr's work on the *de novo* construction of one or two aromatic rings and his key achievement in the diasterodivergent synthesis of arenes with two stereogenic axes [58–60]. In the evolution of organocatalysts, crowned with the Nobel Prize in Chemistry to Benjamin List and David MacMillan in 2021 [61], a large variety of atropisomers have found substantial utilities for catalyzing atroposelective transformations themselves, suggesting that further breakthroughs can still be expected from today's research in expanding fields like organocatalysis and atropisomers.

Enantioselective ring-opening reactions of fused biaryl compounds represent another powerful strategy for constructing axially chiral products. This approach offers practical advantages, including the broad substrate applicability, excellent selectivity control, and high atom efficiency. Experimental observations indicate that inert chemical bonds within tensegrity structures can be selectively cleaved under mild conditions through the ring opening of these structures, attributed to the torsional strain induced by their twisted conformation [45, 62]. In recent years, significant progress has been made in this field, extensively reviewed in existing literature. However, a comprehensive discussion specifically focusing on the synthesis of atropisomers *via* enantioselective ring-opening reactions has been notably absent. In Chapter 6, **Dr. Duan** and **Prof. Gu** provide an insightful historical overview of the asymmetric ring-opening strategy, commencing with the pioneering work of Bringmann [44] and encompassing subsequent key advancements in this domain. The chapter is organized into six sections corresponding to different types of bond cleavage, including the CO—O bond of "Bringmann's Lactone" as well as C—X (X = group 14, 15, 16, and 17 elements) bonds. The final section briefly addresses the ring-opening reactions of transient pentacyclic metal species. The authors elucidate the structural prerequisites of various substrates for effective implementation of this strategy, incorporating dynamic kinetic resolution (DKR), and discuss the impact of torsional strain in bridged biaryls on their efficiency. Within this framework, Chapter 6 systematically explores the use of various metal-based catalysts, including iridium, cobalt, nickel, copper, rhodium, and palladium, along with different ligands and organocatalysts. This structured organization facilitates an understanding of the advancements and challenges in a good context mainly revolving around the synthetic approach rather than the substrate or the obtained product.

1.3 Atropisomerism: Challenges and Applications

Part II of this book delves into the multifaceted applications of scaffolds exhibiting atropisomerism, spanning across diverse realms such as asymmetric catalysis, the total synthesis of natural compounds, medicinal chemistry, and material-oriented applications. By elucidating recent strides in these areas, alongside the obstacles impeding their integration, particularly in domains like drug industry [31, 32], researchers can gain insight into the current situation of the field and discern avenues for prospective advancements.

1.3.1 Axially Chiral Ligands and Organocatalysts

The revolution in asymmetric catalysis, particularly with the pioneering work of Nyori in 1980 utilizing BINAP as a ligand in the rhodium-catalyzed asymmetric hydrogenation, has significantly propelled the field of atropisomerism [18]. This progress underscores the profound significance of scaffolds featuring axial chirality, with predictable spatial projection of functionalities, thereby yielding remarkable organocatalysts, ligands, or auxiliaries [63, 64]. Notably, a considerable array of chiral ligands and organocatalysts stems from a few privileged chiral structures, among which the atropisomeric 1,1′-binaphthyl structure occupies a prominent position. The atropisomerism of the 1,1′-binaphthyl moiety offers several advantages in catalysis. First, both enantiomers of the 1,1′-binaphthyl moiety can be easily accessed from commercially available (*R*)- or (*S*)-BINOL. Second, the atropisomerism of the 1,1′-binaphthyl is notably stable and does not undergo racemization under most reaction conditions. Third, the electronic and steric properties of the 1,1′-binaphthyl moiety can be finely tuned by introducing various substituents at the 3,3′ or 7,7′ positions. Additionally, the solubility of the catalyst can be improved by incorporating lipophilic substituents. Last, the 1,1′-binaphthyl moiety with its C^2-symmetric skeleton reduces the number of potential competing diastereomeric transition states and thereby simplifying the understanding of reaction mechanisms. The axially chiral BINOL, BINAM, and NOBIN represent exemplary binaphthyl molecules, from which a multitude of chiral ligands (Figure 1.4) and organocatalysts (Figure 1.5), including the well-regarded BINAP and phosphoric acids, are derived. In Chapter 7, **Dr. Cen** and **Prof. Zhang** meticulously introduce around 150 representative chiral ligands and organocatalysts derived from axially chiral binaphthyl structures, particularly emphasizing BINOL, BINAM, and NOBIN. Spanning from phosphine and phosphoramidite ligands to Schiff base ligands and from Brønsted acids to Lewis bases and phase-transfer organocatalysts, these privileged axially chiral binaphthyl structures underpin the majority of widely utilized chiral catalytic systems. While it may be impractical to encompass all binaphthyl chiral catalysts within a single chapter, the selected examples by the authors underscore the remarkable enantioinductive capability of these privileged atropisomeric binaphthyl structures. Symbolized by BINOL, BINAM, and NOBIN, axially chiral binaphthyl structures have furnished an exceptional chiral environment for numerous asymmetric transformations [29].

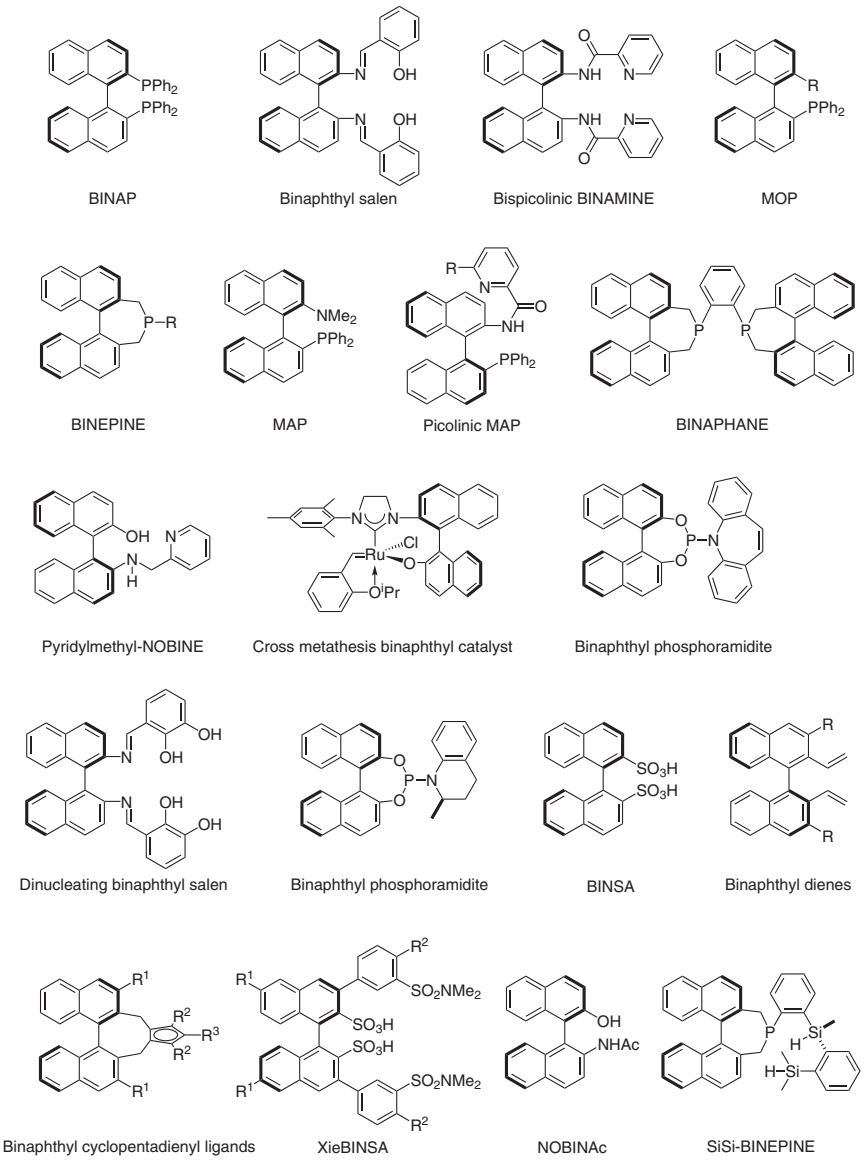

Figure 1.4 Representative chiral ligands derived from atropisomeric binaphthyl structures.

After a comprehensive scope of the role played by axially chiral scaffolds in general, particularly those derived from binaphthyl, the subsequent two chapters delve into a more in-depth and detailed discussion of the role played by two specific families of ligands and organocatalysts that were previously not discussed in depth. Chapter 8 introduces a comprehensive review of various reactions catalyzed by zinc complexes in conjunction with axially chiral ligands, particularly derivatives of BINOL. **Prof. Arai** elucidates in his chapter the significance of specific positions

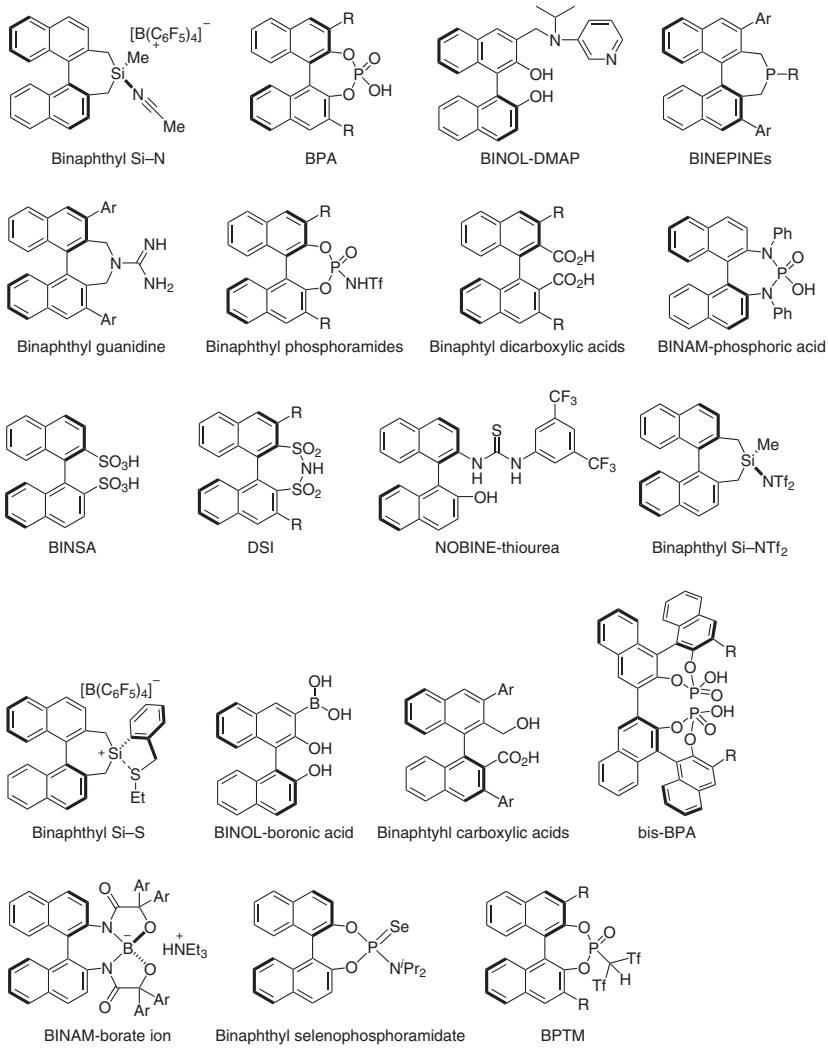

Figure 1.5 Representative chiral organocatalysts derived from atropisomeric binaphthyl structures.

on the ligands, notably the 3,3′ positions, and examines how substituents at these sites influence the overall activity of the zinc catalysts. Furthermore, the chapter expands its scope to encompass other metals, such as lanthanum and barium, which were not extensively discussed in the previous sections of this book. The chapter highlights the significant contributions facilitated by the development of multinuclear zinc catalysts with axial chirality, marking numerous milestones in asymmetric catalysis. Throughout the discussion, mechanisms are scrutinized, providing valuable insights into the underlying processes driving these catalytic transformations.

Chapter 9 covers one of the most rare examples in the domain of atropisomeric organocatalysts, which is nucleophilic catalysis exemplified by binaphthyl-based chiral *N*,*N*-4-dimethyl-4-aminopyridine (DMAP) derivatives [65]. In their chapter, **Prof. Mandai** and **Prof. Suga** explore a range of binaphthyl-based DMAP derivatives and their significant impact on accelerating nucleophilic catalytic reactions. The discussion underscores the favorable outcomes resulting from the incorporation of polar functional groups into the skeleton of the optically active DMAP derivatives. These modifications lead to enhanced catalytic activity and improved enantioselectively, primarily attributed to hydrogen bonding interactions. The chapter delves into the utilization of these derivatives in both intra- and intermolecular enantioselective acylation reactions, highlighting their remarkable efficacy in promoting desired chemical transformations, including different strategies such as kinetic resolution, desymmetrization of alcohols, and DKR.

1.3.2 Natural Product Synthesis

Atropisomeric molecules, imposing a restricted rotational barrier, are not only prevalent in catalysis as chiral ligands or organocatalysts but are also a recurring motif in numerous natural products (Figure 1.6) [22]. The captivating structures and unique features associated with this motif have significantly increased its importance within the synthetic community. The advancement of atroposelective coupling methods, employing various strategies, has contributed to the synthesis of complex molecules [66, 67].

Chapter 10 explores various success stories in the total synthesis of atropisomeric natural products, employing a range of transition-metal-catalyzed asymmetric oxidative coupling reactions coupled with diverse oxidants to augment reactivity and selectivity. **Dr. Kang** and **Prof. Kozlowski**'s contribution to this chapter focuses particularly on copper- and vanadium-catalyzed methodologies. Notably, copper-mediated asymmetric oxidative couplings have utilized poly-substituted naphthols as coupling monomers, while vanadium-catalyzed approaches have expanded the scope to include monocyclic phenols for axial chirality construction in natural product synthesis. The chapter delves into the stereoselectivity of these processes, highlighting the intricate interplay between asymmetric catalysts and the innate stereochemistry of substrates. Additionally, it explores how both catalysts and substrates impact stereochemical outcomes, ultimately enhancing atroposelectivity. The authors shed light on enzyme-based strategies for constructing natural products with chirality axes, encompassing both symmetrical dimers and unsymmetrical coupling products – a feat challenging to achieve *via* conventional chemical means.

1.3.3 Atropisomerism in Drug Discovery and Development

Atropisomerism has garnered an increasing interest in drug design and development within both academia and the pharmaceutical industry over recent decades [68]. The effectiveness of drug action relies heavily on the specific binding

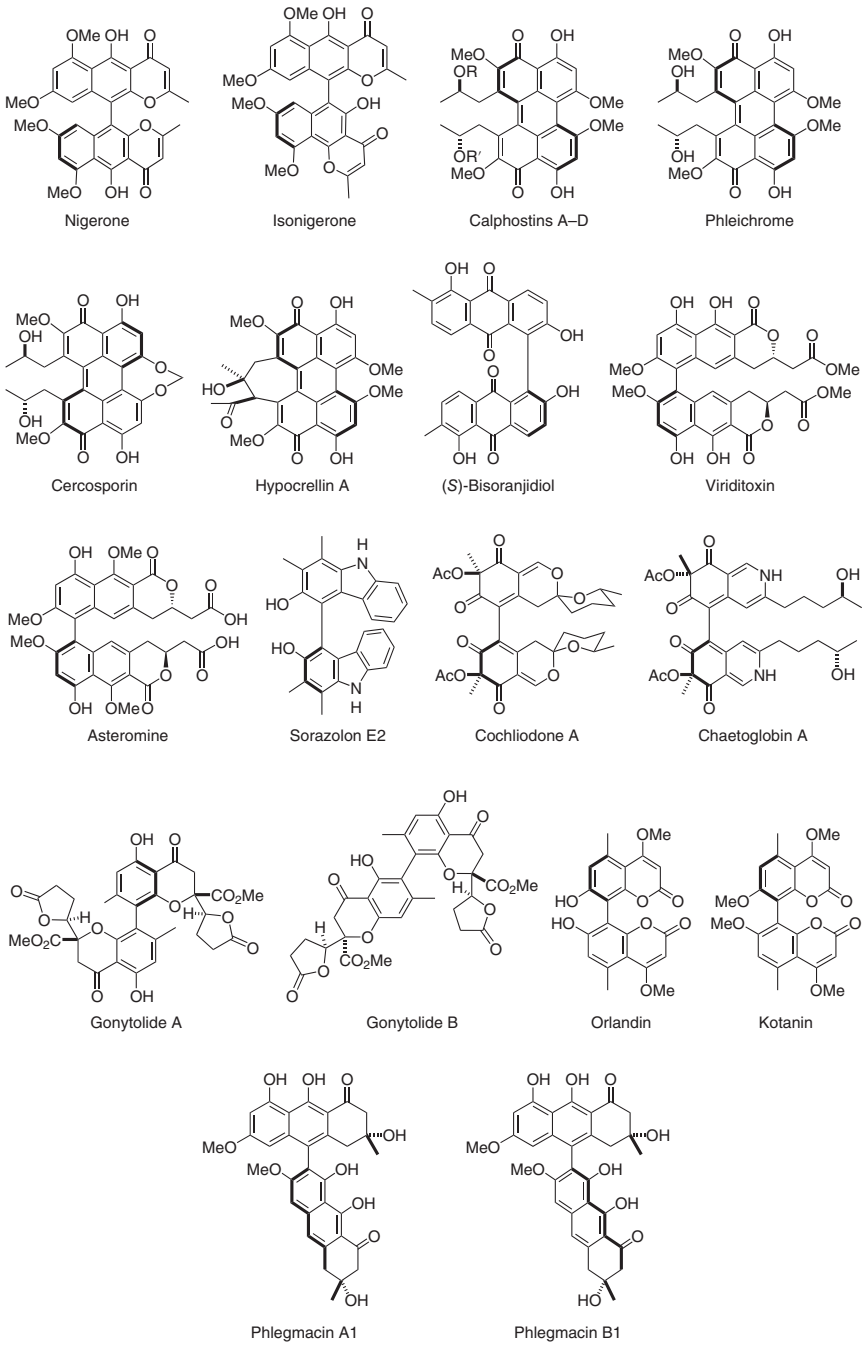

Figure 1.6 Representative natural products featuring chirality axis.

of the bioactive molecule to its protein target, facilitating the formation of crucial chemical interactions that trigger a cascade of biological events culminating in desired bioactivity [8]. Consequently, the influence of axial chirality is anticipated and should be meticulously considered early in the drug design process. It is widely acknowledged that the activity toward a particular target is predominantly dictated by a single atropisomer, with minimal or no contribution from the other enantiomer [69]. "Locking" the molecule in the bioactive atropisomeric form not only enhances activity but also improves selectivity toward the intended biological target. So far, a few FDA-approved drugs stand out as **class III** stable atropisomers, characterized by a high rotational energy barrier (ΔE rotation ≥ 30 Kcal/mol) and slow interconversion between atropisomers ($t_{1/2} > 4.5$ years) [69]. These drugs, including **lesinurad** (urate transporter inhibitor for gout), **telenzepine** (selective M1 receptor blocker for peptic ulcers), **colchicine** (anti-inflammatory/gout agent), and **sotorasib** (KRASG12C covalent inhibitor for non-small cell lung cancer), are either marketed as racemates, single diastereoisomers, or even separated as single atropisomers (Figure 1.7) [24].

In Chapter 11, **Prof. Helal** and his team provide an overview of atropisomerism's utilization in drug discovery, accompanied by examples from recent literature and FDA-approved drugs. These compounds are classified based on their chemical classes into biaryls/heterobiaryls, diaryl ethers or amines, benzamides, and macrocycles. The chapter also discusses the key advantages of controlling atropisomerism in the drug industry and how singular atropisomers offer safer profiles, higher/selective bioactivity, lower administration doses, and reduced off-target activities. Additionally, the authors discuss the main challenges hindering the manufacture of pure atropisomeric drugs, including cost increases and the rapid interconversion of **class I** atropisomers. These compounds, characterized by low ΔE rotation (< 20 Kcal/mol) and quick interconversion at room temperature ($t_{1/2} < 60$ seconds), represent the majority of atropisomeric drug molecules. The chapter concludes by discussing potential opportunities, such as introducing bulkier, sterically hindered scaffolds, which facilitate the switch from **class I** atropisomeric racemates to **class III** atropisomers, easily separable *via* SFC chiral separation [70].

It is worth noting that while this book's structure into two parts facilitates content organization and accessibility for readers, there is a high degree of integration

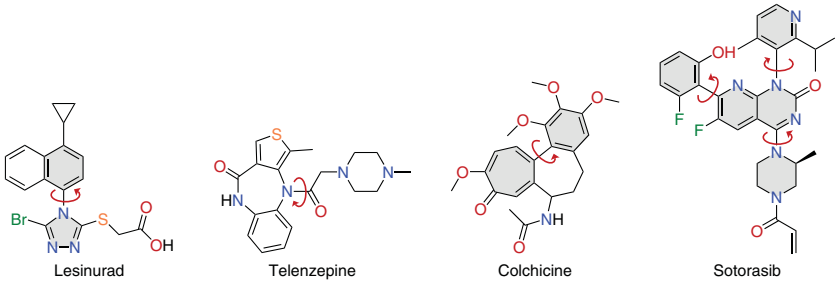

Figure 1.7 Representative FDA-approved drugs featuring class III stable atropisomeric scaffolds.

between the contents and context among the two parts and in each chapter. This book consistently explores different atroposelective synthetic approaches and highlights interconnected parts, whether discussing applications or challenges. For instance, Chapter 3 initiates the first part by delving into vanadium-catalyzed atroposelective synthesis and extends this discussion to the application of this approach in creating functionalized materials such as helicenes and dehydrohelicenes *via* axial-to-helical chirality transfer. These material-based applications are not addressed in other parts of the book. Similarly, some chapters in Part II, dedicated to applications, discuss atroposelective synthetic strategies not previously highlighted in Part I. For example, Chapter 10 delves into copper-catalyzed and enzymatically based atroposelective oxidative coupling of atropisomeric natural products, presenting novel synthetic methodologies not previously discussed in Part I. This integrated context ensures a comprehensive discussion of atropisomerism from various angles, providing readers with a holistic understanding of its applications and implications.

References

1 Pasteur, L. (1848). Memoires sur la relation qui peut exister entre la forme crystalline et al composition chimique, et sur la cause de la polarization rotatoire. *C. R. T.* 26: 535–538.

2 van't Hoff, J.H. (1874). A suggestion looking to the extension into space of the structural formulas at present used in chemistry, and a note upon the relation between the optical activity and the chemical constitution of organic compounds. *Arch. Neerl. Sci. Exactes Nat.* 9: 445–454.

3 Le Bel, J.A. (1874). Sur les relations qui existent entre les formules atomiques des corps organiques et le pouvoir rotatoire de leurs dissolutions. *Bull. Soc. Chim. Fr.* 22: 337–347.

4 Favre, H.A. and Powell, W.H. (2013). *Nomenclature of organic chemistry: IUPAC recommendations and preferred names 2013*. Royal Society of Chemistry.

5 Moss, G.P. (1996). Basic terminology of stereochemistry (IUPAC Recommendations 1996). *Pure Appl. Chem.* 68 (12): 2193–2222.

6 Prelog, V. (1976). Chirality in chemistry. *Science* 193 (4247): 17–24.

7 Bonner, W.A. (1995). Chirality and life. *Orig. Life Evol. Biosph.* 25: 175–190.

8 Brooks, W.H., Guida, W.C., and Daniel, K.G. (2011). The significance of chirality in drug design and development. *Curr. Top. Med. Chem.* 11 (7): 760–770.

9 Zhang, Y., Yu, S., Han, B. et al. (2022). Circularly polarized luminescence in chiral materials. *Matter* 5 (3): 837–875.

10 Salem, M.S.H., Sharma, R., Khalid, M.I. et al. (2023). Data-driven electrochemical one-pot synthesis of double hetero [7] dehydrohelicene. *Electrochemistry* 91 (11): 112015.

11 Salem, M.S.H., Khalid, M.I., Sako, M. et al. (2023). Electrochemical synthesis of hetero[7]helicenes containing pyrrole and furan rings *via* an oxidative heterocoupling and dehydrative cyclization sequence. *Adv. Synth. Catal.* 365 (3): 373–380.

12 Khalid, M.I., Salem, M.S.H., Sako, M. et al. (2022). Electrochemical synthesis of heterodehydro[7]helicenes. *Commun. Chem.* 5 (1): 166.

13 Noyori, R. (2002). Asymmetric catalysis: science and opportunities (Nobel lecture). *Angew. Chem. Int. Ed.* 41 (12): 2008–2022.

14 Walsh, P.J. and Kozlowski, M.C. (2009). *Fundamentals of Asymmetric Catalysis*. University Science Books.

15 Berkessel, A. and Gröger, H. (2006). *Asymmetric Organocatalysis: From Biomimetic Concepts to Applications in Asymmetric Synthesis*. John Wiley & Sons.

16 Salem, M.S.H. and Takizawa, S. (2022). New anionic cobalt (III) complexes enable enantioselective synthesis of spiro-fused oxazoline and iodoacetal derivatives. *Front. Chem.* 10: 1034291. https://doi.org/10.3389/fchem.2022.1034291.

17 Christie, G.H. and Kenner, J. (1922). LXXI—the molecular configurations of polynuclear aromatic compounds. Part I. The resolution of γ-6:6′-dinitro-and 4:6:4′:6′-tetranitro-diphenic acids into optically active components. *J. Chem. Soc. Trans.* 121: 614–620.

18 Miyashita, A., Yasuda, A., Takaya, H. et al. (1980). Synthesis of 2,2′-bis (diphenylphosphino)-1,1′-binaphthyl (BINAP), an atropisomeric chiral bis (triaryl) phosphine, and its use in the rhodium (I)-catalyzed asymmetric hydrogenation of. alpha.-(acylamino) acrylic acids. *J. Am. Chem. Soc.* 102 (27): 7932–7934.

19 Akiyama, T., Itoh, J., Yokota, K., and Fuchibe, K. (2004). Enantioselective Mannich-type reaction catalyzed by a chiral Brønsted acid. *Angew. Chem. Int. Ed.* 43 (12): 1566–1568.

20 Uraguchi, D. and Terada, M. (2004). Chiral Brønsted acid-catalyzed direct Mannich reactions *via* electrophilic activation. *J. Am. Chem. Soc.* 126 (17): 5356–5357.

21 Hu, F. and Xia, Y. (2023). Axial chirality in alkylidene-cyclic molecules. *Eur. J. Org. Chem.* 26 (20): e202300151.

22 Smyth, J.E., Butler, N.M., and Keller, P.A. (2015). A twist of nature–the significance of atropisomers in biological systems. *Nat. Prod. Rep.* 32 (11): 1562–1583.

23 Roos, C.B., Chiang, C.-H., Murray, L.A. et al. (2023). Stereodynamic strategies to induce and enrich chirality of atropisomers at a late stage. *Chem. Rev.* 123 (17): 10641–10727.

24 Basilaia, M., Chen, M.H., Secka, J., and Gustafson, J.L. (2022). Atropisomerism in the pharmaceutically relevant realm. *Acc. Chem. Res.* 55 (20): 2904–2919.

25 Perreault, S., Chandrasekhar, J., and Patel, L. (2022). Atropisomerism in drug discovery: a medicinal chemistry perspective inspired by atropisomeric class I PI3K inhibitors. *Acc. Chem. Res.* 55 (18): 2581–2593.

26 Kozlowski, M.C., Miller, S.J., and Perreault, S. (2023). Atropisomers: synthesis, analysis, and applications. *Acc. Chem. Res.* 56 (3): 187–188.

27 Bai, X.-F., Cui, Y.-M., Cao, J., and Xu, L.W. (2022). Atropisomers with axial and point chirality: synthesis and applications. *Acc. Chem. Res.* 55 (18): 2545–2561.

28 Wan, S.-P., Lu, H.-Y., Li, M., and Chen, C.F. (2022). Advances in circularly polarized luminescent materials based on axially chiral compounds. *J Photochem Photobiol C: Photochem Rev* 50: 100500.

29 Zhou, Q.-L. (2011). *Privileged Chiral Ligands and Catalysts*. John Wiley & Sons.

30 Zamfir, A., Schenker, S., Freund, M., and Tsogoeva, S.B. (2010). Chiral BINOL-derived phosphoric acids: privileged Brønsted acid organocatalysts for C–C bond formation reactions. *Org. Biomol. Chem.* 8 (23): 5262–5276.

31 Toenjes, S.T. and Gustafson, J.L. (2018). Atropisomerism in medicinal chemistry: challenges and opportunities. *Future Med. Chem.* 10 (4): 409–422.

32 Clayden, J., Moran, W.J., Edwards, P.J., and La Plante, S.R. (2009). The challenge of atropisomerism in drug discovery. *Angew. Chem. Int. Ed.* 48 (35): 6398–6401.

33 Wang, Y.-B. and Tan, B. (2018). Construction of axially chiral compounds *via* asymmetric organocatalysis. *Acc. Chem. Res.* 51 (2): 534–547.

34 Cheng, J.K., Xiang, S.-H., Li, S. et al. (2021). Recent advances in catalytic asymmetric construction of atropisomers. *Chem. Rev.* 121 (8): 4805–4902.

35 Tan, B. (2021). *Axially Chiral Compounds: Asymmetric Synthesis and Applications*. John Wiley & Sons.

36 Lassaletta, J.M. and Fernandez, R. (2019). *Atropisomerism and Axial Chirality*. World Scientific.

37 Bringmann, G., Price Mortimer, A.J., Keller, P.A. et al. (2005). Atroposelective synthesis of axially chiral biaryl compounds. *Angew. Chem. Int. Ed.* 44 (34): 5384–5427.

38 Kumarasamy, E., Raghunathan, R., Sibi, M.P., and Sivaguru, J. (2015). Nonbiaryl and heterobiaryl atropisomers: molecular templates with promise for atropselective chemical transformations. *Chem. Rev.* 115 (20): 11239–11300.

39 Kumar, A., Sasai, H., and Takizawa, S. (2022). Atroposelective synthesis of C–C axially chiral compounds *via* mono-and dinuclear vanadium catalysis. *Acc. Chem. Res.* 55 (20): 2949–2965.

40 Baudoin, O. (2005). The asymmetric Suzuki coupling route to axially chiral biaryls. *Eur. J. Org. Chem.* 2005 (20): 4223–4229.

41 Zhang, D. and Wang, Q. (2015). Palladium catalyzed asymmetric Suzuki–Miyaura coupling reactions to axially chiral biaryl compounds: chiral ligands and recent advances. *Coord. Chem. Rev.* 286: 1–16.

42 Kitagawa, O. (2021). Chiral Pd-catalyzed enantioselective syntheses of various N–C axially chiral compounds and their synthetic applications. *Acc. Chem. Res.* 54 (3): 719–730.

43 Sun, H.R., Sharif, A., Chen, J., and Zhou, L. (2023). Atroposelective synthesis of heterobiaryls through ring formation. *Chem Eur J* 29 (27): e202300183.

44 Bringmann, G., Jansen, J.R., and Rink, H.P. (1986). Regioselective and atropoisomeric-selective aryl coupling to give naphthyl isoquinoline alkaloids: the first total synthesis of (−)-ancistrocladine. *Angew. Chem. Int. Ed. Engl.* 25 (10): 913–915.

45 Zhang, X., Zhao, K., and Gu, Z. (2022). Transition metal-catalyzed biaryl atropisomer synthesis *via* a torsional strain promoted ring-opening reaction. *Acc. Chem. Res.* 55 (12): 1620–1633.

46 Zhao, Q., Peng, C., Wang, Y.-T. et al. (2021). Recent progress on the construction of axial chirality through transition-metal-catalyzed benzannulation. *Org. Chem. Front.* 8 (11): 2772–2785.

47 Carmona, J.A., Rodríguez-Franco, C., Fernández, R. et al. (2021). Atroposelective transformation of axially chiral (hetero) biaryls. From desymmetrization to modern resolution strategies. *Chem. Soc. Rev.* 50 (5): 2968–2983.

48 Dyadyuk, A., Vershinin, V., Shalit, H. et al. (2022). A chiral iron disulfonate catalyst for the enantioselective synthesis of 2-amino-2′-hydroxy-1,1′-binaphthyls (NOBINs). *J. Am. Chem. Soc.* 144 (8): 3676–3684.

49 Surgenor, R.R., Liu, X., Keenlyside, M.J. et al. (2023). Enantioselective synthesis of atropisomeric indoles *via* iron-catalysed oxidative cross-coupling. *Nat. Chem.* 15 (3): 357–365.

50 Hayashi, H., Ueno, T., Kim, C., and Uchida, T. (2020). Ruthenium-catalyzed cross-selective asymmetric oxidative coupling of arenols. *Org. Lett.* 22 (4): 1469–1474.

51 Langeslay, R.R., Kaphan, D.M., Marshall, C.L. et al. (2018). Catalytic applications of vanadium: a mechanistic perspective. *Chem. Rev.* 119 (4): 2128–2191.

52 Sako, M., Takeuchi, Y., Tsujihara, T. et al. (2016). Efficient enantioselective synthesis of oxahelicenes using redox/acid cooperative catalysts. *J. Am. Chem. Soc.* 138 (36): 11481–11484.

53 Miyaura, N., Yamada, K., and Suzuki, A. (1979). A new stereospecific cross-coupling by the palladium-catalyzed reaction of 1-alkenylboranes with 1-alkenyl or 1-alkynyl halides. *Tetrahedron Lett.* 20 (36): 3437–3440.

54 Kotha, S., Lahiri, K., and Kashinath, D. (2002). Recent applications of the Suzuki–Miyaura cross-coupling reaction in organic synthesis. *Tetrahedron* 58 (48): 9633–9695.

55 Baudoin, O., Cesario, M., Guenard, D., and Guéritte, F. (2002). Application of the palladium-catalyzed borylation/Suzuki coupling (BSC) reaction to the synthesis of biologically active biaryl lactams. *J. Org. Chem.* 67 (4): 1199–1207.

56 Torborg, C. and Beller, M. (2009). Recent applications of palladium-catalyzed coupling reactions in the pharmaceutical, agrochemical, and fine chemical industries. *Adv. Synth. Catal.* 351 (18): 3027–3043.

57 Patel, N.D., Sieber, J.D., Tcyrulnikov, S. et al. (2018). Computationally assisted mechanistic investigation and development of Pd-catalyzed asymmetric Suzuki–Miyaura and Negishi cross-coupling reactions for tetra-ortho-substituted biaryl synthesis. *ACS Catal.* 8 (11): 10190–10209.

58 Link, A. and Sparr, C. (2014). Organocatalytic atroposelective aldol condensation: synthesis of axially chiral biaryls by arene formation. *Angew. Chem. Int. Ed.* 53 (21): 5458–5461.

59 Zilate, B., Castrogiovanni, A., and Sparr, C. (2018). Catalyst-controlled stereoselective synthesis of atropisomers. *ACS Catal.* 8 (4): 2981–2988.

60 Moser, D. and Sparr, C. (2022). Synthesis of atropisomeric two-axis systems by the catalyst-controlled syn-and anti-selective arene-forming aldol condensation. *Angew. Chem. Int. Ed.* 61 (24): e202202548.

61 García Mancheño, O. and Waser, M. (2023). Recent developments and trends in asymmetric organocatalysis. *Eur. J. Org. Chem.* 26 (1): e202200950.

62 Wang, G., Huang, J., Zhang, J., and Fu, Z. (2022). Catalytically atroposelective ring-opening of configurationally labile compounds to access axially chiral biaryls. *Org. Chem. Front.* 9 (16): 4507–4521.

63 Brandes, S., Niess, B., Bella, M. et al. (2006). Non-biaryl atropisomers in organocatalysis. *Chem Eur J* 12 (23): 6039–6052.

64 Mei, G.-J., Koay, W.L., Guan, C.-Y., and Lu, Y. (2022). Atropisomers beyond the C–C axial chirality: advances in catalytic asymmetric synthesis. *Chem* 8 (7): 1855–1893.

65 Mandai, H., Fujii, K., Yasuhara, H. et al. (2016). Enantioselective acyl transfer catalysis by a combination of common catalytic motifs and electrostatic interactions. *Nat. Commun.* 7 (1): 11297.

66 Bringmann, G., Gulder, T., Gulder, T.A., and Breuning, M. (2011). Atroposelective total synthesis of axially chiral biaryl natural products. *Chem. Rev.* 111 (2): 563–639.

67 Carson, M.C. and Kozlowski, M.C. (2023). Recent advances in oxidative phenol coupling for the total synthesis of natural products. *Nat. Prod. Rep.* https://doi.org/10.1039/D3NP00009E.

68 LaPlante, S.R., Fader, L.D., Fandrick, K.R. et al. (2011). Assessing atropisomer axial chirality in drug discovery and development. *J. Med. Chem.* 54 (20): 7005–7022.

69 LaPlante, S.R., Edwards, P.J., Fader, L.D. et al. (2011). Revealing atropisomer axial chirality in drug discovery. *ChemMedChem* 6 (3): 505–513.

70 Carlsson, A.-C.C., Karlsson, S., Munday, R.H., and Tatton, M.R. (2022). Approaches to synthesis and isolation of enantiomerically pure biologically active atropisomers. *Acc. Chem. Res.* 55 (20): 2938–2948.

2

Iron- and Ruthenium-Catalyzed Atroposelective Synthesis of Axially Chiral Compounds

Tatsuya Uchida

Kyushu University, Faculty of Arts and Science, 744 Motooka, Nishi-ku, Fukuoka, 819-0395, Japan
Kyushu University, International Institute for Carbon-Neutral Energy Research (WPI-I2CNER), 744 Motooka, Nishi-ku, Fukuoka 819-0395, Japan

2.1 Introduction

Aromatic rings are essential motifs for the synthesis of cyclic compounds, in particular, functional organic molecules based on complex cyclic compounds bearing multistereocenters. Therefore, the transformation of aromatic compounds via diverse approaches such as cross-coupling reactions, C–H activation, and enantioselective reduction of aromatic rings has been intensively studied [1–3]. Among these, the oxidative transformation of electron-rich and abundant arenols has received much attention for the synthesis of valuable compounds such as bisarenols. These frameworks are widespread in chiral sources for asymmetric transformations and are common in natural products [4, 5]. Thus, the oxidation as well as the stereoselective transformation of arenols has been the subject of intense research. For this transformation, chiral copper salts, later vanadyl complexes, and complexes based on group 8 elements such as iron and ruthenium have been proven to be efficient catalysts [6]. In this chapter, we focus on group 8 transition-metal complexes as catalysts for the stereoselective oxidation of arenols.

It has been known for a long time that ferric chloride and ferric cyanide oxidize arenols to produce bisarenol derivatives. However, the oxidation of arenols catalyzed by these reagents suffers from a limited substrate scope owing to the occurrence of side reactions such as overoxidation to quinone derivatives and Friedel–Craft substitutions. In contrast, in the past two decades, iron and ruthenium complexes have been demonstrated as unique and efficient catalysts for atroposelective synthetic processes such as oxidative coupling to bisarenols and spirocyclization. These developments are summarized in this chapter.

Atropisomerism in Asymmetric Organic Synthesis: Challenges and Applications, First Edition.
Edited by Shinobu Takizawa and Mohamed S. H. Salem.

2.2 Oxidative Homo-coupling of 2-Naphthols to BINOL and Its Derivatives

Axial chiral binaphthalene derivatives such as 1,1′-bi-2-naphthol (BINOL) and 2,2′-bis(diphenylphosphino)-1,1′-binathyl (BINAP) are widely used as ligands in various highly stereoselective reactions [5]. Therefore, the selective synthesis of optically active BINOLs has attracted widespread interest. Several transition-metal complexes were traditionally used as stoichiometric oxidants or catalysts for the synthesis of BINOLs via coupling reactions until Nakajima et al. reported a highly enantioselective catalytic oxidative coupling in 1999 [7]. They found that chiral diamine-supported copper salts can catalyze the oxidation of methyl 2-hydroxy-3-naphthoate to the corresponding BINOL with 78% enantiomeric excess (ee) using dioxygen in air as the hydrogen acceptor. Subsequently, Katsuki et al. presented (nitrosyl)ruthenium-salen ([ON]Ru-salen) complexes as coupling catalysts (Scheme 2.1) [8]. Prior to this work, they found that chiral (ON)Ru-salen **1** can catalyze oxidative kinetic resolution of racemic secondary alcohols using molecular oxygen as the hydrogen acceptor [9a]. According to the findings from the mechanistic studies, under visible light irradiation conditions, (ON)Ru-salen complexes release NO, and the resulting vacant site at the ruthenium ion is occupied by an alcohol group (Scheme 2.2). These complexes could activate dioxygen to the corresponding ruthenium (superoxide) intermediate via single-electron transfer (SET) from the metal center to dioxygen, followed by dehydrogenation of the coordinated alcohol to the corresponding ketone in a stereoselective manner [9]. Based on the mechanistic considerations, they thought that, in the presence of arenols instead of alcohols, (ON)Ru-salen complexes bearing a binaphthyl framework catalyzed the oxidative coupling to yield the desired bisarenol in a stereoselective manner.

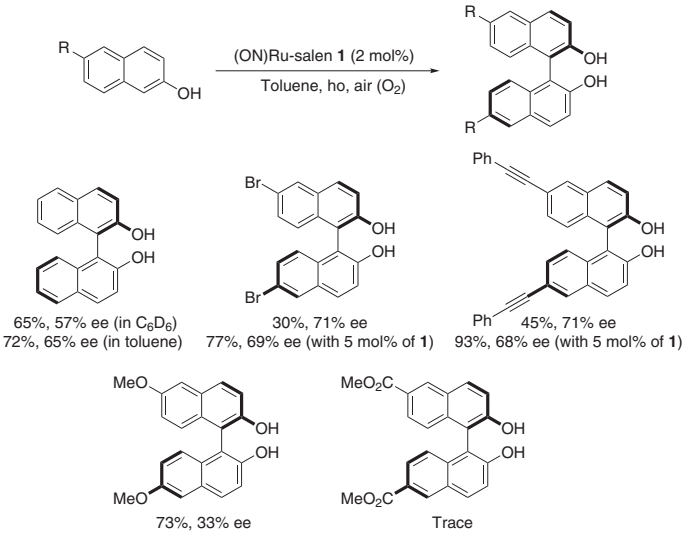

Scheme 2.1 (ON)Ru-salen **1**-catalyzed stereoselective coupling of 2-naphthols.

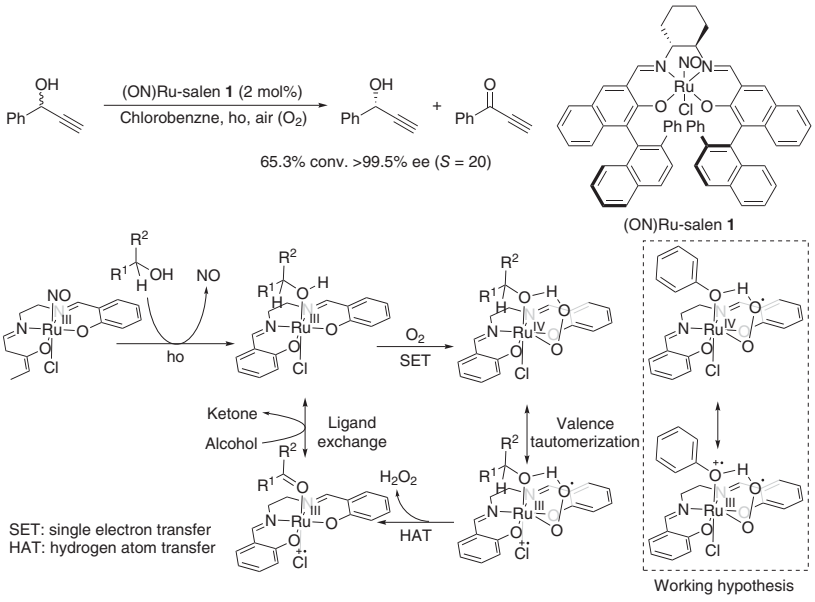

Scheme 2.2 Working hypothesis of oxidation of arenol based on the mechanism of Ru-salen-catalyzed aerobic oxidation of alcohols.

In particular, complex **1**, which exhibits a relative configuration of (*Ra*,*R*) between the binaphthyl and cyclohexanediamine units, afforded better results in terms of yield (65%) and enantioselectivity (57% ee) in C_6D_6. The yield and enantioselectivity were also improved by using toluene as the solvent. These ruthenium-catalyzed reactions were notable for not requiring a directing group such as an ester group at the C3 position on 2-naphthols. Using 2 mol% of complex **1**, the reaction of 6-bromo- and 6-phenyethynyl-2-naphthols yielded the corresponding 6,6′-bisubstituted-1,1′-bi-2-naphthols with 71% ee, albeit in moderate yields. Fortunately, the yields could be improved to 77% and 93% with a slight decrease in stereoselectivity by increasing the catalyst loading to 5 mol%. The homo-coupling product of 6-methoxy-2-naphthol was also produced in 73% yield, with 33% ee using 2 mol% of complex **1**. However, the reaction of a naphthol bearing a methyl carboxylate group was sluggish due to its poor solubility in a less polar solvent and the presence of the electron-withdrawing group.

After that, chiral copper and oxyvanadyl complexes were introduced as catalysts of the oxidative coupling, achieving high enantioselectivities [6]. Egami and Katsuki also reported on the efficacy of the μ-hydroxo-dimer of iron complex bearing a salan ligand, a reduced form of salen, in catalyzing the oxidative coupling of 2-naphthol derivatives (Scheme 2.3) [10]. They found that a salan ligand containing two amino groups could reduce the oxidation potential of the metal complex, and the amino protons regulated the configuration of the coordinated arenol via hydrogen bonding. Consequently, they conducted the aerobic oxidation of 2-naphthols using iron-salan complexes as catalysts. However, most iron-salan complexes exhibited

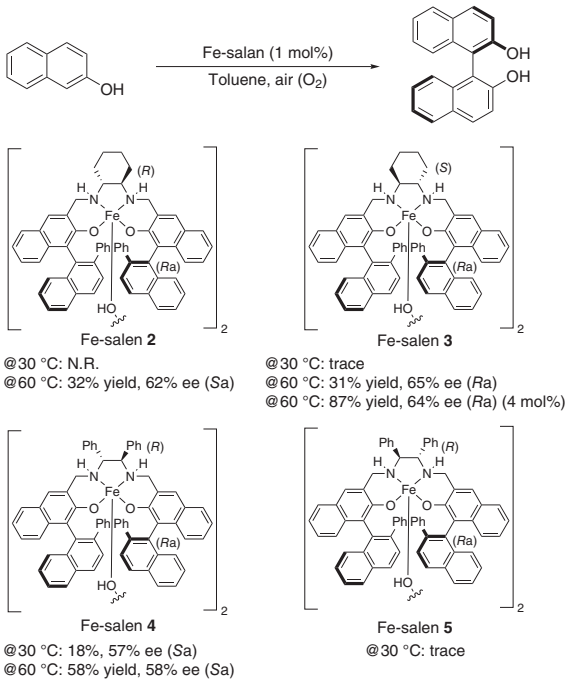

Scheme 2.3 Surveying the efficient iron catalyst for asymmetric aerobic oxidative coupling of 2-naphthol.

poor catalytic performance in this reaction at 30 °C in toluene. Only iron-salan complex **4**, which contained an (*R*a)-binaphthyl moiety and (1*R*,2*R*)-1,2-diphenylethylenediamine, gave (*S*a)-BINOL in 18% yield with 57% ee. Fortunately, increasing the reaction temperature to 60 °C improved the yield to 58% without reducing the enantioselectivity. At 60 °C, other iron-salan complexes bearing the binaphthyl framework gave the product with better enantioselectivity than complex **4**. The reaction with (*R*a,*S*) iron-salan **3** bearing a cyclohexanediamine core as the catalyst afforded the best result in terms of enantioselectivity. Moreover, using 4 mol% of catalyst improved the yield to 87%.

Under the optimized conditions, iron-salan complex **3** catalyzed the reaction of C6-substituted 2-naphthols with moderate enantioselectivity, irrespective of the electronic nature of the substituent (Scheme 2.4). However, when complex **3** was used as the catalyst, the reaction of 3-methyl-2-naphthol afforded an insufficient stereoselectivity of 16% ee. In contrast, a high enantioselectivity of 77% ee was observed in the reaction of 3-methyl-2-naphthol when complex **4** was used as the catalyst. Complex **4** exhibited better catalytic performance in the reaction of C3-substituted 2-naphthols. For instance, the reaction of 3-aryl-2-naphthol yielded 3,3′-diaryl-1,1′-bi(2-naphthol) with excellent enantioselectivity, while 3-phenyl- and 3-trimethylsilylethenyl-2-naphthols also afforded excellent stereoselectivity and yield. Even the presence of electron-withdrawing halogenated substituents at the C3 position resulted in excellent ee, albeit with slightly reduced yields. However,

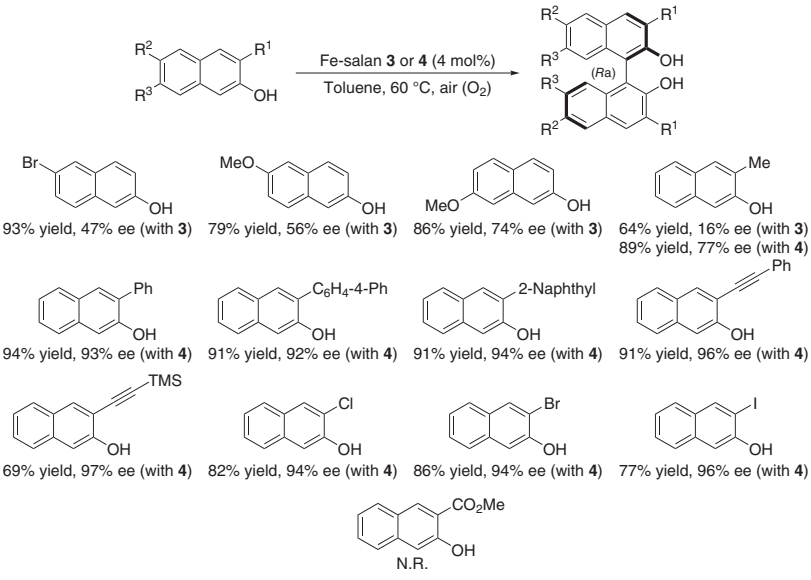

Scheme 2.4 Iron-salan-catalyzed asymmetric aerobic oxidation of 2-naphthols.

no reaction was observed for methyl 2-hydroxynaphthylcarboxylate bearing an electron-deficient functional group.

Later, Pappo et al. reported the enantioselective oxidative coupling of 2-naphthols to BINOLs using chiral iron-phosphate complexes as catalysts (Scheme 2.5) [11]. A screening of the reaction conditions, such as the iron salt, base, phosphate ligand, and oxidant, revealed that the combination of $Fe(ClO_4)_3$,

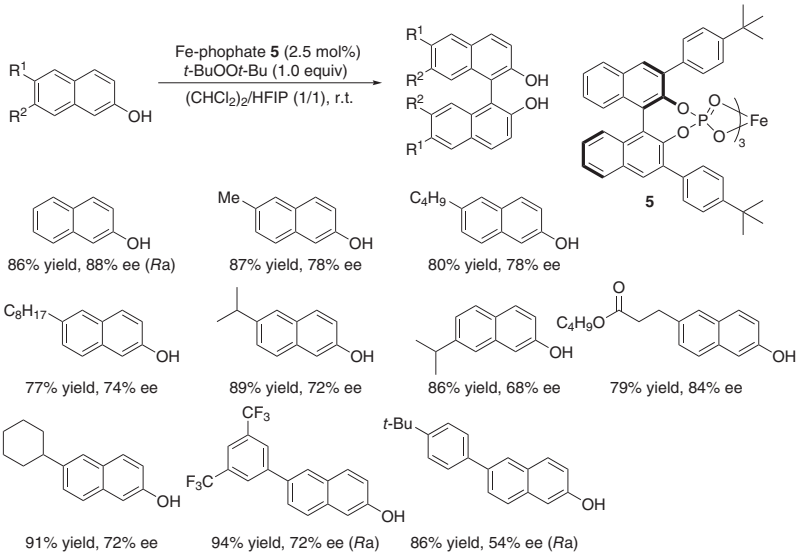

Scheme 2.5 Chiral iron-phosphate-catalyzed oxidative coupling of 2-naphthols.

$CaCO_3$, 3,3′-bis(4-*tert*-butylphenyl)BINOL-phosphate, and di-*tert*-butyl peroxide (*t*-BuOO*t*-Bu) was efficient for the reaction. Under the optimized conditions, the chiral iron-phosphate complex **5** catalyzed the oxidation of 2-naphthol to furnish (*Ra*)-BINOL in 86% yield with 88% ee. 2-Naphthol substituted at the C6 position with either primary or secondary alkyl groups was converted into the desired BINOLs in good to high enantioselectivities and yields. 6,6′-Diarylated BINOLs were also produced with good stereoselectivity under the optimized conditions.

On the basis of a kinetic study, the authors proposed that the oxidative coupling of 2-naphthols catalyzed by chiral iron-phosphate complexes involved the decomposition of the coordinated *t*-BuOO*t*-Bu to high-valent iron species and *tert*-butoxyl radical, resulting in a ligand exchange from phosphate to naphthoxide (Scheme 2.6). Then, valence tautomerization via SET from the naphthoxide ligand to the metal ion produced an electrophilic naphthoxyl radical, and subsequent nucleophilic coupling of arenol and rearomatization via hydrogen abstraction with the *tert*-butoxyl radical furnished the corresponding chiral BINOL, which was released via ligand exchange. However, the SET process in the catalytic cycle resulted in racemization of the product and decreased the enantioselectivity of the resulting BINOL via overoxidation.

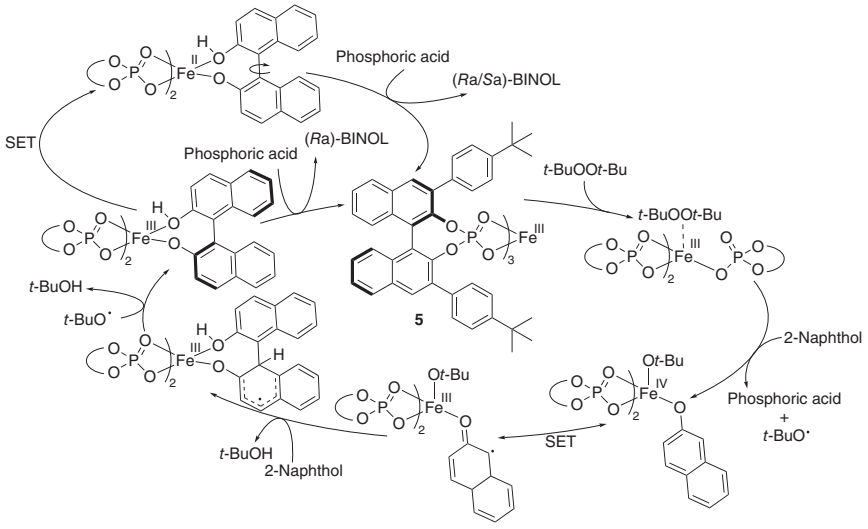

Scheme 2.6 The mechanism of chiral iron-phosphate-catalyzed oxidative coupling of 2-naphthols.

Ishihara et al. described that chiral diphosphine oxide iron complexes catalyzed efficiently the oxidative coupling of 2-naphthol derivatives (Scheme 2.7) [12]. In particular, an (*Sa*)-Xylyl-BIPHEP **A**-supported iron salt catalyzed the oxidative coupling of 2-naphthol in 95% yield with 70% ee using *tert*-butylperoxide as the oxidant at 0 °C. This iron-catalyzed coupling system afforded good to high enantioselectivities with C7-substituted 2-naphthols irrespective of the electronic nature and steric hindrance of the substituents (up to 92% ee). Furthermore, in the reactions of 6-substituted 2-naphthols, (*Sa*)-Xylyl-BIPHEP **B** was more

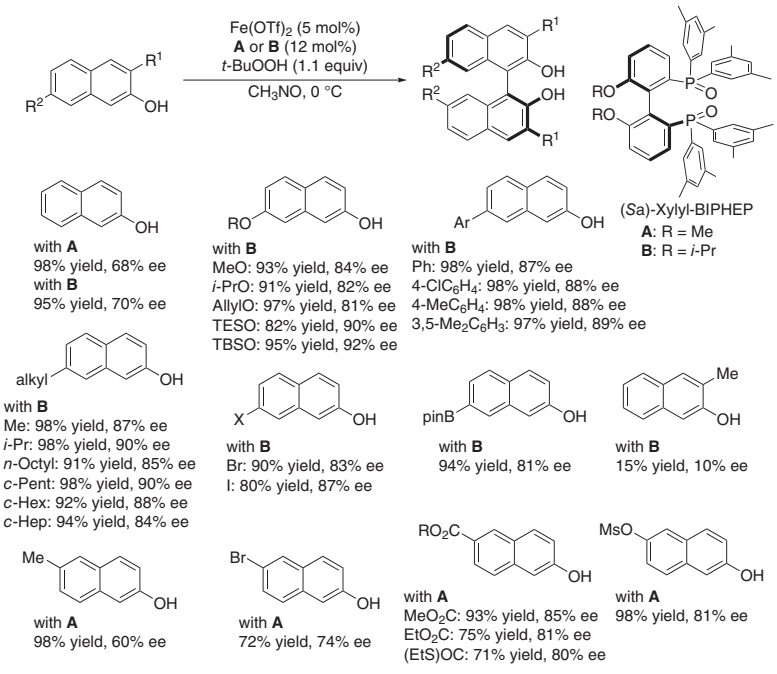

Scheme 2.7 Chiral diphosphine oxide iron complex-catalyzed asymmetric oxidative coupling of 2-naphthols.

effective than (*S*a)-Xylyl-BIPHEP **A**. The reaction of 2-naphthol bearing an electron-donating methyl group at C6 afforded 60% ee, whereas substrates bearing electron-withdrawing groups gave good enantioselectivities.

The authors proposed a catalytic cycle in which the precatalyst iron(II) species **I** was oxidized to the corresponding iron(III) intermediate **II**, producing a naphthoxyl radical cation **III**. Subsequently, its tautomer **III′** underwent the oxidative nucleophilic addition of an arenol to yield coupling intermediate **IV**, which was reoxidized to the iron(III) species with the concomitant formation of iron naphthoxide **II** and the desired BINOL via ligand exchange (Scheme 2.8).

Recently, Liu et al. reported chiral bisquinolyldiamines as efficient ligands in the iron-catalyzed oxidative coupling of 2-naphthols (Scheme 2.9) [13]. Thus, 3- and 6-substituted 2-naphthols gave the corresponding BINOLs with good enantioselectivity. However, 2-naphthols bearing electron-withdrawing carbonyl groups such as carboxylic acid, benzoyl, and benzyl carboxylate groups did not work under the reaction conditions.

Very recently, Knölker applied the iron-catalyzed aerobic oxidative coupling to diarylamine derivatives, finding that using hexadecafluorophthalocyanine iron(II) ($FePcF_{16}$) as the catalyst and a chiral Brønsted acid as the cocatalyst under air yielded the corresponding homo-coupling product in a stereo- and chemoselective manner along with slight production of *N*-aryldibenzo[c,g]carbazole as an overoxidation product (Scheme 2.10) [14]. In the model reaction using *N*-phenyl-2-naphthylamine, 3,3′-bis(triphenylsilyl)BINOL-phosphoric acid

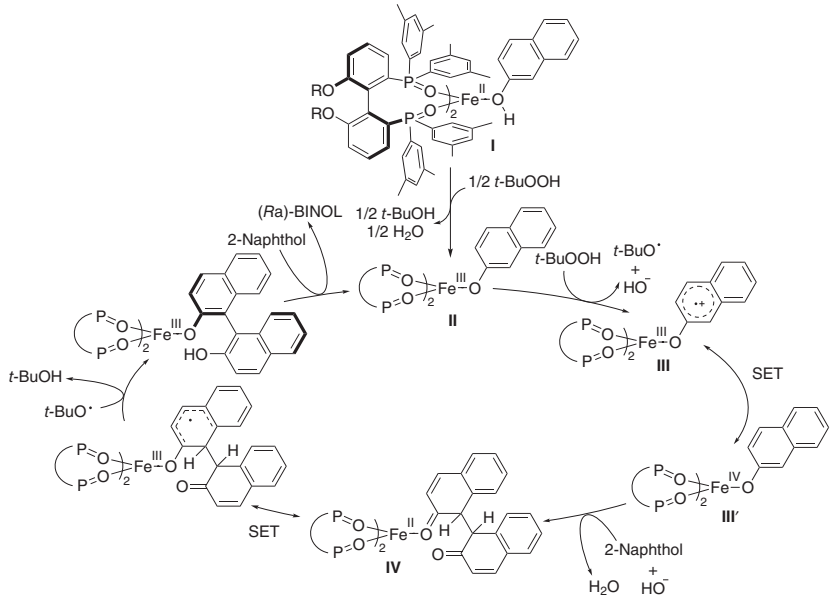

Scheme 2.8 Proposed mechanism of chiral diphosphine oxide iron complex-catalyzed asymmetric oxidative coupling of 2-naphthols.

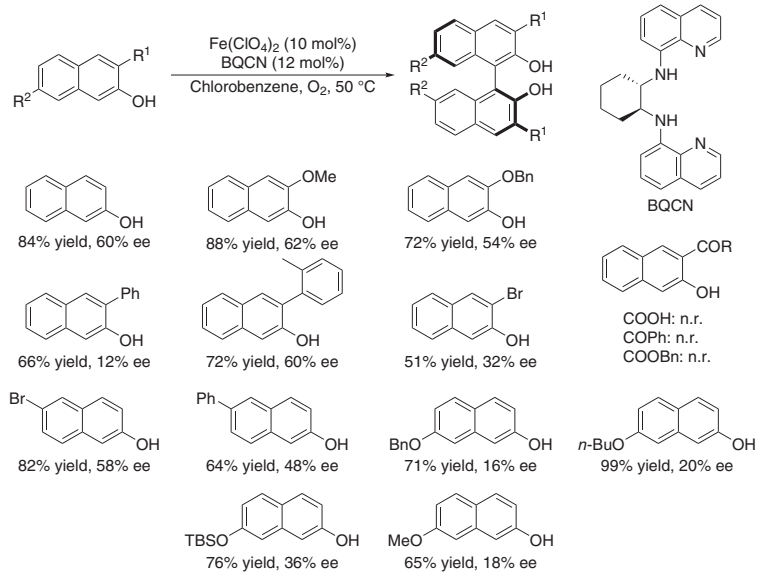

Scheme 2.9 Chiral BQCN iron complex-catalyzed asymmetric aerobic oxidative coupling of 2-naphthols.

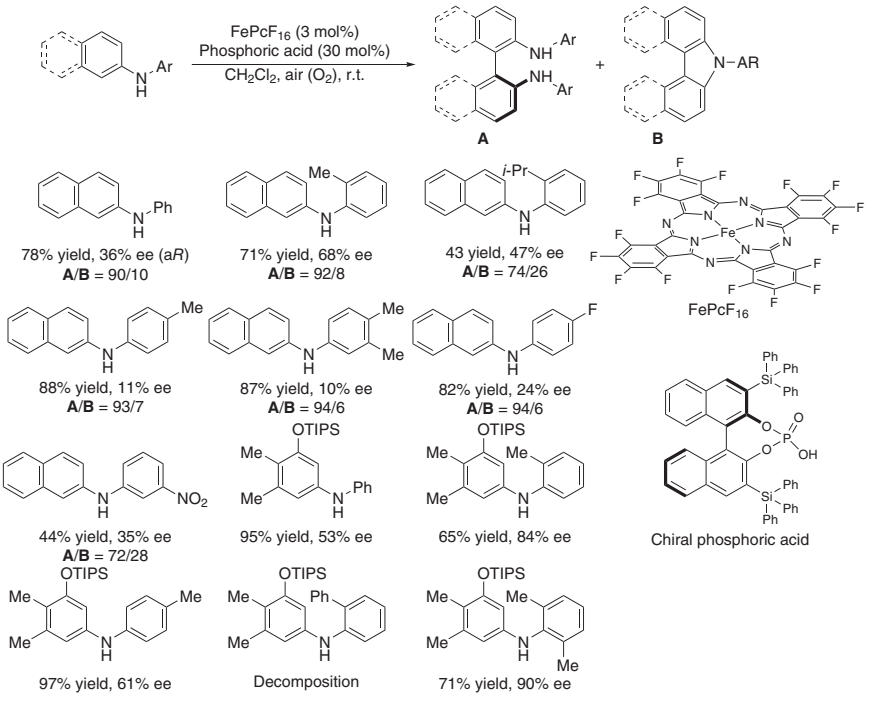

Scheme 2.10 Stereo- and chemoselective aerobic oxidative coupling of diarylamine.

gave 2,2′-bis(phenylamino)-1,1′-binaphthyl in 78% yield with 36% ee and the corresponding carbazole in 7% yield. Under the optimized conditions, several *N*-aryl-2-naphthylamines afforded the corresponding binaphthylamines with high chemoselectivity and moderate to good enantioselectivities. The reaction of biphenylamine derivatives also produced biaryl compounds with better yields and higher enantioselectivities up to 90% ee.

2.3 Oxidative Cross-coupling of 2-Naphthols to Asymmetric BINOLs

Progress in the transition-metal-catalyzed symmetric oxidative homo-coupling of 2-naphthols has led to the synthesis of various C_2-symmetric BINOLs such as 3,3′-, 6,6′-, and 7,7′-disubstituted BINOLs with good to high enantioselectivities, regardless of the electronic nature of the substituents. In contrast, the selective synthesis of C_1-symmetric bisarenols using this strategy still constitutes a challenge because to realize the cross-coupling, one arenol should be oxidized to a radical or a radical cation and subsequently coupled with the other arenol in a chemoselective manner to avoid undesired homo-coupling reactions. However, it is difficult for arenols having similar structures and electronic nature to undergo oxidative coupling. Nevertheless, several selective oxidative cross-couplings have been achieved using

Lewis acid-mediated copper catalysis with substrates such as 2-naphthols bearing esters and ketones at the C3 position [15]. Similarly, iron and ruthenium catalysts also afforded interesting results in this field.

In 2010, Katsuki et al. described a highly selective cross-coupling reaction using a di-μ-hydroxo iron-salan dimer as the catalyst [16]. During the investigation of the reaction mechanism, they found a linear correlation between the optical purity of the catalyst and the ee of the coupling product as well as a first-order dependency between the reaction rate and the substrate concentration. Based on these observations, they proposed that in the coupling reaction, the dimeric iron complex gives a monomeric naphthoxo intermediate that subsequently undergoes a rate-limiting oxidation with molecular oxygen to produce the corresponding radical intermediates, which bind with another naphthol molecule to afford a radical cation intermediate. Then, the monomeric naphthoxo intermediate regenerates via oxidative rearomatization and subsequent ligand exchange. Furthermore, they hypothesized that in the presence of two different naphthols, the more electronically rich, basic one is selectively oxidized to a radical intermediate and the other, more acidic one, acts as a nucleophile and produces the cross-coupling product in a chemoselective manner (Scheme 2.11).

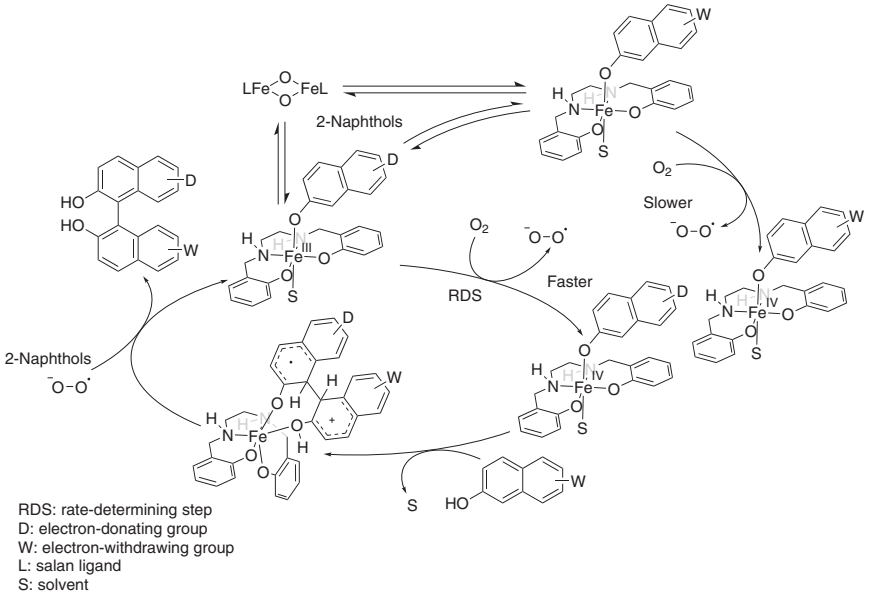

Scheme 2.11 Working hypothesis of Fe-salan-catalyzed oxidative cross-coupling of 2-naphthols.

According to their hypothesis, they conducted the cross-coupling reaction between 3-substituted electron-rich 2-naphthols **A** and 6-substituted electron-deficient naphthols **B** with the iron-salan dimer as the catalyst and achieved an excellent cross-selectivity (up to 91%) and enantioselectivity (up to 95% ee) (Scheme 2.12). In contrast, the reactions between 2-naphthols with slight

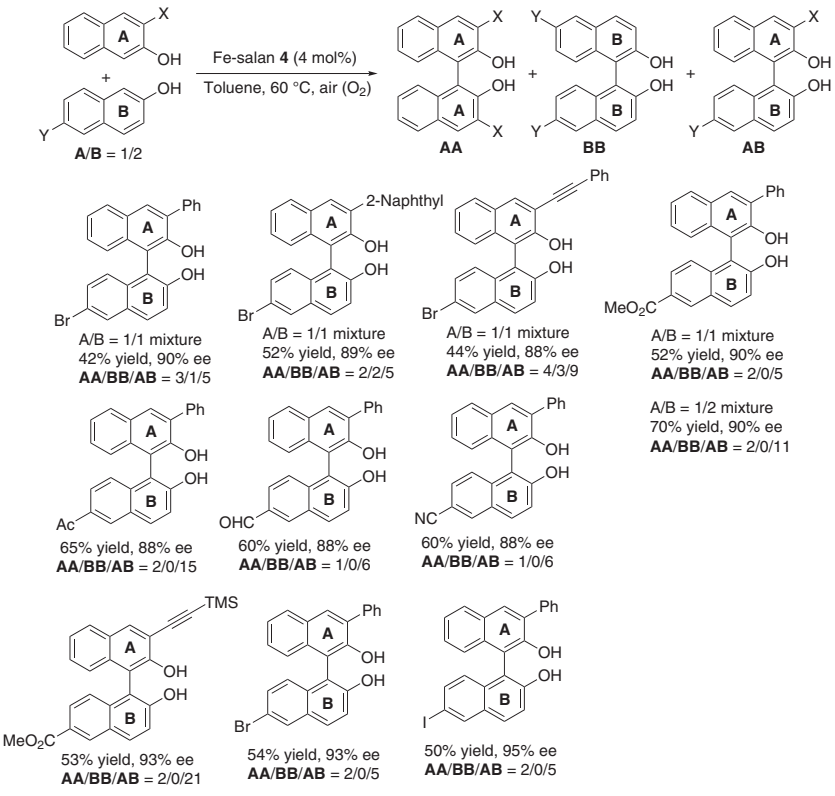

Scheme 2.12 Fe-salan **4**-catalyzed asymmetric aerobic oxidative cross-coupling of 2-naphthols.

differences in their electronic nature proceeded with insufficient cross-selectivity and both homo-coupling products were observed. Meanwhile, the reaction between 3-phenyl-2-naphthol as an electron-rich arenol and methyl 6-hydroxy-2-naphthoate as an electron-deficient arenol exhibited good cross-selectivity; no electron-deficient coupling product was observed. Increasing the amount of electron-deficient naphthol by twofold resulted in an enhancement of the cross-selectivity of 85%. The authors further investigated the effect of electron-withdrawing groups such as acetyl, formyl, and nitrile groups on the reaction, finding that these substituents suppressed the homo-coupling and showed high cross-selectivity (>85%). The combination with electron-deficient methyl 6-hydroxy-2-naphthoate resulted in excellent cross-selectivity. Especially, slight electron-withdrawing bromide and iodide groups at the C2 position gave C_1-symmetric BINOL with excellent cross- and enantioselectivity.

Later, Pappo et al. described an efficient strategy for the cross-coupling of phenols via a coupling mechanism involving a chelated radical anion, according to which a phenol with lower oxidation potential selectively oxidizes to the corresponding phenoxyl radical intermediate and another stronger nucleophilic phenol selectively undergoes an oxidative addition to form the corresponding cross-coupling adducts,

yielding the desired bisarenols via rearomatization [17]. As a proof of concept, they conducted the reaction with iron chloride as the catalyst using bis-*tert*-butylperoxide as the hydrogen acceptor and achieved a systematic cross-selective coupling between a wide range of mixed arenols. Subsequently, they extended this concept to the asymmetric version using 3,3′-bis(4-*tert*-butylphenyl)BINOL-phosphate-iron complex **5**, which was prepared form $Fe(ClO_4)_3$ and the corresponding phosphoric acid with $CaCO_3$ as a base [11]. A 1 : 1 mixture of 2-naphthol and C6- or C7-substituted 2-naphthol showed moderate cross-selectivity (Scheme 2.13).

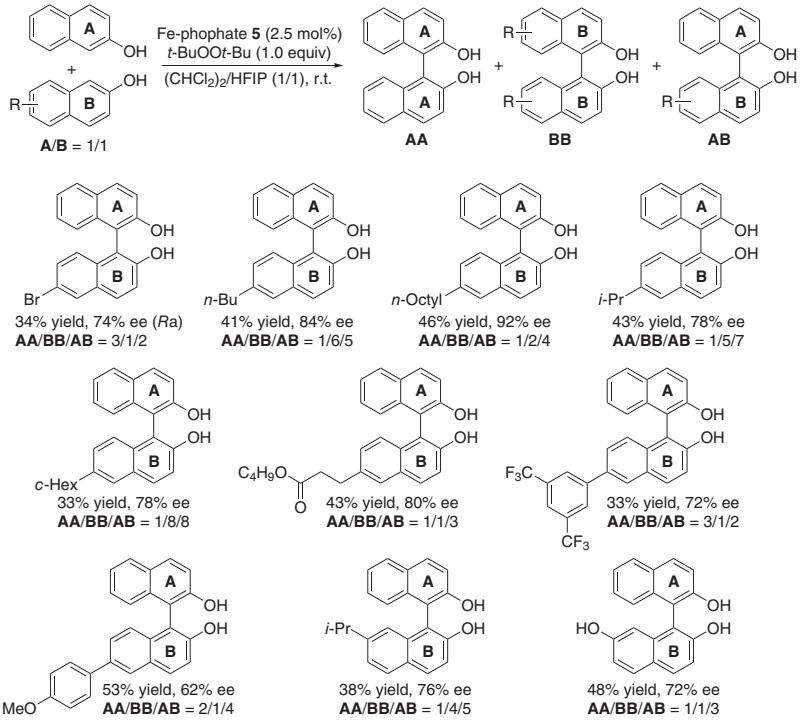

Scheme 2.13 Chiral Fe-phosphate **5**-catalyzed asymmetric aerobic oxidative cross-coupling of 2-naphthols.

Furthermore, they applied the iron-catalyzed cross-coupling method to synthesize an enantiomerically pure 2-amino-2′-hydroxyl-1,1′-binaphthyl (NOBIN), which is used as a chiral source for ligands and catalysts in asymmetric transformations [18, 19]. The reaction between C3-substituted-2-naphthols and 2-naphthylamine derivatives bearing a labile chiral auxiliary with $FeCl_3$ as the catalyst and bis-*tert*-butylperoxide as the oxidant under trifluoroacetic acidic conditions produced the diastereo mixture of the cross-coupling product with moderate to high stereoselectivities (Scheme 2.14). In particular, high diastereoselectivity was observed in the reaction of 3-methoxy-2-naphthylamine derivatives.

Very recently, further developments in the cross-selective synthesis of NOBIN have been achieved by introducing a chiral iron disulfonate complex as the catalyst to realize an inner sphere radical anion/nucleophile coupling (Scheme 2.15) [20]. A 1 : 1.5 mixture of methyl 7-(*tert*-butyl)-3-hydroxy-2-naphthoate

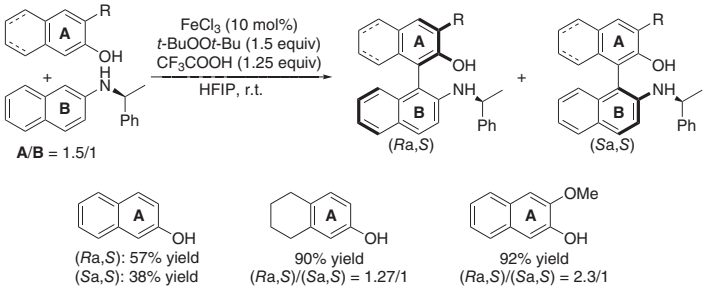

Scheme 2.14 Iron-catalyzed diastereoselective synthesis of chiral NOBINs.

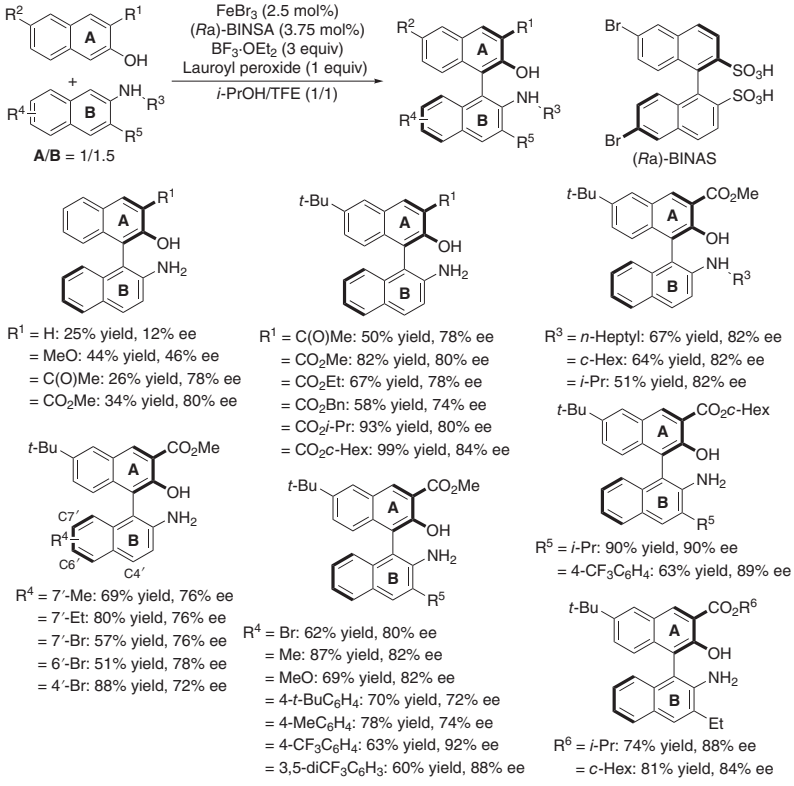

Scheme 2.15 Chiral Fe(BINSate)-catalyzed enantioselective synthesis of chiral NOBINs.

and 2-naphthylamine in the presence of $BF_3{\cdot}OEt_2$ as a binding reagent for the amine moiety using *in situ* generated iron (6,6′-bibromo-1,1′-binaphthalene-2,2′-disulfonate) (Fe[BINSate]) as the catalyst and di(dodecanoyl) peroxide (lauroyl peroxide) as the oxidant produced the desired cross-coupling compound in 82% yield with 80% ee. Under the same conditions, secondary 2-naphthylamine also resulted in a good enantioselectivity of 82% ee. Meanwhile, C4-, C6-, and C7-substituted 2-naphthylamine derivatives were converted into the corresponding products with slightly lower enantioselectivities. The presence of C3-substituents affected the enantioselectivity of the products, with the 3,5-dis(trifluoromethyl)phenyl group affording the best enantioselectivity of 88% ee in 60% yield, whereas modest

reactivity and stereoselectivity were observed in the reaction of 2-naphthol. Directing groups such as methoxy, acyl, and ester groups at the C3 position on 2-naphthol improved the enantioselectivity up to 84% ee. Furthermore, the 6-*tert*-butyl group enhanced the yield of the product without reducing the stereoselectivity.

In 2022, Smith et al. found that the iron Pybox complex is an efficient catalyst for the cross-coupling of 3-hydroxynaphthoates with an indole derivative as a coupling partner using bis(*tert*-butyl) peroxide as the oxidant (Scheme 2.16) [21]. The reaction was successful with various C2-substituted indoles, yielding the desired cross-coupling product with almost complete chemoselectivity and good to high enantioselectivities. Indoles bearing an electron-donating substituent, such as a methyl or methoxy group on the benzene core, provided better yields compared to those with electron-withdrawing substituents. Furthermore, the oxidation potential of indoles strongly influenced the yields and chemoselectivities of the coupling reaction. Specifically, lower oxidation potentials correlated with better chemoselectivity.

The authors proposed that the reaction proceeds with the formation of a high-valent chelate complex. The complex reversibly produces a naphthoxyl radical intermediate via valence tautomerization, which then undergoes nucleophilic addition with indoles to form an adduct (Scheme 2.17). Subsequent rearomatization leads to the desired coupling product.

In 2020, Uchida et al. reported an aerobic oxidative cross-coupling of 2-naphthols using (aqua)ruthenium-salen ([H_2O]Ru-salen) complexes as efficient aerobic

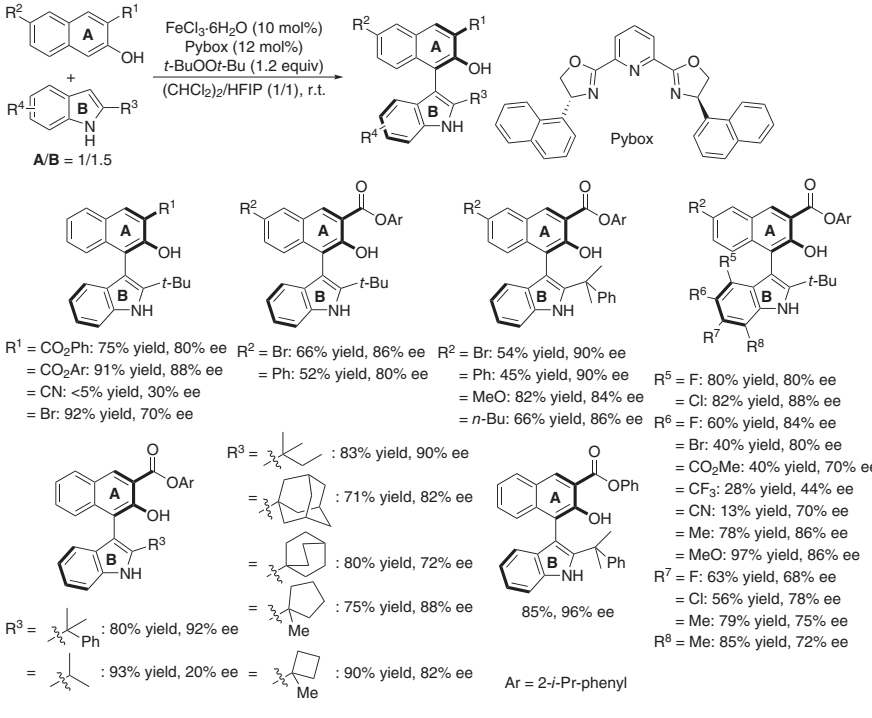

Scheme 2.16 Chiral pybox-supported iron-catalyzed enantioselective cross-coupling between 2-naphthols and indoles.

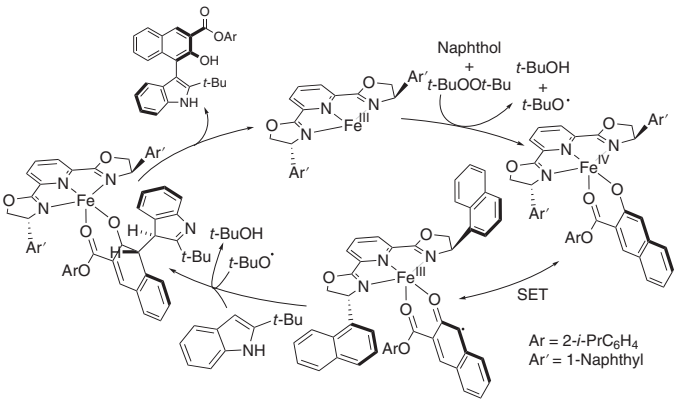

Scheme 2.17 Proposed mechanism of iron-pybox-catalyzed enantioselective cross-coupling between 2-naphthol derivatives and indole derivatives.

oxidation catalysts that do not require any activation such as heating, pressurizing, or photoirradiation [22]. The (H_2O)Ru-salen complexes catalyzed aerobic oxidations, such as olefin epoxidation and alcohol oxidation via SET from the ruthenium ion to molecular oxygen using water or alcohol as a proton and hydrogen bond donor, followed by a radical delocalization to form a radical cation intermediate [22a, b]. Mechanistic studies indicated that an arenol coordinated to the ruthenium ion could be oxidized to the desired radical anion and then undergo oxidative coupling in a stereoselective manner. Furthermore, due to their excellent ability to induce high stereoselectivity in aerobic oxidation, they envisioned that chiral (H_2O)Ru-salen could promote the cross-coupling process preferentially over the homo-coupling process, even in the absence of substantial differences in the electronic nature of the coupling partners.

To confirm their hypothesis, they investigated the homo-coupling reaction of 2-naphthol derivatives, such as 2-naphthol and 3-, 6-, and 7-bromo-2-naphthol, and found that (H_2O)Ru-salen **6** bearing a bulky 3,6-difluoro-4-trimethylsilylphenyl group at the C2″ position achieved the best enantioselectivity of 82% ee in the reaction with 2-naphthol. Moreover, 6-bromo-2-naphthol exhibited better reactivity compared to the others, yielding 87% ee (Scheme 2.18).

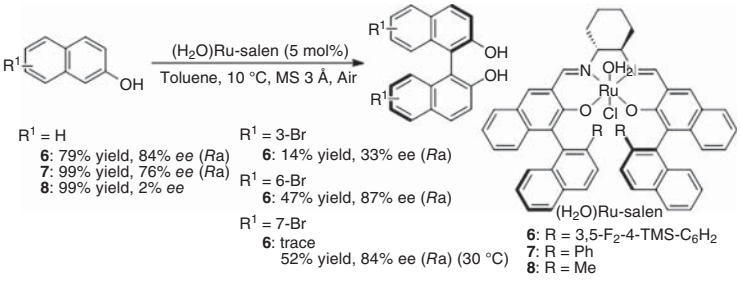

Scheme 2.18 (H_2O)Ru-salen-catalyzed asymmetric aerobic oxidative coupling of 2-naphthol.

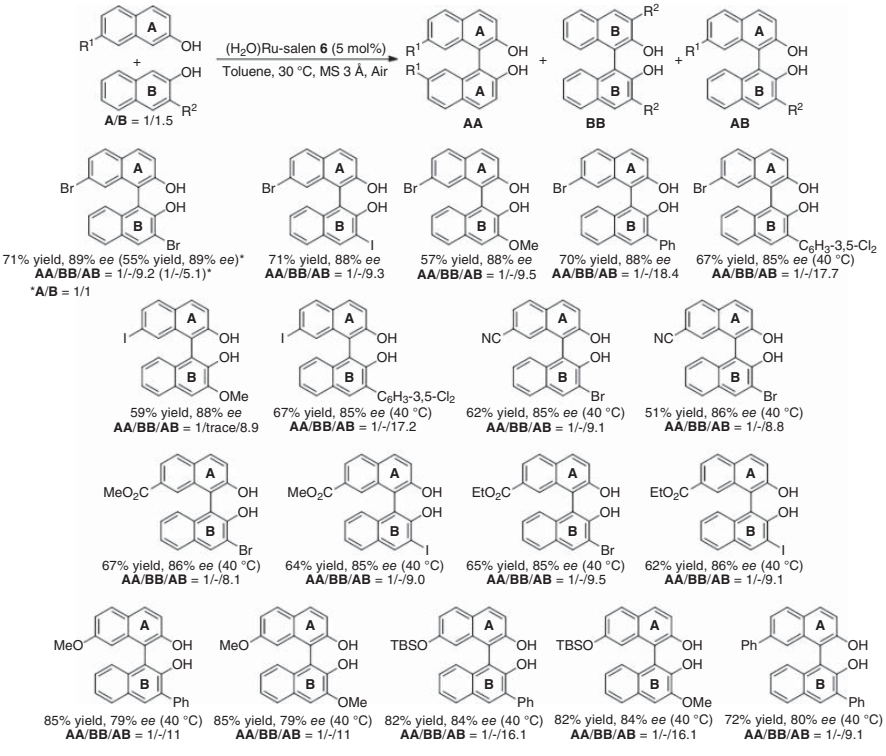

Scheme 2.19 (H_2O)Ru-salen **6**-catalyzed asymmetric oxidative cross-coupling of 2-naphthols.

These observations indicated that complex **6** could distinguish the substitution pattern of 2-naphthols, favoring the oxidation of 6-substituted-2-naphthol. Additionally, the authors proposed that the substituents at the C3 and C7 positions on 2-naphthol might suppress the homo-coupling due to steric repulsion with complex **6** or the naphthoxyl radical cation intermediates. Therefore, the authors investigated the reaction between C3- and C7-substituted-2-naphthols, which showed no considerable differences in their oxidation potential. They used the ruthenium complex **6** as the catalyst at 30 °C under air. A 1 : 1 mixture of 3- and 7-bromo-2-naphthols afforded the corresponding cross-coupling product in 55% yield with 84% cross-selectivity and 89% ee (Scheme 2.19). The cross-selectivity was improved to 92%, and the yield increased to 71% by using 1.5 equivalents of 3-bromo-2-naphthol without reducing the enantioselectivity. Under these conditions, various combinations of C6- and C7-substituted 2-naphthols were converted with excellent cross-selectivity (>70%) and good enantioselectivity. This reaction exhibited a wide functional group tolerance, including bromine, iodide, ester, alkoxyl, phenyl, and nitryl groups at the C6 position and halogen, methoxy, and aryl groups at the C7 position. The best cross-selectivity of 98% was observed in the reaction between 6-bromo-2-naphthol and 3-(3,5-dichlorophenyl)-2-naphthol.

Furthermore, the cross-coupling reaction between 2-naphthols and phenol derivatives, which are less oxidizable than 2-naphthols, was successful (Scheme 2.20). 3-Methoxy- and 3-phenyl-2-naphthol reacted with 3,5-dimethylphenol to give the corresponding coupling products with good to high cross-selectivities, albeit with modest regioselectivity. A high ee of 90% and 79% cross-selectivity were observed in the reaction between 3-phenyl-2-naphthol and 3,5-dimethyl-4-bromophenol.

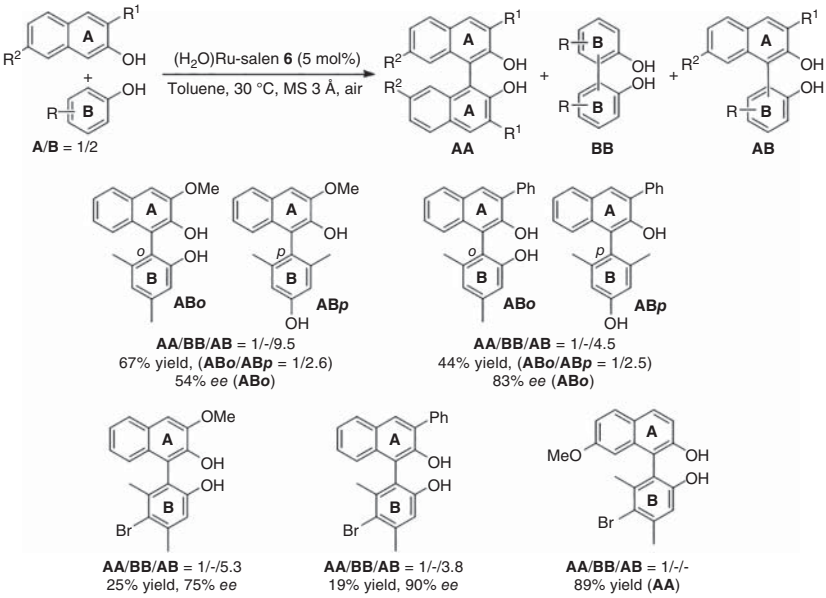

Scheme 2.20 (H_2O)Ru-salen **6**-catalyzed asymmetric oxidative cross-coupling between 2-naphthols and phenols.

2.4 Oxidative Spirocyclization of 2-Naphthols

As mentioned above, the SET-generated arenoxyl radical and radical cation intermediates are highly reactive electrophilic species. They can react with arenols as nucleophiles to produce a dearomatized intermediate, which then undergoes rearomatization to give a bisarenol as a coupling product. Consequently, an appropriate nucleophile rather than an arenol can also undergo dearomatizing nucleophilic addition to yield a substituted arenol through a radical intermediate. In the case of substituted arenols, the construction of a quaternary carbon center via stereoselective oxidative dearomatization has been achieved [23]. Furthermore, this method for the construction of quaternary carbons can be used to synthesize spirocyclic compounds, for which iron-salan complexes are efficient catalysts [24]. In 2014, Oguma and Katsuki proposed that the generation of the radical cation intermediate *ortho*-quinone methide (*o*-QM) could prevent the nucleophilic dearomatization, leading to the formation of a Michael adduct that would undergo spirocyclization (Scheme 2.21) [25].

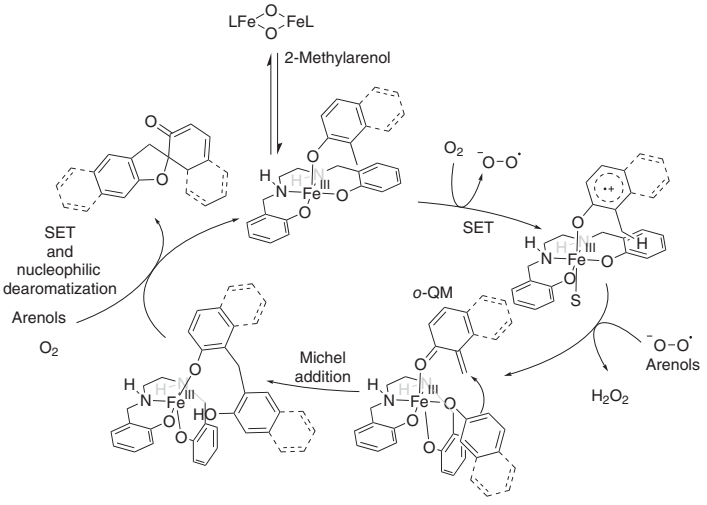

Scheme 2.21 Working hypothesis of oxidative tandem spirocyclization via iron-salan-catalyzed aerobic oxidation.

Based on this hypothesis, they conducted the aerobic oxidation of 1,3-dimethyl-2-naphthol with phenol as the nucleophile using iron-salan catalysts under air (Scheme 2.22). The reaction in the presence of complex **4** yielded the desired spirocyclic compound in moderate yield with 82% ee. Increasing the catalyst amount to 10 mol% improved the yield to an acceptable level. Under the same conditions, complex **9** exhibited better enantioselectivity (92% ee) than complex **4**. Further improvement of the product yield to 86% was achieved by using 1.5 equivalents of 1,3-dimethyl-2-naphthol. High enantioselectivity and a wide functional group tolerance in phenols were observed irrespective of the electron nature, but bulky substituents on phenols afforded the best results, with a 93% ee in the presence of 4-*tert*-butylphenol as a nucleophile. Meanwhile, the product yield depended

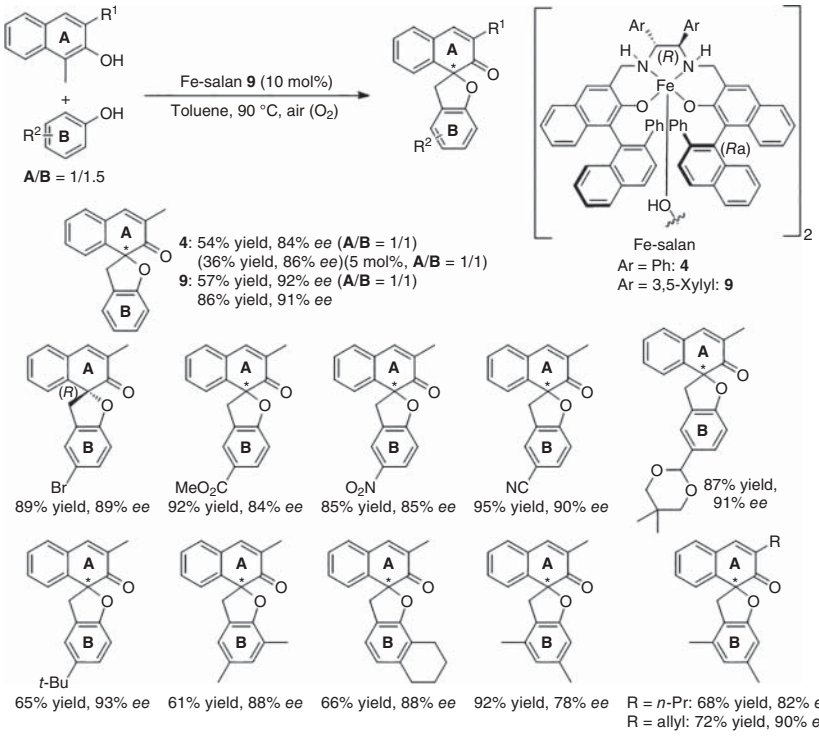

Scheme 2.22 Iron-salan-catalyzed tandem asymmetric spirocyclization of arenols.

considerably on the electron nature of the substituent, with electron-withdrawing groups affording better yields than electron-donating groups.

However, tandem spirocyclization, including *o*-QM formation, Michael addition of phenols, and subsequent intramolecular nucleophilic dearomatization, was limited to 2-naphthols alkylated at the C3 position. These observations indicated that such iron catalysts had limitations in the formation of *o*-QM or methylenebis(arenol) intermediates, hindering the development of an oxidative spirocyclization process. Therefore, they investigated the iron-catalyzed oxidative spirocyclization of methylenebis(arenol) derivatives [26]. The reaction of 1-(2-hydroxybenzyl)naphthalen-2-ols, methylenebis(areno) compounds prepared from 3-substituted naphthols and salicylalcohol, produced the corresponding spirocyclized compound in good to high yields with excellent regioselectivity and good enantioselectivity (Scheme 2.23). During these studies, the regioisomer resulting from the oxidation of the phenolic side was not observed. 2-Naphthols bearing an electron-withdrawing substituent such as bromine and iodine also produced the desired products in good yields with good enantioselectivities. An oxidative spirocyclization of methylenebis(naphthol) bearing arenol units with a similar electron nature was also conducted, finding that the electron-rich naphthol unit preferentially underwent oxidative intramolecular nucleophilic dearomatization reactions, albeit with low regioselectivity. Better stereoselectivity was observed with sterically hindered substituents at the C3 position (Scheme 2.24).

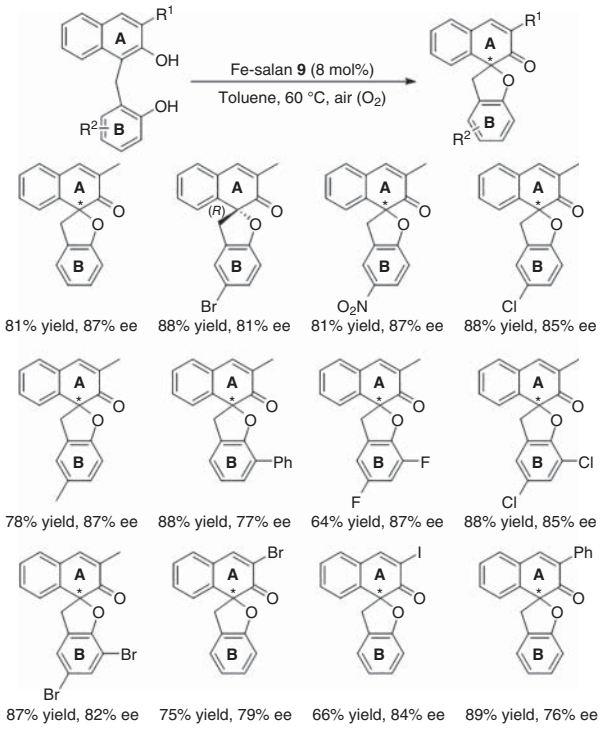

Scheme 2.23 Asymmetric aerobic intramolecular spirocyclization of methylenebis(arenol)s.

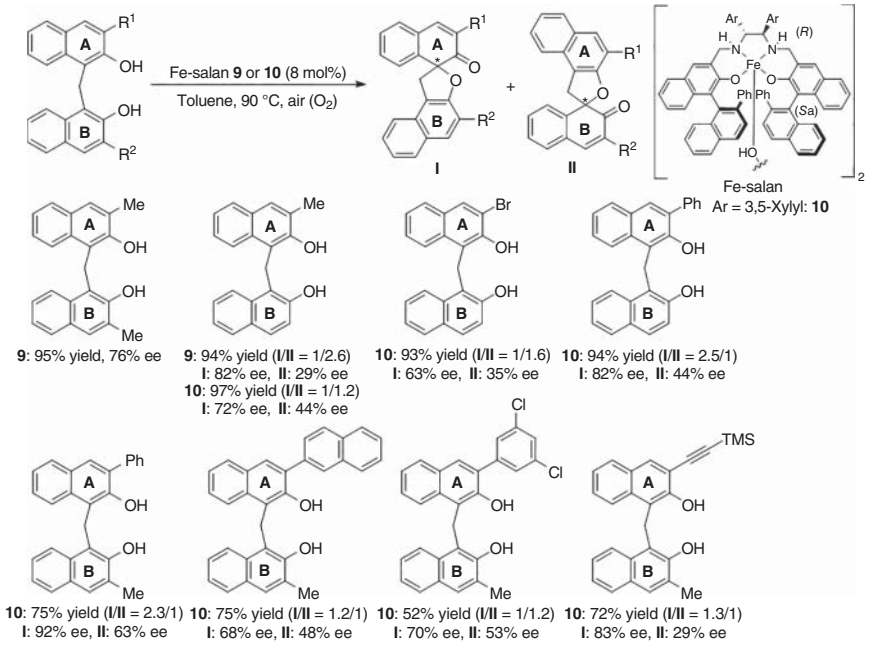

Scheme 2.24 Asymmetric aerobic intramolecular spirocyclization of methylenebis(2-naphthol)s.

2.5 Conclusion

Iron and ruthenium complexes have been demonstrated as efficient catalysts in stereoselective oxidative transformations of arenols such as oxidative homo- and cross-coupling reactions and spirocyclization. In the early stages of the investigation of the asymmetric oxidation of 2-naphthol, (ON)Ru-salen complexes were shown to produce enantiomerically enriched BINOLs with good enantioselectivity using dioxygen in air as the hydrogen acceptor. Later, iron-salen complexes emerged as efficient catalysts in the synthesis of optically active BINOL derivatives, achieving better enantioselectivity, especially in the case of 3-substituted-2-naphthols. The reaction of C6- and C7-substituted 2-naphthols also gave the corresponding BINOLs with good enantioselectivity using a chiral iron-phosphate complex and a diphosphine oxide-supported iron complex as the catalyst, respectively. These coupling systems require a chemical oxidant such as bis(*tert*-butyl)peroxide in the iron-phosphate system reported by Pappo and *tert*-butyl peroxide in the diphosphine oxide system developed by Ishihara. Furthermore, very recently, the coupling of *N*-aryl-2-naphthylamine derivatives co-catalyzed by phthalocyanine iron derivatives and chiral phosphoric acid has been reported. A 90% ee was observed in the reaction of biphenylamine as the substrate in the presence of 3,3′-bis(triphenylsilyl)BINOL-phosphoric acid and $FePcF_{16}$ as a catalyst system.

Along with advances in the enantioselective homo-coupling, highly chemo- and stereoselective cross-coupling reactions of arenols have been achieved. Katsuki et al. revealed the different reactivity between 2-naphthol and 3-bromo-2-naphthol in the iron-salan-catalyzed homo-coupling reaction relative to the cross-coupling and achieved selective C_1-symmetric BINOLs with good to high enantioselectivity. Pappo et al. further clarified the role of the electronic nature of arenols in their cross-coupling reactions. They found that the cross-coupling reaction is favored over the homo-coupling when using an electron-rich arenol and an electron-deficient one. In contrast, Uchida et al. have demonstrated that by using (H_2O)Ru-salen, they can achieve cross-coupling of naphthol derivatives with similar chemical properties by precisely recognizing the positions of the substituents. Moreover, Katsuki and Oguma have demonstrated that by hindering nucleophilic dearomatization after one-electron oxidation, as observed in compounds like 1-methyl-2-naphthol, an *o*-QM intermediate is generated. This generated *o*-QM subsequently leads to the formation of the corresponding spirocyclizing product with good to high enantioselectivity through Michael addition and subsequent oxidative intramolecular nucleophilic dearomatization.

Hence, optically active iron and ruthenium complexes display distinctive catalytic efficacy in the creation of axially asymmetric compounds via enantioselective oxidation of arenols, significantly propelling the field forward. Ongoing research endeavors are anticipated to culminate in the achievement of highly enantioselective biaryl compounds and spirocyclization methodologies.

References

1 (a) Hedouin, G., Hazra, S., Gallou, F., and Handa, S. (2022). *ACS Catal.* 12: 4918–4937. (b) Cheng, J.K., Xiang, S.-H., Li, S. et al. (2021). *Chem. Rev.* 121: 4805–4902. (c) Yang, H., Yang, X., and Tang, W. (2016). *Tetrahedron* 72: 6143–6174. (d) Loxq, P., Manoury, E., Poli, R. et al. (2016). *Coord. Chem. Rev.* 308: 131–190. (e) Zhang, D. and Wang, Q. (2015). *Coord. Chem. Rev.* 286: 1–16. (f) Wencel-Delord, J., Panossian, A., Leroux, F.R., and Colobert, F. (2015). *Chem. Soc. Rev.* 44: 3418–3430. (g) Kočovský, P., Vyskočil, Š., and Smrčina, M. (2003). *Chem. Rev.* 103: 3213–3246.

2 Lapuh, M.I., Mazeh, S., and Besset, T. (2020). *ACS Catal.* 10: 12898–12919.

3 (a) Kim, A.N. and Stoltz, B.M. (2020). *ACS Catal.* 10: 13834–13851. (b) Wiesenfeldt, M.P., Nairoukh, Z., Dalton, T., and Glorius, F. (2019). *Angew. Chem. Int. Ed.* 58: 10460–10476. (c) Luo, Y.-E., He, Y.-M., and Fan, Q.-H. (2016). *Chem. Rec.* 16: 2697–2711. (d) Zhao, D. and Glorius, F. (2013). *Angew. Chem. Int. Ed.* 52: 9616–9618. (e) Wang, D.-S., Chen, Q.-A., Lu, S.-M., and Zhou, Y.-G. (2012). *Chem. Rev.* 112: 2557–2590.

4 (a) Moore, M.J., Qu, S., Tan, C. et al. (2020). *J. Am. Chem. Soc.* 142: 16039–16050. (b) LaPlante, S.R., Fader, L.D., Fandrick, K.R. et al. (2011). *J. Med. Chem.* 54: 7005–7022. (c) Hughes, C.C., Kauffman, C.A., Jensen, P.R., and Fenical, W. (2010). *J. Org. Chem.* 75: 3240–3250. (d) Kozlowski, M.C., Morgan, B.J., and Linton, E.C. (2009). *Chem. Soc. Rev.* 38: 3193–3207. (e) Bringmann, G. and Menche, D. (2001). *Acc. Chem. Res.* 34: 615–624. (f) Hallock, Y.F., Manfredi, K.P., Blunt, J.W. et al. (1994). *J. Org. Chem.* 59: 6349–6355. (g) Kupchan, S.M., Britton, R.W., Ziegler, M.F. et al. (1973). *J. Am. Chem. Soc.* 95: 1335–1336.

5 (a) Parmar, D., Sugiono, E., Raja, S., and Rueping, M. (2014). *Chem. Rev.* 114: 9047–9153. (b) Zhou, Q.-L. (ed.) (2011). *Privileged Chiral Ligands and Catalysts*. Weinheim, Germany: Wiley VCH. (c) Li, Y.-M., Kwong, F.-Y., Yu, W.-Y., and Chan, A.S.C. (2007). *Coord. Chem. Rev.* 251: 2119–2144. (d) Akiyama, T. (2007). *Chem. Rev.* 107: 5744–5758. (e) Tang, W. and Zhang, X. (2003). *Chem. Rev.* 103: 3029–3069. (f) Chen, Y., Yekta, S., and Yudin, A.K. (2003). *Chem. Rev.* 103: 3155–3211. (g) Miyashita, A., Yasuda, A., Takaya, H. et al. (1980). *J. Am. Chem. Soc.* 102: 7932–7934.

6 (a) Wu, J. and Kozlowski, M.C. (2022). *ACS Catal.* 12: 6532–6549. (b) Kumar, A., Sasai, H., and Takizawa, S. (2022). *Acc. Chem. Res.* 55: 2949–2965. (c) Bansal, S., Shabade, A.B., and Punji, B. (2021). *Adv. Synth. Catal.* 363: 1998–2022. (d) Sako, M., Takizawa, S., and Sasai, H. (2020). *Tetrahedron* 76: 131645. (e) Tkachenko, N.V. and Bryliakov, K.P. (2019). *Mini. Rev. Org. Chem.* 16: 392–398. (f) Wang, H. (2010). *Chirality* 22: 827–837. (g) Takizawa, S. (2009). *Chem. Pharm. Bull.* 57: 1179–1188. (h) Brunel, J.M. (2007). *Chem. Rev.* 107: PR1–PR45. (i) Wallace, T.W. (2006). *Org. Biomol. Chem.* 4: 3197–3210.

7 Nakajima, M., Miyoshi, K., Kanayama, K. et al. (1999). *J. Org. Chem.* 64: 2264–2271.

8 Irie, R., Masutani, K., and Katsuki, T. (2000). *Synlett* 2000: 1433–1436.

9 (a) Masutani, K., Uchida, T., Irie, R., and Katsuki, T. (2000). *Tetrahedron Lett.* 41: 5119–5123. (b) Nakamura, Y., Egami, H., Matsumoto, K. et al. (2007). *Tetrahedron* 63: 6383–6387. (c) Shimizu, H., Onitsuka, S., Egami, H., and Katsuki, T. (2005). *J. Am. Chem. Soc.* 127: 5396–5413.

10 Egami, H. and Katsuki, T. (2009). *J. Am. Chem. Soc.* 131: 6082–6083.

11 Narute, S., Parnes, R., Toste, F.D., and Pappo, D. (2016). *J. Am. Chem. Soc.* 138: 16553–16560.

12 Horibe, T., Nakagawa, K., Hazeyama, T. et al. (2019). *Chem. Commun.* 55: 13677–13680.

13 Wu, L.-Y., Usman, M., and Liu, W.-B. (2020). *Molecules* 25: 852.

14 Fritsche, R.F., Schuh, T., Kataeva, O., and Knölker, H.-J. (2023). *Chem. Eur. J.* 29: e202203269.

15 (a) Temma, T. and Habaue, S. (2005). *Tetrahedron Lett.* 46: 5655–5657. (b) Yan, P., Sugiyama, Y., Takahashi, Y. et al. (2008). *Tetrahedron* 64: 4325–4331.

16 (a) Egami, H., Matsumoto, K., Oguma, T. et al. (2010). *J. Am. Chem. Soc.* 132: 13633–13635. (b) Matsumoto, K., Egami, H., Oguma, T., and Katsuki, T. (2012). *Chem. Commun.* 48: 5823–5825.

17 Libman, A., Shalit, H., Vainer, Y. et al. (2015). *J. Am. Chem. Soc.* 137: 11453–11460.

18 Forkosh, H., Vershinin, V., Reiss, H., and Pappo, D. (2018). *Org. Lett.* 20: 2459–2463.

19 (a) Bringmann, G., Mortimer, A.J.P., Keller, P.A. et al. (2005). *Angew. Chem. Int. Ed.* 44: 5384–5427. (b) Chen, Y.H., Qi, L.-W., Fang, F., and Tan, B. (2017). *Angew. Chem. Int. Ed.* 56: 16308–16312.

20 Dyadyuk, A., Vershinin, V., Shalit, H. et al. (2022). *J. Am. Chem. Soc.* 144: 3676–3684.

21 Surgenor, R.R., Liu, X., Keenlyside, M.J.H. et al. (2023). *Nat. Chem.* 15: 357–365.

22 (a) Koya, S., Nishioka, Y., Mizoguchi, H. et al. (2012). *Angew. Chem. Int. Ed.* 51: 8243–8246. (b) Mizoguchi, H., Uchida, T., and Katsuki, T. (2014). *Angew. Chem. Int. Ed.* 53: 3178–3182. (c) Hayashi, H., Ueno, T., Kim, C., and Uchida, T. (2020). *Org. Lett.* 22: 1469–1474.

23 (a) Oguma, T. and Katsuki, T. (2012). *J. Am. Chem. Soc.* 134: 20017–20020. (b) Narute, S. and Pappo, D. (2017). *Org. Lett.* 19: 2917–2920. (c) Zhou, Y.-M., Ping, Y.-J., Xu, Z.-J., and Che, C.-M. (2021). *Asian J. Org. Chem.* 10: 674–678.

24 (a) Sannigrahi, M. (1999). *Tetrahedron* 55: 9007–9071. (b) Rios, R. (2012). *Chem. Soc. Rev.* 41: 1060–1074. (c) Dohi, T. and Kita, Y. (2022). *Iodine Catalysis in Organic Synthesis* (ed. K. Ishihara and K. Muñiz), 211. Weinheim, Germany: Wiley.

25 Oguma, T. and Katsuki, T. (2014). *Chem. Commun.* 50: 5053–5056.

26 Oguma, T., Doiuchi, D., Fujimoto, C. et al. (2020). *Asian J. Org. Chem.* 9: 404–415.

3

Vanadium-Catalyzed Atroposelective Coupling of Arenols and Application in the Synthesis of Polycyclic Heteroaromatics (PHAs)

Mohamed S. H. Salem[1,2] *and Shinobu Takizawa*[1]

[1] *Osaka University, SANKEN, 8-1 Mihogaoka, Ibaraki, Osaka 567-0047, Japan*
[2] *Suez Canal University, Faculty of Pharmacy, Pharmaceutical Organic Chemistry Department, 4.5 KM Ring Road, Ismailia, 41522, Egypt*

3.1 Introduction

Axially chiral molecules bearing rotation-constrained σ-bonds and exhibiting atropisomerism are advantageous synthetic targets [1]. Their significance lies in their high utility as both transition-metal catalysts and organocatalysts [2] as well as their presence in attractive natural products having effective medicinal properties [3]. The value of this unique framework is evident from the fact that the transition-metal-catalyzed enantioselective construction of axially chiral molecules has been extensively investigated to date [4]. Recently, providing efficient ways to perform highly selective synthesis such as chemoselectivity, regioselectivity, and enantioselectivity of axial molecules has been a main goal of chemists [5], which has led to green syntheses by reducing unnecessary by-products and toxic waste emissions [6]. Over the past two decades, optically active vanadium complexes, in particular, those comprising a Schiff base ligand and a tetravalent or pentavalent vanadium metal center, became recognized as low environmental impact catalysts for the formation of axially chiral molecules. This is attributed to the fact that, in comparison to other metal catalysts, vanadium boasts abundant natural reserves that are nearly equivalent to those of zinc, resulting in relatively low toxicity [7].

As shown in Scheme 3.1, Uang [8] and Chen [9] reported the first chiral vanadium complexes **1a** and **1b**–**c** that function as catalysts for the enantioselective oxidative coupling of 2-naphthol derivatives **2**, affording the corresponding 1,1′-binaphthalene-2,2′-diols (BINOLs) **3** in high yields and good enantioselectivities. Uang also found that the addition of acids [8] improved the activity of the vanadium catalyst. After this success, the development of vanadium complex-mediated enantioselective reactions has evolved dramatically [10], parallel to the emerging concept of multifunctional catalysis, with a particular emphasis on the utilization of dinuclear vanadium complexes [11, 12] (Scheme 3.2). In 2002, Gong group presented chiral dinuclear vanadium catalysts (R^a,*S*,*S*)-**1d** and **1e** with

Atropisomerism in Asymmetric Organic Synthesis: Challenges and Applications, First Edition.
Edited by Shinobu Takizawa and Mohamed S. H. Salem.

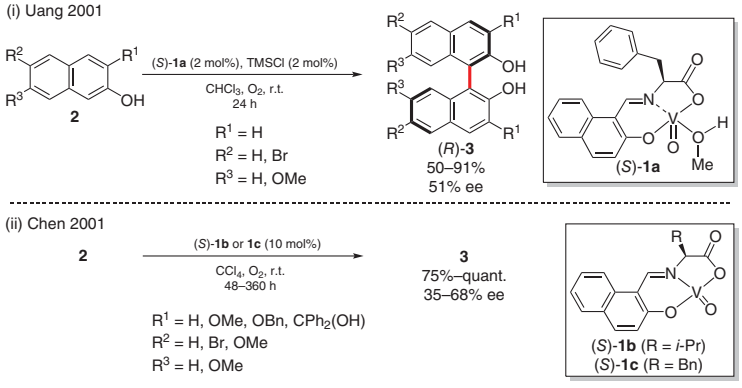

Scheme 3.1 First chiral vanadium complex-catalyzed enantioselective oxidative coupling of 2-naphthols.

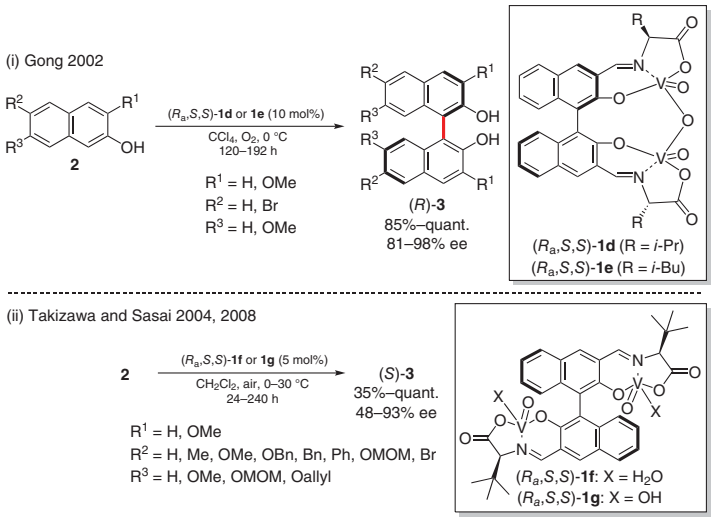

Scheme 3.2 Dinuclear vanadium catalysts for the oxidative coupling of 2-naphthols.

V–O–V linkage, which was prepared from $VOSO_4$, and Schiff base ligands produced from a condensation of 3,3′-formyl-(*R*)-BINOL and (*S*)-*tert*-leucine (Scheme 3.2i) [11b]. Subsequently, Takizawa and Sasai introduced the concept of dual activation to the dinuclear vanadium complexes (R^a,*S*,*S*)-**1f** and **1g** for the homo-coupling of **2** (Scheme 3.2ii) [12]. In the oxidative coupling, the two vanadium metal centers in the chiral complex stimulate two molecules of 2-naphthols simultaneously to generate the radical active species, establishing a high reaction rate and enantiocontrol. Even though the absolute configurations of Gong's catalysts are the same as Takizawa and Sasai's catalysts [both components are as (R^a,*S*,*S*)], the absolute configurations of the obtained BINOLs as major products were opposite to each other. Gong's catalysts produced (*R*)-**3** but the reaction with Takizawa and Sasai's catalysts afforded (*S*)-**3** in both the high yields and enantioselectivities.

As many comprehensive books and reviews on the investigation of enantioselective oxidative coupling of **2** and their relative applications have been reported [13], in this chapter, we focus on the latest advancements in chiral vanadium complex-catalyzed homo- and hetero-couplings, affording C^2- and C^1-symmetrical biarenols involving heteroaromatics. We also discuss their applications in the straightforward synthesis of chiral polycyclic heteroaromatics (PHAs) such as oxa[9]helicenes and hetero[7]dehydohelicenes.

3.2 Chiral Vanadium Catalysis in Homo-Coupling of Hydroxycarbazoles

Carbazoles are tricyclic *N*-heterocycles featuring two benzene rings fused to either side of pyrrole, and their derivatives are commonly found in various natural products [14]. Among them, dimeric hydroxycarbazoles with carbon—carbon (C—C) or carbon—nitrogen (C—N) linked biaryls have attracted much attention due to their potential applications as antibiotics, antibacterial and antifungal agents as well as free radical scavengers (Figure 3.1) [15]. Additionally, bihydroxycarbazoles are also useful as chiral metal ligands [16].

In 2015, Kozlowski group presented the catalytic oxidative homo-coupling of 2-hydroxycarbazole **4a** with the mononuclear vanadium catalyst (*S*)-**1h** for the first time (Scheme 3.3) [17]. The regio- and enantioselective oxidative coupling was challenging due to the plural reactive sites, which led to the formation of many isomers

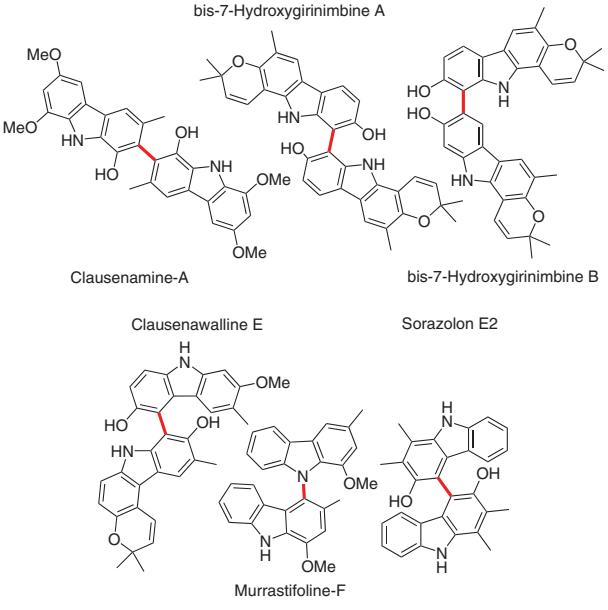

Figure 3.1 Dimeric hydroxycarbazoles in natural products.

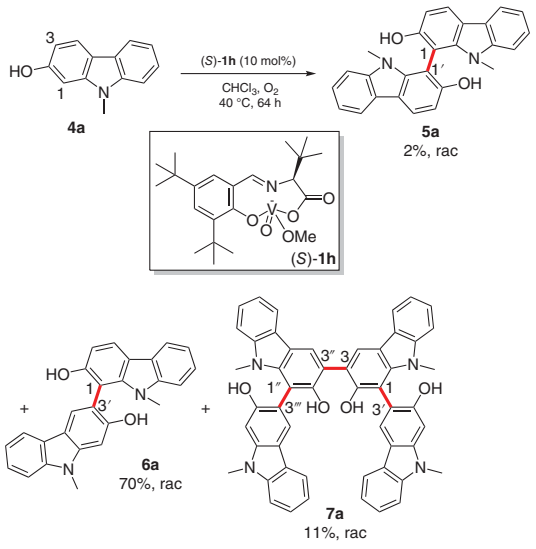

Scheme 3.3 First chiral vanadium complex-catalyzed oxidative coupling of 2-hydroxycarbazole **4a.**

such as dimers **5a** and **6a** and tetramer **7a** with low racemization barrier. Later, Kozlowski and co-workers employed a series of 3-substituted 2-hydroxycarbazoles **4** having bulky substituents on the nitrogen atom of the carbazole to suppress racemization and the over oxidative coupling [18]. Under their optimized conditions with 20 mol% (*S*)-**1i** and 6.5 equiv. AcOH in chlorobenzene, the desired bihydroxycarbazoles **5** were successfully obtained in up to 91% yield with 96% ee (Scheme 3.4i). Takizawa and co-workers reported the first enantioselective homo-coupling of 3- and 4-hydroxycarbazoles **8** and **10**, affording **9** and **11** in up to 90% ee (Scheme 3.4ii–iii) [19]. Since optically active dinuclear vanadium catalyst **1g** distinctively promoted the oxidative coupling of 4-hydroxycarbazole **10a**, compared with that of utilizing mononuclear vanadium complex **1j** (**11a**: 80% yield, 90% ee with 5 mol % of (R^a,*S*,*S*)-**1g**; 25% yield, 56% ee with 10 mol % of (R^a,*S*)-**1j**, Scheme 3.5), a vanadium-mediated dual activation (intramolecular manner radical–radical coupling) might be included in the reaction pathway [12].

As an application of the couplings, Takizawa group employed the mononuclear vanadium catalyst (R^a,*S*)-**1j** bearing a binaphthyl backbone in the oxidative homo-coupling of **4b**, toward forming the natural product, (+)-bi-2-hydroxy-3-carbazole **5b** (Scheme 3.6i). Unfortunately, the reaction yielded **5b** in low optical purity due to the low racemization barrier of biaryl axial chirality even at 25 °C [19b]. Sorazolon E and E2 (dimeric sorazolon E), which were isolated from *Sorangium cellulosum* strain soce375, exhibited a broad-spectrum antibacterial (Gram-positive and Gram-negative) and cytotoxic (mouse fibroblast cell line L929) activities [20]. In 2017, Takizawa and co-workers also established the first short synthesis of 4-deoxycarbazomycin B and sorazolon E using commercially available cyclohexanone **12** and 4-methoxy-2,3-dimethylaniline **13** as starting materials

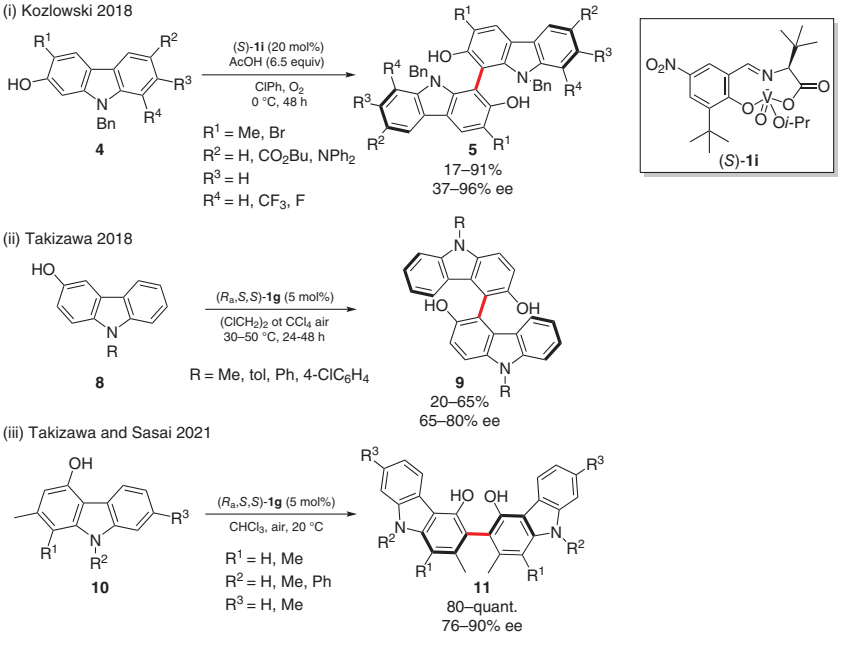

Scheme 3.4 Enantioselective oxidative coupling of hydroxycarbazoles.

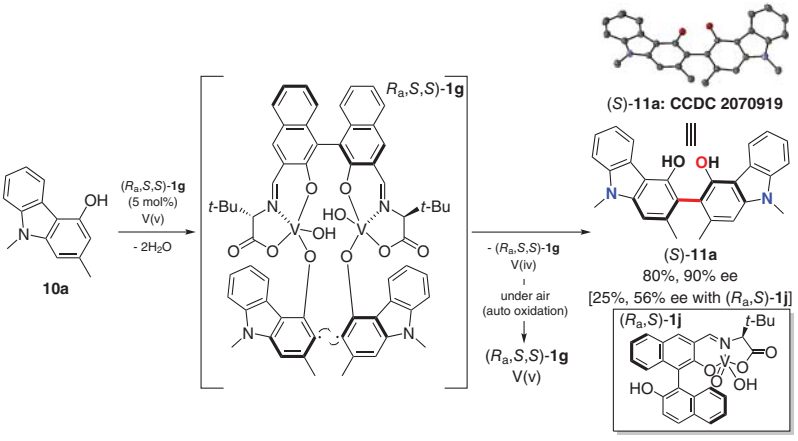

Scheme 3.5 Dual activation in enantioselective homo-coupling of 4-hydroxycarbazoles.

(Scheme 3.6ii) [19a]. Chiral dinuclear vanadium catalyst (R^a,*S*,*S*)-**1g** could promote the oxidative coupling of sorazolon E to afford (+)-sorazolon E2 in 71% yield with 60% ee. After the recrystallization of the product, the absolute configuration of synthetic sorazolon E2 was assigned to be (*R*) by comparison with the circular dichroism (CD) spectrum obtained for optically pure 9*H*,9′*H*-[4,4′-bicarbazole]-3,3′-diol (BICOL) [16] in 5% DMSO/H_2O. Eventually, (R^a,*S*,*S*)-**1g** was found to produce the natural form of sorazolon E2.

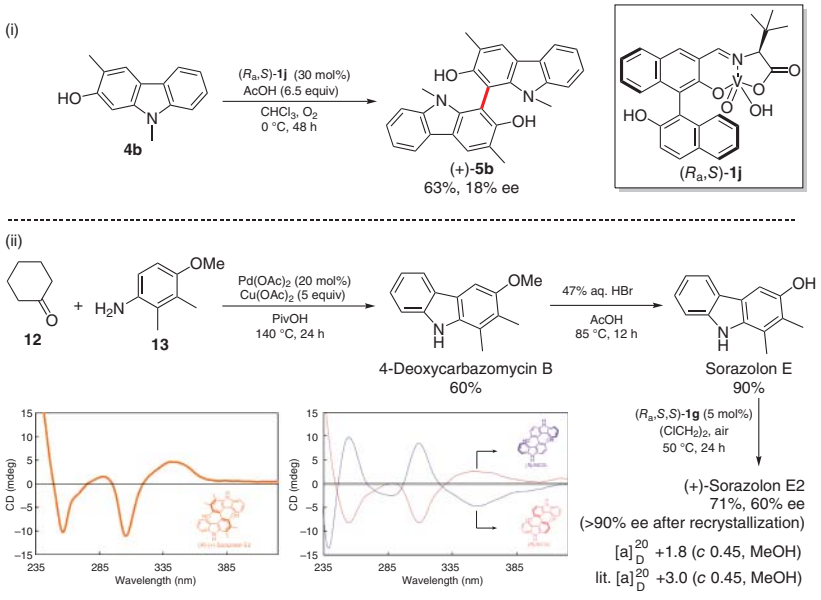

Scheme 3.6 Syntheses of (+)-bi-2-hydroxy-3-carbazole, 4-deoxycarbazomycin B, sorazolon E, and (+)-sorazolon E2.

3.3 Chiral Vanadium Catalysis in Hetero-Coupling of Hydroxycarbazole with 2-Naphthols

The enantioselective homo-coupling of 2-naphthols as coupling precursors was very established using various chiral metal complexes (Cu: Kočovský and Smrčina 1993 [21a], Nakajima 1999 [21b], Kozlowski 2001 [21c], Gao 2003 [21d], Ha 2004 [21e], Habaue 2005 [21f], Sekar 2013 [21g], Cui and Wu 2014 [21h], Breuning 2015 [21i], and Zhang 2022 [21j–k]; Ru: Katsuki 2000 [21l]; V: Uang 2001 [8a], Chen 2001 [9], Gong 2002 [11a], Takizawa and Sasai 2004 [12a], Iwasawa 2004 [21m], Habaue 2005 [21n], Bania 2015 [21o]; Fe: Katsuki 2009 [21p], Pappo 2016 [21q], Ishihara 2019 [21r]). This approach has also been applied to afford the hetero-coupling products so far (Cu: Smrčina and Kočovský 1994 [22a], Kozlowski 2003 [22b], Habaue 2005 [22c], Tian and Tu 2019 [5a], 2021 [5b]; Ru: Uchida 2020 [22d]; Fe: Katsuki 2010 [22e], Pappo 2022 [22f] (Figure 3.2). On the contrary, achieving enantioselective hetero-coupling reactions posed a significant challenge due to the intricate task of effectively suppressing the formation of homo-coupling side products. As mentioned in the previous section, Kozlowski and Takizawa independently studied the first chiral vanadium-catalyzed homo-coupling reactions of hydroxycarbazoles [18, 19]. While chiral vanadium catalysts showed promise in the oxidative coupling of diverse arenols, efficient chiral vanadium catalysis in hetero-couplings remained unreported until the conclusion of the second decade of the twenty-first century.

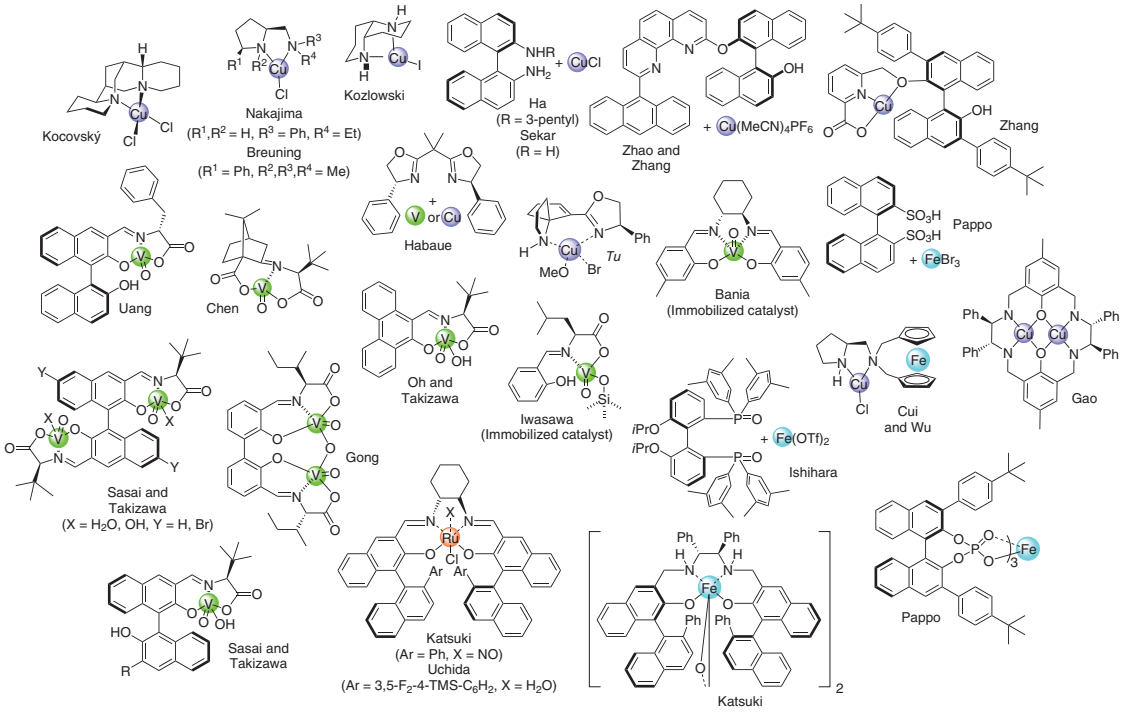

Figure 3.2 Representative chiral transition-metal catalysts for the oxidative coupling of 2-naphthols with high enantiocontrol.

In 2021 [23], Takizawa and co-workers reported the first highly chemo-, regio-, and enantioselective hetero-coupling of 3-hydroxycarbazoles **8** and 2-naphthols **2** catalyzed by a chiral mononuclear vanadium complex, affording various unsymmetrical carbazole-based biaryl molecules **14** (Scheme 3.7). Among the screened catalysts, the mononuclear vanadium catalyst (R^a,*S*)-**1k** with a 2,6-dimethylphenyl substituent resulted in the most promising results for the hetero-coupling of 2-naphthol **2a** and 3-hydroxycarbazole **8a** (R = H). On the coupling reaction with a 1 : 1 molar ratio between **2a** and **8a** under air in 1,1,2,2-tetrachloroethane (TCE), the bulky substituent at the 3′-position on the catalyst showed a crucial role for high enantiocontrol to furnish the corresponding hetero-coupling product **14a** in 92% yield with 64% ee. Upon further optimization, 1,4-dioxane was found to be the optimum solvent for the hetero-coupling to give **14a** in 40% yield with 84% ee together with the recovery of coupling precursors **2a** and **8a**. Finally, the addition of lithium chloride (LiCl) [18] improved the conversion to afford **14a** in 84% yield with 88% ee. Since vanadium complexes easily undergo self-assembly to form their oligomers, LiCl as an additive plays a key role in the dissociation of such oligomers to regenerate highly active monomeric species [24].

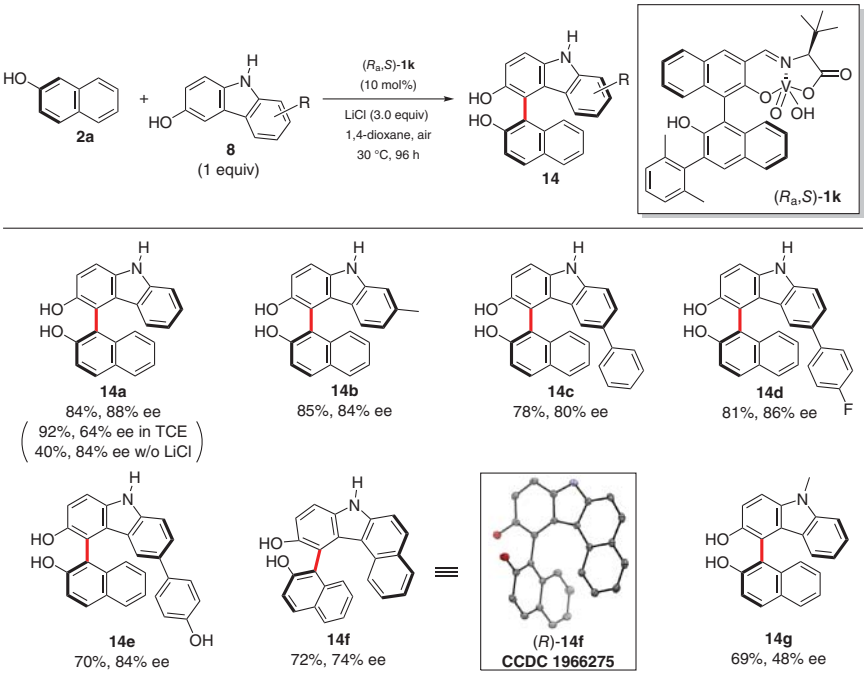

Scheme 3.7 Chiral vanadium complex (R^a,*S*)-**1k** catalyzed hetero-coupling of **2a** and 3-hydroxycarbazoles **8.**

Under the optimized conditions, Takizawa group studied the substrate scope of 3-hydroxycarbazoles **8** as shown in Scheme 3.7. 3-Hydroxycarbazoles **8** with various substituents such as methyl and aryl groups reacted smoothly with **2a** to

afford the hetero-coupling products **14b–e** in up to 85% yields with 86% ees. The hetero-coupling of 7*H*-benzo[*c*]carbazol-10-ol **8f** as a π-expanded hydroxycarbazole and **2a** afforded the hetero-coupling product **14f** in 72% yield with 74% ee. The absolute configuration of the obtained **14f** with (R^a,*S*)-**1k** was determined to be (*R*) based on X-ray crystallographic analysis. Using an *N*-protected 3-hydroxycarbazole such as *N*-methyl 3-hydroxycarbazole, **8g** was found to decrease the enantioselectivity of the resulting hetero-coupling product **14g**.

Takizawa group also studied the scope of 2-naphthols **2** as shown in Scheme 3.8. The reactions of various derivatives of **2** bearing either electron-deficient or -rich substituents such as 6-bromo, 6-iodo, 6-methoxy, 7-methoxymethyl, 7-allyloxy, 6-phenyl, and 6-(pinacolate)boryl-2-naphthols with **8a** gave the desired hetero-couplings **14h**–**s** in up to 98% yield with 90% ee. This system exhibited remarkable tolerance to various functional groups such as halogen, alkoxy, allyl,

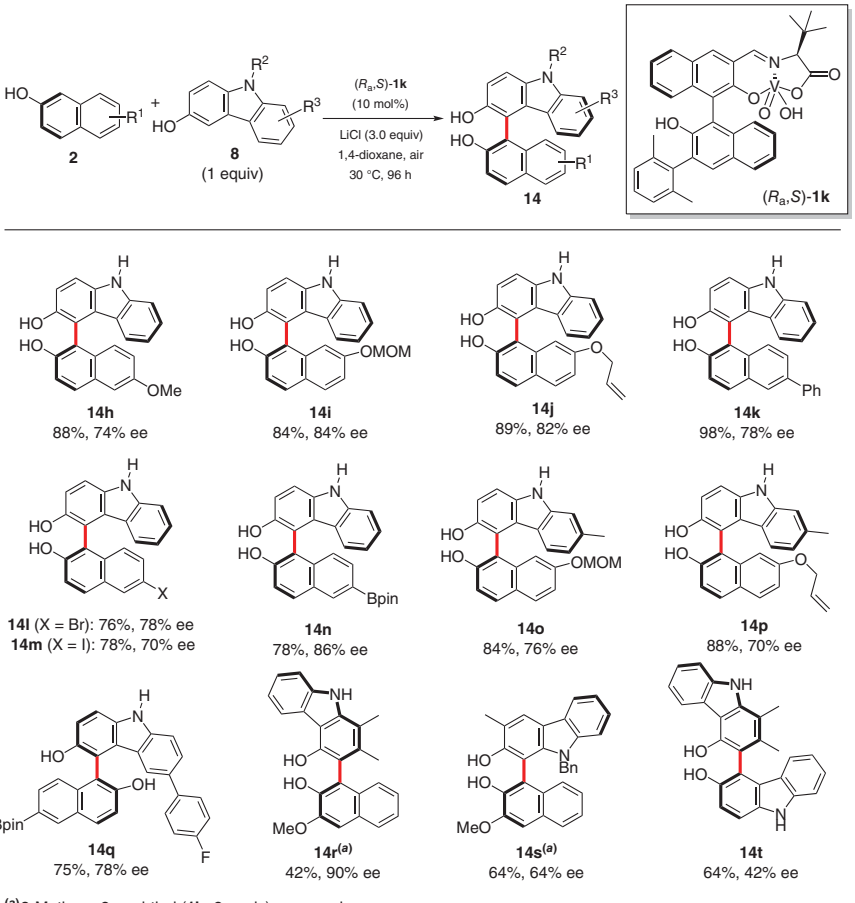

(a)3-Methoxy-2-naphthol (**1b**, 2 equiv) was used.

Scheme 3.8 Various combinations of hydroxycarbazoles and 2-naphthols for the hetero-coupling.

and (pinacolate)boryl groups. It was noted that the oxidative coupling of 3-hydroxycarbazole **8a** and 1,2-dimethyl-4-hydroxycarbazole **10b** in a 1 : 1 molar ratio showed an excellent chemoselectivity to give the corresponding hetero-coupling product **14t** in 64% yield with 42% ee.

In 2018, Kozlowski group performed a mechanistic investigation on the vanadium-catalyzed enantioselective oxidative radical–radical coupling reactions of hydroxycarbazoles. They found a positive nonlinear effect (NLE) between the ee of the catalyst and ee of the coupling product, indicating that the formation of a dimeric cluster, which includes a vanadium complex, played a significant role in the C—C bond formation [18]. The hetero-coupling of naphthols and hydroxycarbazoles reported by the Takizawa group could have proceeded *via* a different activation mode compared to that of Kozlowski's homo-coupling of hydroxycarbazoles. In Takizawa's hetero-coupling system, the linear correlation was observed upon conducting the NLE experiment (Scheme 3.9i). Additionally, when a competing reaction of **8a** with both **2c** containing a MeO group and **2d** containing a Br group was conducted, hetero-coupling product **14h** (56% NMR yield) was preferentially formed rather than **14l** (17% NMR yield) (Scheme 3.9ii). These results suggested that the 2-naphthol **2** nucleophilically attacked the radical cations of **8a** since the more electron-rich nucleophile **2c** exhibited a higher reaction rate than that of **2d** [25].

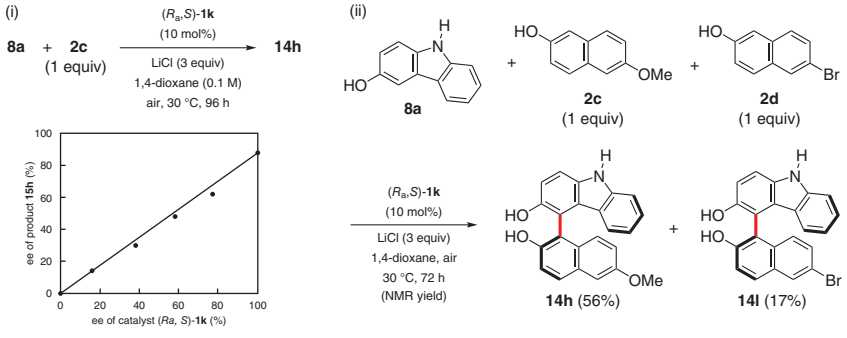

Scheme 3.9 Control experiments. (i) ee of product **14h** as a function of ee of catalyst (R^a,*S*)-**1k** and (ii) hetero-coupling of **8a** in the presence of both **2c** and **2d**.

Takizawa group estimated a plausible catalytic cycle on chiral vanadium complex-mediated hetero-coupling of **8a** with **2a**. Initially, the intermediate **I** was generated *via* the reaction of the mononuclear vanadium complex (R^a,*S*)-**1k** with **8a**, as **8a** is more readily oxidized than **2a** [cyclic voltammetry in MeCN with Bu_4NPF_6: $E_{\mathbf{8a}(ox)} = 0.45$ V; $E_{\mathbf{2a}(ox)} = 0.97$ V]. A single electron transfer (SET) from the carbazole moiety of **I** to vanadium occurred to afford the electrophilic radical intermediate **II**. Next, an intermolecular radical–anion coupling of **II** with **2a** afforded intermediate **III** with a new C—C bond formation *via* the nucleophilic attack of **2a**. The reoxidation of vanadium(IV) to vanadium(V) proceeded *via* molecular oxygen in air, giving the intermediate **IV**, which upon reaction with **8a** afforded the hetero-coupling product **14h** and intermediate **I** to start another catalytic cycle (Scheme 3.10).

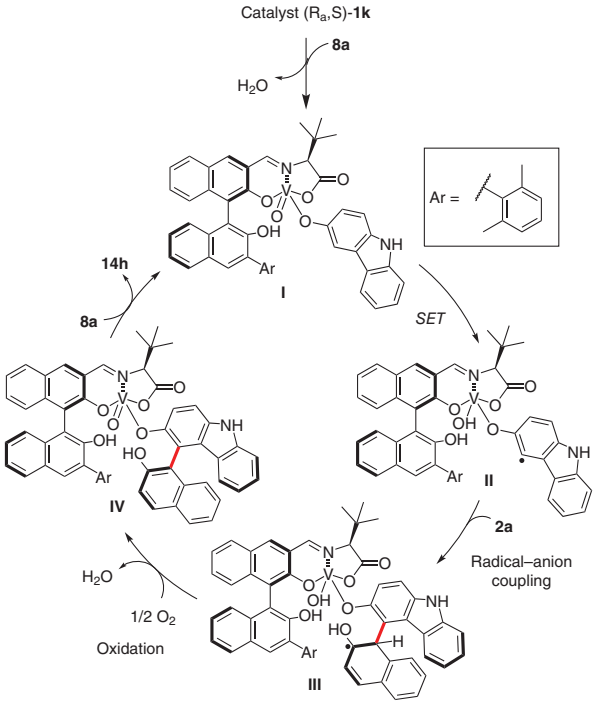

Scheme 3.10 Plausible mechanism for the enantioselective hetero-coupling of **2a** with **8a.**

3.4 Enantioselective Synthesis of Oxa[9]helicenes *via* Chiral Vanadium Complex-Catalyzed Homo-Couplings of Polycyclic Phenols

Heterohelicenes and other screw-shaped helical scaffolds, that can be categorized as PHAs, exhibit helical chirality caused by the steric repulsion of terminal aromatic rings [26]. Over the past few decades, helicenes have attracted attention in the field of synthetic organic chemistry and physical sciences because of their high potential as valuable materials such as liquid crystals, catalysts, and molecular devices [27]. Historically, most helicenes have been synthesized through photochemical processes using stilbene-type molecules as key intermediates [28]. Following a ground-breaking report on the successful synthesis using chiral metal catalysts, the construction of helicenes has drastically improved until now [26, 27]. While metal-assisted synthetic approaches have demonstrated numerous advantages, including efficient synthesis with a high level of stereoselectivity in a short number of steps [28], several challenges persisted. These included the preparation of complex starting substrates with multisteps, high reaction temperature, and high catalyst loading.

In 2016, Takizawa and co-workers developed a mononuclear vanadium complex (R^a,*S*)-**1l**, which cooperatively worked as both an oxidative and Lewis acid catalyst to produce the oxa[9]helicenes **16** in good yields (56–86%) with up to 94% ee. The reaction proceeded *via* the oxidative homo-coupling of

2-hydroxybenzo[*c*]phenanthrenes **15**, followed by the Lewis acid-mediated intramolecular dehydrative cyclization sequence (Scheme 3.11) [29]. Optically pure oxa[9]helicene **16a** (R = H) was readily obtained by a single recrystallization of the enantioenriched product showing a unique optical rotation, $[\alpha]_D^{19} = -2647$ (*c* 0.32, $CHCl_3$). The absolute configuration of **16a** was confirmed to be (*M*) based on the Flack parameter of the obtained crystal.

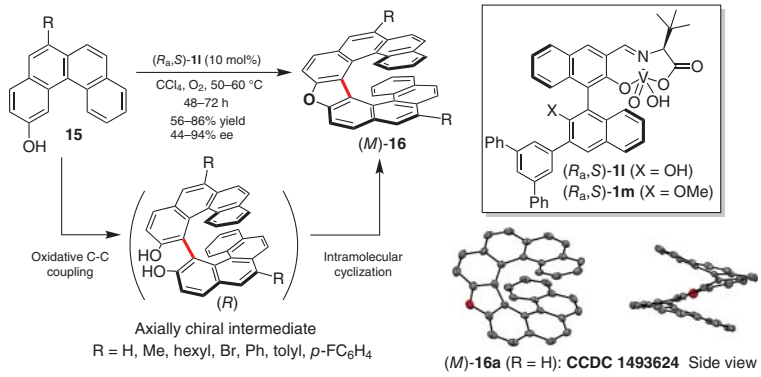

Scheme 3.11 Chiral vanadium complex-catalyzed homo-coupling of polycyclic arenol **15**, followed by intramolecular dehydrative cyclization to produce oxa[9]helicene **16.**

The oxidative coupling reaction could be promoted with one molecule of the mononuclear vanadium complex (R^a,*S*)-**1l** because the rate of the sequential process was first order with respect to the concentration of (R^a,*S*)-**1l**, indicating that the common radical–radical coupling mediated pathway by two chiral metal complexes [8, 9, 11, 21a, b] was not involved in this sequential process. Instead, the reaction of **15a** using a mononuclear vanadium(V) complex (R^a,*S*)-**1l** generated intermediate **I**, which next underwent SET to produce the corresponding electrophilic radical intermediate **II**. Then, a subsequent intermolecular radical–anion coupling of intermediate **II** with another molecule of **15a** occurred to give intermediate **III** with a new C—C bond. After the regeneration of vanadium(IV) to vanadium(V) species **IV** *via* auto-oxidation under oxygen atmosphere, the Lewis acidity of the vanadium catalyst promoted a subsequent dehydrative cyclization to give the desired oxa[9]helicene **16a** along with regeneration of the intermediate **I** (Scheme 3.12i).

Because the methyl-capped mononuclear vanadium catalyst (R^a,*S*)-**1m** (Scheme 3.11) showed a lower reaction rate but maintaining the ee of the product compared to that of (R^a,*S*)-**1l** [29], the hydroxy group in the binaphthyl ligand of the vanadium complex probably make an improvement to the vanadium Lewis acidity through intramolecular hydrogen bonding. As a control experiment, treatment of a 1 : 1 mixture of electron-rich **15a** and electron-poor brominated **15b** with (R^a,*S*)-**1l** (10 mol%) produced a mixture of the hetero-coupling product **16ab** (30% yield, 84% ee) and the homo-coupling products **16a** (28% yield, 69% ee) and **16b** (13% yield, 94% ee) (Scheme 3.12ii). The relative proportions of the products caused by the metal-mediated radical–radical couplings were aligned with the

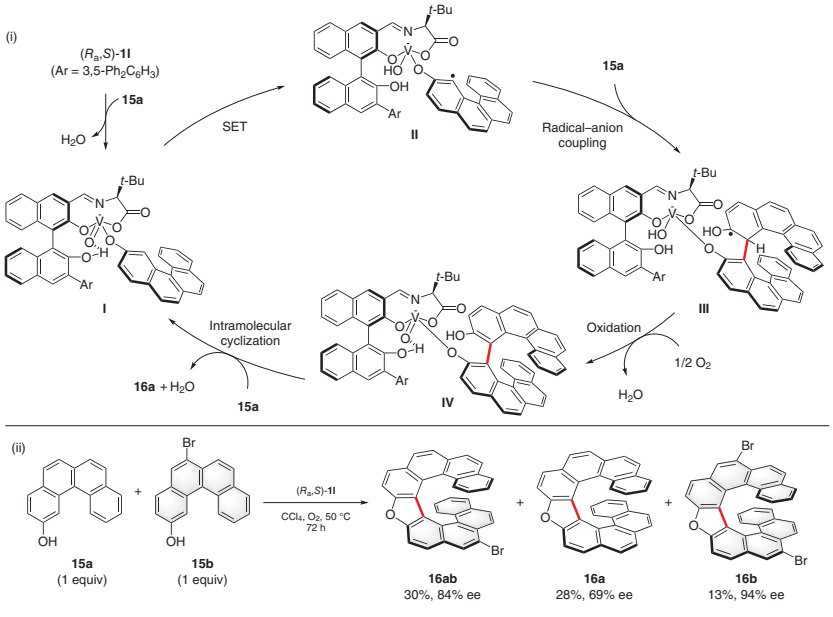

Scheme 3.12 Mechanistic investigations: (i) plausible reaction mechanism for the oxidative coupling/intramolecular dehydrative cyclization sequence and (ii) cross-coupling control experiment with electron-rich and electron-poor substrates.

relative reactivities of the coupling precursors [12, 11, 21c]. In principle, **15b** is less oxidizable than that of **15a**, which should lead to the homo-coupling **16a** as a major product. As shown in Scheme 3.12ii, cross-coupling control experiments and kinetic studies indicated the coupling reaction of **15a** proceeded *via* a nucleophilic attack of **15a** to the radical intermediated **II** (radical–anion coupling) [21f, 21q-r, 22e, 29].

3.5 Enantioselective Synthesis of Oxaza[7] dehydrohelicenes *via* Chiral Vanadium Complex-Catalyzed Hetero-Couplings of 3-Hydroxycarbazoles and 2-Naphthols

Heterodehydrohelicenes, also known as quasi-heterocirculenes with helical chirality, can also be categorized as PHAs in which the two helical ends of a helicene are connected by a sigma bond [30]. The unique helical chirality of heterodehydrohelicenes results in exceptional chiroptical responses [27] that can be implemented in various material-based applications such as field-effect transistors (FETs) and organic light-emitting diodes (OLEDs). Additionally, their excellent chiroptical properties, e.g. CD and circularly polarized luminescence (CPL) open the door to various applications in the storage and transfer of optical information, in such cases, the level of CPL can facilitate additional dimensions of information content transmitted *via* light irradiation. [31]. Although Zander and Franke reported the first synthesis of dehydrohelicenes 50 years ago [32], there are no reports of catalytic and enantioselective synthesis of chiral heterodehydrohelicenes (Figure 3.3).

In 2022, Salem and Takizawa introduced an efficient electrochemical sequential approach for the synthesis of diverse unsymmetrical oxaza[7]dehydrohelicenes **18**. Leveraging the readily available substrates: *N*-tolyl-3-hydroxycarbazole **8b** and 7-methoxy-2-naphthol **2e** as key coupling partners, their differential oxidation potentials ($E_{\mathbf{8b}(ox)} = 0.69$ V, and $E_{\mathbf{2e}(ox)} = 1.32$ V) played a crucial role in orchestrating the chemoselectivity of the oxidative hetero-coupling step, resulting in the exclusive formation of diol derivatives **14u**. Subsequent dehydrative cyclization of these diols yielded oxaza[7]helicene derivatives **17a**, followed by an intramolecular C—C bond formation between the helical termini, ultimately furnishing the corresponding oxaza[7]dehydrohelicene **18a** (Scheme 3.13i) [33]. This protocol presented a highly efficient method for accessing diverse hetero[7]dehydrohelicenes **18** under mild conditions. The green electrochemical process sets itself apart by entirely eliminating metal waste, a notable departure from syntheses catalyzed by transitional metals [4].

Subsequently, Salem and Takizawa extended this approach to demonstrate the stepwise enantioselective scalable synthesis of the optically active dehydrohelicene (Scheme 3.13ii). Mononuclear vanadium complex (R^a,*S*)-**1n** catalyzed oxidative hetero-coupling of **8c** and **2e** giving the diol (*R*)-**14v** in 83% yield with 59% ee. After the recrystallization of the obtained **14v** (91% ee), the diol (*R*)-**14v** underwent

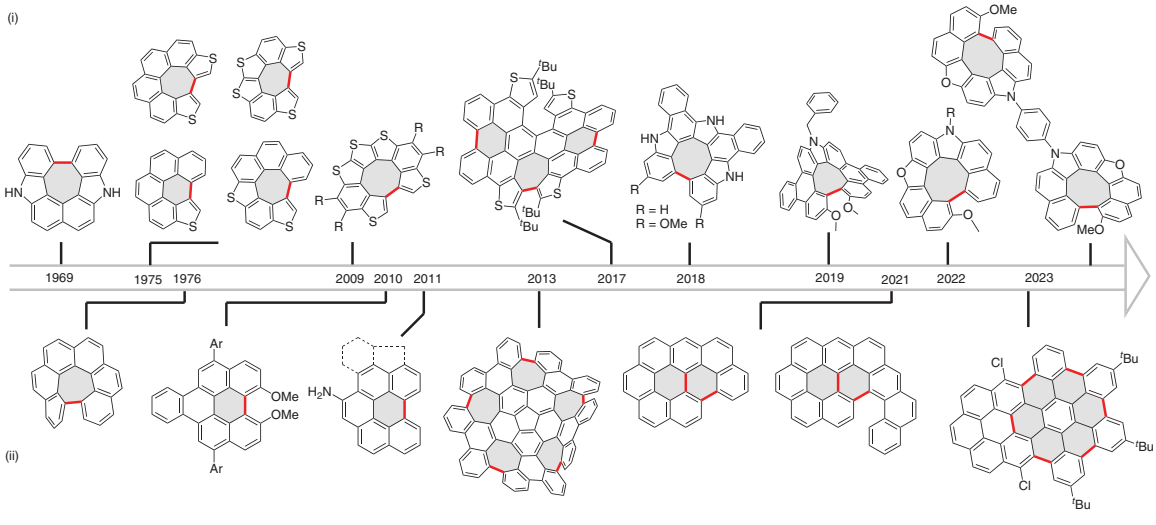

Figure 3.3 Comprehensive overview of the pivotal accomplishments in the chemistry of carbo[*n*]dehydrohelicenes and hetero[*n*]dehydrohelicenes over the past 50 years. (i) hetero[*n*]helicenes, distinguished by their incorporation of sulfur, nitrogen, or oxygen atoms into the helical framework, adding an extra layer of complexity and functionality; (ii) carbo[*n*]dehydrohelicenes, characterized by a dehydrohelicene scaffold composed solely of carbon and hydrogen atoms.

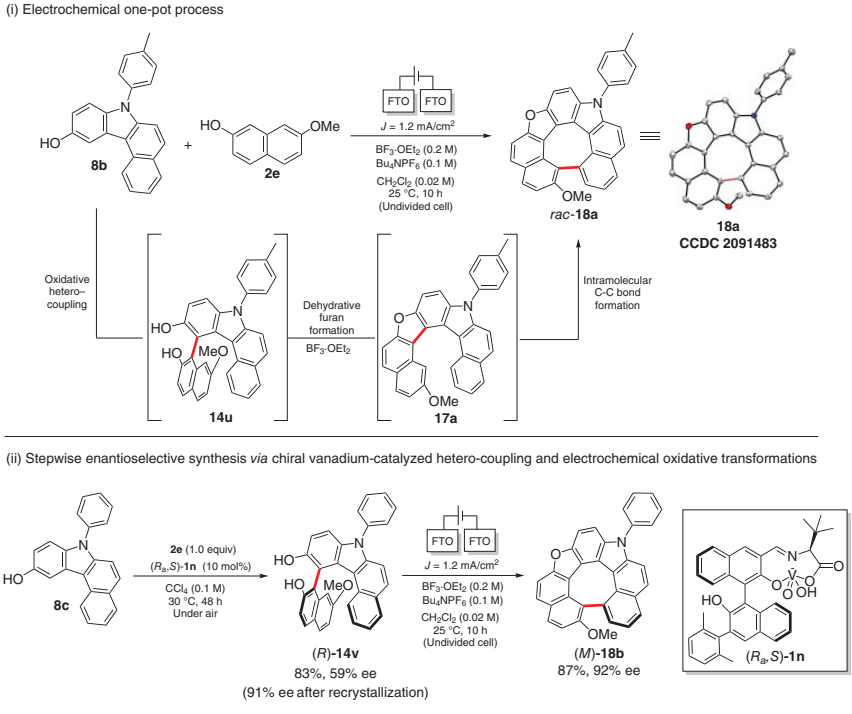

Scheme 3.13 (i) Sequential electrochemical synthesis of oxaza[7]dehydrohelicene and (ii) stepwise enantioselective synthesis of oxaza[7]dehydrohelicene.

an electrochemical dehydrative furan ring formation to give the corresponding oxaza[7]helicene, followed by the intramolecular coupling of the two helical termini to produce the desired oxaza[7]dehydrohelicene (*M*)-**18** in 87% yield maintaining its high optical purity (92% ee) (Scheme 3.13ii). Notably, the protocol was readily scaled up to produce 0.62 g of (*M*)-**18b** (current efficiency = 48%, and overall yield of up to 55%) [32]. Among the synthesized oxaza[7]dehydrohelicenes **18** the authors screened, the dehydrohelicene **18a** showed notable properties (intense blue-colored CPL ($|g_{lum}| \approx 2.5 \times 10^{-3}$ at 433 nm); racemization barrier: $\Delta G^{\ddagger} > 140$ kJ/mol and $t_{1/2} >$ c. 9.5×10^3 years at 25 °C), discernibly higher level of chiral stability when compared to its oxaza[7]helicene counterparts ($\Delta G^{\ddagger} > 110$ kJ/mol and $t_{1/2} >$ c. 5.7 days at 25 °C) [33].

To optimize the electrochemical conditions for the synthesis of double dehydrohelicenes, in 2023, Salem and Takizawa performed a data-driven optimization technique. Bayesian optimization (BO) is one of the robust probabilistic optimization methods for identifying the global maxima of a black-box objective function, particularly suitable for multiparameter systems within minimum data [34]. To efficiently discover the optimal conditions with minimal experimentation, BO operates *via* a series of iterations, balancing exploration by sampling uncharted regions and exploitation by focusing on areas where improvement is expected. Based on their prior works [35], Salem and Takizawa pursued an in-depth study of this electrochemical sequence and performed BO-assisted screening for five numerical synthetic parameters such as concentration of electrolyte, current intensity, concentration of **8d**, $BF_3{\cdot}OEt_2$ concentration, and equivalence of **2e**. While other fundamental parameters showed limited potential for yield enhancing *via* further optimization [33, 36], these five parameters, due to the intricacies of

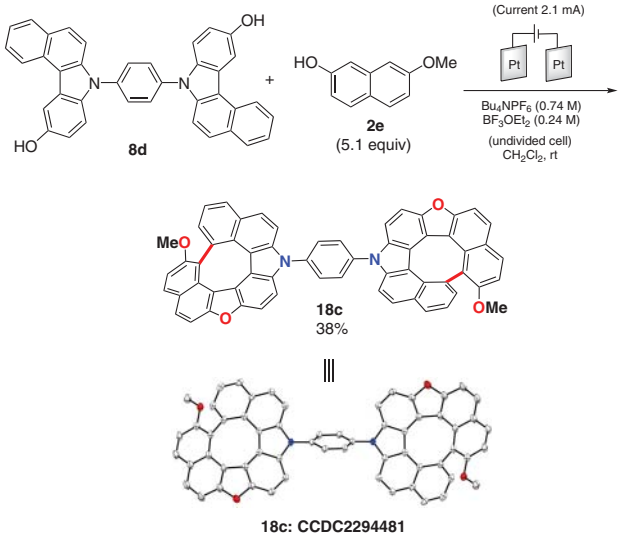

Scheme 3.14 Data-driven electrochemical synthesis of double oxaza[7]dehydrohelicene. Source: Adapted from Langeslay et al. [7].

this electrochemical sequence, held the promise to significantly improve the yields. By fine-tuning the conductivity and cell potential using these specific parameters, Salem and Takizawa eventually achieved the specific optimization context in just 16 trials with judicious switching between acquisition functions tailored to the specific optimization context. This strategic approach led to a remarkable yield of 38% with a faradic efficiency (%FE) of 14.4% [37] (Scheme 3.14).

3.6 Summary and Conclusion

The development of axially chiral biaryl-derived ligands and catalysts has significantly enhanced the efficiency of transition metal and organocatalytic asymmetric processes. While these frameworks are crucial to chemists, some axially asymmetric systems still lack efficient construction techniques, especially for asymmetric metal catalyst systems. In this chapter, recent advances and research on vanadium complex-catalyzed oxidative coupling of arenol and its applications to PHA preparation were discussed. Chiral vanadium complexes, consisting of Schiff base ligands and vanadium center, represented highly active catalysts in various regio- and enantioselective C—C bond formation reactions to construct the axial chirality. The high valency and ability of vanadium to exist in multiple oxidation states enabled vanadium complexes to act as Lewis acid and/or redox catalysts [38]. Moreover, the highly selective and characteristic vanadium activity not only suppressed side reaction pathways and peroxidation but also enabled various functional group tolerances in various organic syntheses [7, 39]. In fact, Takizawa group performed the reaction of aniline **19** and 7-methoxy-1-naphthaldehyde **20** with 10 mol% of the chiral mononuclear vanadium complex (R^a,*S*)-**1j** to give the C_1-symmetrical phenanthridine derivative **21** in 51% yield and 65% ee through a Pictet–Spengler reaction, followed by dehydrogenative aromatization sequence (Scheme 3.15) [40].

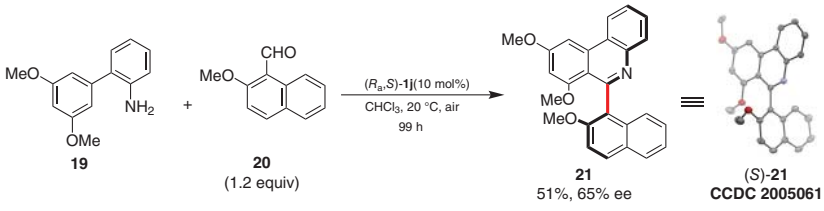

Scheme 3.15 Chiral vanadium complex-catalyzed Pictet–Spengler reaction, followed by dehydrogenative aromatization sequence, producing axial chiral molecules.

Needless to say, continued efforts are required to elucidate the mechanisms, precise active species, and modes of activation as well as the development of new and more challenging C—C bond formations. In 2020, Kozlowski group reported that 1,1,1,3,3,3-hexafluoro-2-propanol (HFIP) as a reaction solvent drastically enhanced the vanadium catalyst activity to promote the coupling of less-activated

phenols efficiently [41]. Hybridization of vanadium, biocatalysts, and/or organocatalysts has sprung new transformation protocols to construct key building blocks in previously unknown pathways [42, 43]. We continue to believe that new chiral vanadium-mediated catalytic processes will promote novel and promising aspects and lead to further breakthrough discoveries in the near future.

References

1 (a) Carson, M.C. and Kozlowski, M.C. (2024). Recent advances in oxidative phenol coupling for the total synthesis of natural products. *Nat. Prod. Rep.* 48: 208–227. (b) Roos, C.B., Chiang, C.-H., Murray, L.A.M. et al. (2023). Stereodynamic strategies to induce and enrich chirality of atropisomers at a late stage. *Chem. Rev.* 123 (17): 10641–10727. (c) Centonze, G., Portolani, C., Righi, P. et al. (2023). Enantioselective strategies for the synthesis of *N–N* atropisomers. *Angew. Chem. Int. Ed.* 62 (31): e202303966.

2 (a) Su, B. and Hartwig, J.F. (2022). Development of chiral ligands for the transition-metal-catalyzed enantioselective silylation and borylation of C–H bonds. *Angew. Chem. Int. Ed.* 61 (9): e202113343. (b) Shibasaki, M., Sasai, H., and Arai, T. (1997). Asymmetric catalysis with heterobimetallic compounds. *Angew. Chem. Int. Ed.* 36 (12): 1236–1256. (c) Maruoka, K. (2008). Practical aspects of recent asymmetric phase-transfer catalysis. *Org. Process Res. Dev.* 12 (4): 679–697.

3 Bringmann, G., Gulder, T., Gulder, T.A.M., and Breuning, M. (2011). Atroposelective total synthesis of axially chiral biaryl natural products. *Chem. Rev.* 111 (2): 563–639.

4 Kumar, A., Sasai, H., and Takizawa, S. (2022). Atroposelective synthesis of C–C axially chiral compounds *via* mono- and dinuclear vanadium catalysis. *Acc. Chem. Res.* 55 (20): 2949–2965.

5 (a)Tian, J.-M., Wang, A.-F., Yang, J.-S. et al. (2019). Copper-complex-catalyzed asymmetric aerobic oxidative cross-coupling of 2-naphthols: enantioselective synthesis of 3,3′-substituted C_1-symmetric BINOLs. *Angew. Chem. Int. Ed.* 58 (32): 11023–11027. (b) Zhao, X.-J., Li, Z.-H., Ding, T.-M. et al. (2021). Enantioselective synthesis of 3,3′-disubstituted 2-amino-2′-hydroxy-1,1′-binaphthyls by copper-catalyzed aerobic oxidative cross-coupling. *Angew. Chem. Int. Ed.* 60 (13): 7061–7065.

6 Walia, P.K., Kumar, M., and Bhalla, V. (2018). Empowering transition-metal-free cascade protocol for the green synthesis of biaryls and alkynes. *ACS Omega* 3 (2): 1983–1990.

7 Langeslay, R.R., Kaphan, D.M., Marshall, C.L. et al. (2019). Catalytic applications of vanadium: a mechanistic perspective. *Chem. Rev.* 119 (4): 2128–2191.

8 (a) Chu, C.-Y., Hwang, D.-R., Wang, S.-K., and Uang, B.J. (2001). Chiral oxovanadium complex catalyzed enantioselective oxidative coupling of 2-naphthols. *Chem. Commun.* 2001 (11): 980–981. (b) Chu, C.-Y. and Uang, B.-J. (2003). Catalytic enantioselective coupling of 2-naphthols by new chiral oxovanadium

complexes bearing a self-accelerating functional group. *Tetrahedron Asymmetry* 14 (1): 53–55.

9 (a) Hon, S.-W., Li, C.-H., Kuo, J.-H. et al. (2001). Catalytic asymmetric coupling of 2-naphthols by chiral tridentate oxovanadium(IV) complexes. *Org. Lett.* 3 (6): 869–872. (b) Barhate, N.B. and Chen, C.-T. (2002). Catalytic asymmetric oxidative couplings of 2-naphthols by tridentate *N*-ketopinidene-based vanadyl dicarboxylates. *Org. Lett.* 4 (15): 2529–2532.

10 Sako, M., Takizawa, S., and Sasai, H. (2020). Chiral vanadium complex-catalyzed oxidative coupling of arenols. *Tetrahedron* 76 (47): 131645.

11 (a) Luo, Z., Liu, Q., Gong, L. et al. (2002). The rational design of novel chiral oxovanadium(iv) complexes for highly enantioselective oxidative coupling of 2-naphthols. *Chem. Commun.* 2002 (8): 914–915. (b)Luo, Z., Liu, Q., Gong, L.-Z. et al. (2002). Novel achiral biphenol-derived diastereomeric oxovanadium(IV) complexes for highly enantioselective oxidative coupling of 2-naphthols. *Angew. Chem. Int. Ed.* 41 (23): 4532–4535. (c) Guo, Q.-X., Wu, Z.-J., Luo, Z.-B. et al. (2007). Highly enantioselective oxidative couplings of 2-naphthols catalyzed by chiral bimetallic oxovanadium complexes with either oxygen or air as oxidant. *J. Am. Chem. Soc.* 129 (45): 13927–13938.

12 (a) Somei, H., Asano, Y., Yoshida, T. et al. (2004). Dual activation in a homolytic coupling reaction promoted by an enantioselective dinuclear vanadium(IV) catalyst. *Tetrahedron Lett.* 45 (9): 1841–1844. (b) Takizawa, S., Katayama, T., Kameyama, C. et al. (2008). Chiral dinuclear vanadium(v) catalysts for oxidative coupling of 2-naphthols. *Chem. Commun.* 2008 (15): 1810–1812. (c) Takizawa, S., Katayama, T., Somei, H. et al. (2008). Dual activation in oxidative coupling of 2-naphthols catalyzed by chiral dinuclear vanadium complexes. *Tetrahedron* 64 (15): 3361–3371. (d) Sako, M., Aoki, T., Zumbrägel, N. et al. (2019). Chiral dinuclear vanadium complex-mediated oxidative coupling of resorcinols. *J. Org. Chem.* 84 (3): 1580–1587.

13 (a) da Silva, E.M., Vidal, H.D.A., Januário, M.A.P. et al. (2023). Advances in the asymmetric synthesis of BINOL derivatives. *Molecules* 28 (1): 12. (b) Chen, P., Chen, H.-N., Wong, H.N.C., and Peng, X.-S. (2023). Recent advances in iron-catalysed coupling reactions for the construction of the C(sp^2)–C(sp^2) bond. *Org. Biomol. Chem.* 21 (30): 6083–6095. (c) Wu, J. and Kozlowski, M.C. (2022). Catalytic oxidative coupling of phenols and related compounds. *ACS Catal.* 12 (11): 6532–6549.

14 Ding, Y.-Y., Zhou, H., Deng, P. et al. (2023). Antimicrobial activity of natural and semi-synthetic carbazole alkaloids. *Eur. J. Med. Chem.* 259: 115627.

15 Yohanes, R., Harneti, D., Supratman, U. et al. (2023). Phytochemistry and biological activities of Murraya species. *Molecules* 28 (15): 5901.

16 Dubois, M.-A., Grandbois, A., Collins, S.K., and Schmitzer, A.R. (2011). Introduction of axial chirality in a planar aromatic ligand results in chiral recognition with DNA. *J. Mol. Recognit.* 24 (2): 288–294.

17 Liu, L., Carroll, P.J., and Kozlowski, M.C. (2015). Vanadium-catalyzed regioselective oxidative coupling of 2-hydroxycarbazoles. *Org. Lett.* 17 (3): 508–511.

18 Kang, H., Herling, M.R., Niederer, K.A. et al. (2018). Enantioselective vanadium-catalyzed oxidative coupling: development and mechanistic insights. *J. Org. Chem.* 83 (23): 14362–14384.

19 (a) Sako, M., Ichinose, K., Takizawa, S., and Sasai, H. (2017). Short syntheses of 4-deoxycarbazomycin B, sorazolon E, and (+)-sorazolon E2. *Chem. Asian J.* 12 (12): 1305–1308. (b) Sako, M., Sugizaki, A., and Takizawa, S. (2018). Asymmetric oxidative coupling of hydroxycarbazoles: facile synthesis of (+)-bi-2-hydroxy-3-methylcarbazole. *Bioorg. Med. Chem. Lett.* 28 (16): 2751–2753. (c) Kamble, G., Salem, M.S.H., Abe, T. et al. (2021). Chiral vanadium (V)-catalyzed oxidative coupling of 4-hydroxycarbazoles. *Chem. Lett.* 50 (10): 1755–1757.

20 Karwehl, S., Jansen, R., Huch, V., and Stadler, M. (2016). Sorazolons, carbazole alkaloids from Sorangium cellulosum strain Soce375. *J. Nat. Prod.* 79 (2): 369–375.

21 (a) Smrčina, M., Polakova, J., Vyskocil, S., and Kocovsky, P. (1993). Synthesis of enantiomerically pure binaphthyl derivatives. Mechanism of the enantioselective, oxidative coupling of naphthols and designing a catalytic cycle. *J. Org. Chem.* 58 (17): 4534–4538. (b) Nakajima, M., Miyoshi, I., Kanayama, K. et al. (1999). Enantioselective synthesis of binaphthol derivatives by oxidative coupling of naphthol derivatives catalyzed by chiral diamine·copper complexes. *J. Org. Chem.* 64 (7): 2264–2271. (c) Li, X., Yang, J., and Kozlowski, M.C. (2001). Enantioselective oxidative biaryl coupling reactions catalyzed by 1,5-diazadecalin metal complexes. *Org. Lett.* 3 (8): 1137–1140. (d) Gao, J., Reibenspies, J.H., and Martell, A.E. (2003). Structurally defined catalysts for enantioselective oxidative coupling reactions. *Angew. Chem. Int. Ed.* 42 (48): 6008–6012. (e) Kim, K.H., Lee, D.-W., Lee, Y.-S. et al. (2004). Enantioselective oxidative coupling of methyl 3-hydroxy-2-naphthoate using mono-*N*-alkylated octahydrobinaphthyl-2,2′-diamine ligand. *Tetrahedron* 60 (41): 9037–9042. (f) Temma, T. and Habaue, S. (2005). Highly selective oxidative cross-coupling polymerization with copper(I)-bisoxazoline catalysts. *J. Polym. Sci. A Polym. Chem.* 43 (24): 6287–6294. (g) Alamsetti, S.K., Poonguzhali, E., Ganapathy, D., and Sekar, G. (2013). Enantioselective oxidative coupling of 2-naphthol derivatives by copper-(*R*)-1,1′-binaphthyl-2,2′-diamine-TEMPO catalyst. *Adv. Synth. Catal.* 355 (14–15): 2803–2808. (h) Zhang, Q., Cui, X., Chen, L. et al. (2014). Syntheses of chiral ferrocenophanes and their application to asymmetric catalysis. *Eur. J. Org. Chem.* 2014 (35): 7823–7829. (i) Prause, F., Arensmeyer, B., Fröhlich, B., and Breuning, M. (2015). In-depth structure–selectivity investigations on asymmetric, copper-catalyzed oxidative biaryl coupling in the presence of 5-cis-substituted prolinamines. *Cat. Sci. Technol.* 5 (4): 2215–2226. (j) Wang, P., Cen, S., Gao, J. et al. (2022). Novel axially chiral ligand-enabled copper-catalyzed asymmetric oxidative coupling of 2-naphthols for the synthesis of 6,6′-disubstituted BINOLs. *Org. Lett.* 24 (12): 2321–2326. (k) Cen, S., Huang, N., Lian, D. et al. (2022). Conformational enantiodiscrimination for asymmetric construction of atropisomers. *Nat. Commun.* 13: 4735. (l) Irie, R., Masutani, K., and Katsuki, T. (2000). Asymmetric aerobic oxidation coupling of 2-naphthol

derivatives catalyzed by photo-activated chiral (NO)Ru(II)-Salen complex. *Synlett* 2000 (10): 1433–1436. (m) Tada, M., Taniike, T., Kantam, L.M. et al. (2004). Chiral self-dimerization of vanadium complexes on a SiO_2 surface: the first heterogeneous catalyst for asymmetric 2-naphthol coupling. *Chem. Commun.* 2004 (22): 2542–2543. (n) Habaue, S., Murakami, S., and Higashimura, H. (2005). New asymmetric vanadium catalyst for highly selective oxidative coupling polymerization. *J. Polym. Sci. A Polym. Chem.* 43 (23): 5872–5878. (o) Mandal, M., Nagaraju, V., Karunakar, G.V. et al. (2015). Electronic, conjugation, and confinement effects on structure, redox, and catalytic behavior of oxido-vanadium(IV) and -(V) chiral Schiff base complexes. *J. Phys. Chem. C* 119 (52): 28854–28870. (p) Egami, H. and Katsuki, T. (2009). Iron-catalyzed asymmetric aerobic oxidation: oxidative coupling of 2-naphthols. *J. Am. Chem. Soc.* 131 (17): 6082–6083. (q) Narute, S., Parnes, R., Toste, F.D. et al. (2016). Enantioselective oxidative homocoupling and cross-coupling of 2-naphthols catalyzed by chiral iron phosphate complexes. *J. Am. Chem. Soc.* 138 (50): 16553–16560. (r) Horibe, T., Nakagawa, K., Hazeyama, T. et al. (2019). An enantioselective oxidative coupling reaction of 2-naphthol derivatives catalyzed by chiral diphosphine oxide–iron(II) complexes. *Chem. Commun.* 55 (91): 13677–13680.

22 (a) Smrčina, M., Vyskočil, Š., Máca, B. et al. (1994). Selective cross-coupling of 2-naphthol and 2-naphthylamine derivatives. A facile synthesis of 2,2′,3-trisubstituted and 2,2′,3,3′-tetrasubstituted 1,1′-binaphthyls. *J. Org. Chem.* 59 (8): 2156–2163. (b) Li, X., Hewgley, J.B., Mulrooney, C.A. et al. (2003). Enantioselective oxidative biaryl coupling reactions catalyzed by 1,5-diazadecalin metal complexes: efficient formation of chiral functionalized BINOL derivatives. *J. Org. Chem.* 68 (14): 5500–5511. (c) Temma, T. and Habaue, S. (2005). Highly selective oxidative cross-coupling of 2-naphthol derivatives with chiral copper(I)–bisoxazoline catalysts. *Tetrahedron Lett.* 46 (34): 5655–5657. (d) Hayashi, H., Ueno, T., Kim, C., and Uchida, T. (2020). Ruthenium-catalyzed cross-selective asymmetric oxidative coupling of arenols. *Org. Lett.* 22 (4): 1469–1474. (e) Egami, H., Matsumoto, K., Oguma, T. et al. (2010). Enantioenriched synthesis of C_1-symmetric BINOLs: iron-catalyzed cross-coupling of 2-naphthols and some mechanistic insight. *J. Am. Chem. Soc.* 132 (39): 13633–13635. (f) Dyadyuk, A., Vershinin, V., Shalit, H. et al. (2022). A chiral iron disulfonate catalyst for the enantioselective synthesis of 2-amino-2′-hydroxy-1,1′-binaphthyls (NOBINs). *J. Am. Chem. Soc.* 144 (8): 3676–3684.

23 Sako, M., Higashida, K., Kamble, G.T. et al. (2021). Chemo- and enantioselective hetero-coupling of hydroxycarbazoles catalyzed by a chiral vanadium(v) complex. *Org. Chem. Front.* 8 (17): 4878–4885.

24 Belokon, Y.N., Maleev, V.I., North, M., and Usanov, D.L. (2006). VO(Salen)(X) catalysed asymmetric cyanohydrin synthesis: an unexpected influence of the nature of anion X on the catalytic activity. *Chem. Commun.* 2006 (44): 4614–4616.

25 Shaik, S.S. and Pross, A. (1989). Nucleophilic attack on cation radicals and cations. A theoretical analysis. *J. Am. Chem. Soc.* 111 (12): 4306–4312.

26 (a) Anderson, H.V., Gois, N.D., and Chalifoux, W.A. (2023). New advances in chiral nanographene chemistry. *Org. Chem. Front.* 10 (16): 4167–4197. (b) Duan, C., Xin, H., and Gao, X. (2023). Recent progress in chemistry of non-benzenoid carbohelicenes. *Tetrahedron Lett.* 123: 154553. (c) Salem, M.S.H., Sharma, R., Suzuki, S. et al. (2024). Impact of helical elongation of symmetric oxa[n]helicenes on their structural, photophysical, and chiroptical characteristics. *Chirality* 36 (5): e23673.

27 (a) Wu, Y.-F., Ying, S.-W., Su, L.-Y. et al. (2022). Nitrogen-embedded quintuple [7]helicene: a helicene–azacorannulene hybrid with strong near-infrared fluorescence. *J. Am. Chem. Soc.* 144 (24): 10736–10742. (b) Pun, S.H., Cheung, K.M., Yang, D. et al. (2022). A near-infrared absorbing and emissive quadruple helicene enabled by the Scholl reaction of perylene. *Angew. Chem. Int. Ed.* 61 (8): e202113203. (c) Mori, T. (2021). Chiroptical properties of symmetric double, triple, and multiple helicenes. *Chem. Rev.* 121 (4): 2373–2412.

28 (a) Crassous, J., Stará, I.G., and Starý, I. (2022). *Helicenes: Synthesis, Properties and Applications*. Wiley-VCH GmbH. (b) Gingras, M., Félix, G., and Peresutti, R. (2013). One hundred years of helicene chemistry. Part 2: stereoselective syntheses and chiral separations of carbohelicenes. *Chem. Soc. Rev.* 42 (3): 1007–1050.

29 Sako, M., Takeuchi, Y., Tsujihara, T. et al. (2016). Efficient enantioselective synthesis of oxahelicenes using redox/acid cooperative catalysts. *J. Am. Chem. Soc.* 138 (36): 11481–11484.

30 Khalid, M.I., Salem, M.S.H., and Takizawa, S. (2024). Synthesis, structural, and optical behavior of dehydrohelicene-containing polycyclic compounds. *Molecules* 29 (2): 296.

31 Peeters, E., Christiaans, M.P.T., Janssen, R.A. et al. (1997). Circularly polarized electroluminescence from a polymer light-emitting diode. *J. Am. Chem. Soc.* 119 (41): 9909–9910.

32 Zander, M. and Franke, W.H. (1969). Über Carbazolo-carbazole. *Chem. Ber.* 102 (8): 2728–2738.

33 Khalid, M.I., Salem, M.S.H., Sako, M. et al. (2022). Electrochemical synthesis of heterodehydro[7]helicenes. *Commun. Chem.* 5: 166.

34 Alvarado, J.I.M., Meinhardt, J.M., and Lin, S. (2022). Working at the interfaces of data science and synthetic electrochemistry. *Tetrahedron Chem* 1: 100012.

35 (a) Kondo, M., Sugizaki, A., Khalid, M.I. et al. (2021). Energy-, time-, and labor-saving synthesis of α-ketiminophosphonates: machine-learning-assisted simultaneous multiparameter screening for electrochemical oxidation. *Green Chem.* 23 (16): 5825–5831. (b) Kondo, M., Wathsala, H.D.P., Salem, M.S.H. et al. (2022). Bayesian optimization-driven parallel-screening of multiple parameters for the flow synthesis of biaryl compounds. *Commun. Chem.* 5: 148. (c) Naito, Y., Kondo, M., Nakamura, Y. et al. (2022). Bayesian optimization with constraint on passed charge for multiparameter screening of electrochemical reductive carboxylation in a flow microreactor. *Chem. Commun.* 58 (24): 3893–3896. (d) Kondo, M., Wathsala, H.D.P., Ishikawa, K. et al. (2023). Bayesian optimization-assisted screening to identify improved reaction conditions for spiro-dithiolane synthesis. *Molecules* 28 (13): 5180.

36 (a) Salem, M.S.H., Khalid, M.I., Sako, M. et al. (2023). Electrochemical synthesis of hetero[7]helicenes containing pyrrole and furan rings *via* an oxidative heterocoupling and dehydrative cyclization sequence. *Adv. Synth. Catal.* 365 (3): 373–380. (b) Salem, M.S.H., Khalid, M.I., Sasai, H., and Takizawa, S. (2023). Two-pot synthesis of unsymmetrical hetero[7]helicenes with intriguing optical properties. *Tetrahedron* 133: 133266. (c) Salem, M.S.H., Sabri, A., Khalid, M.I. et al. (2022). Two-step synthesis, structure, and optical features of a double hetero[7]helicene. *Molecules* 27 (24): 9068.

37 Salem, M.S.H., Sharma, R., Khalid, M.I. et al. (2023). Data-driven electrochemical one-pot synthesis of double hetero[7]dehydrohelicene. *Electrochemistry* 91 (11): 112015.

38 (a) Takizawa, S., Arteaga, F.A., Yoshida, Y. et al. (2013). Vanadium-catalyzed enantioselective Friedel–Crafts-type reactions. *Dalton Trans.* 42 (33): 11787–11790. (b) Zumbrägel, N., Sako, M., Takizawa, S. et al. (2018). Vanadium-catalyzed dehydrogenation of *N*-heterocycles in water. *Org. Lett.* 20 (16): 4723–4727.

39 (a) Pellissier, H. (2020). Enantioselective vanadium-catalyzed transformations. An update. *Coord. Chem. Rev.* 418: 213395. (b) Schober, L., Sako, M., Takizawa, S. et al. (2020). Catalytic and enantioselective oxa-Piancatelli reaction using a chiral vanadium complex. *Chem. Commun.* 56 (70): 10151–10154.

40 Sako, M., Losa, R., Takiishi, T. et al. (2020). Vanadium(V) complex-catalyzed one-pot synthesis of phenanthridines *via* a Pictet–Spengler-dehydrogenative aromatization sequence. *Catalysts* 10 (8): 860.

41 Gilmartin, P.H. and Kozlowski, M.C. (2020). Vanadium-catalyzed oxidative intramolecular coupling of tethered phenols: formation of phenol-dienone products. *Org. Lett.* 22 (8): 2914–2919.

42 Takizawa, S., Gröger, H., and Sasai, H. (2015). Vanadium in asymmetric synthesis: emerging concepts in catalyst design and applications. *Chem. Eur. J.* 21 (25): 8992–8997.

43 Kasama, K., Aoyama, H., and Akai, S. (2020). Enantiodivergent synthesis of axially chiral biphenyls from σ-symmetric 1,1′-biphenyl-2,6-diol derivatives by single lipase-catalyzed acylative and hydrolytic desymmetrization. *Eur. J. Org. Chem.* 2020 (6): 654–661.

4

Atroposelective Suzuki–Miyaura Coupling Toward Axially Chiral Biaryls: Mechanistic Insight

Toshinobu Korenaga

Iwate University, Faculty of Science and Engineering, Department of Chemistry and Biological Sciences, 4-3-5 Ueda, Morioka, Iwate, 020-8551, Japan

4.1 Introduction

Suzuki–Miyaura coupling (SMC) is one of the most important methods for carbon–carbon bond-forming reactions [1]. It was reported in 1979 by Suzuki and Miyaura [2]. Afterward, numerous studies have been conducted on the construction of the sp^2–sp^2, sp–sp^2, sp^3–sp^2, and even sp^3–sp^3 carbon bonds [1, 3, 4]. In 2010, the Nobel Prize in Chemistry was awarded for the reaction [5]. During the formation of biaryls, the steric hindrance of substituents at the *ortho* position slows the axial rotation of sp^2–sp^2 carbon bonds, resulting in atropisomers. Such atropisomeric chirality is observed and used in a wide range of molecular systems, including pharmaceuticals [6], bioactive compounds [7], luminescent materials [8], and chiral ligands [9]. A reasonable rotational barrier is required for the enantiomers of the atropisomer to be present. The enantiomers can be analytically separated if the half-life ($t_{1/2}$) of the interconversion is at least 1000 seconds and if the approximate energy barriers to rotations of (ΔE_{rot}) exceed 20 kcal/mol [10]. However, a larger rotational barrier of $\Delta E_{rot} > 30$ kcal/mol is required to isolate and store the enantiomers in the order of years [6e]. To obtain such a large rotational barrier, three or four substituents are required at the *ortho* position of biaryls. This construction of chiral biaryls is also possible with SMC reactions [11], either by a chiral directing group on the aryl substrates in the presence of an achiral catalyst (diastereoselective SMC) or by the coupling of achiral substrates using an asymmetric catalyst (asymmetric SMC). The latter enables a more straightforward synthesis since many reaction substrates for general SMC reactions can be used without modification if the appropriate asymmetric catalyst is prepared. Thus, asymmetric SMCs continue to be developed, with certain excellent examples; however, they are frequently limited.

This chapter describes an asymmetric SMC using an asymmetric catalyst to afford chiral biaryls. It discusses the mechanism of asymmetric induction based on reported examples to develop better asymmetric catalysts in the future. Since only

Atropisomerism in Asymmetric Organic Synthesis: Challenges and Applications, First Edition.
Edited by Shinobu Takizawa and Mohamed S. H. Salem.

cases where the mechanism was discussed are described in this chapter, see the excellent reviews [11] for a summary of previous asymmetric SMC examples.

In this chapter, the structural diagrams of the mechanism are drawn based on the original papers, and the numbering of compounds, complex intermediates, etc., was independently assigned.

4.2 Mechanism Insight of SMC Reaction and Enantiodetermining Step

During SMC reactions, the axial chirality of the coupling product (**P**) is introduced during the reductive elimination (*RE*) of the Pd-Ar_2 intermediate produced through the oxidative addition (*OA*) of aryl halides (**H**) to zero-valent Pd, followed by the transmetalation (*TM*) of arylboronic acids (**B**) (Scheme 4.1) [1a, 4]. When asymmetric SMC is performed, a chiral catalyst comprising Pd with a chiral ligand is used [11d]. The chiral environment created by the ligand enables the axial chirality of the reacting biaryl groups to develop during the *RE*. Thus, although the *RE* transition state (TS) is considered the most important for determining enantioselectivity (Scheme 4.1) [12], in practice, it is insufficient to compare only the two TSs that afford the *R*- and *S*-enantiomers.

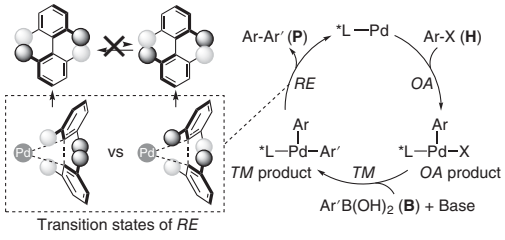

Scheme 4.1 Catalytic cycle of SMC reactions and schematic of asymmetric induction during *RE*.

When considering a *RE* process to produce a C_2-symmetric chiral biaryl, at least eight different TSs must be considered because of differences in the conformation of the aromatic ring to be eliminated. For example, **TS-A**^{S} and **TS-A**^{R} have four substituents at *ortho* position oriented in the same direction (the black circles in the figure are drawn in the foreground). However, the twist of the benzene ring endows one with (*S*)-**P** and the other with (*R*)-**P** (Figure 4.1). When there are many conformations or in C_1-symmetric chiral biaryl-producing reactions, more TSs require consideration.

Furthermore, the asymmetric induction step to be considered changes depending on whether or not equilibrium is achieved during the reaction process. If equilibrium is rapidly achieved between the *TM* products or during the reaction process until the formation of the *TM* products, the Curtin–Hammett principle [13] applies because of the high activation free energy for *RE* giving tri- or tetra-*ortho*-substituted

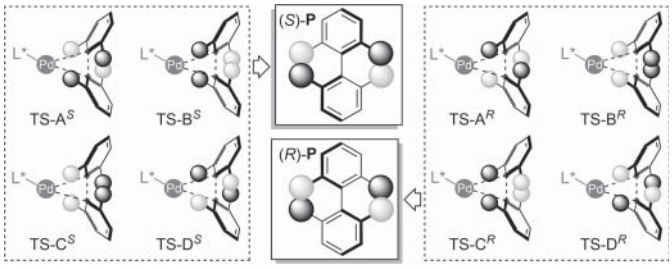

Figure 4.1 Pattern of transition states of *RE* to afford *S*- or *R*-enantiomer.

biaryls, and the enantioselectivity can be evaluated by calculating the activation energy of *RE* (ΔE^{RE}) (Scheme 4.2, gray arrows). Contrarily, in the absence of such equilibrium (no gray arrows), the relative population of *OA* products (**OA**) and *TM* products (**TM**) should be considered [14]. Even at its simplest, during the *OA* step, intermediates of at least two different aryl group orientations are formed ($\mathbf{OA_1}$, $\mathbf{OA_2}$). Considering that the *TM* for these two intermediates introduces aromatic rings from two directions, four intermediates are obtained ($\mathbf{TM_1}$–$\mathbf{TM_4}$). In reality, more conformers require consideration.

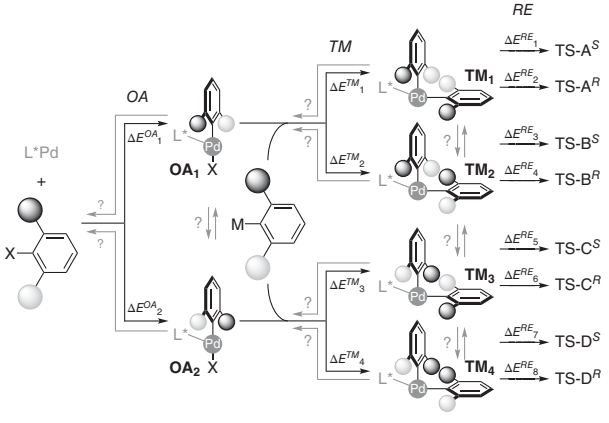

Scheme 4.2 Channel branching in the asymmetric SMC mechanism.

The change in enantioselectivity with and without equilibrium has been reported by Patel et al. [15] During the coupling reaction of 1-bromo-2-methylnaphthalene (**H1**) with 2-methylnaphthyl (2-MeNp)-$B(OH)_2$ (**B1**) (SMC) or 2-MeNp-ZnBr (Negishi coupling) [16], the reactions using the same chiral ligand of NitinPhos (**L1**) afforded different enantioselectivities of 2,2′-dimethyl-1,1′-binaphthalene (**P1**) (89% enantiomeric excess (ee) for SMC vs 61% ee for Negishi coupling) (Scheme 4.3). In addition, the chiral ligands that produced the best results differed for each (**L1** dominance for SMC vs **L2** dominance for Negishi coupling). The different selectivities of both reactions, which proceed *via* the same *RE* process, implied that the enantiodetermining step differed. The authors assumed that the Negishi

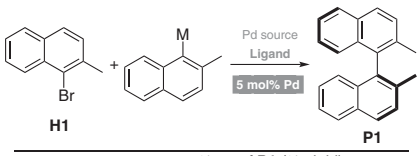

Ligand	% ee of **P1** (% yield)	
	M = ZnBr	M = $B(OH)_2$ (**B1**)
L1	61% ee (10%)	89% ee (97%)
L2	70% ee (93%)	69% ee (73%)

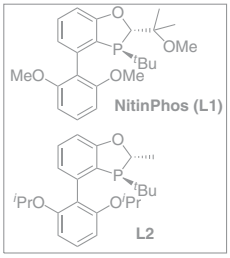

Scheme 4.3 Change in enantioselectivity of **P1** between Negishi coupling and SMC.

coupling and SMC reaction were reversible and irreversible, respectively, and verified this assumption through density functional theory (DFT) calculations. The results showed that *RE* was the enantiodetermining step in the Negishi reaction, whereas all the steps of the catalytic cycle affected enantioselectivity in the SMC (see Scheme 4.20).

Thus, an accurate analysis requires a very large number and cumbersome theoretical investigations [4, 17], although it is occasionally worthwhile to consider a single intermediate or reaction step.

Next, examples of specific considerations for asymmetric induction are provided.

4.3 Asymmetric SMC Reaction

4.3.1 Examples of Early Studies

Asymmetric cross-coupling was attempted from the earliest stages of the reaction development. In 1975, asymmetric Kumada coupling [18] using a Pd/(*S*)-(*R*)-BPPFA [19] catalyst was reported to afford (*R*)-**P1**, although with an optical purity of only 4.6% [20]. In 1988, an improved catalyst, Pd/(*S*)-(*R*)-PPFOMe, afforded (*R*)-**P1** in 95% ee in the same reaction [21]. The results of reactions using the same catalyst with two opposite reaction substrates (1-Np-Br/2-Me-Np-MgBr or 2-Me-Np-Br/1-Np-MgBr) revealed extremely different enantioselectivities (80% and 16% ee, respectively). This indicates that *OA* and/or *TM* play a major role in stereoselectivity. The first example of an asymmetric SMC reaction was reported by Cammidge and Crepy, and the reaction using Pd/(*S*)-(*R*)-PFNMe afforded (*R*)-**P1** in 85% ee [22]. In the same year, a highly enantioselective SMC using a Pd catalyst with Kenphos (**L3**) was performed by Buchwald and co-workers and yielded products in up to 92% ee (see Scheme 4.6, **P3b**) [23]. In the reaction, the aryl coupling partner contained a Lewis basic directing group ($PO(OEt)_2$) at the *ortho* position unlike the aforementioned reaction of Cammidge et al. The presence of such a directing group in the aryl coupling partner was important to achieve high enantioselectivity in the SMC reaction. In 2003, Baudoin and co-workers reported a speculative model for asymmetric induction in the SMC reaction of **H2** with **B2** bearing the NH_2 group using a Pd/**L3** catalyst (Scheme 4.4) [24]. Based on the X-ray structure of the analogs, they hypothesized that the Pd/**L3**

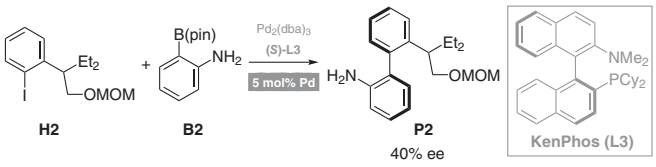

Scheme 4.4 Asymmetric SMC using Pd/**L3**.

complex had a secondary interaction between Pd and the naphthyl group of **L3** that was unique to Buchwald-type ligands and that the benzene ring introduced by the subsequent *OA* was parallel to the naphthyl (Np) group of **L3**, producing $\mathbf{OA_1}$ and $\mathbf{OA_2}$ with the R substituents in opposite directions (Scheme 4.5). It was further assumed that there was equilibrium between the intermediate complexes and that only the thermodynamically stable $\mathbf{OA_1}$ underwent *TM*. They believed that the introduced 2-aminophenyl ring in the *TM* intermediate (**TM**) was twisted in a manner that avoided steric repulsion with **L3**. This rendered $\mathbf{TM_1}^{\boldsymbol{R}}$ more stable and resulted in the formation of (*R*)-**P2**. The insight did not describe any interactions involving a directing group; however, it proposed the idea that the enantiodetermining step preceded *RE*.

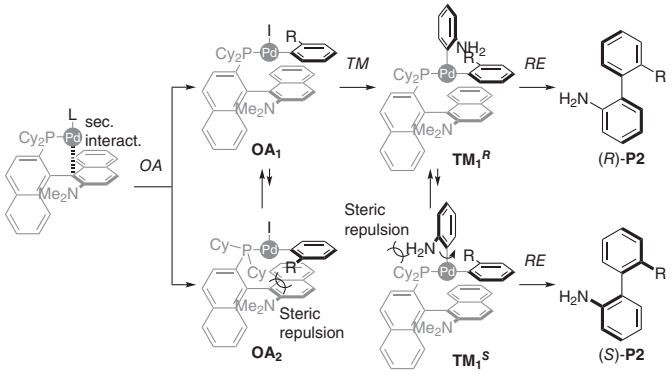

Scheme 4.5 Interconversion between intermediates in *OA* or *TM* products.

Even in recent examples, asymmetric induction is still explained by the steric effects of reaction substrates and chiral ligands. In 2019 and 2020, Qiu and co-workers reported an asymmetric SMC using a chiral-bridged biaryl monophosphine ligand, **L4** [25]. They hypothesized that the eliminating aromatic addends were sterically repulsive to **L4** and that the twist produced by the repulsion affected the enantioselectivity (Figure 4.2) [26, 27]. Similarly, during an asymmetric SMC with **L5** by Zhang and co-workers, the speculative model of TS in *RE* was proposed, in which large substituents were arranged to avoid steric repulsion between large substituents (Np and $POPh_2$ groups) in a sterically chiral environment created by **L5** (Figure 4.2) [28].

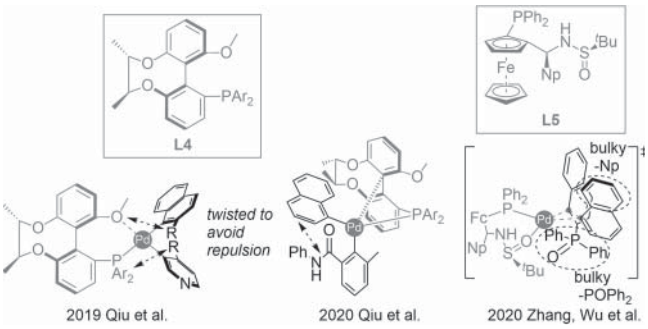

Figure 4.2 Explanation of asymmetric introduction based on steric effects.

4.3.2 Consideration of the Asymmetric SMC: Cases Dependent on a Directing Group

Although the speculative model helps interpret the experimental results, a detailed consideration using computational chemistry is required for catalyst design. A 2010 study by Buchwald and co-workers on the mechanism of asymmetric induction by DFT calculations revealed the importance of the directing group at the *ortho* position of the reacting aromatics and has functioned as a guide for subsequent studies [29]. In the reaction described in Scheme 4.6 [23], although larger R substituents in **H3** and **B3** afforded better enantioselectivity (86% ee and 92% ee for **P3a** and **P3b**, respectively), the consideration by DFT calculations showed that the interaction of the *ortho*-phosphonate group on the naphthyl ring was more important than steric repulsion. First, they focused on *TM* products as an enantiodetermining step, and calculation considerations of the reaction system of **H3a** and **B3a** at the B3LYP/6-31G(d) and LanL2DZ(Pd) levels were performed. Interconversion between *TM* products in T-shaped complexes easily occurs by oscillating and/or rotating the *o*-tolyl group *via* square-planar complexes (Scheme 4.7). The higher activation free energy of *RE* from a T-shaped complex (22.9 kcal/mol), compared with the interconversion energy of 11.5 kcal/mol for the tolyl rotational barrier, indicated that the Curtin–Hammett principle applied and that the TS of *RE* was the enantiodetermining step. After TS search, the authors observed 14 TS structures in the *RE*, and the stable complex structures were naphthylphosphonate addends in the *cis* position of the P atom of **L3**. The most stable TS structure ($\mathbf{TS}^{\mathbf{for}\textit{SP3a}}$) was the structure that formed (*S*)-**P3a**, and the oxygen atoms in the phosphonate group interacted with three C–H in **L3** of -Cy and –Np moiety (C–H···O interactions) and the tolyl addend (Scheme 4.8). Contrarily, the lowest energy TS structure ($\mathbf{TS}^{\mathbf{for}\textit{RP3a}}$) in affording (*R*)-**P3a** had two C–H···O interactions [30]. The C–H···O interactions were expected to be stronger for $\mathbf{TS}^{\mathbf{for}\textit{SP3a}}$, which had a closer linear H···O–P sequence.

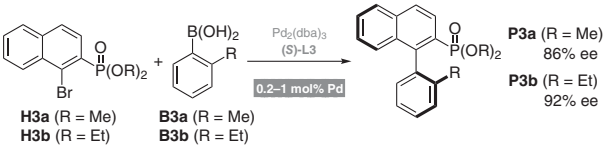

Scheme 4.6 Asymmetric SMC of the substrate having phosphonate group using Pd/**L3**.

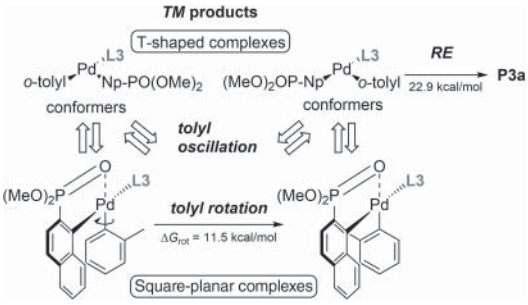

Scheme 4.7 Interconversion between *TM* products.

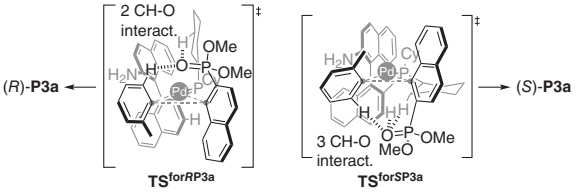

Scheme 4.8 Interactions by phosphonate group in TS of *RE*.

This resulted in $\mathbf{TS}^{\mathbf{for}\mathit{SP}\mathbf{3a}}$ being 0.9 kcal/mol more stable than $\mathbf{TS}^{\mathbf{for}\mathit{RP}\mathbf{3a}}$. The authors concluded that subtle differences in the C–H· · ·O interactions contributed to the relative energies of the TSs.

The weak interactions with the reaction substrates and chiral ligands were shown to strongly influence enantioselectivity, thereby impacting the subsequent reaction design. Tang et al. developed a superior chiral ligand, **L6**, bearing an oxaphosphole moiety and harnessed the weak interactions between the reaction substrates for asymmetric SMC (Scheme 4.9, top) [31]. They proposed that the interaction between a directing group of the aromatic addend and the aromatic

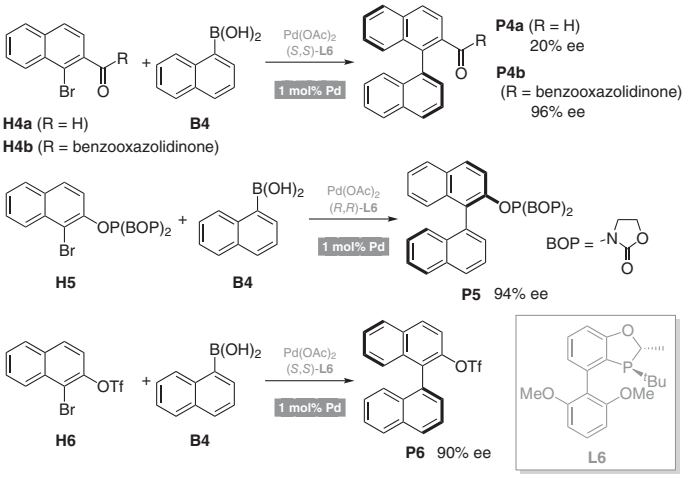

Scheme 4.9 Asymmetric SMCs of the substrate having various directing groups using Pd/**L6**.

face of the other coupling partner in a *TM* product could effectively improve enantioselectivity. The asymmetric SMC of an **H4a**-bearing aldehyde group with **B4** using Pd/(*S*,*S*)-**L6** only afforded **P4a** in 20% ee. When the aldehyde was replaced with carbonyl-benzooxazolidinone (**H4b**), the enantioselectivity significantly improved to 96% ee (**P4b**). The influence of the benzooxazolidinone moiety was analyzed by DFT calculations. Based on the aforementioned analysis of Buchwald et al., the authors considered that the *TM* structures prior to *RE* were important and searched for these optimized structures at the B3LYP/6-31(g) level with the all-electron basis set from the optimization of a face-centered cubic (fcc) Pd bulk for Pd. After optimization, 24 conformers of *TM* products were discovered. Among them, the three lowest energy conformations led to the same chirality in **P4b** that corresponded with the experimental chirality. In the most stable conformer (**TM**$^{\mathbf{forP4b}}$), a π–π interaction existed between the benzooxazolidinone moiety and Np addend (Figure 4.3, left). The authors concluded that the interaction helped to guide the orientation of the two aryl groups at the *RE* step, resulting in good enantioselectivity. Similarly, they showed that the coupling reaction of **H5** bearing a bis(2-oxo-3-oxazolidinyl)phosphinyl (BOP) group using Pd/(*R*,*R*)-**L6** afforded **P5** in 94% ee (Scheme 4.9, middle) [32]. The high enantioselectivity was assumed to be due to the polar–π interaction [33] of the BOP group and the other Np addend in the *TM* product (**TM**$^{\mathbf{forP5}}$) (Figure 4.3, middle). Such polar–π interaction was used in the working hypothesis (**TM**$^{\mathbf{forP6}}$) of the coupling reaction of **H6**, bearing a triflate group (Figure 4.3, right), where **P6** was obtained in 90% ee (Scheme 4.9, bottom) [34].

Kwong and co-workers recently developed a chiral ligand, Cyp-Kin-Phos (**L7**) [35], which was an aryl group introduced to one side of the carbazole ring of the PhenCarPhos ligand [36] in anticipation of a fluctuating secondary interaction between the Pd and carbazole ring during the SMC reaction (Pd–arene-walking coordination) (Scheme 4.10) [35]. The Pd/(*S*)-**L7** catalyst was effective for the reaction of **H7** bearing an *ortho*-1,3-dioxolane group with **B5** bearing an *ortho*-MeO group to afford (*S*)-**P7** in 94% ee. The computational study of SMC steps using the ωB97XD functional, and the Stuttgart–Dresden–Bonn basis sets for Pd with the 6-31G(d) was performed focusing on the consideration of the Pd–arene interaction. The Pd–arene-walking coordination mode in the *OA* step and the MeO group of **L7** in the *TM* step were observed to stabilize the respective TSs. The calculations showed that *RE* was the rate-determining step of the reaction, and the authors stated that these intermediates were free to interconvert with each other, hence

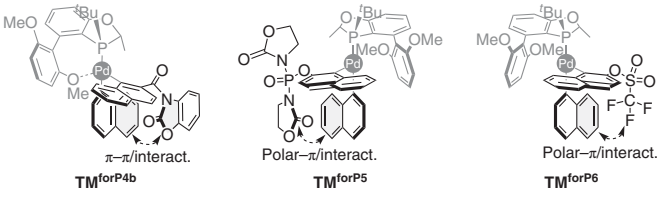

Figure 4.3 Interactions by directing groups in *TM*.

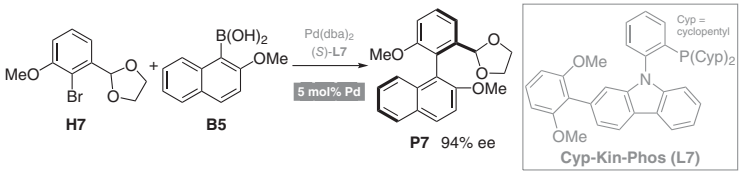

Scheme 4.10 Asymmetric SMC of the substrate having 1,3-dioxolane group using Pd/**L7**.

allowing all the possible TSs accessible before RE. Thus, eight TSs were calculated during the *RE*, and the percentage distribution by Boltzmann distribution was estimated to yield 100% (*S*)-**P7**. The effect of the directing groups in the TS structure was not described in the original paper. However, a detailed check of the structure of the most stable TS, $\mathbf{TS}^{\mathbf{for}SP7}$, revealed that the oxygen of 1,3-dioxolane and the two hydrogen atoms in **L7** were located within the van der Waals radius (rvdW) (Scheme 4.11). Similarly, hydrogen of 1,3-dioxolane and oxygen of MeO in the Np addend were close within the rvdW. Furthermore, CH–π interaction [37] was observed between the proton of the 1,3-dioxolane group and 2,6-dimethoxyphenyl in **L7**. It is speculated that these weak interactions contribute to the stabilization of the TS.

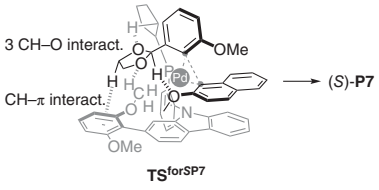

Scheme 4.11 Interactions by 1,3-dioxolane or MeO group in TS of *RE*.

The directing group can achieve conformational control by interaction between reactive aromatic substrates or ligands and by interaction with Pd. Qiu and co-workers conducted DFT investigations of the enantioselectivity of the Pd/**L8**-catalyzed SMC reaction of **H3a** bearing a phosphonate group with **B6** bearing a formyl group (Scheme 4.12) [38]. The authors discovered 64 TS structures after optimization calculations of *RE* at the B3LYP/6-31G(d), LanL2DZ level. The prediction of the ee of (*R*)-**P8** by the distribution analysis of $\Delta G^{\neq}$ calculated from the TSs was 88% ee, which corresponded to the selectivity achieved by the experiment of (*R*)-**P8** in 95% ee. The most stable $\mathbf{TS}^{\mathbf{for}RP8}$, giving (*R*)-**P8**, in which the hydrogen

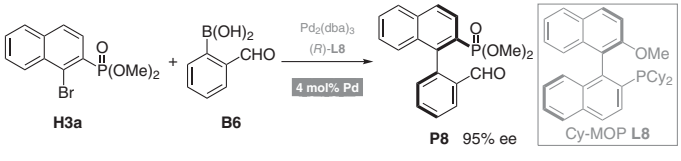

Scheme 4.12 Asymmetric SMC of the substrates having phosphonate or formyl group using Pd/**L8**.

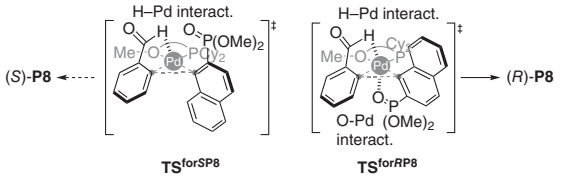

Scheme 4.13 Interactions of Pd with directing groups in TS of *RE*.

atom in the formyl phenyl addend and the oxygen atom of the phosphoryl group in the naphthyl addend interacted with Pd from the opposite directions (Scheme 4.13), resulting in a distorted octahedral structure. Contrarily, in the most stable TS, $\mathbf{TS}^{\mathbf{for}\textit{SP8}}$, giving (*S*)-**P8**, a similar interaction was observed only between Pd and the hydrogen atom in the formyl group, which was 2 kcal/mol more unstable than the case of (*R*)-**P8**. Thus, the authors concluded that the origin of the high enantioselectivity of (*R*)-**P8** was the distorted octahedral configuration derived from the directing group in both aryl addends of the TS of *RE*.

In the examples so far, high enantioselectivity was controlled by the interaction of a directing group in a reactive substrate with an aryl adduct, Pd, and a chiral ligand. As an advanced approach, chiral ligands have been developed to introduce the directing groups to the ligand and actively apply the directing groups to enantioselectivity control. In 2020, Tang et al. redesigned previous ligands (see **L6**) and developed a chiral ligand bearing a hydroxy-directing group (BaryPhos, **L9**) [39]. The asymmetric SMC of **H8** with **B7** using Pd/(*S*,*S*)-**L9** afforded (*S*)-**P9** in 93% ee (Scheme 4.14). The authors considered a stereoselectivity model based on the X-ray structure of an *OA* product using (*R*,*R*)-**L9**. Based on the X-ray structure, the proton of the cyclopentyl (Cyp) group in (*R*,*R*)-**L9** interacted with the formyl group in the aromatic addend, and the interaction was assumed to be present in the subsequent *TM* product ($\mathbf{TM}^{\mathbf{for}\textit{RP9}}$) as well (Scheme 4.15). In $\mathbf{TM}^{\mathbf{for}\textit{RP9}}$, it was assumed that further interaction occurred between the hydroxy group in (*R*,*R*)-**L9** and the formyl group in the other aryl addend. The authors presumed that these interactions contributed to the TS to afford (*R*)-**P9**. The **L9** ligand could provide excellent enantioselectivities for asymmetric SMCs involving noncovalent interactions between **L9** and two coupling partners; it was used in the synthesis of antitumor agent (−)-gossypol [40].

In 2022, Phipps and co-workers utilized the strong electrostatic interaction provided by the sulfonate metal salt in the chiral ligand [41]. Enantiomerically pure sSPhos (**L10**) [42] was synthesized and used for the asymmetric SMC of **H9**

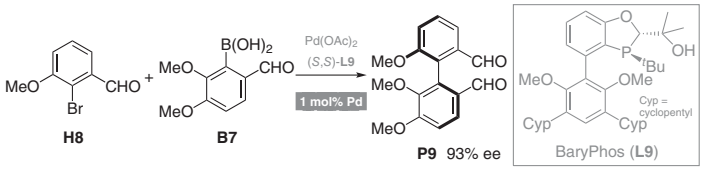

Scheme 4.14 Asymmetric SMC using Pd/**L9** bearing a directing group.

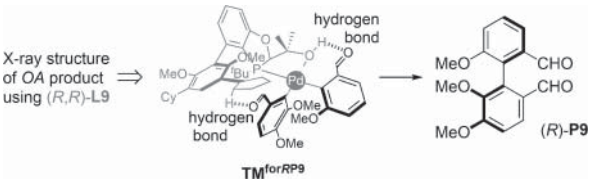

Scheme 4.15 Interactions between the directing groups of both the ligand and the substrate.

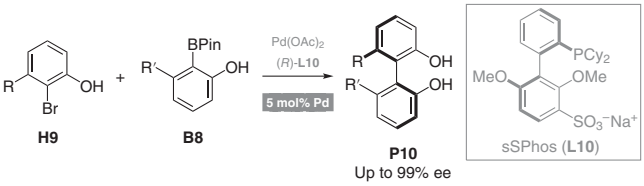

Scheme 4.16 Asymmetric SMC using Pd/**L10** bearing a directing group.

and **B8** to afford chiral biphenol **P10** with up to 99% ee (Scheme 4.16). When the sulfonate group in **L10** was alkylated to convert the $SO_3{}^{i}Bu$ group, the enantioselectivity of **P10** significantly reduced to 8% ee, experimentally indicating that the sulfonate anion played a major role in the asymmetric induction. Based on these results, in the *TM* or *RE* step, the authors considered a speculative model in which the hydrogen bond of the sulfonate anion with the hydroxy group of the aryl addend and an additional hydrogen bond involving the hydroxy group in the other aryl adduct (Scheme 4.17). The authors speculated that the high enantioselectivity was achieved by the cooperation of the two hydrogen bonds.

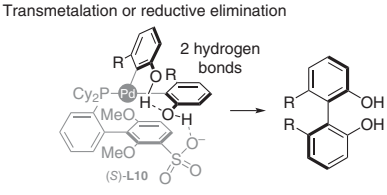

Scheme 4.17 Hydrogen bonds between the directing groups of both the ligand and the substrate.

4.3.3 Consideration of the Asymmetric SMC: Cases Independent of a Directing Group

In the examples discussed thus far, the high enantioselectivity was due to the harnessing of the interaction between directing groups at the *ortho* position in the reaction substrate. However, as mentioned earlier, a highly enantioselective Kumada coupling forming 2,2′-dimethyl-1,1′-binaphthalene (**P1**) in 95% ee without directing groups has been reported [21]. Furthermore, a few examples of highly enantioselective SMCs without directing groups have been reported, and this section discusses the enantioselective introduction of this type of coupling.

In 2008, Lassaletta and co-workers reported an asymmetric SMC using the (*S*,*S*)-**L11** ligand (Scheme 4.18) [43]. The reactions afforded the binaphthyl products, **P11**, with high enantioselectivity with a substrate bearing a directing group (**H10** to **P11a**, R = OMe, 90% ee) and a substrate without a directing group (**H1** to **P11b**, R = Me, 95% ee). The authors considered four types of *TM* products (**TM**), in which two reactive Np addends were differently oriented, to explain the high selectivity (Figure 4.4). Here, Np substituents, X and Y, oriented in the same direction were defined as ***syn***, and those oriented in the opposite direction were defined as ***anti***. The conformation in which the X group of Np faces the front of the paper is $\mathbf{TM_1}$ and vice versa is $\mathbf{TM_2}$. Depending on the orientation of the Np group, π–π stacking interaction [44] between the Np addend and Ph group of (*S*,*S*)-**L11** is possible. The interaction functioned in two places at $\mathbf{TM_2}$-***anti***; therefore, the intermediate was considered to be the most stable. The authors stated that upon subsequent *RE*, the steric effect of the prominent Ph group of (*S*,*S*)-**L11** caused the Np group to twist counterclockwise, thereby forming a highly sterically controlled compound.

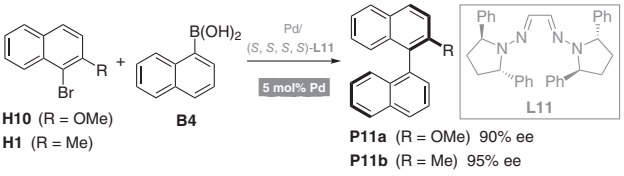

Scheme 4.18 Asymmetric SMC of the substrate having no directing group using Pd/**L11**.

Although the plausible speculations were not theoretically tested, the idea of controlling the aromatic ring surfaces by their interactions explained the experimental results well. On the other hand, control of the asymmetric induction by the steric repulsion of the chiral ligand and the reacting substrate was recently proposed without theoretical calculation. In 2019, Shi et al. reported the asymmetric SMC using a chiral NHC ligand, **L12** (Scheme 4.19) [45]. During the asymmetric SMC reactions using **L12**, highly enantioselective reactions occurred using reaction substrates with various *ortho*-directing groups, e.g. R = OMe (**H10**). However, (*R*)-**P11b** was obtained in 94% ee even when R = Me (**H1**), without an *ortho*-directing group. Most reactions were performed using 1 mol% of the catalyst; however, the gram-scale coupling of 2-Me-Ph and naphthyl derivative

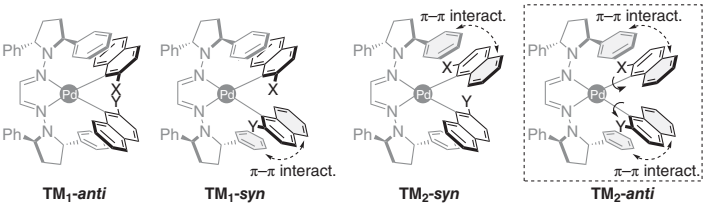

Figure 4.4 Control of the orientation of the Np group by π–π stacking interaction in *TM*.

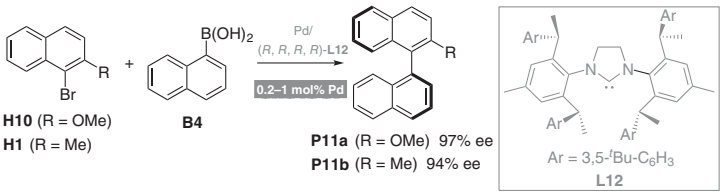

Scheme 4.19 Asymmetric SMC of the substrate having no directing group using Pd/**L12**.

groups was performed with an extremely low catalyst loading (0.2 mol%). Owing to the X-ray structure and topographic steric map analysis of Pd/ligand [46], the bulky 3,5-di-tert-butyl phenyl groups (bulky Ar) on **L12** were believed to play a significant role in the high enantioinduction ability. The authors postulated four *TM* intermediates (**TM**) (Figure 4.5). Here, the R substituent of the Np group described at the front was defined as $\mathbf{TM_1}$ and vice versa as $\mathbf{TM_2}$. In addition, the model with two fused benzene rings of the Np group pointing in the same direction was defined as ***syn***, and the model with the R group and the fused benzene ring in the same direction was defined as ***anti***. In the catalytic system, the repulsion between the R substituent and bulky Ar group of **L12** (R–Ar repulsion) was believed to have a significant destabilizing effect; therefore, $\mathbf{TM_1}$ was more stable than $\mathbf{TM_2}$. Simultaneously, when the fused benzene ring of the naphthyl group on the right side of the figure faces the front, it repels the bulky Ar of **L12** (Np–Ar repulsion). Thus, the authors speculated that the intermediate $\mathbf{TM_1}$-***syn*** would be the most stable.

Although such speculative models not based on theoretical calculations were only valid for the explanation of experimental results in the reaction of reactive substrates without directing groups, the consideration by TS calculations indicated the importance of weak interactions at sites other than directing groups. In 2018, Patel et al. performed a theoretical deep consideration of the asymmetric induction of the SMC of aryls without directing groups [15]. They attempted to modify the P-chiral dihydrobenzooxaphosphole ligand, **L6**, developed by Tang and found that the (*S*,*S*)-NitinPhos (**L1**) ligand was effective in synthesizing (*S*)-2,2′-dimethyl-1,1′-binaphthalene (**P1**) in 89% ee (Scheme 4.3) (In Ref. [15], some depictions of **P1** enantiosense were incorrectly described. In this chapter, the

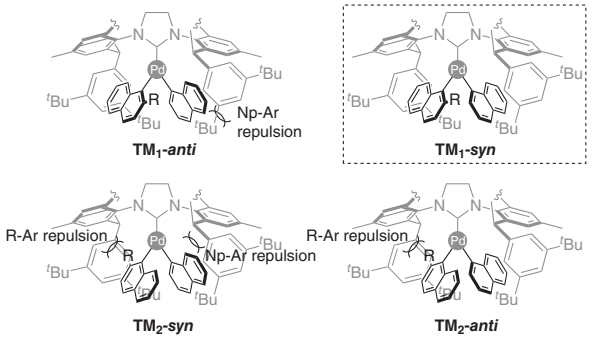

Figure 4.5 Steric control by bulky group of chiral ligand.

enantiosense of **P1** was depicted based on the Supporting Information of Ref. [15] and the calculation results.). As mentioned earlier, asymmetric SMC and Negishi coupling reactions using the same ligand afforded the same product (**P1**) with different enantioselectivities (Scheme 4.3). During the Negishi coupling, it was concluded that only the TS of *RE* affected the asymmetric induction because the reaction process was an equilibrium reaction. In contrast, the authors described that the reaction mechanism during the SMC was irreversible and that interconversion between intermediates was inhibited. Thus, the reaction pathways were identified by energies based on TS calculations at the B3LYP-D3/6-31G(d), LANL2DZ (Pd, Br) level for each reaction step (Scheme 4.20). During the *OA* step, six TSs were considered, leading to two *OA* products ($\mathbf{OA_1}$ and $\mathbf{OA_2}$) with the Np rings oriented in opposite directions to each other. At this time, the reaction pathway branched into two channels because of irreversible *OA*. It then distributed a bifurcation with distributions of 85% and 15% for $\mathbf{OA_1}$ and $\mathbf{OA_2}$, respectively, based on the Boltzmann distribution of the relative enthalpies of the corresponding TSs. Similarly, during the *TM* step, the Boltzmann distribution based on 20 TSs was calculated, revealing the presence of four *TM* products, $\mathbf{TM_1}$-***syn*** (10%) and $\mathbf{TM_1}$-***anti*** (90%) from $\mathbf{OA_1}$ and $\mathbf{TM_2}$-***syn*** (58%) and $\mathbf{TM_2}$-***anti*** (42%) from $\mathbf{OA_2}$. Here, ***syn*** indicates that the two fused benzene rings of the naphthyl group were oriented in the same direction, and ***anti*** indicates that they were oriented in opposite directions. Similar calculations were made for the *RE*. After calculating 32 TSs, the distribution is shown in Scheme 4.20. The only pathway in the eight *RE* pathways that preferentially afforded (*S*)-**P1** was the pathway from $\mathbf{TM_1}$-***anti***, whereas the other pathways preferentially yielded (*R*)-**P1**. However, since this reaction system was irreversible, it was deemed inappropriate to only consider the *RE* step. The selectivity calculated from the distribution of all the branches was 78% ee, considerably lower than the best experimental value of 94% ee. Therefore, the authors assumed that the overall enantioselectivity of the reaction was controlled only by the selectivity of the major branch (thick arrow). In that case, the selectivity was calculated to be 90% ee, close to the experimental value. In this case, the most dominant step was considered to be *TM*, and the authors compared the TS structures of *TM* ($\mathbf{TS^{forTM1}}$) (Figure 4.6). The most stable TS ($\mathbf{TS^{forTM1}}$***anti***) in five TS structures, leading to $\mathbf{TM_1}$-***anti***, and

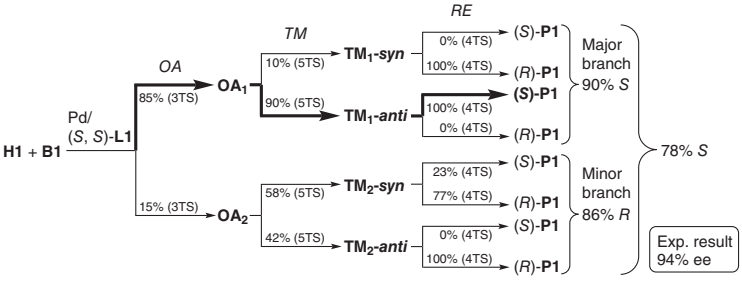

Scheme 4.20 Channel branching in the asymmetric SMC mechanism of the reaction of **H1** with **B1** using Pd/**L1**.

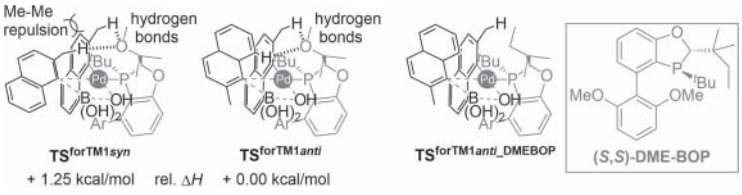

Figure 4.6 Destabilization by steric repulsion and stabilization by weak hydrogen bonds in TS of *TM*.

the most stable TS ($\mathbf{TS}^{\mathbf{forTM1}\textit{syn}}$) in five TS structures, leading to $\mathbf{TM_1}$-***syn***, were compared. The destabilization by 1.25 kcal/mol of $\mathbf{TS}^{\mathbf{forTM1}\textit{syn}}$ appeared to be due to the proximity and repulsion of the two methyl groups (Me–Me repulsion). Early asymmetric SMC studies to obtain **P1** have suggested that such repulsion between the Me groups in Np addends (Me–Me repulsion) significantly impacts chiral induction [21]. $\mathbf{TS}^{\mathbf{forTM1}\textit{anti}}$ and $\mathbf{TS}^{\mathbf{forTM1}\textit{syn}}$ had C–H···O hydrogen bonds between the two reactive Np addends and the oxygen atoms of the methoxy groups of **L1**. The authors stated that these stabilizing interactions contributed to fewer accessible low-energy *TM* TS conformations. Contrarily, it was concluded that using (DME)-BOP ligand, which with an Et group instead of a MeO group, that does not exhibit this interaction in TS ($\mathbf{TS}^{\mathbf{forTM1}\textit{anti}\_\mathbf{DMEBOP}}$) may result in multiple pathways that are accessible at various energy levels, leading to reduced selectivity.

In the aforementioned example, the directing group in the chiral ligand was shown to weakly interact with the reacting substrate without directing groups. However, when using a chiral ligand that is less prone to such interactions, steric repulsion between the chiral ligand and substrate is the most important factor. In 2021, Byrne et al. reported the asymmetric SMC of tetra-*ortho*-substituted biaryls without directing groups using a Buchwald-type biaryl ligand, (*R*,*R*)-**L13**, a SagePhos [47] analog (Scheme 4.21) [48]. Although the enantioselectivity using *o*-tolyl-$B(OH)_2$ (**B3a**) was moderate (54% ee), high enantioselectivity (90% ee) was achieved using 1-Np-$B(OH)_2$ (**B4**). The authors performed DFT calculations at the B3LYP-D3/LACVP* level to elucidate the source of the enantioselectivity. They evaluated the *OA* products (**OA**), *TM* products (**TM**), and TSs of *RE* (**TS-RE**). The 2-Me-Np group of **H1** in **OA** was coordinated in a *cis* position to the phosphine, and the two conformers were observed. $\mathbf{OA_{prox}}$ means that the fused benzene ring of the 2-Me-Np group is "proximal" to the protruding phospholane substituent of the (*R*,*R*)-**L13** ligand, and $\mathbf{OA_{dist}}$ means that the fused benzene ring is "distal" to

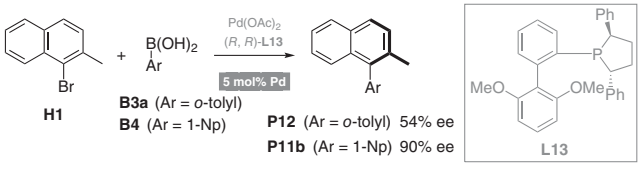

Scheme 4.21 Asymmetric SMC of the substrate having no directing group using Pd/**L13**.

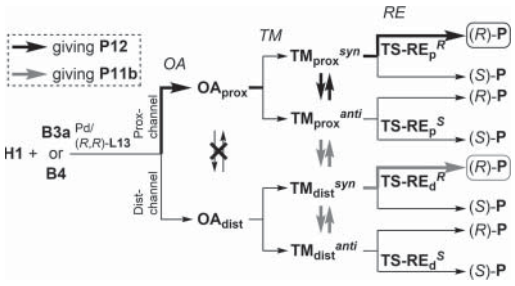

Scheme 4.22 Channel branching in the asymmetric SMC mechanism of the reaction of **H1** with **B3a** or **B4** using Pd/**L13**.

that. Considering that the *OA* was assumed to be irreversible, the reaction pathway was divided into two reaction channels, prox- and dist-channels leading to $\mathbf{OA_{prox}}$ and $\mathbf{OA_{dist}}$, respectively (Scheme 4.22). Furthermore, it was concluded that $\mathbf{OA_{prox}}$ and $\mathbf{OA_{dist}}$ could not be interconverted in dihedral scan calculations. Contrarily, the next **TM** stage allowed interconversion within the same channel; since this interconversion energy was lower than the activation energy of the subsequent *RE*, the Curtin–Hammett rule applied at the *RE* stage. Furthermore, the authors did not assume a crossover between the prox-channel ($\mathbf{TM_{prox}}$) and dist-channel ($\mathbf{TM_{dist}}$) in the case using **B3a**, and the prox-channel was preferred. Thus, the four TSs of *RE* in the prox-channel were compared, and the relatively faster pathway was $\mathbf{TS\text{-}RE_p}^{\boldsymbol{R}}$ (black thick arrow) derived from $\mathbf{TM_{prox}}^{\boldsymbol{syn}}$, where *syn* implies that the Me groups of the 2-Me-Np and *o*-tolyl were oriented in the same direction. The pathway yielded (*R*)-**P12**, whose activation energy was 6.9 kJ/mol lower than the pathway *via* $\mathbf{TS\text{-}RE_p}^{\boldsymbol{S}}$, which had the lowest energy that afforded (*S*)-**P12** in the prox-channel. The Me group of the *o*-tolyl group in $\mathbf{TS\text{-}RE_p}^{\boldsymbol{S}}$ was oriented in the opposite direction to that of $\mathbf{TS\text{-}RE_p}^{\boldsymbol{R}}$, and the Me group appeared to repel the fused benzene ring of the 2-Me-Np group (Me–Np repulsion), resulting in destabilization (Figure 4.7). In the reaction using **B4**, the enantioselectivity was suggested to have been dominated by $\mathbf{TS\text{-}RE_d}^{\boldsymbol{R}}$, which was the lowest energy in both channels and was in the dist-channel, dissimilar to the case of **B3a** (Scheme 4.22). The results of the experimental validation suggested that crossover occurs between both channels in the case using **B4**, although selective *OA* is a possibility. Therefore, it was assumed that all the **TS-RE** were accessible and proceeded *via* the pathway with the lowest energy of $\mathbf{TS\text{-}RE_d}^{\boldsymbol{R}}$ (gray thick arrow) in **TS-RE**, where *syn* implies that the Me group of the 2-Me-Np was closed to the fused benzene ring of the Np group inserted by *TM* from **B4**. The activation energy of the $\mathbf{TS\text{-}RE_d}^{\boldsymbol{R}}$ pathway that yielded (*R*)-**P11b** was 11.0 kJ/mol lower than the $\mathbf{TS\text{-}RE_d}^{\boldsymbol{S}}$ pathway. Thus, the larger energy difference relative to the case of **B3a** (6.9 kJ/mol) corresponded with the experimental selectivities, 90% ee for **P11b** vs 54% ee for **P12** (Scheme 4.21). The large destabilization of $\mathbf{TS\text{-}RE_d}^{\boldsymbol{S}}$ was presumably due to steric repulsion between the 2-Me-Np and Np fused benzene rings (Np–Np repulsion) (Figure 4.7).

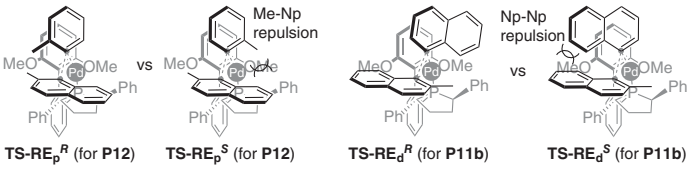

Figure 4.7 Steric repulsion of reactive substrates in TS of *RE*.

4.4 Conclusion

The development of appropriate chiral ligands has enabled highly enantioselective SMC reactions. In many cases, the directing groups of the reaction substrate significantly contribute to asymmetric induction. Computational analyses reveal that even for reactive substrates without oriented groups, weak interactions, such as aromatic ring or C–H interactions, play a role in asymmetric induction. Although many successful examples are presented herein, most of the catalysts were substrate-specific, and further catalyst development will be required for the synthesis of versatile chiral biaryls. Furthermore, a catalyst amount of more than 1 mol% is required in most cases, rendering its industrial use difficult. This is because the activation energy required for *RE* is considerably higher during tetra-*ortho*-biaryl synthesis; therefore, the catalytic activity was considerably lower. For use in process synthesis, it is essential to develop catalysts that enable the synthesis of tetra-*ortho*-biaryls with a low catalyst amount, in addition to the development of advanced asymmetric induction control methods. Therefore, to develop practical asymmetric catalysts, it is necessary to have both high steric control and high catalytic activity. The most promising ligand among the nonchiral SMCs would be Buchwald's ligands, which are biaryl monophosphine [49]. This type of ligand undergoes stabilization by the secondary interaction of palladium with the aromatic ring of the ligand, which facilitates *RE* [50]. By exploiting this secondary interaction, Korenaga recently developed an SMC catalyst for the synthesis of tetra-*ortho*-substituted biaryls that allows the reaction to proceed even with 0.025 mol% of catalyst [51]. It is expected that high-performance asymmetric catalysis for SMC will be produced by combining a chiral unit with such a highly active achiral catalyst in the future.

References

1 (a) Miyaura, N. and Suzuki, A. (1995). Palladium-catalyzed cross-coupling reactions of organoboron compounds. *Chem. Rev.* 95 (7): 2457–2483. (b) Kotha, S., Lahiri, K., and Kashinath, D. (2002). Recent applications of the Suzuki–Miyaura cross-coupling reaction in organic synthesis. *Tetrahedron* 58 (48): 9633–9695. (c) Phan, N.T.S., Sluys, M.V.D., and Jones, C.W. (2006).

On the nature of the active species in palladium catalyzed Mizoroki–Heck and Suzuki–Miyaura couplings – homogeneous or heterogeneous catalysis, a critical review. *Adv. Synth. Catal.* 348 (6): 609–679. (d) Martin, R. and Buchwald, S.L. (2008). Palladium-catalyzed Suzuki–Miyaura cross-coupling reactions employing dialkylbiaryl phosphine ligands. *Acc. Chem. Res.* 41 (11): 1461–1473. (e) Han, F.-S. (2013). Transition-metal-catalyzed Suzuki–Miyaura cross-coupling reactions: a remarkable advance from palladium to nickel catalysts. *Chem. Soc. Rev.* 42 (12): 5270–5298. (f) Maluenda, I. and Navarro, O. (2015). Recent developments in the Suzuki–Miyaura reaction: 2010–2014. *Molecules* 20 (5): 7528–7557. (g) Beletskay, I.P., Alonso, F., and Tyurin, V. (2019). The Suzuki–Miyaura reaction after the Nobel prize. *Coord. Chem. Rev.* 385: 137–173.

2 (a) Miyaura, N., Yamada, K., and Suzuki, A. (1979). A new stereospecific cross-coupling by the palladium-catalyzed reaction of 1-alkenylboranes with 1-alkenyl or 1-alkynyl halides. *Tetrahedron Lett.* 20 (36): 3437–3440. (b) Miyaura, N. and Suzuki, A. (1979). Stereoselective synthesis of arylated (E)-alkenes by the reaction of alk-1-enylboranes with aryl halides in the presence of palladium catalyst. *J. Chem. Soc. Chem. Commun.* 19: 866–867.

3 Recent reviews for SMC: (a) Farhang, M., Akbarzadeh, A.R., Rabbani, M., and Ghadiri, A.M. (2022). A retrospective-prospective review of Suzuki–Miyaura reaction: from cross-coupling reaction to pharmaceutical industry applications. *Polyhedron* 227: 116124. (b) Tsuchiya, N., Sheppard, T.D., and Nishikata, T. (2022). Tertiary alkylative Suzuki–Miyaura couplings. *Synthesis* 54 (10): 2340–2349. (c) Tovar, J.D., Rataboul, F., and Djakovitch, L. (2021). Heterogenization of Pd(II) complexes as catalysts for the Suzuki–Miyaura reaction. *Appl. Catal. A Gen.* 627: 118381. (d) Kadu, B.S. (2021). Suzuki–Miyaura cross coupling reaction: recent advancements in catalysis and organic synthesis. *Cat. Sci. Technol.* 11 (4): 1186–1221. (e) Bhattacherjee, D., Rahman, M., Ghosh, S. et al. (2021). Advances in transition-metal catalyzed carbonylative Suzuki-Miyaura coupling reaction: an update. *Adv. Synth. Catal.* 363 (6): 1597–1624.

4 There were about 6500 reports in the 10 years from 2011–2020: D'Alterio, M.C., Casals-Cruañas, È., Tzouras, N.V. et al. (2021). Mechanistic aspects of the palladium-catalyzed Suzuki-Miyaura cross-coupling reaction. *Chem. Eur. J.* 27 (54): 13481–13493.

5 Suzuki, A. (2011). Cross-Coupling reactions of organoboranes: an easy way to construct C–C bonds (Nobel Lecture). *Angew. Chem. Int. Ed.* 50 (30): 6722–6737.

6 (a) Yang, Y.-D., Yang, B.-B., and Li, L. (2022). A nonneglectable stereochemical factor in drug development: atropisomerism. *Chirality* 34 (10): 1355–1370. (b) Glunz, P.W. (2018). Recent encounters with atropisomerism in drug discovery. *Bioorg. Med. Chem. Lett.* 28 (2): 53–60. (c) Toenjes, S.T. and Gustafson, J.L. (2018). Atropisomerism in medicinal chemistry: challenges and opportunities. *Future Med. Chem.* 10 (4): 409–422. (d) LaPlante, S.R., Fader, L.D., Fandrick, K.R. et al. (2011). Assessing atropisomer axial chirality in drug discovery and development. *J. Med. Chem.* 54 (20): 7005–7022. (e) LaPlante, S.R., Edwards, P.J., Fader, L.D. et al. (2011). Revealing atropisomer axial chirality in drug discovery. *ChemMedChem* 6 (3): 505–513.

7 (a) Wang, Z., Meng, L., Liu, X. et al. (2022). Recent progress toward developing axial chirality bioactive compounds. *Eur. J. Med. Chem.* 243 (5): 114700. (b) Dos Santos, A.R., Pinheiro, A.C., Sodero, A.C.R. et al. (2007). Atropisomerism: the effect of the axial chirality in bioactive compounds. *Quim. Nova* 30 (1): 125–135.

8 Wan, S.-P., Lu, H.-Y., Li, M., and Chen, C.F. (2022). Advances in circularly polarized luminescent materials based on axially chiral compounds. *J Photochem Photobiol C: Photochem Rev* 50: 100500.

9 (a) McCarthy, M. and Guiry, P.J. (2001). Axially chiral bidentate ligands in asymmetric catalysis. *Tetrahedron* 57 (18): 3809–3844. (b) Shimizu, H., Nagasaki, I., and Saito, T. (2005). Recent advances in biaryl-type bisphosphine ligands. *Tetrahedron* 61 (23): 5405–5432.

10 Oki, M. (1983). Recent advances in atropisomerism. *Top. Stereochem.* 14: 1–81.

11 Reviews for asymmetric SMC: (a) Hedouin, G., Hazra, S., Gallou, F., and Handa, S. (2022). The catalytic formation of atropisomers and stereocenters *via* asymmetric Suzuki–Miyaura couplings. *ACS Catal.* 12 (9): 4918–4937. (b) Cheng, J.K., Xiang, S.-H., Li, S. et al. (2021). Recent advances in catalytic asymmetric construction of atropisomers. *Chem. Rev.* 121 (8): 4805–4902. (c) Loxq, P., Manoury, E., Poli, R. et al. (2016). Synthesis of axially chiral biaryl compounds by asymmetric catalytic reactions with transition metals. *Coord. Chem. Rev.* 308: 131–190. (d) Zhang, D. and Wang, Q. (2015). Palladium catalyzed asymmetric Suzuki–Miyaura coupling reactions to axially chiral biaryl compounds: chiral ligands and recent advances. *Coord. Chem. Rev.* 286: 1–16. (e) Cherney, A.H., Kadunce, N.T., and Reisman, S.E. (2015). Enantioselective and enantiospecific transition-metal-catalyzed cross-coupling reactions of organometallic reagents to construct C–C bonds. *Chem. Rev.* 115 (17): 9587–9652. (f) Baudoin, O. (2005). The asymmetric Suzuki coupling route to axially chiral biaryls. *Eur. J. Org. Chem.* 4223–4229.

12 Goetzke, F.W., Dijk, L.V., and Fletcher, S.P. (2019). Catalytic asymmetric Suzuki–Miyaura couplings. In: *PATAI'S Chemistry of Functional Groups*, 1–54. Wiley.

13 (a) Chakraborty, S. and Saha, C. (2016). *Resonance* 21: 151–171. (b) Seeman, J.I. (1983). Effect of conformational change on reactivity in organic chemistry. Evaluations, applications, and extensions of Curtin–Hammett Winstein–Holness kinetics. *Chem. Rev.* 83 (2): 83–134.

14 Jasiński, R., Demchuk, O.M., and Babyuk, D. (2017). A quantum-chemical DFT approach to elucidation of the chirality transfer mechanism of the enantioselective Suzuki–Miyaura cross-coupling reaction. *J. Chem.* 2017: 3617527.

15 Patel, N.D., Sieber, J.D., Tcyrulnikov, S. et al. (2018). Computationally assisted mechanistic investigation and development of Pd-catalyzed asymmetric Suzuki–Miyaura and Negishi cross-coupling reactions for tetra-*ortho*-substituted biaryl synthesis. *ACS Catal.* 8 (11): 10190–10209.

16 Haas, D., Hammann, J.M., Greiner, R., and Knochel, P. (2016). Recent developments in Negishi cross-coupling reactions. *ACS Catal.* 6 (3): 1540–1552.

17 (a) Braga, A.A.C., Ujaque, G., and Maseras, F. (2006). A DFT study of the full catalytic cycle of the Suzuki–Miyaura cross-coupling on a model system. *Organometallics* 25 (15): 3647–3658. (b) Jover, J., Fey, N., Purdie, M. et al. (2010). A computational study of phosphine ligand effects in Suzuki–Miyaura coupling. *J. Mol. Catal. A Chem.* 324 (1–2): 39–47. (c) Huang, Y.-L., Weng, C.-M., and Hong, F.-E. (2008). Density functional studies on palladium-catalyzed Suzuki–Miyaura cross-coupling reactions assisted by N- or P-chelating ligands. *Chem. Eur. J.* 14: 4426–4434. (d) Sperger, T., Sanhueza, I.A., Kalvet, I., and Schoenebeck, F. (2015). Computational studies of synthetically relevant homogeneous organometallic catalysis involving Ni, Pd, Ir, and Rh: an overview of commonly employed DFT methods and mechanistic insights. *Chem. Rev.* 115 (17): 9532–9586. and references therein.

18 Tamao, K., Sumitani, K., and Kumada, M. (1972). Selective carbon-carbon bond formation by cross-coupling of Grignard reagents with organic halides. Catalysis by nickel-phosphine complexes. *J. Am. Chem. Soc.* 94 (12): 4374–4376.

19 Hayashi, T., Yamamoto, K., and Kumada, M. (1974). Asymmetric catalytic hydrosilylation of ketones preparation of chiral ferrocenylphosphines as chiral ligands. *Tetrahedron Lett.* 15 (49–50): 4405–4408.

20 Tamao, K., Minato, A., Miyake, N. et al. (1975). Nickel-phosphine complex catalyzed Grignard synthesis of sterically hindered, unsymmetrical biaryls: an approach to the asymmetric synthesis of biaryl atropisomers. *Chem. Lett.* 4 (2): 133–136.

21 Hayashi, T., Hayashizaki, K., Kiyoi, T., and Ito, Y. (1988). Asymmetric synthesis catalyzed by chiral ferrocenylphosphine-transition-metal complexes. 6. Practical asymmetric synthesis of 1,1′-binaphthyls *via* asymmetric cross-coupling with a chiral [(alkoxyalkyl)ferrocenyl]monophosphine/nickel catalyst. *J. Am. Chem. Soc.* 110 (24): 8153–8156.

22 Cammidge, A.N. and Crepy, K.V.L. (2000). The first asymmetric Suzuki cross-coupling reaction. *Chem. Commun.* 18: 1723–1724.

23 Yin, J. and Buchwald, S.L. (2000). A catalytic asymmetric Suzuki coupling for the synthesis of axially chiral biaryl compounds. *J. Am. Chem. Soc.* 122 (48): 12051–12052.

24 Herrbach, A., Marinetti, A., Baudoin, O. et al. (2003). Asymmetric synthesis of an axially chiral antimitotic biaryl *via* an atropo-enantioselective Suzuki cross-coupling. *J. Org. Chem.* 68 (12): 4897–4905.

25 Wang, S., Li, J., Miao, T. et al. (2012). Highly efficient synthesis of a class of novel chiral-bridged atropisomeric monophosphine ligands *via* simple desymmetrization and their applications in asymmetric Suzuki–Miyaura coupling reaction. *Org. Lett.* 14 (8): 1966–1969.

26 Xia, W., Zhang, Z., Li, Y. et al. (2019). Enantioselective synthesis of chiral heterocyclic biaryls *via* asymmetric Suzuki–Miyaura cross-coupling of 3-bromopyridine derivatives. *Org. Biomol. Chem.* 17: 2351–2355.

27 Li, Y., Pan, B., He, X. et al. (2020). Pd-catalyzed asymmetric Suzuki–Miyaura coupling reactions for the synthesis of chiral biaryl compounds with a large steric substituent at the 2-position. *Beilstein J. Org. Chem.* 16: 966–973.

28 Ji, W., Wu, H.-H., and Zhang, J. (2020). Axially chiral biaryl monophosphine oxides enabled by palladium/WJ-Phos-catalyzed asymmetric Suzuki–Miyaura cross-coupling. *ACS Catal.* 10 (2): 1548–1554.

29 Shen, X., Jones, G.O., Watson, D.A. et al. (2010). Enantioselective synthesis of axially chiral biaryls by the Pd-catalyzed Suzuki–Miyaura reaction: substrate scope and quantum mechanical investigations. *J. Am. Chem. Soc.* 132 (32): 11278–11287.

30 Sosa, G.L., Peruchena, N., Contreras, R.H., and Castro, E.A. (1997). Topological analysis of hydrogen bonding interactions involving CH···O bonds. *J. Mol. Struct. THEOCHEM* 401 (1–2): 77–85.

31 Tang, W., Patel, N.D., Xu, G. et al. (2012). Efficient chiral monophosphorus ligands for asymmetric Suzuki–Miyaura coupling reactions. *Org. Lett.* 14 (9): 2258–2261.

32 Xu, G., Fu, W., Liu, G. et al. (2014). Efficient syntheses of Korupensamines A, B and Michellamine B by asymmetric Suzuki-Miyaura coupling reactions. *J. Am. Chem. Soc.* 136 (2): 570–573.

33 Cozzi, F., Cinquini, F., Annuziata, R., and Siegel, J.S. (1993). Dominance of polar/π over charge-transfer effects in stacked phenyl interactions. *J. Am. Chem. Soc.* 115 (12): 5330–5331.

34 Yang, X., Xu, G., and Tang, W. (2016). Efficient synthesis of chiral biaryls *via* asymmetric Suzuki–Miyaura cross-coupling of ortho-bromo aryl triflates. *Tetrahedron* 72 (34): 5178–5183.

35 Gan, K.B., Zhong, R.-L., Zhang, Z.-W., and Kwong, F.Y. (2022). Atropisomeric phosphine ligands bearing C–N axial chirality: applications in enantioselective Suzuki–Miyaura cross-coupling towards the assembly of tetra-ortho-substituted biaryls. *J. Am. Chem. Soc.* 144 (32): 14864–14873.

36 To, S.C. and Kwong, F.Y. (2011). Highly efficient carbazolyl-derived phosphine ligands: application to sterically hindered biaryl couplings. *Chem. Commun.* 47 (17): 5079–5081.

37 Nishio, M. (2011). The CH/π hydrogen bond in chemistry. Conformation, supramolecules, optical resolution and interactions involving carbohydrates. *Phys. Chem. Chem. Phys.* 13 (31): 13873–13900.

38 Zhou, Y., Zhang, X., Liang, H. et al. (2014). Enantioselective synthesis of axially chiral biaryl monophosphine oxides *via* direct asymmetric Suzuki coupling and DFT investigations of the enantioselectivity. *ACS Catal.* 4 (5): 1390–1397.

39 Yang, H., Sun, J., Gu, W., and Tang, W. (2020). Enantioselective cross-coupling for axially chiral tetra-ortho-substituted biaryls and asymmetric synthesis of gossypol. *J. Am. Chem. Soc.* 142 (17): 8036–8043.

40 Lu, Y., Li, J., Dong, C.-E. et al. (2017). Recent advances in gossypol derivatives and analogs: a chemistry and biology view. *Future Med. Chem.* 9 (11): 1243–1275.

41 Pearce-Higgins, R., Hogenhout, L.N., Docherty, P.J. et al. (2022). An enantioselective Suzuki–Miyaura coupling to form axially chiral biphenols. *J. Am. Chem. Soc.* 144 (33): 15026–15032.

42 Golding, W.A., Pearce-Higgins, R., and Phipps, R.J. (2018). Site-selective cross-coupling of remote chlorides enabled by electrostatically directed palladium catalysis. *J. Am. Chem. Soc.* 140 (42): 13570–13574.

43 Bermejo, A., Ros, A., Fernández, R., and Lassaletta, J.M. (2008). C_2-Symmetric bis-hydrazones as ligands in the asymmetric Suzuki–Miyaura cross-coupling. *J. Am. Chem. Soc.* 130 (47): 15798–15799.

44 Jones, G.B. and Chapman, B.J. (1995). π Stacking effects in asymmetric synthesis. *Synthesis* 5: 475–497.

45 Shen, D., Xu, Y., and Shi, S.-L. (2019). A bulky chiral N-heterocyclic carbene palladium catalyst enables highly enantioselective Suzuki–Miyaura cross-coupling reactions for the synthesis of biaryl atropisomers. *J. Am. Chem. Soc.* 141 (37): 14938–14945.

46 Falivene, L., Credendino, R., Poater, A. et al. (2016). SambVca 2. A web tool for analyzing catalytic pockets with topographic steric maps. *Organometallics* 35 (13): 2286–2293.

47 Saget, T., Lemouzy, S.J., and Cramer, N. (2012). Chiral monodentate phosphines and bulky carboxylic acids: cooperative effects in palladium-catalyzed enantioselective C(sp^3)–H functionalization. *Angew. Chem. Int. Ed.* 51 (9): 2238–2242.

48 Byrne, L., Sköld, C., Norrby, P. et al. (2021). Enantioselective synthesis of atropisomeric biaryls using biaryl 2,5-diphenylphospholanes as ligands for palladium-catalysed Suzuki–Miyaura reactions. *Adv. Synth. Catal.* 363 (1): 259–267.

49 Barder, T.E., Walker, S.D., Martinelli, J.R., and Buchwald, S.L. (2005). Catalysts for Suzuki–Miyaura coupling processes: scope and studies of the effect of ligand structure. *J. Am. Chem. Soc.* 127 (13): 4685–4696.

50 Ingoglia, B.T., Wagen, C.C., and Buchwald, S.L. (2019). Biaryl monophosphine ligands in palladium-catalyzed C–N coupling: an updated user's guide. *Tetrahedron* 75 (32): 4199–4211.

51 Korenaga, T. (2023). Japanese Patent Application No. 2023-142889, filed 4 September 2023.

5

Organocatalytic Enantioselective Formation of Atropisomers

Chiara Portolani, Giovanni Centonze, and Giorgio Bencivenni

Alma Mater Studiorum—University of Bologna, Department of Industrial Chemistry "Toso Montanari", via P. Gobetti 85, Bologna, 40129, Italy

5.1 Introduction

Inspired by enzyme catalysis [1] and representing a valid alternative to asymmetric metal catalysis [2], the use of small organic molecules for promoting enantioselective transformation has become an extremely powerful tool for the synthetic community, in both industry and academia. The use of organocatalysis indeed avoids utilization of expensive, toxic, and polluting metals and makes use of "privileged chiral catalysts" that are more easily synthesized with respect to enzymes and readily available from natural sources.

The primary concept at the base of all the organocatalytic reactions is the activation of the substrate into a more active reagent, by means of making it a better nucleophile or electrophile. The principal classification based on the type of interaction between the catalyst and the substrate is between covalent- and noncovalent-based activation: the first takes place when the organocatalyst is covalently bonded to the substrate with a bonding energy exceeding 15 kcal/mol and is recycled through hydrolysis or displacement by a pendant group on the final product; examples of this activation are amino and carbene catalysis. When the organocatalyst is instead bonded via ion pairing or secondary interactions such as hydrogen bonding, in general lower than 4 kcal/mol, noncovalent-based activation occurs. Inside this class, a further classification according to the mechanistic role of the catalyst distinguishes between donating and removing electrons or protons to or from the substrate or transition states; Brønsted acid/base, Lewis acid/base, and hydrogen bonding activation are included in this class.

Besides numerous asymmetric transformations aimed at obtaining target central-chiral molecules, the applicability of this kind of catalysis appeared highly effective for enantioselective construction of atropisomers [3], the subclass of axially chiral compounds where the stereoisomerism results from a rotationally restricted single bond. In this chapter, we will highlight the role of the different

Atropisomerism in Asymmetric Organic Synthesis: Challenges and Applications, First Edition.
Edited by Shinobu Takizawa and Mohamed S. H. Salem.

types of organocatalytic activation in the enantioselective synthesis of atropisomers. Specifically, distinctions will be made between aminocatalysis, base-catalysis, phase-transfer catalysis, and phosphoric acid catalysis. The adaptability of this catalysis to different synthetic strategies and the orthogonality of the mode of action resulted to be useful for the enantioselective construction of a wide variety of atropisomers bearing different scaffolds. Literature reports a growing number of examples about non-biaryl atropisomers, as well as atropisomers featuring restricted bonds different form C—C. For each activation mode we will focus on selected examples regarding structurally diverse atropisomers, including C—C (biaryls and non-biaryls) and C—N as well as C—O, C—B, and N—N atropisomers.

5.2 Aminocatalysis

Within the category of covalent-based activation, the leading position is occupied by aminocatalysis, a consistent strategy especially for the generation of stereocenters at α and β positions of carbonyl compounds [4]. Primary or secondary chiral amines are exploited, with the catalytic active species being an enamine or iminium ion formed upon condensation of the catalyst with the carbonyl substrate (Scheme 5.1). Enamine activation results in an increased electron density at the reaction center through HOMO (highest occupied molecular orbital) energy raising and possible reactions with electrophiles. Iminium ion activation corresponds to a decrease in electron density at the reaction center due to LUMO (lowest unoccupied molecular orbital) activation and possible reaction with nucleophiles.

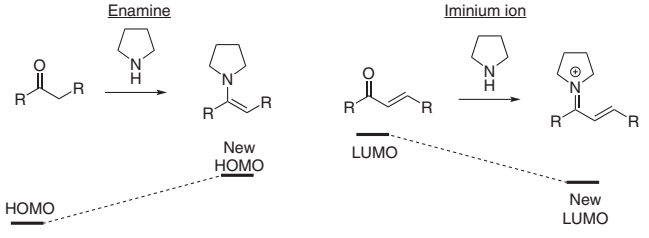

Scheme 5.1 Aminocatalytic activation of carbonyl compounds.

Through this approach, different synthetic strategies are allowed for atroposelective synthesis, including enantioselective *de novo* ring formation, dynamic resolution, desymmetrization, and direct formation of the rotationally restricted bond, as presented in the following sections of this chapter through significant examples.

5.2.1 Atropisomeric Synthesis of C—C Biaryls *via* Aminocatalysis

From its conception, atroposelective synthesis has seen an enormous growth of synthetic strategies for the obtaining of axially chiral biaryls, providing a large variety

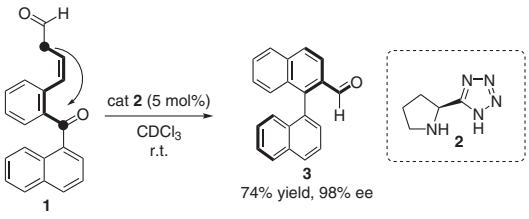

Scheme 5.2 Atroposelective synthesis of biaryls via amine catalyzed aldol condensation. Source: Sparr and Link [6]/with permission of John Wiley & Sons.

of innovative synthetic protocols and possible applications [5]. In this context, Sparr and co-workers conducted a series of studies for the enantioselective synthesis of atropisomeric biaryls where, with respect to approaches where the arene rings are already present in the substrate, they achieved concomitant formation of the chiral axis and *de novo* formation of one or more aromatic rings (Scheme 5.2). They realized the first example of atroposelective synthesis using secondary amine as catalyst, inspired by biosynthesis of aromatic polyketide: [6] promoted by cyclase and aromatase enzymes, the biosynthesis relies on the intramolecular aldol addition to a ketone functionality and final dehydration–aromatization event. Instead of enol formation, they exploited dienamine generation as a new trigger of the aldol reaction. The pyrrolidinyl-tetrazole catalyst **2** can react with the aldehyde functionality of **1** to generate a chiral dienamine that promotes the stereoselective aldol addition to the ketone moiety; central-to-axial chirality transfer occurs during the dehydration–aromatization step, representing the driving force of the transformation.

Two years later, they applied the enamine-catalyzed aldol addition to obtain well-defined 1,2-naphthalene oligomers (Scheme 5.3) [7]. These compounds represent the rotationally stable analogs of stereodynamic helically shaped ortho-phenylenes, where the enhanced hindrance of the building blocks with respect to phenylenes ensures from helix-sense inversion. The geometry of the stable P-helix secondary structure is dictated by the use of a natural amino acid as a catalyst; in this case, the steric encumbrance of the 1,2′-binaphthalen-2-yl (phenyl) ketone **4** requires a primary amine for efficient yield, and 90% enantioselectivity is achieved using L-isoleucine. By adding another building block to the product **6**, quarter naphthalenes **9** could be obtained in an atropo-diastereoisomeric fashion due to substrate-controlled aldol condensation.

Another example reported by Sparr shows a highly atroposelective cascade reaction where noncanonical poly-carbonyls **10** are directly converted to binaphthyls through twofold enantioselective cyclization catalyzed by the aminoethanol-derived proline catalyst **11** (Scheme 5.4) [8]. Double 5-enolexo aldol cyclization leading to hydropentalene **12**, which would occur in nature starting from canonical poly-carbonyls, is suppressed by the presence of the terminal aldehyde groups on the substrate that react with proline catalysis to afford only the final biaryl **13**. This work offers an easy route to atropisomeric biaryls and shows the ability of privileged small-molecule catalysis to promote highly enantioselective transformation not

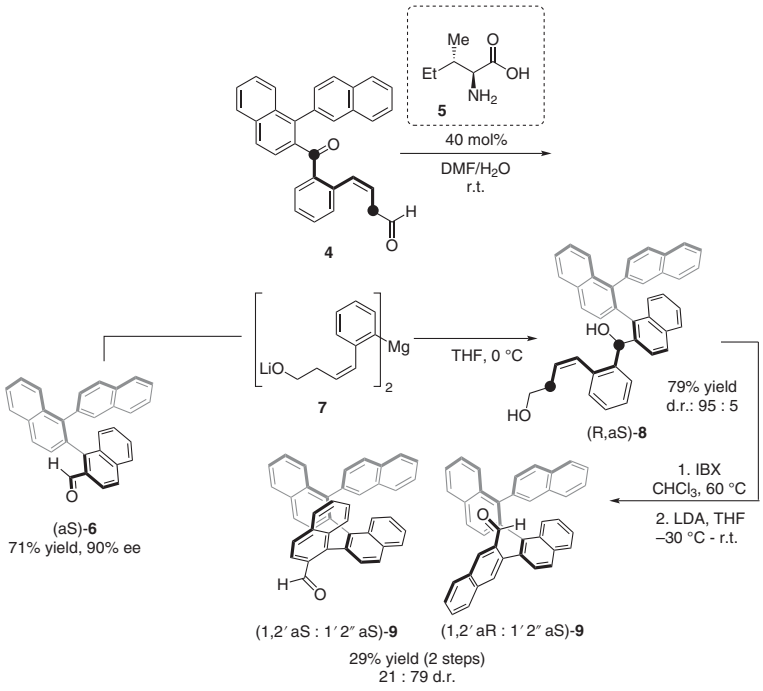

Scheme 5.3 Synthesis of configurationally stable oligonaphthalenes via aldol condensation. Source: Sparr and co-workers [7]/with permission of John Wiley & Sons.

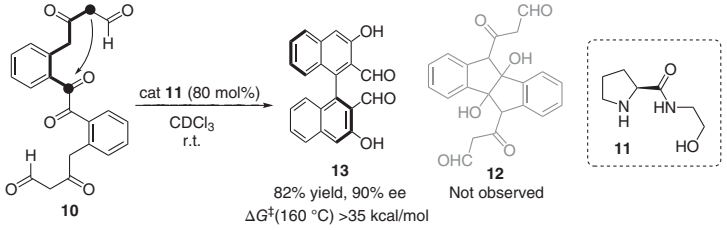

Scheme 5.4 Atroposelective synthesis of tetra-ortho-substituted biaryls via amine catalyzed noncanonical cyclization. Source: Sparr and co-workers [8]/with permission of Springer Nature.

only mimicking natural syntheses but also providing different products from what nature would produce.

5.2.2 Atropisomeric Synthesis of C—C Non-biaryls *via* Aminocatalysis

Non-biaryl atropisomers are molecules defined by a stereogenic axis featuring at least one non-arene moiety. One example of non-biarylic atropisomer is represented by amides, whose first enantioselective synthesis was developed by Koide and Uemura using the desymmetrization of an arene-tricarbonylchromium complex [9]. One year later, Clayden et al. reported the organocatalytic dynamic resolution of naphthamides under thermodynamic control with a chiral diamine resolving agent

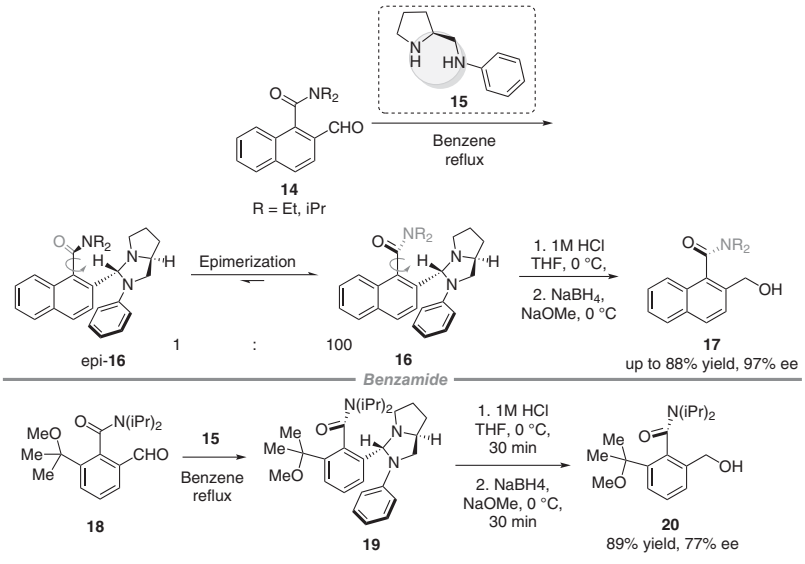

Scheme 5.5 Atropisomeric synthesis of amides via dynamic resolution with L-proline-derived resolving agent. Source: By Clayden.

derived from proline (Scheme 5.5) [10]. Condensation of the secondary amine catalyst **15** on the aldehyde group of the racemic substrate **14** gives rise to just one of the two possible aminal diastereoisomers. Considering the reaction conditions, the authors found that the reason for the atroposelectivity was the rapid epimerization between **16** and epi-**16**, leading to the thermodynamically favored diastereoisomer **16**; hydrolyzation provided the enantioenriched naphthamide and after reduction of the aldehyde moiety, a good stability to rotational racemization was obtained. Benzamides like **18** were also deracemized using this procedure, though with a poorer enantioselectivity due to the lower energy barrier.

In 2004, Walsh and co-workers exploited a L-proline **22** catalyzed aldol reaction to generate an atropisomeric amide by means of increasing the steric hindrance next to the axis, with the formation of the new stereocenter (Scheme 5.6) [11]. A dynamic kinetic resolution character was obtained with high diastereo- and enantioselectivity.

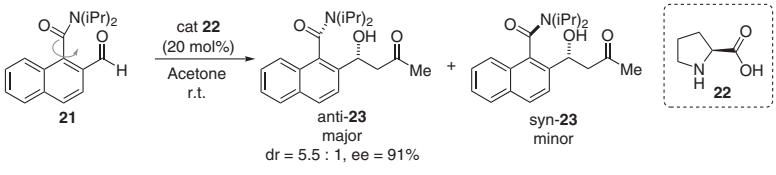

Scheme 5.6 Dynamic kinetic resolution of atropisomeric amides. Source: Walsh and co-workers [11]/with permission of American Chemical Society.

Inside C—C atropisomeric non-biaryls, growing attention is regarding the class of styrenes, whose enantioselective synthesis has remained overlooked for years despite the pivotal work of Adams [12] in 1940 indicating the potential of this type

of axially chiral molecules, further confirmed by Kawabata in 1991 [13]. It is in fact difficult to achieve good enantioselectivity with a low stereochemical stability like one of the styrenes, but significant advances on asymmetric strategies led to overcome these difficulties, with an increase in their atroposelective syntheses in the past years. The first organocatalytic synthesis was developed by Tan in 2017 through a secondary amine-catalyzed direct Michael addition reaction of substituted diones **25** to alkynals **24** (Scheme 5.7) [14]. Through this approach, the proline-derived catalyst **26** selectively forms the chiral iminium ion with the alkynal that upon addition of the nucleophile generates *in situ* the chiral allenamine **29**. Thanks to the control of the covalently bonded catalyst, this intermediate is able to discriminate between the *E*/*Z* configuration of the resulting iminium ion **30** (only one isomer may exhibit axial chirality) that finally transfers the chirality to the rotationally stable styrene. Product **27** was obtained with excellent yield and enantioselectivity, and with a rotational energy barrier around 30.38 kcal/mol at 25 °C, which ensures good stability. This procedure was also applicable to the use of ketone esters and malonitriles as nucleophiles, broadening the scope of this restricted class of compounds.

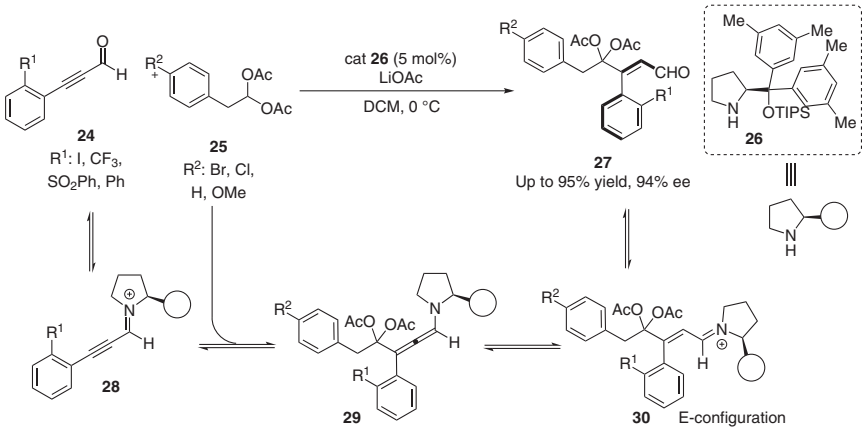

Scheme 5.7 Atroposelective synthesis of styrenes. Source: Tan and co-workers [14]/American Chemical Society.

Other than C(sp^2)–C(sp^2) atropisomers that present the usual planar-orthogonal disposition of the substituents around the rotationally restricted bond, uncommon C(sp^2)–C(sp^3) conformational diastereomeric atropisomers were isolated by Oki [15] and Ford [16] and successively observed by Dubois [17]. The enantioselective synthesis of C(sp^2)–C(sp^3) atropisomers was first obtained by Sparr through transition metal catalysis, where a rhodium complex enabled the formation of more than six stereoisomers of the sole substrate [18]. A first organocatalytic approach to these scaffolds was reported by the group of Bencivenni with the enantioselective Friedel–Crafts addition of β-naphthols to inden-1-ones (Scheme 5.8) [19]. The reaction was catalyzed by the quinine-derived primary amine **33** that after addition to the electrophile forms a chiral iminium ion, which is activated by trifluoroacetic acid cocatalyst for the interaction with the nucleophile giving an already C—C

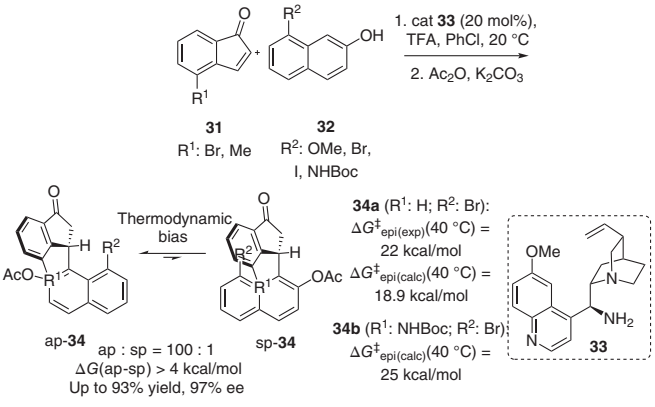

Scheme 5.8 Enantioselective Friedel–Crafts alkylation of β-naphthols with inden-1-ones. Source: Bencivenni and co-workers [19]/with permission of American Chemical Society.

rotationally restricted intermediate; after rapid aromatization, when large enough substituents are placed on both starting materials, the major *ap*-conformational diastereoisomer is formed with total diastereocontrol and with excellent enantioselectivity. This transformation is driven by a complete thermodynamic preference toward the formation of just one of the two conformational diastereoisomers. For this reason, evidence of restricted rotation and determination of the energy barrier was possible only analyzing scaffolds bearing substituents on only one of the two starting materials (Scheme 5.8: $\Delta G^{\ddagger}_{\text{epi(exp)}} = 22$ kcal/mol), where the *sp*-conformer is obtained by simple rotation of the not very stable axis; from calculations, however, an energy barrier of 25 kcal/mol is suggested when both **31** and **32** possess large substituents, as in the case of **34b**.

A rare case of kinetic control was instead found in seminal work developed by Jørgensen et al. in 2022 [20], where a secondary amine **37** catalyzed cycloaddition between 5*H*-benzo[*a*]pyrrolizine-3-carbaldehydes **35** and electron-poor olefins **36** furnished atropisomeric **39** with the simultaneous generation of the C(sp^2)–C(sp^3) stereogenic axis and two stereogenic centers (Scheme 5.9). Atropisomeric cyclazine cores were thus obtained for the first time through an enantioselective synthesis and showed a large variety of possible molecular motives with high level of enantioselectivity. DFT (density functional theory) calculation, together with isolation of a reactive intermediate, demonstrated that the stereogenic axis is formed under a kinetic control in a Curtin–Hammet equilibrium, where the rate-determining elimination step controls the atropo- and enantioselectivity. This made possible the determination of rotational stability of these substrates, with a value of 32.7 kcal/mol on the model substrate.

5.2.3 Atropisomeric Synthesis of C—N Scaffolds *via* Aminocatalysis

Amines proved to be efficient catalysts also for the preparation of molecules with stereogenic axes different from C—C. Chiral anilides featuring a restricted C—N bond were reported by Curran who demonstrated that these structures could exhibit significant stereochemical stability [21].

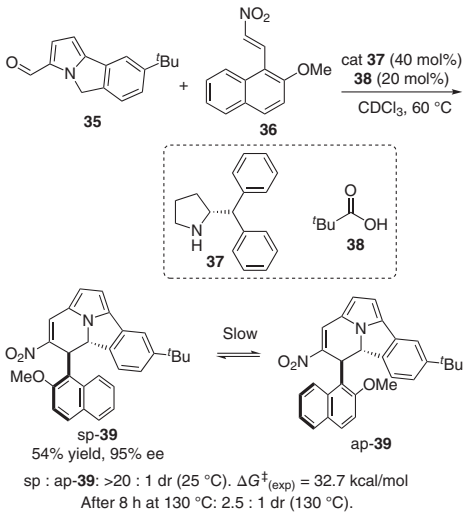

Scheme 5.9 Atroposelective synthesis of C(sp^2)–C(sp^3) configurationally stable cyclazines. Source: Jørgensen and co-workers [20]/with permission of American Chemical Society.

Atropisomeric succinimides were synthesized by Bencivenni and co-workers through an innovative aminocatalytic desymmetrization of maleimides via vinylogous Michael addition with 9-*epi*-9-amino-9-deoxy quinine **33** [22], where the product was obtained with high enantiocontrol on three stereogenic elements: one C—N axis and two stereocenters (Scheme 5.10). The presence on **41** of a bulky substituent at the ortho position of the aryl proved to be fundamental to restrict C—N bond rotation and to direct the nucleophilic attack to the opposite face of the maleimide. Experimental results and DFT analyses precisely explained the mechanism of this transformation [23]. The primary amine catalyst **33** is able to form the chiral dienamine and remotely direct the attack on one of the two

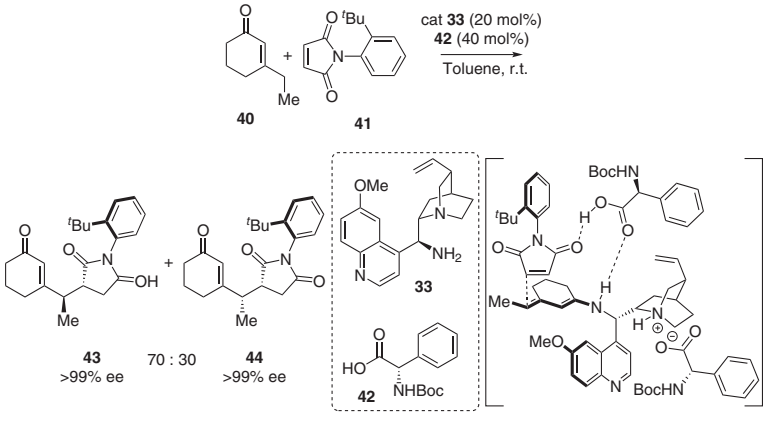

Scheme 5.10 Desymmetrization of *N*-arylmaleimides via vinylogous Michael addition. Source: Bencivenni and co-workers [23]/with permission of American Chemical Society.

electrophilic carbons of the maleimide, controlling the atroposelectivity of the reaction; the presence of 2 equiv of *N*-Boc-L-phenylglycine **42** with respect to the catalyst enhances the effectiveness of the transformation: the first molecule reacts with the catalyst forming the catalytic salt and the second bridges reacting partners in a cyclical fashion.

The atroposelective desymmetrization of *N*-arylmaleimides was realized through an aminocatalyzed Diels–Alder reaction of enones exploiting the same catalyst **33** [24], where the chirality of the C—N axis is determined by the remote control of the catalyst.

While existing organocatalytic approaches regarded the synthesis of atropisomers where the C—N bond is already preformed, direct formation of the C—N bond was developed for the first time by the group of Jørgensen through an amino catalysis (Scheme 5.11) [25]. Atroposelective coupling between indole-2-carboxaldehydes **45** and ortho-quinones **46** was promoted by a new fluorine-substituted proline-derived catalyst **47** that was designed and synthetized *ad hoc* with an increased outer sphere bulk to ensure good levels of enantioselectivity and, especially, perfect regiocontrol between C_3 and N_1 sites on the indole core (**49** : **48** – 20 : 1). Final central-to-axial chirality transfer promoted by DDQ (2,3-dichloro-5,6-dicyano-1,4-benzoquinone) resulted in the atropisomeric C—N scaffold.

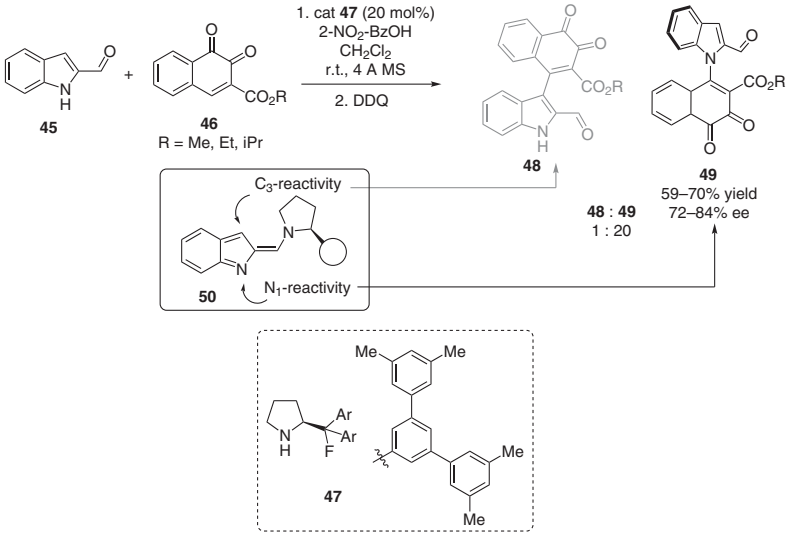

Scheme 5.11 Enantioselective addition of indole-2-carboxaldehydes to *ortho*-quinone derivatives via amine catalysis. Source: Jørgensen and co-workers [25]/with permission of John Wiley & Sons.

5.3 Brønsted Base Catalysis

Prominent role inside base catalysis activation is represented by Brønsted base catalysis, as the one promoted by chiral tertiary amines. The key to the activation is the

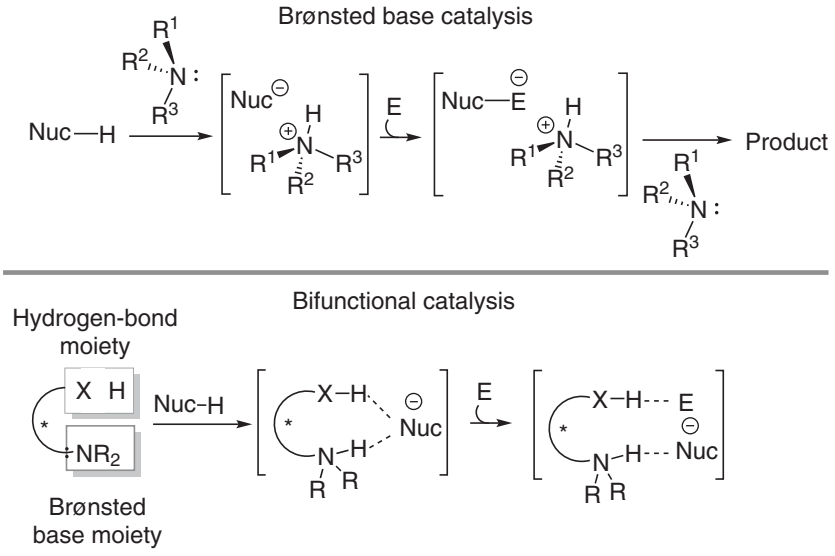

Scheme 5.12 Brønsted base and bifunctional catalysis activation.

proton transfer from a pro-nucleophile or charged nucleophile–electrophile adduct to the basic catalyst; the substrate is situated within a chiral pocket formed by the catalyst, and the enantioselective attack depends on the conformation of this complex (Scheme 5.12). However, stereoselectivity based only on this ion pairing interactions can become challenging, hence catalysts combining both a basic moiety and a second activation site were required as they would provide bifunctional activation that greatly enhances the final enantioselectivity. Brønsted base-hydrogen donor bifunctional catalysts were designed to obtain such organized activation states where the nucleophile is activated and stabilized, or both nucleophile and electrophile are stabilized. Selected examples of simple Brønsted base and bifunctional catalysis are reported for the synthesis of atropisomers.

5.3.1 Atropisomeric Synthesis of C—C Biaryls and Heterobiaryls *via* Base Catalysis

In 2010, Miller reported the atroposelective electrophilic aromatic substitution of a racemic biaryl with simple bromination reagents, catalyzed by a tripeptide-derived small-molecule catalyst **52** (Scheme 5.13) [26]. The presence of bromine substituents at the ortho position in fact attributes to the stereogenic axis a high enough barrier to rotation to preclude product racemization. From single-crystal X-ray analysis of the major enantiomer and awareness of the possible conformation of the catalyst, a docking model of the substrate–catalyst interactions was proposed (Scheme 5.13). The bifunctional catalyst can deprotonate the carboxylic acid moiety of the substrate **51** through the tertiary amine group and simultaneously coordinate the phenolic proton through hydrogen bonding with the amide diacetate. These interactions, together with the folding properties of the catalyst and conformation of the *N*-acyl

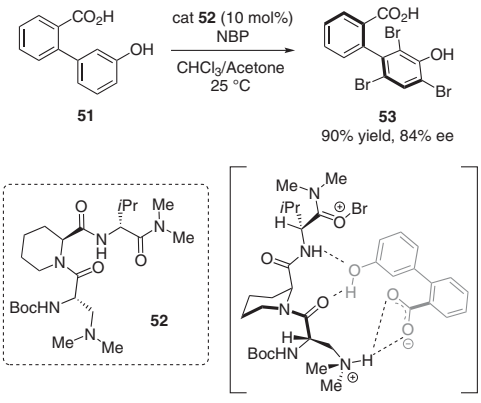

Scheme 5.13 Atropisomeric synthesis of biaryls via peptide-catalyzed dynamic kinetic resolution. Source: Miller and co-workers [26]/with permission of American Association for the Advancement of Science.

piperidine, ensure high level of enantioselectivity in a dynamic kinetic resolution strategy to obtain optically enantioenriched biaryls.

Atroposelective addition of naphthols **55** to halogenated quinones **54** was reported by Bella in 2016 [27], where simple quinine **56** as organocatalyst promoted the transformation with high level of enantioselectivity in mild reaction conditions (Scheme 5.14). Non-C2-symmetrical biaryls were obtained through this approach, where mono- and disubstituted quinones ensured a high enough energy barrier to rotation on the final product. To impart atroposelectivity, a possible rationalization regards the interactions between the deprotonated hydroxyl group on the naphthol unit and the protonated quinuclidine unit on the quinine as well as the hydrogen bonding between the quinone carbonyl and the 9-hydroxy moiety of the catalyst. It was in fact observed experimentally and from DFT calculations that a catalyst missing free 9-hydroxy group led to inversion of stereoinduction.

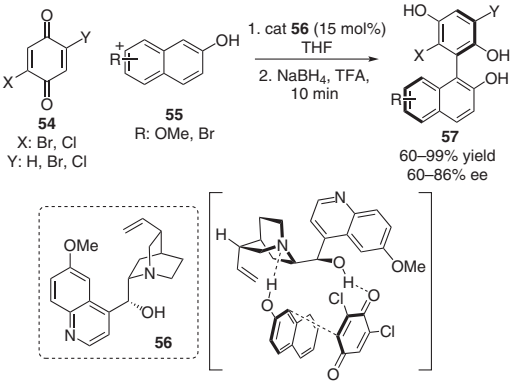

Scheme 5.14 Enantioselective synthesis of biaryls via quinine catalysis. Source: Bella and co-workers [27]/with permission of John Wiley & Sons.

A similar transformation was reported by Miller [28], who developed the coupling of naphthols **59** and ester-bearing quinones **58** to achieve non-C_2-symmetric BINOL-type scaffolds (Scheme 5.15). As a catalytic approach, they used a tetrameric peptide **60** featuring the basic residue β-dimenthylaminoalanine (Dmaa), which proved to be highly effective in the synthesis of a large variety of substrates with different frameworks with good yield and enantioselectivity.

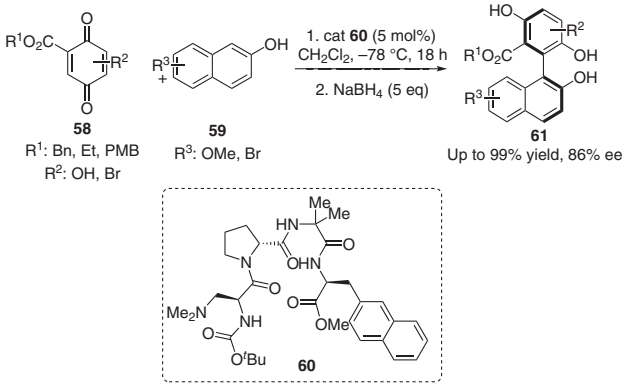

Scheme 5.15 Synthesis of axially chiral non-C_2-symmetric biaryls via peptide catalysis. Source: Miller and co-workers [28]/with permission of John Wiley & Sons.

In 2017, Rodriguez and Bonne developed the first enantioselective synthesis of unknown furan atropisomers through a domino Michael/O-alkylation reaction between chloronitroalkenes **63** and 2-naphthols **62** (Scheme 5.16) [29]. The originality of the sequence lies in the central-to-axial chirality conversion based on the enantioselective formation of dihydrofuran heterocycles *sp*-**65** and *ap*-**65** promoted by the bifunctional squaramide organocatalyst **64**, and subsequent

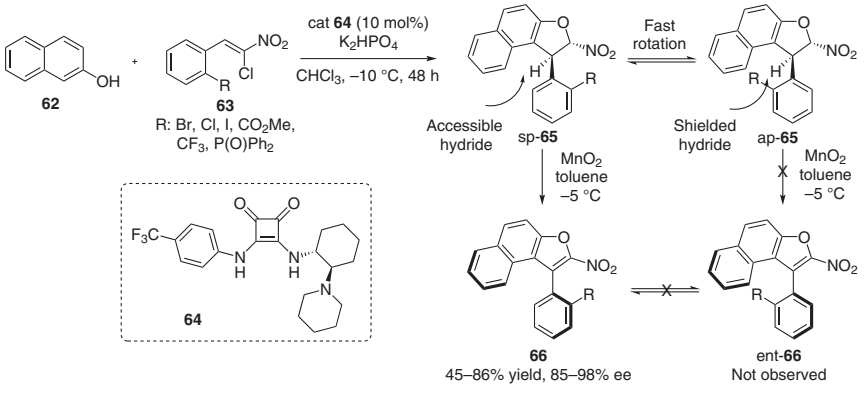

Scheme 5.16 Enantioselective synthesis of furan-based atropisomers via base-catalyzed point-to-axial chirality conversion. Source: Rodriguez and co-workers [29]/with permission of American Chemical Society.

atroposelective oxidative dehydrogenation with MnO_2. From mechanistic investigation, a Curtin–Hammet equilibrium seems present between the two conformations, and selective oxidation in favor of the intermediate with the most accessible hydride leads to atroposelective formation of the rotationally stable product **66** (26.4–36.5 kcal/mol).

This strategy was exploited by the same group for the formation of *S*- and *E*-shaped bis-benzofuran atropisomeric oligoarenes **71** and **72** with two C—C stereogenic axes (Scheme 5.17) [30]. A double central-to-axial chirality transfer was promoted by the unique bifunctional squaramide catalyst **70** with subsequent oxidative aromatization, achieving a wide range of differently substituted structures. By using the enantiomer of catalyst, the opposite stereogenic axis could be obtained, resulting in an elegant stereodivergent approach that enabled the formation of all four diastereoisomers of the final atropisomeric oligomer.

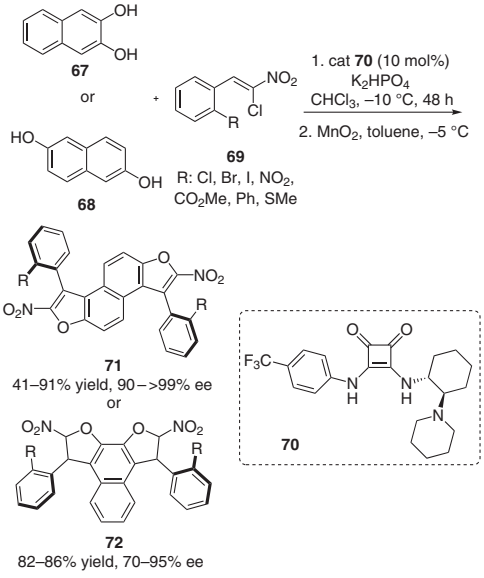

Scheme 5.17 Atroposelective synthesis of bis-benzofuran oligoarenes via base catalysis. Source: Rodriguez and co-workers [30]/with permission of Royal Society of Chemistry.

The group of Yan reported several examples of atropisomeric heterobiaryls obtained through vinylidene *ortho*-quinone methide (VQM) intermediates (Scheme 5.18a). The strategy consists in initial tautomerization of an alkyne **73** promoted by a quinine-derived catalyst **74** provided with a hydrogen bonding moiety that imparts stereoinformation to the newly formed allene **75**. Axially chiral aryl-C2-indoles **76** were obtained for the first time by the group through this organocatalytic approach with excellent enantioselectivity in the final nucleophilic intramolecular annulation [31]; the final products were found to be useful for further functional-group transformations as well as a possible key skeleton for organocatalysts for reactions as enantioselective aza-Bayliss–Hillman and [4 + 2]

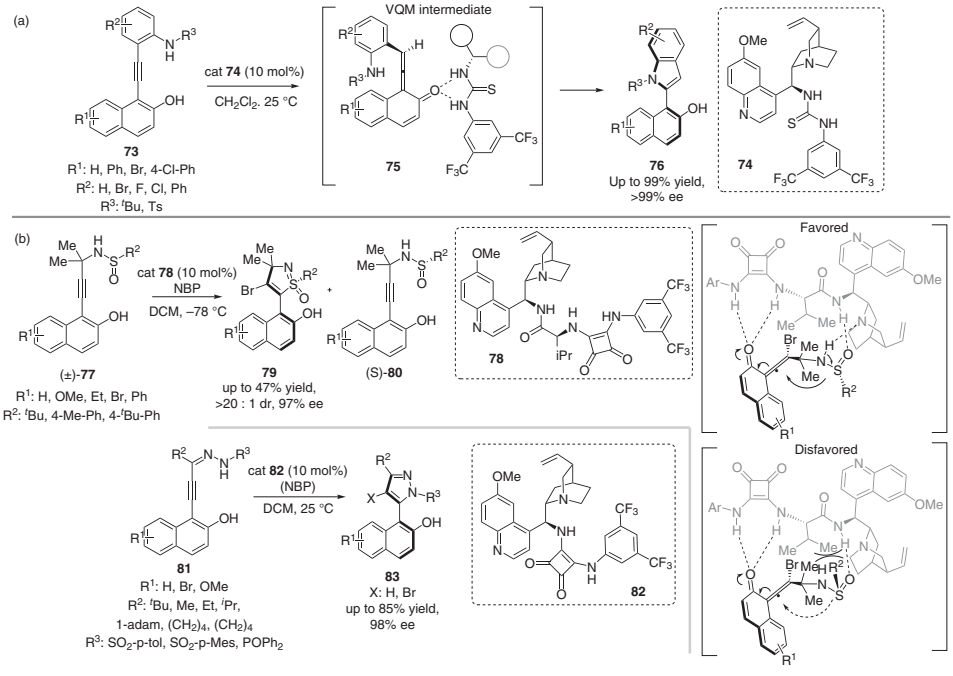

Scheme 5.18 (a) Atroposelective syntheses of axially chiral aryl-C2-indoles. Source: Yan and co-workers [31]/with permission of John Wiley & Sons. (b) Atroposelective syntheses of axially chiral *N*,*N*- and *N*,*S*-1,2-azoles. Source: Yan and co-workers [32]/Springer Nature/CC BY 4.0.

tandem cyclization. Few years later, they developed the synthesis of axially chiral *N*,*N*- and *N*,*S*-1,2-azoles using the same VQM method (Scheme 5.18b) [32]. Racemic mixture of *N*-naphthyl propargylsulfinamides **77** with a stereogenic sulfur center underwent kinetic resolution leading to the final atropisomeric 1,2-azole **79** with excellent enantioselectivity, which is possibly due to the favored nucleophilic attack from the less sterically hindered side of the intermediate. Axially chiral naphthyl-pyrazoles **83** were also obtained through this highly atroposelective protocol with excellent results; interestingly, biological tests showed that this kind of scaffold seems to have promising action as a therapeutic agent.

5.3.2 Atropisomeric Synthesis of C—C Non-biaryls *via* Base Catalysis

Yan and co-workers posed a milestone on the asymmetric synthesis of atropisomeric styrenes [33]. In 2018, they developed a methodology to obtain chiral sulfone-containing styrenes through the formal nucleophilic addition of an activated nucleophile to the VQM intermediate (Scheme 5.19). In this example, the

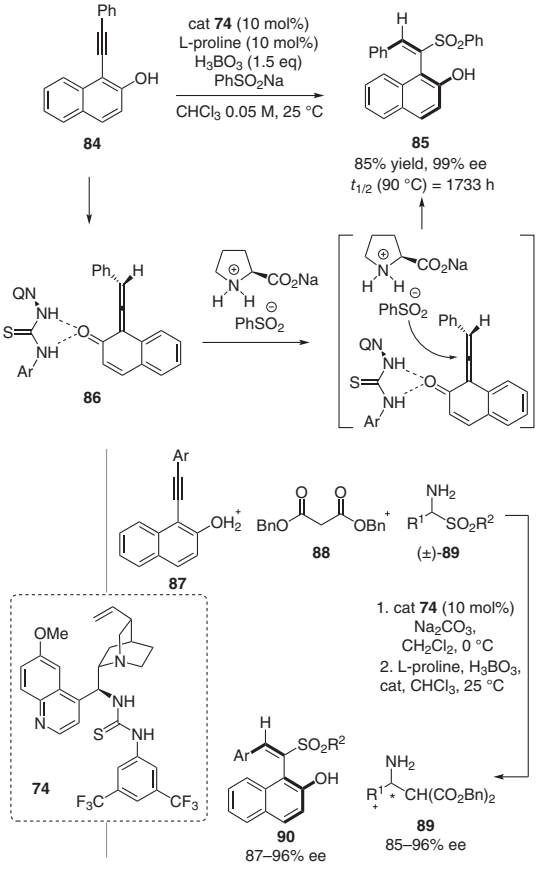

Scheme 5.19 Atroposelective syntheses of axially chiral styrenes. Source: Yan (co-author).

nucleophile sulfinate salt is activated by L-proline that upon formation of the quaternary ammonium salt increases the nucleophile solubility; after addition of the sulfonate to the chiral allene **86**, atropisomeric styrenes **85** were obtained with high yields, enantioselectivity, and *E*/*Z* ratio. Notably, the use of D-proline furnished the same enantioselectivity as L-proline, suggesting that only the bifunctional thiourea catalyst **74** is responsible for the enantioinduction. This methodology was used by the same group for the one-pot formation of similar axially chiral sulfone-containing styrenes, where the nucleophile was *in situ* generated by the same thiourea-catalyzed Mannich reaction [34]. Squaramide-derived cinchona catalysts were exploited by the group for the synthesis of a large variety of functionalized styrenes featuring one or more than one stereogenic axis [35–37].

Another relevant example of thiourea-catalyzed atroposelective formation of chiral styrenes was reported by Tan as extension of the methodology developed for organocatalytic dihalogenation of alkenes and alkynes (Scheme 5.20) [38]. Axially chiral vicinal dihaloalkenes **93** and **94** were obtained in high yield and enantiomeric excess in exclusive *E* configuration. The role of the catalyst **92** consists of facilitating the initial transfer of the bromonium ion to the alkyne by interaction with the quinuclidine group, while the substrate is able to orientate the halide ion via hydrogen bonds with the urea group for the addition to the bromirenium species.

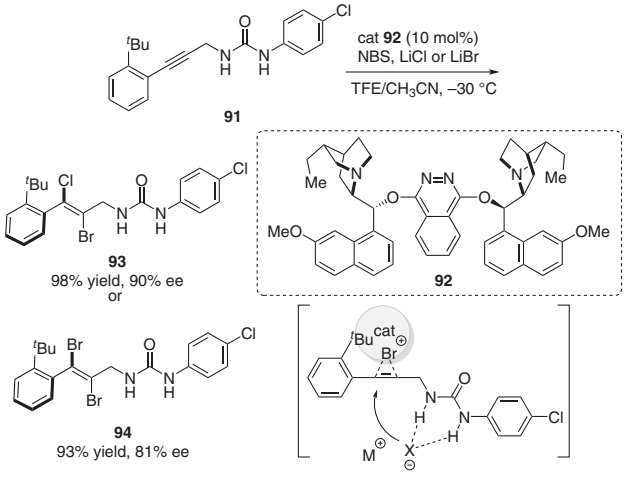

Scheme 5.20 Enantioselective dihalogenation of alkynes to obtained axially chiral styrenes. Source: Tan and co-workers [38]/with permission of Springer Nature.

5.3.3 Atropisomeric Synthesis of C—N Scaffolds *via* Base Catalysis

The first report about an atropisomeric anilide **97**, where the nitrogen atom is directly attached to the aromatic ring, was described by Jørgensen [39]. His group in fact developed an unprecedent organocatalytic asymmetric Friedel–Crafts amination of 2-naphthols **95** with azodicarboxylates using cinchona-alkaloid **96** (Scheme 5.21); the final atropisomer showed a good stability to rotation, as from

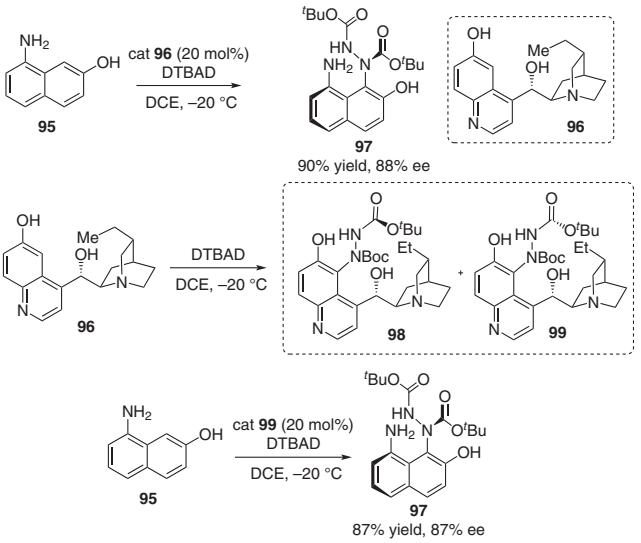

Scheme 5.21 Atropisomeric synthesis of C—N non-biaryl compounds via base catalysis. Source: Jørgensen and co-workers [39]/with permission of John Wiley & Sons.

HPLC (high-performance liquid chromatography) analysis only a decrease of 3% ee was observed leaving the compound at r.t. for 10 days; the barrier to rotation was measured experimentally and computationally on the substrate missing the amino group on the naphthol, giving values of $\Delta G^{\ddagger}_{(\mathrm{exp})} = 20$ kcal/mol and $\Delta G^{\ddagger}_{(\mathrm{cal})} = 22$ kcal/mol. Interestingly, the same transformation could be performed on the quinine-derived catalyst **96** as substrate, and the resulting aminated product **99** was effective for catalyzing the reaction itself.

As reported for the enantioselective formation of atropisomeric biaryls, Miller exploited small peptide catalysis for the asymmetric construction of axially chiral anilides by bromination of 3-hydroxyl 1-benzamides **100** via electrophilic aromatic substitution (Scheme 5.22) [40]. The tertiary amine moiety of catalyst **101** is again able to deprotonate the quinazolinone hydroxyl group, while the binding interactions with the β-turned peptide impart chirality to the substrate, with the first bromination event being stereodetermining and resulting in rotationally stable mono-*ortho*-substituted isomer **103**.

A bifunctional organocatalyst **105** was used by the group of Tan for the asymmetric tyrosine click-like reaction for the formation of axially chiral urazole **106** with N—Ar bond restricted rotation (Scheme 5.23) [41]. This example shows desymmetrization of the triazoledione **104** by means of remote control of the catalyst, able to discriminate between the two reactive sites and imparting excellent enantioselectivity by hydrogen bonding interactions.

As a similar approach, base-catalyzed desymmetrization of maleimides was reported by Bencivenni and co-workers exploring the reactivity of 1,3-dicarbonyls **108** and cyanoesters **109** using pyrimidine-bridged cinchona alkaloid catalyst **110** (Scheme 5.24a) [43], and the year later with the study on Michael addition of oxindoles **113** to maleimides using catalyst **114** (Scheme 5.24b) [42]. These examples are

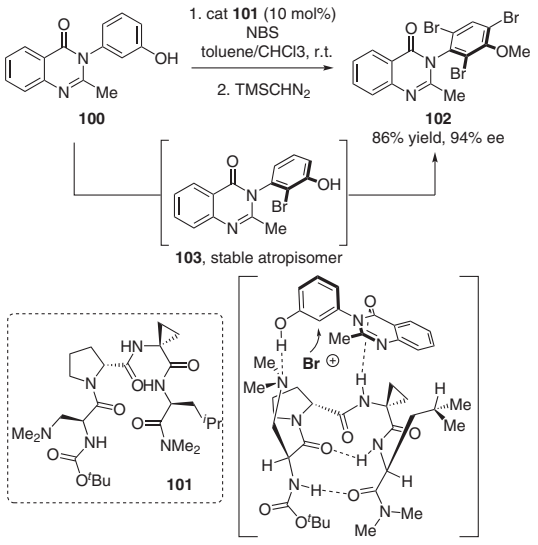

Scheme 5.22 Atroposelective synthesis of 3-arylquinazolin-4(3H)-ones via peptide catalyzed bromination. Source: Miller and co-workers [40]/with permission of American Chemical Society.

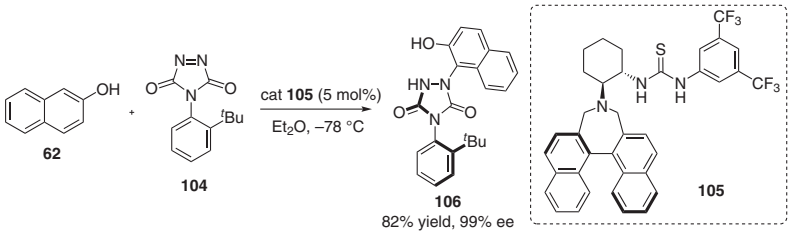

Scheme 5.23 Enantioselective synthesis of axially chiral urazole via thiourea-catalyzed tyrosine click reaction. Source: Tan and co-workers [41]/Springer Nature/CC BY 4.0.

complementary to the amino-catalyzed desymmetrization of maleimides previously mentioned, showing the versatility of organocatalysts in promoting orthogonal approaches for the synthesis of similar scaffolds.

Various axially chiral anilides were obtained by the group of Li via asymmetric *N*-allylic alkylation with achiral Morita–Bayliss–Hillman adducts (Scheme 5.25). Different cinchona alkaloids (**110**, **120**, and **123**) were able to promote the atroposelective synthesis of C—N axially chiral anilides **118** (Scheme 5.25a) [44], phosphonamides **121** (Scheme 5.25c) [45], and sulfinamides **124** (Scheme 5.25b) [46]. The ortho-iodine derivative of atropisomeric phosphamide **121** was found to be effective as chiral hypervalent iodine catalyst for the asymmetric oxidative dearomatization of phenols. Axially chiral sulfonamides **128** were also obtained by Zhao and co-workers through an asymmetric allylic alkylation promoted by the cinchona dimers **127** and **110** (Scheme 5.25d), strategy that proved to be useful also for obtaining enantiopure NOBIN derivative (*R*)-**126** via kinetic resolution [47].

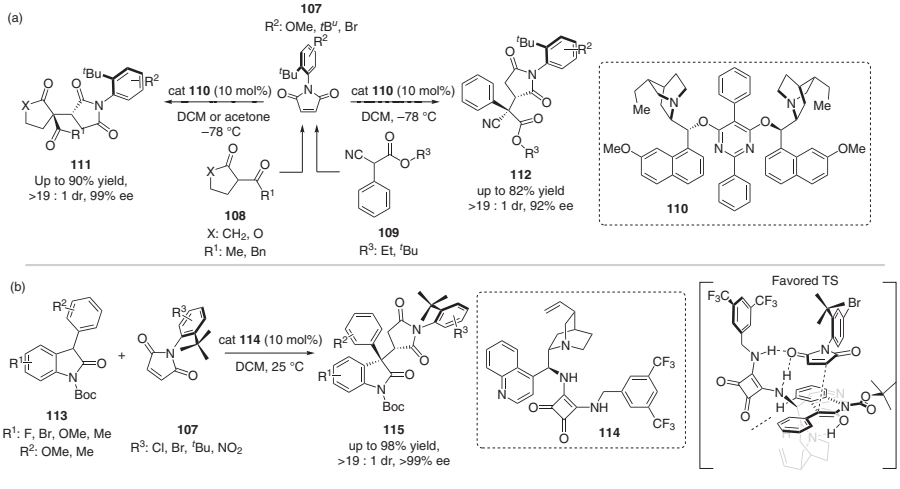

Scheme 5.24 (a) Desymmetrization strategies to obtain axially chiral maleimides by the addition of 1,3-dicarbonyls and cyanoesters. (b) Desymmetrization strategies to obtain axially chiral maleimides by addition of oxindoles. Source: Bencivenni and co-workers [42]/with permission of Georg Thieme Verlag KG.

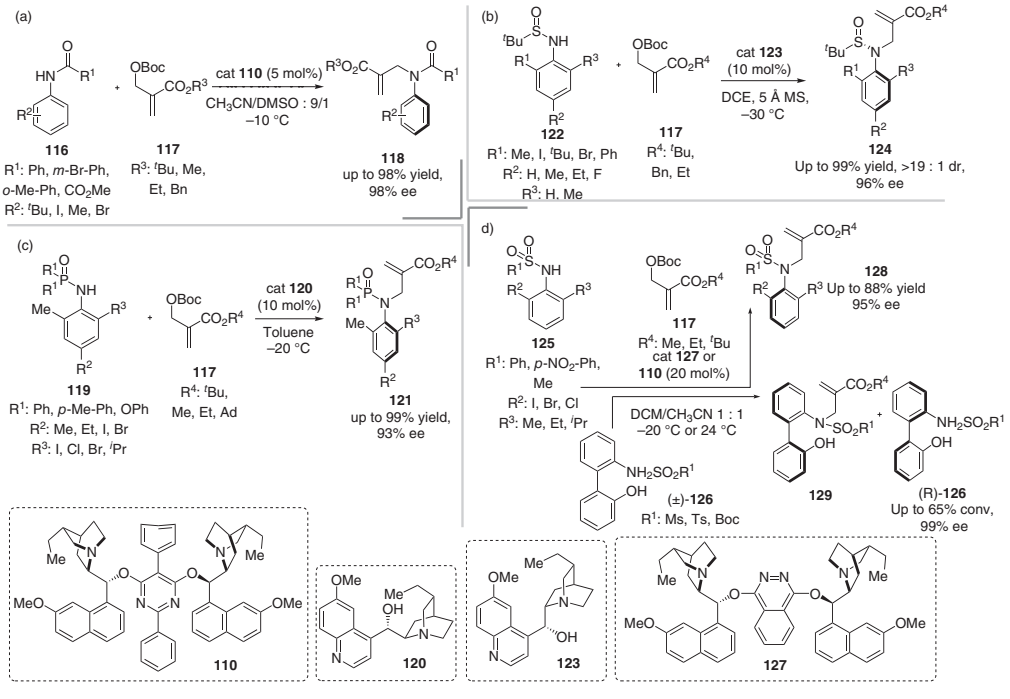

Scheme 5.25 (a) synthesis of C—N axially chiral anilides; (b) synthesis of C—N axially chiral sulfinamides; (c) synthesis of C—N axially chiral phosphonamides; and (d) synthesis of C—N axially chiral sulfonamides.

As analogs of anilides, atropisomeric lactams were synthesized one of the first times by the group of Taguchi in 2000 [48]. Interestingly, they reported variation in stereochemical stability when different ring sizes were considered: a difference of 4–5 kcal/mol between six- and five-membered lactams was found, highlighting that when a smaller ring is present, external bond angles of substituents cause them to position further away from the axis compared to larger rings. In this scenario, Tan developed an organocatalytic synthesis where chiral guanidine **131** was found to promote a tandem isomerization-Michael reaction toward atropisomeric six-membered lactams **132** (Scheme 5.26) [49]. Alkynamide **130** was converted to the product via a conjugated allenoate intermediate, followed by a highly enantioselective aza-Michael addition.

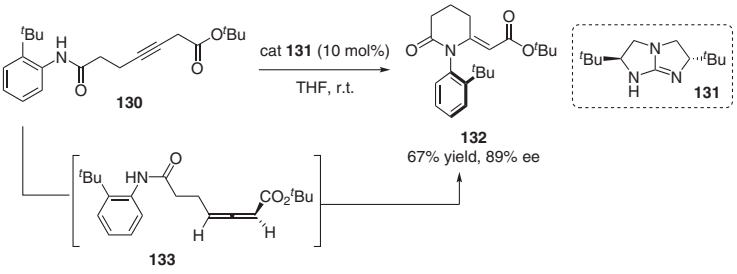

Scheme 5.26 Tandem isomerization–Michael reactions of alkynes to obtain axially chiral lactams. Source: Tan and co-workers [49]/with permission of John Wiley & Sons.

5.3.4 Atropisomeric Synthesis of N—N Scaffolds *via* Base Catalysis

A recently expanding field in atropisomeric synthesis regards the construction of N—N atropisomers, which has seen a significant growth in the past two years with the development of new and various synthetic strategies, with organocatalysis being one of the most exploited [50].

Cinchona-catalyzed asymmetric *N*-alkylation was an efficient method to synthesize for one of the first times this type of rotationally restricted molecules. In 2021, Lu and Houk presented the first enantioselective synthesis of N—N axially chiral scaffolds by quinidine catalysis (Scheme 5.27) [51]. The transformation was applicable to both aminopyrroles **134** and aminoquinazolinones **137** as substrates, which undergo MBH alkylation to obtain rotationally stable atropisomers. High enantiocontrol was ensured by hydrogen bonding interactions between the acceptor and donating groups on the substrate and the catalyst, through an extremely efficient remote control on the stereogenic axis. Computational calculation further confirmed the origin of enantioselectivity from these secondary interactions.

Isothiourea-catalyzed *N*-acylation of amides **139** with anhydrides was described by Li in 2022 (Scheme 5.28) [52]. Axially chiral quinazolinone scaffolds with aromatic substituents at C2 were obtained in high enantioselectivity, with a high enough energy barrier to rotation (see **142**), although slightly lower than the one obtained by Lu and Houk. Computational analyses showed strong stabilizing

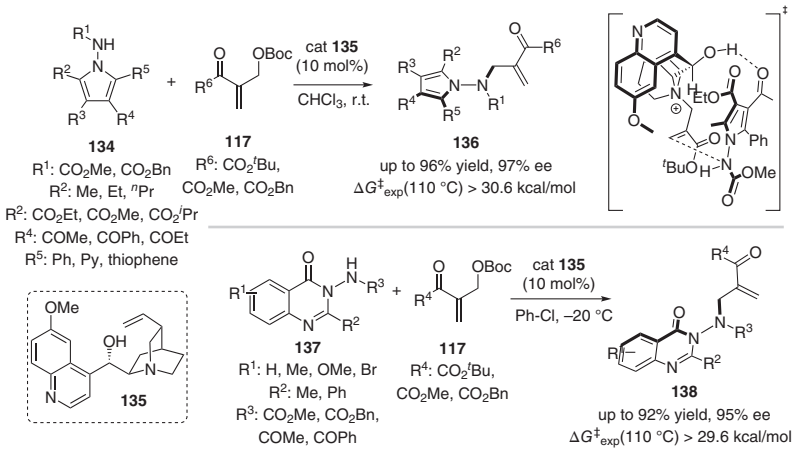

Scheme 5.27 Morita–Bayliss–Hillman alkylation to obtain N—N atropisomers. Source: Lu and co-workers [51]/with permission of Elsevier.

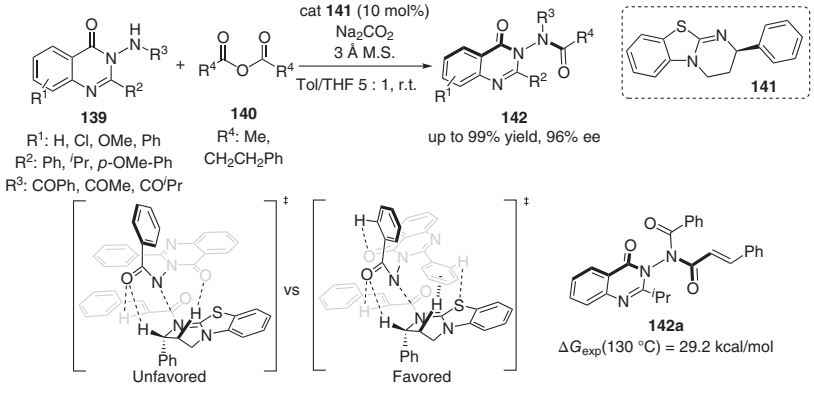

Scheme 5.28 Enantioselective acylation for the construction of N-N atropisomeric quinazolinones. Source: Li and co-workers [52]/Royal Society of Chemistry/CC BY 3.0.

hydrogen bonding interaction between catalyst **141** and substrate **139**, while two noncovalent interactions between the catalyst and the aryl group of the substrate led to discrimination between the two final enantiomers.

5.4 Phase Transfer Catalysis

Phase transfer catalysis (PTC) [53] represents a valid and widely employed synthetic tool for both industry and academia due to the mild reaction conditions, the easiness of operations, and the adaptability to large-scale synthesis [54]. The general strategy for the asymmetric approach relies on generating the reactive species from the starting substrate within a biphasic mixture and taking advantage of its different partition coefficient in the reaction medium compared to its reaction partner, in order to prevent their chemical interaction without the assistance of the chiral catalyst.

Nucleophilic substitution reactions are the most developed and studied processes where the anion of the nucleophilic species arises from an alkaline environment; besides, chiral organic salts based on quaternary ammonium or phosphonium scaffolds are commonly employed as catalysts for possessing a large ionic radius which allows them to dissolve in both phases. Indeed, catalysis is realized when the chiral cation matches the anion of the nucleophile and forms a new species that can reach and interact with the electrophilic partner in a stereoselective way. Despite the sole ionic generally noncovalent interactions involved in the asymmetric ionic pair, the chiral counterion has widely proved to exert elevated levels of chirality transfer over the stereocontrolled formation of the products. PTC was initially conceived for the asymmetric synthesis of non-natural amino acid derivatives (Scheme 5.29) [55], but recently has found application in several different purposes, such as the construction of axially chiral architectures.

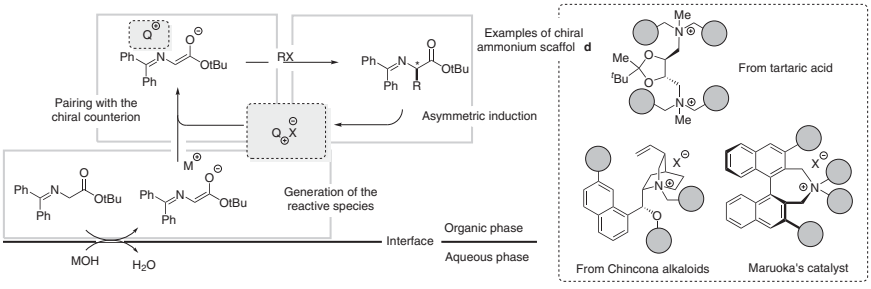

Scheme 5.29 Phase transfer catalysis general mechanism and most common examples of phase transfer catalysts. Source: Takashi and Maruoka [55]/with permission of John Wiley & Sons.

5.4.1 Atropisomeric Synthesis of C—C Biaryls, Heterobiaryls, and Non-biaryls *via* PTC

The desymmetrization of achiral dichloropyrimidine derivatives conducted by Smith's group in 2014 represents a milestone in the history of PTC employed in the preparation of axially chiral biaryls [56]. This was realized with thiophenols as nucleophile and quinine-based salt as catalyst in a biphasic mixture of CCl_4/water (Scheme 5.30). The single C—C bond of **144** involved in the plane of symmetry is converted into a stereogenic axis thanks to the excellent ability of the catalyst in recognizing the pseudo atropisomeric sides of the substrate and directing thiophenol toward the regioselective replacement of one of its chlorine atoms. The arising diastereoisomeric Meisenheimer intermediate possesses also a stereogenic carbon, before its rapid loss in favor of the rearomatization event. Interestingly, pseudoenantiomers of the chiral catalyst showed a preference of delivering the same configuration of the axis; the opposite configuration is achievable changing the pendant group of the quaternary ammonium. A slight excess of tiophenol reacts exclusively with the minor enantiomer **ent-146**, provoking the enhancement of the enantiomeric excess of the desired product.

Later in 2017, the same group realized the first general enantioselective and catalytic approach to enable access to various C_2 biaryl compounds possessing the

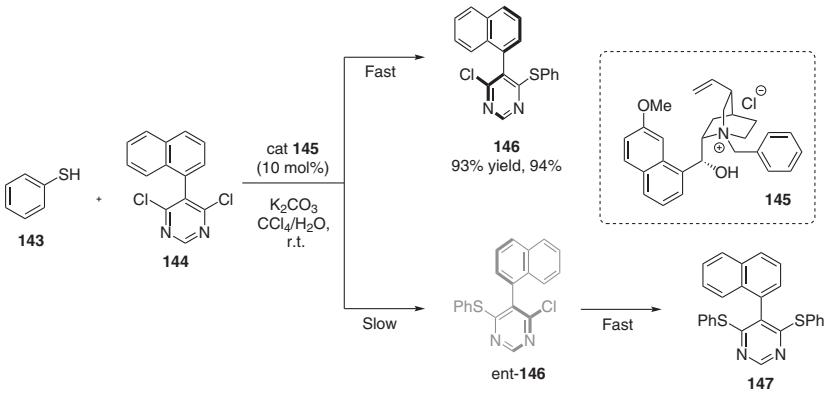

Scheme 5.30 Enantioselective synthesis of atropisomeric biaryls via phase transfer catalyzed nucleophilic aromatic substitution. Source: Smith and co-workers [56]/with permission of John Wiley & Sons.

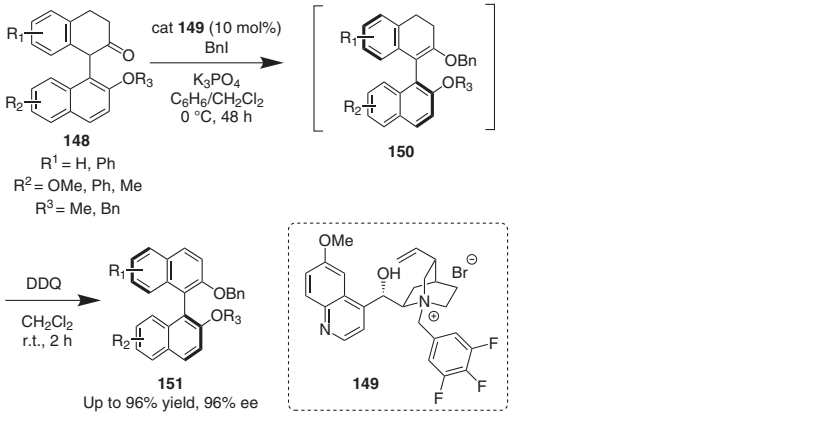

Scheme 5.31 Atroposelective synthesis of biaryls via O-alkylation. Source: Smith and co-workers [57]/with permission of Springer Nature.

BINOL scaffolds via dynamic kinetic resolution of racemic substituted tetralones **148** [57]. The strategy relies on the conversion of the racemic starting material into a biarylic architecture with a defined configuration via two consecutive steps conducted in a one-pot fashion (Scheme 5.31). Within a biphasic alkaline mixture, the racemic mixture of tetralone with point chirality is converted into an equilibrium mixture of two axially chiral enolates. Afterward, the reversible matches with the chiral cation of the quinidine-based catalyst generate two diastereomeric salts possessing yet a fixed configuration of the axis which eventually undergoes the following benzylation under kinetic resolution control. Indeed, the O-alkylation takes place preferentially onto one chiral pair with the effect of definitively locking the free rotation around the C—C bond. The biaryl motif is finally obtained after the oxidation mediated by DDQ, furnishing the desired BINOL scaffold **151**.

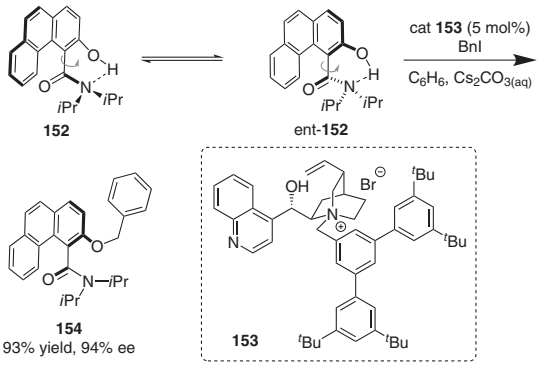

Scheme 5.32 Atroposelective synthesis of axially chiral amides via hydrogen bond-mediated dynamic kinetic resolution. Source: Smith and co-workers [58]/with permission of John Wiley & Sons.

Later in 2019, Smith's group exploited the same approach in the atroposelective synthesis of chiral benzamide derivatives (Scheme 5.32) [58]. The dynamic kinetic resolution is realized thanks to an intramolecular H-bond of the benzamide **152**, which allows the fast rotation of the axis within the reaction time. Computational studies suggested that this interaction lowers the energy of the TS (transition state) of the bond's rotation stabilizing the transient sp^3 character of the nitrogen atom. Erasing this interaction via O-alkylation also provides more steric hindrance around the C—C bond and contributes to enhance the rotational barrier. This strategy was carried out with solid cesium carbonate in benzene and with the assistance of cinchonidinium-based catalyst **153**, which promotes the O-benzylation in an enantioselective fashion.

In 2022, Smith realized the enantioconvergent synthesis of medium-size lactams, which bear both point and axial chirality (Scheme 5.33) [59]. The starting **155** potentially possesses three rotationally restricted bonds and one stereogenic center and

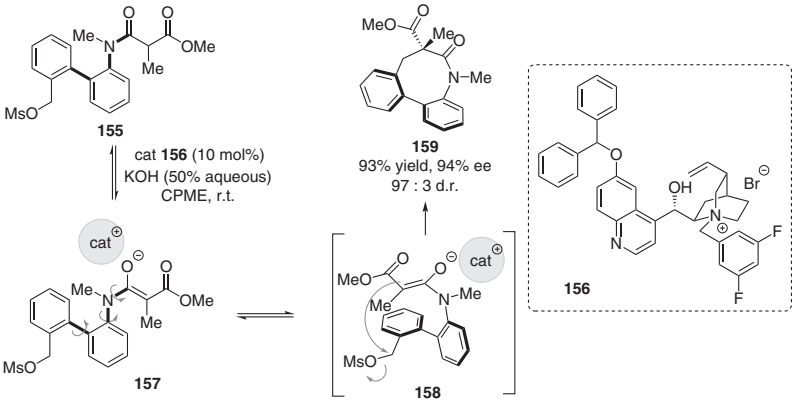

Scheme 5.33 Atroposelective synthesis of medium-size lactams via enantioconvergent PTC. Source: Smith and co-workers [59]/American Chemical Society/CC BY 4.0.

thus exists as a mixture of diastereoisomeric conformers. Nevertheless, when subjected to a basic environment the enolate of **157** is formed, causing both the loss of the stereogenic carbon and the release of the torsional constriction around C—N bond due to the pyramidalization of the amide's nitrogen [60]. At this stage, the conformational isomers are paired with the chiral cation of **157** and all converge into the thermodynamic stereoisomer through rotation of different unlocked bonds. Eventually the enolate is quenched undergoing the stereoselective intramolecular nucleophilic substitution under the control of the chiral counterion of **156**, which establishes the concomitant configuration of both the axis and the center.

When prochiral substrates take part in additional reactions, multiple diastereoisomers may form. Having access to all the stereoisomers is still a current and hard challenge in the field of catalysis, also because often diastereoselectivity is substrate dependent. In 2022, Sparr achieved for the first time the diastereodivergent synthesis of arenes **165** bearing two stereogenic axes (Scheme 5.34) [61]. Intramolecular aldol condensation followed by dehydration and final aromatization carried out in a basic environment allowed the smooth conversion of 1,5 diketone derivatives into ortho disubstituted beta-naphthols. Quinidine/quinine-based catalysts **161**–**164** operating in PTC conditions promoted the two steps in an enantioselective fashion. While pseudoenantiomers of the catalyst led to the formation of opposite enantiomers of the product, changing the benzyl moiety on the quaternary amine with the anthracene motif interestingly allowed the desired diastereodivergence.

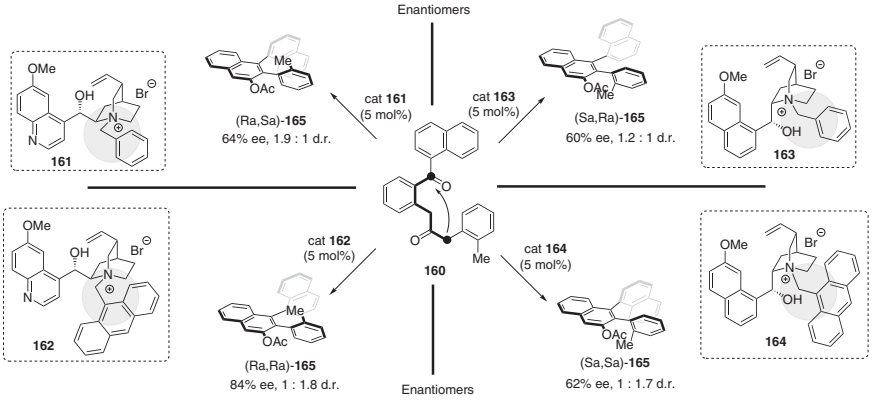

Scheme 5.34 Phase transfer catalyzed arene-forming aldol condensation for the construction of two-axis systems. Source: Sparr and co-workers [61]/with permission of John Wiley & Sons.

In 2019, Bin Tan recognized rotationally restricted alkenes **166** as precursors for the construction of axially chiral 2-arylpyrroles **170** or **176** (Scheme 5.35) [62], whose synthesis lacked any approach until then. The strategy relies on a two-step procedure. The first *N*-allylation/propargylation occurs stereodefinitely promoted by the unusual chiral phase transfer catalyst **167** and is designed for providing sufficient hindrance to lock the rotation around the alkene-arene bond. The resulting enantioenriched intermediate **169** or **175** being activated on the benzylic either

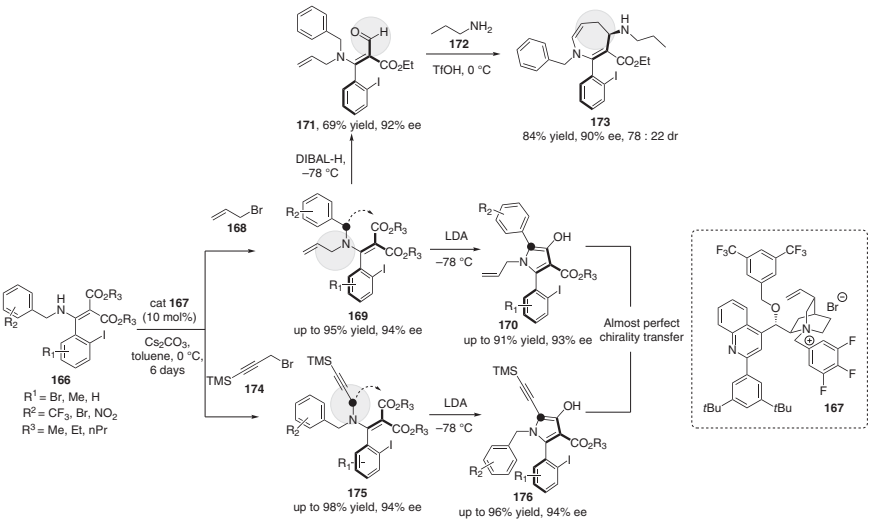

Scheme 5.35 Atroposelective synthesis of 2-arylpyrroles from axially chiral alkenes. Source: Tan and co-workers [62]/with permission of John Wiley & Sons.

propargylic moiety (when available), undergoes a regioselective annulation via LDA-mediated deprotonation. Moreover, 2-arylazepine **173** is achievable through facile manipulation of the noncyclic intermediate **169** followed by the ene reaction.

5.4.2 Atropisomeric Synthesis of C—N Scaffolds *via* PTC

Axially chiral anilides are widely found in nature and may display biological activity [63]. Moreover, the planarization of the nitrogen atom beside sufficiently hindered substituents placed in the ortho position of the aryl ring can cause torsional constrain around the C—N bond. Since 2002 [64, 65], several strategies have been developed to deliver axially chiral anilide derivatives in highly enantioselective fashion, but the scope was limited to *o*-^{t}Bu substituted arenes which allows higher rotational barriers. Nevertheless, during 2012 Maruoka demonstrated the feasibility of chiral salt **179** in the construction of the more valuable ortho-iodo anilide **180** as configurationally stable C—N atropisomers (Scheme 5.36a) [66]. The catalytic cycle begins with the deprotonation of amide **177** with solid KOH followed by ion pairing with the chiral quaternary ammonium cation, which locks the rotation of the pseudo stereogenic C—N axis. The determination of the absolute configuration through X-rays of the product allowed the authors to suggest that the enantioselective addition of the alkylbromide to the chiral salt is controlled by two main features: the preference of the chiral counterion in matching one enantiomer of the anions and its ability to effectively shield one side of the anion with its aryl substituents. In fact, high enantiocontrol is observed when the difference in the bulkiness of the ortho groups of the aryl ring is evident and when catalysts with large substituents are employed. Later, in 2013 Maruoka's group also demonstrated

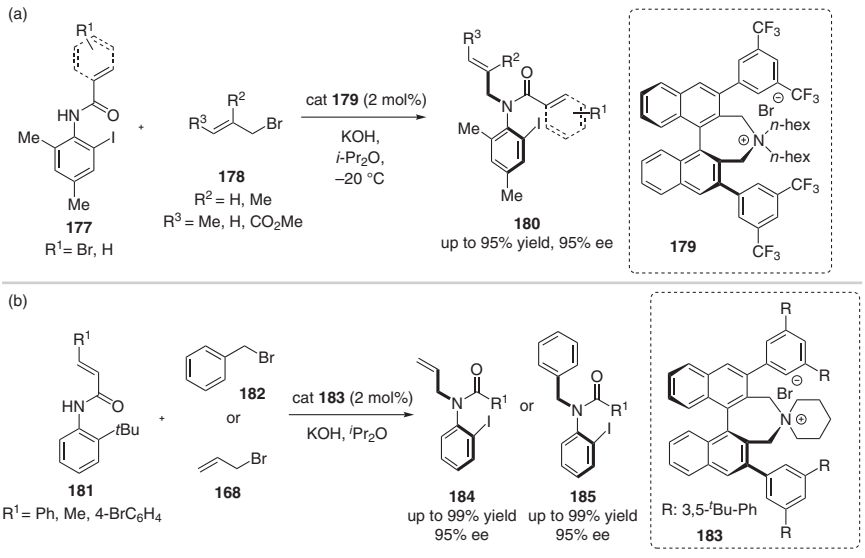

Scheme 5.36 (a) Asymmetric synthesis of atropisomeric o-iodoanilides by PTC. Source: Maruoka and co-workers [66]/with permission of American Chemical Society.
(b) Atroposelective synthesis of anilides via enantioselective alkylation. Source: Maruoka and co-workers [67]/John Wiley & Sons.

that a similar approach is feasible for the atroposelective synthesis of *o*-^{t}Butyl anilide **184** and **185** with **183** as the catalyst (Scheme 5.36b) [67].

5.4.3 Atropisomeric Synthesis of C—O Scaffolds *via* PTC

Despite diaryl ethers may exhibit atropisomerism around C—O bonds, their asymmetric synthesis is still overlooked mainly due to their poor configuration stability. The pioneering studies conducted by Clayden [68] highlighted the steric hindrance factors necessary to increase the rotational barrier around the ether bonds. Afterward, his group was the first to successfully employ a catalytic approach to build configurationally stable diarylethers via enantioselective desymmetrization reaction promoted by enzymes [69]. Following these recent developments, Gustafson and co-workers [70] exploited for the first time the organocatalyst **187** to perform the conversion of substrate **186** into stable atropisomers by phase transfer methylation (Scheme 5.37). The catalyst is a chiral salt provided also of a pivotal thiourea motif which proved to engage critical hydrogen bonds with the anion of **186**, locking its configuration before the moderate enantiocontrolled addition of the nitroalkane occurring toward the side not shielded by the catalyst. This allows the formation of the product **188**-exo, which rapidly equilibrates through gearing mechanism into the more stable conformer **189**-endo.

5.4.4 Atropisomeric Synthesis of N—N Scaffolds *via* PTC

N—N rotationally hampered bonds have been detected in several natural compounds such as Schischkiniin and Dixiamycin B. Although extensive studies on

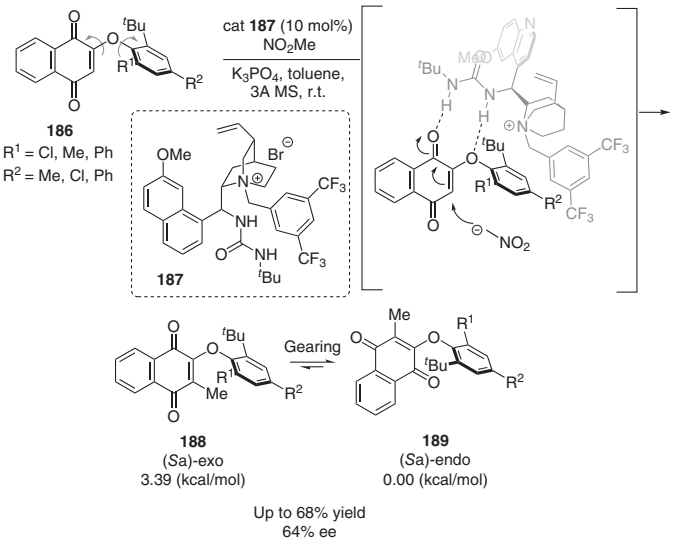

Scheme 5.37 Synthesis of atropisomeric diaryl ethers via PTC alkylation. Source: Gustafson and co-workers [70]/with permission of Georg Thieme Verlag KG.

the nature of atropisomerism arising from such compounds [71] and the evidence that they may exist as configurationally stable enantiomers, the development of asymmetric strategies that described their synthesis have been reported only within the past few years, soon after the pilot work of Rinaldi [72]. In 2022, Bencivenni's group demonstrated an organocatalytic approach to access rotationally restricted tetrasubstituted hydrazides [73]. The one-pot procedure relies on a sequential catalysis promoted by two quinine/quinidine-based catalysts which operate in different reaction conditions (Scheme 5.38). The first stereoselective amination step

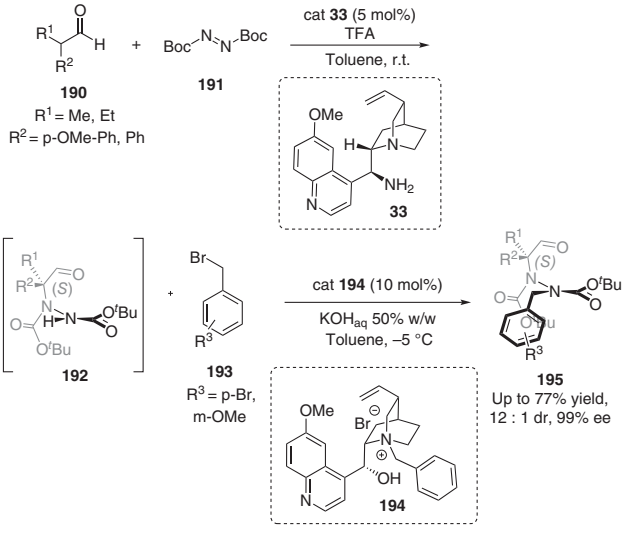

Scheme 5.38 One-pot synthesis of atropisomeric hydrazides with construction of axially chiral N—N bond via PTC. Source: Bencivenni (author).

is mediated by catalyst **33,** which activates the racemic substrate **190** forming the chiral enamine; the following *N*-alkylation is assisted by catalyst **194** in a biphasic mixture and is effective in hampering the free rotation around the trisubstituted hydrazide, furnishing a diastereoenriched mixture of tetrasubstituted hydrazide **195** possessing both point and axial chirality.

In 2022, Li's group employed quinazolinone amides **196** as precursors for the construction of NN atropisomers **199** (Scheme 5.39): [74] the *N*-benzylation performed in PTC conditions is indeed sufficient to restrict the free rotation of the pseudo-stereogenic bond. The authors accurately designed a quinine-based catalyst **198** capable of installing multiple hydrogen bonds to better control the enantioselection. Indeed, computational studies highlight how catalyst **198** in toluene establishes critical bifurcated hydrogen bonds along with π–π interactions, which are responsible for the high level of enantioselection detected.

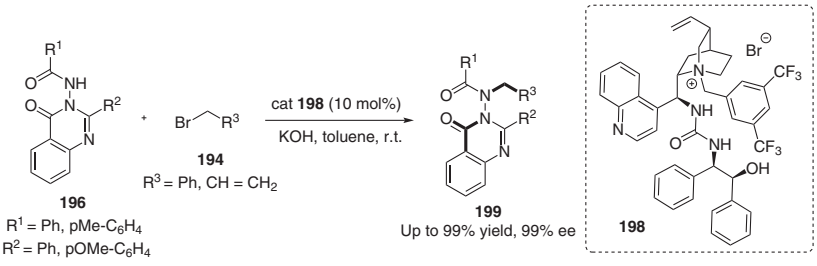

Scheme 5.39 Alkylation in PTC for the construction of atropisomeric quinazolinone derivatives. Source: Li and co-workers [74]/with permission of American Chemical Society.

5.5 Chiral Phosphoric Acids

In 2004, Akyama [75] and Terada [76] showed, independently, the feasibility of chiral phosphoric acid (CPA) possessing a BINOL backbone, of promoting the enantioselective Mannich-type reaction. Since this disclosure, CPAs became progressively a landmark in the field of asymmetric synthesis for their versatility toward such different reactions. Numerous explorations and computational studies during the years suggested different modes of activation [77]; nevertheless, among this variety, activation of the LUMO of the electrophile is supposed to be the most common to happen. Indeed, the phosphoric acid moiety could act as simple hydrogen bond donor either as Brønsted acid along with offering the P=O motif as Lewis basic site, interacting with the reaction partners via dual or bifunctional activation (Scheme 5.40). Although the most employed backbone involves a BINOL scaffold, which further allows to easily install substituent in 3,3′ thus creating a surrogate of the enzyme's chiral pocket, many other skeletons are feasible in bearing the phosphoric acid moiety thus broadening the scope of such class of catalysts.

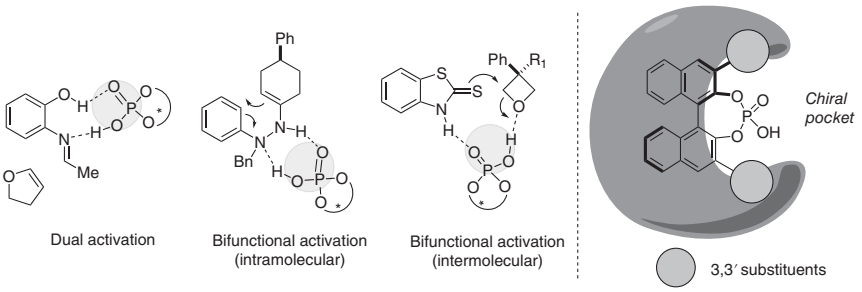

Scheme 5.40 General activation of chiral phosphoric acid catalysis.

5.5.1 Atropisomeric Synthesis of C—C Biaryls and Heterobiaryls *via* CPA

Akyama in 2013 accessed biaryl derivatives via a CPA-mediated desymmetrization reaction (Scheme 5.41) [78]. The achiral tetra-*ortho*-substituted biaryl **200** is voluntarily designed to create an intramolecular network of hydrogen bonds, which provide more structural rigidity and enable interactions with the chiral catalyst in the transition state. The desymmetrization strategy is pursued involving *N*-bromosuccinimide as a source of bromide which is delivered enantioselectively onto the diphenoxy arene by **201**. The product is obtained with excellent

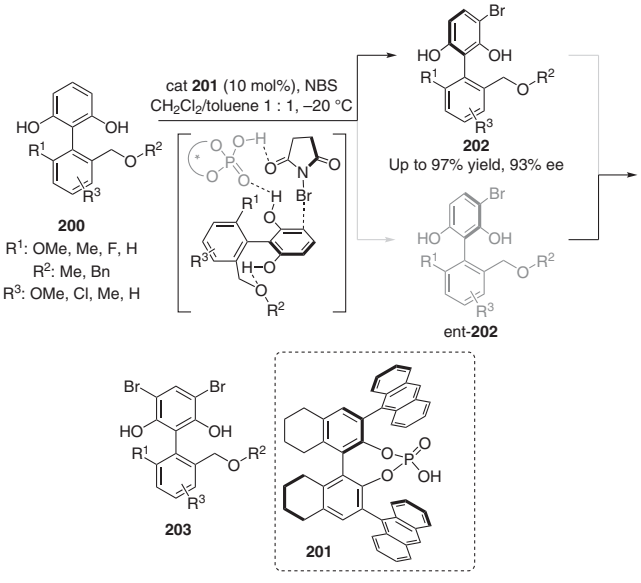

Scheme 5.41 Atroposelective synthesis of biaryls via CPA-catalyzed desymmetrization/kinetic resolution. Source: Akyama and co-workers [78]/with permission of American Chemical Society.

enantiomeric excesses thanks to an efficient kinetic resolution occurring onto the minor enantiomer ent-**202**, which is converted into the achiral dibromide **203**. When the reaction is performed with the corresponding substrate provided by masked OH group, a worse enantioselection along with lower conversion is observed, highlighting the role of hydrogen bonds in both promoting the reaction and arranging a better-organized transition state.

In 2013, Kurti disclosed the first enantioselective synthesis of BINAM derivatives via [3] rearrangement (Scheme 5.42) [79]. Starting from the previous noncatalytic trial reported by Sannicolo in 1985 [80], Kurti designed the asymmetric catalytic strategy employing CPAs. Notably, the best catalysts in terms of yield and enantioselectivity are the more acidic **205** and **206**; in fact, according to computational investigations, the substrate **204** needs to be protonated instead of just engaging hydrogen bonds. Therefore, the catalyst acts as chiral counterion, controlling the spatial approaching of the two aryl rings which occurs within its chiral pocket. The configuration of the stereogenic axis arising from the C—C formation is maintained through a very fast rearomatization event before any further bond rotation occurs, avoiding any loss of chiral information. This remarkable reaction enables the direct construction of the axis with good to high level of enantiocontrol starting from common 1,2-diaryl hydrazines.

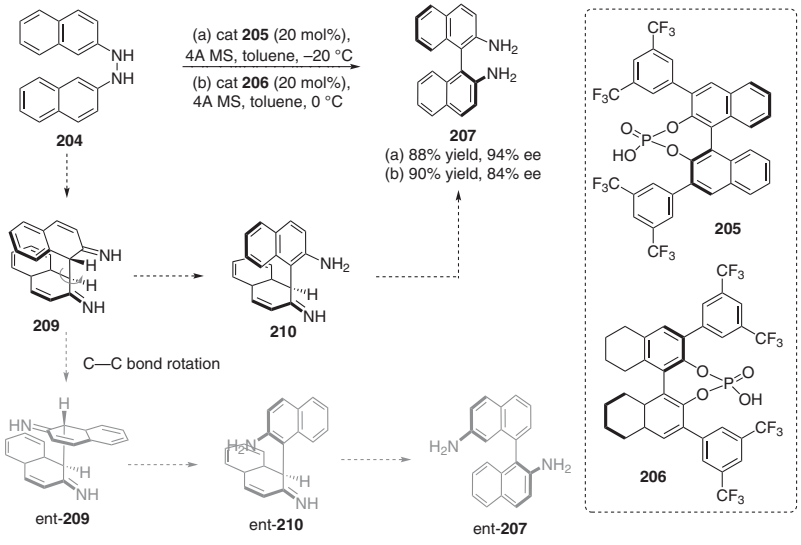

Scheme 5.42 Enantioselective synthesis of BINAM derivatives via direct construction of chiral axis through CPA catalysis. Source: Kurti and co-workers [79]/with permission of American Chemical Society.

After the pioneering work of Akyama and Kurti, in 2015 Tan described a general procedure to access privileged axially chiral biarylic diols via CPA-mediated addition of β-naphthols to quinones [81]. The chiral **213** is supposed to behave as a dual catalyst, guiding the addition of the enantiotopic faces of the reaction partners stereoselectively. The stereogenic center on **241** arising along with the C—C formation

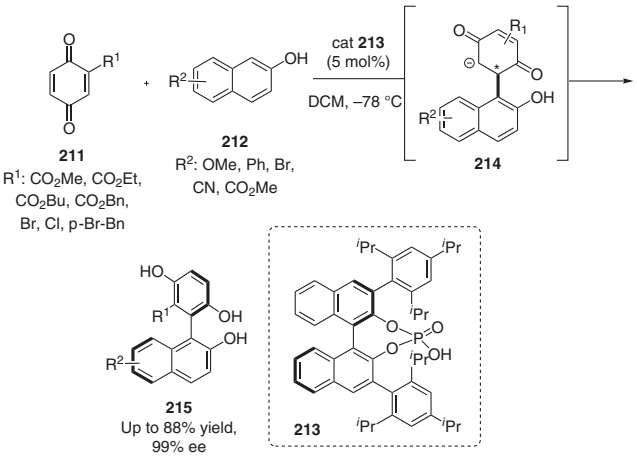

Scheme 5.43 Asymmetric synthesis of biaryldiols via CPA-catalyzed arylation of naphthols. Source: Tan (co-author).

is rapidly lost in favor of the aromatization process, furnishing the desired biaryl motif. Such protocols will tolerate a halogen atom placed instead of the ester moiety, allowing further derivatization of the product (Scheme 5.43).

In 2022, List reported a benchmark work on the enantioselective synthesis of tertiary silyl ethers bearing chirality on the silicon atom [82]. Inspired by this approach, in 2023 Bin Tan's group exported such knowledge into the development of the asymmetric synthesis of axially chiral siloxanes [83]. The strategy relies on the releasing of relatively high tension of the five-membered ring of **216** involving the silicon atom through a ring-opening event triggered by the regioselective protonation of the alpha carbon (Scheme 5.44). In this context, *N*-triflylphosphoramides **218** realized the rate- and stereodetermining protonation step, indeed providing the proper chiral environment that guaranteed excellent enantiocontrol over the formation of the axially chiral biaryl. In the case of nonsymmetrical biaryl, a mixture of regioisomers is generated (**220a** and **220b**); besides, not symmetrical silafluorenes are converted into siloxanes **220c** bearing a chiral silicon atom diastereoselective.

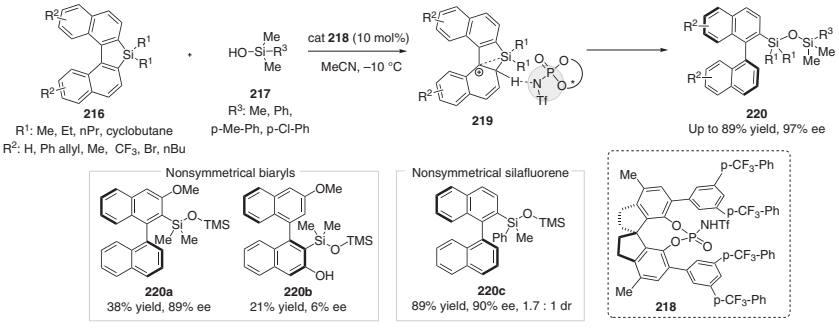

Scheme 5.44 Enantioselective synthesis of axially chiral biaryl siloxanes via Si—C_{Aryl} bond functionalization. Source: Tan (co-author).

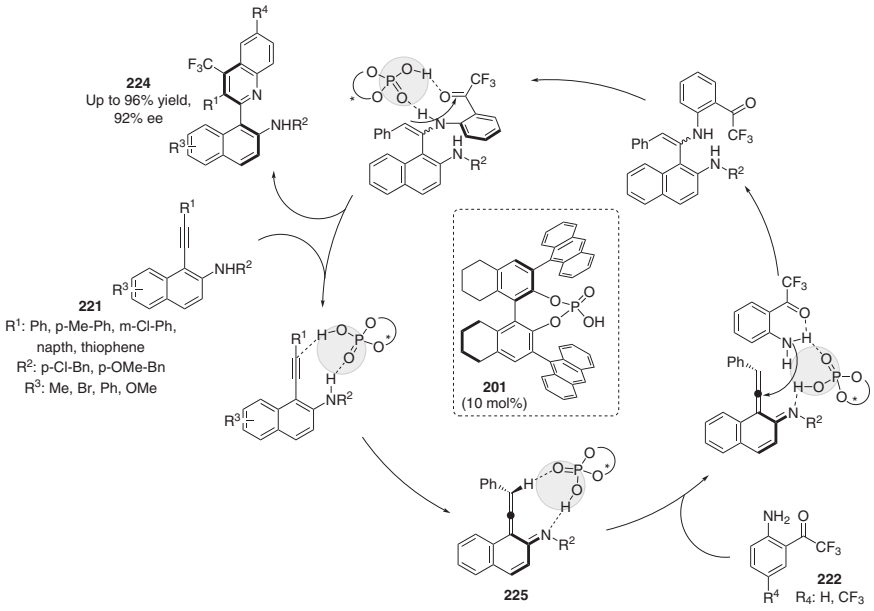

Scheme 5.45 Asymmetric heteroannulation of alkenes via CPA catalysis for the construction of axially chiral IAN analogs. Source: Tan (co-author).

In 2020, Tan exploited CPAs to access enantioenriched IAN analogs **224** through the transient formation of VQM intermediate (Scheme 5.45) [84]. Such compounds represent promising catalysts because of their architecture that has the Lewis basic site of the nitrogen atom in proximity to the stereogenic axis. CPA **201** is supposed to generate the reactive VQM **225** via 1,5-H transfer from ortho-alkynyl-naphthylamine **221** and assist, through a hydrogen network, the addition of ortho trifluoroacetyl aniline **222** and the following stereodetermining annulation event. The scope was revealed to be very broad, but the protocol is limited to anilines provided of CF_3 moiety and *N*-benzylated naphthylamine.

In 2022, Zhou's group recognized CPA as a bifunctional catalyst to promote the [3 + 2] cycloaddition between 3-alkynil-indole derivatives **226** and azonaphthalenes **227** [85]. Various alkynyl indoles smoothly undergo the annulation to provide highly enantioenriched products at −50 °C in chloroform (Scheme 5.46). Moreover, 2- and 7-substituted indoles yielded diastereisomeric mixtures (**229a** and **229b**), which indicates that the free rotation of the other C—C could be hampered. The first C—C bond formation, which forges two contiguous stereogenic elements (point and axis), is the stereodetermining event. This former stereogenic center is retained during the evolution of subsequent different intermediates and converted into a single stereogenic axis after the last rearomatization event.

5.5.2 Atropisomeric Synthesis of C—N Scaffolds *via* CPA

In 2019, Miller reported the same ability of a peptide-based phosphoric acid **231** and a more common BINOL-based phosphoric acid **232** in promoting the intramolecular

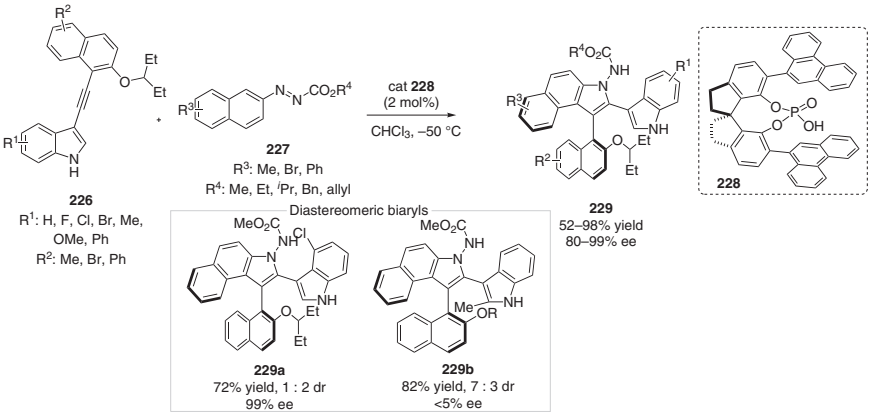

Scheme 5.46 Axially chiral indole-based biaryls via asymmetric cycloaddition with CPA. Source: Zhou (co-author).

cyclodehydration of ortho-substituted aniline derivative **230**, delivering the heterobiaryl **233** in high enantioenriched form (Scheme 5.47) [86]. Besides the excellent results in yielding the desired benzimidazoles with high enantiomeric excess, this study offers a deep insight into the different modes of action exploited by the chiral catalysts. Although in both cases the catalysis is promoted by the phosphoric acid moiety, experimental investigations along with computational calculations, suggested that the more flexible peptide-based phosphoric acid could arrange its conformation following the steric demand of the substrates, thus sometimes performing better than the BINOL-based phosphoric acid which is shown to discriminate the stereogenic axis via classical steric repulsion. Moreover, this study demonstrated how the strategic assembly of the amino acids gives rise to diverse peptides, which may be more versatile with respect to the common catalyst known so far.

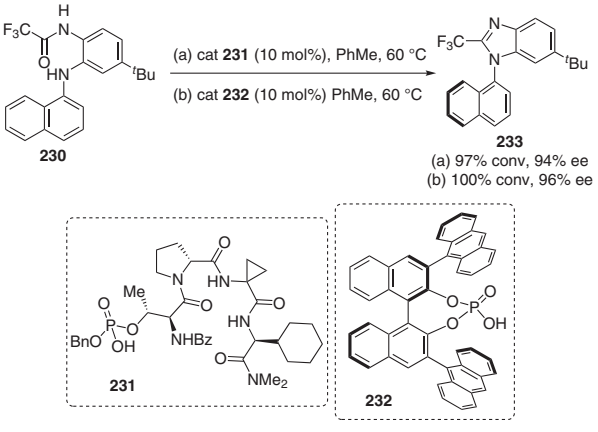

Scheme 5.47 Atroposelective synthesis of heterobiaryls via CPA catalyzed cyclodehydration of aniline derivatives. Source: Miller and co-workers [86]/with permission of American Chemical Society.

Later, in 2021 Bin Tan pursued the enantioselective synthesis of *N*-arylbenzylimidazoles via domino catalysis (Scheme 5.48) [87]. The reaction proceeds smoothly in six days at room temperature or three days at 45 °C in the presence of the CPA **237**, which promotes the last stereodetermining intramolecular annulation step. During the reaction, a first C—N bond is forged between the reaction partners, followed by oxidation mediated by an excess of nitroarene or via 1,5 hydrogen shift, delivering the crucial intermediate **241** which undergoes the intramolecular annulation via the construction of the C—N bond. The consecutive oxidative rearomatization enables the formation of the desired axially chiral C—N atropisomer. Despite for *N*-arylglycine **234** is sufficient an excess of nitroarene which also works as an oxidant, *N*-benzyl-2-naphthylamines **235** generates, during the reaction, a more inert intermediate that requires biscyclopentylcarbonyl copper as an external oxidant to proceed through the ring formation. Noteworthy, the catalyst induces the opposite configuration of the stereogenic axis starting from *N*-benzyl-2-naphthylamines with respect to *N*-arylglycine, maybe due to π–π interaction in the TS.

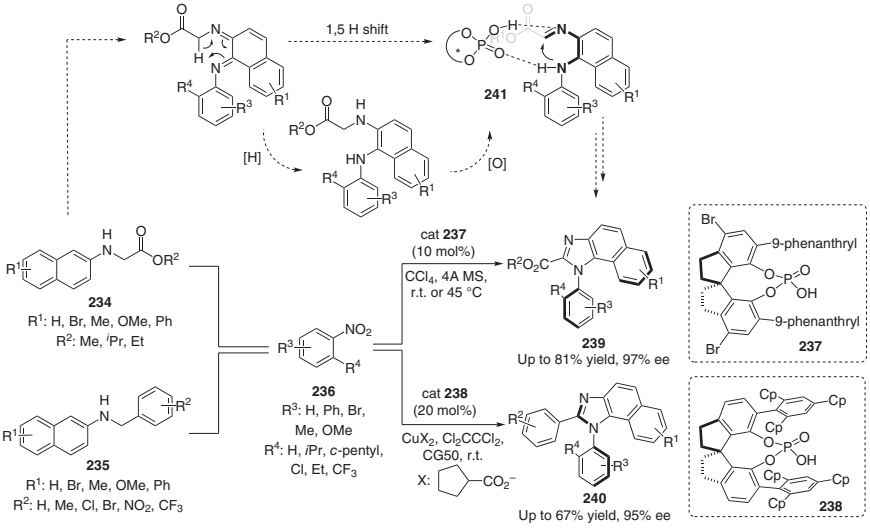

Scheme 5.48 Enantioselective synthesis of axially chiral *N*-arylbenzimidazoles. Source: Tan and co-workers [87]/with permission of John Wiley & Sons.

o-Alkynylanilines have been considered a privileged scaffold to access substituted indoles via metal-catalyzed *5-endo-dig* cyclization [88]. Moreover, within the last century numerous reports described the enantioselective version of such transformation [89], but only two examples involved chiral organic molecules as catalysts. In 2019, Yan for first demonstrated that a Brønsted base could effectively replace the role of the metal in the cyclization process, which proceeds through a strategic VQM intermediate [31]. Afterward, in 2022 Ye's group disclosed the atroposelective annulation of *o*-anylino ynamide mediated by CPAs (Scheme 5.49) [90]. The CPA catalyst **243** works in mild conditions to deliver the atropisomeric indoles **244** with excellent yield and enantiomeric excess within one hour at −40 °C. Computational

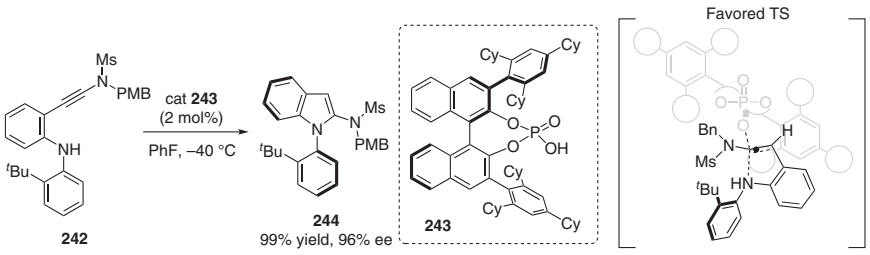

Scheme 5.49 Atroposelective cyclization of ynamides catalyzed by chiral phosphoric acid. Source: Ye and co-workers [90]/with permission of John Wiley & Sons.

studies along with experimental observations suggested a novel mode of activation, which relies on the addition of the OH moiety of the catalyst onto the alkyne group, followed by an irreversible and stereodetermining nucleophilic vinylic substitution carried out by the nitrogen of the diarylamine. Further investigations revealed that the ortho *tert*-butyl group is the element that discriminates the energy of the two diastereomeric TSs, in fact when it is replaced with a less steric hindered group a lower enantioselection is observed.

After the landmark work of Jørgensen [39] in the atroposelective synthesis of axially chiral C—N bond involved in non-biaryl compounds, in 2019 Zhang reported the enantioselective amination of 2-aminonaphthol derivatives **245** mediated by CPA **247** (Scheme 5.50) [91]. The substrate **245** was accurately designed to possess a free NH provided of a benzylic moiety to better interact with the catalyst via H-bonds and π–π packing in the transition state. The formation of the addition intermediate that also possesses a stereogenic carbon is followed by a rapid tautomerization, which finally realizes the point to axial chirality transfer. Besides the critical importance of the NH in installing tight interaction with the catalyst

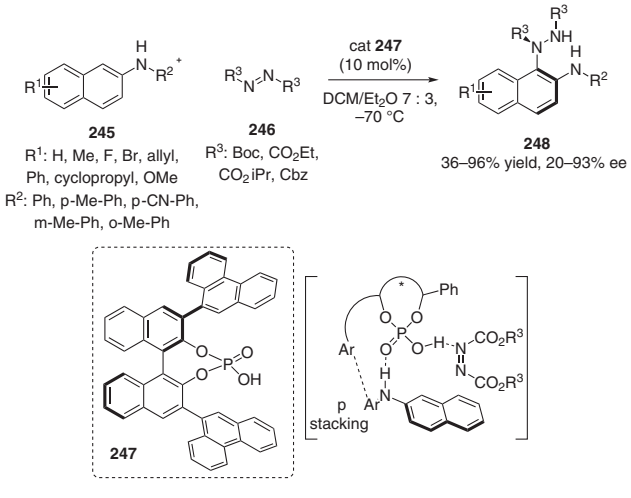

Scheme 5.50 Synthesis of atropisomeric C—N non-biaryls via CPa-catalyzed amination. Source: Zhang and co-workers [91]/with permission of Springer Nature.

thus enhancing the enantiocontrol, it was proved that the intramolecular H-bond between the NH and the carbamate moiety is beneficial for the configurational stability of the product.

In 2009, Kawabata showed that diaryl amines could exist as configurationally stable atropisomers [92]. Despite the potential to exhibit a dual contiguous axis, a strategic intramolecular hydrogen bond may simplify the number of conformers and also raise the rotational barrier, along with excluding the gearing effect. Taking these considerations in mind, in 2020 Gustafson designed, for the first time, an enantioselective synthesis of diarylamine-like scaffolds via halogenation strategy (Scheme 5.51) [93]. The catalyst **250** is found to establish critical hydrogen bonds with the reaction partners, both activating the source of the halogen donor and the nucleophile which acts as an enamine. π–π interaction among the catalyst and the quinone **249** is the origin of the discrimination between S_a and R_a axes of the product. As expected, computational studies demonstrated the presence of a tight intramolecular bond on the *exo* product **251**, which is responsible for higher rotational barrier.

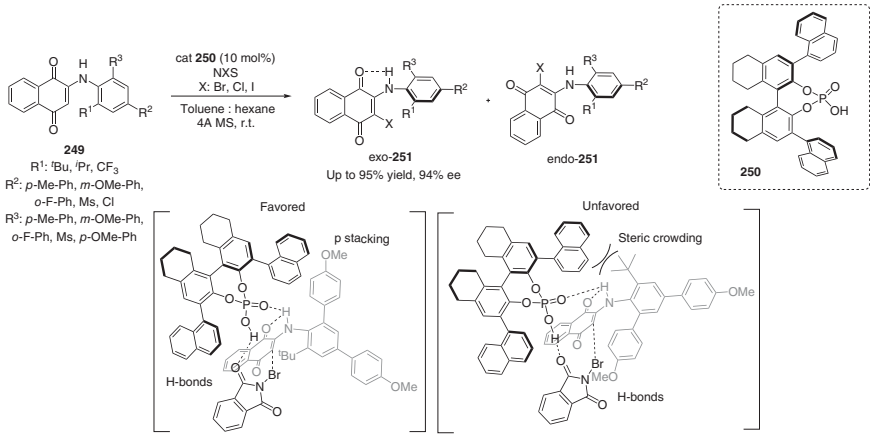

Scheme 5.51 Atroposelective synthesis of *N*-aryl quinoid derivatives via CPA catalysis. Source: Gustafson and co-workers [93]/with permission of American Chemical Society.

5.5.3 Atropisomeric Synthesis of C—O Scaffolds *via* CPA

The pioneering investigations conducted by Clayden [13] in 2006 officially opened the route to the comprehension of the atropisomerism arising from hindered diarylethers. Such disclosure triggered the appeal to obtain these compounds in an asymmetric fashion. Clayden for first accomplished the enantioselective synthesis of axially chiral diarylethers through an enzymatic approach [14], followed by Gustafson [15] in 2018 who successfully hampered the free rotation of *exo*-**188** (Scheme 5.37) around the C—O axis exploiting PTC catalysis. After these pivotal reports, in 2023 Zeng [94] and Yang [95] independently developed the synthesis of tetrasubstituted diarylethers mediated by CPAs. Inspired by the enzymatic desymmetrization of diacarbaldehydes realized by Clayden, the Zeng's group performed a similar transformation but via an asymmetric transfer hydrogenation

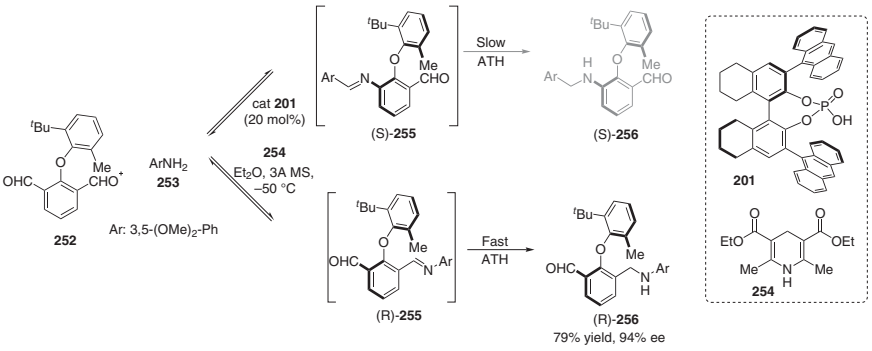

Scheme 5.52 Asymmetric transfer hydrogenation with CPA for the construction of diaryl ethers. Source: Zeng (co-author).

(ATH) approach (Scheme 5.52). The combination of **201** and Hantzsch ester **254** and arylamine **252** in diethylether at −50 °C allowed the preparation of stable axially chiral diarylethers **256** (around 29.9 kcal/mol) via reductive amination of the dicarbaldehydes. Insight into the mechanism revealed a dynamic kinetic resolution regime: the formation of the imine **255** is not stereocontrolled and just one of the enantiomers is selectively converted into the product.

Shortly after, Yang exploited the desymmetrization strategy for the conversion of the rigid achiral diaryl ethers **257** into stable atropisomers (Scheme 5.53) [95]. In this case, a complementary approach takes place, where the electron-rich arene of the starting material is subjected to electrophilic aromatic substitution in the presence of azodicarboxylates. The CPA **259** promotes the desymmetrization event

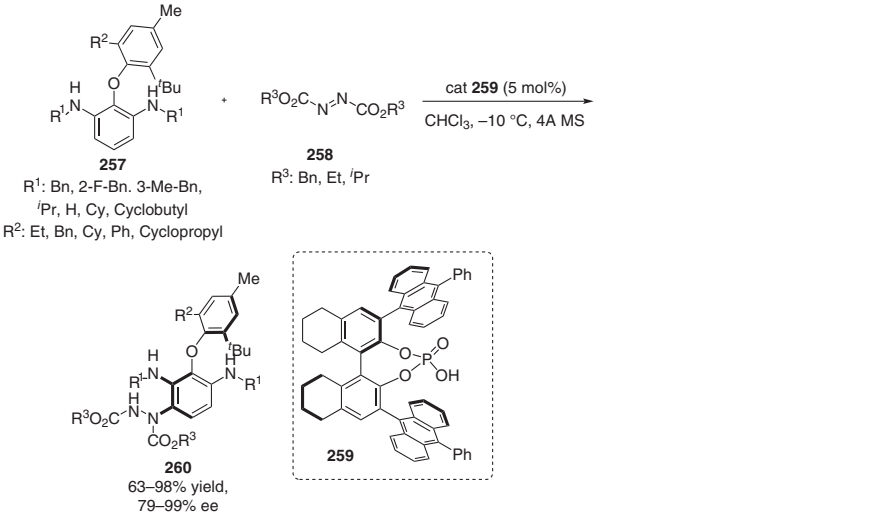

Scheme 5.53 CPA-catalyzed desymmetrization for the enantioselective synthesis of atropisomeric diaryl ethers. Source: Yang and co-workers [95]/with permission of John Wiley & Sons.

in an excellent stereoselective fashion, being able to recognize the enantiotopic sides of the aryl ring. Although electron-deficient aryls are not suitable for the amination, this method was revealed to be highly tolerant toward both diverse functional groups installed into the inert arene ring and different substituents bore by the amine moiety. The same catalyst could also resolve a racemic mixture of nonsymmetrical diarylether, with an *s* factor up to 198.

5.5.4 Atropisomeric Synthesis of C—B Scaffolds *via* CPA

Compounds possessing rotational constrain around C—B bond are still little explored. In this context, B-aryl-1,2-azaborines represent a potential C—B atropisomer but their asymmetric syntheses still lack a general approach. The B—N motif makes the six-membered ring isoelectronic to benzene [96]; therefore, the entire scaffold may be treated as a biaryl system. Nevertheless, the unique features of the heteroaromatic ring and the longer C—B bond [97] compared to C—C [78] and C—N [86] bonds make their asymmetric synthesis challenging. Indeed, before the pioneering contribution of Bin Tan, configurationally stable B-aryl-1,2-azaborine have been isolated only via HPLC resolution on a chiral stationary phase. In 2021, Tan's group recognized the desymmetrization strategy as the best approach to achieve enantiomerically pure B-aryl-1,2-azaborines **263** [98]. The substrate was rationally designed to be provided of strategic NH and OH moieties, which may establish a network of hydrogen bonds with both the catalyst and the electrophile. This proved to be crucial in achieving high enantiocontrol. Indeed, the CPA **262** guides the approach of **260** to **261** delivering the product within only 10 minutes in an elevated enantioenriched form, despite the presence of a strong background reaction (Scheme 5.54). Investigation of the mechanism evidenced a linear effect; therefore, it is noteworthy to highlight how just one molecule of the catalyst is involved in the TS and could effectively transfer remotely its chiral information.

5.5.5 Atropisomeric Synthesis of N—N Scaffolds *via* CPA

The N—N bond is ubiquitous in nature and its configurational stability has been widely proven. The first enantioselective synthesis of heterobiarylic N—N compounds was carried out by Zhang and Shi in 2022 who proposed a *de novo* ring construction via Paal–Knorr reaction to prepare both atropisomeric indole-pyrrole and bispyrrole scaffolds [99]. Starting from indoles **264** or pyrrole **268** already provided of the N—N bond, the CPA **266** promotes the stereoselective cyclization process that involves the free amino group and the tricarbonyl compound. The products are delivered with elevated yields and enantiomeric excesses and exhibit a high rotational barrier (up to 52.20 kcal/mol), which makes them suitable for different purposes, such as novel drugs or catalysts (Scheme 5.55).

A similar strategy was exploited by Liu for the atropisomeric synthesis of C2 symmetrical bisquinazoline analogs via ring formation [100]. The CPA promotes the condensation of the aldehyde in order to furnish the quinazoline scaffold and the stereogenic N—N axis.

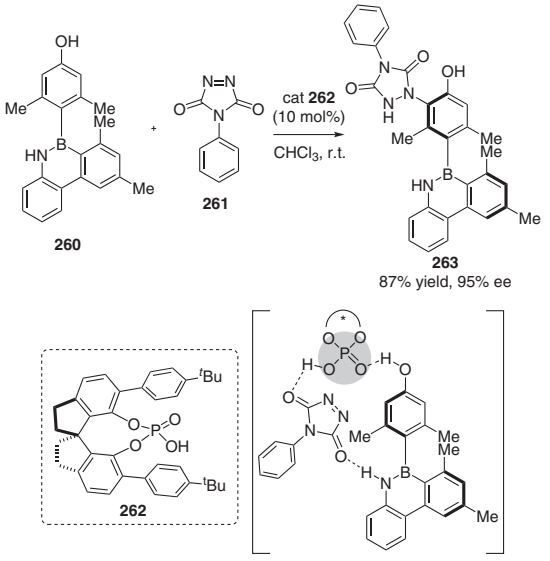

Scheme 5.54 Atroposelective synthesis of B-aryl-1,2-azaborines through CPA-catalyzed desymmetrization. Source: Tan (co-author).

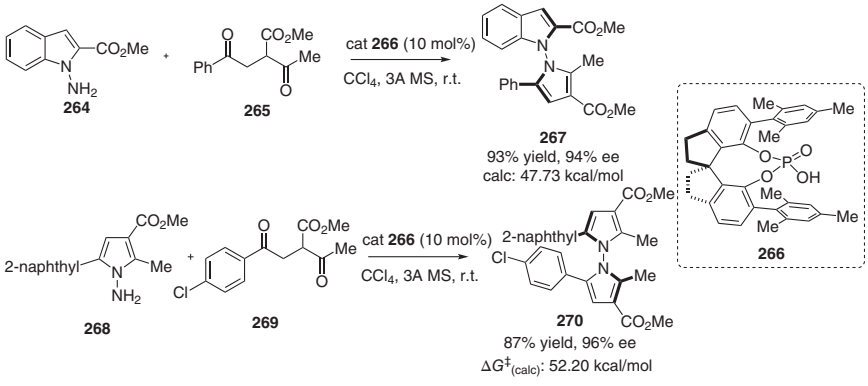

Scheme 5.55 Atroposelective synthesis of axially chiral pyrrolindoles and bispyrroles through CPA-catalyzed *de novo* ring formation. Source: Zhang and Shi (co-author).

5.6 Conclusions

The literature selection presented herein aims to offer an overview of the excellent feasibility of small organic molecules in promoting a wide range of enantioselective transformations involving the formation of a stereogenic axis, beyond the more common organocatalytic strategies previously designed to form new stereogenic centers. Atropisomers featuring diverse restricted bonds (C—C, C—N, C—O, C—B, and N—N) as well as bearing different scaffolds can be efficiently obtained through organocatalytic protocols exploiting the complementary activation methods that these molecules can provide.

Remarkably, in the noteworthy evolution of organocatalysts, a large variety of atropisomers have found significant utilities for catalyzing atroposelective transformations themselves, suggesting that further breakthroughs can still be expected from nowadays research in expanding fields like organocatalysis and atropisomers.

References

1 Wagner, J., Lerner, R.A., and Barbas, C.F. (1995). *Science* 270: 1797–1800.
2 Vogel, P., Lam, Y.H., Simon, A., and Houk, K.N. (2016). *Catalysts* 6: 128.
3 Portolani, C., Centonze, G., Righi, P., and Bencivenni, G. (2022). *Acc. Chem. Res.* 55: 3551–3571.
4 Melchiorre, P., Marigo, M., Carlone, A., and Bartoli, G. (2008). *Angew. Chem. Int. Ed.* 47: 6138–6171.
5 Bringmann, G., Mortimer, A.J., Keller, P.A. et al. (2005). *Angew. Chem. Int. Ed.* 44: 5384–5427.
6 Link, A. and Sparr, C. (2014). *Angew. Chem. Int. Ed.* 53: 5458–5461.
7 Lotter, D., Neuburger, M., Rickhaus, M. et al. (2016). *Angew. Chem. Int. Ed.* 55: 2920–2923.
8 Witzig, R.M., Fäseke, V.C., Häussinger, D., and Sparr, C. (2019). *Nat. Catal.* 2: 925–930.
9 Koide, H. and Uemura, M. (1998). *Chem. Commun.* 2483–2484.
10 Clayden, J. and Wah, L.L. (1999). *Angew. Chem. Int. Ed.* 38 (17): 2556–2558.
11 Chan, V., Kim, J.G., Jimeno, C. et al. (2004). *Org. Lett.* 6 (12): 2051–2053.
12 Adams, R. and Miller, M.W. (1940). *J. Am. Chem. Soc.* 62: 53–56.
13 Kawabata, T., Yahiro, K., and Fuji, K. (1991). *J. Am. Chem. Soc.* 113: 9694–9696.
14 Zheng, S.C., Wu, S., Zhou, Q. et al. (2017). *Nat. Commun.* 8: 15238.
15 (a) Nakamura, M. and Oki, M. (1975). *Bull. Chem. Soc. Jpn.* 48: 2106–2111. (b) Yamamoto, G., Nakamura, M., and Oki, M. (1975). *Bull. Chem. Soc. Jpn.* 48: 2592–2596.
16 Ford, W.T., Thompson, T.B., Snoble, K.A.J., and Timko, J.M. (1975). *J. Am. Chem. Soc.* 97: 95.
17 Lomas, J.S. and Dubois, J.E. (1976). *J. Org. Chem.* 41: 3033.
18 Wu, X., Witzig, R.M., Beaud, R. et al. (2021). *Nat. Catal.* 4: 457.
19 Di Iorio, N., Filippini, G., Mazzanti, A. et al. (2017). *Org. Lett.* 19: 6692–6695.
20 Bertuzzi, G., Corti, V., Izzo, J.A. et al. (2022). *J. Am. Chem. Soc.* 144 (2): 1056–1065.
21 Curran, D.P., Qi, H., Geib, S.J., and DeMello, N.C. (1994). *J. Am. Chem. Soc.* 116: 3131.
22 Di Iorio, N., Righi, P., Mazzanti, A. et al. (2014). *J. Am. Chem. Soc.* 136: 10250.
23 Tampellini, N., Righi, P., and Bencivenni, G. (2021). *J. Org. Chem.* 86: 11782.
24 Eudier, F., Righi, P., Mazzanti, A. et al. (2015). *Org. Lett.* 17: 1728–1731.
25 Corti, V., Thøgersen, M.K., Enemærke, V.J. et al. (2022). *Chem. Eur. J.* 28: e202202395.
26 Gustafson, J.L., Lim, D., and Miller, S.J. (2010). *Science* 328: 1251–1255.

27 Moliterno, M., Cari, R., Puglisi, A. et al. (2016). *Angew. Chem. Int. Ed.* 55: 6525–6529.

28 Coombs, G., Sak, M.H., and Miller, S.J. (2020). *Angew. Chem. Int. Ed.* 59: 2875–2880.

29 Raut, V.S., Jean, M., Vanthunye, N. et al. (2017). *J. Am. Chem. Soc.* 139: 2140–2143.

30 Bao, X., Rodriguez, J., and Bonne, D. (2020). *Chem. Sci.* 11: 403–408.

31 Peng, L., Xie, C., Li, S. et al. (2019). *Angew. Chem. Int. Ed.* 58: 17199–17204.

32 Chang, Y., Xie, C., Liu, H. et al. (2022). *Nat. Commun.* 13: 1933.

33 Jia, S., Chen, Z., Zhang, N. et al. (2018). *J. Am. Chem. Soc.* 140: 7056–7060.

34 Li, D., Tan, Y., Peng, L. et al. (2018). *Org. Lett.* 20 (16): 4959–4963.

35 Huang, A., Zhang, L., Li, D. et al. (2019). *Org. Lett.* 21: 95–99.

36 Li, S., Xu, D., Hu, F. et al. (2018). *Org. Lett.* 20 (23): 7665–7669.

37 Tan, Y., Jia, S., Hu, F. et al. (2018). *J. Am. Chem. Soc.* 140: 16893–16898.

38 Wu, S., Xiang, S.H., Li, S. et al. (2021). *Nat. Catal.* 4: 692–702.

39 Brandes, S., Bella, M., Kjoersgaard, A., and Jørgensen, K.A. (2006). *Angew. Chem. Int. Ed.* 45: 1147–1151.

40 Diener, M.E., Metrano, A.J., Kusano, S., and Miller, S.J. (2015). *J. Am. Chem. Soc.* 137: 12369–12377.

41 Zhang, J.W., Xu, J.H., Cheng, D.J. et al. (2016). *Nat. Commun.* 7: 10677.

42 Di Iorio, N., Soprani, L., Crotti, S. et al. (2017). *Synthesis* 49: 1519–1530.

43 Di Iorio, N., Champavert, F., Erice, A. et al. (2016). *Tetrahedron* 72 (34): 5191–5201.

44 Li, S.L., Yang, C., Wu, Q. et al. (2018). *J. Am. Chem. Soc.* 140: 12836–12843.

45 Yang, G.H., Zheng, H., Li, X., and Cheng, J.P. (2020). *ACS Catal.* 10: 2324–2233.

46 Zheng, G., Li, X., and Cheng, J.P. (2021). *Org. Lett.* 23: 3997–4001.

47 Lu, S., Ng, S.V., Lovato, K. et al. (2019). *Nat. Commun.* 10: 3061.

48 Kitagawa, O., Fujita, M., Kohriyama, M. et al. (2000). *Tetrahedron Lett.* 41: 8539–8544.

49 Liu, H., Feng, W., Kee, C.W. et al. (2010). *Adv. Synth. Catal.* 352: 3373.

50 Centonze, G., Portolani, C., Righi, P., and Bencivenni, G. (2023). *Angew. Chem. Int. Ed.* 62: e202303966.

51 Mei, G.J., Wong, J.J., Zheng, W. et al. (2021). *Chem* 7: 2743–2757.

52 Lin, W., Zhao, Q., Li, Y. et al. (2022). *Chem. Sci.* 13: 141–148.

53 Starks, C.M. (1971). *J. Am. Chem. Soc.* 93: 195–199.

54 Sasson, Y. and Neumann, R. (ed.) (1997). *Handbook of Phase-Transfer Catalysis*. London: Blackie Academic & Professional.

55 Takashi, O. and Maruoka, K. (2007). *Angew. Chem. Int. Ed.* 46: 4222–4266.

56 Armstrong, R.J. and Smith, M.D. (2014). *Angew. Chem. Int. Ed.* 53: 12822–12826.

57 Jolliffe, J.D., Armstrong, R.D., and Smith, M.D. (2017). *Nat. Chem.* 9: 558–562.

58 Fugard, J.A., Lahdenperä, S.K.A., Tan, S.J.J. et al. (2019). *Angew. Chem. Int. Ed.* 58: 2795–2798.

59 Du, J.Y., Balan, T., Claridge, T.D.W., and Smith, M.D. (2022). *J. Am. Chem. Soc.* 144: 14790–14797.

60 Mandel, J., Pan, X., Hay, E.B. et al. (2013). *J. Org. Chem.* 78: 4083–4089.
61 Moser, D. and Sparr, C. (2022). *Angew. Chem. Int. Ed.* 61: e202202548.
62 Wang, Y.B., Wu, Q.H., Zhou, Z.P. et al. (2019). *Angew. Chem. Int. Ed.* 58: 13443–13447.
63 Paul, B., Butterfoss, G.L., Boswell, M.G. et al. (2011). *J. Am. Chem. Soc.* 133: 10910–10919.
64 Osamu, K., Kohriyama, M., and Taguchi, T. (2002). *J. Org. Chem.* 67: 8682–8684.
65 Ken, T., Takeishi, K., and Noguchi, K. (2006). *J. Am. Chem. Soc.* 128: 4586–4587.
66 Seiji, S., Liu, K., and Maruoka, K. (2012). *J. Am. Chem. Soc.* 134: 916–919.
67 Liu, K., Wu, X., Kan, S.J. et al. (2013). *Chem. Asian J.* 8: 3214–3221.
68 Betson, M.S., Clayden, J., Worrall, C.P., and Peace, S. (2006). *Angew. Chem. Int. Ed.* 45: 5803–5807.
69 Yuan, B., Page, A., Worrall, C.P. et al. (2010). *Angew. Chem. Int. Ed.* 49: 7010–7013.
70 Dinh, A.N., Noorbehesht, R.R., Toenjes, S.T. et al. (2018). *Synlett* 29: 2155–2160.
71 (a) Srivastava, A., Srivastava, V., Verma, S.M., and Subramanian, E. (1994). *J. Org. Chem.* 59: 3560–3563. (b) Atkinson, R.S., Barker, E., Price, C.J., and Russell, D.R. (1994). *J. Chem. Soc. Chem. Commun.* 10: 1159–1160.
72 Amabili, P., Amici, A., Campisi, G. et al. (2018). *Eur. J. Chem.* 2018: 6524–6536.
73 Portolani, C., Centonze, G., Luciani, S. et al. (2022). *Angew. Chem. Int. Ed.* 61: e202209895.
74 Pan, M., Shao, Y.B., Zhao, Q., and Li, X. (2021). *Org. Lett.* 24: 374–378.
75 Akiyama, T., Itoh, J., Yokota, K., and Fuchibe, K. (2004). *Angew. Chem. Int. Ed.* 43: 1566–1568.
76 Uraguchi, D. and Terada, M. (2004). *J. Am. Chem. Soc.* 126: 5356–5357.
77 Rajat, M., Mallojjala, S.C., and Wheeler, S.E. (2018). *Chem. Soc. Rev.* 47: 1142–1158.
78 Mori, K., Ichikawa, Y., Kobayashi, M. et al. (2013). *J. Am. Chem. Soc.* 135: 3964–3970.
79 Li, G.Q., Gao, H., Keene, C. et al. (2013). *J. Am. Chem. Soc.* 135: 7414–7417.
80 Sannicolò, F. (1985). *Tetrahedron Lett.* 26: 119–120.
81 Chen, Y.H., Cheng, D.J., Zhang, J. et al. (2015). *J. Am. Chem. Soc.* 137: 15062–15065.
82 Zhou, H., Han, J.T., Nöthling, N. et al. (2022). *J. Am. Chem. Soc.* 144: 10156–10161.
83 Wu, M., Chen, Y.W., Lu, Q. et al. (2023). *J. Am. Chem. Soc.* 145: 20646–20654.
84 Zhang, L., Shen, J., Wu, S. et al. (2020). *Angew. Chem. Int. Ed.* 59: 23077–23082.
85 Yang, H., Sun, H.R., He, R.Q. et al. (2022). *Nat. Commun.* 13: 632.
86 Kwon, Y., Li, J., Reid, J.P. et al. (2019). *J. Am. Chem. Soc.* 141: 6698–6705.
87 An, Q.J., Xia, W., Ding, W.Y. et al. (2021). *Angew. Chem. Int. Ed.* 60: 24888–24893.
88 Ototake, N., Morimoto, Y., Mokuya, A. et al. (2010). *Chem. Eur. J.* 16: 6752–6755.

89 (a) Tian, M., Bai, D., Zheng, G. et al. (2019). *J. Am. Chem. Soc.* 141: 9527–9532. (b) He, Y.P., Wu, H., Wang, Q., and Zhu, J. (2020). *Angew. Chem. Int. Ed.* 59: 2105–2109. (c) Yang, W.C., Chen, X.B., Song, K.L. et al. (2021). *Org. Lett.* 23: 1309–1314. (d) Wang, C.S., Wei, L., Fu, C. et al. (2021). *Org. Lett.* 23: 7401–7406.

90 Wang, Z.S., Zhu, L.J., Li, C.T. et al. (2022). *Angew. Chem. Int. Ed.* 61: e202201436.

91 Bai, H.Y., Tan, F.X., Liu, T.Q. et al. (2019). *Nat. Commun.* 10: 3063.

92 (a) Jiang, C., Hayashi, K., Tsubaki, K. et al. (2009). *J. Am. Chem. Soc.* 131: 54–55. (b) Hayashi, K., Matubayasi, N., Jiang, C. et al. (2010). *J. Org. Chem.* 75: 5031–5036.

93 Vaidya, S.D., Toenjes, S.T., Yamamoto, N. et al. (2020). *J. Am. Chem. Soc.* 142: 2198–2203.

94 Dai, L., Liu, Y., Xu, Q. et al. (2023). *Angew. Chem. Int. Ed.* 62: e202216534.

95 Bao, H., Chen, Y., and Yang, X. (2023). *Angew. Chem. Int. Ed.* 62: e202300481.

96 (a) Liu, Z. and Marder, T.B. (2008). *Angew. Chem. Int. Ed.* 47: 242–244. (b) Bosdet, M.J.D. and Piers, W.E. (2009). *Can. J. Chem.* 87: 8–29. (c) Campbell, P.G., Marwitz, A.J.V., and Liu, S.-Y. (2012). *Angew. Chem. Int. Ed.* 51: 6074–6092.

97 (a) Mazzanti, A., Boffa, M., Marotta, E., and Mancinelli, M. (2019). *J. Org. Chem.* 84: 12253–11225. (b) Mancinelli, M., Bencivenni, G., Pecorari, D., and Mazzanti (2020). *Eur. J. Org. Chem.* 4070–4086.

98 Yang, J., Zhang, J.W., Bao, W. et al. (2021). *J. Am. Chem. Soc.* 143: 12924–12929.

99 Chen, K.W., Chen, Z.H., Yang, S. et al. (2022). *Angew. Chem. Int. Ed.* 61: e202116829.

100 Pu, L.Y., Zhang, Y.J., Liu, W., and Teng, F. (2022). *Chem. Commun.* 58: 13131–13134.

6

Synthesis of Atropisomers *via* Enantioselective Ring-Opening Reactions

Longhui Duan and Zhenhua Gu

University of Science and Technology of China, School of Chemistry and Materials Science, Department of Chemistry, 96 Jinzhai Road, Hefei, 230026, Anhui, China

6.1 Introduction

Enantioselective ring-opening reactions of fused biaryl compounds are effective methods for producing axially chiral products, offering practical advantages such as a wide range of applicable substrates, precise selectivity control, and high atom efficiency. These reactions selectively break inert chemical bonds under mild conditions by opening tensegrity structures, facilitated by torsional strain from twisted conformations. Recent significant progress in this field has been well documented in various reviews and books [1–3]. This chapter delves into the historical background of asymmetric ring-opening strategies for accessing atropisomers, highlighting key advancements. This chapter is organized into six sections based on different types of bond cleavage, including the C(O)—O bond of "Bringmann's Lactone" and various C—X (X = group 17, 16, 15, 14 elements) bonds. The final section briefly touches upon ring-opening reactions of transient pentacyclic metal species.

6.2 Asymmetric Ring Opening of Biaryl Lactones and Their Derivatives

6.2.1 Preliminary Findings

The presence of a six-membered bridge in biaryl compounds is typically considered an advantageous factor in facilitating rotation around the biaryl axis between different conformations due to ring strain, thus enabling the dynamic kinetic resolution (DKR) of such compounds. Biaryl lactones are exemplary and the earliest molecules that have been thoroughly examined [4–7].

In 1986, Bringmann et al. discovered the equilibrium of two conformers of biaryl lactones containing two *ortho* substituents adjacent to the axis. Subsequently, they realized DKR by transforming the lactones into configurationally stable benzyl alcohols with high enantioselectivity using chiral aluminum hydride [6, 8],

Atropisomerism in Asymmetric Organic Synthesis: Challenges and Applications, First Edition.
Edited by Shinobu Takizawa and Mohamed S. H. Salem.

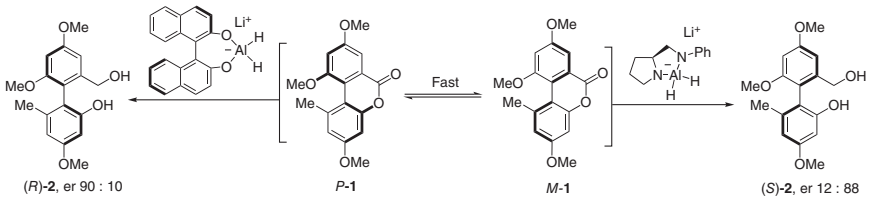

Scheme 6.1 Tautomeric equilibria of biaryl lactones and enantioselective reduction.

as shown in Scheme 6.1. This transformation was made possible by the spontaneous internal racemization of lactones, which created a "*pro*-chiral" axis between the ***P*-1** and ***M*-1** conformers via a planarized transition state. The degree of helical distortion in these lactones was found to vary based on the size of the *ortho* substituents [4].

In 1993, Miyano and co-workers observed that optically biaryl phenolic acids, which possessed highly restricted stable configurations, would undergo racemization in acidic conditions via lactone intermediates **4** [9]. In addition, treatment of the racemic lactone **4** with sodium (−)-methoxide could obtain the optically pure (−)-menthyl-(*R*)-2′-hydroxy-1,1′-binaphthyl-2-carboxylate with varying degrees of stereoselectivity (0–70% ee) depending on the reaction conditions (Scheme 6.2).

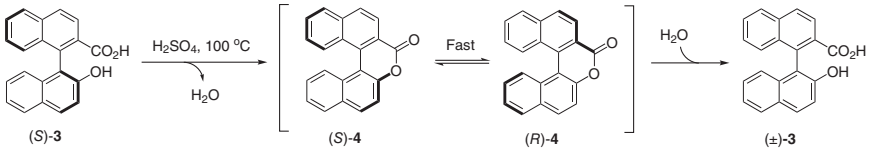

Scheme 6.2 Racemization of optically biaryl phenolic acids.

Investigating the influence of substituents on rotational barriers of lactones revealed a quick atropisomerization with small to moderate-size substituents adjacent to the axis, as is shown in Scheme 6.3 [5]. The rotational barrier $\Delta G^{\#}$

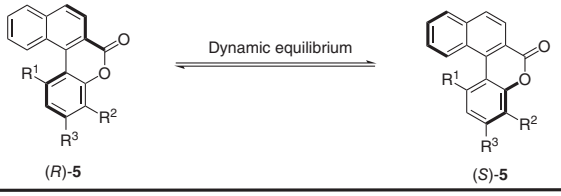

	5a	5b	5c	5d	5e	5f
R^1	H	OMe	Me	Et	*i*Pr	*t*Bu
R^2	*i*Pr	Et	*i*Pr	*i*Pr	Me	H
R^3	H	H	H	H	H	*t*Bu
$\Delta G_{(298\ K)}$ (kJ/mol)	–	54.4	73.9	83.7	92.3	104.4
$\tau_{(298\ K)}$	< ms	0.4 ms	1.0 s	52 s	28 min	2.2 d

Scheme 6.3 The substituent effect on the rotational barriers of biaryl lactones.

(298 K) increased with the enlargement of steric hindrance. The equilibria between two isomers (*R*)-**5** and (*S*)-**5** occurred rapidly at room temperature with a half-life being less than one minute at 298 K when the *ortho* substituents were H, OMe, Me, or Et. The half-life could be increased to 28 minutes by enlarging the steric size (*i*Pr) at the *ortho* position. Only when the substituent was the highly steric hindered tert-butyl group, the half-life could be prolonged to 2.2 days, which was thought to be configurationally stable and resolvable.

In 1999, Bringmann et al. investigated an atrop-diastereoselective ring-opening reaction of configurationally unstable lactones with chiral alkali metal-activated primary 1-arylethylamines [10]. A significant effect of the diastereomeric ratio on the activating metal was observed. Compared with the lithium amide, which proceeded with a low diastereomeric ratio of 59 : 41, the higher homologs Na and K exhibited excellent diastereomeric ratios of up to 95 : 5. Notably, the steric hindrance at the biaryl axis had minimal impact on the diastereomeric ratio, as only a slight difference in asymmetric induction was observed between methyl and methoxy substituents (Scheme 6.4).

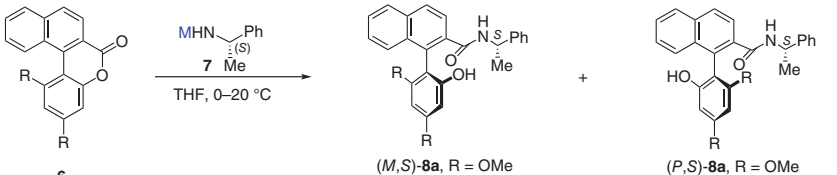

R	d.r. (yield [%])			
	M = H	M = Li	M = Na	M = K
OMe (**8a**)	No reaction	51 : 49 (93)	89 : 11 (98)	91 : 9 (70)
Me (**8b**)	No reaction	59 : 41 (95)	92 : 8 (99)	95 : 5 (85)

Scheme 6.4 Ring-opening reaction of the lactones with chiral metal-activated amines.

6.2.2 Catalytic Asymmetric Reactions

During the past two decades, several catalytic protocols for atrop-enantioselective ring cleavage of biaryl lactones have been developed. The most commonly implemented strategies have utilized metal/chiral ligand complexes to facilitate hydrogenation processes. In 2002, Bringmann and Hurtung reported the first enantioselective ring opening of biaryl lactones by using 10 mol% of the CBS reagent as the catalyst with BH_3·THF as the reduction reagent to yield a range of chiral biaryl alcohols with high yields and selectivity (up to 94% yield, up to 88% ee) [11]. In 2008, Yamada's group realized a versatile atroposelective borohydride reduction of biaryl lactones catalyzed by an optically active β-ketoiminatocobalt(II) complex [12a]. To achieve optimum results, a significant surplus of alcohol was added to the mixture. Dynamic chiral high-performance liquid chromatography revealed a rapid equilibrium between the conformers of biaryl lactones. The study revealed that

the addition of $NaBH_4$ in diglyme was crucial in achieving elevated yields and enantioselectivity. In 2016, Wang and co-workers reported a development for the catalytic asymmetric ring-opening reaction of Bringmann lactones with achiral alcohols or phenols using a chiral bifunctional amino thiourea as the catalyst [12b]. Zhang, Yin and co-workers introduced an efficient Ir-catalyzed direct asymmetric hydrogenation of Bringmann's lactones with H_2 in 2018 [13]. They found that the structurally unique ligands with oxa-spirocyclic diphenol skeletons were effective in iridium-catalyzed asymmetric hydrogenation of biaryl lactones, providing an atom-economic and facile method for synthesizing chiral biaryl benzyl alcohols. In 2019, the same group developed a CuH-catalyzed atroposelective reduction of Bringmann's lactones with poly(methylhydrosiloxane) (PMHS) as the hydride source [14], yielding good to high stereoselectivity (Scheme 6.5).

Organo-catalyzed atrop-enantioselective ring-opening reactions of biaryl lactones were also explored by Miller and co-workers in 2020 [15]. They developed a novel class of peptide-based guanidine catalysts that were found to be effective for the enantioselective ring opening of lactones and asymmetric halogenations. Through a two-step cascade reaction of asymmetric ring opening and halogenations at the *ortho* position to the axis, terphenyl scaffolds with two chiral axes could be constructed with approximately 70% yields and up to 99 : 1 de (Scheme 6.6).

In 2021, Liao and co-workers reported an unprecedented atroposelective DKR of Bringmann's lactones with C-nucleophiles [16]. Activated isocyanides were used to access axially chiral oxazole-substituted biaryl phenols in high yields and enantioselectivity via an Ag-catalyzed tandem atroposelective addition of isocyanides to the lactone substrate followed by a rapid cyclization. In 2022, the same group further developed a ring-opening reaction of biaryl thionolactones with activated isocyanides [17]. The torsional strain of bridged biaryls was found to be critical for high efficiency, with lower reactivity of low-strain substrates (for details of the relations between the reactivity and torsional strain, see Figure 6.1). The possible mechanism involved the deprotonation of isocyanides with the assistance of [Ag] to form [Ag]-intermediate **A1** and its tautomer **A1′**, which then underwent nucleophilic addition to lactones selectively, generating the *S*,*O*-ketal **Int1** with both axial and central chirality. Subsequent intramolecular cyclization produced the thiazolinyl-silver intermediate **Int2** and then protonation to generate the intermediate **Int3**. Finally, further elimination of **Int3** led to the desired products (Scheme 6.7).

Derivatives of biaryl lactones possess characteristics similar to those of Bringmann's lactones, making them ideal substrates or key intermediates for the DKR process. In 2016, Akiyama and co-workers described an asymmetric synthesis of chiral hydroxy aniline derivatives via chiral phosphine acid-catalyzed ring opening of active cyclic biaryl *N*,*O*-acetals [18]. The ring-opening/ring-closing equilibrium between the biaryl *N*,*O*-acetal **20**, and biaryl imine **21** played a crucial role in the DKR, and the strong hydrogen bonding interaction between biaryl imines and CPAs facilitated enantioselectivity for the asymmetric transfer hydrogenation. Notably, the atroposelectivity of the products was entirely controlled by the choice of hydroxy aniline derivatives. The proposed mechanism indicated two crucial

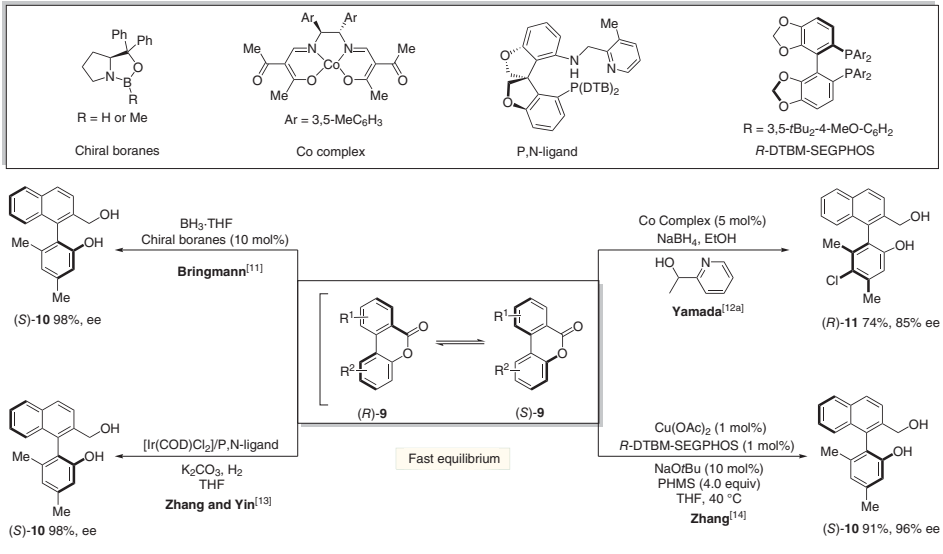

Scheme 6.5 Catalytic asymmetric reduction via ring opening of biaryl lactones.

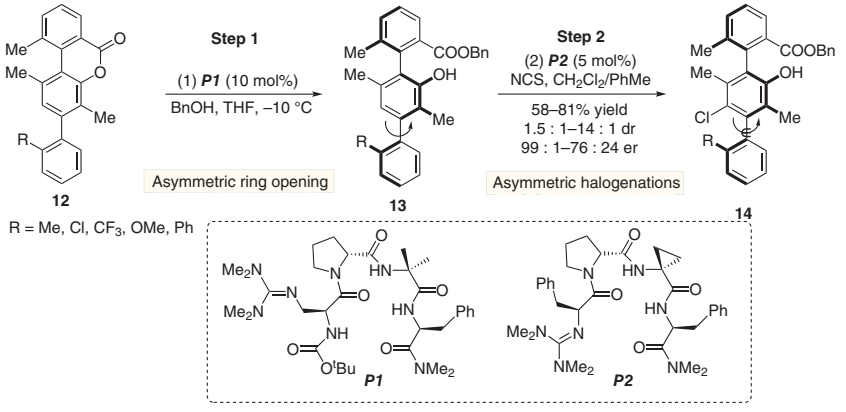

Scheme 6.6 Organo-catalyzed atroposelective ring-opening reactions of biaryl lactones.

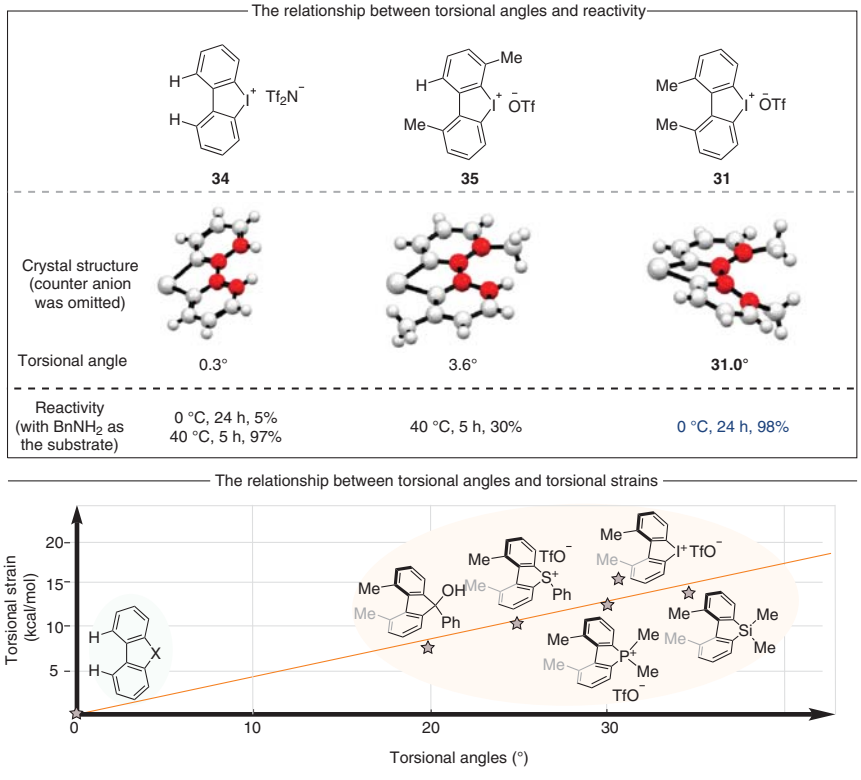

Figure 6.1 The relationship between torsional angles, torsional strains, and reactivity.

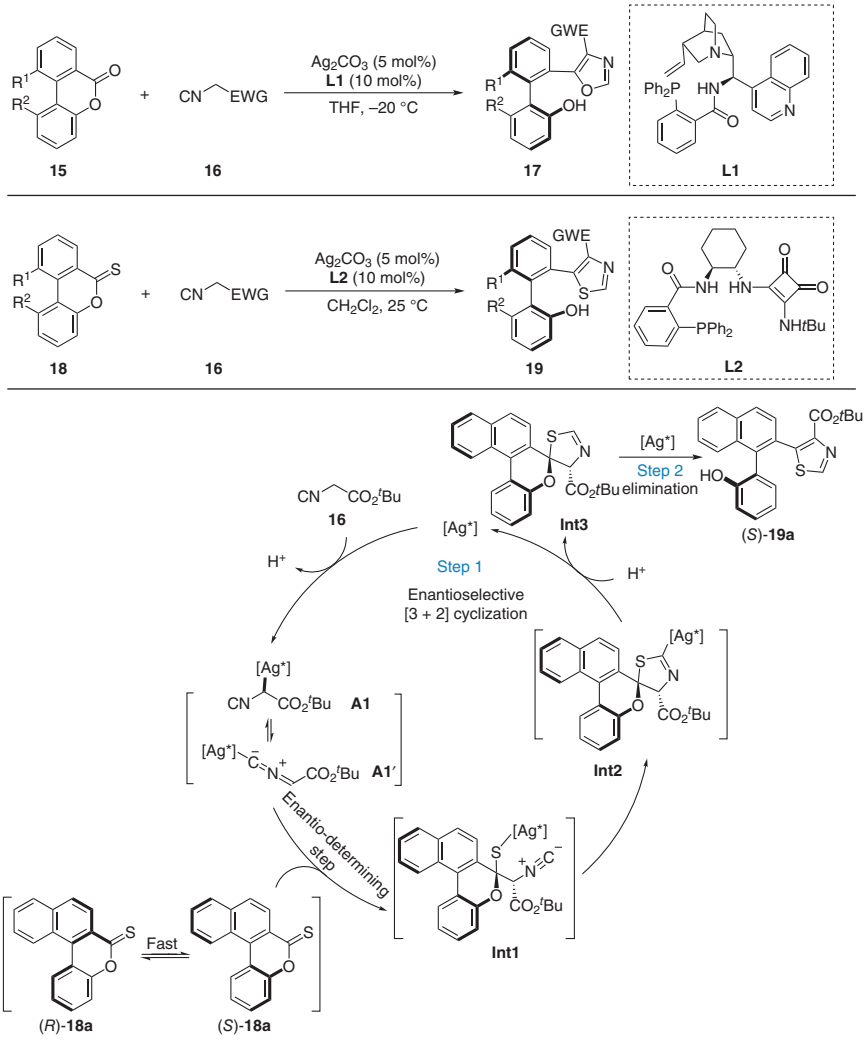

Scheme 6.7 C-nucleophiles involved enantioselective ring-opening reactions of biaryl lactones.

factors for achieving excellent selectivity. First, the fast equilibrium between the biaryl *N*,*O*-acetal **20**, and biaryl imine **21** led to a quicker interconversion than the transfer of hydrogenation to imines. Second, an appropriate difference in transfer hydrogenation rate and the equilibrium rate between **21** and *ent*-**21** resulted in the rapid consumption of the single isomer (Scheme 6.8).

In 2018, Wang and Zhang reported an atroposelective redox-neutral amination of biaryl compounds through a cascade-borrowing hydrogen process under the cooperative catalysis of a chiral iridium complex and an achiral Bronsted acid (Scheme 6.9) [19]. The DKR process was achieved via the dynamic equilibriums of the cyclic biaryl *N*,*O*-acetal intermediate. High yields, broad substrate scopes,

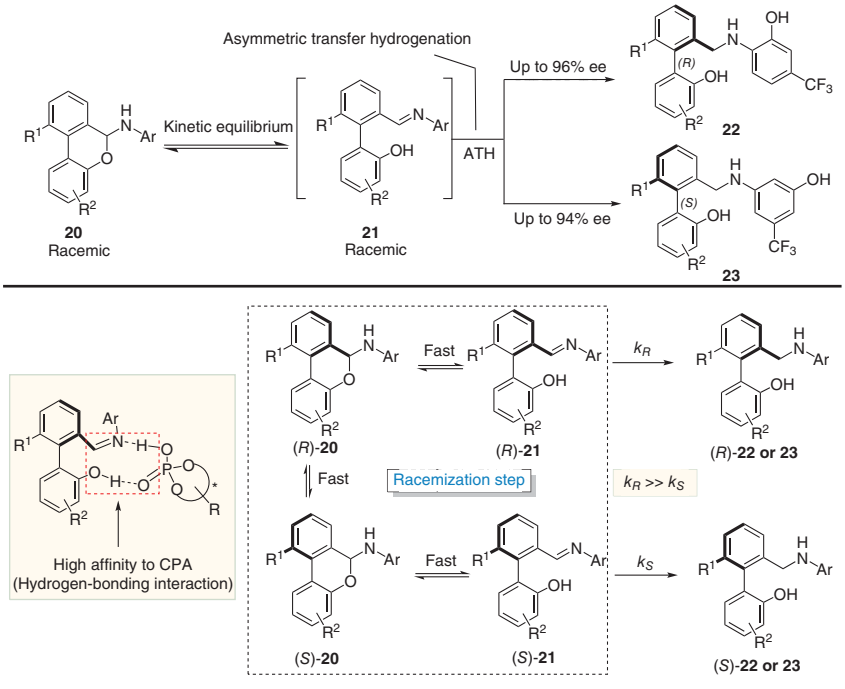

Scheme 6.8 Enantioselective ring opening of *N*,*O*-acetals via transfer hydrogenation.

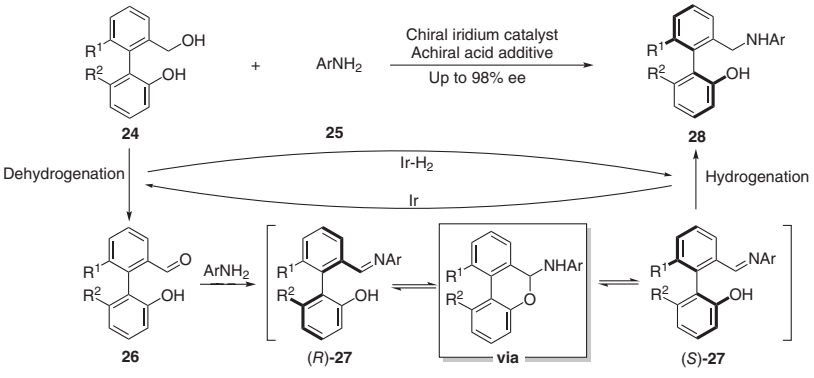

Scheme 6.9 Atroposelective redox-neutral amination of biaryl alcohols.

and good functional-group tolerance enabled the synthesis of a large number of biaryl compounds via the methods discussed, achieving impressive levels of stereoselectivity.

Recently, Trapp and co-workers investigated the equilibrium between the aldehyde alcohols and hemiacetal forms via enantioselective dynamic HPLC analysis, which could be strong evidence for the interconversion of the hemiacetal enantiomers [20].

The rapid equilibrium displayed by biaryl lactones and their derivatives enables the development of asymmetric ring-opening reactions as a useful strategy for preparing diverse biaryl atropisomers. These reactions involve the use of chiral substrate induction, metal-chiral ligand complexes, and organo-catalysts to induce selectivity and provide practical ways of rapidly assembling axially chiral biaryl molecules. Stereoselective cleavage of configurationally unstable bridged biaryl lactones crucially relies on two main factors: (1) the rapid interconversion between two lactone-bridged conformers enables the DKR process and (2) the effective protocols are employed for the stereoselective ring opening. Nonetheless, it is essential to recognize that the scope of biaryl atropisomers currently is limited to alcohols, esters, or amines, which emphasizes the necessity for developing innovative strategies for biaryls with different skeletons.

6.3 Asymmetric Ring-Opening Reactions *via* C—I Bond Cleavage

Cyclic diaryliodonium salts exhibit distinctive structures that render them well-suited substrates for the enantioselective synthesis of atropisomers [21, 22]. The rapid interconversion between two conformations enables the DKR, while the presence of an iodine atom broadens the derivatization of the products. In 2004, Hayashi and co-workers performed a palladium-catalyzed asymmetric ring-opening carbonylation insertion reaction. Under the induction of (*R*)-(+)-2, 2′-bis(diphenylphosphino)-1,1′-binaphthyl, the best result they achieved was a 36% yield accompanied by 28% ee (Scheme 6.10) [23].

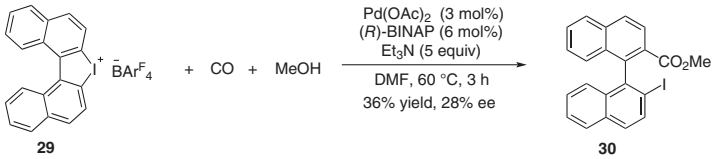

29 30

Scheme 6.10 Palladium-catalyzed asymmetric ring opening of binaphthalonium iodide salts.

A breakthrough was developed in 2018 when Gu and co-workers disclosed that the chiral Cu-bis(oxazolinyl)pyridine complexes **cat1** and **cat2** had extremely high catalytic activity and excellent discrimination to the conformers of cyclic diaryliodonium salts, resulting in high yields and enantiomeric excess (Scheme 6.11) [24]. Density functional theory (DFT) calculations exhibited a small energy barrier between two conformations of cyclic diaryliodonium salts, which was just 8.6 kcal/mol, revealing a fast equilibrium between the two conformers (*S*)-**31** and (*R*)-**31**. A series of diaryliodoniums and substituted aromatic amines were utilized with a broad functional-group tolerance, and up to 99% yields were obtained with up to 99% ee. Although ring-opening reactions can also be carried out with benzyl

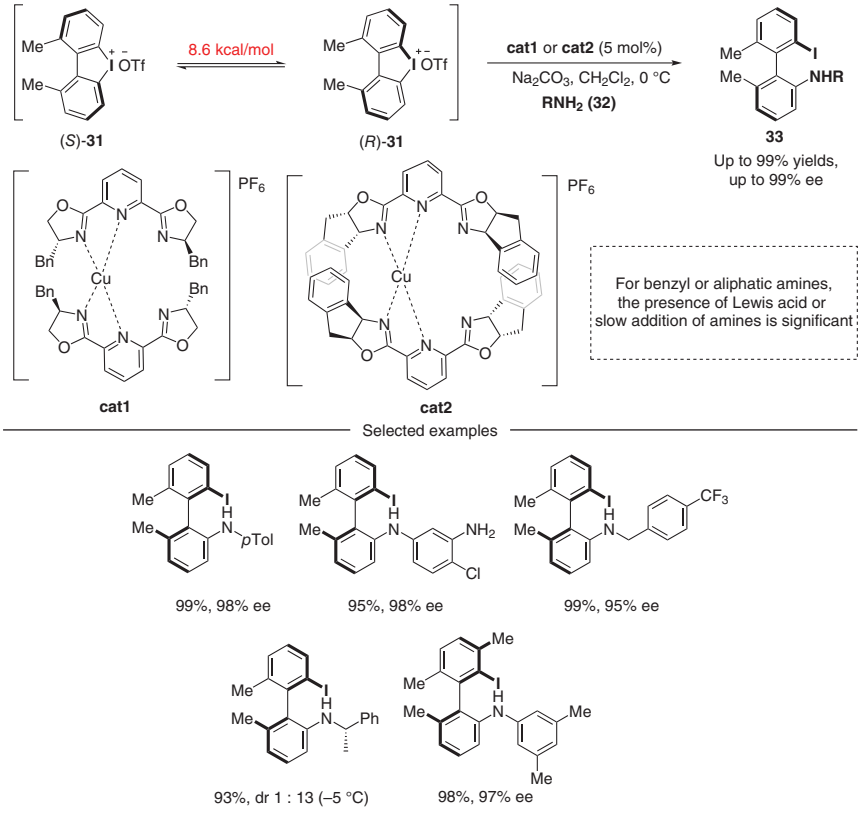

Scheme 6.11 Copper-catalyzed enantioselective ring opening of cyclic diaryliodonium salts.

or aliphatic amines, the high degree of competitive coordination necessitated the presence of a Lewis acid or a slow addition of the amines for optimal results [25].

They also investigated the torsional strain effect of copper-catalyzed ring-opening reactions (Figure 6.1). The crystal structure revealed that the axially *ortho*-dimethyl substituted diaryliodonium (**31**) underwent a distortion of 31.0°, indicating the presence of intramolecular torsional strain. However, the corresponding structures without the *ortho*-methyl group (**34**) or with one *ortho*-methyl group (**35**) had distortion of 0.3° or 3.6°, respectively. The control experiments additionally substantiated a strong correlation between the torsional angle and reaction activity, indicating that the reaction activity escalated with an increase in the torsional angle. Subsequently, the torsional strains of cyclic diaryliodoniums and other distorted compounds were calculated, which were around 8.5–15.1 kcal/mol. To gain a deeper understanding of the relationship between the torsional angle of cyclic molecules and torsional strain, Xue made further efforts to calculate various types of pentacyclic compounds, revealing a positive correlation [26]. These discoveries are highly significant and will serve as valuable guidance for further investigations into asymmetric ring-opening reactions of pentacyclic compounds.

The reaction was postulated to proceed via the DKR. Initially, the copper/di-ligand complex **cat1** released one ligand to form the active catalyst **cat3**, which would further coordinate with amines **32** to give **Int4**. Then, the **Int4** underwent oxidative addition with cyclic diaryliodonium salts **31** to furnish **Int5**, where rapid interconversion of the two conformers of iodonium moieties was expected. Finally, the **Int5** would undergo reductive elimination to form biaryl amines **33a**, releasing the active catalyst for the next cycle. It was also reasonable that oxidative addition may occur before amine coordination to form **Int6**. Since there was no chiral ligand coordinated with copper, **cat4** would give racemic products, thus resulting in decreased enantioselectivity (Scheme 6.12).

The subsequent research has further enriched the copper-catalyzed ring-opening reactions. Gu and co-workers developed a series of enantioselective ring-opening reactions with different nucleophiles, such as thiocarboxylic acids [27], carboxylic acids [28], hydroxyl amines [29], 1,2,3-triazoles [30], oximes [31], and trifluoromethylthio salts [32] (Figure 6.2).

Significant contributions also came from several other research groups in recent years (Figure 6.2). In 2019, Zhang and co-workers developed enantioselective ring-opening reactions with various carboxylic acids [33]. In 2020, the same group achieved ring-opening of cyclic diaryliodonium salts with heterocyclic thiophenols [34]. Recently, Zhang's and He's groups independently reported copper-catalyzed enantioselective ring opening with halogen anions [35, 36]. In 2022, Wang and co-workers developed an efficient copper-catalyzed asymmetric ring-opening reaction of diaryliodonium salts with imides, affording a wide range of axially chiral 2-imido biaryl compounds, which were ready to give primary anilines [37].

In 2019, Gu and co-workers revealed that with the assistance of 2,2,6,6-tetramethylpiperidin-1-oxyl, ring-cleavage reactions involving diarylphosphine oxides would afford diarylphosphates via a cascade ring-opening/oxidative phosphorylation process in high yields and enantioselectivity [38]. The ^{18}O-labeled experiments exhibited that the oxidation reaction occurred before the C—O bond formation step, presumably through the key intermediate **Int7**. It is worth noting that the enantiopure diarylphosphates can be transformed to atropisomers 2′-hydroxy biaryl phosphine oxides through an efficient intramolecular synergism phosphorus transfer reaction with high enantioretention via **Int8**, which could be further reduced to 2-(diphenylphosphine)-2′-methoxy-1,1-binaphthyl (MOP)-type ligands (Scheme 6.13).

Recently, diols activation through a boronic acid strategy was developed and applied in the enantioselective ring-opening reactions by Gu and co-workers. Low nucleophilic diols benefited from a coordination–dissociation equilibrium between diols and boronic acids, which remarkably enhanced their nucleophilicity and reactivity [39]. Notably, the activation of diols was found to be highly dependent on the structure of boronic acids, with the six-membered boronic acid **B2** being suitable for the activation of 1,2-diols, and the five-membered boronic acid **B1** selectively activating 1,4-diols (Scheme 6.14).

The efficacy of the chiral Cu/Box or Cu/PyBox catalytic systems was limited in the presence of bulky amines, such as 2,6-dimethylaniline **57**, due to significant steric

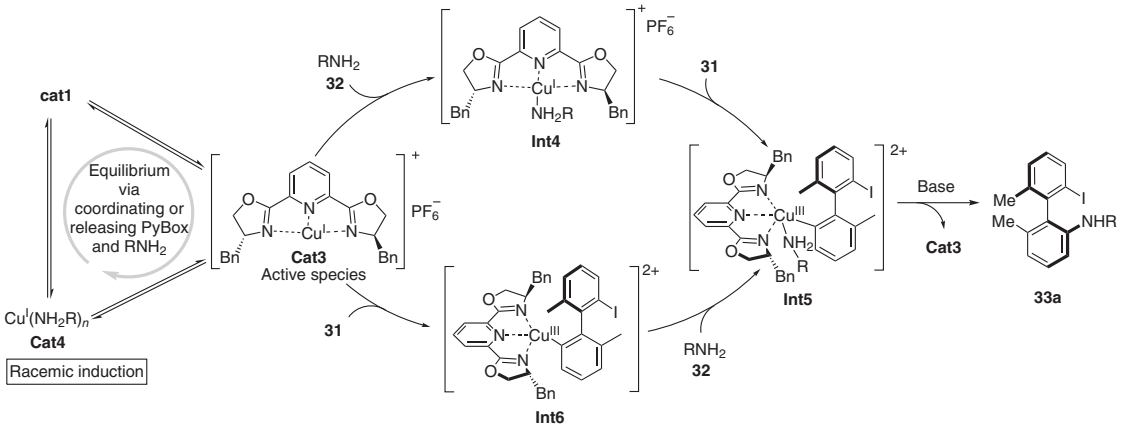

Scheme 6.12 The rationale of the copper-catalyzed ring-opening reaction.

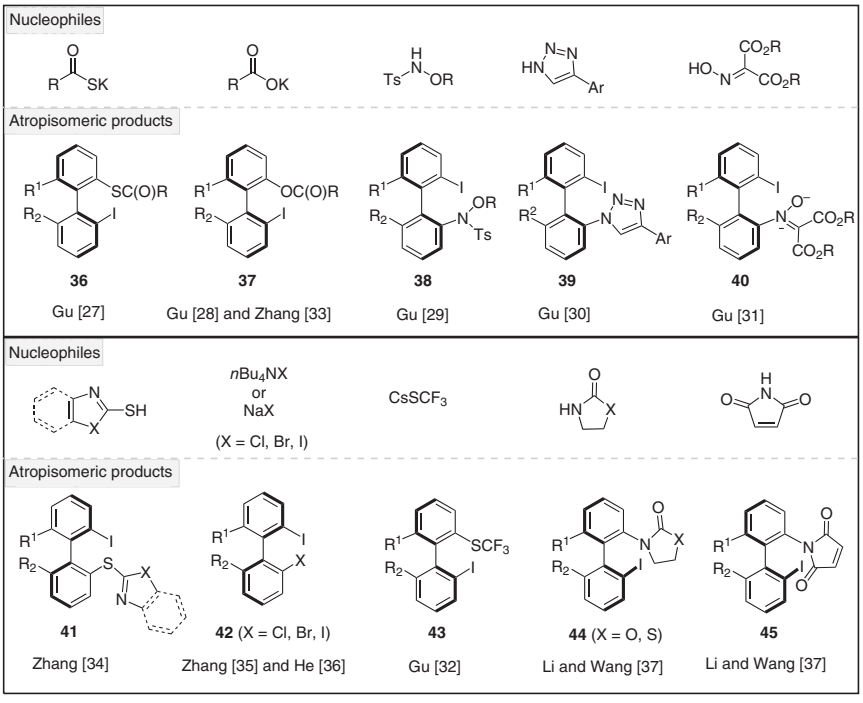

Figure 6.2 Nucleophiles utilized in enantioselective ring-opening reactions.

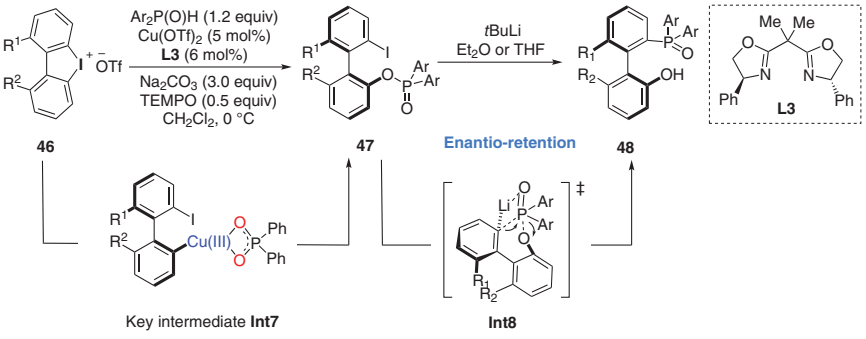

Scheme 6.13 Copper-catalyzed ring-opening/oxidative phosphorylation and subsequent migration.

hindrance that hampered the reaction. This was attributed to the hard formation of crowded intermediates. In 2021, Gu and co-workers employed the chiral cobalt(III) anion to control the enantioselectivity in the ring opening of cyclic diaryliodonium salts with bulky anilines (Scheme 6.15) [40]. The protocol relied on the interaction between chiral anions and cations to achieve elevated reactivity and enantioselective induction. The single crystal of chiral cobalt(III) anion with cyclic diaryliodonium cation complex **59** revealed a close connection between two parts, and the chiral anion could induce the diaryliodonium to form a single conformer. Additionally,

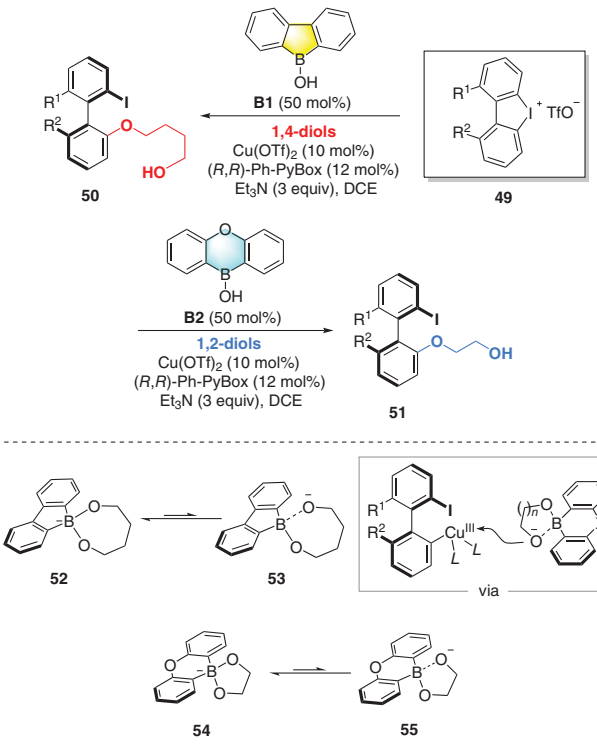

Scheme 6.14 Copper-catalyzed ring-opening reactions with diols activated by boronic acids.

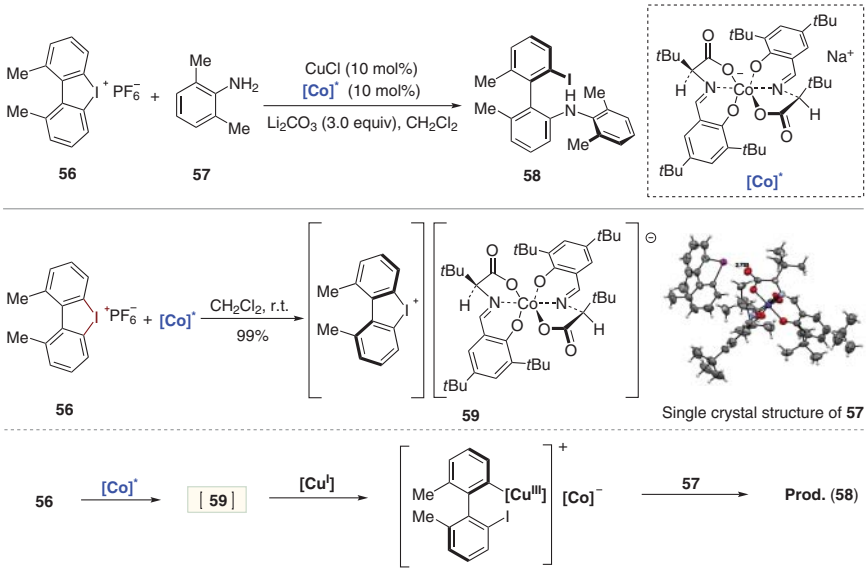

Scheme 6.15 Chiral cobalt anions controlled enantioselective ring opening of cyclic diaryliodonium salts.

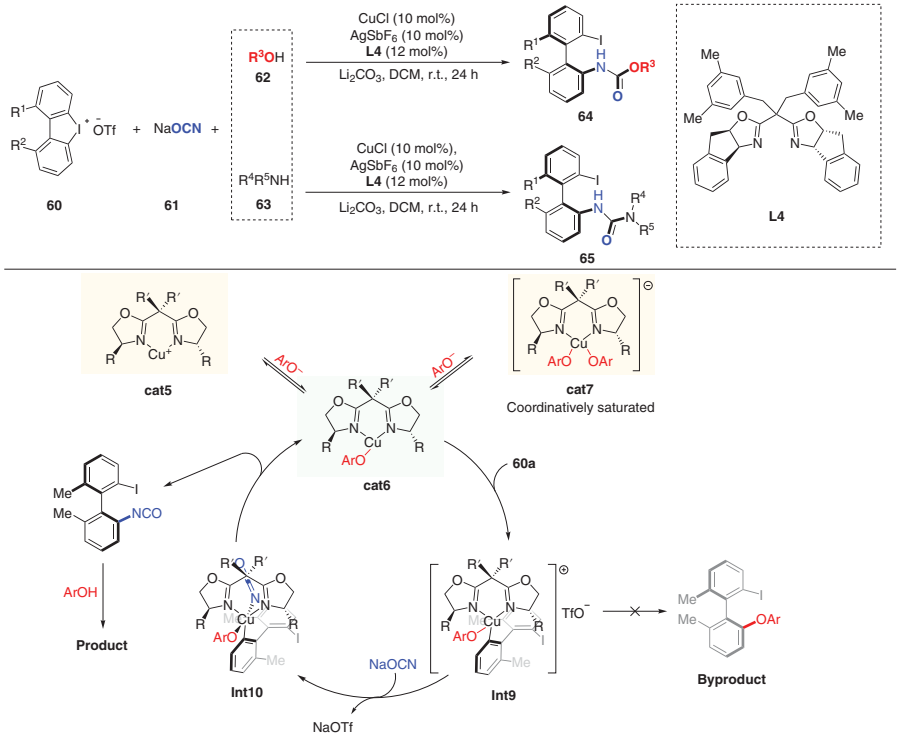

Scheme 6.16 Enantioselective three-component coupling reaction of cyclic diaryliodoniums.

they found the addition of anionic chiral cobalt(III) dramatically accelerated the reaction to achieve good to excellent enantioselectivity.

Very recently, the Gu group developed an enantioselective ring-opening/three-component coupling reaction of cyclic diaryliodoniums with sodium cyanate and phenols (or alcohols) for the synthesis of atropisomeric carbamates (Scheme 6.16) [41]. A process involving phenol-activated chemoselective isocyanation was proposed due to the acceleration of ring-opening reactions with the addition of phenols. It was proposed that phenols not only served as reagents to trap highly active intermediate isocyanates but also activated the copper catalyst as oxygen ligands, generating the active spice **cat6**.

In 2022, Liao and co-workers described a palladium-catalyzed enantioselective carbonylation reaction of cyclic diaryliodoniums enabled by high-valent palladium catalysis (Scheme 6.17) [42]. The sulfoxide dialkylphosphine ligands (SOPs) were found to be privileged frameworks for this reaction. High reactivity and excellent enantioselectivity have been demonstrated with broad substrate scopes in high yields and enantioselectivity (up to 93% yield, up to 99% ee). When *N*-aryl anilines **67** were used, monocarbonylation products were obtained with moderate to excellent yields and high selectivity (63–93% yields and up to 99% ee). In contrast, benzyl or aliphatic primary amines **68** selectively formed double CO insertion products. Mechanism studies in combination with DFT calculations exhibited a nonclassical Pd(II)/Pd(IV) process. Initially, coordination with imines to the Pd(II) catalyst with subsequent CO insertion gave the Pd(II) intermediate **Int11**, which could undergo oxidative addition with diaryliodonium salts to form Pd(IV) intermediate

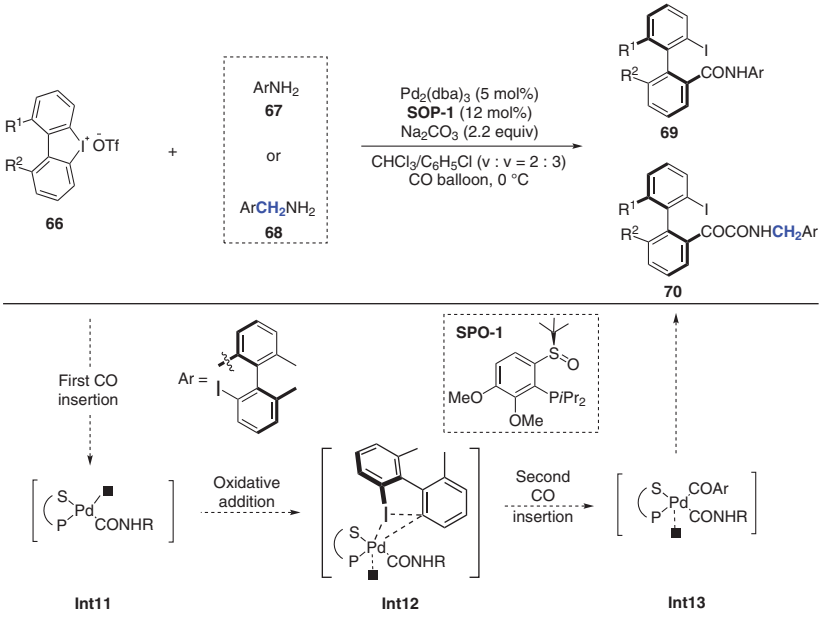

Scheme 6.17 High-valent palladium-catalyzed enantioselective ring-opening reactions.

Int12. The **Int12** could immediately undergo a second CO insertion and reductive elimination to give the final products.

Transition-metal-catalyzed enantioselective ring-opening reactions of cyclic diaryliodonium salts offer effective strategies for the synthesis and utilization of atropisomers. The addition of diverse nucleophiles enables the formation of different chemical bonds, considerably enhancing the range of atropisomers. Three primary advantages should be highlighted for optimal protocols: (i) The ring-opening reaction of cyclic diaryliodonium is highly atom economic. (ii) The derived aryl-I bond can be adapted for various further modifications. (iii) The molecule's torsional strain significantly enhances the reaction by relieving ring strain.

6.4 Asymmetric Ring-Opening Reactions *via* C—N and C—P Bonds Cleavage

While atroposelective ring opening of Bringmann's lactones and their derivatives has achieved great success, investigations with the corresponding lactams are still infrequent. This situation is largely attributed to the low reactivity of the C—N bond. In 2010, Furuta et al. developed an optically active alcohol-induced asymmetric ring-opening of *N*-Boc lactams, and the optical binaphthyl amino ester could be obtained with 99% de values from the separation of diastereomers via proper recrystallization [43]. In 2020, Fu and co-workers reported a catalytic cleavage of C—N bonds in *N*-sulfonyl biaryl lactams by using a bifunctional thiourea catalyst [44]. The strong electron-withdrawing substituent (Ts) on the nitrogen atoms of the lactams was found to be crucial for the activation of the C—N bond, as no reaction was observed when using other substituents such as Boc or Cbz. They discovered the cooperative effects of the bifunctional moieties of the Cinchona-alkaloid-derived thiourea catalyst played a critical role in achieving high yields and enantioselectivity (Scheme 6.18).

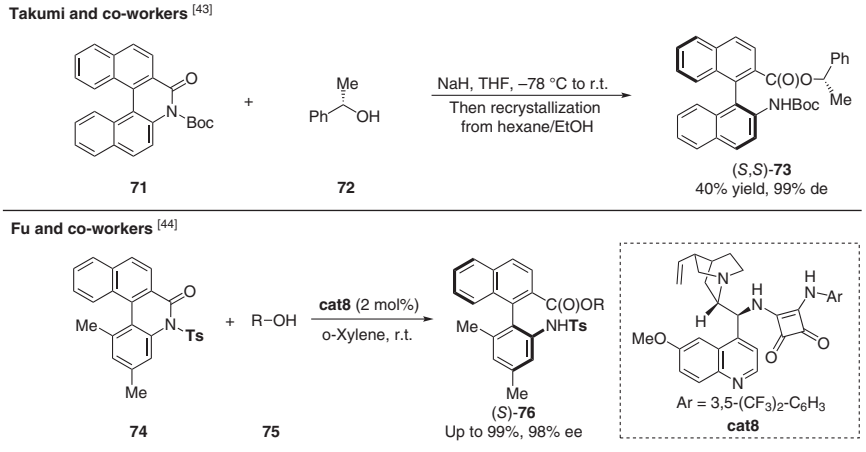

Scheme 6.18 Organo-catalyzed asymmetric ring-opening of lactams.

Recently, Fu and co-workers further extended the substrate to *N*-arylindole lactams, which delivered axially chiral amino acids bearing C—N chiral axes upon asymmetric ring opening [45]. Notably, several novel skeletons, such as *N*-aryl indole, thieno[3,2-*b*]pyrrole, furo[3,2-*b*]pyrrole, and pyrrolo[2,3-*b*]pyridine, are compatible with the reactions, thus demonstrating a considerable structural diversity (Scheme 6.19).

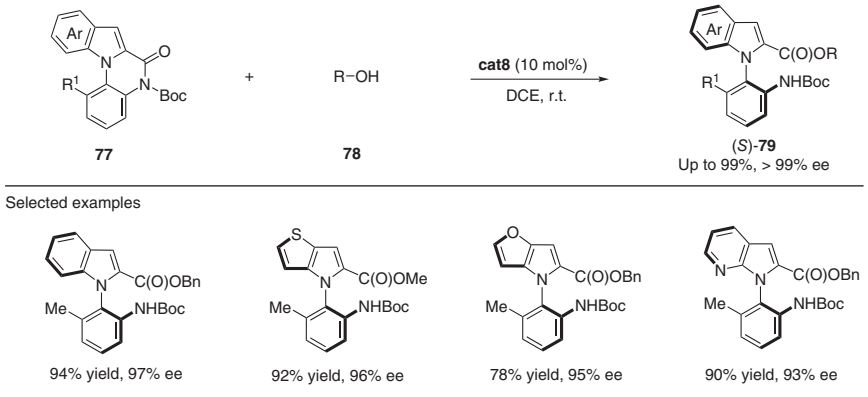

Scheme 6.19 Organo-catalytic atroposelective ring-opening of *N*-arylindole lactams.

In 2022, the Li group reported a palladium-catalyzed stereoselective cleavage of the C—P bond via asymmetric ring-opening reactions for the construction of atropisomers bearing a P-stereogenic center (Scheme 6.20) [46]. The products were obtained in moderate to high yields (up to 82%) and exhibited high

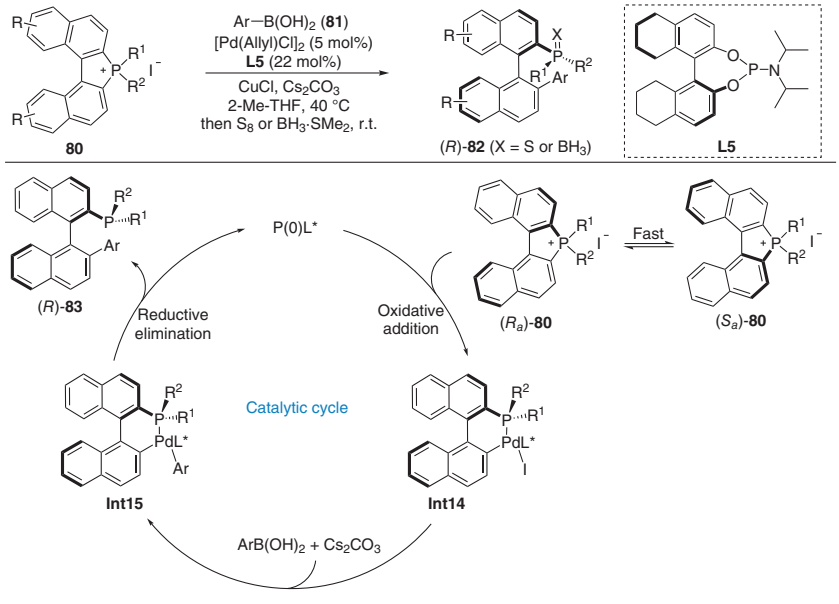

Scheme 6.20 Palladium-catalyzed stereoselective cleavage of C—P bond.

diastereo/enantioselectivity (up to 25 : 1 dr and up to 99% ee). Control experiments demonstrated the significant impact of additive copper on both the reactivity and enantioselectivity of the reaction, suggesting its crucial role in promoting the coordination of $[Pd(Allyl)Cl]_2$ with the chiral ligand **L5**. A plausible mechanism was proposed wherein the oxidative addition of the chiral Pd(0)/ligand complex with phosphonium salts formed optically active intermediates **Int14**. Subsequent transmetallation with the arylboronic acid followed by reductive elimination to furnish the chiral phosphine products (*R*)-**83**, which could be further stabilized through coordination with S_8 or BH_3 to deliver (*R*)-**82**.

6.5 Asymmetric Ring-Opening Reactions *via* C—C and C—Si Bond Cleavage

Catalytic transformations involving the cleavage of carbon–carbon bonds have served as practical strategies for synthesizing various compounds. However, it seems to be a particular challenge due to the high bond dissociation energy (BDE) of C—C bonds. On the basis of torsional strain-promoted ring-opening reactions, the Gu group developed an enantioselective carbon–carbon bond cleavage of 9-aryl-9*H*-fluoren-9-ols via palladium-catalyzed decarbonyl coupling (Scheme 6.21) [47]. They observed a significant dependence of reactivity on the *ortho* substituent, particularly with *ortho*-dihydrogen (**87**) or difluoro substituents (**88**) as

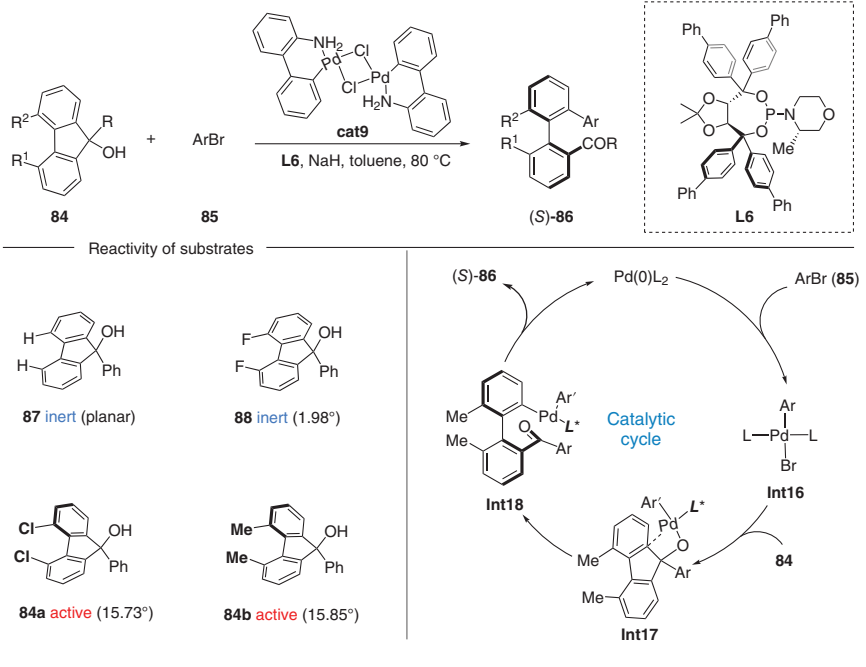

Scheme 6.21 Palladium-catalyzed enantioselective ring opening via carbon–carbon bond cleavage.

substrates, which displayed inert results under standard conditions. The reaction involved the oxidative addition of palladium (0) to an aryl bromide to produce palladium(II) species **Int16**. This intermediate underwent ligand exchange with sodium alkoxide to generate **Int17**, which further underwent β-C elimination to form the carbon–palladium(II) complex **Int18**. Eventually, the desired products were obtained through reductive elimination of the palladium(II) spice **Int18** (Scheme 6.21).

This concept was further applied to a palladium-catalyzed kinetic resolution/ring-opening reaction of 8*H*-indeno[1,2-*c*]thiophen-8-ols [48]. The reaction exhibited highly enantioselective control with high regioselectivity of β-aryl elimination, which selectively eliminated thiophene motifs, and both optically active thiophene-phenyl atropisomers and stereogenic substrates were obtained with excellent enantiomeric excess. Control experiments demonstrated that both the steric hindrance and electronic properties of the thiophene unit have an impact on the regioselectivity of the ring opening of substrates (Scheme 6.22). The authors proposed models for achieving regio/stereoselective β-aryl elimination with three major requirements. First, the palladium catalyst coordinated with the hydroxyl group with excellent directional selectivity to form **Int19′** and **Int20′** (vs **Int19** and **Int20**). Second, an empty orbital of the Pd atom must overlap with the σ-orbital of the C—C bond for effective bond cleavage, which would promote the proximity of carbon–carbon bonds to the metal center to benefit axial chirality induction. Third, according to previous reports, the reaction favors breaking the C—C bond attached to the thiophene ring [49].

On the basis of these findings, the authors further developed a practical synthesis of axially chiral biaryls via chirality transfer reactions from a stereogenic center to axial chirality [50]. The synthesis was based on a palladium-catalyzed carbon–carbon bond cleavage/ring-opening reaction of optically active substrates using an achiral ligand. The researchers employed a series of coupling partners, including benzyl bromides [C(sp^3)-Br], aryl halides [C(sp^2)-Br], and alkynyl bromides [C(sp)-Br], all of which gave excellent yields and selectivity. The reactions showed excellent chemical specificity recognition, with a preference for breaking the C—C bond of thiophene. Furthermore, palladium-catalyzed selective domino cyclization/ring-opening reactions between 8*H*-indeno[1,2-c]thiophen-8-ols and *N*-(2-bromophenyl)propiolamide derivatives are also applicable to this point to axial chirality transfer process (Scheme 6.23) [51].

Narasaka acylation is a practical method for synthesizing α,β-unsaturated ketones, but its sensitivity to silyl coupling partners limits the application [52, 53]. Generally, only vinyl silanes were active enough to undergo Narasaka acylation. In 2020, the Gu group reported a torsional strain-promoted aryl Narasaka acylation through Rh-catalyzed ring-opening of dimethyl silafluorenes [54]. They found that the torsional strain of five-membered silafluorenes enabled selective cleavage of the cyclic C—Si bond, resulting in the production of various α-silyl biaryl atropisomers with high enantioselectivity (Scheme 6.24). Mechanism studies exhibited poor reactivity when employing silanol **98** as the almost planar substrate. The use of a phosphoramidite ligand derived from (*S*)-3-methyl-1-((2,4,6-triisopropylphenyl)-

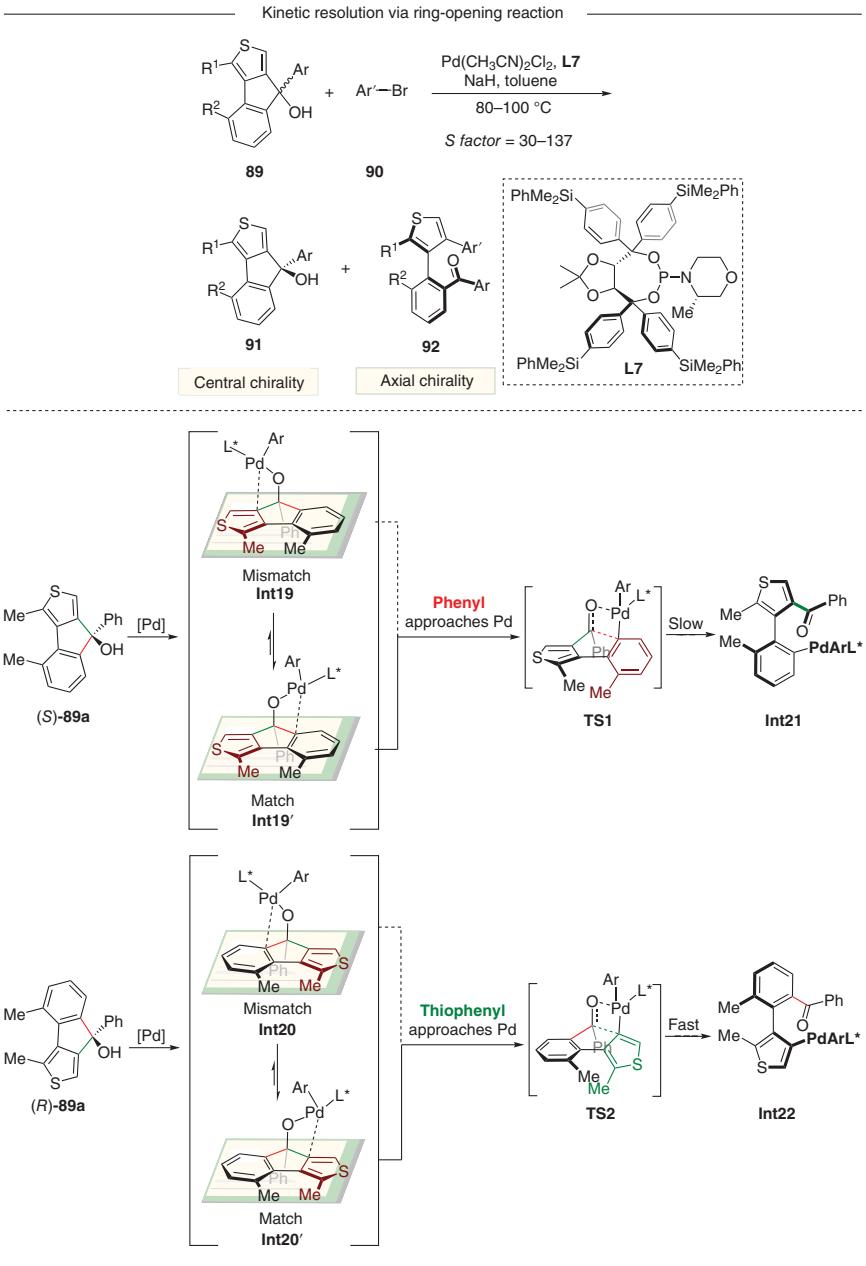

Scheme 6.22 Palladium-catalyzed kinetic resolution/ring-opening reaction.

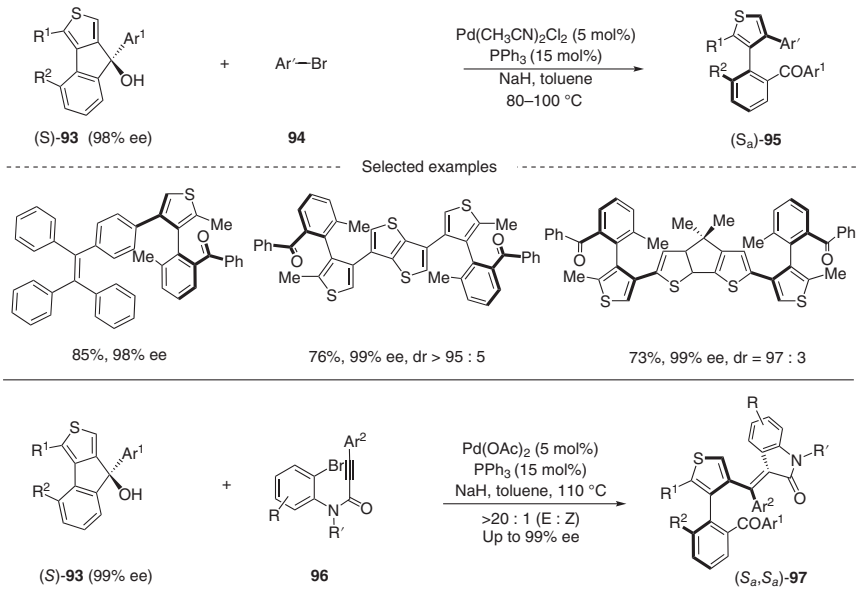

Scheme 6.23 Asymmetric carbon–carbon bond cleavage via ring-opening reactions. Source: Gu et al. [51]/with permission of American Chemical Society.

sulfonyl)-piperazine was crucial for stereochemistry control. A possible catalytic cycle was tentatively proposed for the reaction. First, ligand substitution of the chiral ligand with $[Rh(CO)_2Cl]_2$ gave the catalyst **Cat10** via the precipitation of KCl, which acted as an active spice. Enantioselective oxidative addition of cyclic C—Si bond afforded the biaryl rhodium complex **Int23**. Reductive elimination delivered the ester **Int24** which reacted with the acid anhydride to produce Rh(III) complex **Int25**. The products were obtained through further reductive elimination and subsequent hydrolysis.

Building upon this work, the same research group reported an Rh-catalyzed asymmetric ring-opening of chiral silafluorenes to simultaneously create an axial chirality and a silicon-stereogenic center with high selectivity [55]. They discovered that the addition of methanol was crucial for achieving high diastereoselectivity, although the exact role of MeOH remained unclear. The authors hypothesized that the chiral rhodium complex would dissociate to the monomer via coordination with MeOH, which may undergo deprotonation in the presence of K_2CO_3 to give the rhodium anion complex as the active catalyst (Scheme 6.24).

In conclusion, transition-metal-catalyzed asymmetric ring-opening reactions via C—C/C—Si bonds cleavage have been shown to be a superior method for facile access to a series of axially chiral biaryls in an atom-economical fashion. Notably, the torsional strain created by the steric repulsion between two *ortho* substituents of the biaryl skeleton considerably facilitated the cleavage of the C—C/C—Si bonds, increasing not only the reactivity of the substrates but also the enantio-/regioselectivity control.

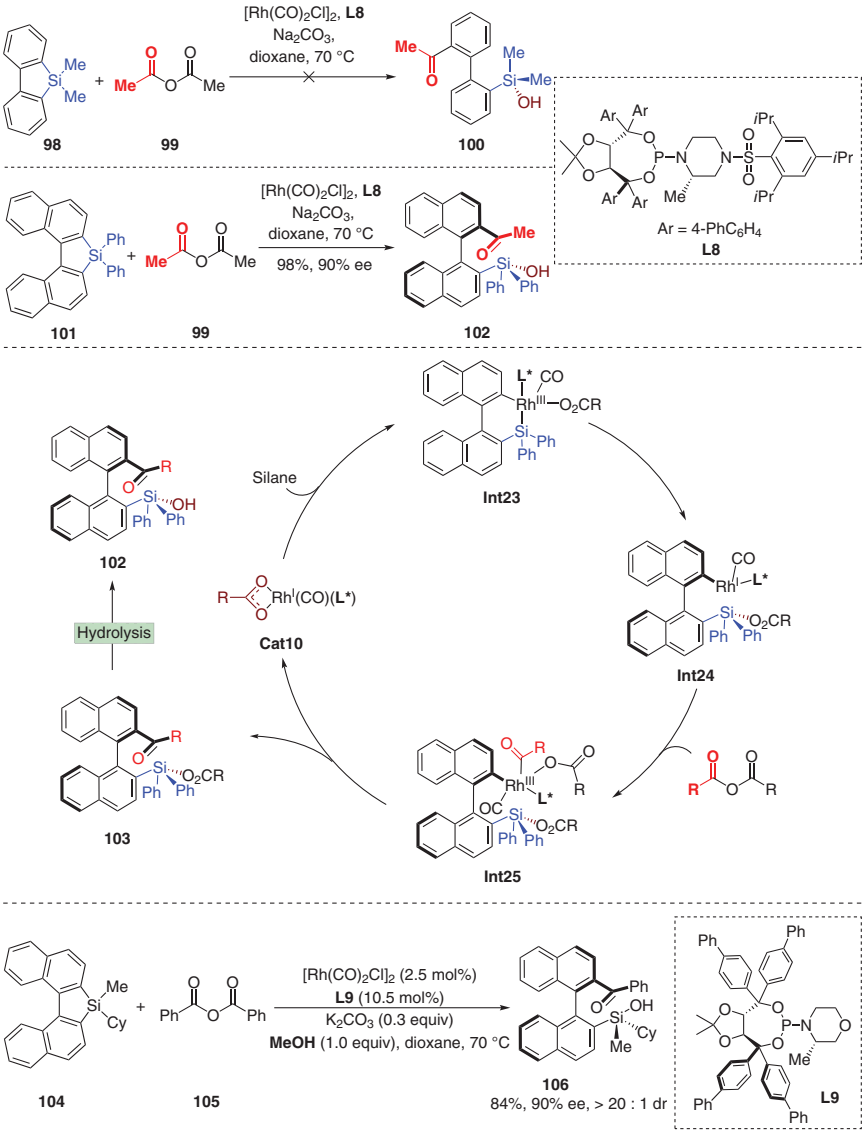

Scheme 6.24 Torsional strain-promoted Rh-catalyzed aryl Narasaka acylation.

6.6 Asymmetric Ring-Opening Reactions *via* C–O and C–S Bond Cleavage

As early as 2002, Hayashi and co-workers reported a nickel-catalyzed asymmetric Grignard cross-coupling reaction via the ring opening of dinaphthothiophene with Grignard reagents [56]. The reaction proceeded well with high enantioselectivity at 20 °C in the presence of 3 mol% of a nickel catalyst generated from $Ni(cod)_2$ and a chiral oxazoline-phosphine ligand **L10**, giving axially chiral 1,1′-binaphthyls with

high yields and enantioselectivity (Scheme 6.25). However, the Grignard reagents were limited to aromatic compounds.

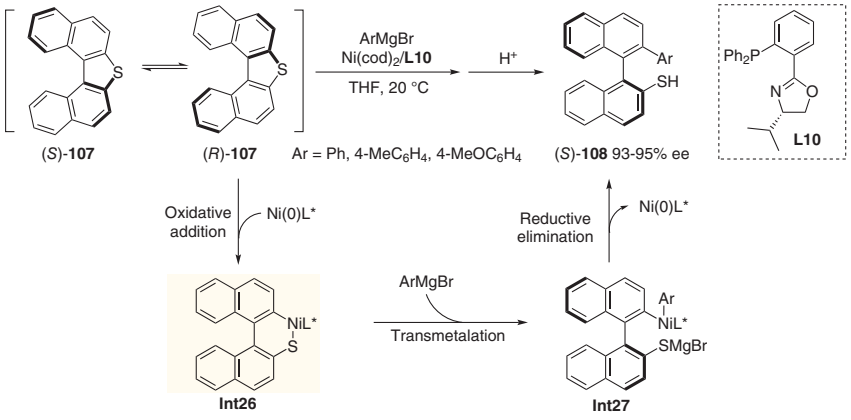

Scheme 6.25 Nickel-catalyzed asymmetric coupling via the ring opening of dinaphthothiophene.

Sulfonium salts **109** were anticipated to exhibit elevated reactivity in comparison with thioethers; however, the cleavage of the exocyclic S-aryl bond of sulfonium salts is usually regarded with a significant preference for the cyclic S-aryl bond. In 2022, Gu and co-workers described an asymmetric ring-opening reaction via a Pd-catalyzed atroposelective carbonylation of dibenzothiopheniums [57]. However, in their study, they observed notable selectivity of the reaction with a significant preference for cleaving the cyclic C—S bonds with higher steric hindrance over the exocyclic C—S bonds. The inversed chemoselectivity was attributed to the torsional strain effect. Concurrently, a slow reaction rate was observed under standard conditions when the substrate containing two adjacent hydrogen atoms on the biaryl axis **112** was used, in which 50% of starting material was recovered even with a prolonged reaction time (five days), along with the formation of *N*-(*p*-tolyl)benzamide **114** (Scheme 6.26).

In 2021, Cao and co-workers developed an efficient enantioselective ring-opening reaction by cleavage of a more challenging C—O ether bond in the presence of $Ni(cod)_2$ and chiral *N*-heterocyclic carbene (NHC) ligands [58]. The transformation exhibited good enantioselectivity control (up to 92% ee) with various aryl Grignard reagents, providing a practical way for the synthesis of naphthol derivatives. Ulteriorly, they developed an enantioselective alkylative ring-opening reaction of cyclic dinaphthylfuran with alkyl Grignard reagent nucleophiles in 2022 [59]. The chiral NHC ligand (**L12**–**L14**) was found to greatly facilitate the reaction with nickel catalysis. Recently, they extended the method to the Grignard reagents containing β-hydrogen [60]. Based on the experimental findings, it was observed that solvents play a crucial role in influencing the competition between β-H elimination and reductive elimination (Scheme 6.27).

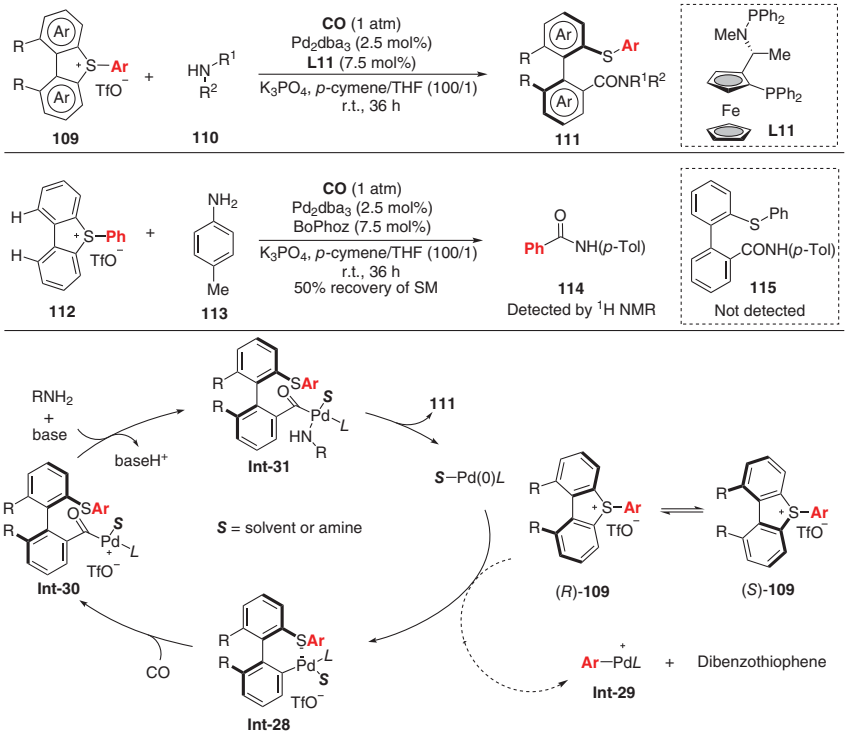

Scheme 6.26 Pd-catalyzed atroposelective carbonylation of dibenzothiopheniums.

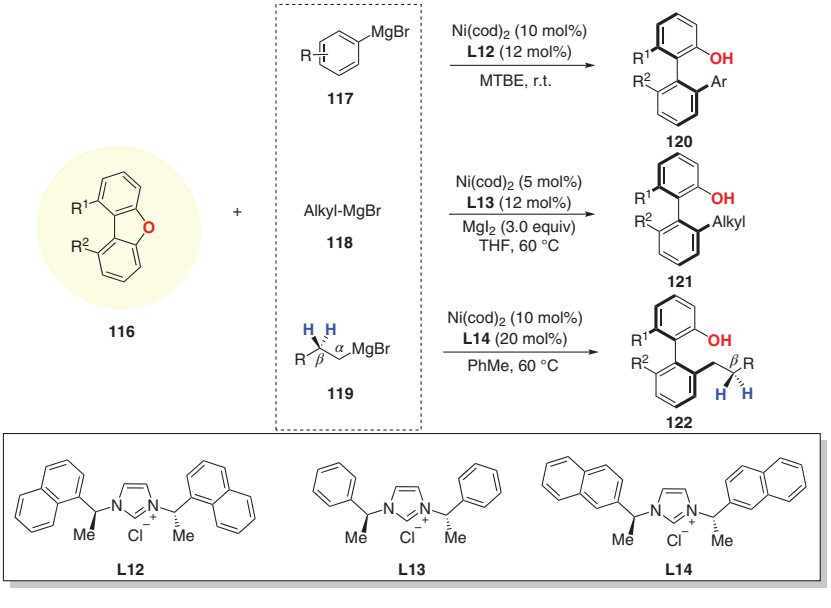

Scheme 6.27 Ni-catalyzed enantioselective ring opening of inactivated cyclic dinaphthylfuran.

6.7 Oriented Asymmetric Ring Opening *via* Transient Pentacyclic Metal Species

Despite the tremendous achievements of the DKR process in various cyclic reactants, there has been a recent surge in interest in utilizing pentacyclic metal intermediates for the synthesis of optically active biaryl compounds. This increased attention is attributed to the distinct reactivity exhibited by these metal-centered cyclic intermediates. In 2013, Stoltz and co-workers reported a Pd-catalyzed atroposelective C–P coupling process via nitrogen atom-oriented asymmetric cross-coupling reaction for the asymmetric synthesis of the 1-(2-(diphenylphosphino)naphthalen-1-yl)isoquinoline and its derivatives in high yields and high enantioselectivity (Scheme 6.28) [61]. Slow addition of diphenylphosphine was demonstrated to greatly improve the overall effectiveness of the DKR process, which allowed more time for the isomerization of arylpalladium intermediate before its subsequent reaction with diphenylphosphine.

In the same year, Lassaletta and co-workers developed a Pd(0)-catalyzed coupling of racemic 2-triflates with aryl boroxines, employing an α,α,α,α-tetraaryl-2,2-dimethyl-1,3-dioxolane-4,5-dimethanol-derived phosphoramidite **L16** as the ligand [62]. A dynamic kinetic asymmetric transformation (DYKAT) was assumed via the configurational equilibrium of cationic palladacyclic intermediates (**Int32** and *ent*-**Int32**) as a consequence of the widening of the concerned angles, which was further demonstrated by the isolated oxidative addition intermediate. This protocol has been demonstrated to be effective with various coupling partners developed subsequently, such as alkynes [63], amines [64], and alkenes [65] (Scheme 6.28).

In 2016, You and co-workers disclosed a rhodium-catalyzed oxidative coupling of biaryl compounds with alkenes via the pentacyclic metal intermediate [66]. The reaction exhibited a wide range of substrate scopes with various electronically and sterically varied styrenes, leading to the corresponding chiral biaryls in reasonable yields (37–91%) and excellent er values (93 : 7 to 98 : 2). In addition, they introduced a new class of chiral cyclopentadiene (Cp) ligands based on 1,1′-spirobiindane, which were demonstrated to be excellent ligands in asymmetric oxidative coupling reactions. Recently, they further applied the strategy to a rhodium-catalyzed enantioselective C–H iodination of 1-aryl isoquinolines with *N*-iodosuccinimide (NIS), affording practical access toward a series of axially chiral biaryl iodides (Scheme 6.29) [67].

Pentacyclic metal intermediates formed through either oxidative addition or C—H metalation serve as an effective supplement to enantioselective ring-opening reactions via DKR. This strategy provides access to a range of functionalized hetero-biaryls with appealing structures, which may serve as ligands in asymmetric catalysis. In situations where the standard DKR is not feasible due to slow substrate isomerization, isomerization of the aryl palladium intermediates is a practical alternative that can be further modified with various reaction pathways.

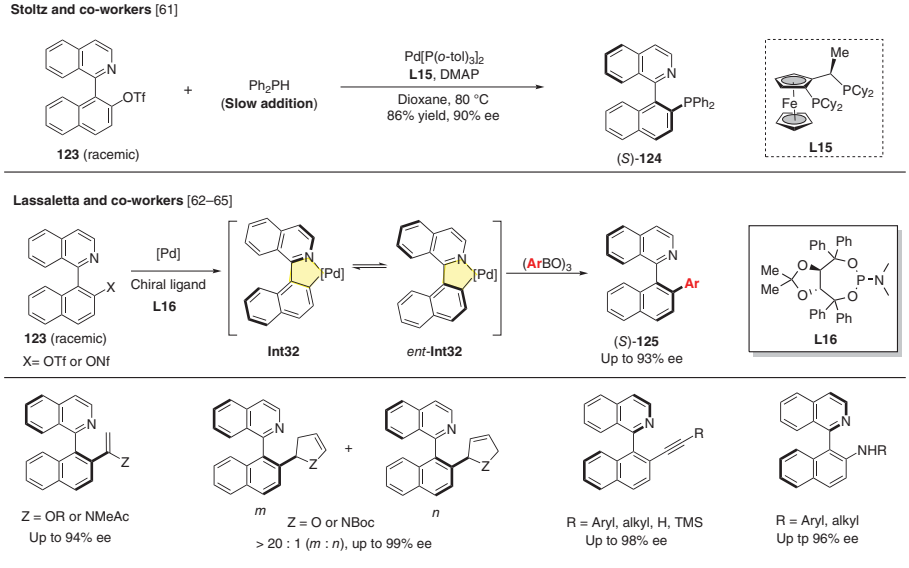

Scheme 6.28 Palladium-catalyzed stereoselective cross-coupling reactions.

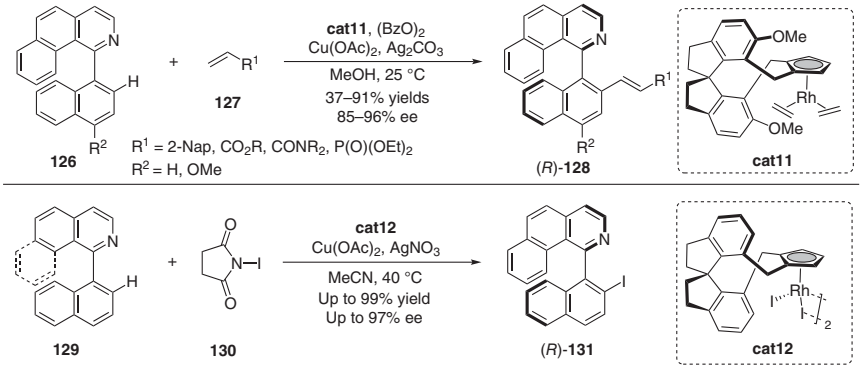

Scheme 6.29 Rh-catalyzed oxidative coupling reaction of biaryl compounds.

6.8 Summary and Conclusions

After a long period of effort, asymmetric ring-opening reactions of fused biaryls have emerged as a potent strategy for the synthesis of biaryl atropisomers with the aid of chiral catalysts. Notably, a diverse range of atropisomers with high enantioselectivity have been obtained via the cleavage of a C—C or C—X (X = I, S, P, Si, O, N) bond under mild conditions. Such advancements facilitate the streamlined construction of pivotal molecular frameworks and diverse chemical bonds. We hope that this chapter not only showcases original discoveries and state-of-the-art achievements in the field of asymmetric synthesis for biaryl atropisomers via ring-opening reactions but also provides readers with valuable insights, guiding the development of more effective strategies for crafting atropisomers and other chiral molecules.

References

1 Wang, G., Huang, J., Zhang, J., and Fu, Z. (2022). Catalytically atroposelective ring-opening of configurationally labile compounds to access axially chiral biaryls. *Org. Chem. Front.* 9 (16): 4507–4521.

2 Zhang, X., Zhao, K., and Gu, Z. (2022). Transition metal-catalyzed biaryl atropisomer synthesis via a torsional strain promoted ring-opening reaction. *Acc. Chem. Res.* 55 (12): 1620–1633.

3 Zhou, T. and Shi, B.F. (2021). *Metal-catalyzed asymmetric synthesis of biaryl atropisomers*. In: *Axially Chiral Compounds* (ed. B. Tan), 13–45. Hoboken, NJ: Wiley.

4 Bringmann, G., Hartung, T., Göbel, L. et al. (1992). Novel concepts in directed biaryl synthesis, IX. Synthesis and structure of benzonaphthopyranones, useful bridged model precursors for stereoselective biaryl syntheses. *Liebigs Ann. Chem.* 1992 (3): 225–232.

5 Bringmann, G., Price Mortimer, A.J., Keller, P.A. et al. (2005). Atroposelective synthesis of axially chiral biaryl compounds. *Angew. Chem. Int. Ed.* 44 (34): 5384–5427.

6 Bringmann, G., Walter, R., and Weirich, R. (1990). The directed synthesis of biaryl compounds: modern concepts and strategies. *Angew. Chem. Int. Ed.* 29 (9): 977–991.

7 Bringmann, G., Breuning, M., Pfeifer, R.M. et al. (2002). The lactone concept – a novel approach to the metal-assisted atroposelective construction of axially chiral biaryl systems. *J. Organomet. Chem.* 661 (1): 31–47.

8 Bringmann, G., Jansen, J.R., and Rink, H.P. (1986). Regioselective and atropoisomeric-selective aryl coupling to give naphthyl isoquinoline alkaloids: the first total synthesis of (−)-ancistrocladine. *Angew. Chem. Int. Ed.* 25 (10): 913–915.

9 Shuichi, O., Kazumasa, K., and Sotaro, M. (1993). Acid-catalyzed facile racemization of axially dissymmetric 2′-hydroxy-1,1′-binaphthyl-2-carboxylic acid. *Chem. Lett.* 22 (1): 79–80.

10 Bringmann, G., Breuning, M., Tasler, S. et al. (1999). Atropo-diastereoselective cleavage of configurationally unstable biaryl lactones with alkali metal activated primary 1-arylethylamines. *Chem. Eur. J.* 5 (10): 3029–3038.

11 Bringmann, G., Breuning, M., Henschel, P., and Hinrichs, J. (2002). Asymmetric synthesis of (*M*)-2-hydroxymethyl-1-(2-hydroxy-4,6-dimethylphenyl)naphthalene via a configurationally unstable biaryl lactone. *Org. Synth.* 79: 72.

12 (a) Ashizawa, T., Tanaka, S., and Yamada, T. (2008). Catalytic atropo-enantioselective reduction of biaryl lactones to axially chiral biaryl compounds. *Org. Lett.* 10 (12): 2521–2524. (b) Yu, C., Huang, H., Li, X. et al. (2016). Dynamic kinetic resolution of biaryl lactones via a chiral bifunctional amine thiourea-catalyzed highly atropo-enantioselective transesterification. *J. Am. Chem. Soc.* 138 (22): 6956–6959.

13 Chen, G.Q., Lin, B.J., Huang, J.M. et al. (2018). Design and synthesis of chiral oxa-spirocyclic ligands for Ir-catalyzed direct asymmetric reduction of Bringmann's lactones with molecular H_2. *J. Am. Chem. Soc.* 140 (26): 8064–8068.

14 Hu, L.a., Zhang, Y., Chen, G.Q. et al. (2019). CuH-catalyzed atropoenantioselective reduction of bringmann's lactones via dynamic kinetic resolution. *Org. Lett.* 21 (14): 5575–5580.

15 Beleh, O.M., Miller, E., Toste, F.D., and Miller, S.J. (2020). Catalytic dynamic kinetic resolutions in tandem to construct two-axis terphenyl atropisomers. *J. Am. Chem. Soc.* 142 (38): 16461–16470.

16 Qian, L., Tao, L.F., Wang, W.T. et al. (2021). Catalytic atroposelective dynamic kinetic resolution of biaryl lactones with activated isocyanides. *Org. Lett.* 23 (13): 5086–5091.

17 Luo, Z.H., Wang, W.T., Tang, T.Y. et al. (2022). Torsional strain-independent catalytic enantioselective synthesis of biaryl atropisomers. *Angew. Chem. Int. Ed.* 61 (43): https://doi.org/10.1002/ange.202211303.

18 Mori, K., Itakura, T., and Akiyama, T. (2016). Enantiodivergent atroposelective synthesis of chiral biaryls by asymmetric transfer hydrogenation: chiral phosphoric acid catalyzed dynamic kinetic resolution. *Angew. Chem. Int. Ed.* 55 (38): 11642–11646.

19 Zhang, J. and Wang, J. (2018). Atropoenantioselective redox-neutral amination of biaryl compounds through borrowing hydrogen and dynamic kinetic resolution. *Angew. Chem. Int. Ed.* 57 (2): 465–469.

20 Heitsch, S., Mayer, L.C., Pignot, Y.L., and Trapp, O. (2023). Synthesis and stereodynamics of intramolecular hemiacetals in biaryl aldehyde-alcohols. *Chirality* https://doi.org/10.1002/chir.23560.

21 Peng, X., Rahim, A., Peng, W. et al. (2023). Recent progress in cyclic aryliodonium chemistry: syntheses and applications. *Chem. Rev.* 123 (4): 1364–1416.

22 Robidas, R., Huber, S.M., and Legault, C.Y. (2021). Computational investigation of cyclic substituted iodine(III) halogen bond donors. *ARKIVOC* 2021 (7): 128–140.

23 Kina, A., Miki, H., Cho, Y.-H., and Hayashi, T. (2004). Palladium-catalyzed Heck and carbonylation reactions of a dinaphthaleneiodonium salt forming functionalized 2-iodo-1,1′-binaphthyls. *Adv. Synth. Catal.* 346 (13–15): 1728–1732.

24 Zhao, K., Duan, L., Xu, S. et al. (2018). Enhanced reactivity by torsional strain of cyclic diaryliodonium in Cu-catalyzed enantioselective ring-opening reaction. *Chem* 4 (3): 599–612.

25 Xu, S., Zhao, K., and Gu, Z. (2018). Copper-catalyzed asymmetric ring-opening of cyclic diaryliodonium with benzylic and aliphatic amines. *Adv. Synth. Catal.* 360 (20): 3877–3883.

26 Xue, X. (2022). Study on ring-opening reaction based on torsional strain of fused biaryl compounds. Doctoral thesis. University of Science and Technology of China.

27 Hou, M., Deng, R., and Gu, Z. (2018). Cu-catalyzed enantioselective atropisomer synthesis via thiolative ring opening of five-membered cyclic diaryliodoniums. *Org. Lett.* 20 (18): 5779–5783.

28 Xue, X. and Gu, Z. (2019). Synthesis of bridged biaryl atropisomers via sequential Cu- and Pd-catalyzed asymmetric ring opening and cyclization. *Org. Lett.* 21 (11): 3942–3945.

29 Li, Q., Zhang, M., Zhan, S., and Gu, Z. (2019). Copper-catalyzed enantioselective ring-opening of cyclic diaryliodoniums and *O*-alkylhydroxylamines. *Org. Lett.* 21 (16): 6374–6377.

30 Chao, Z., Ma, M., and Gu, Z. (2020). Cu-catalyzed site-selective and enantioselective ring opening of cyclic diaryliodoniums with 1,2,3-triazoles. *Org. Lett.* 22 (16): 6441–6446.

31 Guo, W., Gu, J., and Gu, Z. (2020). Catalytic asymmetric synthesis of atropisomeric nitrones: versatile intermediate for axially chiral biaryls. *Org. Lett.* 22 (19): 7622–7628.

32 Duan, L., Wang, Z., Zhao, K., and Gu, Z. (2021). Enantioselective preparation of atropisomeric biaryl trifluoromethylsulfanes via ring-opening of cyclic diaryliodoniums. *Chem. Commun.* 57 (32): 3881–3884.

33 Zhu, K., Xu, K., Fang, Q. et al. (2019). Enantioselective synthesis of axially chiral biaryls via Cu-catalyzed acyloxylation of cyclic diaryliodonium salts. *ACS Catal.* 9 (6): 4951–4957.

34 Zhu, K., Wang, Y., Fang, Q. et al. (2020). Enantioselective synthesis of axially chiral biaryls via copper-catalyzed thiolation of cyclic diaryliodonium salts. *Org. Lett.* 22 (5): 1709–1713.

35 Zhu, K., Song, Z., Wang, Y., and Zhang, F. (2020). Synthesis of 2,2′-dihalobiaryls via Cu-catalyzed halogenation of cyclic diaryliodonium salts. *Org. Lett.* 22 (23): 9356–9359.

36 Ke, J., Zu, B., Guo, Y. et al. (2021). Hexafluoroisopropanol-enabled copper-catalyzed asymmetric halogenation of cyclic diaryliodoniums for the synthesis of axially chiral 2, 2′-dihalobiaryls. *Org. Lett.* 23 (2): 329–333.

37 Cheng, F., Duan, D.S., Jiang, L.M. et al. (2022). Copper-catalyzed asymmetric ring-opening reaction of cyclic diaryliodonium salts with imides. *Org. Lett.* 24 (6): 1394–1399.

38 Duan, L., Zhao, K., Wang, Z. et al. (2019). Enantioselective ring-opening/oxidative phosphorylation and p-transfer reaction of cyclic diaryliodoniums. *ACS Catal.* 9 (11): 9852–9858.

39 Zhao, K., Yang, S., Gong, Q. et al. (2021). Diols activation by Cu/borinic acids synergistic catalysis in atroposelective ring-opening of cyclic diaryliodoniums. *Angew. Chem. Int. Ed.* 60 (11): 5788–5793.

40 Zhang, X., Zhao, K., Li, N. et al. (2020). Atroposelective ring opening of cyclic diaryliodonium salts with bulky anilines controlled by a chiral cobalt(III) anion. *Angew. Chem. Int. Ed.* 132 (45): 20071–20076.

41 Yang, S., Zheng, T., Duan, L. et al. (2023). Atroposelective three-component coupling of cyclic diaryliodoniums and sodium cyanate enabled by the dual-role of phenol. *Angew. Chem. Int. Ed.* 62 (21): https://doi.org/10.1002/anie.202302749.

42 Han, J., Xiao, B., Sun, T.Y. et al. (2022). Enantioselective double carbonylation enabled by high-valent palladium catalysis. *J. Am. Chem. Soc.* 144 (47): 21800–21807.

43 Furuta, T., Yamamoto, J., Kitamura, Y. et al. (2010). Synthesis of axially chiral amino acid and amino alcohols via additive-ligand-free Pd-catalyzed domino coupling reaction and subsequent transformations of the product Amidoaza[5]helicene. *J. Org. Chem.* 75 (20): 7010–7013.

44 Wang, G., Shi, Q., Hu, W. et al. (2020). Organocatalytic asymmetric *N*-sulfonyl amide C-N bond activation to access axially chiral biaryl amino acids. *Nat. Commun.* 11: 946.

45 Hong, X., Guo, J., Liu, J. et al. (2022). Organocatalytic dynamic kinetic resolution of *N*-arylindole lactams: atroposelective construction of axially chiral amino acids bearing a C-N chiral axis. *Sci. China Chem.* 65 (5): 905–911.

46 Pang, L., Sun, Q., Huang, Z. et al. (2022). Palladium-catalyzed stereoselective cleavage of C−P bond: enantioselective construction of atropisomers containing a P-stereogenic center. *Angew. Chem. Int. Ed.* 61 (47): https://doi.org/10.1002/anie.202211710.

47 Deng, R., Xi, J., Li, Q., and Gu, Z. (2019). Enantioselective carbon-carbon bond cleavage for biaryl atropisomers synthesis. *Chem* 5 (7): 1834–1846.

48 Xi, J., Yang, H., Li, L. et al. (2022). Atroposelective kinetic resolution of 8H-Indeno[1,2-c]thiophen-8-ols via Pd-catalyzed C–C bond cleavage reaction. *Org. Lett.* 24 (12): 2387–2392.

49 (a) Shih, F.Y., Choi, D., Wu, Q. et al. (2019). ipso-Arylative ring-opening polymerization as a route to electron-deficient conjugated polymers. *Angew. Chem. Int. Ed.* 58 (1): 288–291. (b) Terao, Y., Wakui, H., Nomoto, M. et al. (2003). Palladium-catalyzed arylation of α,α-disubstituted arylmethanols via cleavage of a C−C or a C−H bond to give biaryls. *J. Org. Chem.* 68 (13): 5236–5243.

50 Li, L., Xi, J., Hong, B., and Gu, Z. (2023). From peripheral stereogenic center to axial chirality: synthesis of 3-arylthiophene atropisomers. *Adv. Synth. Catal.* 365 (4): 594–599.

51 Gu, J., Hong, B., Xue, X. et al. (2022). Synthesis of atropisomers with biaryl and vinylaryl chirality via Pd-catalyzed point-to-axial chirality transfer ring-opening. *Org. Lett.* 24 (49): 9097–9101.

52 Motoki, Y., Kazuyoshi, U., and Koichi, N. (2004). Rhodium-catalyzed acylation of vinylsilanes with acid anhydrides: application to the transformation of α-acyloxy vinylsilanes to unsymmetrical 1,2-diketones. *Chem. Lett.* 33 (4): 424–425.

53 Yamane, M., Uera, K., and Narasaka, K. (2005). Rhodium-catalyzed acylation of vinylsilanes with acid anhydrides. *Bull. Chem. Soc. Jpn.* 78 (3): 477–486.

54 Feng, J., Bi, X., Xue, X. et al. (2020). Catalytic asymmetric C–Si bond activation via torsional strain-promoted Rh-catalyzed aryl-Narasaka acylation. *Nat. Commun.* 11: 4449.

55 Bi, X., Feng, J., Xue, X., and Gu, Z. (2021). Construction of axial chirality and silicon-stereogenic center via Rh-catalyzed asymmetric ring-opening of silafluorenes. *Org. Lett.* 23 (8): 3201–3206.

56 Shimada, T., Cho, Y.H., and Hayashi, T. (2002). Nickel-catalyzed asymmetric Grignard cross coupling of dinaphthothiophene giving axially chiral 1,1′-binaphthyls. *J. Am. Chem. Soc.* 124 (45): 13396–13397.

57 Zhang, Q., Xue, X., Hong, B., and Gu, Z. (2022). Torsional strain inversed chemoselectivity in a Pd-catalyzed atroposelective carbonylation reaction of dibenzothiophenium. *Chem. Sci.* 13 (13): 3761–3765.

58 Zhang, J., Sun, T., Zhang, Z. et al. (2021). Nickel-catalyzed enantioselective arylative activation of aromatic C–O bond. *J. Am. Chem. Soc.* 143 (44): 18380–18387.

59 Zhang, Z., Zhang, J., Gao, Q. et al. (2022). Enantioselective alkylative cross-coupling of unactivated aromatic C–O electrophiles. *Nat. Commun.* 13: 2953.

60 Sun, T., Zhang, J., Fang, Y. et al. (2023). Enantioselective alkylation of unactivated C–O bond: solvent molecule affects competing β-H elimination and reductive elimination dynamics. *ACS Catal.* 13 (6): 3702–3709.

61 Bhat, V., Wang, S., Stoltz, B.M., and Virgil, S.C. (2013). Asymmetric synthesis of QUINAP via dynamic kinetic resolution. *J. Am. Chem. Soc.* 135 (45): 16829–16832.

62 Ros, A., Estepa, B., Ramirez-Lopez, P. et al. (2013). Dynamic kinetic cross-coupling strategy for the asymmetric synthesis of axially chiral heterobiaryls. *J. Am. Chem. Soc.* 135 (42): 15730–15733.

63 Hornillos, V., Ros, A., Ramírez-López, P. et al. (2016). Synthesis of axially chiral heterobiaryl alkynes via dynamic kinetic asymmetric alkynylation. *Chem. Commun.* 52 (98): 14121–14124.

64 Ramirez-Lopez, P., Ros, A., Romero-Arenas, A. et al. (2016). Synthesis of IAN-type *N*, *N*-ligands via dynamic kinetic asymmetric Buchwald–Hartwig amination. *J. Am. Chem. Soc.* 138 (37): 12053–12056.

65 Carmona, J.A., Hornillos, V., Ramirez-Lopez, P. et al. (2018). Dynamic kinetic asymmetric Heck reaction for the simultaneous generation of central and axial chirality. *J. Am. Chem. Soc.* 140 (35): 11067–11075.

66 Zheng, J., Cui, W.J., Zheng, C., and You, S.L. (2016). Synthesis and application of chiral spiro Cp ligands in rhodium-catalyzed asymmetric oxidative coupling of biaryl compounds with alkenes. *J. Am. Chem. Soc.* 138 (16): 5242–5245.

67 Zheng, D.S., Zhang, W.W., Gu, Q., and You, S.L. (2023). Rh(III)-catalyzed atroposelective C–H iodination of 1-aryl isoquinolines. *ACS Catal.* 13 (8): 5127–5134.

Part II

Challenges and Applications

7

Axially Chiral Ligands and Catalysts Derived from Atropisomeric Binaphthyl Structures

Shouyi Cen and Zhipeng Zhang

East China University of Science and Technology, School of Chemistry and Molecular Engineering, Feringa Nobel Prize Scientist Joint Research Center, Key Laboratory for Advanced Materials and Joint International Research Laboratory of Precision Chemistry and Molecular Engineering, 130 Meilong Road, Shanghai, 200237, China

7.1 Introduction

Asymmetric organic synthesis is among the core research areas in chemistry and has provided very efficient methods for the construction of numerous chiral molecules in the past decades. The key to this success is the development of a large variety of chiral ligands, which in combination with metals form catalytically active complexes, and organocatalysts as well as enzymes. It is worth noting that considerable amounts of chiral ligands and organocatalysts are derived from a few privileged chiral structures [1–3], and atropisomeric binaphthyl structure is one of them. Axially chiral 1,1′-bi-2-naphthol (BINOL), 2,2′-diamino-1,1′-binaphthalene (BINAM), and 2-amino-2′-hydroxy-1,1′-binaphthyl (NOBIN) are the most representative binaphthyl molecules (Figure 7.1) [4–8]. A large number of chiral ligands and organocatalysts, such as the privileged 2,2′-bis(di-phenylphosphino)-1,1′-binaphthyl (BINAP) and phosphoric acids, are derived from BINOL, BINAM, or NOBIN. In this chapter, we will trace the source of chirality and introduce about 150 representative chiral ligands and organocatalysts derived from axially chiral binaphthyl structures, especially BINOL, BINAM, and NOBIN. Some of the ligands/catalysts were not originally synthesized from BINOL, BINAM, or NOBIN. As enantiopure BINOL, BINAM, and NOBIN are commercially available nowadays, they can be easily synthesized from these chiral starting materials, especially BINOL which is a low-cost privileged chiral molecule. Therefore, chiral ligands and organocatalysts are mainly classified into three types according to their source of chirality.

The following items are suggested to be kept in mind when the readers proceed to explore these amazing chiral ligands and organocatalysts:

(1) Although only binaphthyl-containing chiral ligands and organocatalysts are included in this chapter, similar variants of them have been or can be developed from other axially chiral motifs such as biphenyl atropisomers and the privileged 1,1′-spirobiindane-7,7′-diol (SPINOL) [3].

Atropisomerism in Asymmetric Organic Synthesis: Challenges and Applications, First Edition.
Edited by Shinobu Takizawa and Mohamed S. H. Salem.

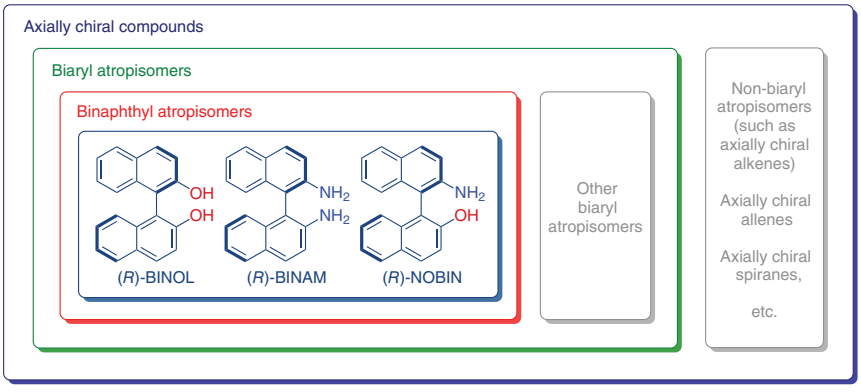

Figure 7.1 BINOL, BINAM, NOBIN, and their relationship to atropisomers and axially chiral compounds.

(2) The focus of this chapter is on the structural diversity of the chiral catalysts derived from binaphthyl motifs and the timeline for their development. Although a very limited number of enantioselective reactions are illustrated, a certain catalyst can possibly catalyze dozens of, hundreds of, or even thousands of asymmetric transformations.

7.2 Chiral Ligands Derived from BINOLs

The synthesis of BINOL can be traced back to about 100 years ago, whereas the utilization of BINOL as a chiral ligand was reported by Noyori et al. in 1979 [9]. One year later in 1980, Noyori and co-workers reported the development and application of BINAP (Figure 7.2) [10]. This milestone brings the axially chiral binaphthyl structures to the stage of asymmetric catalysis and inspires the development of a large variety of chiral ligands and organocatalysts possessing axial chirality.

7.2.1 Phosphorus-Containing Ligands

The eminent BINAP (**L1)** was first utilized as an axially chiral diphosphine ligand to generate a BINAP–rhodium complex that is capable of catalyzing asymmetric hydrogenation of α-(acylamino)acrylic acids **1** (Scheme 7.1) with excellent efficiency and enantioselectivity (up to 99% yield and 100% ee) [10]. This kind of privileged binaphthyl diphosphine ligands have proven to be capable of forming catalytically active and highly enantioselective species in combination with various transition metals, thus promoting thousands of reactions [11]. Apart from BINAP, a lot of elegant phosphorus-containing ligands have also been developed in the past decades (Figure 7.2).

In 1991, Hayashi and co-workers developed monodentate phosphines MOP (**L2**) and applied them in Pd-catalyzed asymmetric hydrosilylation of styrene [12]. MOP ligands have also found applications in many other enantioselective

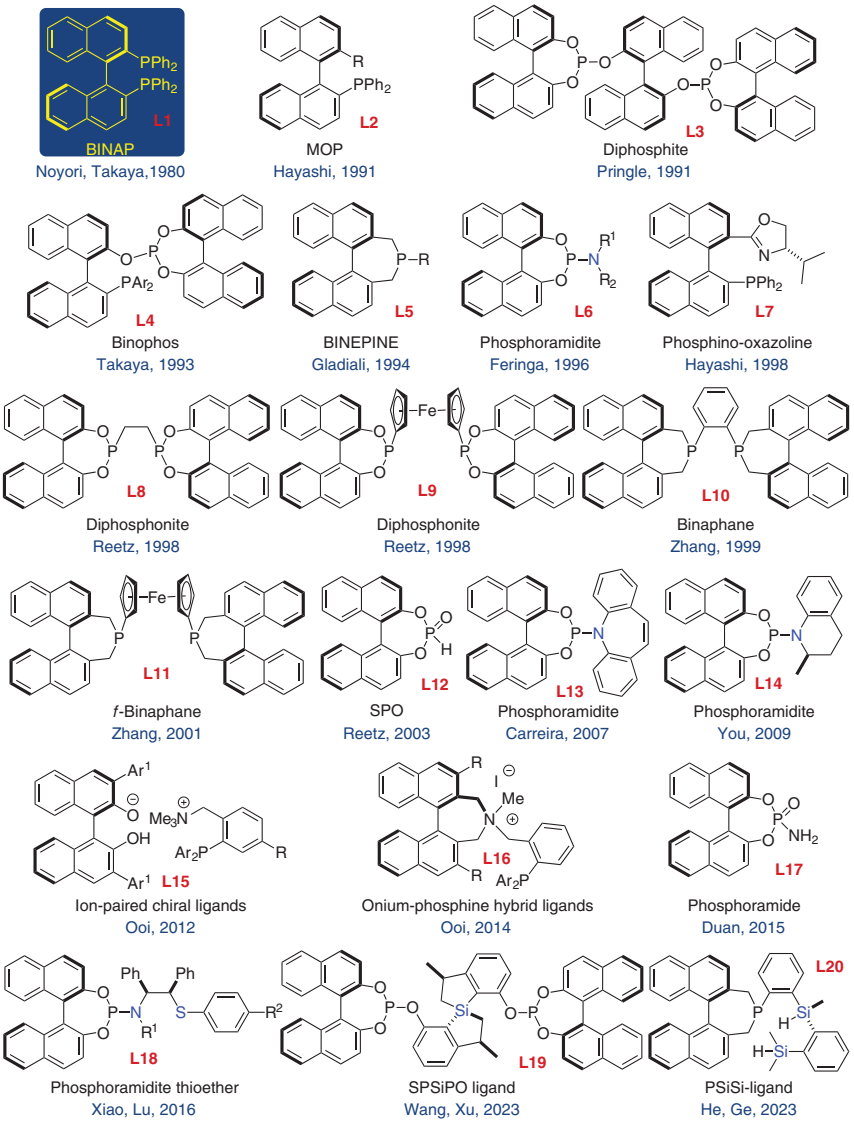

Figure 7.2 Phosphorus-containing ligands derived from BINOLs.

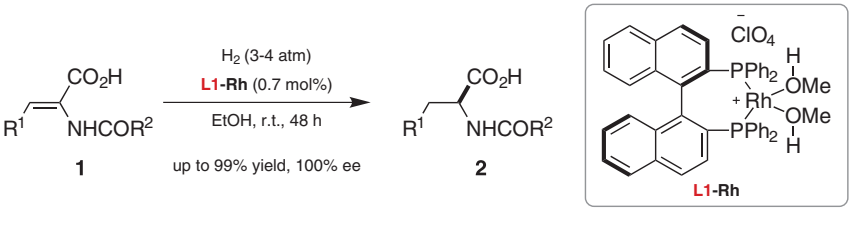

Scheme 7.1 Rh-catalyzed asymmetric hydrogenation of α-(acylamino)acrylic acids.

reactions [13]. In the same year, Pringle and co-workers developed a diphosphite ligand **L3**, which is composed of three binaphthyl units [14]. Later in 1993, Takaya and co-workers reported Binophos ligand **L4** and applied it in the hydroformylation of olefins [15]. Gladiali et al. reported the development of monodentate BINEPINE ligands **L5** [16]. In 1996, Feringa and co-workers developed axially chiral phosphoramidite ligand **L6** from BINOL and applied it in Cu-catalyzed conjugate addition of dialkylzinc reagents to unsaturated ketones [17]. This work is a milestone in the development of chiral phosphoramidite ligands and has inspired the design of a vast variety of phosphoramidite ligands bearing axially chiral backbone and diverse amines including the chiral ones. The ease of synthesis and modification of the ligands, the high catalytic reactivity, and excellent enantioinduction of the corresponding transition-metal complexes make phosphoramidites a privileged class of chiral ligands [18, 19]. Hayashi and co-workers synthesized C_1-symmetric phosphino-oxazoline ligand **L7** bearing both a binaphthyl skeleton and an oxazoline unit. The ligand was applied in Pd-catalyzed asymmetric allylic alkylation and the product was obtained in up to 91% ee [20]. Diphosphonite ligands **L8** and **L9** linked by ethano- or ferroceno-bridges were synthesized from BINOL by Reetz et al. in 1998 [21]. The corresponding rhodium complexes of these ligands are excellent catalysts for the hydrogenation of prochiral olefins such as itaconic acid dimethyl ester and 2-acetamido methyl acrylate, and the products were synthesized in 90–99.5% ee. In 1999, Zhang and co-workers reported the synthesis of chiral binaphthyl phosphane **L10** and its application in highly enantioselective hydrogenation of enamides [22]. Two years later, Zhang and co-workers developed binaphthyl phosphane possessing a ferrocene backbone **L11**, the Ir complex of which can catalyze enantioselective hydrogenation of acyclic imines (up to 99% ee) [23]. Reetz et al. reported the application of BINOL-based secondary phosphine oxide (SPO) **L12** in Rh-catalyzed hydrogenation of olefins and imines (up to 85% ee) [24]. In 2007, Carreira and co-workers developed binaphthyl phosphoramidite-olefin ligand **L13**, which enabled direct synthesis of an enantiomerically enriched primary allylic amine (70% yield, 70% ee) from an allylic alcohol [25]. This phosphoramidite-olefin ligand has proved to be very powerful in many transition metal-catalyzed asymmetric reactions [26]. You and co-workers synthesized 2-methyl-1,2,3,4-tetrahydroquinoline-derived phosphoramidite ligand **L14** and used it in Ir-catalyzed Friedel–Crafts reaction of indoles with allylic carbonates in 2009 [27]. This ligand was found to be very efficient and highly enantioselective in several Ir-catalyzed allylic substitution reactions [28–30].

In 2012, Ooi and co-workers reported a new strategy for design of chiral ligands for asymmetric transition-metal catalysis. An achiral cationic ammonium–phosphine hybrid ligand paired with a chiral binaphtholate anion (**L15**) showed remarkable stereo-controlling ability in Pd-catalyzed allylic alkylation of α-nitrocarboxylates (up to 97% ee) [31]. Two years later, Ooi and co-workers developed onium-phosphine hybrid ligands (arylphosphine, chiral ammonium ion, and counterion) **L16** [32]. The palladium complexes of this kind of ligands were found to be capable of promoting highly enantio- and diastereoselective [3 + 2] annulation reaction of 5-vinyloxazolidinones and activated trisubstituted alkenes to afford

five-membered heterocyclics with contiguous all-carbon quaternary stereocenters (up to 99% ee). BINOL-derived chiral phosphoramide **L17** was utilized as ligand by Duan and co-workers in 2015 to control the enantioselectivity in Pd-catalyzed asymmetric arylation of secondary β-C(sp^3)–H bonds of 8-aminoquinoline amides (up to 82% ee) [33]. In 2016, Xiao and co-workers developed binaphthyl-based phosphoramidite-thioether ligands **L18** [34]. These hybrid *P*,*S*-ligands were applied to Pd-catalyzed asymmetric decarboxylative [4 + 2] cycloaddition [34], indole allylic alkylation [35], and Cu-catalyzed regio-reversed asymmetric [3 + 2] cycloaddition of iminoesters with nitroolefins [36]. Recently, Wang and co-workers reported their development of the SPSiOL-derived bisphosphite ligand **L19** and realized Ni-catalyzed asymmetric hydrosilylation of 1,1-disubstituted allenes for the first time [37]. He and co-workers developed chiral PSiSi-ligand **L20** and applied it in the first Ir-catalyzed atroposelective intermolecular C–H silylation of 2-arylisoquinolines (up to 99% yield, 99% ee) [38].

7.2.2 Rare Earth-Alkali Metal–BINOL (REMB) Complexes and Linked BINOLs

BINOL and substituted BINOLs bear two phenolic hydroxy groups; therefore, they can directly form various metal complexes in combination with metals such as lanthanum, zinc, titanium, aluminum, gallium, and zirconium [4, 5]. A representative example is the REMB complexes developed by Shibasaki and co-workers in 1992 (**C1** in Figure 7.3) [39]. This class of monomeric and multimetallic complexes are composed of one rare earth metal, three alkali metals, and three BINOLates. The first REMB catalyst (RE = La) was applied to the catalytic asymmetric nitroaldol reaction of nitromethane (up to 90% ee). The broad utility of REMB turns it into one of the most successful multimetallic catalysts in asymmetric catalysis [40–42].

Besides the REMB catalysts, Shibasaki and co-workers also developed linked-BINOL ligands **L21** [43], which can form complexes with metals such

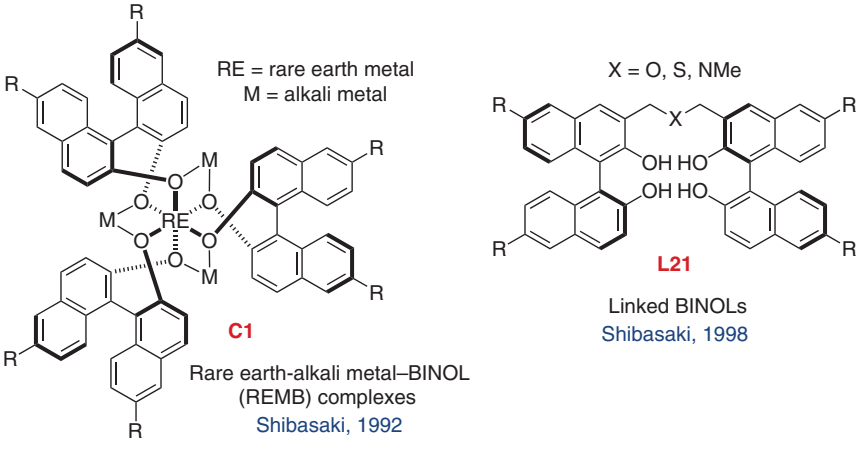

Figure 7.3 Rare earth-alkali metal–BINOL (REMB) complexes and linked BINOLs.

as Ga^{3+}, La^{3+}, Y^{3+}, Li^{+}, Zn^{2+}, and In^{3+}. The coordinative heteroatom (X) in the linker plays a crucial role in generating a unique and effective chiral environment for related transformations. The linked-BINOL ligands have been applied to various catalytic asymmetric reactions including epoxide opening reactions, Michael reactions, direct aldol reactions, direct Michael reactions of hydroxyketone, and direct Mannich-type reactions of hydroxyketones and *N*-acylpyrrole [44].

7.2.3 BINOL-Derived Salen Ligands

The binaphthyl motifs have also been incorporated into the privileged Salen type of ligands (Figure 7.4). Early in the 1990s, Brunner and co-workers [45, 46] and Katsuki and co-workers [47, 48] synthesized acyclic and cyclic BINOL-derived Salen ligands (**L22–24**) and utilized them in Cu-catalyzed enantioselective cyclopropanation of styrene and Mn-catalyzed enantioselective epoxidation of unfunctionalized olefins, respectively. A number of BINOL-derived Salen complexes incorporating Ni^{2+}, Cu^{2+}, Zn^{2+}, or Pd^{2+} were synthesized and characterized by Kozlowski and co-workers [49]. These complexes were found to be capable of catalyzing the asymmetric addition of benzyl malonate to cyclohexenone (up to 90% ee).

7.2.4 Sulfur-Containing Ligands

In 1993, Lucchi and co-workers reported the practical synthesis of enantiomerically pure 1,1′-binaphthalene-2,2′-dithiol **L25** (binas) from (*R*)-BINOL (Figure 7.5) [50]. In the same year, Gladiali and co-workers utilized **L25** (binas) or the dimethyl sulfide **L26** as a ligand to promote Rh-catalyzed hydroformylation of styrene, albeit low enantioselectivity (15% ee) [51]. Dorta and co-workers reported the application of chiral bis-sulfoxide (BINASO) ligand **L27** derived from binaphthyl backbone in Rh-catalyzed asymmetric addition of arylboronic acids to electron-deficient olefins (up to 99% ee) [52]. In 2008, Ishihara and co-workers disclosed a practical synthesis of 1,1-binaphthyl-2,2-disulfonic acid (BINSA) **L28** from (*R*)-BINOL [53]. One year later, Ishihara and co-workers developed a chiral lanthanum(III) complex from BINSA and utilized it to catalyze the enantioselective Strecker reaction (up to 92% ee) [54]. As an anionic ligand, BINSA is capable of forming complexes with various metals to catalyze a range of enantioselective reactions [55]. In 2021,

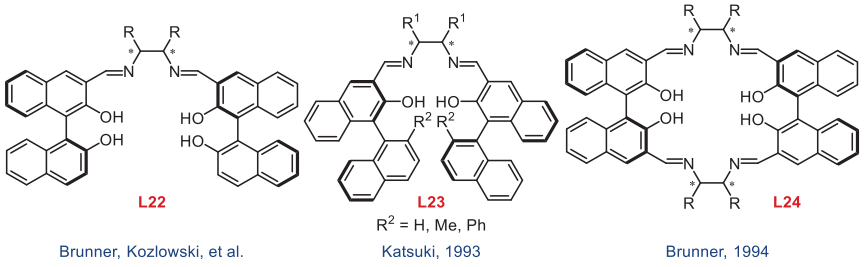

Figure 7.4 Representative BINOL-derived Salen ligands.

Figure 7.5 Sulfur-containing ligands.

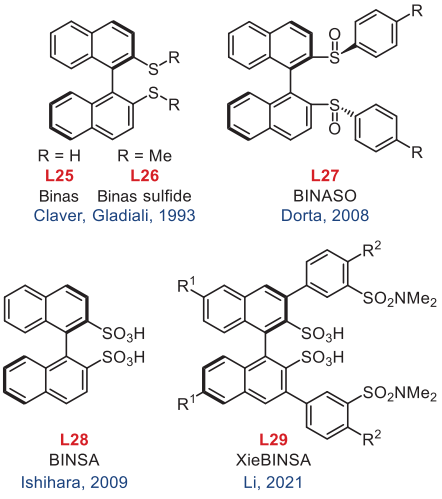

Li and co-workers designed and synthesized a series of chiral binaphthyl disulfonic acid ligands **L29** and applied them in Ti-catalyzed enantioselective intramolecular hydroalkoxylation of nonactivated alkenes (up to 97% ee) [56].

7.2.5 Oxazoline-Containing Ligands

Chiral oxazolines have been widely utilized as ligands in a large variety of asymmetric reactions. Oxazoline-containing ligands based on binaphthyl backbone have also been developed (Figure 7.6). In 1996, Hayashi and co-workers developed axially chiral bis(oxazolyl) ligands **L30** and applied them in Cu-catalyzed asymmetric cyclopropanation of styrene with diazoacetates (up to 97% ee) [57]. Shibatomi et al. developed chiral pyridyl spirooxazoline ligands bearing a binaphthyl backbone **L31**. These ligands show high enantioinduction in Pd-catalyzed allylic alkylation [58], and Cu-catalyzed fluorination and chlorination of β-keto esters [59]. In 2016, Wang and co-workers reported the synthesis of BINOL-derived bisoxazoline (BOX) ligand **L32**, the copper complex of which promoted the Friedel–Crafts reaction of indoles with isatin-derived β,γ-unsaturated α-keto esters with excellent enantioselectivities (up to 99% ee) [60]. Maruoka and co-workers synthesized chiral binaphthyl–BOX hybrid ligand **L33** in 2020. An enantioselective three-component radical relay coupling of alkylsilyl peroxides, vinylarenes, and arylboronic acids was achieved with the copper complex of this binaphthyl–BOX hybrid ligand **L33** (up to 93% ee) [61].

7.2.6 Vanadium Complexes for Enantioselective Oxidative Coupling of Phenols

Oxidative coupling of phenols, in particular 2-naphthols, provides a very efficient and straightforward approach for the construction of biaryl atropisomers. Various

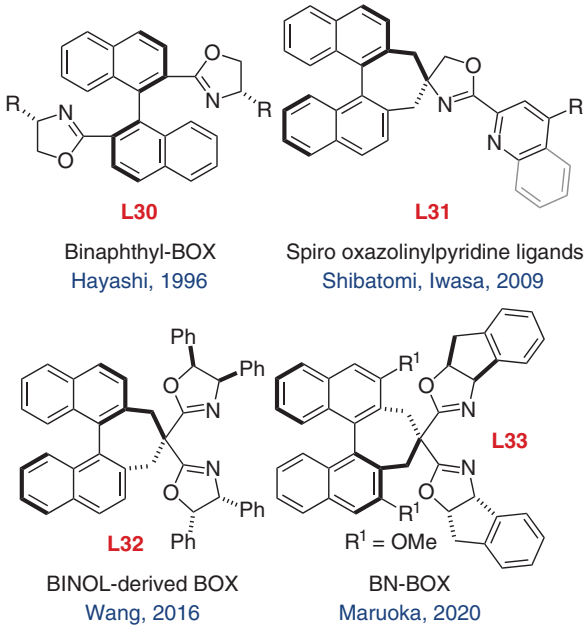

Figure 7.6 Oxazoline-containing ligands.

dinuclear and mononuclear vanadium complexes derived from binaphthyl ligands have been developed by Gong (**C2**) [62, 63], Uang (**C3**) [64], and Sasai and Takizawa (**C4**, **C5** in Figure 7.7) [65, 66]. These complexes have been proven to be efficient and highly enantioselective catalysts for the oxidative homocoupling and cross-coupling of various phenolic compounds including 2-naphthols to afford various substituted BINOLs and other axially chiral compounds [67]. Mononuclear vanadium complexes **C5** were reported to be capable of catalyzing oxidative coupling/intramolecular cyclization of polycyclic phenols **3** to afford oxa[9]helicenes **4** (Scheme 7.2) with ee values up to 94% (refer to Chapter 3 for more details) [66].

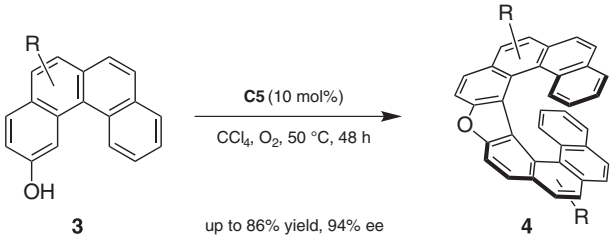

Scheme 7.2 Oxidative coupling/intramolecular cyclization of polycyclic phenols.

7.2.7 Binaphthyl-Based Chiral Diene Ligands and Cyclopentadienyl Ligands

In 2010, Du and co-workers synthesized various binaphthyl-based chiral dienes **L34** (Figure 7.8). These axially chiral dienes were utilized as ligands in Rh-catalyzed

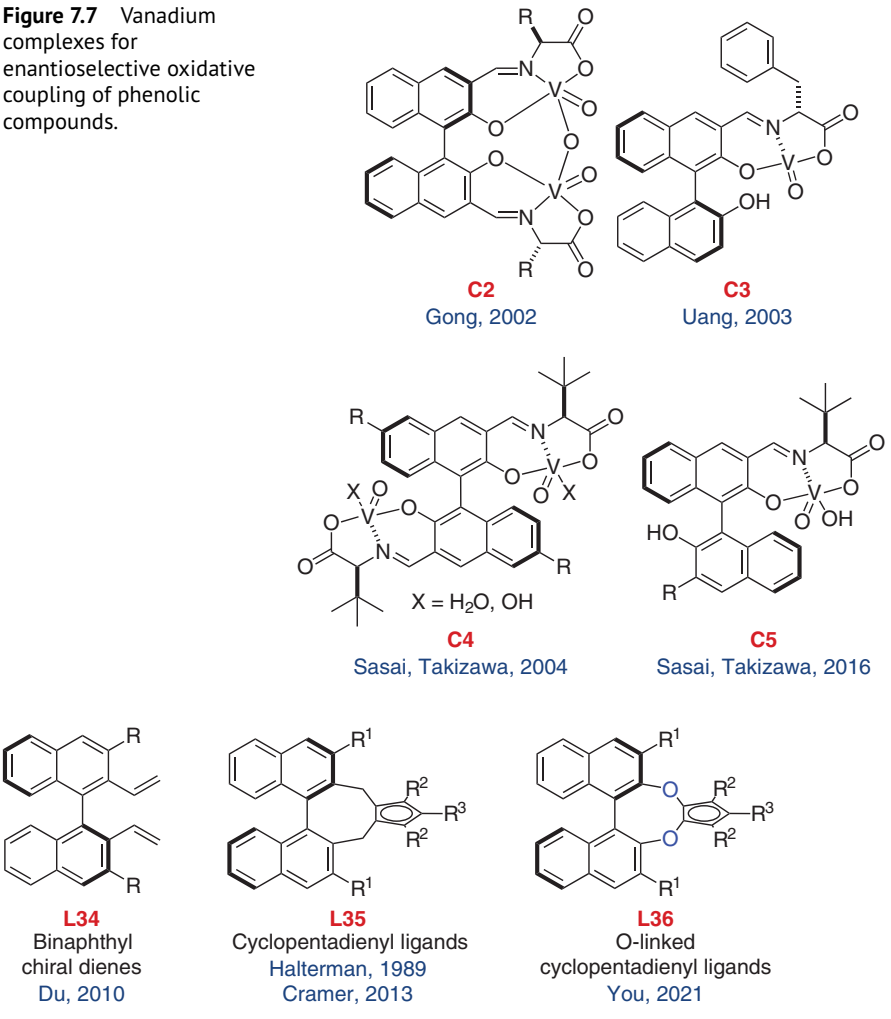

Figure 7.7 Vanadium complexes for enantioselective oxidative coupling of phenolic compounds.

Figure 7.8 Binaphthyl-based chiral diene ligands and cyclopentadienyl ligands.

asymmetric arylations of *N*,*N*-dimethylsulfamoyl-protected aldimines with aryl-boronic acids (up to 84% ee) [68]. Early in 1989, Halterman reported the synthesis of an unsubstituted binaphthyl cyclopentadienyl ligand using an asymmetric Ni-catalyzed coupling reaction as the key step [69]. Cramer in 2013 developed a practical and efficient method for the synthesis of highly tunable cyclopentadienyl ligands **L35** from (*R*)- or (*S*)-BINOL and applied them in Rh-catalyzed C–H allylations of benzamides [70]. After 10 years of explorations, binaphthyl-based cyclopentadienyl ligands (**L35**) have proven to be able to form catalysts with various transition metals (such as Rh, Ru, Ir, and Co) and rare-earth metals (Sc, Y, La, Sm, Gd, etc.) and promote dozens of enantioselective transformations [71]. The sterically and electronically tunable *ortho*-substituents (R^1) on the binaphthyl backbone prove to be crucial to its success. In 2021, You and co-workers reported

the synthesis of oxygen-linked cyclopentadienyl ligands **L36** from enantiomerically pure BINOL. The corresponding rhodium(III) complexes have proved to be very efficient and highly enantioselective catalysts for asymmetric C–H arylation of benzo-[*h*]quinolines with 1-diazonaphthoquinones (up to 99% yield, 97% ee) [72].

7.2.8 Binaphthyl-Based Monocarboxylic Acid Ligands

Chiral carboxylic acid-containing compounds can serve as ligands for transition-metal catalyzed reaction, especially for C–H functionalization reactions. In 2015, Hintermann and co-workers developed a chiral titanium catalyst from binaphthyl-based monocarboxylic acid ligand **L37** and utilized it to promote the cycloisomerization of 2-allylphenols to 2-methyl-2,3-dihydrobenzofurans (2-methylcoumarans) at uncommonly high temperatures (220–240 °C) with ee up to 87% (Figure 7.9) [73]. Baudoin and co-workers developed carboxylic acid-containing bifunctional ligands **L38** in 2018 [74]. The ligands displayed excellent enantioinduction in several Pd(0)-catalyzed C(sp^2)–H arylation reactions (Scheme 7.3a) [75, 76].

Matsunaga and co-workers reported the utilization of carboxylic acid ligand **L39** to control the enantioselectivity (up to 97% ee) of achiral Cp*Rh(III)-catalyzed C–H alkylation of diarylmethanamines **7** with diazomalonate **8** (Scheme 7.3b) [77]. Matsunaga and co-workers also realized enantioselective directed methylene C(sp^3)–H amidation reactions of 8-alkylquinolines by using a catalyst formed from Cp*Rh(III) and carboxylic acid **L40** [78]. In 2021, the authors developed pseudo-C_2-symmetric chiral binaphthyl monocarboxylic acids **L41** with reduced conformational flexibility. The ligands were applied to Rh(III)-catalyzed enantioselective C(sp^3)–H amidation reactions of 2-alkylpyridine derivatives and related heteroaromatic compounds (up to 92% ee) [79]. Shi and co-workers reported the

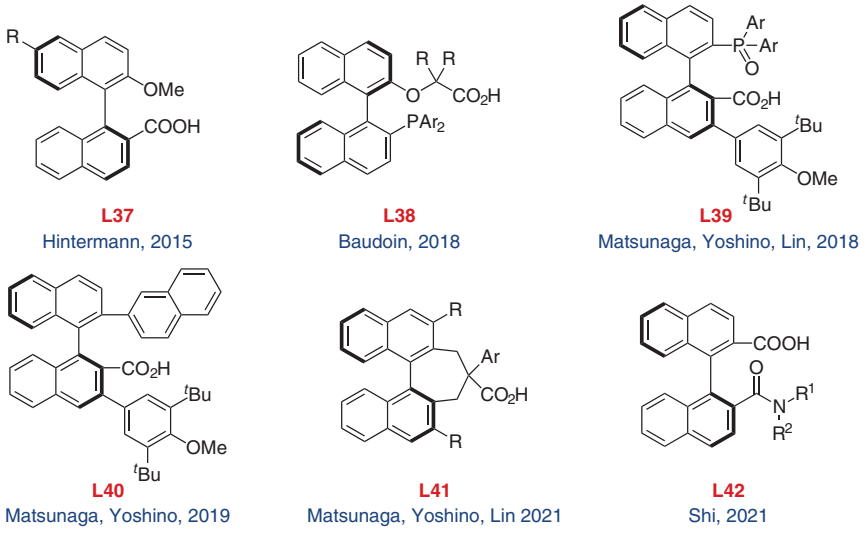

Figure 7.9 Binaphthyl-based monocarboxylic acid ligands.

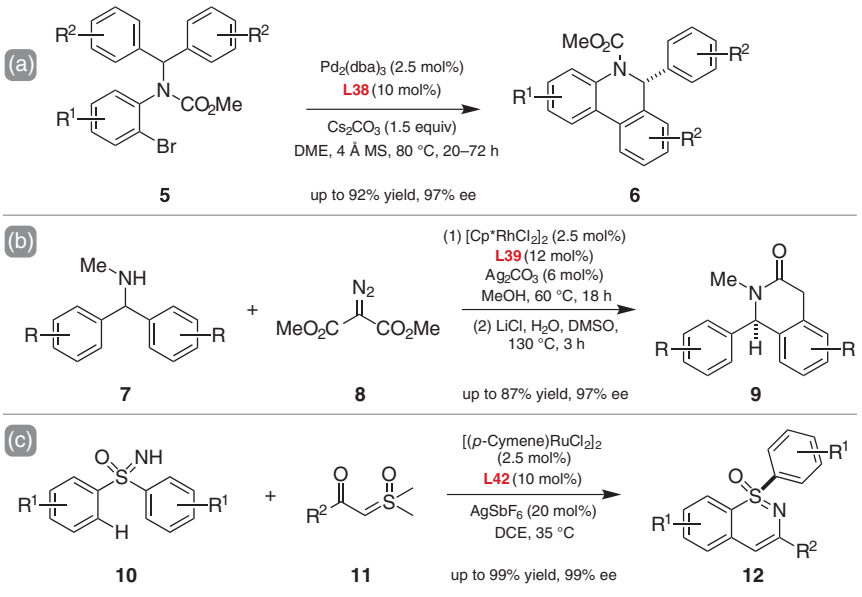

Scheme 7.3 C–H functionalization promoted by **L38**, **L39**, or **L42**.

application of monocarboxylic acids **L42** in Ru(II)-catalyzed enantioselective C–H activation/annulation of sulfoximines **10** with α-carbonyl sulfoxonium ylides **11** (Scheme 7.3c) and Ir(III)-catalyzed enantioselective C–H activation/annulation of sulfoximines with diazo compounds [80, 81]. These examples show the great potential of binaphthyl-based carboxylic acid ligands in C–H activation reactions.

7.2.9 Axially Chiral Ligands and Catalysts Containing a Phenanthroline or Pyridine Unit

Coordinating heterocycles such as phenanthroline and pyridine have been incorporated into binaphthyl backbones to develop novel chiral ligands that possess both greater coordination ability and excellent chiral environment. Representative examples are shown in Figure 7.10. In 2014, Nishiyama and co-workers developed binaphthyl-based *N*,*N*,*O*-tridentate phenanthroline ligands **L43** [82]. The ligands are able to form highly enantioselective catalysts with various metals (such as Zn, Cu, Ni, and Rh) and have been applied to a range of asymmetric reactions including 1,2-addition of organozinc reagents to aldehydes, amination of β-keto carbonyl compounds with azodicarboxylate, Davis oxidation and Michael addition of *N*-Boc-3-phenyloxindole, and desymmetrization of substituted hydrosilanes **13** (Scheme 7.4a) [83].

Zhang and co-workers designed multivariant axially chiral catalysts (MACCs) by incorporating various chelating subunits into binaphthyl backbones to form highly tunable chiral ligands, which then coordinate with various metals to form chiral complexes. Preliminary applications of this catalytic system in asymmetric construction of axially chiral molecules (BINOL, BINAM, and NOBIN derivatives)

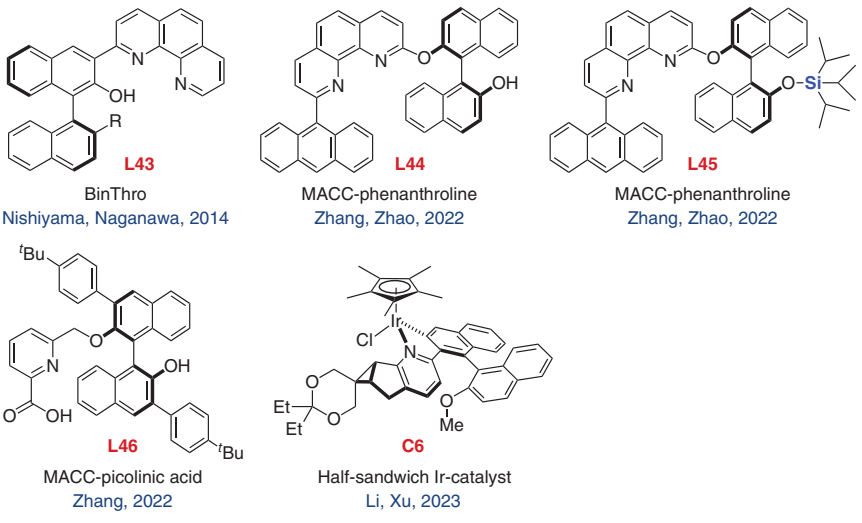

Figure 7.10 Axially chiral ligands and catalysts containing a phenanthroline or pyridine unit.

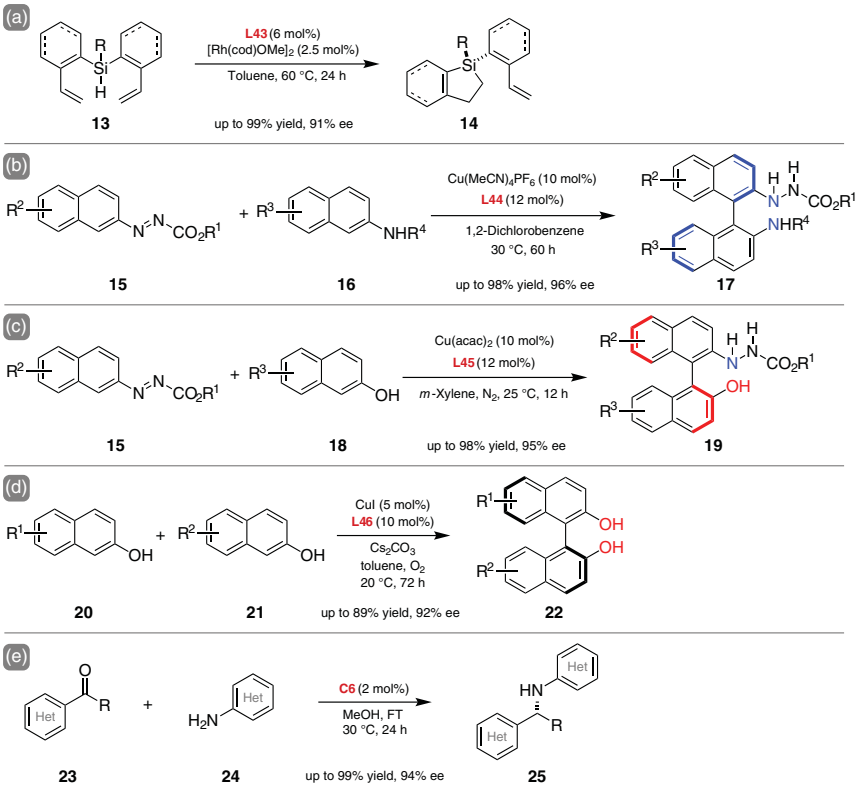

Scheme 7.4 Transformations promoted by ligands and catalysts shown in Figure 7.10.

were disclosed in 2022. The copper catalyst *in situ* prepared from ligand **L44** and $Cu(MeCN)_4PF_6$ was able to catalyze the enantioselective cross-coupling of azonaphthalenes **15** with *N*-benzyl-2-naphthylamines **16**, affording (*R*)-BINAM derivatives in excellent yield and ee (Scheme 7.4b). The copper catalyst prepared from ligand **L45** and $Cu(acac)_2$ catalyzed the cross-coupling of azonaphthalenes **15** with 2-naphthols **18** to produce (*S*)-NOBIN derivatives also in excellent yield and ee (Scheme 7.4c) [84]. Interestingly, the absolute configuration of the products was found to be determined by the conformation of the catalysts rather than the absolute configuration of the BINOL unit. The results show the importance of conformational dynamics of chiral catalysts in asymmetric catalysis. These two redox neutral coupling reactions for the synthesis of BINAM and NOBIN derivatives were first developed by Tan and co-workers in 2019, using a chiral phosphoric acid-salt complex or $Ni(OTf)_2$/chiral bis(oxazoline) complex as a catalyst [85]. Axially chiral ligand **L46** bearing a chelating picolinic acid unit reacts with CuI to generate an efficient catalyst for the asymmetric oxidative coupling of various 2-naphthols (Scheme 7.4d) [86]. In 2023, Li and co-workers developed a chiral half-sandwich iridium catalyst **C6** bearing a binaphthyl skeleton and applied it to transfer hydrogenative direct asymmetric reductive amination (Scheme 7.4e) [87].

7.3 Chiral Ligands Derived from BINAMs

BINAM possesses very similar axially chiral binaphthyl structure to BINOL, whereas it bears two chelating amino groups rather than two phenolic hydroxy groups. These features turn enantiopure BINAM into an excellent chiral diamine (such as *trans*-1,2-cyclohexanediamine and 1,2-diphenylethylenediamine) for designing nitrogen-containing ligands. Representative examples of chiral ligands derived from BINAMs are shown in Figure 7.11.

As a subclass of privileged Salen ligands, BINAM-derived ligand **L47** can be easily synthesized through the condensation of salicylaldehyde with enantiopure BINAM. Early in the 1980s, Brunner and co-workers [88] and Nishinaga et al. [89] prepared copper and cobalt complexes from **L47**, respectively, and tested them as chiral catalysts. Che and co-workers [90] and Moberg and co-workers [91] have synthesized tetradentate binaphthyl bis-amide ligand **L48** and utilized it to prepare transition-metal complexes for asymmetric transformation, respectively. In 1994, Mikami and co-workers developed chiral titanium catalyst from binaphthyl bis-sulfonamide ligand **L49** and tested it in the carbonyl-ene reaction of glyoxylate [92, 93]. Suga et al. employed binaphthyldiimine **L50** as ligand in Cu-catalyzed enantioselective cyclopropanation of olefins with diazoacetates (98% ee) [94]. Ytterbium catalysts were prepared from BINAM-derived bis-amide ligands **L51** by Nakagawa and co-workers for the Diels–Alder reaction between cyclopentadiene and crotonyl-1,3-oxazolidin-2-one and excellent ee was obtained (up to >98%) [95]. In 2000, Shi and Sui developed binaphthyl thiophosphoramide ligands **L52** [96]. These ligands have been applied to several reactions such as Ag-catalyzed allylation

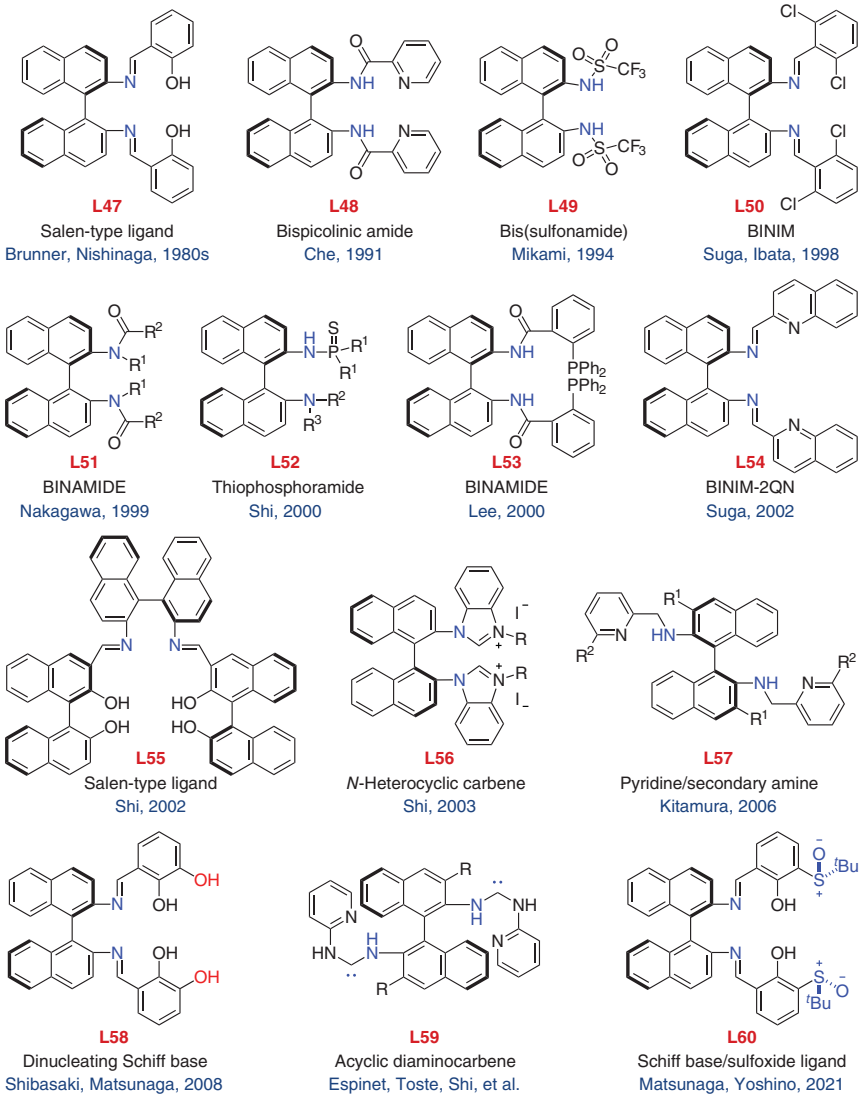

Figure 7.11 Representative axially chiral ligands derived from BINAMs.

of aldehydes with allyltributyltin (up to 98% ee) [97], Cu-catalyzed addition of diethylzinc to sulfonylimines (up to 93% ee) [98], and diphenylphosphinoylimines (up to 85% ee) [99]. Lee and co-workers synthesized bisphosphine ligands **L53** and tested them in Pd-catalyzed desymmetrization of meso cyclic carbamates (up to 76% ee) [100]. In 2002, Suga et al. synthesized binaphthyldiimine **L54** bearing two quinoline units and used it in Ni-catalyzed Diels–Alder reactions between cyclopentadiene and 3-alkenoyl-2-oxazolidinones (up to 94% ee) [101]. In the same year, Shi et al. synthesized a Salen-type ligand **L55** bearing three binaphthyl units and tested it in the addition reaction of diethylzinc to aldehydes (up to 83% ee) [102].

In 2003, Shi and co-workers developed axially chiral *N*-heterocyclic carbene precursors **L56** and corresponding rhodium complexes. In the hydrosilylation of methyl ketones, these rhodium catalysts displayed excellent enantioinduction (up to 98% ee) [103]. Kitamura and co-workers developed tetradentate ligands **L57** containing both sp^2 and sp^3 nitrogen atoms from BINAM in 2006 [104]. Excellent enantioselectivities (up to 99% ee) were achieved in Ru-catalyzed hydrogenation of aromatic ketones using **L57** as ligands. In 2008, Shibasaki and co-workers designed dinucleating Schiff base ligand **L58**, which can coordinate with two Ni to form dinuclear complex [105]. Excellent enantioselectivities (up to 99% ee) were achieved in the Mannich-type reaction of *N*-Boc imines with β-keto phosphonates with this dinuclear nickel catalyst. Acyclic diaminocarbene ligands **L59** were utilized to generate gold catalysts by several groups to catalyze asymmetric reactions such as cyclopropanation of styrene with propargyl pivaloate [106] and enantioselective synthesis of chromenyl pivalate from phenol ethers [107]. In 2021, Matsunaga and co-workers developed a BINAM-based Salen-type ligand bearing sulfoxide units **L60** and applied it in Pd-catalyzed intramolecular allylic C–H amination (up to 82% ee) [108].

7.4 Chiral Ligands Derived from NOBINs

NOBIN is regarded as a hybrid of BINOL and BINAM as it bears one phenolic hydroxy group and one amino group located at a chelating position. With a binaphthyl backbone, NOBIN has also been utilized to develop various axially chiral ligands (Figure 7.12). The tridentate Schiff base ligands **L61** are a representative class of ligands developed from NOBIN. This type of ligand was first reported by Carreira et al. in 1994 and can be easily synthesized through the condensation of enantiopure NOBINs with salicylaldehydes [109]. The corresponding titanium complexes have been proven to be very efficient and highly enantioselective catalysts for aldol additions of acetate-derived silyl enolates [109], 2-methoxypropene [110], and O-TMS dienolate [111]. Ding and co-workers prepared a library of tridentate Schiff base ligands **L61** and applied them in Ti-catalyzed hetero-Diels–Alder reaction of Danishefsky's diene with aldehydes (up to >99% yield, >99% ee) [112, 113].

The MAP ligand **L62** was developed by Kočovský and co-workers [114, 115] and Ding et al. [116], independently in the late 1990s. In 1999, Zhang and co-workers designed *P*,*N*-ligands **L63** and applied them in Cu-catalyzed conjugate addition of diethylzinc to enones (up to 98% ee) [117]. In 2002, Ding and co-workers synthesized pyrrolidino-MAP ligand **L64**, which bears both axial and central chirality. Good enantioselectivity (up to 86% ee) was achieved in the Pd-catalyzed allylic alkylation of allyl acetates [118]. Brunner et al. synthesized axially chiral imine **L65** and amine **L66** ligands from NOBIN and applied them in Ru-catalyzed transfer hydrogenation of acetophenone. Both of these ligands exhibit excellent enantioinduction (up to 97% ee) [119]. Also in 2002, Hoveyda and co-workers developed chiral Ru-catalyst **C7** for enantioselective olefin metathesis [120]. This ruthenium complex was synthesized from a NOBIN-based *N*-heterocyclic carbene and can promote asymmetric ring-opening/cross metathesis (AROM/CM) in air, with undistilled solvents (up

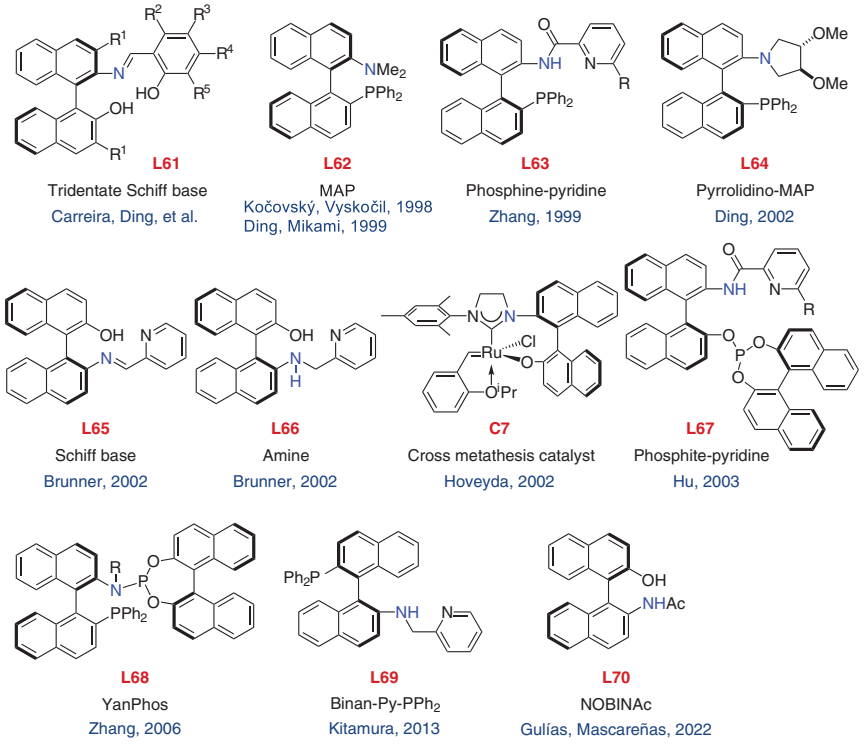

Figure 7.12 Representative axially chiral ligands derived from NOBINs.

to >98% ee) [121]. In 2003, Hu and co-workers developed phosphite-pyridine ligand **L67** from NOBIN and BINOL and employed it in Cu-catalyzed 1,4-conjugate additions of diethylzinc to acyclic enones (up to 97% ee) [122].

In 2006, Zhang and co-workers designed a hybrid phosphorus ligand (YanPhos) **L68** from NOBIN and BINOL. In the Rh-catalyzed asymmetric hydroformylations of styrene derivatives and vinyl acetate, this ligand exhibits excellent enantioinductive capability (up to 99% ee) [123]. In 2013, Kitamura and co-workers designed C_1-symmetric *P*,*N*,*N*-ligand **L69** for Ru-catalyzed hydrogenation of *tert*-alkyl ketones (up to 98% ee) [124]. Recently in 2022, Gulías and co-workers reported the utilization of simple acylated NOBIN **L70** in controlling the enantioselectivity (up to 98% ee) of a Pd-catalyzed C–H activation reaction (Scheme 7.5) [125].

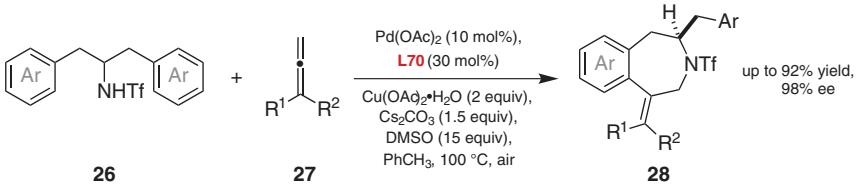

Scheme 7.5 Synthesis of benzazepines through a formal [5 + 2] annulation using **L70** as a ligand.

7.5 Chiral Organocatalysts Derived from BINOLs

With the development of asymmetric organocatalysis, a large variety of chiral organocatalysts including Brønsted acids, Brønsted bases, Lewis acids, Lewis bases, phase-transfer catalysts, and bifunctional catalysts have been developed in the past decades. Considerable amount of these chiral organocatalysts bear at least one atropisomeric binaphthyl unit, especially those derived from enantiopure BINOLs.

7.5.1 Acid Organocatalysts Derived from BINOLs

In 2004, Akiyama et al. [126] (Scheme 7.6a) and Terada and co-workers [127] (Scheme 7.6b) independently reported pioneering work on the utilization of BINOL-derived phosphoric acids **C8** as Brønsted acid catalysts in Mannich-type reactions (Figure 7.13). During the past twenty years, chiral phosphoric acids have drawn extremely broad attention from the community of asymmetric catalysis and have been successfully applied in hundreds of enantioselective reactions [128–131]. In 2006, Yamamoto and co-workers designed chiral *N*-triflyl phosphoramides **C9** and applied them in asymmetric Diels–Alder reaction of α,β-unsaturated ketone with silyloxydiene (up to 93% ee) [132]. Yamamoto and co-workers developed Brønsted acid-assisted chiral Brønsted acid catalyst **C10**, which catalyzed Mannich-type reaction of ketene silyl acetals with aldimines to give β-amino esters with moderate to good ee (up to 87%) [133]. In 2007, Maruoka and co-workers designed axially chiral dicarboxylic acids **C11** and applied them to the Mannich reaction of arylaldehyde *N*-Boc imines and diazo compounds (up to 96% ee) [134]. These axially chiral dicarboxylic acids **C11** can also promote several other asymmetric reactions [135]. Ishihara and co-workers used BINSA **C12** as Brønsted

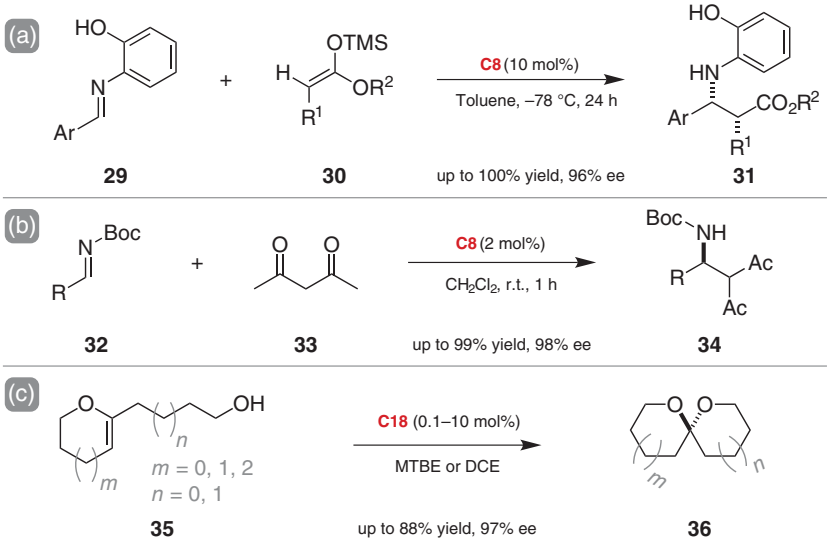

Scheme 7.6 Transformations promoted by organocatalyst **C8** or **C18**.

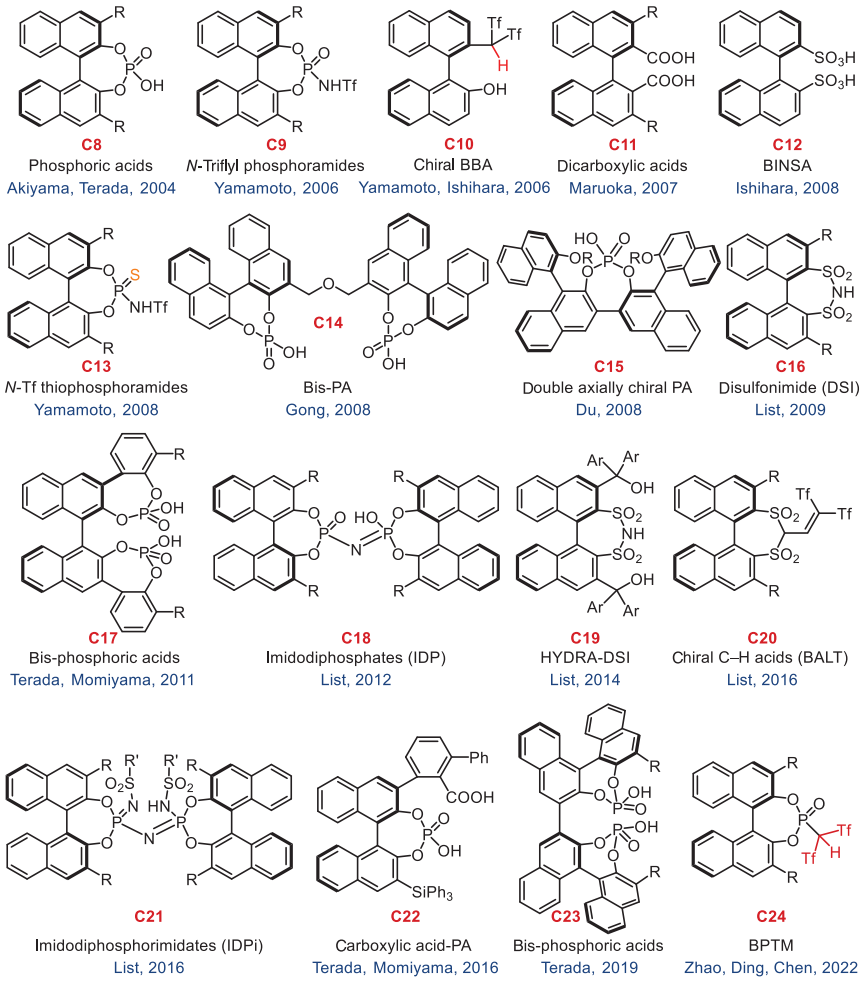

Figure 7.13 Acid organocatalysts derived from BINOLs.

acid in combination with a 2,6-diarylpyridine to form a combined salt catalyst for Mannich-type reactions [53]. Several axially chiral Brønsted acids, including *N*-triflyl thiophosphoramides **C13** (by Yamamoto) [136], bis-phosphoric acid **C14** (by Gong) [137], and double axially chiral phosphoric acid **C15** (by Du) [138] were also developed in 2008.

List and co-workers designed and synthesized axially chiral disulfonimides (DSIs) **C16** in 2009 [139]. DSI catalysts can serve as both Brønsted acids and Lewis acids (after silylation) to promote a broad range of reactions with excellent enantioselectivities [140]. In 2011, Momiyama et al. designed chiral bis-phosphoric acids **C17** [141]. In the Diels–Alder reaction of α,β-unsaturated aldehydes with amidodienes, bis-phosphoric acids **C17** are catalytically more active and enantioselective than mono-phosphoric acids **C8**. In 2012, List and Čorić designed and developed confined Brønsted acids imidodiphosphates (IDP) **C18**

by connecting two BINOL-derived chiral phosphoric units through the formation of an imidodiphosphoric acid motif. These Brønsted acids possess an extremely sterically demanding chiral environment and demonstrate exceptionally high enantioinduction in the extremely challenging catalytic enantioselective spiroacetalization reaction (Scheme 7.6c) [142]. List and co-workers also developed internal hydrogen bond-assisted disulfonimide catalyst **C19** [143]. The authors investigated the relative catalytic activity of **C19** and **C16** in the Mukaiyama aldol reaction of benzophenone and it turned out that internal hydrogen-bond-assisted DSI **C19** is several orders of magnitude more active than **C16**.

In 2016, List and co-workers reported the development of chiral super Brønsted C–H acids binaphthyl-allyl-tetrasulfones (BALTs) **C20**, which possess a binaphthyl-allyl-tetrasulfone structure and turn into highly active Lewis acid catalysts after in situ silylation, for the Diels–Alder reaction of cinnamates with cyclopentadiene (up to 94% ee) [144]. In the same year, List and co-workers developed highly acidic and extremely active imidodiphosphorimidate (IDPi) Brønsted acids **C21** and applied them in enantioselective addition of allyltrimethylsilane to aldehydes [145]. IDPi have been proven to be very powerful Brønsted acid catalysts and "silylium" Lewis acid precatalysts for a large number of very challenging transformations [146].

Momiyama and co-workers designed a chiral Brønsted acid **C22** containing two different acidic sites (both carboxylic acid and monophosphoric acid), which has proven to be a highly regio-, diastereo-, and enantioselective catalyst for the asymmetric hetero-Diels–Alder reaction between 6-trifluoromethyl-2-azopyridinecarboxylates and *N*-H-amidodienes [147]. In 2019, Terada et al. synthesized bis-phosphoric acid **C23** from a dimeric BINOL backbone [148]. Recently in 2022, Zhao and co-workers developed BINOL-derived chiral super Brønsted C–H acids **C24** (BINOL-derived phosphoryl bis-((trifluoromethyl)sulfonyl) methane, BPTM) [149]. In comparison with BINOL-derived chiral phosphoric acids **C8** and *N*-triflyl phosphoramides (**C9**), BPTM exhibited much higher activity and enantioselectivity in several reactions such as asymmetric Mukaiyama–Mannich reaction, allylic amination, and protonation of silyl enol ether.

A few binaphthyl-based silicon Lewis acids have been developed from BINOL (Figure 7.14). In 1998, Jørgensen and co-workers reported an acetonitrile-stabilized silicon cation catalyst **C25** for the enantioselective Diels–Alder reaction [150]. Although the obtained ee is very low (10%), this work inspires the development of other silicon Lewis acid catalysts. Hatanaka and co-workers reported pentacoordinate silyl triflimides **C26** for a highly enantioselective Diels–Alder reaction (up to 97% ee) [151]. Oestreich and co-workers developed thioether-stabilized silicon cation catalysts **C27** and **C28** [152, 153]. In 2013, Du and co-workers developed axially chiral frustrated Lewis pair catalysts **C29** through *in situ* hydroboration of chiral dienes with $HB(C_6F_5)_2$ and achieved highly enantioselective metal-free hydrogenation of imines (up to 89% ee) [154]. In 2015, Maruoka and co-workers reported a boronic acid catalyst **C30** for the aza-Michael addition of hydroxamic acid to quinone imine ketals (up to 97% ee) [155]. In 2021, Hall and co-workers designed

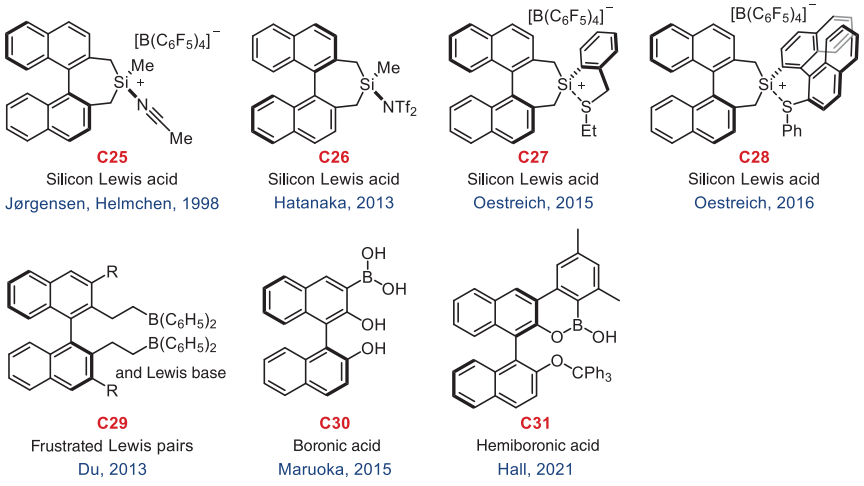

Figure 7.14 Silicon- and boron-containing organocatalysts derived from BINOLs.

a chiral hemiboronic acid catalyst **C31** and employed it in the desymmetrization of 2-aryl-1,3-diols through direct *O*-alkylation [156].

7.5.2 Base Organocatalysts Derived from BINOLs

Various Lewis base, Brønsted Base, and bifunctional catalysts have been designed and developed from BINOLs (Figure 7.15). Tertiary phosphine **C32** was previously prepared as ligands for asymmetric hydrogenation reactions [16]. In 2005, Fu and co-workers reported the utilization of **C32** as nucleophilic organocatalysts in the [4 + 2] annulation of imines with allenes (up to 99% ee) [157]. Maruoka and co-workers developed binaphthyl amino acid **C33** [158] and amino sulfonamide **C34** [159] and applied them in direct aldol reaction of aldehydes with acetone (up to 96% ee) and Mannich reaction between aldehydes and α-imino ester (up to >99% ee), respectively. Although binaphthyl-based secondary amine **C35** was tested in several reactions, poor reactivity and stereoselectivity were observed. In 2015, Maruoka and co-workers found this sample amine **C35** (R = H) was able to promote regio-, diastereo-, and enantioselective conjugate addition of aldehydes to β-tosyl enones (*syn*/*anti* > 20:1, up to 94% ee) [160].

Sasai and co-workers developed bifunctional organocatalysts **C36** and **C37** and applied them in the aza-Morita–Baylis–Hillman reaction (up to 95% ee) [161, 162]. Terada et al. designed two classes of axially chiral guanidine catalysts **C38** and **C39**. Excellent enantioselectivities have been achieved in the 1,4-addition of 1,3-dicarbonyl compounds with conjugated nitroalkenes (up to 98% ee) [163] and amination of 1,3-dicarbonyl compounds with azodicarboxylate (up to 98% ee) [164]. In 2008, Shao and co-workers [165] and Kim and co-workers [166, 167] reported the utilization of bifunctional amine-thiourea organocatalysts **C40** in asymmetric transformations, independently.

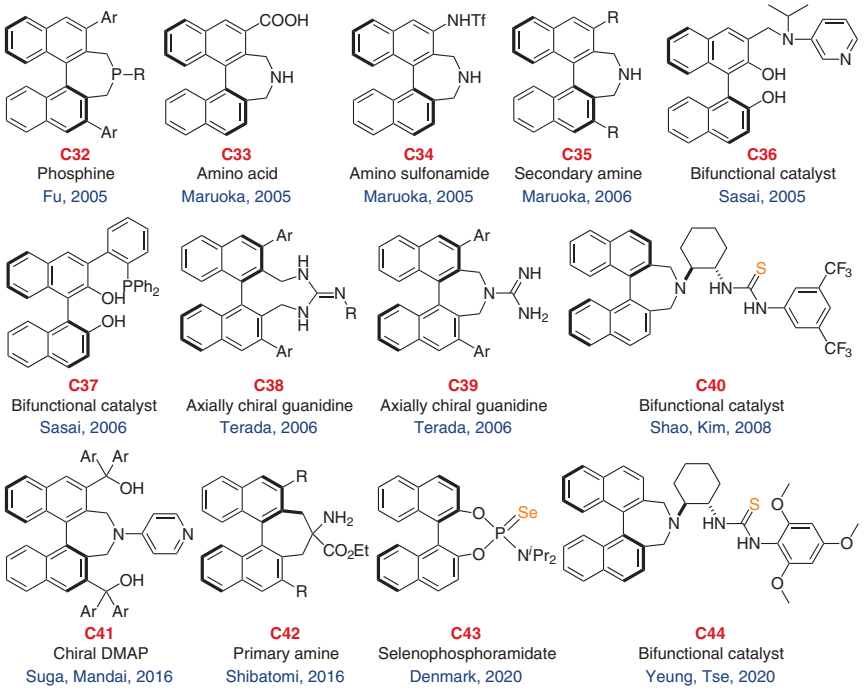

Figure 7.15 Base and bifunctional organocatalysts derived from BINOLs.

In 2016, Suga and co-workers combined the binaphthyl backbone with the 4-aminopyridyl unit to develop axially chiral DMAP-type organocatalysts **C41** for enantioselective acyl transfer reactions (up to >98% yield, 98% ee) (refer to Chapter 9 for more details) [168]. Primary amine **C42** was utilized as an organocatalyst in the fluorination of α-branched aldehydes (up to 95% ee) by Shibatomi and co-workers [169]. As a variant of the BINAM-derived selenophosphoramidate, BINOL-derived selenophosphoramidate **C43** was also synthesized by Denmark and Panger in 2020 [170]. In the sulfenoamidation of electron-deficient alkenes, **C43** worked well (up to 78% yield, 94% ee), whereas the BINAM-derived catalyst did not work. In 2020, Yeung and coworkers developed a highly enantioselective domino halocyclization and spiroketalization of olefinic keto acids **37** (Scheme 7.7). The key to this success is the utilization of electron-rich thiourea **C44** as the catalyst [171].

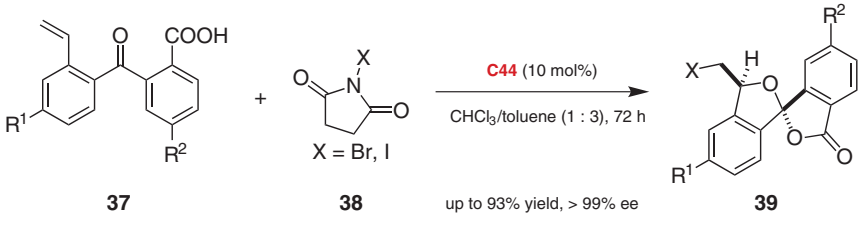

Scheme 7.7 Domino halocyclization and spiroketalization of olefinic keto acids.

7.5.3 Phase-Transfer, Cation-Bonding, and Ammonium Betaine Catalysts

Chiral quaternary ammonium and phosphonium salts have been utilized as phase-transfer catalysts in asymmetric catalysis and various binaphthyl-based quaternary ammonium and phosphonium organocatalysts have been designed and developed (Figure 7.16). In 1999, Maruoka and co-workers developed C_2-symmetric quaternary ammonium salts **C45** and **C46**, for practical synthesis of α-amino acids through asymmetric alkylation of the benzophenone Schiff base of glycine esters (up to 96% ee) [172]. Maruoka and co-workers also synthesized quaternary phosphonium salts **C47** and utilized them as organocatalysts in the asymmetric amination of β-keto esters [173]. Ooi and co-workers developed quaternary ammonium betaine **C48** and employed it as an organic base catalyst in the direct Mannich-type reaction of α-substituted α-nitrocarboxylates with various *N*-Boc-imines (up to 99% ee) [174]. In 2009, Maruoka and co-workers developed chiral phase-transfer catalysts **C49**, which catalyzed the enantioselective conjugate addition of 3-aryloxindoles to β-nitrostyrene under neutral conditions [175]. In the same year, Song and co-workers developed multifunctional organocatalysts **C50** bearing a bis(hydroxy) polyether structure and two BINOL units [176]. This type of catalyst acts as excellent chiral-anion generator to promote a range of reactions such as the desilylative kinetic resolution of silyl-protected secondary alcohols, asymmetric Strecker reaction, and silylative kinetic resolution of racemic alcohols [177]. The Ooi and co-workers also reported chiral ammonium betaine **C51** in 2010, which also served as an organic base catalyst for the direct Mannich-type reaction of 2-alkoxythiazol-5(4H)-ones [178]. In 2015, Hamashima and co-workers designed binaphthyl monocarboxylic acids **C52** and utilized them as anionic phase-transfer catalysts in fluoro-difunctionalization of C–C double bonds (Scheme 7.8a) (up to 94% ee) [179]. Three years later, Hamashima and co-workers reported a dianionic phase-transfer catalyst **C53** bearing two binaphthyl units for asymmetric fluoro-cyclization reactions (Scheme 7.8b) (up to 99% ee) [180].

7.5.4 Chiral Ketone and Aldehyde Organocatalysts Derived from BINOLs

Very early in 1996, Yang and co-workers developed a class of C_2-symmetric chiral ketone organocatalysts **C54** (Figure 7.17) bearing a binaphthyl backbone and successfully applied them in the asymmetric epoxidation of unfunctionalized olefins (up to 95% ee) [181, 182]. In 2014, Guo and co-workers reported the utilization of BINOL-based chiral aldehydes **C55** as organocatalysts to promote direct α-functionalization of *N*-unprotected amino esters [183]. In 2018, Guo, Ouyang, and co-workers developed another class of aldehyde catalyst **C56** [184] and realized the direct asymmetric α-functionalization of *N*-unprotected glycine esters (Scheme 7.9).

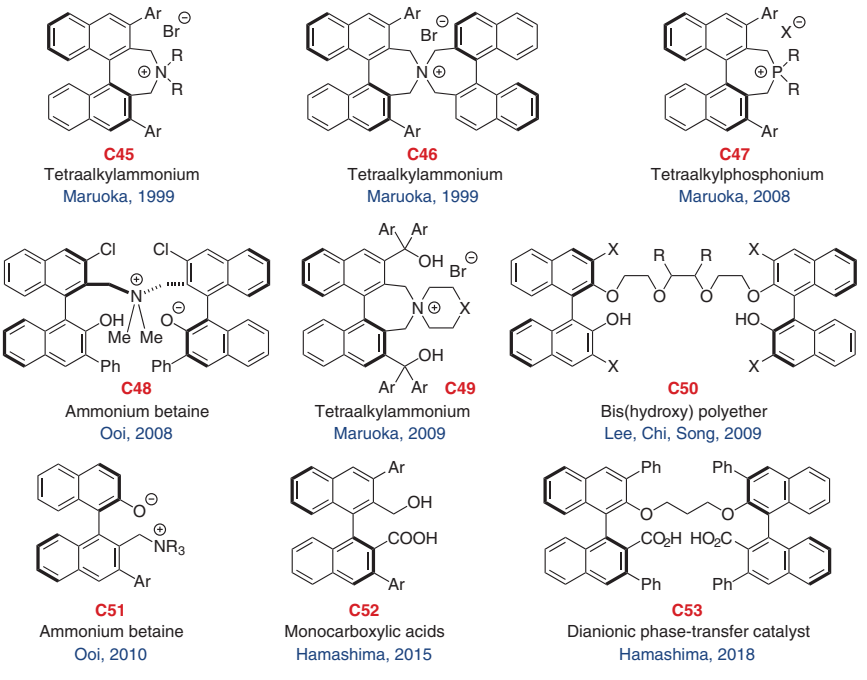

Figure 7.16 Phase-transfer, cation-bonding, and ammonium betaine catalysts.

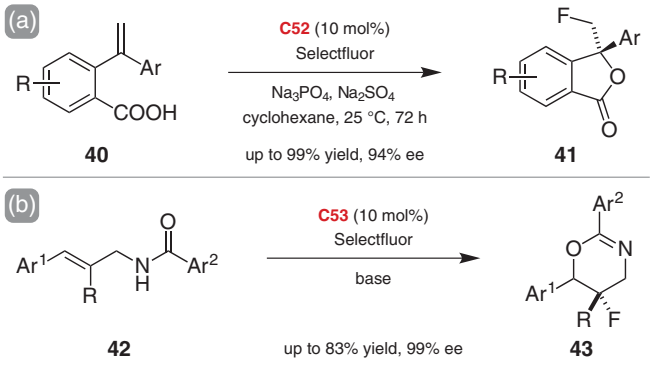

Scheme 7.8 Fluoro-difunctionalization and fluoro-cyclization catalyzed by **C52** and **C53**.

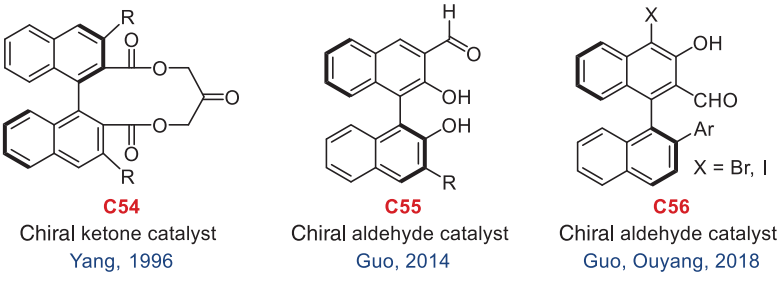

Figure 7.17 Chiral ketone and aldehyde organocatalysts derived from BINOLs.

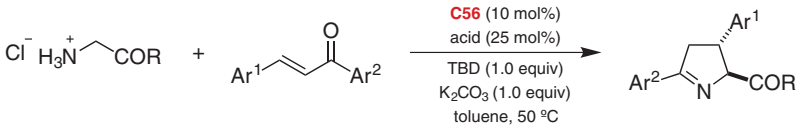

Scheme 7.9 Direct asymmetric α-functionalization of *N*-unprotected glycine esters.

7.5.5 BINOL-Derived Catalysts for Hypervalent Iodine Organocatalysis

Chiral hypervalent iodines have been proven to be very promising organocatalysts for enantioselective oxidative transformations, owing to their attractive features such as high stability, low toxicity, and ease of handling. Several binaphthyl-based iodine-containing catalysts have been developed in recent years (Figure 7.18). In 2009, Quideau and co-workers synthesized iodoarene **C57** and employed it as hypervalent iodine precursor to mediate hydroxylative dearomatization of 2-methylnaphthol in the presence of *m*CPBA (up to 50% ee) [185]. In 2010, Ishihara and co-workers creatively utilized a chiral quaternary ammonium iodite **C58** as a precursor to catalyze the oxidative cycloetherification of ketophenols **47** to 2-acyl-2,3-dihydrobenzofuran derivatives **48** with hydrogen peroxide as the oxidant (Scheme 7.10a) [186]. Berthiol and co-workers synthesized 3,3-diiodo-BINOL-fused maleimides **C59** and tested them in the α-oxytosylation of propiophenone (up to 46% ee) [187]. In 2014, Kita and co-workers reported their test of iodoarene **C60** as a catalyst in the intramolecular aminofluorination of alkenes (up to 70% ee) and the nucleophilic fluorination of β-ketoesters (up to 56% ee) [188].

Recently in 2023, Zhang and co-workers developed a confine chiral aryl iodide catalyst **C61** by incorporating two bulky BINOL-derived units, which form the

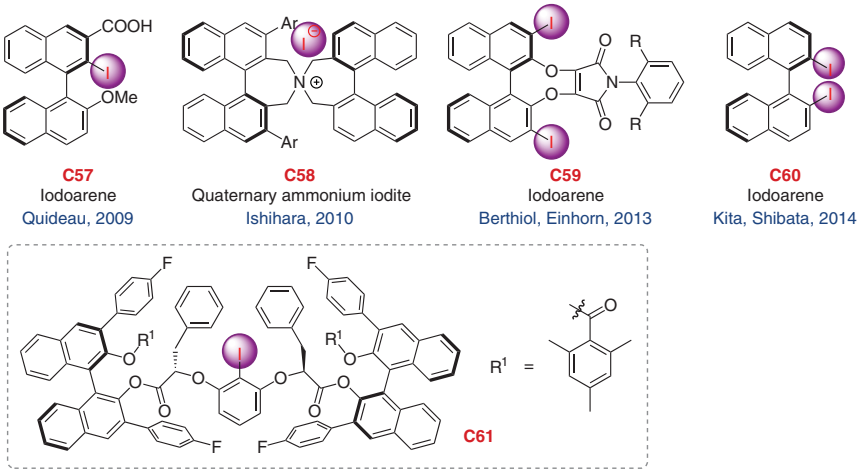

Figure 7.18 BINOL-derived catalysts for hypervalent iodine organocatalysis.

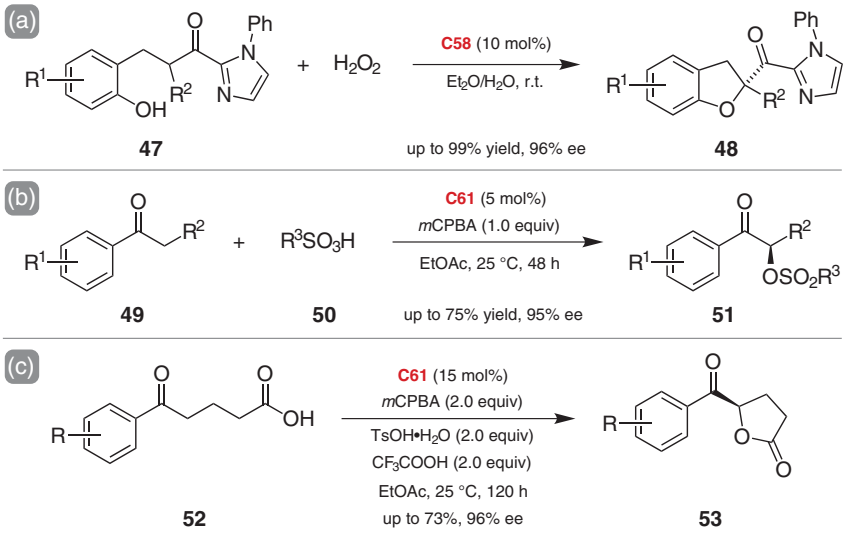

Scheme 7.10 Transformations promoted by organocatalyst **C58** or **C61**.

second-layer chiral environment, to lock down the conformation of the catalyst and create a compact chiral environment around the catalytically active site. With this catalyst, good to excellent enantioselectivities have been achieved in the α-oxysulfonylation of ketones (up to 95% ee, Scheme 7.10b) and the oxidative cyclization of 5-oxo-5-arylpentanoic acids **52** to γ-butyrolactones **53** (up to 96% ee, Scheme 7.10c) [189].

7.6 Chiral Organocatalysts Derived from BINAMs

BINAMs have been employed as a source of chirality to design various organocatalysts such as phosphoramides, thiophosphoramides, selenophosphoramides, ureas, thioureas, and squaramides (Figure 7.19). In 2001, Denmark and Wynn developed bis-phosphoramide catalyst **C62** and used it in the allylation and propargylation of aldehydes (up to 97% ee) [190]. In 2005, Wang and co-workers developed a binaphthyl-derived amine thiourea **C63** and employed it to catalyze the enantioselective Morita–Baylis–Hillman reaction of cyclohexenone with aldehydes (up to 94% ee) [191]. In 2006, Connon and co-workers reported the application of axially chiral bis-thiourea **C64** and bis-urea **C65** in the Friedel–Crafts type addition of indole and *N*-methylindole to nitroolefins (up to 50% ee) [192]. Shi and Liu also applied similar bis-thioureas in the Henry reaction (up to 75% ee) [193] and Morita–Baylis–Hillman reaction (up to 88% ee) [194].

Terada et al. synthesized phosphorodiamidic acids **C66** from BINAM and studied their capability of catalyzing the direct Mannich reaction of *N*-acyl imines with 1,3-dicarbonyl compounds (up to 97% yield, 56% ee) [195]. In 2008, Ishihara and co-workers tested lithium salt of BINAM-derived phosphoric acid **C67** as a

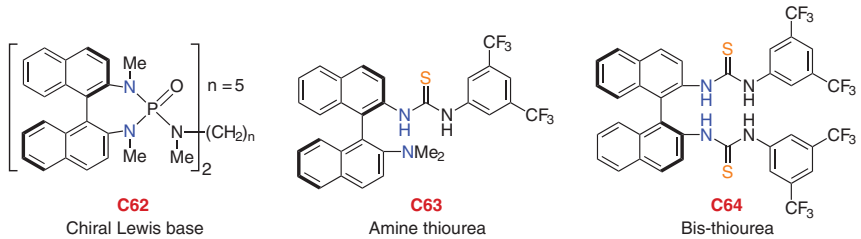

C62
Chiral Lewis base
Denmark, 2001

C63
Amine thiourea
Wang, 2005

C64
Bis-thiourea
Connon, 2006

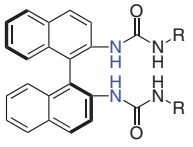

C65
Bis-urea
Connon, 2006

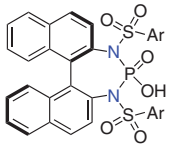

C66
Phosphorodiamidic acids
Terada, 2006

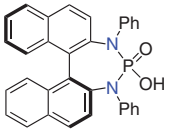

C67
BINAM-phosphoric acid
Ishihara, 2008

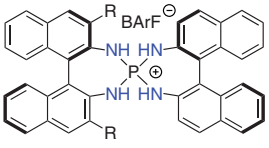

C68
Arylaminophosphonium barfates
Ooi, 2009

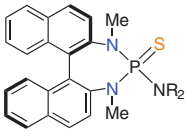

C69
Chiral Lewis base
Denmark, 2010

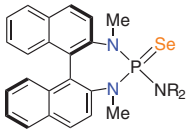

C70
Chiral Lewis base
Denmark, 2010

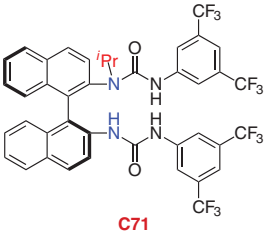

C71
Bis-urea
Gouverneur, 2018

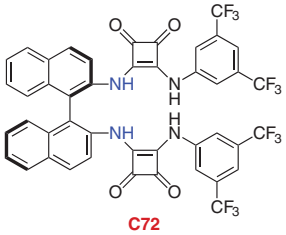

C72
Bis-squaramide
Ema, Takaishi, 2019

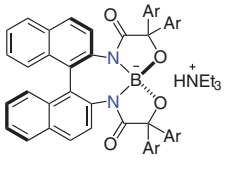

C73
Chiral borate ion
Ooi, 2020

Figure 7.19 Representative chiral organocatalysts derived from BINAMs.

catalyst in the cyanosilylation of acetophenone and obtained the corresponding tertiary cyanohydrin in 83% yield with 68% ee [196]. In 2015, Toste and co-workers utilized BINAM-derived phosphoric acids as a phase-transfer catalyst to promote the α-diazenation of enolate derivatives (up to 93% ee) [197]. In 2009, Ooi and co-workers identified arylaminophosphonium barfates **C68** as charged Brønsted acids to catalyze conjugate addition of arylamines to nitroolefins (up to 97% ee) [198].

In 2010, Denmark et al. developed thiophosphoramides **C69** and selenophosphoramides **C70** and tested their performance as Lewis base catalysts in the cyclization of unsaturated alcohols in the presence of *N*-(2-nitrophenylselenenyl)succinimide and methanesulfonic acid (up to 70% ee) [199]. These BINAM-derived thiophosphoramides and selenophosphoramides have proved to be very powerful Lewis base

catalysts for many other asymmetric transformations. In 2018, Gouverneur and co-workers employed bis-urea **C71** as a hydrogen bonding phase-transfer catalyst to promote asymmetric nucleophilic fluorination (Scheme 7.11) (up to 94 % ee) [200]. Ema and co-workers reported the synthesis of bis-squaramide **C72** and tested it in the kinetic resolution of styrene oxide, albeit with low enantioselectivity [201]. In 2022, Ooi and co-workers designed chiral borate ion **C73** consisting of a BINAM backbone and demonstrated the application of it as catalyst in the Prins-type cyclization of vinylic ethers (up to 95 % ee) [202].

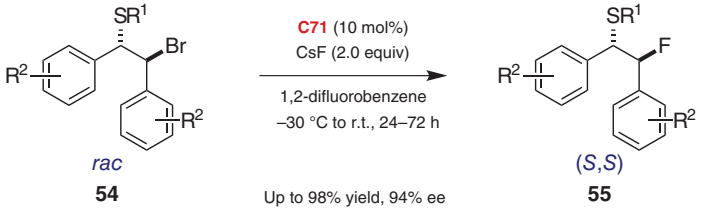

Scheme 7.11 Asymmetric nucleophilic fluorination catalyzed by **C71**.

7.7 Chiral Organocatalysts Derived from NOBINs

NOBINs also have been used to design organocatalysts such as thioureas, ureas, and squaramides (Figure 7.20). In 2007, Shi and co-workers developed thiourea-phosphine organocatalysts **C74** and applied them to several asymmetric transformations [203, 204]. In 2010, Ooi and co-workers developed diaminodioxaphosphonium barfates **C75** for enantioselective protonation of α-amino acid-derived ketene disilyl acetals (up to 97% ee) [205]. In 2011, Herrera and co-workers synthesized a thiourea organocatalyst **C76** and tested it in the Friedel–Crafts alkylation of indoles with nitroalkenes during the catalyst screening (7% ee) [206]. In 2014, Sibi and co-workers used NOBIN-derived thiourea **C77** to promote [2 + 2] photocycloaddition of 4-alkenyl-substituted coumarins **56** (Scheme 7.12) (up to 96% ee) [207]. Herrera and co-workers synthesized various unsymmetrical squaramides including **C78** in 2015 and then used it to catalyze the Henry reaction in 2016 (up to 94% ee) [208, 209]. In 2017, Shirakawa and co-workers reported the development of binaphthyl-derived chiral tertiary sulfonium salts **C79** and their application as phase-transfer catalysts in the asymmetric conjugate addition of 3-substituted oxindoles to maleimides (up to 93% ee) [210].

7.8 Chiral Ligands and Catalysts Derived from Other Binaphthyl Motifs

In this section, two chiral ligands developed by the Yamamoto and co-workers and one iodoarene organocatalyst developed by Kita and co-workers were selected as examples to briefly introduce how they were synthesized. As shown in

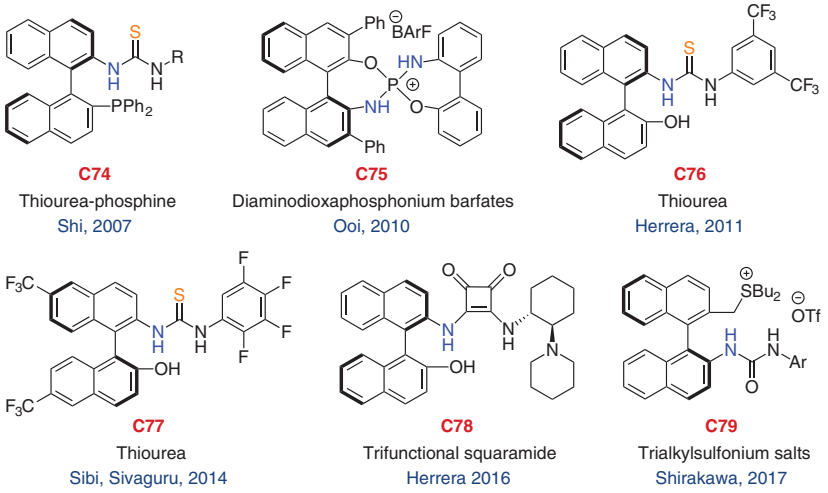

Figure 7.20 Representative chiral organocatalysts derived from NOBINs.

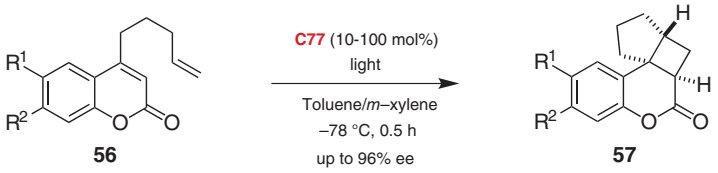

Scheme 7.12 Photocycloaddition of 4-alkenyl-substituted coumarins catalyzed by **C77**.

Scheme 7.13a, the tethered bis(8-quinolinolato) ligand (TBO_x) **L71** was synthesized from (*R*)-2,2′-diiodo-1,1′-binaphthalene **58**. A chromium complex of **L71** was used to catalyze the asymmetric pinacol coupling reactions of aldehydes (up to 98% ee) [211]. Besides chromium complex, **L71** can also form a chiral catalyst with aluminum to promote various asymmetric transformations [212]. In 2011, Yamamoto and Nishikawa designed a class of chiral bidentate ligands **L72** bearing both a phenanthroline unit and a binaphthyl motif [213]. These ligands were synthesized from (*R*)-2,2′-dibromo-1,1′-binaphthalene **60** (Scheme 7.13b) and used to generate iron catalysts for asymmetric epoxidation of acyclic β,β-disubstituted enones (up to 92% ee). In 2017, Kita and co-workers designed a new type of axially chiral iodoarenes **C80** (Scheme 7.13c) and tested them as hypervalent iodine organocatalyst precursors to promote asymmetric dearomatizing spirocyclizations of 1-naphthol-2-propionic acid (62% yield, 64% ee) [214]. In the synthesis of iodoarenes **C80**, Ni-catalyzed reductive coupling of 8-amino-1-bromonaphthalenes **62** was used to construct the racemic binaphthyl diamine intermediate **63**. After chiral resolution with preparative HPLC, the obtained enantiopure diamine was converted to **C80** through Sandmeyer-type iodination. Although the enantioselectivity is yet to be improved and the synthesis of the catalysts requires a chiral resolution procedure, this type of promising iodoarene represents novel axially

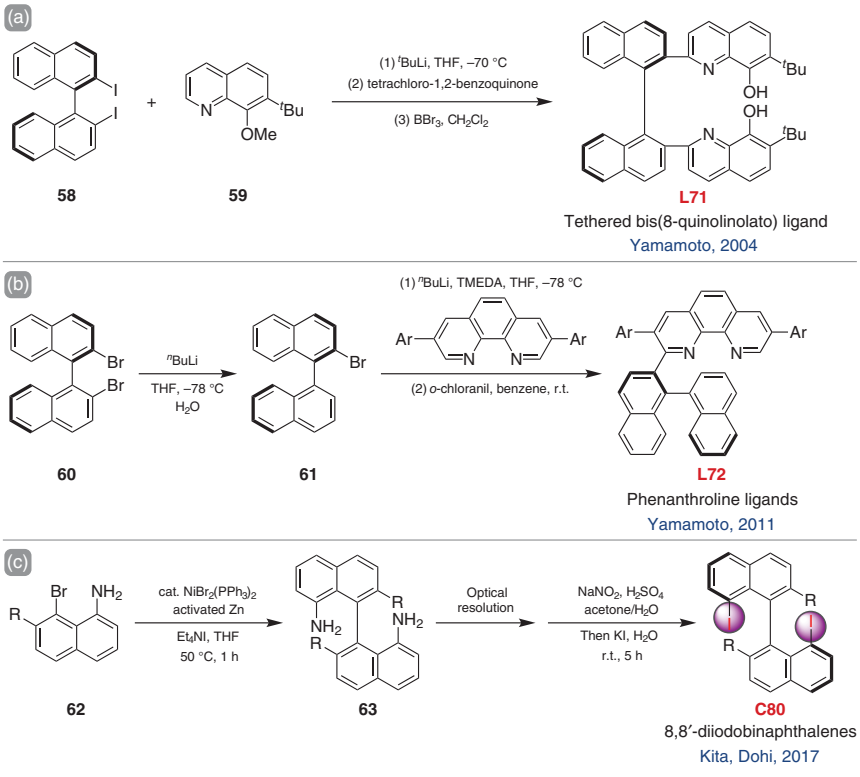

Scheme 7.13 Syntheses of ligands **L71**, **L72**, and organocatalyst **C80**.

chiral catalysts derived from binaphthyl starting materials other than BINOL, BINAM, and NOBIN.

7.9 Summary and Outlook

Illustrated in this chapter are more than 150 axially chiral ligands and organocatalysts derived from atropisomeric BINOLs, BINAMs, NOBINs, or other binaphthyl structures. From phosphine and phosphoramidite ligands to Schiff base ligands, from Brønsted acid to Lewis base and phase-transfer organocatalysts, the privileged axially chiral binaphthyl structures present in most of the widely utilized chiral catalytic systems. Although it is nearly impossible to include all the binaphthyl chiral catalysts in one chapter, it is believed that these representative examples are sufficient to demonstrate the amazing enantioinductive capability of the privileged atropisomeric binaphthyl structures. A chiral catalyst not only promotes a certain reaction by reducing its activation energy, but also provides a crucial chiral environment for the enantioinduction. In fact, the nature of asymmetric catalysis is bond beak and formation in a chiral environment provided by the catalyst, despite the diverse classifications of numerous chiral metal catalysts and organocatalysts, and

the very different catalytic modes. Represented by BINOL, BINAM, and NOBIN, axially chiral binaphthyl structures have provided a wonderful chiral environment for numerous asymmetric transformations. With the rapid development in the asymmetric syntheses of highly diversified axially chiral molecules [215, 216], we believe that more novel and powerful axially chiral catalysts will be developed, and tremendous new asymmetric transformations will be realized in the future.

References

1 Yoon, T.P. and Jacobsen, E.N. (2003). Privileged chiral catalysts. *Science* 299 (5613): 1691–1693.
2 List, B. and Yang, J.W. (2006). The organic approach to asymmetric catalysis. *Science* 313 (5793): 1584–1586.
3 Zhou, Q.-L. (ed.) (2011). *Privileged Chiral Ligands and Catalysts*. Weinheim: Wiley.
4 Chen, Y., Yekta, S., and Yudin, A.K. (2003). Modified BINOL ligands in asymmetric catalysis. *Chem. Rev.* 103 (8): 3155–3211.
5 Brunel, J.M. (2005). BINOL: a versatile chiral reagent. *Chem. Rev.* 105 (3): 857–897.
6 Kočovský, P., Vyskočil, Š., and Smrčina, M. (2003). Non-symmetrically substituted 1,1′-binaphthyls in enantioselective catalysis. *Chem. Rev.* 103 (8): 3213–3245.
7 Ding, K., Li, X., Ji, B., and Kitamura, M. (2005). Ten years of research on NOBIN chemistry. *Curr. Org. Synth.* 2 (4): 499–545.
8 Ding, K., Guo, H., Li, X. et al. (2005). Synthesis of NOBIN derivatives for asymmetric catalysis. *Top. Catal.* 35: 105–116.
9 Noyori, R., Tomino, I., and Tanimoto, Y. (1979). Virtually complete enantioface differentiation in carbonyl group reduction by a complex aluminum hydride reagent. *J. Am. Chem. Soc.* 101 (11): 3129–3131.
10 Miyashita, A., Yasuda, A., Takaya, H. et al. (1980). Synthesis of 2,2′-bis(diphenylphosphino)-1,1′-binaphthyl (BINAP), an atropisomeric chiral bis(triaryl)phosphine, and its use in the rhodium(I)-catalyzed asymmetric hydrogenation of α-(acylamino)acrylic acids. *J. Am. Chem. Soc.* 102 (27): 7932–7934.
11 Berthod, M., Mignani, G., Woodward, G., and Lemaire, M. (2005). Modified BINAP: the how and the why. *Chem. Rev.* 105 (5): 1801–1836.
12 Uozumi, Y. and Hayashi, T. (1991). Catalytic asymmetric synthesis of optically active 2-alkanols via hydrosilylation of 1-alkenes with a chiral monophosphine-palladium catalyst. *J. Am. Chem. Soc.* 113 (26): 9887–9888.
13 Hayashi, T. (2000). Chiral monodentate phosphine ligand MOP for transition-metal-catalyzed asymmetric reactions. *Acc. Chem. Res.* 33 (6): 354–362.

14 Baker, M.J. and Pringle, P.G. (1991). Chiral aryl diphosphites: a new class of ligands for hydrocyanation catalysis. *J. Chem. Soc. Chem. Commun.* 18: 1292–1293.

15 Sakai, N., Mano, S., Nozaki, K., and Takaya, H. (1993). Highly enantioselective hydroformylation of olefins catalyzed by new phosphine phosphite-rhodium(I) complexes. *J. Am. Chem. Soc.* 115 (15): 7033–7034.

16 Gladiali, S., Dore, A., Fabbri, D. et al. (1994). Novel atropisomeric phosphorus ligands: 4,5-dihydro-3H-dinaphtho[2,1-c;1′,2′-e]phosphepine derivatives. *Tetrahedron Asymmetry* 5 (4): 511–514.

17 De Vries, A.H.M., Meetsma, A., and Feringa, B.L. (1996). Enantioselective conjugate addition of dialkylzinc reagents to cyclic and acyclic enones catalyzed by chiral copper complexes of new phosphorus amidites. *Angew. Chem. Int. Ed.* 35 (20): 2374–2376.

18 Minnaard, A.J., Feringa, B.L., Lefort, L., and de Vries, J.G. (2007). Asymmetric hydrogenation using monodentate phosphoramidite ligands. *Acc. Chem. Res.* 40 (12): 1267–1277.

19 Teichert, J.F. and Feringa, B.L. (2010). Phosphoramidites: privileged ligands in asymmetric catalysis. *Angew. Chem. Int. Ed.* 49 (14): 2486–2528.

20 Ogasawara, M., Yoshida, K., Kamei, H. et al. (1998). Synthesis and application of novel chiral phosphino-oxazoline ligands with 1,1′-binaphthyl skeleton. *Tetrahedron Asymmetry* 9 (10): 1779–1787.

21 Reetz, M.T., Gosberg, A., Goddard, R., and Kyung, S.-H. (1998). Diphosphonites as highly efficient ligands for enantioselective rhodium-catalyzed hydrogenation. *Chem. Commun.* 19: 2077–2078.

22 Xiao, D., Zhang, Z., and Zhang, X. (1999). Synthesis of a novel chiral binaphthyl phospholane and its application in the highly enantioselective hydrogenation of enamides. *Org. Lett.* 1 (10): 1679–1681.

23 Xiao, D. and Zhang, X. (2001). Highly enantioselective hydrogenation of acyclic imines catalyzed by Ir–f-binaphane complexes. *Angew. Chem. Int. Ed.* 40 (18): 3425–3428.

24 Reetz, M.T., Sell, T., and Goddard, R. (2003). Chiral phosphoric acid diesters as ligands in asymmetric transition metal catalyzed hydrogenation. *Chimia* 57 (5): 290–292.

25 Defieber, C., Ariger, M.A., Moriel, P., and Carreira, E.M. (2007). Iridium-catalyzed synthesis of primary allylic amines from allylic alcohols: sulfamic acid as ammonia equivalent. *Angew. Chem. Int. Ed.* 46 (17): 3139–3143.

26 Rössler, S.L., Petrone, D.A., and Carreira, E.M. (2019). Iridium-catalyzed asymmetric synthesis of functionally rich molecules enabled by (phosphoramidite,olefin) ligands. *Acc. Chem. Res.* 52 (9): 2657–2672.

27 Liu, W.-B., He, H., Dai, L.-X., and You, S.-L. (2009). Synthesis of 2-methylindoline- and 2-methyl-1,2,3,4-tetrahydroquinoline-derived phosphoramidites and their applications in iridium-catalyzed allylic alkylation of indoles. *Synthesis* 2009 (12): 2076–2082.

28 Yang, Z.-P., Zheng, C., Huang, L. et al. (2017). Iridium-catalyzed intramolecular asymmetric allylic dearomatization reaction of benzoxazoles, benzothiazoles, and benzimidazoles. *Angew. Chem. Int. Ed.* 56 (6): 1530–1534.

29 Liu, X.-J., Jin, S., Zhang, W.-Y. et al. (2020). Sequence-dependent stereodivergent allylic alkylation/fluorination of acyclic ketones. *Angew. Chem. Int. Ed.* 59 (5): 2039–2043.

30 Nie, Y.-H., Komatsuda, M., Yang, P. et al. (2022). Pd-catalyzed asymmetric dearomative arylation of indoles via a desymmetrization strategy. *Org. Lett.* 24 (7): 1481–1485.

31 Ohmatsu, K., Ito, M., Kunieda, T., and Ooi, T. (2012). Ion-paired chiral ligands for asymmetric palladium catalysis. *Nat. Chem.* 4 (6): 473–477.

32 Ohmatsu, K., Imagawa, N., and Ooi, T. (2014). Ligand-enabled multiple absolute stereocontrol in metal-catalysed cycloaddition for construction of contiguous all-carbon quaternary stereocentres. *Nat. Chem.* 6 (1): 47–51.

33 Yan, S.-B., Zhang, S., and Duan, W.-L. (2015). Palladium-catalyzed asymmetric arylation of C(sp^3)–H bonds of aliphatic amides: controlling enantioselectivity using chiral phosphoric amides/acids. *Org. Lett.* 17 (10): 2458–2461.

34 Wei, Y., Lu, L.-Q., Li, T.-R. et al. (2016). P,S ligands for the asymmetric construction of quaternary stereocenters in palladium-catalyzed decarboxylative [4+2] cycloadditions. *Angew. Chem. Int. Ed.* 55 (6): 2200–2204.

35 Feng, B., Pu, X.-Y., Liu, Z.-C. et al. (2016). Highly enantioselective Pd-catalyzed indole allylic alkylation using binaphthyl-based phosphoramidite-thioether ligands. *Org. Chem. Front.* 3 (10): 1246–1249.

36 Feng, B., Lu, L.-Q., Chen, J.-R. et al. (2018). Umpolung of imines enables catalytic asymmetric regio-reversed [3+2] cycloadditions of iminoesters with nitroolefins. *Angew. Chem. Int. Ed.* 57 (20): 5888–5892.

37 Liu, T., Mao, X.-R., Song, S. et al. (2023). Enantioselective nickel-catalyzed hydrosilylation of 1,1-disubstituted allenes. *Angew. Chem. Int. Ed.* 62 (11): e202216878.

38 Yang, B., Gao, J., Tan, X. et al. (2023). Chiral PSiSi-ligand enabled iridium-catalyzed atroposelective intermolecular C–H silylation. *Angew. Chem. Int. Ed.* 62 (36): e202307812.

39 Sasai, H., Suzuki, T., Arai, S. et al. (1992). Basic character of rare earth metal alkoxides. Utilization in catalytic carbon-carbon bond-forming reactions and catalytic asymmetric nitroaldol reactions. *J. Am. Chem. Soc.* 114 (11): 4418–4420.

40 Shibasaki, M., Kanai, M., Matsunaga, S., and Kumagai, N. (2009). Recent progress in asymmetric bifunctional catalysis using multimetallic systems. *Acc. Chem. Res.* 42 (8): 1117–1127.

41 Kumagai, N., Kanai, M., and Sasai, H. (2016). A career in catalysis: Masakatsu Shibasaki. *ACS Catal.* 6 (7): 4699–4709.

42 Panetti, G.B., Robinson, J.R., Schelter, E.J., and Walsh, P.J. (2021). Expanding the rare-earth metal BINOLate catalytic multitool beyond enantioselective organic synthesis. *Acc. Chem. Res.* 54 (11): 2637–2648.

43 Vogl, E.M., Matsunaga, S., Kanai, M. et al. (1998). Linking BINOL: C_2-symmetric ligands for investigations on asymmetric catalysis. *Tetrahedron Lett.* 39 (43): 7917–7920.

44 Shibasaki, M. and Matsunaga, S. (2006). Design and application of linked-BINOL chiral ligands in bifunctional asymmetric catalysis. *Chem. Soc. Rev.* 35 (3): 269–279.

45 Brunner, H. and Wutz, K. (1992). Optically active binaphthyl derivatives in the Cu-catalyzed enantioselective cyclopropanation. *New J. Chem.* 16 (1–2): 57–61.

46 Brunner, H. and Schieβling, H. (1994). Acyclic and macrocyclic binaphthyl derivatives. *Bull. Soc. Chim. Belg.* 103 (3): 119–126.

47 Sasaki, H., Irie, R., and Katsuki, T. (1993). Catalytic asymmetric epoxidation with (Salen)manganese(III) complex bearing binaphthyl groups of axial chirality. *Synlett* 1993 (4): 300–302.

48 Hosoya, N., Hatayama, A., Irie, R. et al. (1994). Rational design of Mn-Salen epoxidation catalysts: preliminary results. *Tetrahedron* 50 (15): 4311–4322.

49 DiMauro, E.F. and Kozlowski, M.C. (2001). BINOL–Salen metal catalysts incorporating a bifunctional design. *Org. Lett.* 3 (11): 1641–1644.

50 Fabbri, D., Delogu, G., and Lucchi, O.D. (1993). Preparation of enantiomerically pure 1,1′-binaphthalene-2,2′-diol and 1,1′-binaphthalene-2,2′-dithiol. *J. Org. Chem.* 58 (7): 1748–1750.

51 Claver, C., Castillbn, S., Ruiz, N. et al. (1993). Asymmetric hydroformylation of styrene by rhodium(I) catalysts with chiral ligands containing sulfur donors. *J. Chem. Soc. Chem. Commun.* 24: 1833–1834.

52 Mariz, R., Luan, X., Gatti, M. et al. (2008). A chiral bis-sulfoxide ligand in late-transition metal catalysis; rhodium-catalyzed asymmetric addition of arylboronic acids to electron-deficient olefins. *J. Am. Chem. Soc.* 130 (7): 2172–2173.

53 Hatano, M., Maki, T., Moriyama, K. et al. (2008). Pyridinium 1,1′-binaphthyl-2,2′-disulfonates as highly effective chiral Brønsted acid–base combined salt catalysts for enantioselective Mannich-type reaction. *J. Am. Chem. Soc.* 130 (50): 16858–16860.

54 Hatano, M., Hattori, Y., Furuya, Y., and Ishihara, K. (2009). Chiral lanthanum(III)-binaphthyldisulfonate complexes for catalytic enantioselective Strecker reaction. *Org. Lett.* 11 (11): 2321–2324.

55 Satake, S., Kurihara, T., Nishikawa, K. et al. (2018). Pentamethylcyclopentadienyl rhodium(III)–chiral disulfonate hybrid catalysis for enantioselective C–H bond functionalization. *Nat. Catal.* 1 (8): 585–591.

56 Xie, W.-B. and Li, Z. (2021). Bis(μ-oxo)–dititanium(IV)–chiral binaphthyldisulfonate complexes for highly enantioselective intramolecular hydroalkoxylation of nonactivated alkenes. *ACS Catal.* 11 (10): 6270–6275.

57 Uozumi, Y., Kyota, H., Kishi, E. et al. (1996). Homochiral 2,2′-bis(oxazolyl)-l,l′-binaphthyls as ligands for copper(I)-catalyzed asymmetric cyclopropanation. *Tetrahedron Asymmetry* 7 (6): 1603–1606.

58 Shibatomi, K., Muto, T., Sumikawa, Y. et al. (2009). Development of a new chiral spiro oxazolinylpyridine ligand (Spymox) for asymmetric catalysis. *Synlett* 2009 (2): 241–244.

59 Shibatomi, K., Narayama, A., Soga, Y. et al. (2011). Enantioselective *gem*-chlorofluorination of active methylene compounds using a chiral spiro oxazoline ligand. *Org. Lett.* 13 (11): 2944–2947.

60 Li, N.-K., Kong, L.-P., Qi, Z.-H. et al. (2016). Friedel–Crafts reaction of indoles with isatin-derived β,γ-unsaturated α-keto esters using a BINOL-derived bisoxazoline (BOX)/copper(II) complex as catalyst. *Adv. Synth. Catal.* 358 (19): 3100–3112.

61 Sakurai, S., Matsumoto, A., Kano, T., and Maruoka, K. (2020). Cu-catalyzed enantioselective alkylarylation of vinylarenes enabled by chiral binaphthyl–BOX hybrid ligands. *J. Am. Chem. Soc.* 142 (45): 19017–19022.

62 Luo, Z., Liu, Q., Gong, L. et al. (2002). The rational design of novel chiral oxovanadium(IV) complexes for highly enantioselective oxidative coupling of 2-naphthols. *Chem. Commun.* 8: 914–915.

63 Guo, Q.-X., Wu, Z.-J., Luo, Z.-B. et al. (2007). Highly enantioselective oxidative couplings of 2-naphthols catalyzed by chiral bimetallic oxovanadium complexes with either oxygen or air as oxidant. *J. Am. Chem. Soc.* 129 (45): 13927–13938.

64 Chu, C.-Y. and Uang, B.-J. (2003). Catalytic enantioselective coupling of 2-naphthols by new chiral oxovanadium complexes bearing a self accelerating functional group. *Tetrahedron Asymmetry* 14 (1): 53–55.

65 Somei, H., Asano, Y., Yoshida, T. et al. (2004). Dual activation in a homolytic coupling reaction promoted by an enantioselective dinuclear vanadium(IV) catalyst. *Tetrahedron Lett.* 45 (9): 1841–1844.

66 Sako, M., Takeuchi, Y., Tsujihara, T. et al. (2016). Efficient enantioselective synthesis of oxahelicenes using redox/acid cooperative catalysts. *J. Am. Chem. Soc.* 138 (36): 11481–11484.

67 Kumar, A., Sasai, H., and Takizawa, S. (2022). Atroposelective synthesis of C–C axially chiral compounds via mono- and dinuclear vanadium catalysis. *Acc. Chem. Res.* 55 (20): 2949–2965.

68 Cao, Z. and Du, H. (2010). Development of binaphthyl-based chiral dienes for rhodium(I)-catalyzed asymmetric arylation of *N*,*N*-dimethylsulfamoyl-protected aldimines. *Org. Lett.* 12 (11): 2602–2605.

69 Colletti, S.L. and Halterman, R.L. (1989). Binaphthylcyclopentadiene: a C_2-symmetric annulated cyclopentadienyl ligand with axial chirality. *Tetrahedron Lett.* 30 (27): 3513–3516.

70 Ye, B. and Cramer, N. (2013). A tunable class of chiral Cp ligands for enantioselective rhodium(III)-catalyzed C–H allylations of benzamides. *J. Am. Chem. Soc.* 135 (2): 636–639.

71 Mas-Roselló, J., Herraiz, A.G., Audic, B. et al. (2021). Chiral cyclopentadienyl ligands: design, syntheses, and applications in asymmetric catalysis. *Angew. Chem. Int. Ed.* 60 (24): 13198–13224.

72 Pan, C., Yin, S.-Y., Wang, S.-B. et al. (2021). Oxygen-linked cyclopentadienyl rhodium(III) complexes-catalyzed asymmetric C–H arylation of benzo[*h*]quinolines with 1-diazonaphthoquinones. *Angew. Chem. Int. Ed.* 60 (28): 15510–15516.

73 Schlüter, J., Blazejak, M., Boeck, F., and Hintermann, L. (2015). Asymmetric hydroalkoxylation of non-activated alkenes: titanium-catalyzed cycloisomerization of allylphenols at high temperatures. *Angew. Chem. Int. Ed.* 54 (13): 4014–4017.

74 Yang, L., Neuburger, M., and Baudoin, O. (2018). Chiral bifunctional phosphine-carboxylate ligands for palladium(0)-catalyzed enantioselective C–H arylation. *Angew. Chem. Int. Ed.* 57 (5): 1394–1398.

75 Savary, D. and Baudoin, O. (2021). Enantioselective Pd0-catalyzed C(sp^2)–H arylation for the synthesis of chiral warped molecules. *Angew. Chem. Int. Ed.* 60 (10): 5136–5140.

76 Guo, S.-M., Huh, S., Coehlo, M. et al. (2023). A C–H activation-based enantioselective synthesis of lower carbo[*n*]helicenes. *Nat. Chem.* 15 (6): 872–880.

77 Lin, L., Fukagawa, S., Sekine, D. et al. (2018). Chiral carboxylic acid enabled achiral rhodium(III)-catalyzed enantioselective C–H functionalization. *Angew. Chem. Int. Ed.* 57 (37): 12048–12052.

78 Fukagawa, S., Kojima, M., Yoshino, T., and Matsunaga, S. (2019). Catalytic enantioselective methylene C(sp^3)–H amidation of 8-alkylquinolines using a Cp*RhIII/chiral carboxylic acid system. *Angew. Chem. Int. Ed.* 58 (50): 18154–18158.

79 Kato, Y., Lin, L., Kojima, M. et al. (2021). Development of Pseudo-C_2-symmetric chiral binaphthyl monocarboxylic acids for enantioselective C(sp^3)–H functionalization reactions under Rh(III) catalysis. *ACS Catal.* 11 (7): 4271–4277.

80 Zhou, T., Qian, P.-F., Li, J.-Y. et al. (2021). Efficient synthesis of sulfur-stereogenic sulfoximines via Ru(II)-catalyzed enantioselective C–H functionalization enabled by chiral carboxylic acid. *J. Am. Chem. Soc.* 143 (18): 6810–6816.

81 Li, J.-Y., Xie, P.-P., Zhou, T. et al. (2022). Ir(III)-catalyzed asymmetric C–H activation/annulation of sulfoximines assisted by the hydrogen-bonding interaction. *ACS Catal.* 12 (15): 9083–9091.

82 Naganawa, Y., Namba, T., Aoyama, T. et al. (2014). Design of novel chiral *N*,*N*,*O*-tridentate phenanthroline ligands and their application to enantioselective addition of organozinc reagents to aldehydes. *Chem. Commun.* 50 (87): 13224–13227.

83 Naganawa, Y. and Nishiyama, H. (2016). Renovation of optically active phenanthrolines as powerful chiral ligands for versatile asymmetric metal catalysis. *Chem. Rec.* 16 (6): 2573–2584.

84 Cen, S., Huang, N., Lian, D. et al. (2022). Conformational enantiodiscrimination for asymmetric construction of atropisomer. *Nat. Commun.* 13: 4735.

85 Qi, L.-W., Li, S., Xiang, S.-H. et al. (2019). Asymmetric construction of atropisomeric biaryls via a redox neutral cross-coupling strategy. *Nat. Catal.* 2 (4): 314–323.

86 Wang, P., Cen, S., Gao, J. et al. (2022). Novel axially chiral ligand-enabled copper-catalyzed asymmetric oxidative coupling of 2-naphthols for the synthesis of 6,6′-disubstituted BINOLs. *Org. Lett.* 24 (12): 2321–2326.

87 Gao, Y., Wang, Z., Zhang, X. et al. (2023). Additive-free transfer hydrogenative direct asymmetric reductive amination using a chiral pyridine-derived half-sandwich catalyst. *Angew. Chem. Int. Ed.* 135 (31): e202303709.

88 Brunner, H. and Miehling, W. (1984). Enantioselektive cyclopropanierung von 1,1-diphenylethylen und diazoessigester mit kupfer-katalysatoren. *Monatsh. Chem.* 115 (10): 1237–1254.

89 Nishinaga, A., Yamato, H., Abe, T. et al. (1988). Asymmetric induction in oxygenation of styrene catalyzed by cobalt Schiff base complex. *Tetrahedron Lett.* 29 (48): 6309–6312.

90 Lin, J.-H., Che, C.-M., Lai, T.-F. et al. (1991). An approach to chiral metal catalysts; the synthesis and X-ray crystal structures of a chiral tetradentate binaphthyl bis-amide ligand and its osmium(VI)-oxo derivative. *J. Chem. Soc. Chem. Commun.* 7: 468–470.

91 Adolfsson, H. and Moberg, C. (1995). Chiral Lewis acid catalysed asymmetric nucleophilic ring opening of cyclohexene oxide. *Tetrahedron Asymmetry* 6 (8): 2023–2031.

92 Terada, M., Motoyama, Y., and Mikami, K. (1994). Diastereoselective and enantioselective glyoxylate-ene reaction catalyzed by new class of binaphthol-derived titanium complex. *Tetrahedron Lett.* 35 (36): 6693–6696.

93 Mikami, K., Motoyama, Y., and Terada, M. (1994). Designed binaphthyl-derived titanium complexes: a new type of asymmetric catalyst for the carbonyl-ene reaction with glyoxylate. *Inorg. Chim. Acta* 222 (1-2): 71–75.

94 Suga, H., Fudo, T., and Ibata, T. (1998). Cu(I)-binaphthyldiimine catalyzed asymmetric cyclopropanation of olefin with diazoacetate. *Synlett* 1998 (8): 933–935.

95 Nishida, A., Yamanaka, M., and Nakagawa, M. (1999). Enantioselective Diels-Alder reactions catalyzed by chiral 1,1′-(2,2′-bisacylamino)binaphthalene-ytterbium complex. *Tetrahedron Lett.* 40 (8): 1555–1558.

96 Shi, M. and Sui, W.-S. (2000). Chiral diphenylthiophosphoramides: a new class of chiral ligands for the silver(I)-promoted enantioselective allylation of aldehydes. *Tetrahedron Asymmetry* 11 (3): 773–779.

97 Wang, C.-J. and Shi, M. (2003). Highly enantioselective allylation of arylaldehydes catalyzed by a silver(I)-chiral binaphthylthiophosphoramide. *Eur. J. Org. Chem.* 2003 (15): 2823–2828.

98 Wang, C.-J. and Shi, M. (2003). Chiral binaphthylthiophosphoramide–Cu(I)-catalyzed asymmetric addition of diethylzinc to *N*-sulfonylimines. *J. Org. Chem.* 68 (16): 6229–6237.

99 Shi, M. and Wang, C.-J. (2003). The catalytic asymmetric addition of diethylzinc to *N*-(diphenylphosphinoyl) imines catalyzed by $Cu(OTf)_2$-chiral *N*-(binaphthyl-2-yl)thiophosphoramide ligands. *Adv. Synth. Catal.* 345 (8): 971–973.

100 Lim, C.W. and Lee, S.-G. (2000). C_2-symmetric bisphosphine ligands derived from 1,1′-binaphthyldiamines and diphenylphosphinobenzoic acid for palladium catalyzed desymmetrizations. *Tetrahedron* 56 (29): 5131–5136.

101 Suga, H., Kakehi, A., and Mitsuda, M. (2002). Asymmetric Diels–Alder reactions catalyzed by chiral Ni(II)-binaphthyldiimine complexes. *Chem. Lett.* 31 (9): 900–901.

102 Shi, M. and Wang, C.-J. (2002). Axially dissymmetric binaphthyldiimine chiral Salen-type ligands for catalytic asymmetric addition of diethylzinc to aldehyde. *Tetrahedron Asymmetry* 13 (19): 2161–2166.

103 Duan, W.-L., Shi, M., and Rong, G.-B. (2003). Synthesis of novel axially chiral Rh–NHC complexes derived from BINAM and application in the enantioselective hydrosilylation of methyl ketones. *Chem. Commun.* 23: 2916–2917.

104 Huang, H., Okuno, T., Tsuda, K. et al. (2006). Enantioselective hydrogenation of aromatic ketones catalyzed by Ru complexes of Goodwin–Lions-type sp^2N/sp^3N hybrid ligands R-BINAN-R′-Py. *J. Am. Chem. Soc.* 128 (27): 8716–8717.

105 Chen, Z., Yakura, K., Matsunaga, S., and Shibasaki, M. (2008). Direct catalytic asymmetric Mannich-type reaction of β-keto phosphonate using a dinuclear Ni_2–Schiff base complex. *Org. Lett.* 10 (15): 3239–3242.

106 Bartolomé, C., García-Cuadrado, D., Ramiro, Z., and Espinet, P. (2010). Synthesis and catalytic activity of gold chiral nitrogen acyclic carbenes and gold hydrogen bonded heterocyclic carbenes in cyclopropanation of vinyl arenes and in intramolecular hydroalkoxylation of allenes. *Inorg. Chem.* 49 (21): 9758–9764.

107 Wang, Y.-M., Kuzniewski, C.N., Rauniyar, V. et al. (2011). Chiral (acyclic diaminocarbene)gold(I)-catalyzed dynamic kinetic asymmetric transformation of propargyl esters. *J. Am. Chem. Soc.* 133 (33): 12972–12975.

108 Bunno, Y., Tsukimawashi, Y., Kojima, M. et al. (2021). Metal-containing Schiff base/sulfoxide ligands for Pd(II)-catalyzed asymmetric allylic C–H aminations. *ACS Catal.* 11 (5): 2663–2668.

109 Carreira, E.M., Singer, R.A., and Lee, W. (1994). Catalytic, enantioselective aldol additions with methyl and ethyl acetate O-silyl enolates: a chiral tridentate chelate as a ligand for titanium(IV). *J. Am. Chem. Soc.* 116 (19): 8837–8838.

110 Carreira, E.M., Lee, W., and Singer, R.A. (1995). Catalytic, enantioselective acetone aldol additions with 2-methoxypropene. *J. Am. Chem. Soc.* 117 (12): 3649–3650.

111 Singer, R. and Carreira, E.M. (1995). Catalytic, enantioselective dienolate additions to aldehydes: preparation of optically active acetoacetate aldol adducts. *J. Am. Chem. Soc.* 117 (49): 12360–12361.

112 Yuan, Y., Long, J., Sun, J., and Ding, K. (2002). Dramatically synergetic effect of carboxylic acid additive on tridentate titanium catalyzed enantioselective hetero-Diels–Alder reaction: additive acceleration and nonlinear effect. *Chem. Eur. J.* 8 (21): 5033–5042.

113 Yuan, Y., Li, X., Sun, J., and Ding, K. (2002). To probe the origin of activation effect of carboxylic acid and (+)-NLE in tridentated titanium catalyst systems. *J. Am. Chem. Soc.* 124 (50): 14866–14867.

114 Vyskočil, Š., Smrčina, M., Hanuš, V. et al. (1998). Derivatives of 2-amino-2′-diphenylphosphino-1,1′-binaphthyl (MAP) and their application in asymmetric palladium(0)-catalyzed allylic substitution. *J. Org. Chem.* 63 (22): 7738–7748.

115 Vyskočil, Š., Smrčina, M., and Kočovský, P. (1998). Synthesis of 2-amino-2′-diphenylphosphino-1,1′-binaphthyl (MAP) and its accelerating effect on the Pd(0)-catalyzed *N*-arylation. *Tetrahedron Lett.* 39 (50): 9289–9292.

116 Ding, K., Wang, Y., Yun, H. et al. (1999). Highly efficient and practical optical resolution of 2-amino-2′-hydroxy-1,1′-binaphthyl by molecular complexation with *N*-benzylcinchonidium chloride: a direct transformation to binaphthyl amino phosphine. *Chem. Eur. J.* 5 (6): 1734–1737.

117 Hu, X., Chen, H., and Zhang, X. (1999). Development of new chiral P,N ligands and their application in the Cu-catalyzed enantioselective conjugate addition of diethylzinc to enones. *Angew. Chem. Int. Ed.* 38 (23): 3518–3521.

118 Wang, Y., Li, X., and Ding, K. (2002). The synthesis of a new generation of MAP ligands containing two types of chiral elements for asymmetric catalysis. *Tetrahedron Lett.* 43 (1): 159–161.

119 Brunner, H., Henning, F., and Weber, M. (2002). Enantioselective catalysis. Part 143: astonishingly high enantioselectivity in the transfer hydrogenation of acetophenone with 2-propanol using Ru complexes of the Schiff base derived from (S)-2-amino-2′-hydroxy-1,1′-binaphthyl (NOBIN) and 2-pyridinecarbaldehyde. *Tetrahedron Asymmetry* 13 (1): 37–42.

120 Van Veldhuizen, J.J., Garber, S.B., Kingsbury, J.S., and Hoveyda, A.H. (2002). A recyclable chiral Ru catalyst for enantioselective olefin metathesis. efficient catalytic asymmetric ring-opening/cross metathesis in air. *J. Am. Chem. Soc.* 124 (18): 4954–4955.

121 Van Veldhuizen, J.J., Gillingham, D.G., Garber, S.B. et al. (2003). Chiral Ru-based complexes for asymmetric olefin metathesis: enhancement of catalyst activity through steric and electronic modifications. *J. Am. Chem. Soc.* 125 (41): 12502–12508.

122 Hu, Y., Liang, X., Wang, J. et al. (2003). Readily prepared chiral P,N ligands and their applications in Cu-catalyzed enantioselective conjugate additions. *J. Org. Chem.* 68 (11): 4542–4545.

123 Yan, Y. and Zhang, X. (2006). A hybrid phosphorus ligand for highly enantioselective asymmetric hydroformylation. *J. Am. Chem. Soc.* 128 (22): 7198–7202.

124 Yamamura, T., Nakatsuka, H., Tanaka, S., and Kitamura, M. (2013). Asymmetric hydrogenation of *tert*-alkyl ketones: DMSO effect in unification of stereoisomeric ruthenium complexes. *Angew. Chem. Int. Ed.* 52 (35): 9313–9315.

125 González, J.M., Vidal, X., Ortuño, M.A. et al. (2022). Chiral ligands based on binaphthyl scaffolds for Pd-catalyzed enantioselective C–H activation/cycloaddition reactions. *J. Am. Chem. Soc.* 144 (47): 21437–21442.

126 Akiyama, T., Itoh, J., Yokota, K., and Fuchibe, K. (2004). Enantioselective Mannich-type reaction catalyzed by a chiral Brønsted acid. *Angew. Chem. Int. Ed.* 43 (12): 1566–1568.

127 Uraguchi, D. and Terada, M. (2004). Chiral Brønsted acid-catalyzed direct Mannich reactions via electrophilic activation. *J. Am. Chem. Soc.* 126 (17): 5356–5357.

128 Terada, M. (2010). Chiral phosphoric acids as versatile catalysts for enantioselective transformations. *Synthesis* 2010 (12): 1929–1982.

129 Yu, J., Shi, F., and Gong, L.-Z. (2011). Brønsted-acid-catalyzed asymmetric multicomponent reactions for the facile synthesis of highly enantioenriched structurally diverse nitrogenous heterocycles. *Acc. Chem. Res.* 44 (11): 1156–1171.

130 Parmar, D., Sugiono, E., Raja, S., and Rueping, M. (2014). Complete field guide to asymmetric BINOL-phosphate derived Brønsted acid and metal catalysis: history and classification by mode of activation; Brønsted acidity, hydrogen bonding, ion pairing, and metal phosphates. *Chem. Rev.* 114 (18): 9047–9153.

131 Akiyama, T. and Mori, K. (2015). Stronger Brønsted acids: recent progress. *Chem. Rev.* 115 (17): 9277–9306.

132 Nakashima, D. and Yamamoto, H. (2006). Design of chiral *N*-triflyl phosphoramide as a strong chiral Brønsted acid and its application to asymmetric Diels–Alder reaction. *J. Am. Chem. Soc.* 128 (30): 9626–9627.

133 Hasegawa, A., Naganawa, Y., Fushimi, M. et al. (2006). Design of Brønsted acid-assisted chiral Brønsted acid catalyst bearing a bis(triflyl)methyl group for a Mannich-type reaction. *Org. Lett.* 8 (15): 3175–3178.

134 Hashimoto, T. and Maruoka, K. (2007). Design of axially chiral dicarboxylic acid for asymmetric Mannich reaction of arylaldehyde *N*-Boc imines and diazo compounds. *J. Am. Chem. Soc.* 129 (33): 10054–10055.

135 Hashimoto, T., Uchiyama, N., and Maruoka, K. (2008). Trans-selective asymmetric aziridination of diazoacetamides and *N*-Boc imines catalyzed by axially chiral dicarboxylic acid. *J. Am. Chem. Soc.* 130 (44): 14380–14381.

136 Cheon, C.H. and Yamamoto, H. (2008). A Brønsted acid catalyst for the enantioselective protonation reaction. *J. Am. Chem. Soc.* 130 (29): 9246–9247.

137 Chen, X.-H., Zhang, W.-Q., and Gong, L.-Z. (2008). Asymmetric organocatalytic three-component 1,3-dipolar cycloaddition: control of stereochemistry via a chiral Brønsted acid activated dipole. *J. Am. Chem. Soc.* 130 (17): 5652–5653.

138 Guo, Q.-S., Du, D.-M., and Xu, J. (2008). The development of double axially chiral phosphoric acids and their catalytic transfer hydrogenation of quinolines. *Angew. Chem. Int. Ed.* 47 (4): 759–762.

139 García-García, P., Lay, F., García-García, P. et al. (2009). A powerful chiral counteranion motif for asymmetric catalysis. *Angew. Chem. Int. Ed.* 48 (24): 4363–4366.

140 James, T., van Gemmeren, M., and and. List, B. (2015). Development and applications of disulfonimides in enantioselective organocatalysis. *Chem. Rev.* 115 (17): 9388–9409.

141 Momiyama, N., Konno, T., Furiya, Y. et al. (2011). Design of chiral bis-phosphoric acid catalyst derived from (*R*)-3,3′-di(2-hydroxy-3-arylphenyl)binaphthol: catalytic enantioselective Diels–Alder reaction of α,β-unsaturated aldehydes with amidodienes. *J. Am. Chem. Soc.* 133 (48): 19294–19297.

142 Čorić, I. and List, B. (2012). Asymmetric spiroacetalization catalysed by confined Brønsted acids. *Nature* 483 (7389): 315–319.

143 Ratjen, L., van Gemmeren, M., Pesciaioli, F., and List, B. (2014). Towards high-performance Lewis acid organocatalysis. *Angew. Chem. Int. Ed.* 53 (33): 8765–8769.

144 Gatzenmeier, T., van Gemmeren, M., Xie, Y. et al. (2016). Asymmetric Lewis acid organocatalysis of the Diels–Alder reaction by a silylated C–H acid. *Science* 351 (6276): 949–952.

145 Kaib, P.S.J., Schreyer, L., Lee, S. et al. (2016). Extremely active organocatalysts enable a highly enantioselective addition of allyltrimethylsilane to aldehydes. *Angew. Chem. Int. Ed.* 55 (42): 13200–13203.

146 Schreyer, L., Properzi, R., and List, B. (2019). IDPi Catalysis. *Angew. Chem. Int. Ed.* 58 (37): 12761–12777.

147 Momiyama, N., Tabuse, H., Noda, H. et al. (2016). Molecular design of a chiral Brønsted acid with two different acidic sites: regio-, diastereo-, and enantioselective hetero-Diels–Alder reaction of azopyridinecarboxylate with amidodienes catalyzed by chiral carboxylic acid–monophosphoric acid. *J. Am. Chem. Soc.* 138 (35): 11353–11359.

148 Terada, M., Gupta, Y., and Kikuchi, J. (2019). Bis-phosphoric acid derived from BINOL dimer as a chiral Brønsted acid catalyst for enantioselective transformations. *Chem. Lett.* 48 (3): 260–263.

149 Peng, B., Ma, J., Guo, J. et al. (2022). A powerful chiral super Brønsted C–H acid for asymmetric catalysis. *J. Am. Chem. Soc.* 144 (7): 2853–2860.

150 Johannsen, M., Jørgensen, K.A., and Helmchen, G. (1998). Synthesis and application of the first chiral and highly Lewis acidic silyl cationic catalyst. *J. Am. Chem. Soc.* 120 (30): 7637–7638.

151 Sakaguchi, Y., Iwade, Y., Sekikawa, T. et al. (2013). Chiral silicon Lewis acids having a pentacoordinate stereogenic silicon center: ^{29}Si NMR studies and application to asymmetric Diels–Alder reactions. *Chem. Commun.* 49 (95): 11173–11175.

152 Rohde, V.H.G., Müller, M.F., and Oestreich, M. (2015). Intramolecularly sulfur-stabilized silicon cations with chiral binaphthyl backbones: synthesis of three different motifs and their application in enantioselective Diels–Alder reactions. *Organometallics* 34 (13): 3358–3373.

153 Shaykhutdinova, P. and Oestreich, M. (2016). Enantioselective Diels–Alder reactions of cyclohexa-1,3-diene and chalcones catalyzed by intramolecular silicon–sulfur Lewis pairs as chiral Lewis acids. *Organometallics* 35 (16): 2768–2771.

154 Liu, Y. and Du, H. (2013). Chiral dienes as "ligands" for borane-catalyzed metal-free asymmetric hydrogenation of imines. *J. Am. Chem. Soc.* 135 (18): 6810–6813.

155 Hashimoto, T., Gálvez, A.O., and Maruoka, K. (2015). Boronic acid-catalyzed, highly enantioselective aza-Michael additions of hydroxamic acid to quinone imine ketals. *J. Am. Chem. Soc.* 137 (51): 16016–16019.

156 Estrada, C.D., Ang, H.T., Vetter, K.-M. et al. (2021). Enantioselective desymmetrization of 2-aryl-1,3-propanediols by direct *O*-alkylation with a rationally

designed chiral hemiboronic acid catalyst that mitigates substrate conformational poisoning. *J. Am. Chem. Soc.* 143 (11): 4162–4167.

157 Wurz, R.P. and Fu, G.C. (2005). Catalytic asymmetric synthesis of piperidine derivatives through the [4 + 2] annulation of imines with allenes. *J. Am. Chem. Soc.* 127 (35): 12234–12235.

158 Kano, T., Takai, J., Tokuda, O., and Maruoka, K. (2005). Design of an axially chiral amino acid with a binaphthyl backbone as an organocatalyst for a direct asymmetric aldol reaction. *Angew. Chem. Int. Ed.* 44 (20): 3055–3057.

159 Kano, T., Yamaguchi, Y., Tokuda, O., and Maruoka, K. (2005). Anti-selective direct asymmetric Mannich reactions catalyzed by axially chiral amino sulfonamide as an organocatalyst. *J. Am. Chem. Soc.* 127 (47): 16408–16409.

160 Kano, T., Sugimoto, H., Maruyama, H., and Maruoka, K. (2015). Regio- and stereoselective conjugate addition of aldehydes to β-tosyl enones under the catalysis of a binaphthyl-modified chiral amine. *Angew. Chem. Int. Ed.* 54 (29): 8462–8465.

161 Matsui, K., Takizawa, S., and Sasai, H. (2005). Bifunctional organocatalysts for enantioselective aza-Morita–Baylis–Hillman reaction. *J. Am. Chem. Soc.* 127 (11): 3680–3681.

162 Matsui, K., Takizawa, S., and Sasai, H. (2006). A Brønsted acid and Lewis base organocatalyst for the aza-Morita-Baylis-Hillman reaction. *Synlett* 2006 (5): 761–765.

163 Terada, M., Ube, H., and Yaguchi, Y. (2006). Axially chiral guanidine as enantioselective base catalyst for 1,4-addition reaction of 1,3-dicarbonyl compounds with conjugated nitroalkenes. *J. Am. Chem. Soc.* 128 (5): 1454–1455.

164 Terada, M., Nakano, M., and Ube, H. (2006). Axially chiral guanidine as highly active and enantioselective catalyst for electrophilic amination of unsymmetrically substituted 1,3-dicarbonyl compounds. *J. Am. Chem. Soc.* 128 (50): 16044–16045.

165 Peng, F.-Z., Shao, Z.-H., Fan, B.-M. et al. (2008). Organocatalytic enantioselective Michael addition of 2,4-pentandione to nitroalkenes promoted by bifunctional thioureas with central and axial chiral elements. *J. Org. Chem.* 73 (13): 5202–5205.

166 Kim, S.M., Lee, J.H., and Kim, D.Y. (2008). Enantioselective direct amination of α-cyanoketones catalyzed by bifunctional organocatalysts. *Synlett* 2008 (17): 2659–2662.

167 Jung, S.H. and Kim, D.Y. (2008). Catalytic enantioselective electrophilic α-hydrazination of β-ketoesters using bifunctional organocatalysts. *Tetrahedron Lett.* 49 (38): 5527–5530.

168 Mandai, H., Fujii, K., Yasuhara, H. et al. (2016). Enantioselective acyl transfer catalysis by a combination of common catalytic motifs and electrostatic interactions. *Nat. Commun.* 7: 11297.

169 Shibatomi, K., Kitahara, K., Okimi, T. et al. (2016). Enantioselective fluorination of α-branched aldehydes and subsequent conversion to α-hydroxyacetals via stereospecific C–F bond cleavage. *Chem. Sci.* 7 (2): 1388–1392.

170 Panger, J.L. and Denmark, S.E. (2020). Enantioselective synthesis of γ-lactams by Lewis base catalyzed sulfenoamidation of alkenes. *Org. Lett.* 22 (7): 2501–2505.

171 Zheng, T., Wang, X., Ng, W.-H. et al. (2020). Catalytic enantio- and diastereoselective domino halocyclization and spiroketalization. *Nat. Catal.* 3 (12): 993–1001.

172 Ooi, T., Kameda, M., and Maruoka, K. (1999). Molecular design of a C_2-symmetric chiral phase-transfer catalyst for practical asymmetric synthesis of α-amino acids. *J. Am. Chem. Soc.* 121 (27): 6519–6520.

173 He, R., Wang, X., Hashimoto, T., and Maruoka, K. (2008). Binaphthyl-modified quaternary phosphonium salts as chiral phase-transfer catalysts: asymmetric amination of β-keto esters. *Angew. Chem. Int. Ed.* 47 (49): 9466–9468.

174 Uraguchi, D., Koshimoto, K., and Ooi, T. (2008). Chiral ammonium betaines: a bifunctional organic base catalyst for asymmetric Mannich-type reaction of α-nitrocarboxylates. *J. Am. Chem. Soc.* 130 (33): 10878–10879.

175 He, R., Shirakawa, S., and Maruoka, K. (2009). Enantioselective base-free phase-transfer reaction in water-rich solvent. *J. Am. Chem. Soc.* 131 (46): 16620–16621.

176 Lee, J.W., Yan, H., Jang, H.B. et al. (2009). Bis-terminal hydroxy polyethers as all-purpose, multifunctional organic promoters: a mechanistic investigation and applications. *Angew. Chem. Int. Ed.* 48 (41): 7683–7686.

177 Jadhav, A.P., Park, S.Y., Lee, J.-W. et al. (2021). Cooperative asymmetric cation-binding catalysis. *Acc. Chem. Res.* 54 (23): 4319–4333.

178 Uraguchi, D., Koshimoto, K., and Ooi, T. (2010). Flexible synthesis, structural determination, and synthetic application of a new C_1-symmetric chiral ammonium betaine. *Chem. Commun.* 46 (2): 300–302.

179 Egami, H., Asada, J., Sato, K. et al. (2015). Asymmetric fluorolactonization with a bifunctional hydroxyl carboxylate catalyst. *J. Am. Chem. Soc.* 137 (32): 10132–10135.

180 Egami, H., Niwa, T., Sato, H. et al. (2018). Dianionic phase-transfer catalyst for asymmetric fluoro-cyclization. *J. Am. Chem. Soc.* 140 (8): 2785–2788.

181 Yang, D., Yip, Y.-C., Tang, M.-W. et al. (1996). A C_2 symmetric chiral ketone for catalytic asymmetric epoxidation of unfunctionalized olefins. *J. Am. Chem. Soc.* 118 (2): 491–492.

182 Yang, D., Wang, X.-C., Wong, M.-K. et al. (1996). Highly enantioselective epoxidation of trans-stilbenes catalyzed by chiral ketones. *J. Am. Chem. Soc.* 118 (45): 11311–11312.

183 Xu, B., Shi, L.-L., Zhang, Y.-Z. et al. (2014). Catalytic asymmetric direct α-alkylation of amino esters by aldehydes via imine activation. *Chem. Sci.* 5 (5): 1988–1991.

184 Wen, W., Chen, L., Luo, M.-J. et al. (2018). Chiral aldehyde catalysis for the catalytic asymmetric activation of glycine esters. *J. Am. Chem. Soc.* 140 (30): 9774–9780.

185 Quideau, S., Lyvinec, G., Marguerit, M. et al. (2009). Asymmetric hydroxylative phenol dearomatization through in situ generation of iodanes from chiral iodoarenes and *m*-CPBA. *Angew. Chem. Int. Ed.* 48 (25): 4605–4609.

186 Uyanik, M., Okamoto, H., Yasui, T., and Ishihara, K. (2010). Quaternary ammonium (hypo)iodite catalysis for enantioselective oxidative cycloetherification. *Science* 328 (5984): 1376–1379.

187 Brenet, S., Berthiol, F., and Einhorn, J. (2013). 3,3′-Diiodo-BINOL-fused maleimides as chiral hypervalent iodine(III) organocatalysts. *Eur. J. Org. Chem.* 2013 (36): 8094–8096.

188 Suzuki, S., Kamo, T., Fukushi, K. et al. (2014). Iodoarene-catalyzed fluorination and aminofluorination by an Ar-I/HF·pyridine/*m*CPBA system. *Chem. Sci.* 5 (7): 2754–2760.

189 Zhang, X., Liu, M., Ge, H., and Zhang, Z. (2023). Second-layer chiral environment-induced steric hindrance enables catalyst conformation lockdown in enantioselective hypervalent iodine organocatalysis. *ACS Catal.* 13 (12): 8273–8280.

190 Denmark, S.E. and Wynn, T. (2001). Lewis base activation of Lewis acids: catalytic enantioselective allylation and propargylation of aldehydes. *J. Am. Chem. Soc.* 123 (25): 6199–6200.

191 Wang, J., Li, H., Yu, X. et al. (2005). Chiral binaphthyl-derived amine-thiourea organocatalyst-promoted asymmetric Morita–Baylis–Hillman reaction. *Org. Lett.* 7 (19): 4293–4296.

192 Fleming, E.M., McCabe, T., and Connon, S.J. (2006). Novel axially chiral bis-arylthiourea-based organocatalysts for asymmetric Friedel–Crafts type reactions. *Tetrahedron Lett.* 47 (39): 7037–7042.

193 Liu, X.-G., Jiang, J.-J., and Shi, M. (2007). Development of axially chiral bis(arylthiourea)-based organocatalysts and their application in the enantioselective Henry reaction. *Tetrahedron Asymmetry* 18 (23): 2773–2781.

194 Shi, M. and Liu, X.-G. (2008). Asymmetric Morita-Baylis-Hillman reaction of arylaldehydes with 2-cyclohexen-1-one catalyzed by chiral bis(thio)urea and DABCO. *Org. Lett.* 10 (6): 1043–1046.

195 Terada, M., Sorimachi, K., and Uraguchi, D. (2006). Phosphorodiamidic acid as a novel structural motif of Brønsted acid catalysts for direct Mannich reaction of *N*-acyl imines with 1,3-dicarbonyl compounds. *Synlett* 2006 (1): 133–136.

196 Hatano, M., Ikeno, T., Matsumura, T. et al. (2008). Chiral lithium salts of phosphoric acids as Lewis acid–base conjugate catalysts for the enantioselective cyanosilylation of ketones. *Adv. Synth. Catal.* 350 (11–12): 1776–1780.

197 Nelson, H.M., Patel, J.S., Shunatona, H.P., and Toste, F.D. (2015). Enantioselective α-amination enabled by a BINAM-derived phase-transfer catalyst. *Chem. Sci.* 6 (1): 170–173.

198 Uraguchi, D., Nakashima, D., and Ooi, T. (2009). Chiral arylaminophosphonium barfates as a new class of charged Brønsted acid for the enantioselective activation of nonionic Lewis bases. *J. Am. Chem. Soc.* 131 (21): 7242–7243.

199 Denmark, S.E., Kalyani, D., and Collins, W.R. (2010). Preparative and mechanistic studies toward the rational development of catalytic, enantioselective selenoetherification reactions. *J. Am. Chem. Soc.* 132 (44): 15752–15765.

200 Pupo, G., Ibba, F., Ascough, D.M.H. et al. (2018). Asymmetric nucleophilic fluorination under hydrogen bonding phase-transfer catalysis. *Science* 360 (6389): 638–642.

201 Takaishi, K., Okuyama, T., Kadosaki, S. et al. (2019). Hemisquaramide tweezers as organocatalysts: synthesis of cyclic carbonates from epoxides and CO_2. *Org. Lett.* 21 (5): 1397–1401.

202 Uraguchi, D., Ueoka, F., Tanaka, N. et al. (2020). A structurally robust chiral borate ion: molecular design, synthesis, and asymmetric catalysis. *Angew. Chem. Int. Ed.* 59 (28): 11456–11461.

203 Shi, Y.-L. and Shi, M. (2007). Chiral thiourea-phosphine organocatalysts in the asymmetric aza-Morita–Baylis–Hillman reaction. *Adv. Synth. Catal.* 349 (13): 2129–2135.

204 Zhang, X.-N. and Shi, M. (2013). Phosphine-catalyzed [3 + 2] cycloaddition of 4,4-dicyano-2-methylenebut-3-enoates with benzyl buta-2,3-dienoate and penta-3,4-dien-2-one. *ACS Catal.* 3 (4): 507–512.

205 Uraguchi, D., Kinoshita, N., and Ooi, T. (2010). Catalytic asymmetric protonation of α-amino acid-derived ketene disilyl acetals using P-spiro diaminodioxaphosphonium barfates as chiral proton. *J. Am. Chem. Soc.* 132 (35): 12240–12242.

206 Marqués-López, E., Alcaine, A., Tejero, T., and Herrera, R.P. (2011). Enhanced efficiency of thiourea catalysts by external Brønsted acids in the Friedel–Crafts alkylation of indoles. *Eur. J. Org. Chem.* 2011 (20-21): 3700–3705.

207 Vallavoju, N., Selvakumar, S., Jockusch, S. et al. (2014). Enantioselective organo-photocatalysis mediated by atropisomeric thiourea derivatives. *Angew. Chem. Int. Ed.* 53 (22): 5604–5608.

208 Alegre-Requena, J.V., Marqués-López, E., and Herrera, R.P. (2015). One-pot synthesis of unsymmetrical squaramides. *RSC Adv.* 5 (42): 33450–33462.

209 Alegre-Requena, J.V., Marqués-López, E., and Herrera, R.P. (2016). Trifunctional squaramide catalyst for efficient enantioselective Henry reaction activation. *Adv. Synth. Catal.* 358 (11): 1801–1809.

210 Liu, S., Maruoka, K., and Shirakawa, S. (2017). Chiral tertiary sulfonium salts as effective catalysts for asymmetric base-free neutral phase-transfer reactions. *Angew. Chem. Int. Ed.* 56 (17): 4819–4823.

211 Takenaka, N., Xia, G., and Yamamoto, H. (2004). Catalytic, highly enantio- and diastereoselective pinacol coupling reaction with a new tethered bis(8-quinolinolato) ligand. *J. Am. Chem. Soc.* 126 (41): 13198–13199.

212 Abell, J.P. and Yamamoto, H. (2010). Development and applications of tethered bis(8-quinolinolato) metal complexes (TBOxM). *Chem. Soc. Rev.* 39 (1): 61–69.

213 Nishikawa, Y. and Yamamoto, H. (2011). Iron-catalyzed asymmetric epoxidation of β,β-disubstituted enones. *J. Am. Chem. Soc.* 133 (22): 8432–8435.

214 Dohi, T., Sasa, H., Miyazaki, K. et al. (2017). Chiral atropisomeric 8,8′-diiodobinaphthalene for asymmetric dearomatizing spirolactonizations in hypervalent iodine oxidations. *J. Org. Chem.* 82 (22): 11954–11960.

215 Cheng, J.K., Xiang, S.-H., Li, S. et al. (2021). Recent advances in catalytic asymmetric construction of atropisomers. *Chem. Rev.* 121 (8): 4805–4902.

216 Tan, B. (ed.) (2021). *Axially Chiral Compounds: Asymmetric Synthesis and Applications*. Weinheim: Wiley-VCH.

8

Multinuclear Zinc Catalysts with Axial Chirality

Takayoshi Arai

Chiba University, Graduate School of Science, Department of Chemistry, 1-33 Yayoi, Inage-ku, Chiba, 263-8522, Japan

This chapter details the development of zinc catalysts using axially chiral ligands. The hard nature of the zinc element has led to the development of many catalysts by employing the axial chiral 1,1′-bi-2-naphthol (BINOL) ligands (Figure 8.1) [1]. Let us look at some representative studies that have been established along with the development of asymmetric catalysis.

8.1 Pioneering Works on BINOL-Zn System

The first chiral Lewis acidic BINOL-Zn system was pioneered by Yamamoto et al. In 1985, an enantioselective cyclization of prochiral unsaturated aldehydes was reported using a zinc binaphthoxide complex prepared from dimethylzinc and (*R*)-(+)-1,1′-bi-2-naphthol (BINOL: **L1**) (Scheme 8.1) [2].

Renaud and co-workers applied Yamamoto's reagent to an enantioselective Diels–Alder reaction (Scheme 8.2) [3]. The zinc binaphthoxide reagent promoted the reaction of *N*-alkoxyacrylamide substrates with cyclopentadiene to give the *endo*-selective Diels–Alder adduct with up to 96% ee. Yamamoto's zinc binaphthoxide complex was also promoted the asymmetric aza-Diels–Alder reaction of Danishefsky's diene with imine to give the products with up to 93% ee [4].

In these pioneering works, the real catalyst structure was unclear and typically stoichiometric amount of zinc binaphthoxide complex was required in order to ensure acceptable enantioselectivity and chemical yields.

8.2 Enantioselective Addition Reaction of Dialkylzinc to Aldehydes Using BINOL Additive

Another early-stage stream of the BINOL-Zn system is shown in the enantioselective addition of dialkylzinc to aldehydes. For the addition of dialkylzinc to aldehydes,

Atropisomerism in Asymmetric Organic Synthesis: Challenges and Applications, First Edition.
Edited by Shinobu Takizawa and Mohamed S. H. Salem.

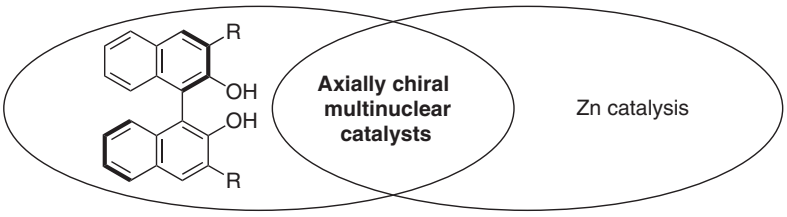

Figure 8.1 Multinuclear zinc catalysts with axial chirality.

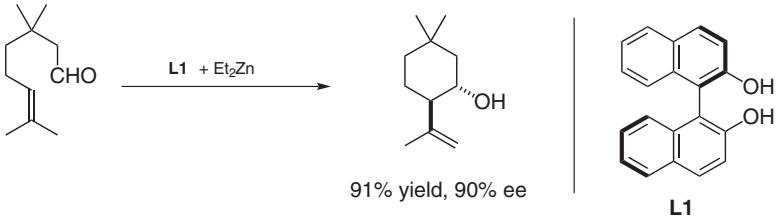

Scheme 8.1 Asymmetric enantioselective cyclization of unsaturated aldehydes promoted by zinc binaphthoxide.

Renaud and co-workers [3]

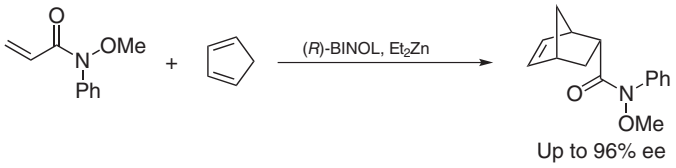

Whiting and et al. [4]

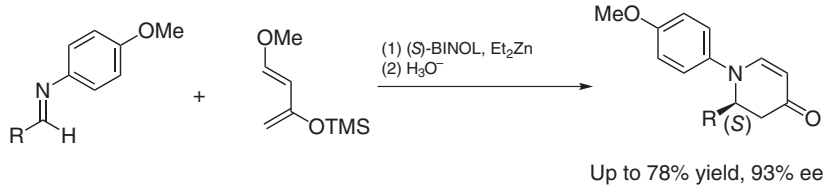

Scheme 8.2 Asymmetric enantioselective Diels–Alder reactions promoted by zinc binaphthoxide.

Oguni et al. reported the first enantioselective reaction using a bis((−)-camphorquinone-α-dioximato: **L2**) palladium(II) metal complex in 1983 [5], and the reaction using an (*S*)-leucinol (**L3**) in 1984 [6]. Noyori and co-workers reported a (−)-3-*exo*-dimethylaminoisobornenol [(−)-DAIB (**L4**)] as a quite efficient catalyst for giving the product in a highly enantioselective manner (Scheme 8.3) [7].

Among the survey of various chiral ligands for zinc reagents, BINOL as a C_2-symmetric chiral diol was reasonably examined. Although Salvadori and co-workers reported that the BINOL (**L1**) itself promoted the reaction of diethylzinc

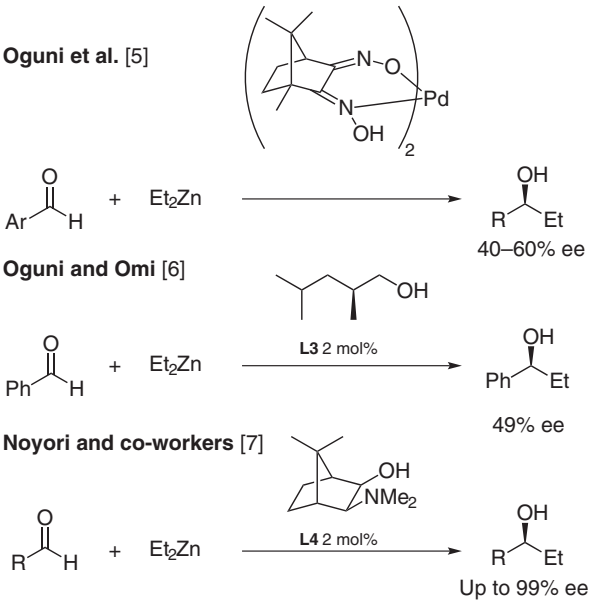

Scheme 8.3 Examples of asymmetric diethylzinc addition to aldehydes.

with aromatic aldehydes to give the products ranging from 48% ee to 77% ee [8], Joshi and Prasad concluded that the reaction was not promoted [9]. The obscure results would be due to the aggregation nature of the zinc binaphthoxide.

Katsuki and co-workers reported an *N*,*N*,*N*′,*N*′-tetraisopropyl-2,2′-dihydroxy-1,1′-binaphthyl-3,3′-dicarboxamide (**L5**)-catalyzed addition of diethylzinc to benzaldehyde with enantioselectivity of up to 99% ee (Scheme 8.4). A monomeric seven-membered 2,2′-dihydroxy-1,1′-binaphthyl-3,3′-dicarboxamide–Zn complex is proposed on the basis of nuclear magnetic resonance (NMR) experiments [10]. In the paper, catalytic asymmetric Simmons–Smith cyclopropanation of allylic alcohols was also examined.

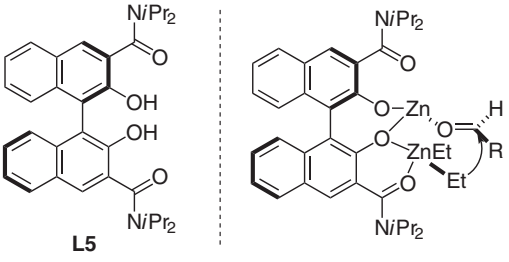

Scheme 8.4 *N*,*N*,*N*′,*N*′-tetraisopropyl-2,2′-dihydroxy-1,1′-binaphthyl-3,3′-dicarboxamide (**L5**)-catalyzed addition of diethylzinc to benzaldehyde.

Pu and co-workers prepared a unique BINOL polymer (**L6**). The rigid and sterically regular chiral polybinaphthyl (5 mol% based on the binaphthyl unit) was applied to the asymmetric addition of diethylzinc to aldehydes to record up to 95% yield with 94% ee, which would be the result on prevention of the undesired aggregation of zinc binaphthoxide (Scheme 8.5) [11].

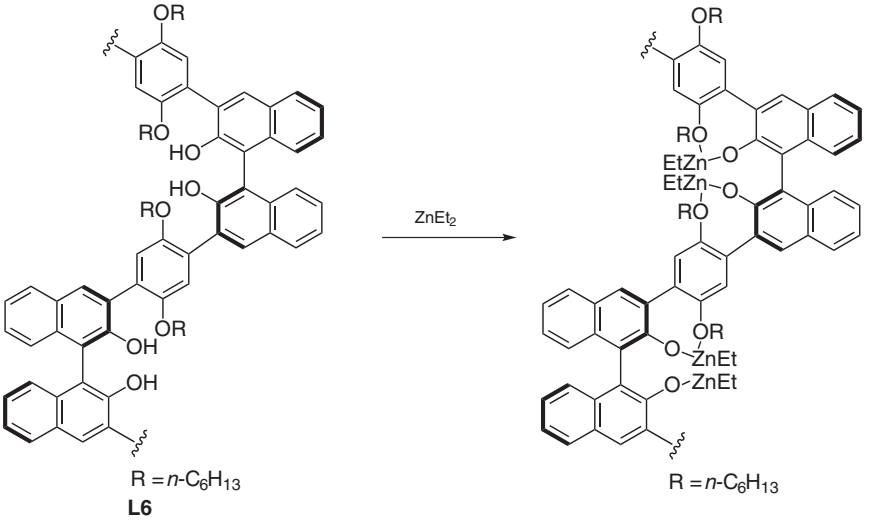

Scheme 8.5 BINOL polymers **(L6)** for diethylzinc addition to aldehydes.

The early stage of asymmetric zinc binaphthoxide system has indicated the importance of some bulky substituents at the 3- and/or 3′-positions of BINOL to get high catalytic activity. In many cases, the substituents would reduce the complicated aggregation to form the polynuclear zinc complexes.

Impressive approach for exploring the efficient zinc binaphthoxide catalyst came from the study on "Asymmetric Activation" [12]. In the strategy of asymmetric activation, one enantiomer of catalyst can be activated by adding a compound for improving the catalyst efficiency and enantioselectivity.

Mikami et al. and Walsh et al. have independently studied the use of a "chiral/achiral activator" for the zinc binaphthoxide catalysts and discovered the combination use of 3,3′-diphenylbinaphthol (**L7**) with diminines (**L8**, **L9**) gave the excellent catalysts (Figure 8.2). For example, in Mikami's combination, only 2 mol% of **L7**/diphenylethylene-derived diimine **L8** gave (*S*)-phenylpropanol in 100% yield with 97% ee [13, 14].

Ishihara and co-workers reported 3,3′-diphosphoryl-binaphthol (**L10**) for the enantioselective dialkylzinc addition to aldehydes [15]. Using a zinc 3,3′-diphosphoramide binaphthoxide, highly enantioselective dialkylzinc addition was achieved for a series of aromatic, aliphatic, and heteroaromatic aldehydes with up to >99% ee (Figure 8.3).

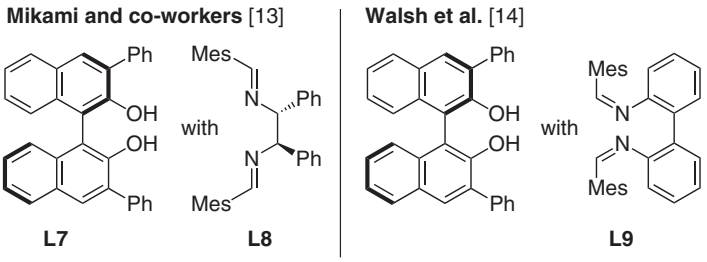

Figure 8.2 Asymmetric activation system for diethylzinc addition to aldehydes.

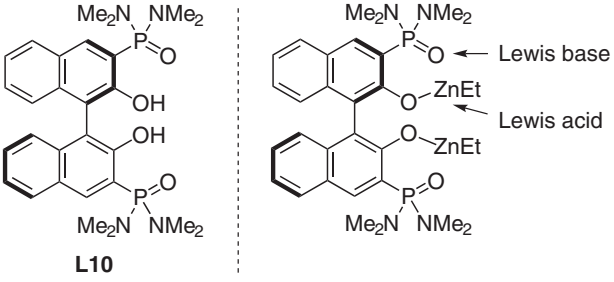

Figure 8.3 3,3′-Diphosphoryl-binaphthol (**L10**).

8.3 Catalytic Asymmetric Alkynylation of Aldehydes

Pedro and co-workers reported a 3,3-bis(3,5-ditrifluoromethylphenyl)binaphthol (**L11**) for the first enantioselective alkynylation of *N*-sulfonyl aldimines to give *N*-sulfonyl-protected propargylic amines via *in situ* formation of zinc acetylide from dimethylzinc with the terminal alkynes (Scheme 8.6) [16]. **L11** drastically improved the asymmetric induction to 96% ee from **L1**-catalyzed reaction (8% ee).

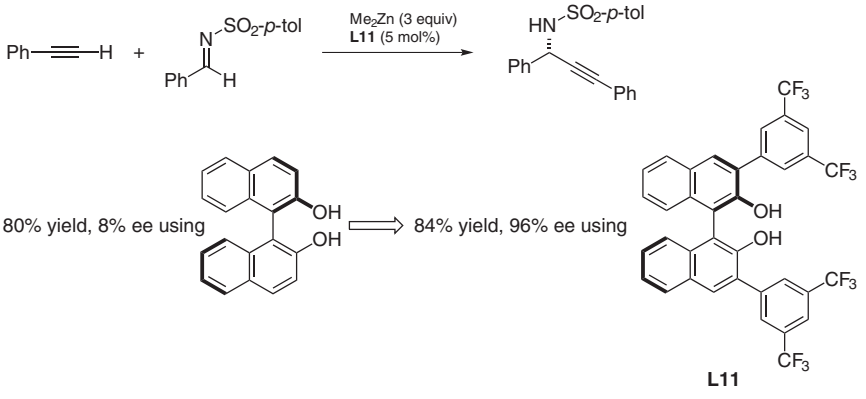

Scheme 8.6 3,3-Bis(3,5-ditrifluoromethylphenyl)binaphthol (**L11**)-catalyzed asymmetric alkynylation.

Without the use of an activator, the reaction worked nicely with various aromatic and heteroaromatic *N*-sulfonyl aldimines. The *N*-tosyl amines derived from alkyl acetylenes can be efficiently transformed into the corresponding propargylic amines by a treatment with SmI_2.

8.4 Catalytic Asymmetric Diels–Alder Reaction

From the study on the asymmetric activation, Ding and co-workers discovered a combination use of 3,3′-dibromobinaphthol (**L12**) and cyclohexyldiamine-derived diimine (**L13**) provided an efficient zinc catalyst for the hetero Diels–Alder reaction of Danishefsky's diene with aldehydes to give the 2-substituted 2,3-dihydro-4H-pyran-4-one in up to quantitative yield with 98% ee (Scheme 8.7) [17].

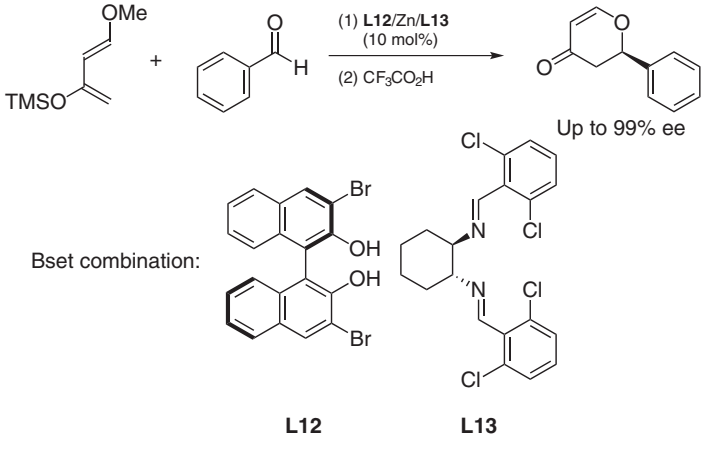

Scheme 8.7 Asymmetric activation of zinc 3,3′-dibromobinaphthoxide-catalyzed hetero Diels–Alder reaction.

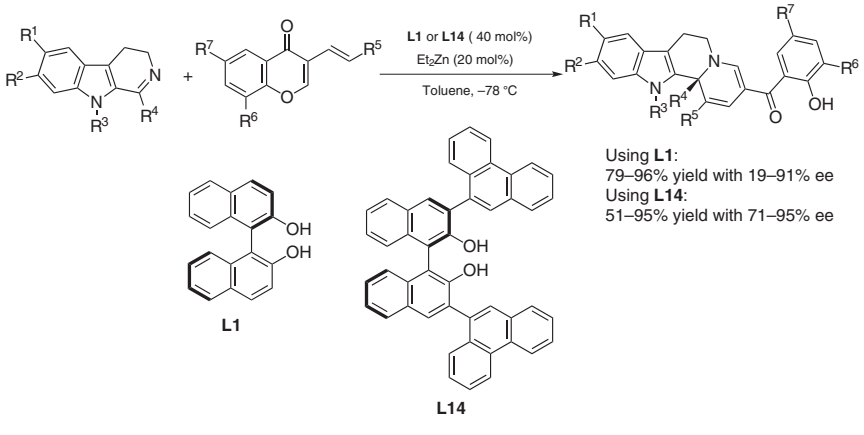

Scheme 8.8 Catalytic asymmetric inverse-electron-demand imino Diels–Alder reaction.

We have realized the importance of introducing some substituents at the 3,3′-poisition of BINOL to get high catalytic activity, but it is not always essential. Interestingly, Kumar and Waldmann reported first an asymmetric inverse-electron-demand imino Diels–Alder (IEDIDA) reaction that is the cycloaddition of the electron-rich cyclic imine with the chromone-derived diene in the presence of zinc binaphthoxides [18]. In this study, both the original simple BINOL (**L1**) and the 3,3′-diphenanthrenylbinaphthol (**L14**) showed comparable catalytic activities (Scheme 8.8). The large and highly polar substrates themselves might act as the achiral asymmetric activator.

8.5 Catalytic Asymmetric Epoxidation of Enones

Asymmetric epoxidation of enones is one of the well-studied reactions using the zinc binaphthoxide system. After Shibasaki's lanthanoid binaphthoxide-catalyzed asymmetric epoxidation of enones, a wide range of efficient catalysts have been developed (Scheme 8.9) [19, 20]. Among them, Pu and co-workers applied their binaphthyl polymer (**L6**) for the zinc-catalyzed epoxidation of enone substrates using *tert*-butyl hydroperoxide (TBHP) [21]. From the structure–activity relationship of the polymer ligands, interaction of the neighboring catalytic sites in the polymer chain was proposed.

Later, Dötz and co-workers discovered that the zinc-catalyzed enantioselective epoxidation of α,β-enones was possible to be conducted using a simple BINOL (**L1**) [22]. An observation of asymmetric amplification for the epoxidation of chalcone suggests the dimeric or oligomeric zinc binaphthoxide complexes as the active species.

Shibasaki et al. [19, 20]

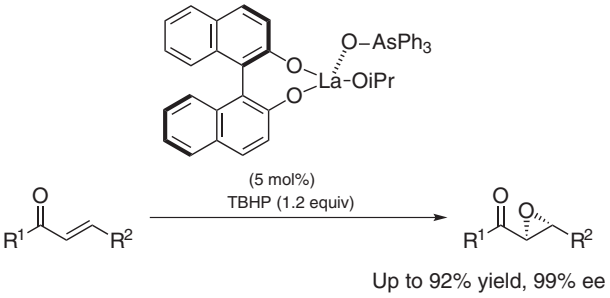

Up to 92% yield, 99% ee

Pu and co-workers [21]

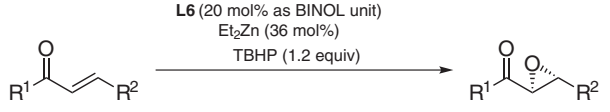

Up to 81% yield with 79% ee

Scheme 8.9 Catalytic asymmetric epoxidation of enones.

Dötz and Minatti [22]

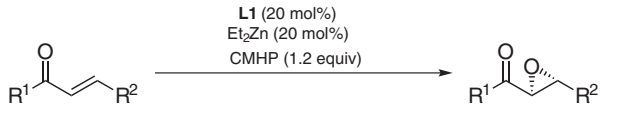

Scheme 8.9 (*Continued*)

8.6 Catalytic Asymmetric Direct Aldol Reaction

Catalytic asymmetric direct aldol reaction using nonactivated simple ketones is an important reaction for accessing the chiral α-hydroxy ketones [1]. Shibasaki et al. pioneered the first intermolecular direct catalytic aldol of simple ketones using their famous heterobimetallic multifunctional $LaLi_3$tris-(binaphthoxide) (LLB) complex [23]. The addition of an equimolar amount of KHMDS to the LLB complex improved the catalytic activity for reducing the catalyst amount in 8 mol% (Scheme 8.10) [24].

Shibasaki and co-workers have also carried out the direct aldol reaction using barium binaphthoxide catalysts [25]. The barium binaphthoxide derived from monomethyl ether of BINOL (**L15**) became the efficient catalyst for the direct aldol reaction of acetophenone with alkyl aldehydes [26]. More simply obtainable barium binaphthoxide is useful for the enolate formation from α,β-unsaturated esters to give Baylis–Hillman-type adducts, in which a dynamic kinetic asymmetric transformation (DYKAT) through isomerization of the initial aldol adduct is observed [27].

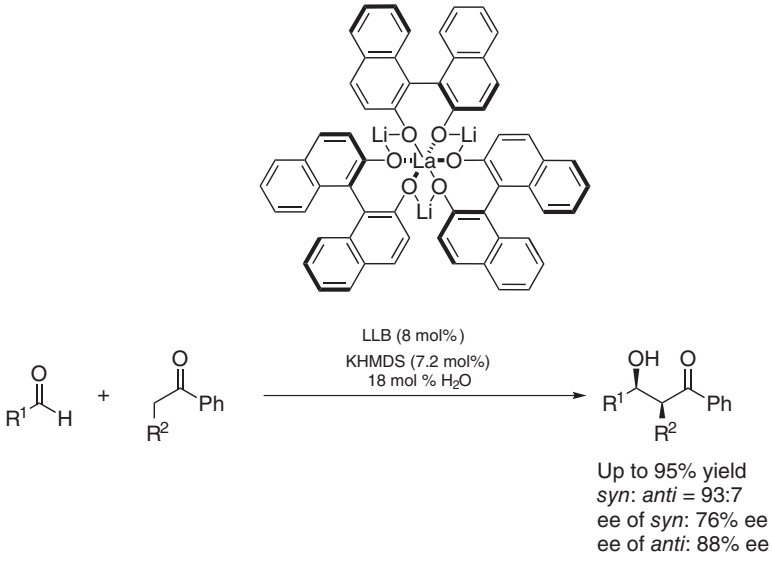

Scheme 8.10 Shibasaki's catalytic asymmetric direct aldol reactions.

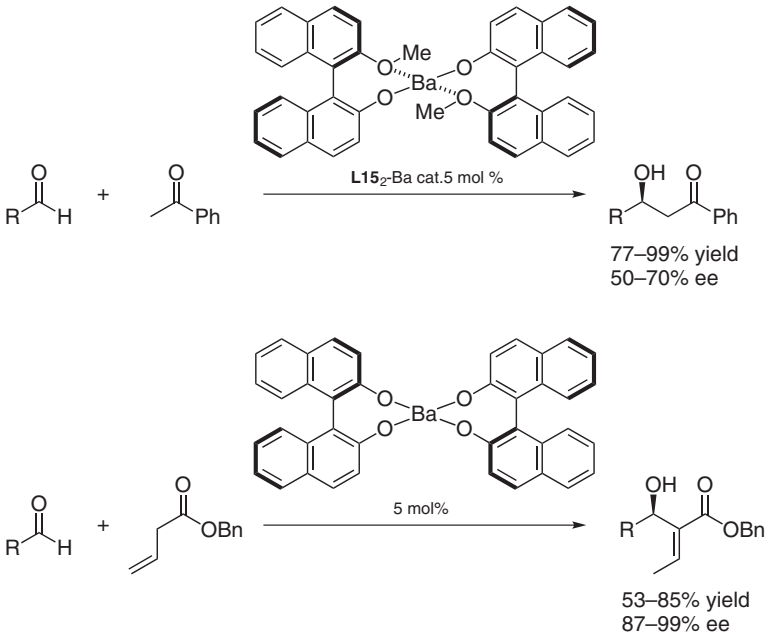

Scheme 8.10 (*Continued*)

Regarding the multinuclear Zn catalysts, Trost's catalyst is impressive. In 2000, a bisproline-substituted phenol ligand (**L16**) was developed for dinuclear Zn catalyst systems (Scheme 8.11) [28]. After the first demonstration of the asymmetric aldol reaction, the unique dinuclear Zn platform has been applied to a wide range of asymmetric reactions. Because Trost's Zn catalyst is missing the concept of atrope chirality, here the utility is just summarized in a showcase (Figure 8.4) [29].

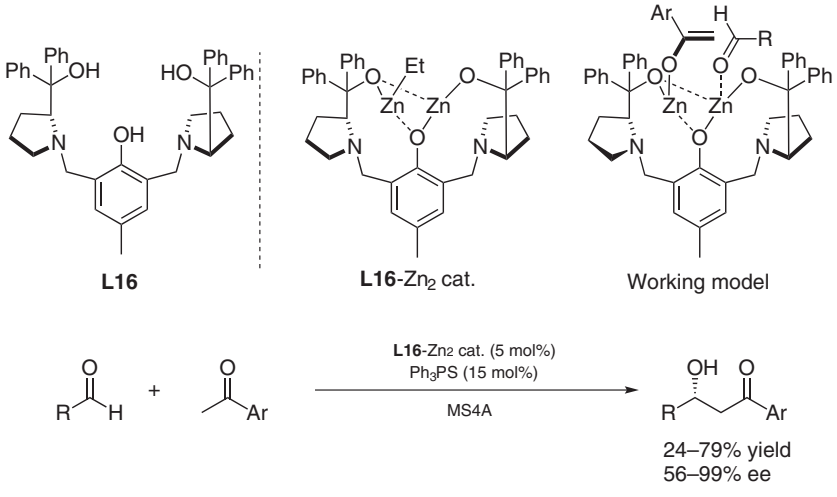

Scheme 8.11 Zinc bisproline-substituted phenoxide catalyst for direct aldol reaction.

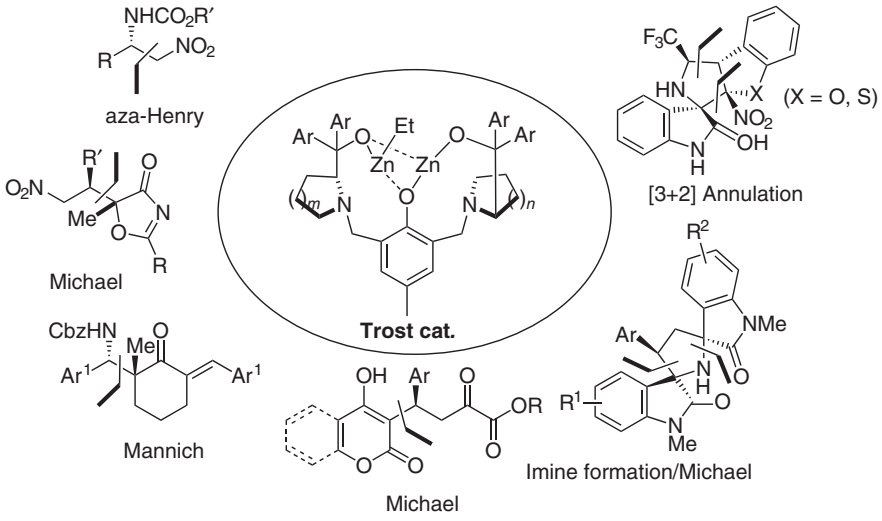

Figure 8.4 Showcase of Trost's Zn catalyses.

Da et al. developed a BINOL ligand having (*S*)-diphenylprolinol unit at the 3,3′-posision (**L17**) [30]. Using the 20 mol% dinuclear zinc complex prepared from **L17**, the direct aldol reaction of acetophenone was catalyzed to give the product with up to 80% ee (Scheme 8.12).

Especially, α-hydroxy ketones are important substrates for the multinuclear zinc-catalyzed asymmetric direct aldol reaction, because the multinuclear zinc platform has been studied as a mimic of class II zinc metalloenzymes. The feature of bifunctional aldolases, classified as class I (peptide base) and class II (zinc metalloenzyme), have received much attention as a potentially advantageous strategy

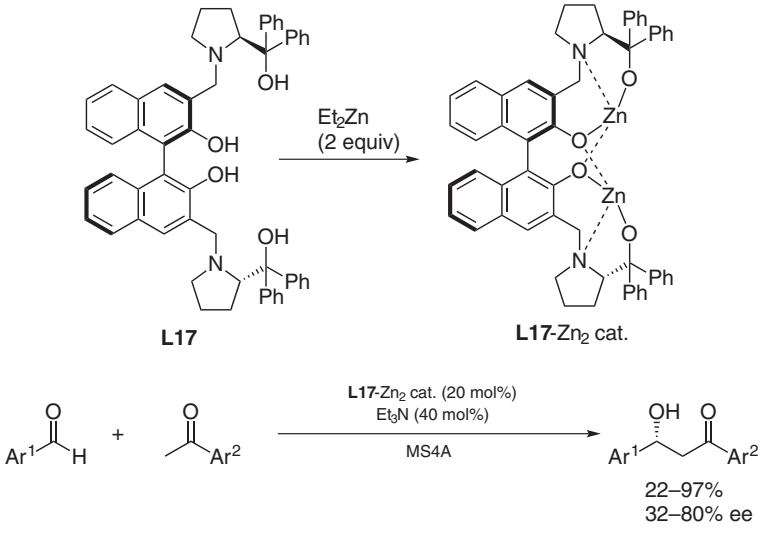

Scheme 8.12 Diphenylprolinol-substituted BINOL (**L17**) for zinc-catalyzed asymmetric aldol reaction.

to develop efficient and atom-economic artificial asymmetric enzymes. In the mechanism of the class II Zn^{2+}-dependent aldolases, chelation of the *cis*-enediolate form of dihydroxyacetone phosphate is proposed (Scheme 8.13) [31].

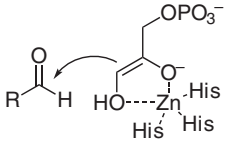

Scheme 8.13 Working hypothesis of Zn^{2+}-dependent aldolases.

Trost et al. applied their multinuclear Zn-catalysts (**L16**-Zn_2) to the aldol reaction of α-hydroxy ketones to give the products in a highly *syn*-selective manner (Scheme 8.14) [32].

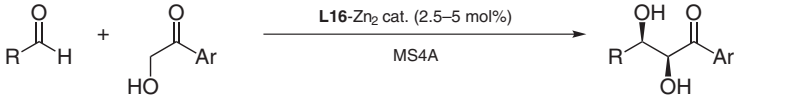

Scheme 8.14 Dinuclear zinc prophenoxide-catalyzed aldol for *syn*-diols.

From the continuous efforts of Shibasaki group for developing multinuclear cooperative asymmetric catalysts, a (*S*,*S*)-linked-BINOL (**L18**) was synthesized and applied to the Zn-catalyzed asymmetric aldol reaction of α-hydroxyketones (Scheme 8.15) [33]. The complex prepared in a ratio of 4 : 1 for Et_2Zn/**L18**

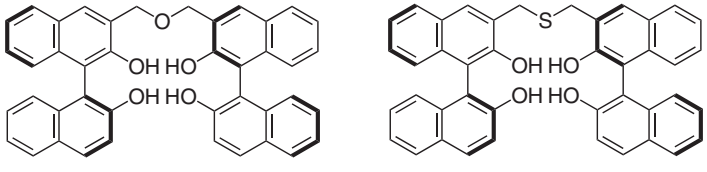

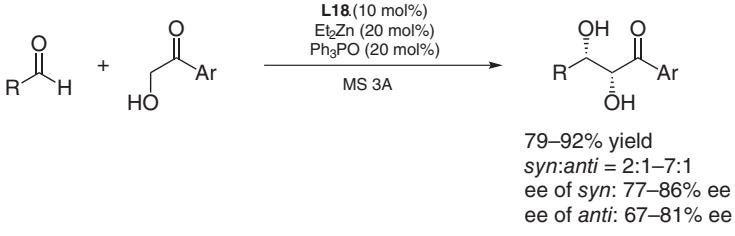

Scheme 8.15 Linked BINOLs for zinc-catalyzed asymmetric aldol reaction of α-hydroxyketones.

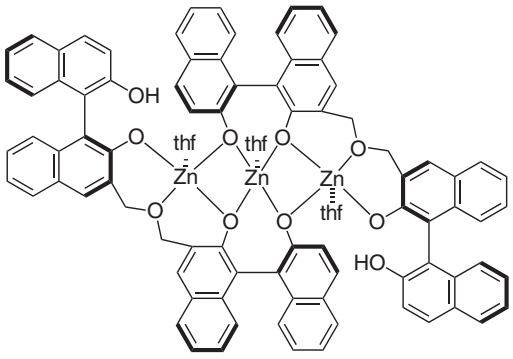

Scheme 8.15 (*Continued*)

with molecular sieves 3A (MS 3A) worked effective catalyst for the direct aldol reaction albeit in a *syn*-selective manner. From the mechanistic study, the formation of trinuclear Zn complex having two molecules of **L18** was suggested. A sulfur-linked-BINOL (**L19**) was also effective in the direct aldol reaction of α-hydroxyketones to give the aldol adducts in an *anti*-selective manner with up to 93% ee.

8.7 Catalytic Asymmetric Iodofunctionalization of Alkenes

In 2014, a 3,3′-bis(aminoimino)BINOL ligand (**L20**) prepared from (*R*, *R*)-diphenylethylenediamine and (*R*)-3,3′-diformylbinaphthol was developed for making a trinuclear Zn complex by a reaction with $Zn(OAc)_2$. The structure of chiral $Zn_3(OAc)_4$-3,3′-bis(aminoimino)binaphthoxide complex (***tri-Zn***) was unequivocally determined by an X-ray crystallographic analysis. Using 1 mol% ***tri-Zn*** catalyst up to 99.9% ee of iodolactones were obtained (Scheme 8.16) [34].

The diastereomeric ligand (**L21**) prepared from (*S*, *S*)-diphenylethylenediamine and (*R*)-3,3′-diformylbinaphthol reduced asymmetric induction with 68% ee. Interestingly, a **L22** prepared using an achiral amine also provided an efficient chiral zinc catalyst to afford chiral iodolactone with 98% ee. The catalyst prepared using (*R*, *R*)-diphenylethylenediamine-derived bis(aminoimino)biphenol (**L23**) gave (*R*)-enriched iodolactone in 75% yield with 72% ee. From density functional theory (DFT) calculations of the **L23**-$Zn(OAc)_2$ complex, the conformation with the (*R*)-axis **L23**-Zn_3 complex is more stable by 6.0 kcal/mol than the (*S*)-axis configuration. Further experimental analysis of the reaction mechanism and the DFT calculation revealed the catalyst role. In the ***tri-Zn*** catalysis, carboxylic acid substrate was converted to zinc carboxylates. The halolactonization is significantly enhanced by the addition of catalytic I_2. DFT calculation suggested that a catalytic amount of I_2 mediates the alkene portion of the substrates and *N*-Iodosuccinimide (NIS) to achieve highly enantioselective iodolactonization [35].

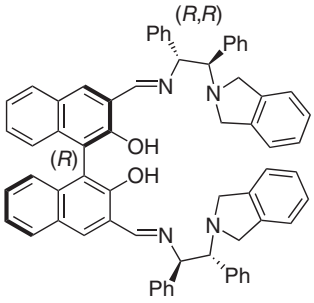

L20: (*R*,*R*,*R*)-Bis(aminoimino)BINOL

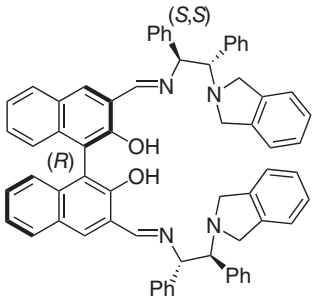

L21: (*R*,*S*,*S*)-Bis(aminoimino)BINOL

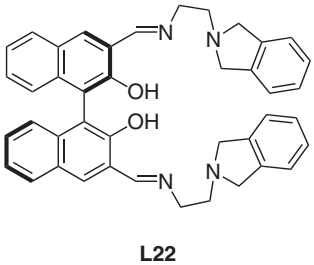

L22

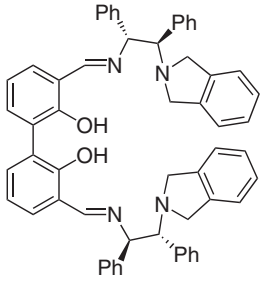

L23

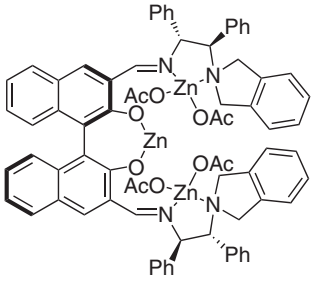

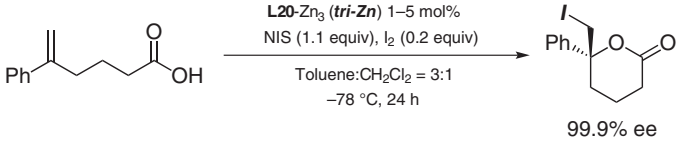

99.9% ee

Scheme 8.16 $Zn_3(OAc)_4$-3,3′-bis(aminoimino)binaphthoxide complex (***tri-Zn***) catalyzed the asymmetric iodolactonization.

Compared to the well-examined halolactonaization, the intermolecular haloesterification was hard to be conducted. Although haloesterification using easily obtainable alkenes and carboxylic acids has a clear industrial advantage, the successful examples of catalytic asymmetric haloesterification are limited due to the difficulty of controlling the intermolecular reaction.

The first catalytic asymmetric iodoesterification of simple alkenes was achieved using the (*R*,*S*,*S*)-3,3′-bis(aminoimino)BINOL ligand (**L21**). The reaction of **L21** with zinc carboxylate formed a dinuclear zinc-(*R*,*S*,*S*)-3,3′-bis(aminoimino)

binaphthoxide (***di-Zn***) complex. For iodoesterification using *p*-methoxybenzoic acid, the *N*-iodonaphthalenimide (NIN)-I_2 system was effective for producing iodoesters in a highly enantioselective manner (Scheme 8.17) [36].

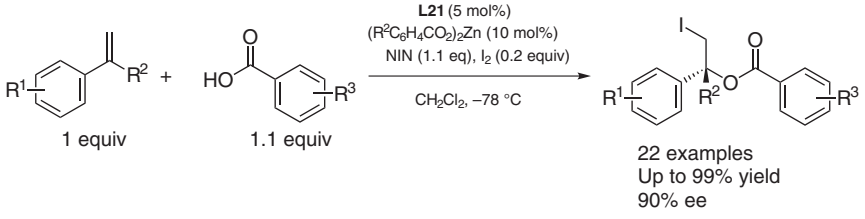

Scheme 8.17 Dinuclear zinc-(*R*,*S*,*S*)-3,3′-bis(aminoimino)binaphthoxide (***di-Zn***) catalyzed the asymmetric iodoesterification.

Recently, a similar catalyst system was applied to the intermolecular iodoetherification. Although the previously reported ***tri-Zn*** and ***di-Zn*** were resulted in poor asymmetric induction in the iodoetherification, further optimization of the catalyst structure achieved the development of a new **tri-Zn II** for highly enantioselective iodoetherification of the simple alkenes with *o*-nitrophenols (Scheme 8.18). The DFT calculation reveals that on the **tri-Zn II** catalyst, zinc-phenoxide formation, chelation of the *o*-nitro functionality, halogen-bonding between NIP and I_2, hydrogen-bonding, and π–π-stacking were merged for accomplishing the intermolecular catalytic asymmetric iodoetherification [37].

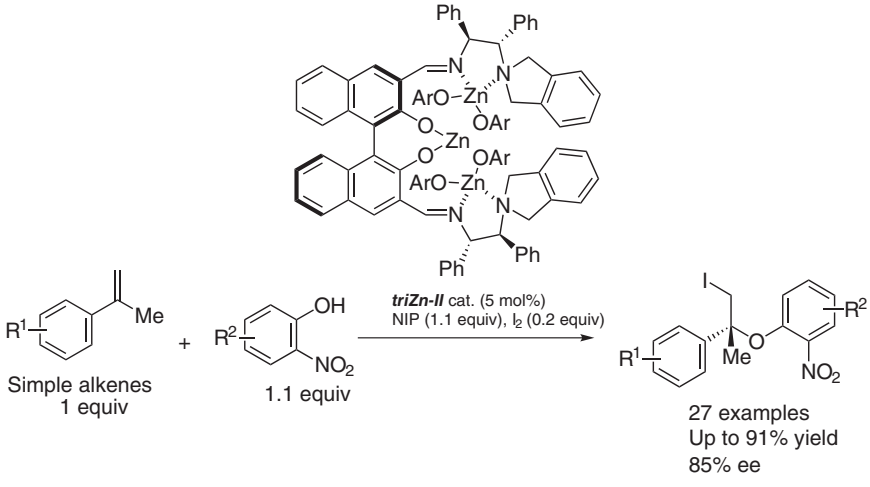

Scheme 8.18 $Zn_3(OAc)_4$-3,3′-bis(aminoimino)binaphthoxide complex (***tri-Zn***) catalyzed the asymmetric iodoetherification.

8.8 Conclusions

In this chapter, epoch-making researches on the multinuclear zinc catalysts having axial chirality were surveyed. The introduction of substituents at the 3,3′-position of BINOL has been a trend for getting high catalytic activity and stereoselectivity. Advanced 3,3′-funactionalized BINOLs have also been developed for employing cooperative effects and for incorporating the plural zinc atoms. Not only zinc atoms, the highly ordered axially chiral ligand spheres are fascinating platforms for various metal elements (e.g. V [38], Cu [39], and Pd [40]). As learned the mechanism in the class II Zn^{2+}-dependent aldolases, the axially chiral 3,3′-funactionalized BINOLs have further potential to cleating next-generation catalysts for contributing sustainable and biofriendly catalyses.

References

1 Thankachana, A., Ashaa, P.S., Sindhua, K.S., and Anilkumara, G. (2015). An overview of Zn-catalyzed enantioselective aldol type C–C bond formation. *RSC Adv.* 5: 62179–62193.

2 Sakane, S., Maruoka, K., and Yamamoto, H. (1985). Asymmetric cyclization of unsaturated aldehydes catalyzed by a chiral Lewis acid. *Tetrahedron Lett.* 26: 5535–5538.

3 Corminboeuf, O. and Renaud, P. (2002). *N*-Alkoxyacrylamides as substrates for enantioselective Diels–Alder reactions. *Org. Lett.* 4: 1735–1738.

4 Bari, L.D., Guillarme, S., Hanan, J. et al. (2007). Application of zinc(II)–binol for the formal aza-Diels–Alder reaction of *N*-arylimines with Danishefsky's Diene: CD-based absolute stereochemistry determination, origin of asymmetric induction and mechanistic considerations. *Eur. J. Org. Chem.* 2007: 5771–5779.

5 Oguni, N., Omi, T., Yamamoto, Y., and Nakamura, A. (1983). Enantioselective addition of diethylzinc to arylaldehydes catalyzed by chiral cobalt(II) and palladium(II) complexes. *Chem. Lett.* 12: 841–842.

6 Oguni, N. and Omi, T. (1984). Enantioselective addition of diethylzinc to benzaldehyde catalyzed by a small amount of chiral 2-amino-1-alcohols. *Tetrahedron Lett.* 25: 2823–2824.

7 Masato, K., Suga, S., Kawai, K., and Noyori, R. (1986). Catalytic asymmetric induction. Highly enantioselective addition of dialkylzincs to aldehydes. *J. Am. Chem. Soc.* 108: 6071–6607.

8 Rosini, C., Franzini, L., Pini, D., and Salvadori, P. (1990). Enantioselective alkylation of prochiral aldehydes by diethylzinc promoted by (*S*,*S*)-1,2-diphenylethan-1,2-diol. *Tetrahedron Asymmetry* 1: 587–588.

9 Prasad, K.R.K. and Joshi, N.N. (1996). C_2-Symmetric chiral zinc alkoxides as catalysts for the enantioselective addition of diethylzinc to aryl aldehydes. *Tetrahedron Asymmetry* 7: 1957–1960.

10 Kitajima, H., Ito, K., Aoki, Y., and Katsuki, T. (1997). *N*,*N*,*N*′,*N*′-Tetraalkyl-2,2′-dihydroxy-1,1′-binaphthyl-3,3′-dicarboxamides: novel chiral

auxiliaries for asymmetric Simmons–Smith cyclopropanation of allylic alcohols and for asymmetric diethylzinc addition to aldehydes. *Bull. Chem. Soc. Jpn.* 70: 207–217.

11 Hu, Q.-S., Huang, W.-S., Vitharana, D. et al. (1997). Functionalized Major-Groove and Minor-Groove chiral polybinaphthyls: application in the asymmetric reaction of aldehydes with diethylzinc. *J. Am. Chem. Soc.* 119: 12454–12464.

12 Mikami, K., Terada, M., Korenaga, T. et al. (2000). Asymmetric activation. *Angew. Chem. Int. Ed.* 39: 3515–3710.

13 Ding, K., Ishii, A., and Mikami, K. (1999). Super high throughput screening (SHTS) of chiral ligands and activators: asymmetric activation of chiral diol-zinc catalysts by chiral nitrogen activators for the enantioselective addition of diethylzinc to aldehydes. *Angew. Chem. Int. Ed.* 38: 497–501.

14 Balsells, J., Davis, T.J., Carroll, P., and Walsh, P.J. (2002). Insight into the mechanism of the asymmetric addition of alkyl groups to aldehydes catalyzed by titanium-BINOLate species. *J. Am. Chem. Soc.* 124: 10336–10348.

15 Hatano, M., Miyamoto, T., and Ishihara, K. (2006). 3,3′-Diphosphoryl-1,1¢-bi-2-naphthol-Zn(II) complexes as conjugate acid-base catalysts for enantioselective dialkylzinc addition to aldehydes. *J. Org. Chem.* 71: 6474–6484.

16 Blay, G., Cardona, L., Climent, E., and Pedro, J. (2008). Highly enantioselective zinc/binol-catalyzed alkynylation of *N*-sulfonyl aldimines. *Angew. Chem. Int. Ed.* 47: 5593–5596.

17 Du, H., Long, J., Hu, J. et al. (2002). 3,3′-Br_2-BINOL-Zn complex: a highly efficient catalyst for the enantioselective hetero-Diels–Alder. *Org. Lett.* 4: 4349–4352.

18 Eschenbrenner-Lux, V., Küchler, P., Ziegler, S. et al. (2014). An enantioselective inverse-electron-demand imino Diels–Alder reaction. *Angew. Chem. Int. Ed.* 53: 2134–2137.

19 Bougauchi, M., Watanabe, S., Arai, T. et al. (1997). Catalytic asymmetric epoxidation of α,β-unsaturated ketones promoted by lanthanoid complexes. *J. Am. Chem. Soc.* 119: 2329–2330.

20 Nemoto, T., Ohshima, T., Yamaguchi, K., and Shibasaki, M. (2001). Catalytic asymmetric epoxidation of enones using La−BINOL−triphenylarsine oxide complex: structural determination of the asymmetric catalyst. *J. Am. Chem. Soc.* 123: 2725–2732.

21 Yu, H.-B., Zheng, X.-F., Lin, Z.-M. et al. (1999). Asymmetric epoxidation of α,β-unsaturated ketones catalyzed by chiral polybinaphthyl zinc complexes: greatly enhanced enantioselectivity by a cooperation of the catalytic sites in a polymer chain. *J. Org. Chem.* 64: 8149–8155.

22 Minatti, A. and Dötz, K.H. (2006). Enantioselective epoxidation of α,β-Enones by electrophilic activation with a BINOL–zinc catalyst. *Eur. J. Org. Chem.* 268–276.

23 Shibasaki, M., Sasai, H., and Arai, T. (1997). Asymmetric catalysis with heterobimetallic compounds. *Angew. Chem. Int. Ed.* 36: 1236–1256.

24 Yamada, Y.M.A., Yoshikawa, N., Sasai, H., and Shibasaki, M. (1997). Direct catalytic asymmetric aldol reactions of aldehydes with unmodified ketones. *Angew. Chem. Int. Ed.* 36: 1871–1873.

25 Yamada, Y.M.A. and Shibasaki, M. (1998). Direct catalytic asymmetric aldol reactions promoted by a novel barium complex. *Tetrahedron Lett.* 39: 5561–5564.

26 Yoshikawa, N., Yamada, Y.M.A., Das, J. et al. (1999). Direct catalytic asymmetric aldol reaction. *J. Am. Chem. Soc.* 121: 4168–4278.

27 Yamaguchi, A., Matsunaga, S., and Shibasaki, M. (2009). Catalytic asymmetric synthesis of α-alkylidene-β-hydroxy esters via dynamic kinetic asymmetric transformation involving Ba-catalyzed direct aldol reaction. *J. Am. Chem. Soc.* 131: 10842–10843.

28 Trost, B.M. and Ito, H. (2000). A direct catalytic enantioselective aldol reaction via a novel catalyst design. *J. Am. Chem. Soc.* 122: 12003–12004.

29 Trost, B.M., Hung, C.-I., and Mata, G. (2020). Dinuclear metal-ProPhenol catalysts: development and synthetic applications. *Angew. Chem. Int. Ed.* 59: 4240–4261.

30 Li, H., Da, C.-S., Xiao, Y.-H. et al. (2008). Direct asymmetric aldol reaction of aryl ketones with aryl aldehydes catalyzed by chiral BINOL-derived zincate catalyst. *J. Org. Chem.* 73: 7398–7401.

31 Fessner, W.-D., Schneider, A., Held, D.-C.H. et al. (1996). The mechanism of Class II, metal-dependent aldolases. *Angew. Chem. Int. Ed.* 35: 2219–2221.

32 Trost, B.M., Ito, H., and Silcoff, E.R. (2001). Asymmetric aldol reaction via a dinuclear zinc catalyst: α-hydroxyketones as donors. *J. Am. Chem. Soc.* 123: 3367–3368.

33 Kumagai, N., Matsunaga, S., Kinoshita, T. et al. (2003). Direct catalytic asymmetric aldol reaction of hydroxyketones: asymmetric Zn catalysis with a Et_2Zn/linked-BINOL complex. *J. Am. Chem. Soc.* 125: 2169–2178.

34 Arai, T., Sugiyama, N., Masu, H. et al. (2014). Trinuclear $Zn_3(OAc)_4$-3,3′-bis(aminoimino)binaphthoxide complex for highly efficient catalytic asymmetric iodolactonization. *Chem. Commun.* 42: 8287–8290.

35 Arai, T., Horigane, K., Watanabe, O. et al. (2019). Association of halogen bonding and hydrogen bonding in metal acetate-catalyzed asymmetric halolactonization. *iScience* 280–292.

36 Arai, T., Horigane, K., Suzuki, T.K. et al. (2020). Catalytic asymmetric iodoesterification of simple alkenes. *Angew. Chem. Int. Ed.* 59: 12680–12683.

37 Suzuki, T.K., Yamanaka, M., and Arai, T. (2022). Intermolecular catalytic asymmetric iodoetherification of unfunctionalized alkenes. *Org. Lett.* 24: 3872–3877.

38 Kumar, A., Sasai, H., and Takizawa, S. (2022). Atroposelective synthesis of C–C axially chiral compounds via mono- and dinuclear vanadium catalysis. *Acc. Chem. Res.* 55: 2949–2965.

39 Cen, S., Huang, N., Lian, D. et al. (2022). Conformational enantiodiscrimination for asymmetric construction of atropisomers. *Nat. Commun.* 13: 4735.

40 Arai, T., Sato, K., Nakamura, A. et al. (2018). Dinuclear phosphoiminoBINOL-Pd container for malononitrile: catalytic asymmetric double Mannich reaction for chiral 1,3-diamine synthesis. *Sci. Rep.* 8: 837.

9

Binaphthyl-Based Chiral DMAP Derivatives in Enantioselective Transformations

Hiroki Mandai[1] *and Seiji Suga*[2]

[1] *Gifu University of Medical Science, Faculty of Pharmacy, Department of Pharmacy, 4-3-3 Nijigaoka, Kani, Gifu 509-0293, Japan*
[2] *Okayama University, Faculty of Environmental, Natural Science and Technology, 3-1-1 Tsushima-naka, Kita-ku, Okayama 700-8530, Japan*

9.1 Introduction

Atropisomerism of the binaphthyl moiety has been widely used as a chiral source in organocatalysts, such as chiral phase transfer catalysts [1–3], chiral Brønsted acid catalysts [4–9], and chiral Brønsted base catalysts (Figure 9.1) [10, 11].

Some advantages of using the atropisomerism of the 1,1′-binaphthyl moiety include the following: (i) both enantiomers of the 1,1′-binaphthyl moiety are readily obtained from (*S*)- or (*R*)-(−)-1,1′-bi-2-naphthol [12] (BINOL), which is available commercially. (ii) The atropisomerism of the 1,1′-binaphthyl is relatively stable and does not racemize under most reaction conditions. (iii) 1,1′-Binaphthyl moiety can be tuned electronically and sterically by introducing various substituents at the 3,3′ or 7,7′ positions (Figure 9.2). (iv) The solubility of the catalyst can also be enhanced by introducing lipophilic substituents. (v) An easily accessible C_2-symmetric catalyst decreases the potential number of possible competing transition states (compared to C_1-symmetric catalyst) and simplifies the understanding of the reaction mechanism. Despite these advantages, the 1,1′-binaphthyl moiety has rarely been applied to nucleophilic catalysis, including acylation of alcohol.

N,*N*-4-Dimethyl-4-aminopyridine (DMAP) has been used as a powerful nucleophilic catalyst in organic synthesis for acylation of alcohols. In 1967, Litvinenko and Kirichenko reported that DMAP dramatically increased the rate of benzoylation of aniline compared to triethylamine or pyridine [13]. Soon after, Steglich and Höfle established the general protocol for the acylation of alcohols with a catalytic amount of DMAP in the presence of an auxiliary base [14]. The generally accepted mechanism of alcohol acylation, based on both experimental and computational results, is shown in Scheme 9.1 [15–18]. The DMAP rapidly reacts with the acylating reagent

Atropisomerism in Asymmetric Organic Synthesis: Challenges and Applications, First Edition.
Edited by Shinobu Takizawa and Mohamed S. H. Salem.

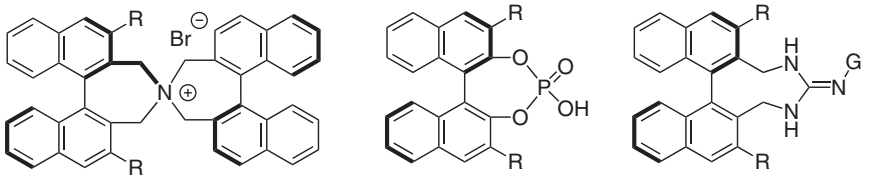

Figure 9.1 Selected examples of organocatalysts with binaphthyl moiety.

i (e.g. acetic anhydride**)** to form *N*-acyl pyridinium salt **ii**. This salt then reacts with the alcohol (R^2OH) via transition state **iii**, facilitated by deprotonation by the counter anion ($^-OOCR^1$), resulting in the formation of ester **iv** and pyridinium salt **v**. The pyridinium salt **v** is subsequently neutralized by base B: (e.g. Et_3N) to regenerate DMAP.

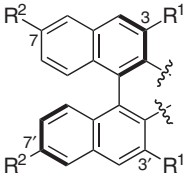

Figure 9.2 Substituted 1,1′-binaphthyl moiety.

Selected enantiomerically pure variants of DMAPs or their related scaffolds [19] are listed in Figure 9.3. These catalysts fall into several categories based on the origin of chirality. For example, catalysts having stereogenic carbon(s) [20–25],

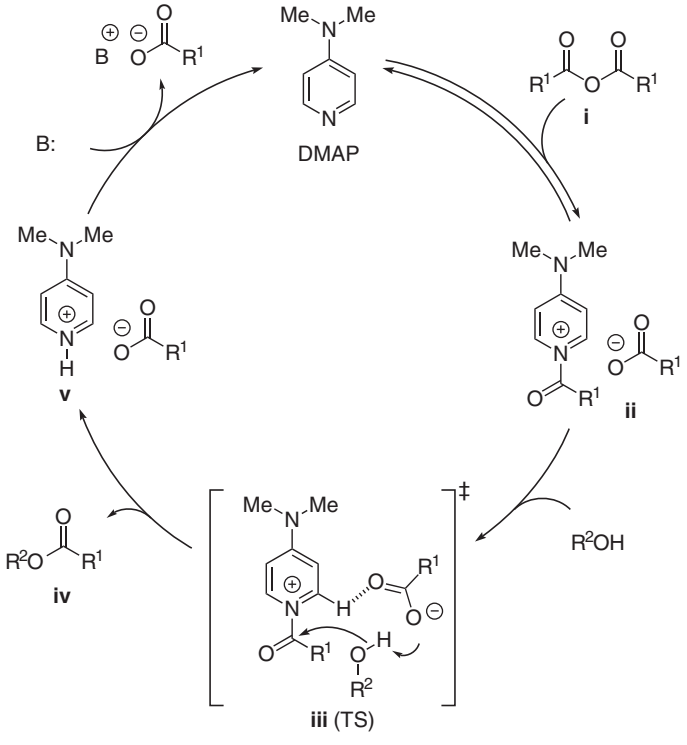

Scheme 9.1 A plausible mechanism for DMAP-catalyzed acylation of alcohols using acid anhydride.

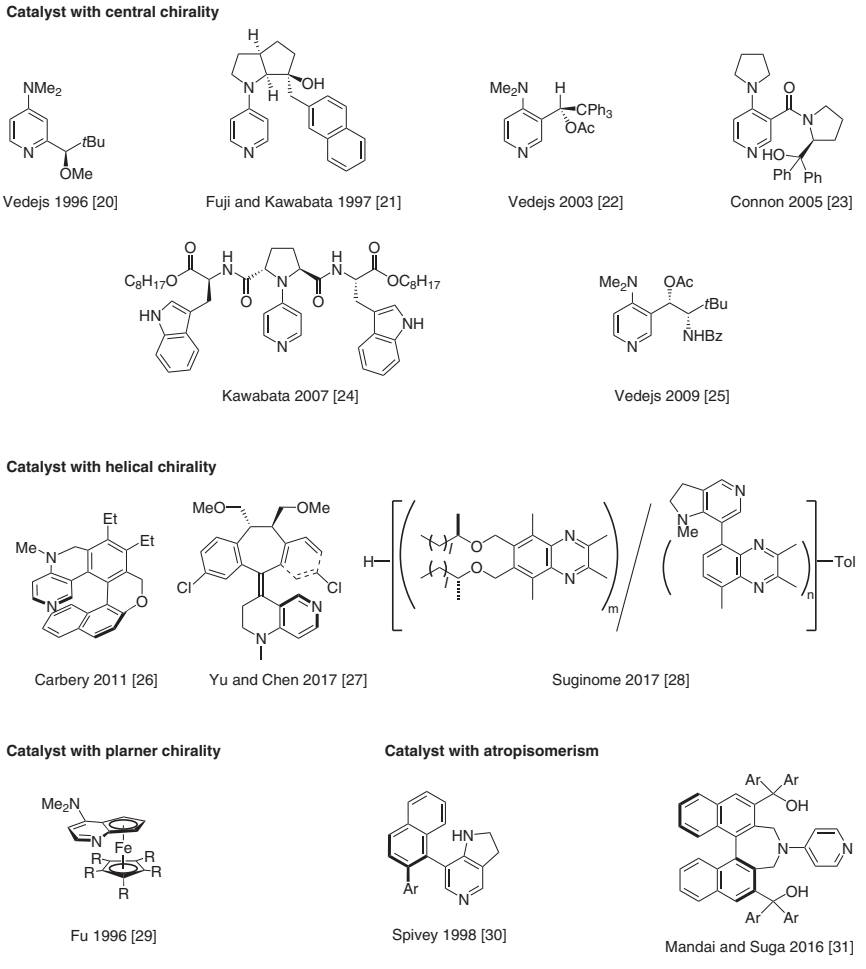

Figure 9.3 Selected examples of chiral DMAPs and related compounds.

helical chirality [26–28], planar chirality [29, 30], and atropisomerism [31, 32]. Such catalysts have been successfully applied to various nonenzymatic approaches [33] for the enantioselective acyl transfer reactions [e.g. the kinetic resolution [34–37], dynamic kinetic resolution (DKR) [38], desymmetrization [37, 39–42], rearrangements [43], and opening *meso* anhydride [44] and regioselective acylations of carbohydrates [45, 46].

This chapter will mainly focus on binaphthyl-based chiral DMAPs in inter- or intramolecular acyl transfer reactions. Furthermore, concepts related to catalyst design and mechanistic insights including hydrogen bonding [47, 48] will also be discussed for a better understanding of the mechanism. We believe that the insights (e.g. reaction mechanism and/or mode of enantiodiscrimination) from binaphthyl-based chiral DMAP derivatives could offer helpful information for the future development of novel binaphthyl-based catalysts.

9.2 Binaphthyl-Based Chiral DMAP Derivatives

9.2.1 Catalyst Design

In 2016, Mandai and Suga reported a new class of chiral DMAP derivatives with atropisomerism of the binaphthyl moiety [32]. The catalyst structure allows rapid access to a range of optically active DMAP derivatives and exploits the positive, noncovalent interaction between catalyst and substrate for reaction acceleration (Figure 9.4).

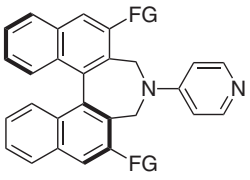

1

Figure 9.4 Binaphthyl-based chiral DMAP derivatives (FG = polar functional group).

This catalyst design would have some advantages: [1] both enantiomers of optically active BINOL, the starting material for catalyst synthesis, are readily available and do not require optical resolution during catalyst synthesis, even if they carry various polar functional groups (FGs) on the binaphthyl moiety. Therefore, [2] gram-scale synthesis of catalysts might be possible without complicated operations, and [3] various substituents (FG) can be installed on the binaphthyl unit. [4] The chiral environment at C4 of pyridine might not decrease its catalytic activity. Furthermore, [5] the FG might serve as a positive effect on the fixation of the transition state (Figure 9.5). For example, if the counter anion of the *N*-acyl pyridinium ion intermediate serves as the nucleophile (Nu^-) (**design option 1**), the interaction between FG and the counter anion (Nu^-) forms a rigid transition state and some reaction acceleration and high enantioselectivity can be expected. On the other hand, if the nucleophile is effectively activated by FG (**design option 2**), reaction acceleration and high enantioselectivity can also be expected. Such universal catalyst designs (**design options 1 and 2**) could cover different types of reactions.

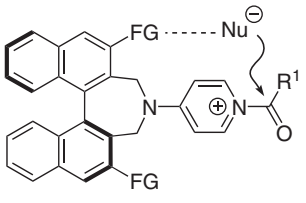

Design option 1
Counteranion = Nu^-

Possible application: Steglich-type reactions

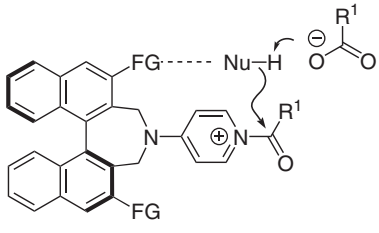

Design option 2
Counteranion = $R^1CO_2^-$

Possible application: alcohol acylation

Figure 9.5 Two possible modes of activations by FG of binaphthyl-based chiral DMAP derivatives.

9.2.2 Catalyst Synthesis

The synthesis of optically active DMAPs **1j** from (*S*)-BINOL is summarized in Scheme 9.2. MOM-protected compound **2** prepared from (*S*)-BINOL in 98% yield was subjected to *O*-lithiation, and installation of ester group at 3,3′-position, followed by deprotection of MOM group to give **3** in 98% yield in two steps. Then, Migita–Kosugi–Stille cross-coupling of compound **4**, obtained from triflation of **3** in 98% yield, afforded compound **5** in 83% yield. Putala reported that Migita–Kosugi–Stille cross-coupling of a simple BINOL (an unsubstituted 3,3′-position) with tetramethyl tin resulted in no reaction [49]. However, the reaction of compound **4** with two ester groups at 3,3′-position proceeded smoothly to give **5** without racemization. Thus obtained **5** was subjected to bromination to give **6** in 97% yield, followed by formation of cyclic amine **7** and deprotection of allyl group gave cyclic free amine **8** in 95% yield. The installation of the pyridine ring was achieved by the Buchwald–Hartwig cross-coupling of amine **8** with 4-bromopyridine to give the key intermediate **9**. Finally, the reaction of ester **9** with aryl lithium

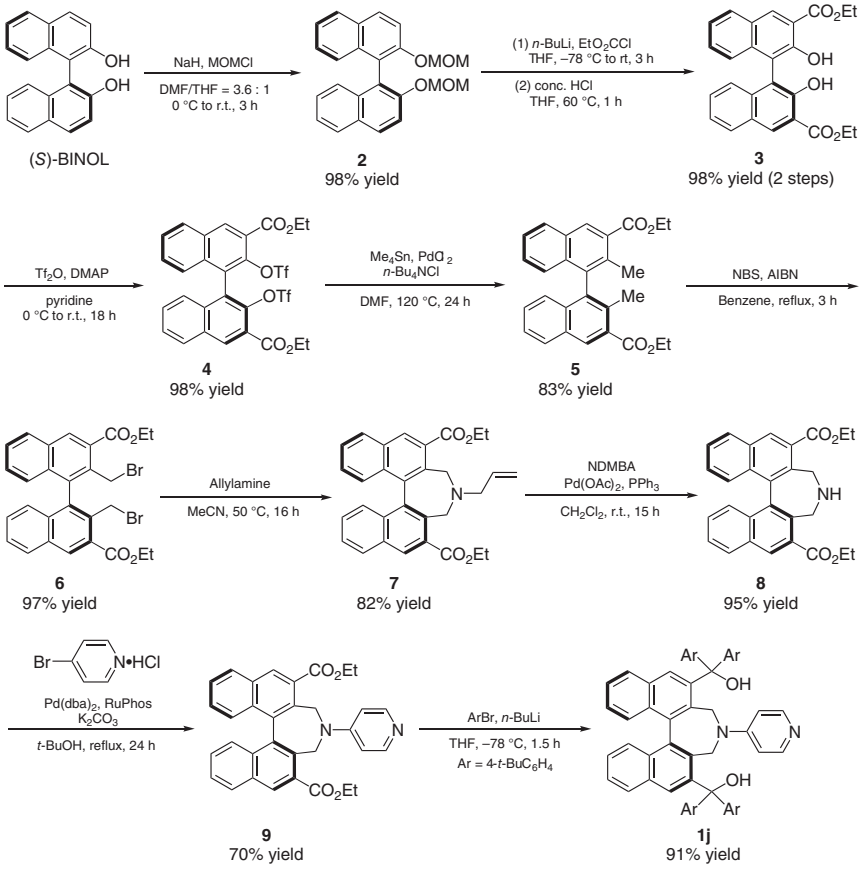

Scheme 9.2 Synthetic route to binaphthyl-based chiral nucleophilic catalyst.

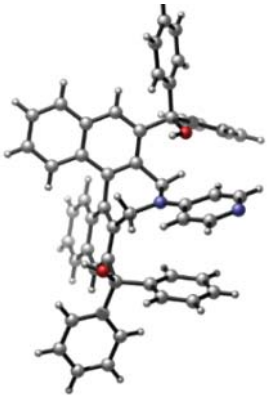

Figure 9.6 X-ray structure of chiral DMAP derivative **1g** (Ar = Ph).

(ArLi prepared *in situ* from ArBr and *n*-BuLi) afforded an optically active DMAP derivative **1j** with tertiary alcohol at the 3,3′ position of the binaphthyl moiety. Although the synthesis of this catalyst requires 10 steps from (*S*)-BINOL in 38% total yield (average yield of each step >90%), time-consuming purification steps could be omitted and only four times of column chromatographic purifications were required. Furthermore, the advantage of this synthetic route is that key intermediate **9** can lead to optically active DMAP derivatives with various structures at the 3,3′ position in the final step (e.g. **9** to **1j**). Accordingly, key intermediate **9** can be used as a starting point to lead a series of binaphthyl-based DMAPs (FG = *tert*-alcohols, esters, amides, etc.).

Single crystal X-ray structure analysis of catalyst **1g** (Ar = Ph) shows that the tertiary alcohol moiety at the 3,3′ position is located toward the pyridine ring and substituents (Ph) protrude above and below the pyridine ring, suggesting that a suitable chiral environment has been established (Figure 9.6).

9.3 Intramolecular Acyl Transfer Reactions

9.3.1 *O*- to *C*-Acyl Transfer Reaction

To confirm the above working hypothesis (**design option 1**, Figure 9.5), a new type of catalyst was tested in the *O*- to *C*-acyl transfer reaction because the reaction mechanism of this reaction has been partially elucidated [50–52]. In this reaction, the catalyst and substrate form an *N*-acyl pyridinium ion, and its counter anion acts as a nucleophile (Nu^-). Thus, the *O*- to *C*-acyl transfer reaction would be an ideal reaction to evaluate the capability of the binaphthyl-based catalyst.

First, Mandai and Suga group investigated the importance of catalyst structure (C_1- or C_2-symmetric) and its substituent(s) at the 3,3′-position of catalyst for *O*- to *C*-acyl transfer reaction [32]. The transformation of **10a** to **11a** was carried out in THF (0.1 M) at 0 °C using catalysts **1a**–**p** (5 mol%) for 12 hours (Scheme 9.3).

The use of C_2-symmetric catalysts **1a**–**f** (e.g. methoxy, aryl, ester, or amide) gave product but generated low or nearly racemic products [up to 99% Conv. and up to 72 : 28 enantiomeric ratio (er)]. The surprising breakthrough was observed with catalysts **1g**–**m** containing tertiary alcohols led to the formation of the all-carbon quaternary stereogenic center with high enantioselectivity. On the other hand, the C_1-symmetric catalyst (**1n**, **1o**, or **1p**) was significantly less efficient, affording a racemic mixture of products. Two *tert*-alcohol units (**1j** vs **1p**) are essential for efficient enantiofacial discrimination. After optimizing the reaction conditions, the authors finally found that the reactions proceeded smoothly with only 0.5 mol%

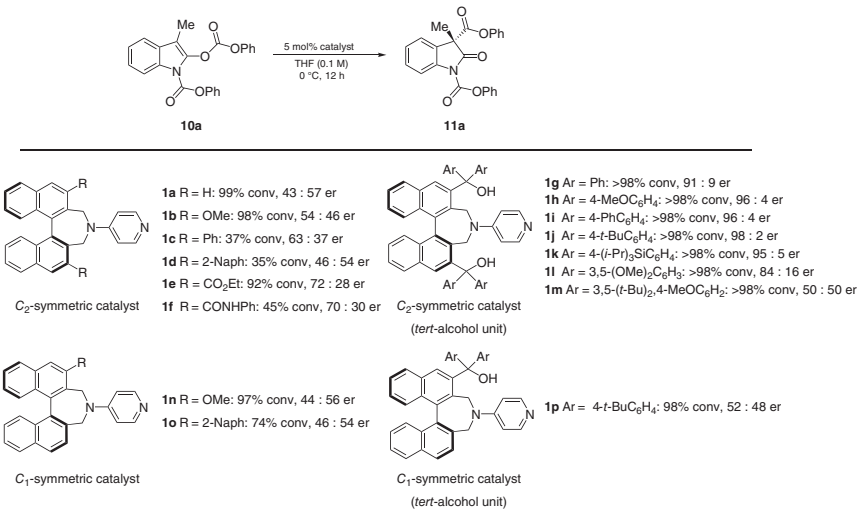

Scheme 9.3 Screening of various catalyst candidates.

of a catalyst having a *tert*-alcohol unit at 3,3′ position in THF for five hours, and the system could be applied to various substrates with substituents (alkyl, allyl, propargyl, aryl, heteroatom-, and bromo-containing, etc.) without decreasing the enantioselectivity (Scheme 9.4). In some cases, substrates **10c**, **10j**, and **10k** with a sterically bulky group required a 3 mol% catalyst and a higher reaction temperature, but the desired products were still obtained with good enantioselectivity. According to the results obtained with substrate **10m**, the *N*-methyl moiety was not as good as the *N*-acyl moiety for achieving high enantioselectivity (87 : 13 er).

To further elucidate the effects of tertiary alcohol moiety of the catalyst, the correlation between the 3,3′ position of the catalyst and catalytic activity and/or enantioselectivity was investigated (Scheme 9.5). The catalyst with tertiary alcohol moieties, an optimal catalyst, was the most effective in accelerating the reaction ($k_{\mathbf{1j}} = 1.22$ h). It was 47 times more active than the methyl-protected catalyst **1j′** (no alcohol moiety), and 16 times more active than DMAP. Furthermore, the enantioselectivity of the product was 98 : 2 er for catalyst **1j**, while the enantioselectivity was 66 : 34 er for catalyst **1j′**, in which the hydroxy group was protected by a methyl group.

Density functional theory (DFT) calculations were performed at the B3LYP/6-31G(d) level of theory with substrate **10a** and catalyst **1g**, which serves as a simplified of **1j** (Figure 9.7). The lowest energy transition state **I**, consistent with experimental findings and leading to the major enantiomer, suggests hydrogen bonding between the enolate oxygen of the ion pair and the hydroxy unit of the catalyst. This is likely due to the conformational rigidity imposed by the presence of two aryl units on the same carbon, which ensures the correct orientation of the hydroxyl unit for interaction with the negatively charged oxygen. Additionally, there is an electrostatic attraction [53, 54] between the enolate and an *ortho*-hydrogen of one of the aryl units at the C3 site of the chiral catalyst. The second lowest energy transition state, labeled **II** in the DFT calculations, exhibits similar electrostatic

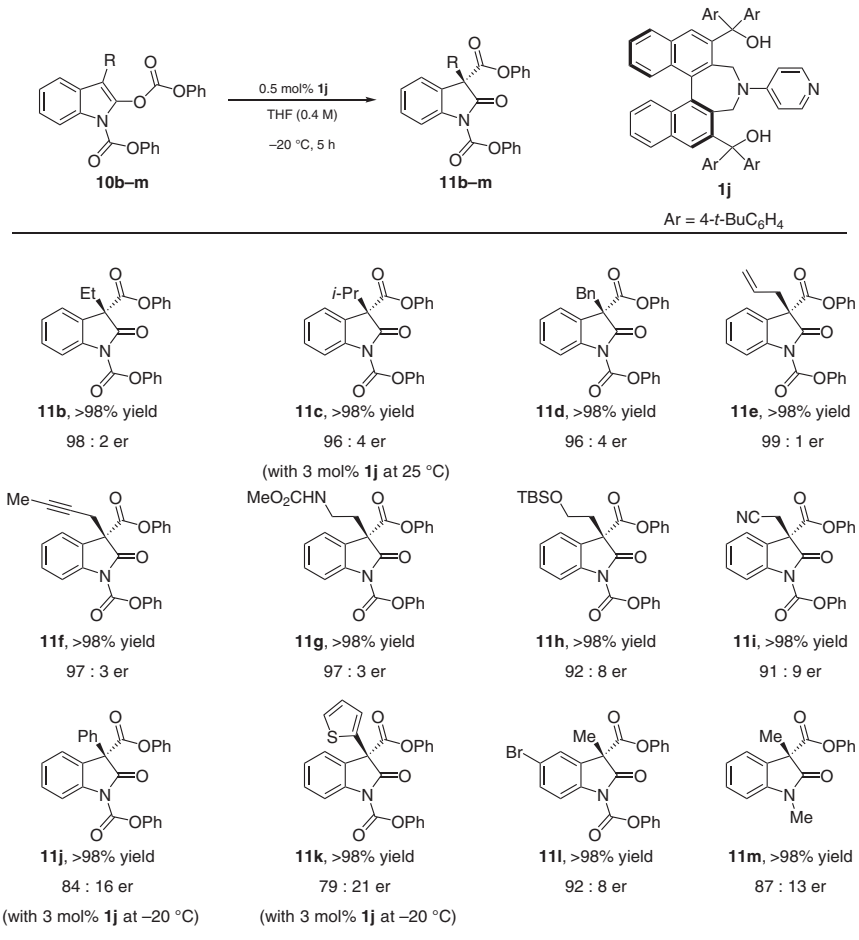

Scheme 9.4 The reaction of various substrates bearing different substituents.

attractions but faces substantial steric repulsion between the binaphthyl moiety of the catalyst and the phenoxy unit of the substrate. Both experimental and computational results emphasize the key role of the tertiary alcohol moieties of the catalyst in accelerating the reaction rate and achieving high enantioselectivity.

In 2019, the Mandai and Suga group also reported a similar type of transformation using furanyl carbonates (Scheme 9.6) [55]. They efficiently obtained various optically active 3,3′-disubstituted benzofuranone derivatives (15 examples achieving >98% yield and up to >99 : 1 er), which are valuable intermediates for synthesizing various pharmaceuticals and natural products.

Surprisingly, extremely low amounts of catalyst (0.05 mol% [500 ppm]) are sufficient to promote the reaction with substrates **12a**, **12g**, **12i**, **12l**, and **12n**. The highest turnover frequency (TOF) (3640 h^{-1}) still maintains high enantioselectivity. Control experiments and computational calculations also showed that the presence

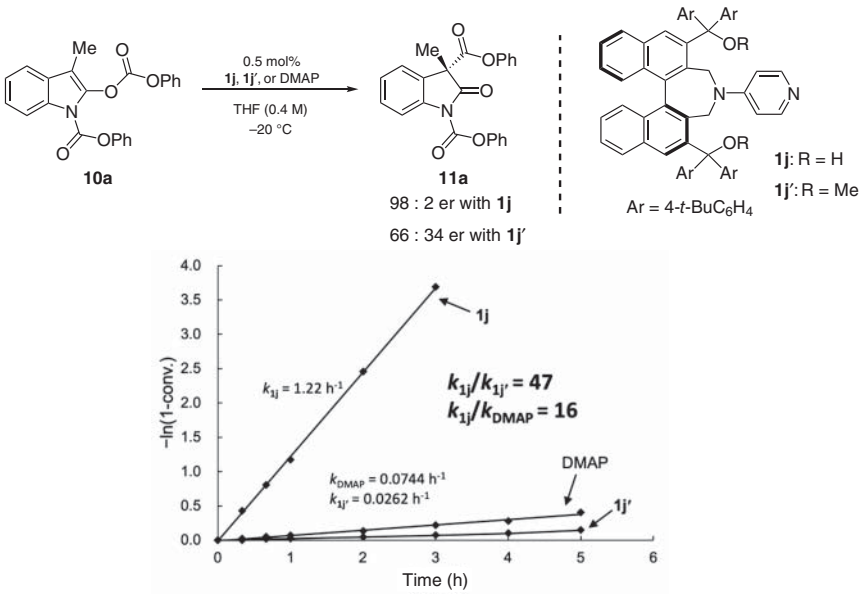

Scheme 9.5 Kinetic studies with catalyst **1j**, **1j′,** and DMAP.

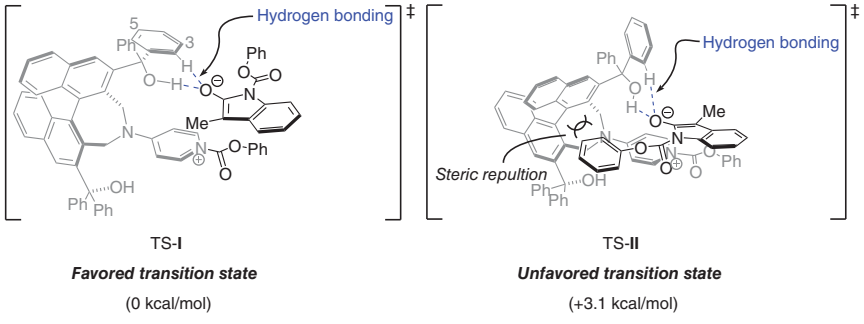

Figure 9.7 DFT calculations for two transition states.

of hydrogen bonding between a catalyst and a substrate is crucial for achieving both high catalytic activity and excellent enantioselectivity.

In addition, a more challenging regioselective migration reaction of furanyl carbonate **14** was demonstrated, which can give two products, α isomer **15** and γ isomer **16**. As shown in Scheme 9.7, the C_2-symmetric catalyst with two alcohol units only gave the product with high γ-selectivity and high enantioselectivity (α : γ = 10 : 90, 95 : 5 er). Under identical conditions except for the catalyst and its loading, the use of the catalyst without two *tert*-alcohol units (1 mol%) resulted in no reaction, and achiral DMAP (5 mol%) gave almost trace amounts of products and mainly formed α isomer (α : γ = 66 : 34). The reasons for these observations were unclear, but it indicated again that the *tert*-alcohol unit of the catalyst demonstrated a significant role for achieving high γ selectivity and high enantioselectivity.

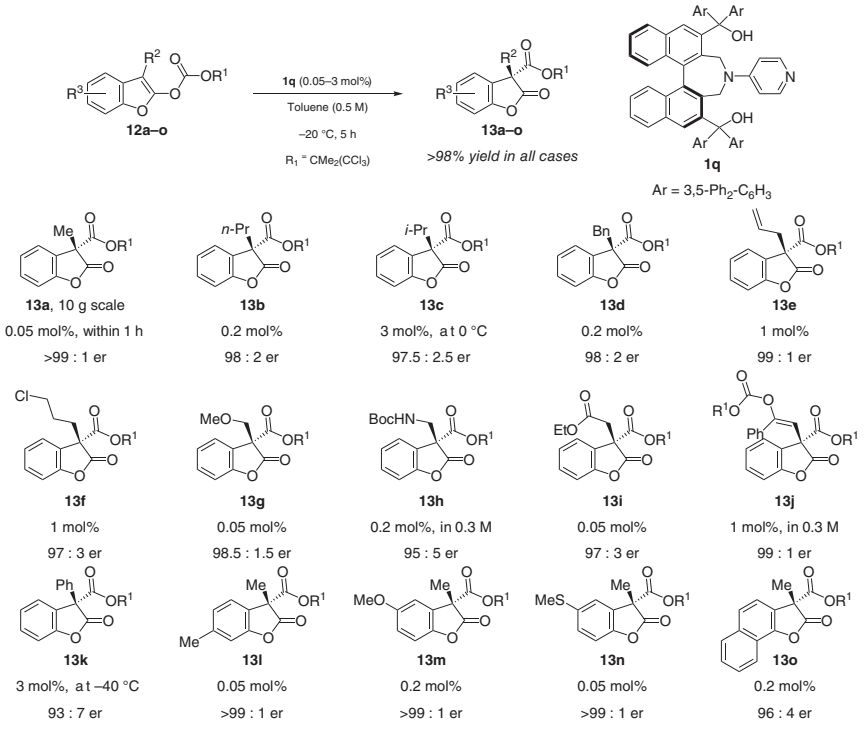

Scheme 9.6 Enantioselective acyl migration reactions of furanyl carbonates.

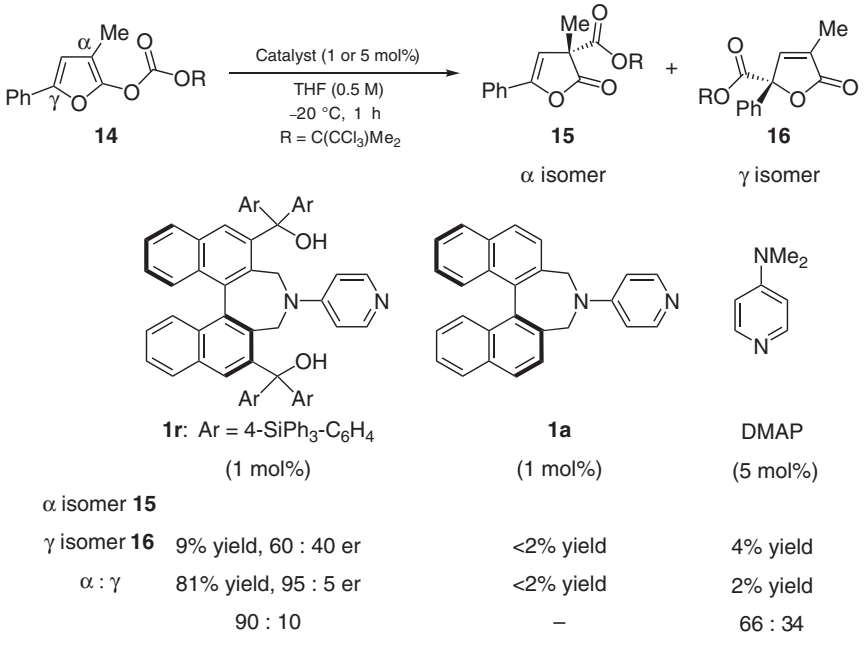

Scheme 9.7 Rearrangement of furanyl carbonate.

In this section, binaphthyl-based chiral DMAP derivatives were efficiently applied to two types of intermolecular acyl transfer reactions (**design option 1**, Figure 9.5), *O*- to *C*-acyl transfer reaction of oxindole and furanyl derivatives. Several control experiments and DFT calculations highlighted the key role of the polar FG at the 3,3′ position (*tert*-alcohol moiety) in achieving both high enantioselectivity and acceleration of the reaction rate due to noncovalent hydrogen bonding between catalyst and substrate.

9.4 Intermolecular Acyl Transfer Reactions

9.4.1 Kinetic Resolution of Alcohols

To evaluate the performance of binaphthyl-based DMAP catalysts in other types of reactions, such as intermolecular acylation reactions (**design option 2**, Figure 9.5), Mandai and Suga selected the kinetic resolution reaction of mono-ols, which is the benchmark reaction of catalyst evaluation. In general, catalyst efficiency is judged by the selectivity factor (s) [56]. When the catalyst shows $s > 20$, it indicates that the catalyst almost separates two enantiomers and $s > 50$ indicates the complete separation of two enantiomers.

After several attempts to find optimal conditions for kinetic resolution of mono-ol, they finally found the following conditions: 5 mol% catalyst **1j**, isobutyric anhydride as an acylating agent, and cesium carbonate as a base in toluene as solvent at −60 °C [57]. As the results shown in Scheme 9.8, the reaction with various benzylic alcohol derivatives gave moderate to excellent *s*.

While the exact mechanism of acceleration remains unclear, the authors hypothesize based on several experimental findings. These include observations of the leaving group effect on the acylating reagent (−Cl versus −OAc), the influence of hydrogen bonding on enantioselectivity (evaluated by solvent screening), the effects of base and kinetic studies, and the remarkably high enantioselectivities observed with isobutyric anhydride. Taking into account the findings of Spivey [58], Zipse [16], and Kawabata [59, 60], the transition state appears to favor the configuration shown in Figure 9.8. This configuration involves two hydrogen bonds formed between the carboxylate anion and both the hydroxy group of the catalyst and the *ortho*-hydrogen of the pyridine moiety.

Contrary to their initial assumption, the reaction with secondary alcohols (mono-ols) showed moderate to good reaction acceleration and enantioselectivity. The reason for this was thought to be the lack of proper intermolecular interaction between the catalyst with tertiary alcohol and the reaction substrate. Therefore, they decided to investigate the kinetic resolution of 1,2-diol [61–65] 1,2-diols, which have additional hydrogen bonding sites (donor and acceptor).

As expected, the reaction is applied to a wide range of *d,l*-1,2-diols as illustrated in Scheme 9.9 [66]. For example, monoacylation was selectively obtained with good reactivity and good *s*-value (s = 54–180) even with different hydrobenzoin derivatives **19a–j**. When cyclic diols **19k–o** with six- to eight-membered rings were used as

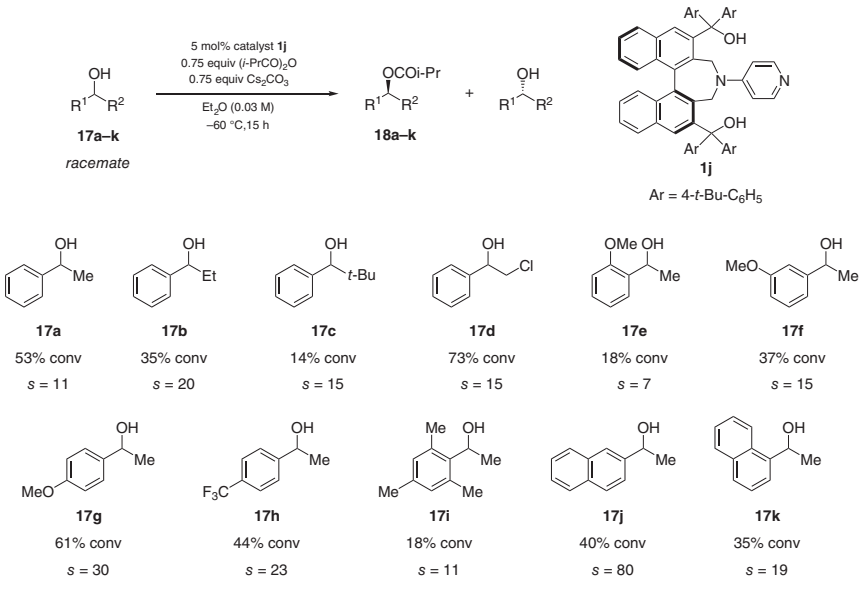

Scheme 9.8 Substrate scope in the kinetic resolution of mono-ols with catalyst **1j.**

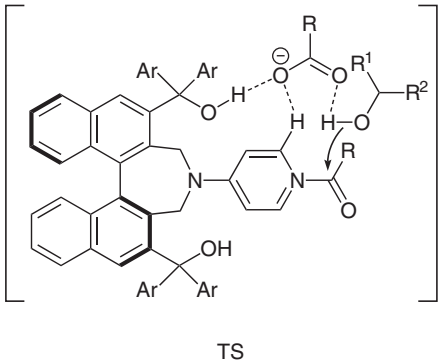

Figure 9.8 Possible transition states for kinetic resolution of mono-ol.

reaction substrates, good *s* values ($s = 20.1–146.1$) were obtained but diols **19p** and **19q** with a five-membered ring resulted in low *s* values. There is no good explanation for this observation, but it might be due to the rigidity of the conformation of the five-membered ring. Furthermore, the reaction of acyclic diols **19r**–**t** proceeded with good *s* values ($s = 9.7–36.3$) even with chain 1,2-diols containing alkyl, allyl, and vinyl groups. Alternatively, acyclic diols **19u** and **19v** with polar FGs (ester and ether) on their side chain resulted in poor *s* value ($s = 2.0–2.3$). Such a polar FG might hinder the hydrogen bonding formation between the catalyst and the substrate.

Next, the authors conducted further investigations into the impact of hydrogen bonding formation between the hydroxy groups of the catalyst and two hydroxy groups of the substrate. Their focus was on analyzing the substrate's structure and conducting kinetic resolution of various substrates (as depicted in Scheme 9.10). These trials demonstrated that achieving a high *s*-factor and conversion requires

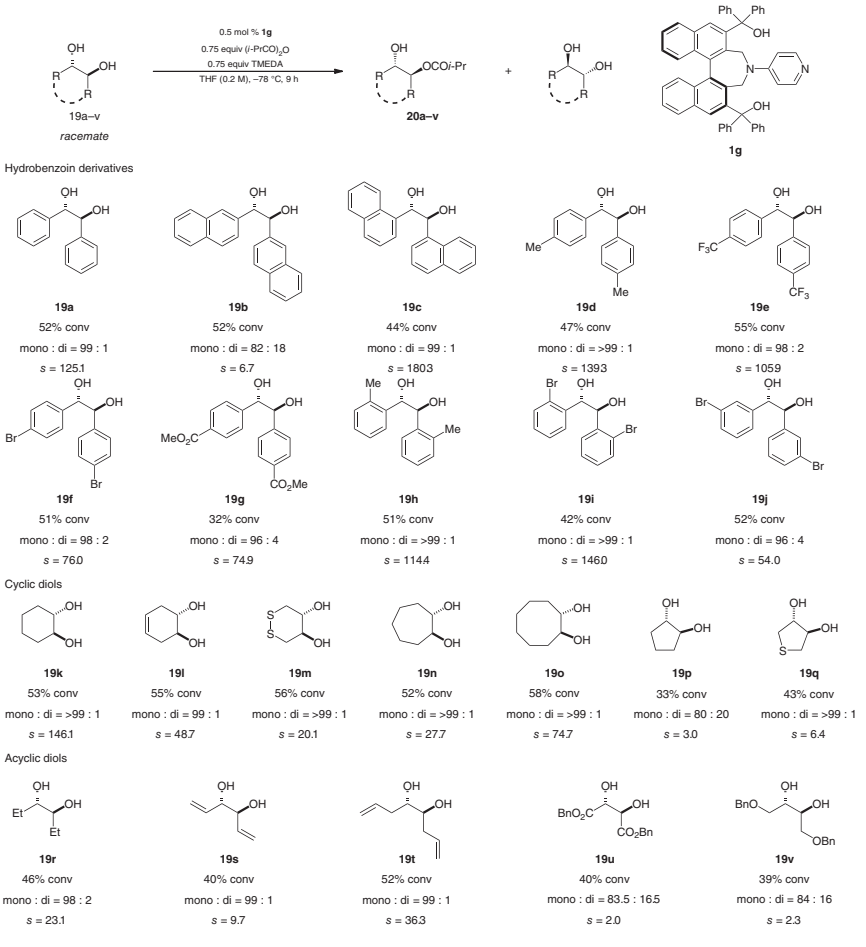

Scheme 9.9 Substrate scope in kinetic resolution of *d,l-1,2*-diols with catalyst **1g.**

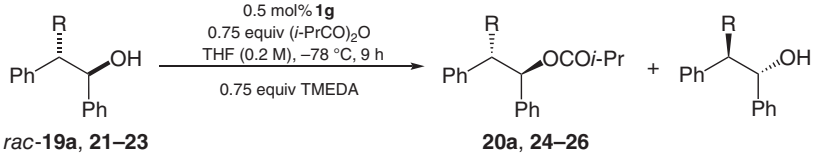

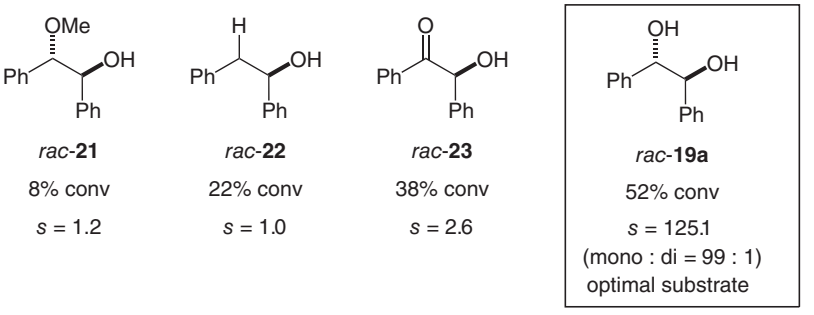

Scheme 9.10 Control experiment with various substrates.

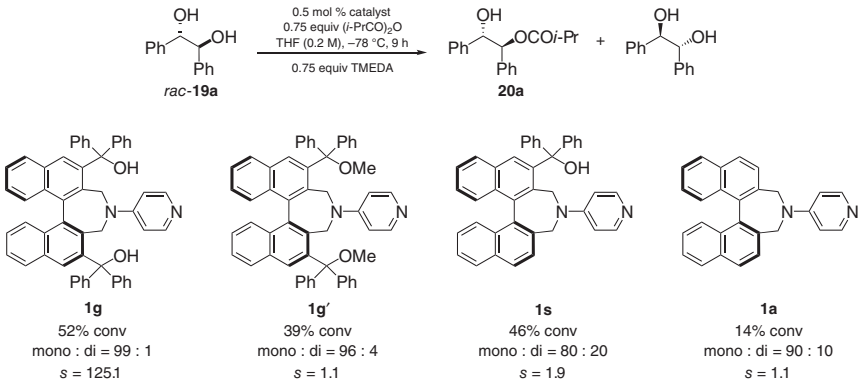

Scheme 9.11 Control experiment with various catalysts with/without *tert*-alcohol unit.

racemic substrates featuring two neighboring free hydroxy groups. For instance, employing racemic monomethyl-capped 1,2-diol **21**, benzyl phenyl carbinol **22**, and benzoin **23** as substrates resulted in relatively low *s*-factors (s = 1.0–2.6) and conversions (8–38% conv.) under optimal conditions. They pointed out that catalyst **1g** recognizes the presence of two adjacent hydroxy groups on the substrate (e.g. **19a**), which accelerates the reaction and enables discrimination between the substrate's two enantiomers.

The study investigated the catalyst structure (Scheme 9.11) by testing three catalyst analogs: the methyl ether analog **1g′**, the C_1-symmetric analog **1s**, and analog **1a** without *tert*-alcohol moiety, in comparison to the optimal catalyst **1g**, for the acylative kinetic resolution of **19a**. The use of catalyst **1g′** gave a rather low *s*-factor (s = 1.1 with **1g′** vs s = 125.1 with **1g**). Catalyst **1s** showed a low *s*-factor and a substantial diacylate formation (s = 1.9 with a mono : di ratio of 80 : 20). Surprisingly, catalyst **1a** exhibited the lowest catalytic activity and almost no enantioselectivity (s = 1.1). These findings suggest that the catalyst featuring two hydroxyl moieties is the most effective in the enantioselective monoacylation of the *d*,*l*-1,2-diol series.

After reviewing mechanistic insight from Spivey [58], Zipse [16], and Kawabata [59, 60], the authors hypothesized that there are several interconnected hydrogen bonding networks included in the transition states. These networks connect the *tert*-alcohol moiety of the catalyst, the carboxylate anion, the *ortho*-hydrogen of the pyridine moiety, and a hydroxy group of the substrate (Figure 9.9). In the favored transition state, the more acidic proton of one of the hydroxy groups through *intermolecular* hydrogen bonding is deprotonated by the carboxylate anion (*i*-PrCOO$^-$) and then reacts with *N*-acyl pyridinium salt to give **20a**. The unfavorable transition state involves steric repulsion between the phenyl group and the isopropyl group of the acylating agent (Figure 9.9). These transition states account for all the results observed in the control experiments at this stage. Previous studies by Miller (hydrogen bonding between the catalyst and a vicinal amino alcohol [67, 68] or carbinol [69]) and Seidel (hydrogen bonding between thiourea-DMAP system and a vicinal amine) [70] also clearly illustrated the impact of the hydrogen bonding network in the design of highly enantioselective acyl transfer reactions.

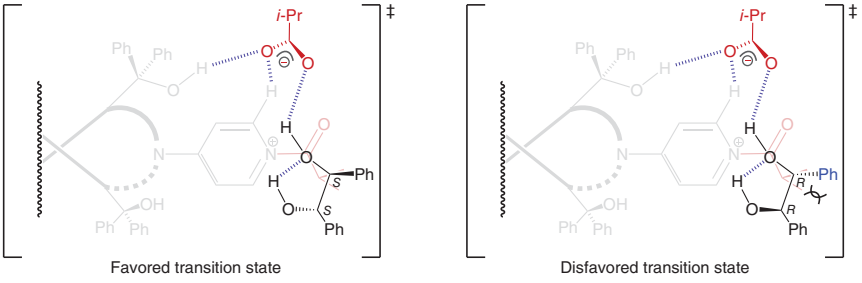

Figure 9.9 Possible transition states for kinetic resolution of *d*,*l*-1,2-diol.

The kinetic resolution of tertiary alcohols poses a significant challenge. Therefore, the new catalyst was used for the kinetic resolution of tertiary alcohols **27a**–**n** (Scheme 9.12) [71]. The reactions with allyl-, alkyl-, vinyl-, or alkynyl-substituted substrates **27a**, **27b**, **27e**, and **27f** were efficiently resolved with high *s*-factors (s = 41–60), and the reaction with **27c** or **27d** with a sterically demanding substituent (R = *i*-Pr or Cy) resulted in maintaining good *s*-factors (s = 27 and 17, respectively). However, the reaction with aryl- or heteroaryl-substituted substrates **27g**–**j** showed higher *s*-factors (s = 49–60) compared to **27a**–**f** (s = 17–60). The substrates **27h** or **27i** with an electron-donating or -withdrawing substituent on the aryl group did not significantly affect the *s*-factor (s = 63 or **27h** and s = 60, for **27i**).

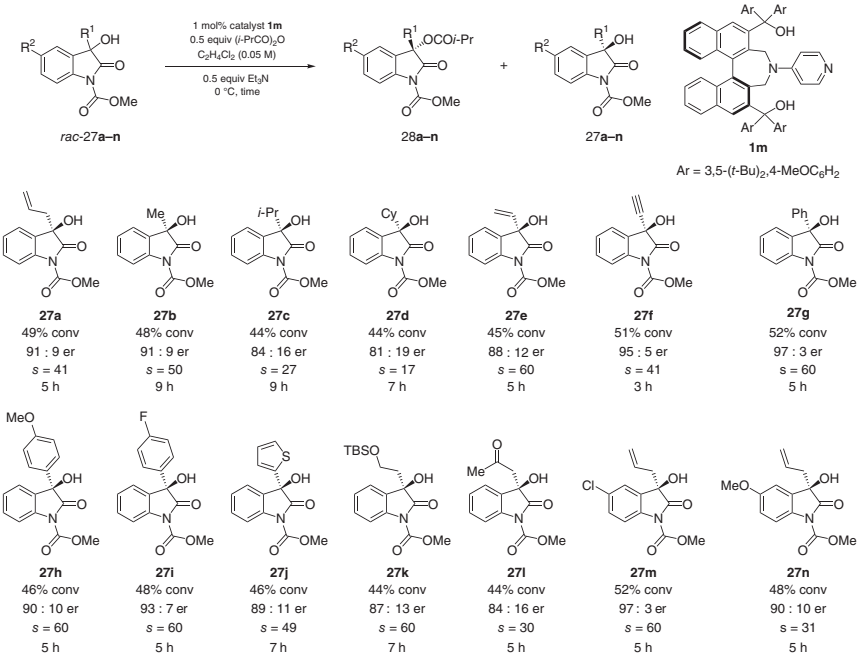

Scheme 9.12 Substrate scope in kinetic resolution of 3-hydroxy-3-substituted 2-oxindoles with catalyst **1m**.

Furthermore, a polar FG within the substrate could be tolerated. The reaction with **27k** with a silyl ether showed an excellent *s*-factor ($s = 60$), and β-hydroxyketone **27l** showed a good *s*-factor ($s = 30$). The 5-Cl- and 5-MeO substituted substrates **27m** and **27n** also showed good to excellent *s*-factors ($s = 60$ for **27m** and $s = 31$ for **27n)**. Overall, various enantio-enriched 3-hydroxy-3-substituted 2-oxindoles were obtained in 3–9 hours with high efficiency ($s = 17$–60).

Next, the Mandai and Suga group directed their focus toward the significance of *tert*-alcohol moiety of the catalyst for enantioselective reactions. They conducted the kinetic resolution of *rac*-**27a** via pseudo-C_2-symmetric catalyst **1m′** (one hydroxy group replaced hydrogen), C_2-symmetric catalyst **1m′** (two hydroxy groups replaced hydrogen), and **1a** (lack of two *tert*-alcohol moieties) employing the ideal conditions for **1f** (Scheme 9.13). Catalyst **1m′** exhibited moderate conversion (41% conv.) and *s*-factor ($s = 27$), whereas **1m′′** and **1a** showed diminished catalytic activity and enantioselectivity. Notably, two sterically demanding -$CHAr_2$ moieties within **1m′′** did not have catalytic activity (4% conv.). Thus, the hydroxy group within the catalyst **1m** facilitates hydrogen bonding-mediated kinetic resolution, enhancing the overall reaction efficiency compared to **1m′′** or **1m′**. Similar observations were made in their previous studies as well [32, 57, 66, 72].

Based on mechanistic insights provided by Spivey and Zipse et al. [58], Zipse [16], and Yamanaka and Kawabata et al. [59, 60], as well as the authors' previous transition state models [32, 57, 66], the authors speculated that the *N*-methoxycarbonyl group within the substrate is positioned away from the catalyst backbone to avoid steric repulsion (Figure 9.10). The efficient hydrogen bonding network in the favored transition state facilitated the fixation of counter anion (*i*-$PrCOO^-$) [57–60, 73] in the right place, which deprotonate from the hydroxy group in the substrate (Figure 9.10, left), followed by acylation to give (*S*)-**28a** and recovered alcohol (*R*)-**27a**. On the other hand, in the disfavored transition state (Figure 9.10, right), there are large

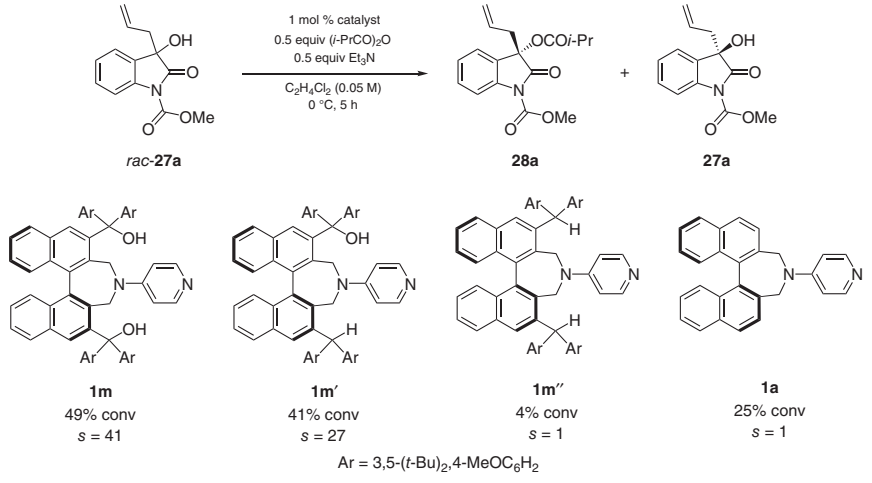

Scheme 9.13 Control experiment with various catalysts with/without *tert*-alcohol unit.

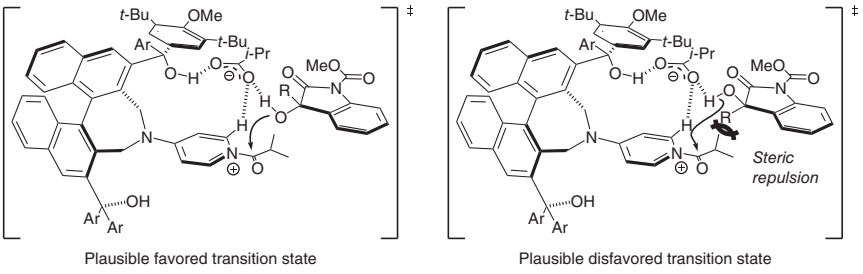

Figure 9.10 Possible transition states for kinetic resolution of 3-hydroxy-3-substituted 2-oxindole.

steric repulsion between the substituent (R in substrate) and the isopropyl group of the *N*-acyl pyridinium ion.

9.4.2 Desymmetrization of Alcohols

The successful desymmetrization of *meso*-1,2-diols was also achieved by Mandai and Suga (Scheme 9.14) [72]. Reactions of *meso*-hydrobenzoin derivatives **29a–d**

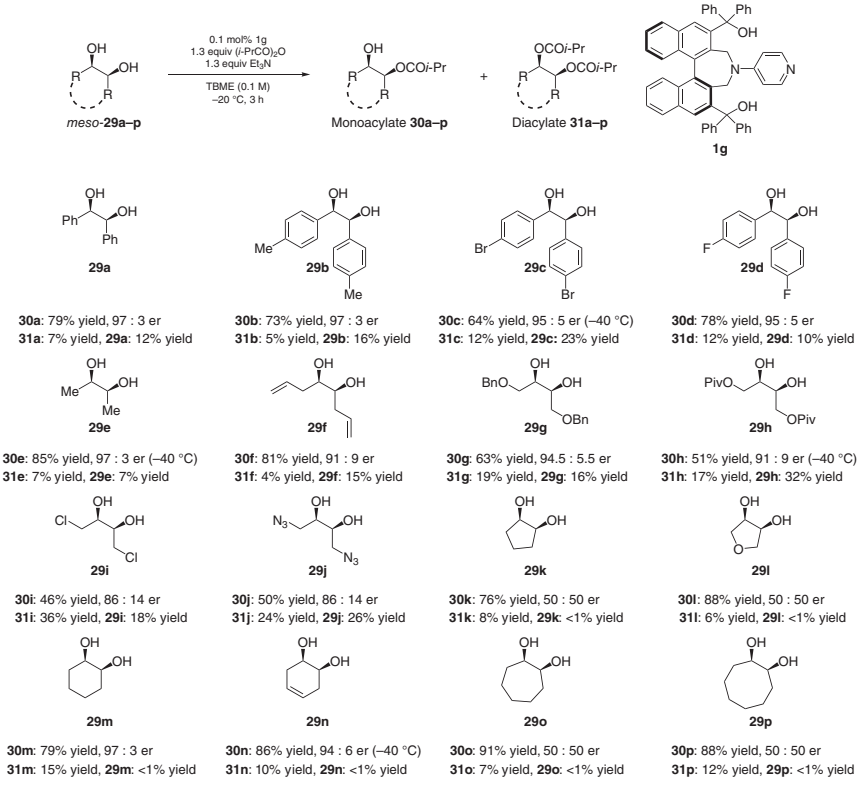

Scheme 9.14 Desymmetrization reactions of various *meso*-1,2-diol derivatives promoted by **1g** catalyst.

yielded **30a**–**d** with excellent enantioselectivities (up to 97 : 3 er) and high chemoselectivities (**30**/**31** = 5.3–14.6). Acyclic diols with allyl-, alkyl-, and heteroatom functionalized alkyl moieties **29e**–**j** could be desymmetrized to afford monoacylates **30e**–**j** with high enantioselectivities (er ranging from 86 : 14 to 97 : 3 er). Notably, substrates **29i** and **29j** bearing electron-withdrawing groups yielded not negligible amounts of diacylates **31i** and **31j**; however, the exact reason for this undesired diacylate formation remains unclear. Next, the cyclic substrates **29k**–**29p** were tested and high enantioselectivity was observed with the six-membered ring 1,2-diols **29m** and **29n** (**30m** with 97 : 3 er, and **30n** with 94 : 6 er), whereas the other cyclic substrates **29k**, **29l**, **29o**, and **29p** gave racemates of monoacylates, albeit with high chemoselectivity (**30**/**31** = 7.3–14.7).

Mandai and Suga also investigated the desymmetrization reaction of cyclic *meso*-1,3-diols (Scheme 9.15) [74]. The reaction of **32a** gave the monoacylate **33a** (95% yield, 98 : 2 er) along with trace amounts of the diacylate **34a**. Conversely, the employment of the other enantiomer of catalyst **1t** (*ent*-**1t**) yielded **33a** in 93% yield with 2 : 98 er. These results demonstrate the usefulness of the method where both enantiomers of the monoacylate are easily accessible in a single step from the same starting material **32a**. The reaction of substrate **32b** resulted in **33b** in 66% yield with 62 : 38 er, possibly due to a sterically congested conformation of **32b**

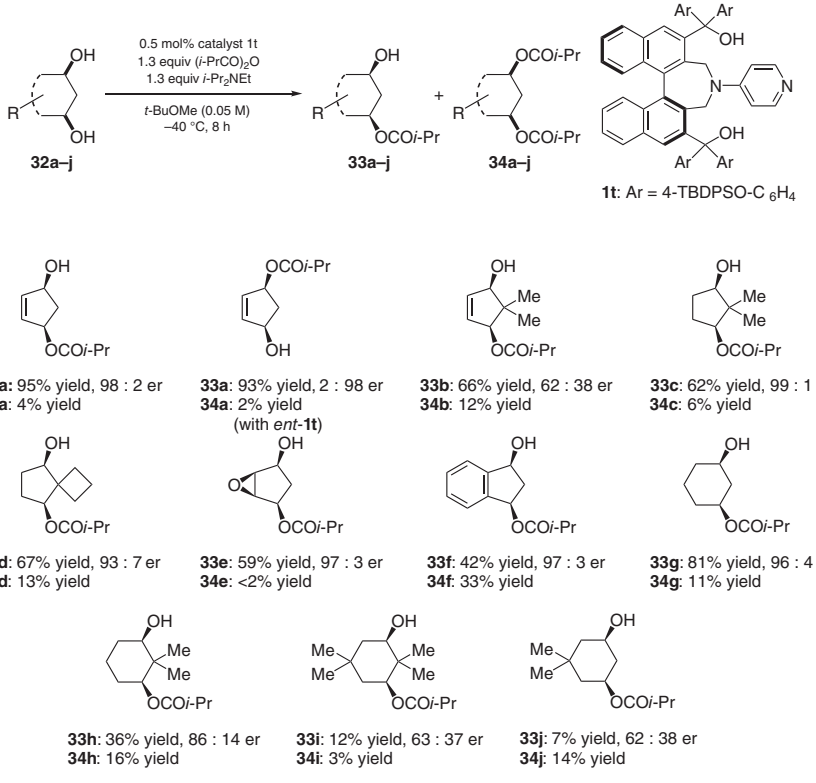

Scheme 9.15 Desymmetrization of various cyclic *meso*-1,3-diols promoted by catalyst **1t**.

from the cyclopentene scaffold. Consequently, saturated variant **32c** was used for desymmetrization reaction, leading to **33c** in 62% yield with 99 : 1 er. Employing **32c** with a spiro-system or **32e** with an epoxide gave monoacylate **33d** or **33e** in 67% yield with 93 : 7 er and 59% yield with 97 : 3 er, respectively. The substrate **32f** yielded **33f** in 42% yield with 97 : 3 er along with a significant amount of diacylate **34f** (33% yield). The lower solubility of **32f** compared to its product **33f** contributed significantly to generating **34f**; i.e. once **33f** was formed, it readily converted to diacylate **34f**. In the case of cyclic *meso*-1,3-diols with a six-membered ring, the reaction of **32g** gave **33g** in 81% yield with 96 : 4 er. However, substrates **32h–j** with a 2,2-dimethyl-, 2,2,5,5-tetramethyl-, or 5,5-dimethyl substrate yielded unsatisfactory results (7–36% yield, up to 86 : 14 er), with the reasons for these low yields and enantioselectivities of these products remaining obscure.

Enantioselective desymmetrization of 1,3-propanediol derivatives is a considerable challenge. Distinguishing the enantiotropic alcohols is challenging because the pro-stereogenic center is distant from the reaction site (Scheme 9.16; target reaction in the solid-line box). Additionally, the desired monoacylated product retains a free primary alcohol, which could undesirably react with the acylating agent to produce the diacylate (Scheme 9.16; over-acylation in the dotted-line box). It is important to note that both the enantiomeric ratio (er) and yield of the monoacylate are significantly affected by the second acylation, either through **path A** (major enantiomer acylation) or **B** (minor enantiomer acylation).

Scheme 9.17 demonstrates that the reaction involving **35a** (R^1 = Ph, R^2 = Me) gave monoacylate **36a** in 90% yield with 94 : 6 er along with a small amount of diacylate **37a** and unreacted **35a** [75]. The reaction of substrates bearing a bulkier alkyl or allyl group **35b**, **35c**, or **35d** (R^1 = Ph, R^2 = Et, *i*-Pr, or allyl) afforded monoacylates **36b–d** in high yield with moderate enantioselectivity (84 : 16 er for **36b**, 66 : 34 er for **36c**, and 79 : 21 er for **36d**, respectively). With these substrates, undesired diacylates were approximately suppressed. The use of substrates **35e–g** (R^1 = aryl, R^2 = Me) afforded monoacylate **36e–g** with moderate to high enantioselectivities. However, the use of 1,3-diol **35e** bearing an electron-rich aryl group (R^1 = *p*-$MeOC_6H_4$, R^2 = Me) resulted in a significant amount of diacylate **37e**, likely due to the high solubility and reactivity of the monoacylate **36e**. Conversely, substrate **35g** with an electron-deficient group (R^1 = *p*-$NO_2C_6H_4$, R^2 = Me) exhibited poor chemoselectivity (monoacylate/diacylate) with the low solubility of 1,3-diol **35g** compared

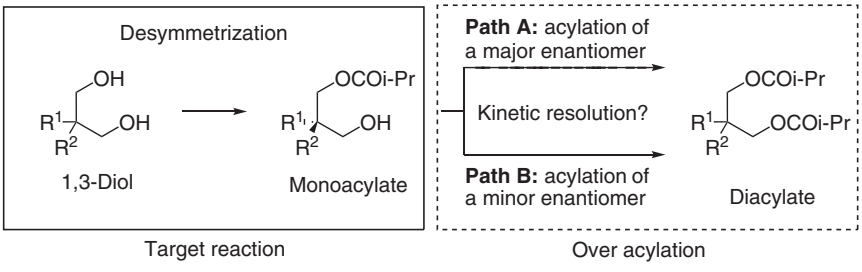

Scheme 9.16 General scheme for the acylative desymmetrization of 1,3-diol.

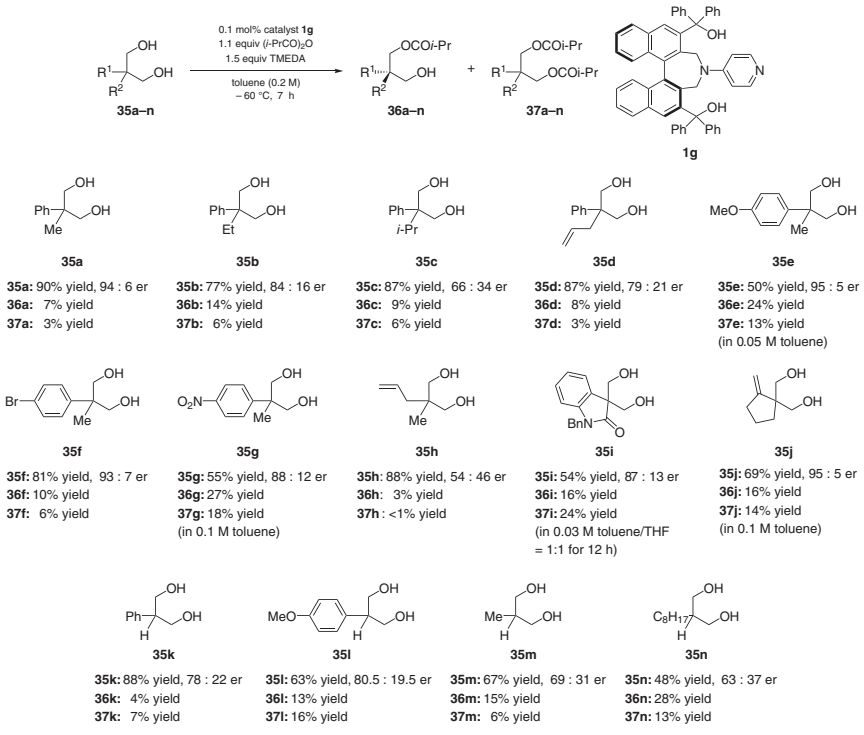

Scheme 9.17 Desymmetrization of various 1,3-diols promoted by catalyst **1g**.

to monoacylate **36g** leading to its rapid conversion to diacylate **37g** once formed. The reaction with substrates **35h–j** gave monoacylates **36h–j** with moderate to high enantioselectivity (from 54 : 46 to 95 : 5 er). The low solubility of the substrates also impacted the chemoselectivity (e.g., **35i** and **35j**). Next, substrates **35k–n** containing tertiary carbon atom (R^1 = aryl or alkyl, R^2 = H) were subjected to the optimal conditions, yielding monoacylates with moderate enantioselectivities (up to 80.5 : 19.5 er). The reasons for this poor chemo- and enantioselectivity of monoacylates **35k–n** are still obscure at present.

Control experiments were conducted to elucidate the second acylation process by the authors (Table 9.1). As previously mentioned, managing such an over-reaction poses a significant challenge due to the high reactivity of primary alcohols, making it difficult to prevent undesirable over-acylation, which could greatly impact the yields and enantioselectivities of the monoacylate (e.g. Scheme 9.16). Hence, the reaction with the racemates **36a** (R^1 = Ph, R^2 = Me) or **36k** (R^1 = Ph, R^2 = H) under the reaction conditions was tested. Over-acylation proceeded smoothly to yield the corresponding diacylate **37a** or **37k** in ~50% conversion with low *s*-factor (s = 1.8–2.0). According to the analysis of the recovered starting materials **36a** and **36k**, minor enantiomers were mainly consumed in the enantioselective desymmetrization of 1,3-diols **35a** and **35k**. This finding suggests that over-acylation in Scheme 9.16 occurred preferentially via **path B** (the pathway that tends to enhance enantioenrichment of the monoacylate), but its selectivity was rather low.

Table 9.1 Investigation of the second acylation step.

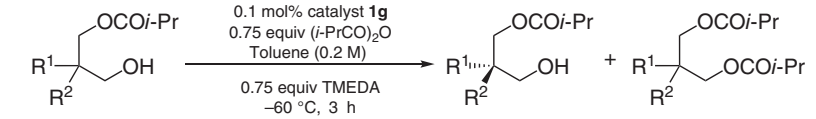

36a: R^1 = Ph, R^2 = Me
36k: R^1 = Ph, R^2 = H

36a or **36k** **37a** or **37k**

Entry	Monoacylate	Conv (%)	er of monoacylate	s
1	**36a**	50	62 : 38	2.0
2	**36k**	59	63 : 37	1.8

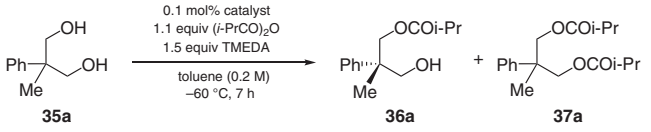

35a **36a** **37a**

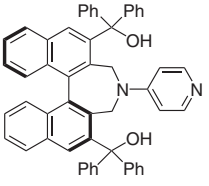

1g

36a: 90% yield, 94 : 6 er
37a: 7% yield
35a: 3% yield

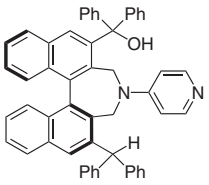

1g″

36a: 65% yield, 88.5 : 11.5 er
37a: 6% yield
35a: 31% yield

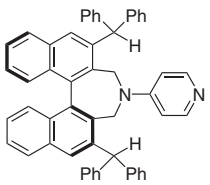

1g‴

36a: 31% yield, 46 : 54 er
37a: 7% yield
35a: 60% yield

Scheme 9.18 Control experiment with various catalysts with/without *tert*-alcohol unit.

The key role of the hydroxy groups within the catalyst was also investigated by the same authors. The desymmetrization reaction of **35a** was conducted using catalyst **1g″** (lacking one hydroxy group) and catalyst **1g‴** (lacking two hydroxy groups) under identical conditions (Scheme 9.18). Catalysts **1g″** and **1g‴** showed significantly lower catalytic activity and enantioselectivity than the optimal catalyst **1g** (65% yield with 88.5 : 11.5 er for catalyst **1g″** and 31% yield with 46 : 54 er for catalyst **1g‴**, respectively). These results highlighted catalyst **1g** with two *tert*-alcohol units in achieving both high catalytic activity and enantioselectivity.

A similar transformation, the desymmetrization of glycerol derivatives with different protecting groups, was also reported by the Mandai and Suga group (Scheme 9.19) [76].

The reaction of **38a** (PG = TBS) gave monoacylate **39a** in good yield (86% isolated yield) with high enantioselectivity (94 : 6 er) along with a detectable amount

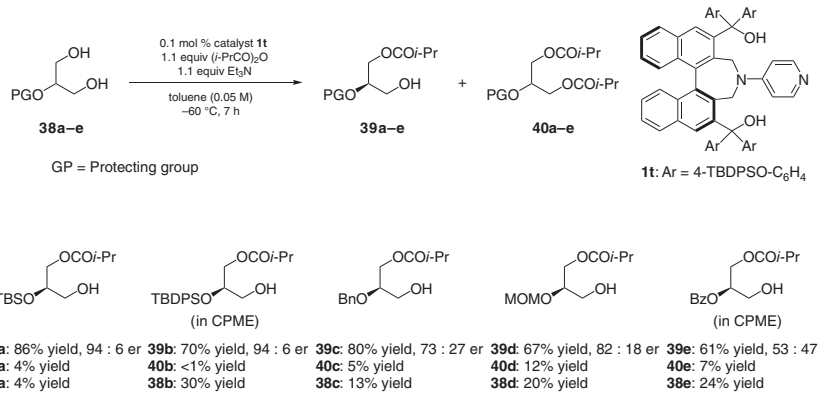

Scheme 9.19 Desymmetrization of various glycerol derivatives by catalyst **1t**.

of diacylate **40a**. In addition, the use of a bulkier silyl protecting group **38b** (PG = TBDPS) gave acceptable results (70% yield of **39b** with 94 : 6 er and 30% recovery of **38b**), but in this case, a more polar solvent, cyclopentyl methyl ether (CPME), was required to dissolve the diol **38b**. Other protecting groups, such as **38c** (PG = Bn), **38d** (PG = MOM), and **38e** (PG = Bz), gave moderate to good yields of monoacylates **39c–e** with lower enantioselectivities, and detectable amounts of diacylates and unreacted diols were observed. A possible reason for such poor results could be the poorly soluble diols **38c–e**, leading to incomplete enantiodiscrimination by catalyst **1t**. The solubility of the monoacylate **39c–e** was much higher than that of diols **38c–e**. Accordingly, once **39c–e** was generated, it was readily converted to diacylate **40c–e**. For the successful enantioselective desymmetrization of glycerol derivatives, a silyl-protecting group (e.g. diol **38a**) is indispensable to improve the solubility of glycerol derivatives.

9.4.3 Dynamic Kinetic Resolution

To further expand the applications of chiral DMAP derivatives in enantioselective reactions, the Mandai and Suga group use their catalysts for different types of reactions. They considered the DKR of azlactones, resulting in α-amino acids, as a benchmark reaction to evaluate the catalytic performance. Several organocatalytic approaches have been documented for the DKR of azlactones, utilizing a range of catalysts such as a planar chiral DMAP derivative [77], benzotetramisole [78], urea-based-bifunctional catalysts [79, 80], chiral phosphoric acid [81], a peptide catalyst [82], and a chiral bisguanidinium salt catalyst [83]. However, most of the reported methods achieved moderate enantioselectivities (less than <95 : 5 er) and required high catalyst loading (up to 20 mol%) with extended reaction time (>24 hours). Therefore, some improvements are still needed to achieve higher enantioselectivities (>95 : 5 er), reduce the loading of the catalyst (<5 mol%), and shorten the reaction times.

The authors first identified the optimal catalyst from a catalyst library for the DKR of azlactone **41a** using 5 equiv of methanol (nucleophile) and 10 mol% of benzoic

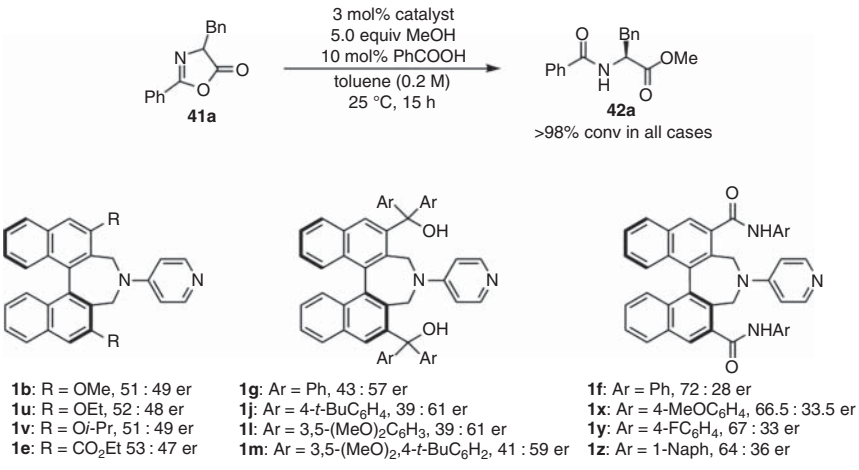

Scheme 9.20 Initial screening of catalyst structure.

acid co-catalyst [77] in toluene at 25 °C for 15 hours (Scheme 9.20) [84]. Reactions with 3 mol% of catalysts **1b**, **1u**, **1v**, and **1e**, which have alkyl ethers or ethyl esters at the 3,3′-positions of the binaphthyl moiety, afforded a nearly racemic mixture of **42a** (up to 53 : 47 er). Those with **1g**, **1j**, **1l**, and **1m**, having *tert*-alcohol moieties, showed a slight increase in the enantioselectivity of **42a** (up to 39 : 61 er). Conversely, catalysts **1f**, **1x–z** with amide groups yielded **42a** with moderate enantioselectivities (up to 72 : 28 er). Based on these results, **1f** was selected as the optimal catalyst for the DKR of azlactone.

Following optimization of the other reaction parameters, they identified the following conditions to be optimal: the use of 3 mol% of **1f** as a catalyst, 3 equiv of *i*-PrOH as a nucleophile, 10 mol% benzoic acid as an additive in $CHCl_3$ at 25 °C for 24 hours. The DKR of different azlactones was studied under the optimal conditions (Scheme 9.21). The reactions of the azlactone **41a–e** yielded the products **43a–e** with excellent enantioselectivities (er ranging from 95.5 : 4.5 to 96 : 4). Conversely, the results with **41f** (tryptophan derivative with free –NH) exhibited poorer results in terms of yield and enantioselectivity (28% yield with 61.5 : 38.5 er), probably because the –NH hampers the formation of hydrogen bonding network between the catalyst and substrate. Additionally, they conducted the reactions involving **41g–n**, including allyl-, thiomethyl-, and ester groups to afford products **43g**, **43h**, and **43j–n** in satisfactory yields with good-to-excellent enantioselectivities (er ranging from 86 : 14 to 95 : 5 er). In certain cases (**41h–m**), the procedures were modified (with MS3A and/or extended reaction time 48 hours) to obtain a satisfactory result. Notably, substrate **41i**, containing an α-branched alkyl moiety (*i*-Pr), remained unreactive due to the steric hindrance. Interestingly, the reaction of **41n** ($-CO_2Me$ might interfere with the hydrogen bonding network) did not have a significant impact on the enantioselectivity (95 : 5 er for **43n**), and **41o** did not give any desired product. Based on these experiments, these methods enabled to access α-amino acid derivatives (natural or unnatural type). Despite most of the typical transformations requiring a longer

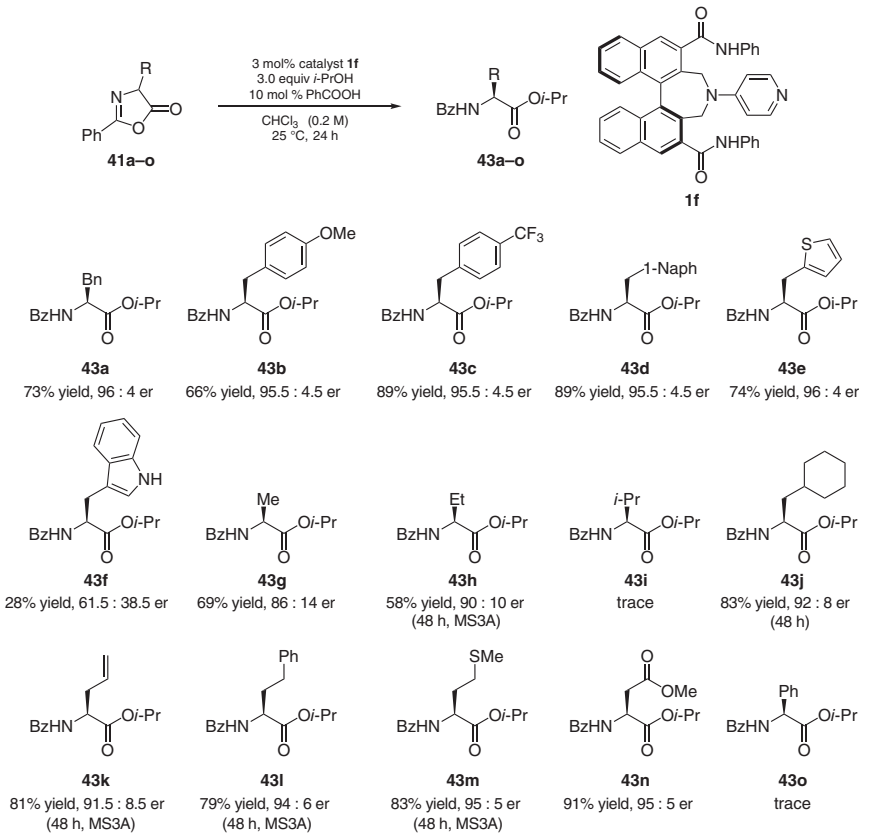

Scheme 9.21 Dynamic kinetic resolution of azlactone promoted by catalyst **1f**.

reaction time (>48 hours) and/or a higher catalyst loading (5–20 mol%) [77–80], it is noteworthy that catalyst **1f** featuring amide exhibited exceptional catalytic activity (3 mol% catalyst) in the DKR of azlactone, even in the presence of a sterically demanding nucleophile (*i*-PrOH).

9.5 Summary and Conclusions

In summary, binaphthyl-based DMAP derivatives provide efficient and dramatic acceleration effects in various acyl transfer reactions. This new class of catalysts allows for (i) the rapid synthesis of optically active DMAPs and (ii) the acceleration of nucleophilic catalytic reactions. By introducing a polar FG into the catalytic structure of optically active DMAP derivatives, a reaction system can exhibit excellent catalytic activities and high enantioselectivities through hydrogen bonding interactions, in intra- and intermolecular enantioselective acylation reactions. We hope that the various phenomena and considerations described in this chapter will be useful for the future development of organocatalysts.

References

1 Hashimoto, T. and Maruoka, K. (2007). Recent development and application of chiral phase-transfer catalysts. *Chem. Rev.* 107: 5656–5682.
2 Maruoka, K. (2007). Design of c2-symmetric chiral phase-transfer catalysts for practical asymmetric synthesis. *Chimia* 61: 263–268.
3 Ooi, T. and Maruoka, K. (2007). Recent advances in asymmetric phase-transfer catalysis. *Angew. Chem. Int. Ed.* 46: 4222–4266.
4 Akiyama, T., Itoh, J., and Fuchibe, K. (2006). Recent progress in chiral bronsted acid catalysis. *Adv. Synth. Catal.* 348: 999–1010.
5 Terada, M. (2008). Binaphthol-derived phosphoric acid as a versatile catalyst for enantioselective carbon-carbon bond forming reactions. *Chem. Commun.* 35: 4097–4112.
6 Akiyama, T. (2007). Stronger Brønsted acids. *Chem. Rev.* 107: 5744–5758.
7 Terada, M. (2010). Chiral phosphoric acids as versatile catalysts for enantioselective transformations. *Synthesis* (12): 1929–1982.
8 Akiyama, T. and Mori, K. (2015). Stronger Brønsted acids: recent progress. *Chem. Rev.* 115: 9277–9306.
9 Parmar, D., Sugiono, E., Raja, S., and Rueping, M. (2014). Complete field guide to asymmetric binol-phosphate derived bronsted acid and metal catalysis: history and classification by mode of activation; bronsted acidity, hydrogen bonding, ion pairing, and metal phosphates. *Chem. Rev.* 114: 9047–9153.
10 Palomo, C., Oiarbide, M., and Lopez, R. (2009). Asymmetric organocatalysis by chiral Brønsted bases: implications and applications. *Chem. Soc. Rev.* 38: 632–653.
11 Kondoh, A. and Terada, M. (2022). Asymmetric base organocatalysis. In: *Catalytic Asymmetric Synthesis* (ed. T. Akiyama and I. Ojima), 81–115. UK: Wiley.
12 Brunel, J.M. (2007). Update 1 of: Binol: a versatile chiral reagent. *Chem. Rev.* 107: PR1–PR45.
13 Litvinenko, L.M. and Kirichenko, A.I. (1967). Basicity and stereospecificity in nucleophilic catalysis by tertiary amines. *Dokl. Akad. Nauk SSSR* 176: 97–100.
14 Steglich, W. and Höfle, G. (1969). *N*,*N*-dimethyl-4-pyridinamine, a very effective acylation catalyst. *Angew. Chem. Int. Ed.* 8: 981.
15 Spivey, A.C. and Arseniyadis, S. (2004). Nucleophilic catalysis by 4-(dialkylamino)pyridines revisited—the search for optimal reactivity and selectivity. *Angew. Chem. Int. Ed.* 43: 5436–5441.
16 Xu, S., Held, I., Kempf, B. et al. (2005). The DMAP-catalyzed acetylation of alcohols—a mechanistic study (DMAP = 4-(dimethylamino)pyridine). *Chem. Eur. J.* 11: 4751–4757.
17 Larionov, E. and Zipse, H. (2011). Organocatalysis: acylation catalysts. *Wiley Interdiscip. Rev. Comput. Mol. Sci.* 1: 601–619.
18 De Rycke, N., Couty, F., and David, O.R.P. (2011). Increasing the reactivity of nitrogen catalysts. *Chem. Eur. J.* 17: 12852–12871.
19 Wurz, R.P. (2007). Chiral dialkylaminopyridine catalysts in asymmetric synthesis. *Chem. Rev.* 107: 5570–5595.

20 Vedejs, E. and Chen, X. (1996). Kinetic resolution of secondary alcohols. Enantioselective acylation mediated by a chiral (dimethylamino)pyridine derivative. *J. Am. Chem. Soc.* 118: 1809–1810.

21 Kawabata, T., Nagato, M., Takasu, K., and Fuji, K. (1997). Nonenzymatic kinetic resolution of racemic alcohols through an "induced fit" process. *J. Am. Chem. Soc.* 119: 3169–3170.

22 Shaw, S.A., Aleman, P., and Vedejs, E. (2003). Development of chiral nucleophilic pyridine catalysts: applications in asymmetric quaternary carbon synthesis. *J. Am. Chem. Soc.* 125: 13368–13369.

23 Dalaigh, C.O., Hynes, S.J., Maher, D.J., and Connon, S.J. (2005). Kinetic resolution of *sec*-alcohols using a new class of readily assembled (*s*)-proline-derived 4-(pyrrolidino)-pyridine analogues. *Org. Biomol. Chem.* 3: 981–984.

24 Kawabata, T., Muramatsu, W., Nishio, T. et al. (2007). A catalytic one-step process for the chemo- and regioselective acylation of monosaccharides. *J. Am. Chem. Soc.* 129: 12890–12895.

25 Duffey, T.A., Shaw, S.A., and Vedejs, E. (2009). Acoledmap and bnoledmap: conformationally restricted nucleophilic catalysts for enantioselective rearrangement of indolyl acetates and carbonates. *J. Am. Chem. Soc.* 131: 14–15.

26 Crittall, M.R., Rzepa, H.S., and Carbery, D.R. (2011). Design, synthesis, and evaluation of a helicenoidal DMAP Lewis base catalyst. *Org. Lett.* 13: 1250–1253.

27 Chen, C.-T., Tsai, C.-C., Tsou, P.-K. et al. (2017). Enantiodivergent Steglich rearrangement of *O*-carboxylazlactones catalyzed by a chirality switchable helicene containing a 4-aminopyridine unit. *Chem. Sci.* 8: 524–529.

28 Yamamoto, T., Murakami, R., and Suginome, M. (2017). Single-handed helical poly(quinoxaline-2,3-diyl)s bearing achiral 4-aminopyrid-3-yl pendants as highly enantioselective, reusable chiral nucleophilic organocatalysts in the Steglich reaction. *J. Am. Chem. Soc.* 139: 2557–2560.

29 Ruble, J.C. and Fu, G.C. (1996). Chiral π-complexes of heterocycles with transition metals: a versatile new family of nucleophilic catalysts. *J. Org. Chem.* 61: 7230–7231.

30 Ruble, J.C., Latham, H.A., and Fu, G.C. (1997). Effective kinetic resolution of secondary alcohols with a planar−chiral analogue of 4-(dimethylamino)pyridine. Use of the Fe(C_5Ph_5) group in asymmetric catalysis. *J. Am. Chem. Soc.* 119: 1492–1493.

31 Spivey, A.C., Fekner, T., and Adams, H. (1998). Synthesis of atropisomeric analogues of DMAP. *Tetrahedron Lett.* 39: 8919–8922.

32 Mandai, H., Fujii, K., Yasuhara, H. et al. (2016). Enantioselective acyl transfer catalysis by a combination of common catalytic motifs and electrostatic interactions. *Nat. Commun.* 7: 11297.

33 Taylor, J.E., Bull, S.D., and Williams, J.M.J. (2012). Amidines, isothioureas, and guanidines as nucleophilic catalysts. *Chem. Soc. Rev.* 41: 2109–2121.

34 Müller, C.E. and Schreiner, P.R. (2011). Organocatalytic enantioselective acyl transfer onto racemic as well as *meso* alcohols, amines, and thiols. *Angew. Chem. Int. Ed.* 50: 6012–6042.

35 Pellissier, H. (2011). Catalytic non-enzymatic kinetic resolution. *Adv. Synth. Catal.* 353: 1613–1666.

36 Krasnov, V.P., Gruzdev, D.A., and Levit, G.L. (2012). Nonenzymatic acylative kinetic resolution of racemic amines and related compounds. *Eur. J. Org. Chem.* 2012: 1471–1493.

37 Seidel, D. (2014). The anion-binding approach to catalytic enantioselective acyl transfer. *Synlett* 25: 783–794.

38 Alba, A.-N.R. and Rios, R. (2011). Oxazolones in organocatalysis, new tricks for an old reagent. *Chem. Asian J.* 6: 720–734.

39 Diaz-de-Villegas, M.D., Galvez, J.A., Badorrey, R., and Lopez-Ram-de-Viu, M.P. (2012). Organocatalyzed enantioselective desymmetrization of diols in the preparation of chiral building blocks. *Chem. Eur. J.* 18: 13920–13935.

40 Enriquez-Garcia, A. and Kündig, E.P. (2012). Desymmetrisation of *meso*-diols mediated by non-enzymatic acyl transfer catalysts. *Chem. Soc. Rev.* 41: 7803–7831.

41 Zeng, X.-P., Cao, Z.-Y., Wang, Y.-H. et al. (2016). Catalytic enantioselective desymmetrization reactions to all-carbon quaternary stereocenters. *Chem. Rev.* 116: 7330–7396.

42 Suzuki, T. (2017). Recent topics in the desymmetrization of *meso*-diols. *Tetrahedron Lett.* 58: 4731–4739.

43 Lupton, D., Candish, L., and Nakano, Y. (2014). Lewis base catalysis of three n–π^* mediated reactions with N-heterocyclic carbenes (NHCs), isothioureas, bicyclic tertiary amines, and electron-rich pyridyls. *Synthesis* 46: 1823–1835.

44 Atodiresei, I., Schiffers, I., and Bolm, C. (2007). Stereoselective anhydride openings. *Chem. Rev.* 107: 5683–5712.

45 Lee, D. and Taylor, M.S. (2012). Catalyst-controlled regioselective reactions of carbohydrate derivatives. *Synthesis* 44: 3421–3431.

46 Lawandi, J., Rocheleau, S., and Moitessier, N. (2016). Regioselective acylation, alkylation, silylation and glycosylation of monosaccharides. *Tetrahedron* 72: 6283–6319.

47 Taylor, M.S. and Jacobsen, E.N. (2006). Asymmetric catalysis by chiral hydrogen-bond donors. *Angew. Chem. Int. Ed.* 45: 1520–1543.

48 Doyle, A.G. and Jacobsen, E.N. (2007). Small-molecule H-bond donors in asymmetric catalysis. *Chem. Rev.* 107: 5713–5743.

49 Kasák, P. and Putala, M. (2004). Elaboration of a novel effective approach to enantiopure functionalised 2,2′-dialkyl-1,1′-binaphthyls by stereoconservative cross-couplings at positions 2 and 2′. *Tetrahedron Lett.* 45: 5279–5282.

50 Black, T.H., Arrivo, S.M., Schumm, J.S., and Knobeloch, J.M. (1986). A novel oxygen-to-carbon ester migration catalyzed by 4-(*N*,*N*-dimethylamino)-pyridine in the benzofuranone ring-system. *J. Chem. Soc. Chem. Commun.* (20): 1524–1525.

51 Black, T.H., Arrivo, S.M., Schumm, J.S., and Knobeloch, J.M. (1987). 4-(Dimethylamino)pyridine as a catalyst for carbon acylation. 2. Control of carbon vs. oxygen acylation in benzofuranones. *J. Org. Chem.* 52: 5425–5430.

52 Hills, I.D. and Fu, G.C. (2003). Catalytic enantioselective synthesis of oxindoles and benzofuranones that bear a quaternary stereocenter. *Angew. Chem. Int. Ed.* 42: 3921–3924.

53 Lippert, K.M., Hof, K., Gerbig, D. et al. (2012). Hydrogen-bonding thiourea organocatalysts: the privileged 3,5-bis(trifluoromethyl)phenyl group. *Eur. J. Org. Chem.* 2012: 5919–5927.

54 Yang, H. and Wong, M.W. (2013). Oxyanion hole stabilization by C-H···O interaction in a transition state—a three-point interaction model for cinchona alkaloid-catalyzed asymmetric methanolysis of *meso*-cyclic anhydrides. *J. Am. Chem. Soc.* 135: 5808–5818.

55 Fujii, K., Mitsudo, K., Mandai, H. et al. (2019). Enantioselective acyl migration reactions of furanyl carbonates with chiral DMAP derivatives. *Chem. Eur. J.* 25: 2208–2212.

56 Kagan, H.B. and Fiaud, J.C. (1988). Kinetic resolution. *Top. Stereochem.* 18: 249–330.

57 Fujii, K., Mitsudo, K., Mandai, H., and Suga, S. (2016). Kinetic resolution of secondary carbinols by a chiral *N*,*N*-4-dimethylaminopyridine derivative containing a 1,1′-binaphthyl unit: hydrogen bonding affects catalytic activity and enantioselectivity. *Bull. Chem. Soc. Jpn.* 89: 1081–1092.

58 Larionov, E., Mahesh, M., Spivey, A.C. et al. (2012). Theoretical prediction of selectivity in kinetic resolution of secondary alcohols catalyzed by chiral DMAP derivatives. *J. Am. Chem. Soc.* 134: 9390–9399.

59 Yamanaka, M., Yoshida, U., Sato, M. et al. (2015). Origin of high *E*-selectivity in 4-pyrrolidinopyridine-catalyzed tetrasubstituted α,α′-alkenediol: a computational and experimental study. *J. Org. Chem.* 80: 3075–3082.

60 Imayoshi, A., Yamanaka, M., Sato, M. et al. (2016). Insights into the molecular recognition process in organocatalytic chemoselective monoacylation of 1,5-pentanediol. *Adv. Synth. Catal.* 358: 1337–1344.

61 Mizuta, S., Ohtsubo, Y., Tsuzuki, T. et al. (2006). Kinetic resolution of *d,l*-1,2-diols catalyzed by amine-phosphinite bifunctional organocatalysis derived from quinidine. *Tetrahedron Lett.* 47: 8227–8229.

62 Muller, C.E., Wanka, L., Jewell, K., and Schreiner, P.R. (2008). Enantioselective kinetic resolution of *trans*-cycloalkane-1,2-diols. *Angew. Chem. Int. Ed.* 47: 6180–6183.

63 Hrdina, R., Muller, C.E., and Schreiner, P.R. (2010). Kinetic resolution of *trans*-cycloalkane-1,2-diols via Steglich esterification. *Chem. Commun.* 46: 2689–2690.

64 Muller, C.E., Zell, D., Hrdina, R. et al. (2013). Lipophilic oligopeptides for chemo- and enantioselective acyl transfer reactions onto alcohols. *J. Org. Chem.* 78: 8465–8484.

65 Kuwano, S., Harada, S., Kang, B. et al. (2013). Enhanced rate and selectivity by carboxylate salt as a basic cocatalyst in chiral *N*-heterocyclic carbene-catalyzed asymmetric acylation of secondary alcohols. *J. Am. Chem. Soc.* 135: 11485–11488.

66 Fujii, K., Mitsudo, K., Mandai, H., and Suga, S. (2017). Hydrogen bonding-assisted enhancement of the reaction rate and selectivity in the kinetic

resolution of *d*,*l*-1,2-diols with chiral nucleophilic catalysts. *Adv. Synth. Catal.* 359: 2778–2788.

67 Jarvo, E.R., Copeland, G.T., Papaioannou, N. et al. (1999). A biomimetic approach to asymmetric acyl transfer catalysis. *J. Am. Chem. Soc.* 121: 11638–11643.

68 Vasbinder, M.M., Jarvo, E.R., and Miller, S.J. (2001). Incorporation of peptide isosteres into enantioselective peptide-based catalysts as mechanistic probes. *Angew. Chem. Int. Ed.* 40: 2824–2827.

69 Copeland, G.T. and Miller, S.J. (2001). Selection of enantioselective acyl transfer catalysts from a pooled peptide library through a fluorescence-based activity assay: an approach to kinetic resolution of secondary alcohols of broad structural scope. *J. Am. Chem. Soc.* 123: 6496–6502.

70 Mittal, N., Lippert, K.M., De, C.K. et al. (2015). A dual-catalysis anion-binding approach to the kinetic resolution of amines: insights into the mechanism via a combined experimental and computational study. *J. Am. Chem. Soc.* 137: 5748–5758.

71 Mandai, H., Shiomoto, R., Fujii, K. et al. (2021). Kinetic resolution of tertiary alcohols by chiral DMAP derivatives: enantioselective access to 3-hydroxy-3-substituted 2-oxindoles. *Org. Lett.* 23: 1169–1174.

72 Mandai, H., Yasuhara, H., Fujii, K. et al. (2017). Desymmetrization of *meso*-1,2-diols by a chiral *N*,*N*-4-dimethylaminopyridine derivative containing a 1,1′-binaphthyl unit: importance of the hydroxy groups. *J. Org. Chem.* 82: 6846–6856.

73 Kattnig, E. and Albert, M. (2004). Counterion-directed regioselective acetylation of octyl beta-D-glucopyranoside. *Org. Lett.* 6: 945–948.

74 Mandai, H., Hironaka, T., Mitsudo, K., and Suga, S. (2021). Acylative desymmetrization of cyclic meso-1,3-diols by chiral DMAP derivatives. *Chem. Lett.* 50: 471–474.

75 Mandai, H., Ashihara, K., Mitsudo, K., and Suga, S. (2018). Enantioselective desymmetrization of 1,3-diols by a chiral DMAP derivative. *Chem. Lett.* 47: 1360–1363.

76 Mandai, H., Ashihara, K., Mitsudo, K., and Suga, S. (2021). Acylative desymmetrization of glycerol derivatives by chiral DMAP derivatives. *Heterocycles* 102: 1083–1090.

77 Liang, J., Ruble, J.C., and Fu, G.C. (1998). Dynamic kinetic resolutions catalyzed by a planar-chiral derivative of DMAP: enantioselective synthesis of protected α-amino acids from racemic azlactones. *J. Org. Chem.* 63: 3154–3155.

78 Yang, X., Lu, G., and Birman, V.B. (2010). Benzotetramisole-catalyzed dynamic kinetic resolution of azlactones. *Org. Lett.* 12: 892–895.

79 Berkessel, A., Cleemann, F., Mukherjee, S. et al. (2005). Highly efficient dynamic kinetic resolution of azlactones by urea-based bifunctional organocatalysts. *Angew. Chem. Int. Ed.* 44: 807–811.

80 Peschiulli, A., Quigley, C., Tallon, S. et al. (2008). Organocatalytic asymmetric addition of alcohols and thiols to activated electrophiles: efficient dynamic kinetic resolution and desymmetrization protocols. *J. Org. Chem.* 73: 6409–6412.

81 Lu, G. and Birman, V.B. (2011). Dynamic kinetic resolution of azlactones catalyzed by chiral Brønsted acids. *Org. Lett.* 13: 356–358.

82 Metrano, A.J. and Miller, S.J. (2014). Peptide-catalyzed conversion of racemic oxazol-5(4h)-ones into enantiomerically enriched α-amino acid derivatives. *J. Org. Chem.* 79: 1542–1554.

83 Yu, K., Liu, X., Lin, X. et al. (2015). Organocatalytic dynamic kinetic resolution of azlactones to construct chiral *N*-acyl amino acid oxime esters. *Chem. Commun.* 51: 14897–14900.

84 Mandai, H., Hongo, K., Fujiwara, T. et al. (2018). Dynamic kinetic resolution of azlactones by a chiral *N*,*N*-dimethyl-4-aminopyridine derivative containing a 1,1′-binaphthyl unit: importance of amide groups. *Org. Lett.* 20: 4811–4814.

10

Catalytic Atroposelective Oxidative Coupling in Natural Product Synthesis

Houng Kang[1] *and Marisa C. Kozlowski*[2]

[1] *Chungbuk National University, Department of Chemistry Education, 1 Chungdae-ro, Seowon-gu, Cheongju, Chungbuk, 28644, South Korea*
[2] *University of Pennsylvania, Department of Chemistry, 231 South 34th Street, Philadelphia, PA, 19104, USA*

10.1 Introduction

A chiral axis, possessing a restricted rotational barrier, is not only prevalent in catalysis in the form of chiral ligands but is also a recurring motif in numerous natural products (Figure 10.1) [1, 2]. The captivating structures and unique properties associated with this motif have captivated the synthetic community, including academia and pharmaceutical companies. Intriguing findings from pharmacological research have revealed that axial chiral biaryl-containing complex molecules exhibit promising biological activities, encompassing antibiotic, anti-HIV, antispermatogenic, antitumor, and antimalarial activities, among others [3–7]. Additionally, highly conjugated atropopure biaryl compounds are known for their photochemical properties, making them suitable for applications such as photodynamic therapy in cancer treatment and as photosensitizers [8, 9].

Over the past three decades, extensive endeavors have been directed toward the development of methods related to the introduction of axial chiral bonds. Well-established strategies employing transition-metal catalysis have been utilized to construct both homo-coupled and hetero-coupled biaryl compounds [10, 11]. Conventional transition-metal-assisted coupling approaches can be categorized based on the origin of stereoselectivity: (a) axial chiral bonds induced by catalysis and (b) asymmetric induction arising from the inherent chirality of a substrate or from the incorporation of a chiral auxiliary (Scheme 10.1). For instance, Suzuki–Miyaura and Negishi coupling reactions stand as prominent methods for creating biaryl bonds, and with chiral ligands the generation of a chiral axis is possible in such couplings. Indeed, the efficiency of the enantioselective Suzuki–Miyaura coupling reaction, a key step in the synthesis of the tetra-*ortho*-substituted biaryl natural product, gossypol, was demonstrated by the Tang group in 2020 [12]. In addition, direct C–H activation strategies using various catalysts such as Pd, Rh, Ir, and Cu have been developed to build axial chiral bonds [13–16]. These approaches

Atropisomerism in Asymmetric Organic Synthesis: Challenges and Applications, First Edition.
Edited by Shinobu Takizawa and Mohamed S. H. Salem.

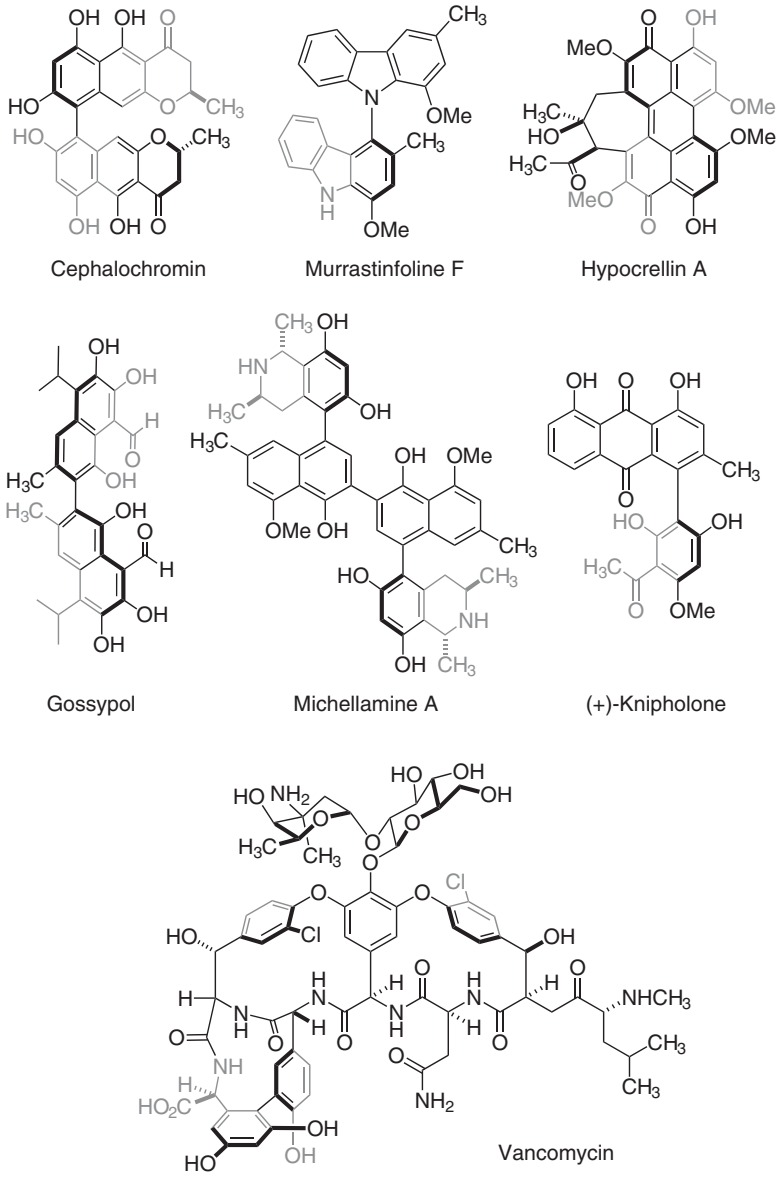

Figure 10.1 Natural products featuring axial chiral bonds.

circumvent the need for aryl halides and organometallic nucleophiles, which would often require conditions that are less compatible with functional groups. The latter methods, entailing central-to-axial chirality transfer, have been primarily used in bridged biaryl compounds as well as with artificial chiral auxiliaries. The Lipshutz group utilized chiral diols to construct tethered biaryl compounds, followed by Ullmann-type coupling reactions to establish the chiral axis [17]. When oxazoline, a well-known chiral transfer moiety, is located at the *ortho* position to a forming axial

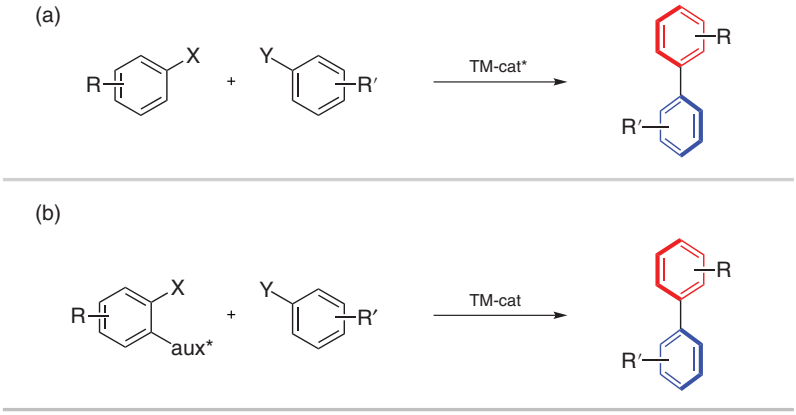

Scheme 10.1 Transition-metal-mediated coupling reaction to install a chiral axis. (a) Catalyst-controlled enantioselective coupling reaction. (b) Substrate-controlled stereoselective coupling reaction.

chiral bond, Ullmann or Kumada coupling reactions proceed with good stereoselectivity [18–20]. This approach has enabled the enantioselective synthesis of naturally occurring axial chiral compounds such as mastigophorene A and (+)-gossypol [21, 22].

An alternative effective approach for installing axial chiral bonds involves desymmetrization of achiral substrates (Scheme 10.2). For example, stereoselective functionalization to replace one of the *ortho* substituents via a transition-metal-catalyzed or an organocatalyzed reaction breaks the symmetry plane of the substrate [23–25]. When a directing group is present, desymmetrization can be executed through C–H activation, facilitating stereoselective functionalization [26–30]. Furthermore, in the context of cyclic biaryl compounds,

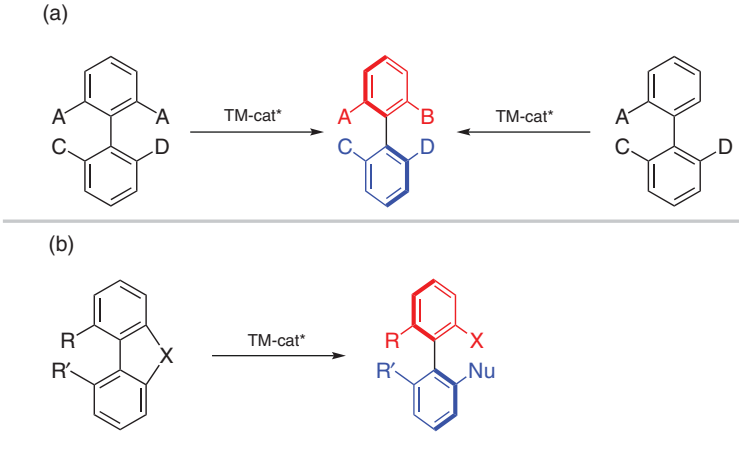

Scheme 10.2 Stereogenic axis generation by desymmetrization. (a) Asymmetric functionalization by substitutions. (b) Enantioselective fused biaryl ring-opening reactions.

heterocyclic ring-opening reactions have proven successful in generating axial chiral bonds [31–34]. Various ring-opening processes, including Pd-catalyzed carbonylation [35], Cu-catalyzed amination [33], and acyloxylation [34], have been reported thus far. Notably, atroposelective lactone ring-opening reactions have been firmly established by the Bringmann group [36]. Employing an asymmetric reductive lactone ring-opening reaction in conjunction with the Corey–Bakshi–Shibata catalyst and borane has enabled access to axial chiral natural products such as (+)-knipholone after several subsequent steps [37, 38].

Several other methods have been reported for the introduction of a chiral axis including kinetic resolution, nucleophilic aromatic substitution reactions, intramolecular lactonization coupled with dynamic kinetic resolution, and oxidative coupling reactions [10, 11]. Recently, particular attention has been garnered by the oxidative coupling process. This attention arises from both the substrate accessibility, given that it obviates the need for pre-functionalized substrates, and its overall atom economy.

Early reports of asymmetric oxidative coupling methods focused on 2-naphthol due to (i) its low oxidation potential, (ii) the absence of regioselectivity issues, (iii) the resistance to further oxidation, and (iv) the structural importance of the products, BINOL derivatives, which are chiral ligands used across diverse organic transformations. Over the past 30 years, various transition-metal-catalyzed oxidative protocols have been unveiled, including those based on copper, vanadium, iron, and ruthenium. Several research groups, from Nakajima (1995) to Tu (2019), have explored copper-catalyzed atroposelective oxidative coupling reactions (Table 10.1) [39–43]. In 1995, the Nakajima group showcased promising levels of stereoselectivity using a chiral pyrrolidine diamine ligand [44]. Their initial attempts involved a TMEDA/CuCl complex, inspired by the Glaser–Hay coupling [45]. Subsequent successful high-yielding conditions led them to opt for a chiral tertiary diamine, (−)-sparteine, for an asymmetric protocol, providing moderate selectivity in the presence of 2-naphthols with a C-3 ester group. Extensive ligand modifications revealed that an *L*-proline-based diamine backbone provided the best results for constructing BINOL derivatives. Interestingly, enhanced selectivity was obtained by employing a combination of secondary pyrrolidine amine and tertiary amine on the side chain, deviating from a tertiary diamine system [41]. The Kozlowski group later demonstrated that the secondary diamine ligand, 1,5-diaza-*cis*-decalin, in combination with copper, substantially improved enantioselectivity [42]. Cross-coupling experiments not only elucidated the reaction mechanism but also underscored the necessity of an additional coordination group to attain optimal stereoselectivity. The Ha and Sekar group employed BINAM derivatives as chiral ligands, enabling the corresponding asymmetric transformation to install the chiral axis from 3-substituted-2-naphthols [39, 40]. More recently, the Tu group reported the successful construction of axial chiral bonds through the utilization of a spirocyclic pyrrolidine in synergy with a chiral oxazoline system. This system stands out due to its success in the challenging cross-coupling process to furnish C_1-symmetric BINOL derivatives in high yields and stereoselectivities [43].

Table 10.1 Cu-catalyzed asymmetric oxidative coupling reaction.

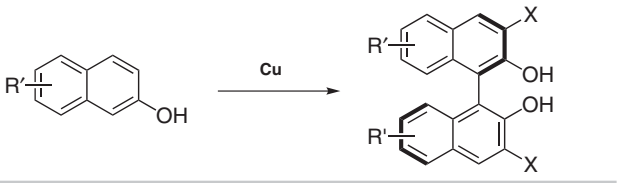

Nakajima et al. [39]

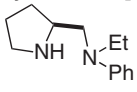

X = H, Me, *i*-Pr
OBn, COOR
58–95% yield
5–78% ee

Kozlowski (2001)

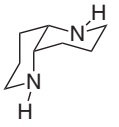

X = H, OBn, COOR
77–85% yield
13–93% ee

Ha and co-workers [39]

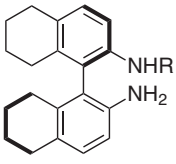

X = COOMe
R = H, *i*-Pr, 3-pentyl,
Bn, 3,5-xylyl
60–99% yield
4–94% ee

Sekar and co-workers [40]

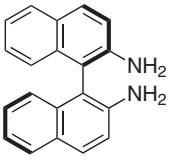

X = COOR
R′ = 6-Br, 6-naphthyl,
6-phenylacetyl
77–98% yield
48–97% ee

Tu (2019)[a]

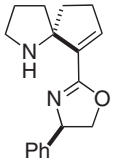

X = CHO, COOR
R′ = 6-Br, 6-Me, 6-OMe
3-Cl, 3-Br, 3-OR
34–92% yield
20–99% ee

a) This system produced both homo- and hetero-coupling products.

In 2009, Katsuki and coworkers delved into atroposelective oxidative coupling reactions using an earth-abundant iron metal approach (Table 10.2) [46]. The combination of iron and salan ligand facilitated the creation of axial chiral BINOL derivatives using air as the oxidant. Intriguingly, the iron/salan system yielded hetero-coupled products with high enantioselectivity, capitalizing on differences in the oxidation potentials of the substrates [47]. In contrast to Cu-catalyzed asymmetric oxidative coupling reactions, the presence of an additional coordination group at the C3-position of 2-naphthol impeded the formation of oxidative homo-coupled products within the Fe/salan complex system. The Toste and Pappo groups established that iron metal with C_2-symmetric phosphate furnished both homo- and hetero-coupled BINOL derivatives with high atroposelectivities in the presence of *tert*-butyl peroxide [48]. Notably, the Fe/phosphate complex successfully enabled the synthesis of 3,3′-unsubstituted BINOLs, a feat previously unattainable in high enantiopurity via either copper- or iron-catalyzed direct oxidative coupling strategies.

Table 10.2 Fe-catalyzed asymmetric oxidative coupling reaction.

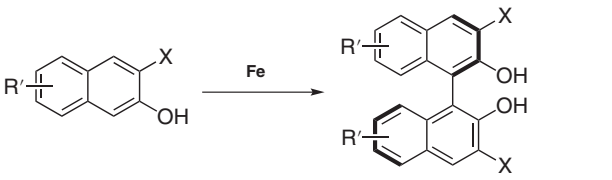

Katsuki [46][a]	Toste, Pappo [47][a]
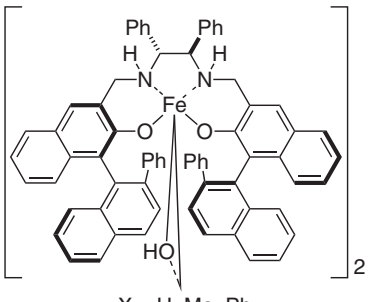	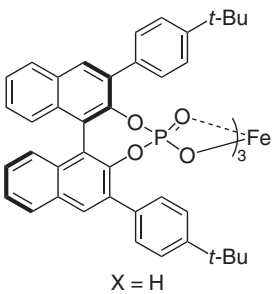
X = H, Me, Ph 2-naphthyl, Cl, Br, I 64–94% yield 16–96% ee	X = H R′= H, Me, *i*-Pr, butyl octyl, cyclohexyl 77–94% yield 54–88% ee

a) This system produced both homo- and hetero-coupling products.

Inspired by the early achievements of the Uang group, a myriad of chiral vanadium complexes have been developed since 2001 to facilitate the installation of axial chiral bonds [49–54]. An array of vanadium complex modes has been reported for the construction of axial chiral biaryl bonds, as shown in Table 10.3. Both monomeric and dimeric vanadyl complexes have found utility in establishing a chiral axis between 2-naphthol derivatives, displaying notable efficiency and enantioselectivity. Initial attempts into vanadium-catalyzed oxidative coupling reactions, however, suffered from extended reaction times [49, 51]. Improvements emerged upon ligand backbone modifications. For example, the Gong group revealed a dramatic acceleration in the reaction rate by transitioning from the conformationally flexible biphenyl to H_8-BINOL [50]. Mechanistic insights into the vanadium-mediated oxidative coupling process suggest that the high enantioselectivity originated from each vanadium center in the bisvanadium catalysts coordinating a substrate.

Other asymmetric oxidative coupling methods have been documented, encompassing the enzymatic route [55, 56], Ru-catalyzed asymmetric oxidative coupling reaction [57], transition metal-free atroposelective cross-coupling of quinones with chiral phosphoric acids [58, 59], and V-catalyzed oxidative coupling of simple phenols and hydroxycarbazoles [60, 61].

Within this chapter, our discussion will revolve around synthetic efforts pertinent to natural products that feature axial chiral bonds. Our emphasis will be placed on

Table 10.3 V-catalyzed asymmetric oxidative coupling reaction.

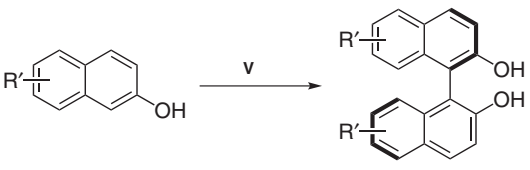

Gong [49]

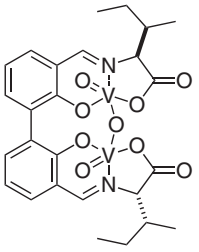

R′ = H, Br, OR, Ph
62–99% yield
89–97% ee

Gong [50]

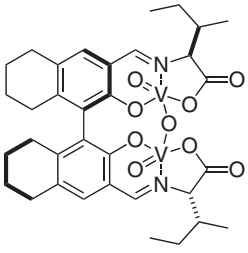

R′ = H, Br, OR
58–99% yield
60–97% ee

Chen [51]

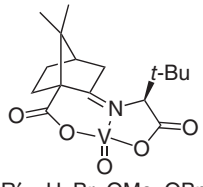

R′ = H, Br, OMe, OBn
61–99% yield
42–87% ee

Uang [52]

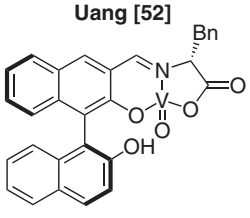

R′ = H, Br, OMe, OEt
40–96% yield
18–73% ee

Sasai [53, 54][a]

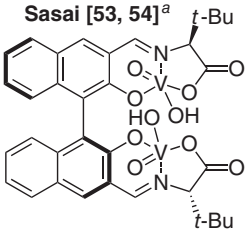

R′ = H, Br, Ph, OR
83–99% yield
81–90% ee

a) This system produced (*S*)-BINOL instead of (*R*)-BINOL.

describing the strategies for constructing a chiral axis through asymmetric oxidative methods among the various approaches discussed above.

10.2 Copper-Catalyzed Asymmetric Oxidative Coupling to Construct a Chiral Axis

10.2.1 Nigerone

The bisnaphthopyrone natural product, nigerone (**1**), exhibits a range of antibacterial and antitumor biological activities [62, 63]. Nigerone (**1**), a pigment isolated from mold, and isomeric isonigerone (**2**) feature a chiral axis between two highly oxygenated tricyclic fused heterocyclic ring systems (Figure 10.2). The first atroposelective synthesis of **1** was reported by Kozlowski group in 2007 [64].

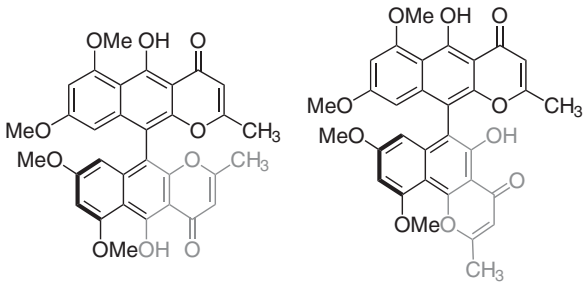

Figure 10.2 Structure of nigerone and isonigerone natural products.

Retrosynthetic analysis of the naturally occurring bisnaphthopyrone compounds envisioned rearrangement of bisisonigerone compound (**3**), which could be prepared by copper-catalyzed enantioselective oxidative coupling of flavasperone (**4**). In turn, oxidative coupling monomer **4** could be synthesized from carboxylic acid (**5**) in nine steps (Scheme 10.3).

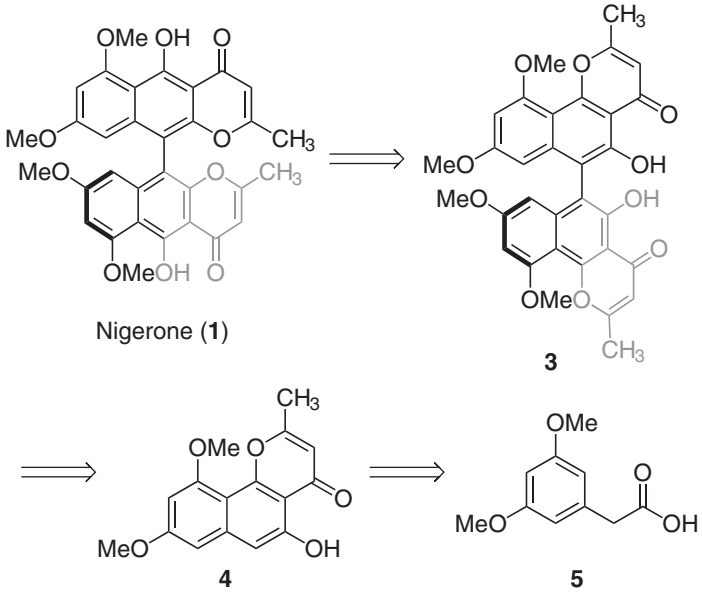

Scheme 10.3 Retrosynthetic analysis of nigerone (**1**).

Kozlowski and coworkers had discovered earlier that a 1,5-diaza-*cis*-decalin and Cu(II) complex is highly effective in the construction of the axial chiral bonds of BINOL derivatives. However, a coordinating group at C-3 position is necessary to obtain high enantioselectivity. Thus, the derivatives **7a–d** in Table 10.4 were examined to determine the optimal oxidative coupling monomer [65]. With the copper catalyst, less crowded naphthols provided higher enantioselectivity. For example, no substituent at C-5 naphthol gave 90% ee (Table 10.4, **7a**). In contrast, **7b** with a substituent at C-5 resulted in a dramatic decrease in atroposelectivity (27% ee).

Table 10.4 Cu-catalyzed asymmetric oxidative coupling of naphthols.

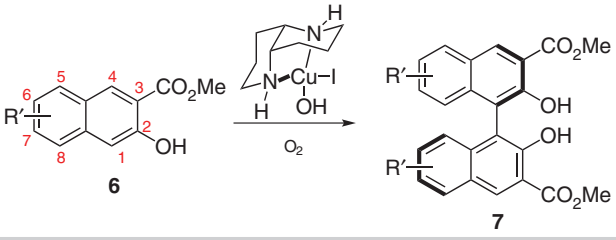

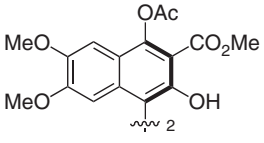

7a, 90% ee

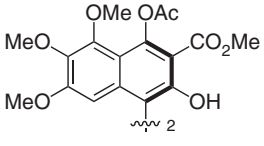

7b, 27% ee

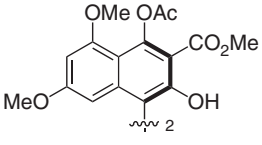

7c, 45% ee

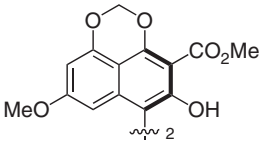

7d, 66% ee

The removal of a substituent even more distal from the coupling site (**7c**) reinforces the premise that gearing interactions between the substituents disrupt the alignment of the C3-group with the C-2 hydroxyl. Naphthol **7d** with a cyclic ketal limits this conformational gearing to allow a coplanar arrangement of the C3-group with the C-2 hydroxyl, thereby improving the enantioselectivity.

Based on these findings, the synthetic route toward nigerone outlined in Scheme 10.3 was proposed. Naturally occurring flavasperone (**4**), which features a constrained ring system with coordinating carbonyl in the C-3 position, could be synthesized from carboxylic acid (**5**) in nine steps (Scheme 10.4). Late-stage atroposelective copper-catalyzed oxidative coupling afforded bisisonigerone (**3**) in good yield and enantioselectivity. A catalytic amount of base promoted the isomerization of both pyrone rings to furnish desired nigerone (**1**). This isomerization was driven by the greater thermodynamic stability of nigerone (**1**), which stems from the lower degree of steric hindrance between the C-2 and C-1 aryl group in nigerone (**1**) vs the coplanar relationship between C-4 and C-5 in bisisonigerone (**3**). In line with this analysis, energy calculations found nigerone (**1**) as the lowest energy isomer. There was very little erosion in the enantioselectivity of the chiral access during this process (less than 3% ee change) and trituration upgraded the final product to 90%. Circular dichroism studies with bisisonigerone (**3**) and nigerone (**1**) revealed that the assignment of the natural product as (*S*)-nigerone was incorrect [66]. The calculated CD spectrum of (*R*)-nigerone matched both the synthesized and isolated natural product confirming the (*R*) absolute configuration.

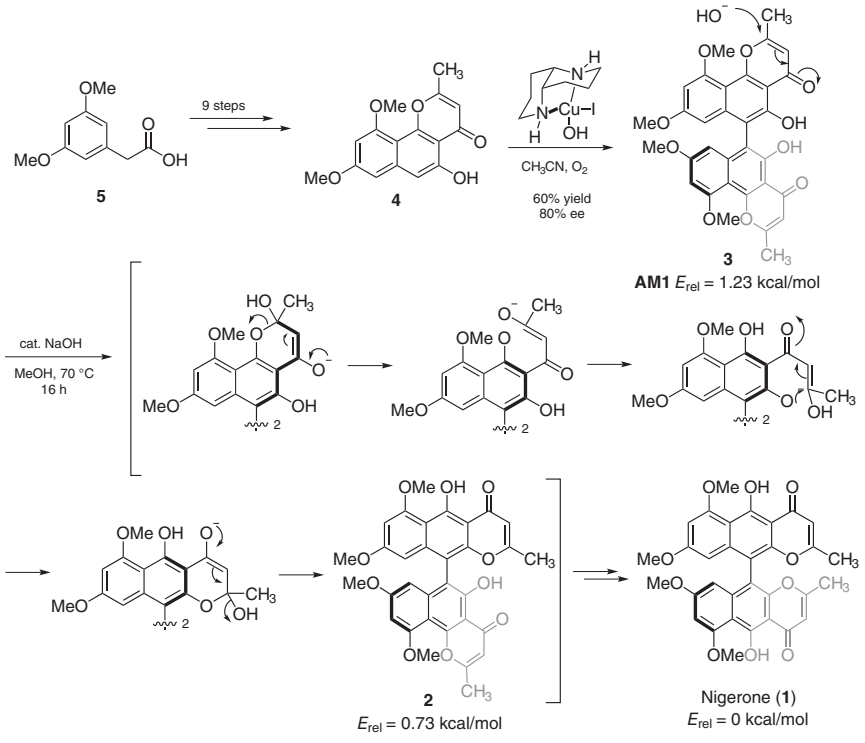

Scheme 10.4 Total synthesis of nigerone (**1**) via Cu-catalyzed oxidative coupling and isomerization.

10.2.2 Perylenequinones

Perylenequinones are highly conjugated pentacyclic natural products incorporating helical chirality. They exhibit photosensitizing properties and inhibit protein kinase C (Figure 10.3) [67]. Calphostins (**8**) and phleichrome (**9**) are diastereomers, each of which is atropisomerically stable due to the substituents at the C2,C2′ and C7,C7′ positions, which increase the rotational barrier. The strain afforded by the additional seven-membered rings in cercosporin (**10**) and hypocrellin A (**11**), however, lowers the rotational barriers substantially allowing isomerization under conditions used in synthesis. In the case of hypocrellin A (**11**), atropisomerization occurs rapidly at ambient temperature (only major atropisomer shown).

Notably, all the perylenequinone natural products can be synthesized from the common naphthol intermediate (**13**) (Scheme 10.5) [68, 69]. Late-stage introduction of central chirality at C7, C7′ substituents has permitted access to a diverse array of natural products with complete stereocontrol instead of using extant sp^3

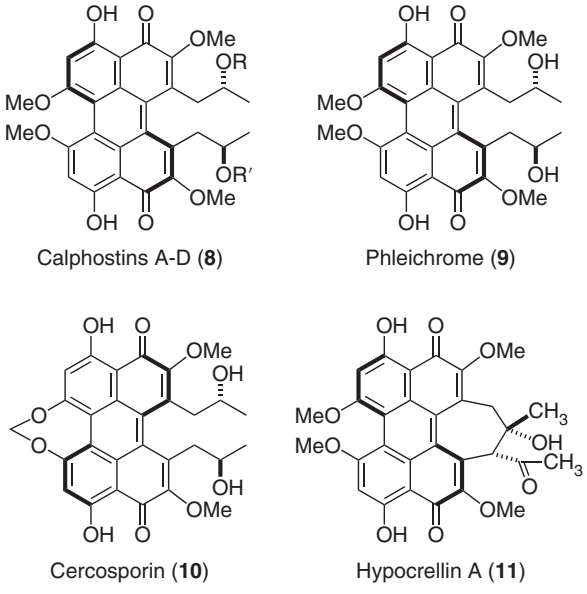

Figure 10.3 Perylenequinone natural products.

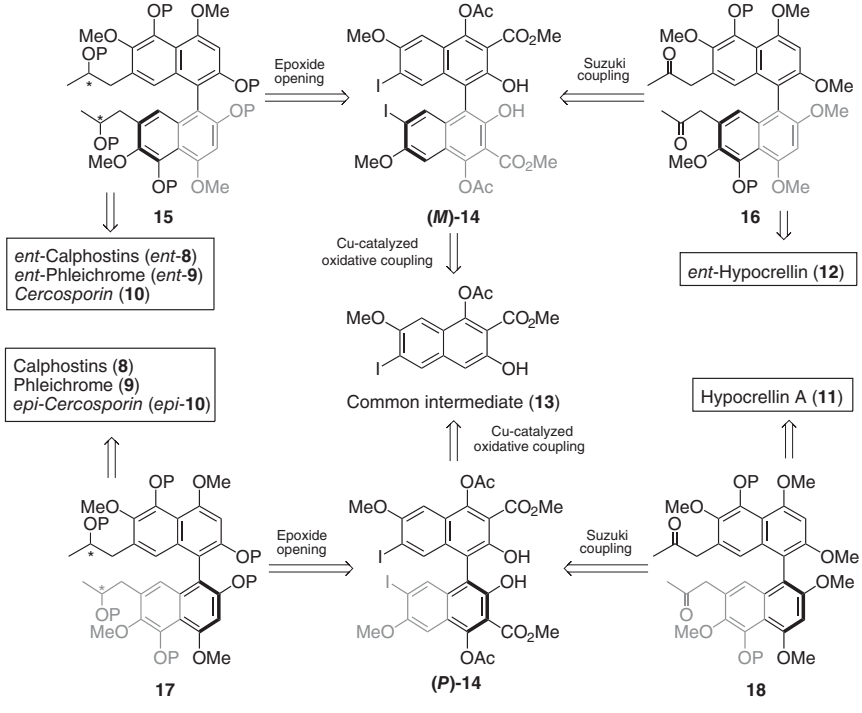

Scheme 10.5 Common intermediate to synthesize the perylenequinone natural products.

stereocenters to direct formation of the chiral axis via a diastereoselective oxidative coupling pathway, which only provides moderate stereoselectivity. Natural products and their derivatives could be obtained via either epoxide ring-opening process [68, 70, 71] or Suzuki coupling reaction [69, 72] with the corresponding axial chiral dimers **14**. Both enantiomeric dimers could be prepared from naphthol **13** via catalyst-controlled atroposelective oxidative biaryl coupling reactions. In combination, these transformations permitted access to all the stereoisomers of the perylenequinone natural products including variants not found in natural sources.

Common intermediate **13** could be prepared over five steps from the commercial compound **19** (Scheme 10.6) [69]. With the (*S*,*S*)-1,5-diaza-*cis*-decalin copper complex, the corresponding dimer (*M*)-**14** was generated with good yield and selectivity. A subsequent single trituration provided >99% ee bisiodide (*M*)-**14**. Installation of the stereogenic 2-hydroxypropyl group was achieved by epoxide ring opening via an organocuprate. Alternative methods to install the 2-hydroxypropyl groups via diastereoselective diketone reduction or asymmetric methylation of a dialdehyde provided low yields and selectivities [68]. Although many reported cuprate-mediated epoxide alkylation reactions are known, no examples with such highly complex substrates, especially involving dianions, have been disclosed. By screening, conditions for the epoxide ring-opening reactions with various highly functionalized biaryl systems were identified allowing either stereochemistry of the 2-hydroxypropyl group to be introduced in the presence of the C3,C3′ esters [71]. Subsequent steps, featuring C5 functionalization, mild decarboxylation, oxidative cyclization, and selective demethylation with MgI_2, provided both *ent*-calphostin D (*ent*-**8**) and *ent*-phleichrome (*ent*-**9**) in ~5% overall yield (total 17 steps).

In contrast to calphostin and phleichrome which are atropisomerically stable, no synthetic efforts had been published with respect to cercosporin which is characterized by a low atropisomerization barrier. Half-life studies revealed that the

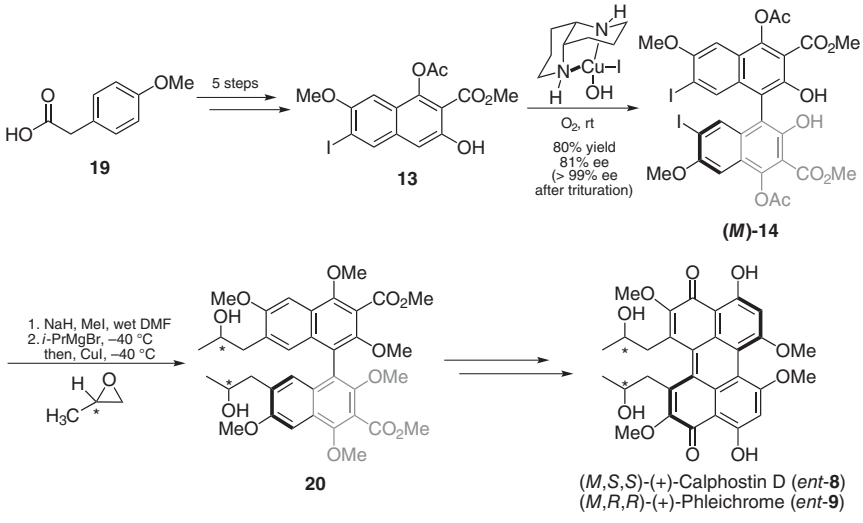

Scheme 10.6 Synthesis of *ent*-calphostin D and *ent*-phleichrome.

large substituent at the C7,C7′ positions in calphostin and phleichrome protected them from axial chiral bond isomerization [68]. The methylene bridge present in the seven-membered ring of cercosporin, however, produces additional strain resulting in a lower atropisomerization barrier. In order to determine the contributions of each of the structural elements to the atropisomerization barrier, measurements were made for the compounds in Table 10.5. A simple binaphthyl **21** containing the seven-membered ring found in cercosporin is quite stable even at 60 °C. In contrast, the strain of the perylenequinone as in *ent*-**8** caused a greater lowering of the barrier. Analysis of cercosporin (**10**) itself shows that an extended reaction time at 60 °C would cause atropisomerization. Based on this data, a route was selected that delayed formation of the greatest contributor to atropisomeric instability (the perylenequinone core) to as late as possible. In addition, any reactions after formation of both the perylenequinone core and the seven-membered ring needed to be as mild as possible.

With the common intermediate **13**, axial chiral dimer **(*M*)-14** was prepared by means of copper-catalyzed asymmetric oxidative coupling reaction (Scheme 10.7). Epoxide ring opening installed the appropriate stereochemistry of the propyl chain on both rings. Subsequent debenzylation of the more labile benzyl ethers at the C2,C2′ positions occurred with excellent selectivity. Formation of the seven-membered ring of **23** was accomplished by employing bromochloromethane as an optimal methylene source, which balances leaving group ability and steric size. The formation of the pentacycle could thus be reserved as late as possible. Subsequent removal of the methoxycarbonyl, oxidation, and directed demethylation accomplished the first total synthesis of cercosporin (**10**) [68, 70].

The hypocrellin family of the perylenequinone natural products is differentiated from others by an unsymmetrical seven-membered carbocyclic ring containing two stereocenters. In this system, atropisomerization occurs rapidly at room temperature complicating the assignment of the structures. For example, there are four possible isomeric forms for hypocrellin A arising from rapid enol–keto tautomerism and a low atropisomerization barrier (Figure 10.4) [72].

Table 10.5 Selected examples of atropisomerization barrier and half-lives.

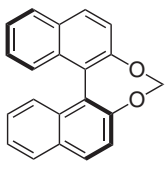	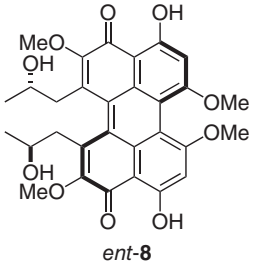	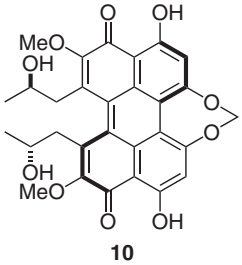
21	*ent*-**8**	**10**
$\Delta G^{\ddagger}$ = 33 kcal/mol $t_{1/2}$ = 13.7 y at 60 °C	$\Delta G^{\ddagger}$ = 30.2 kcal/mol $t_{1/2}$ = 75 d at 60 °C	$\Delta G^{\ddagger}$ = 27.4 kcal/mol $t_{1/2}$ = 25 h at 60 °C

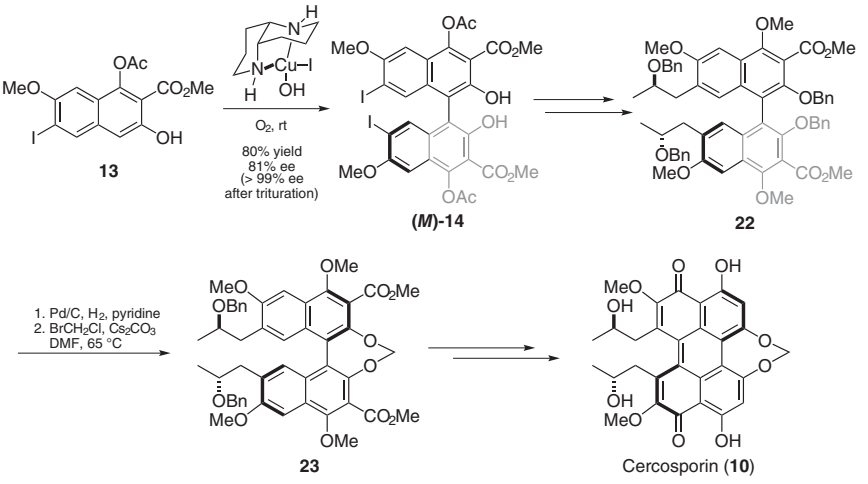

Scheme 10.7 Total synthesis of cercosporin.

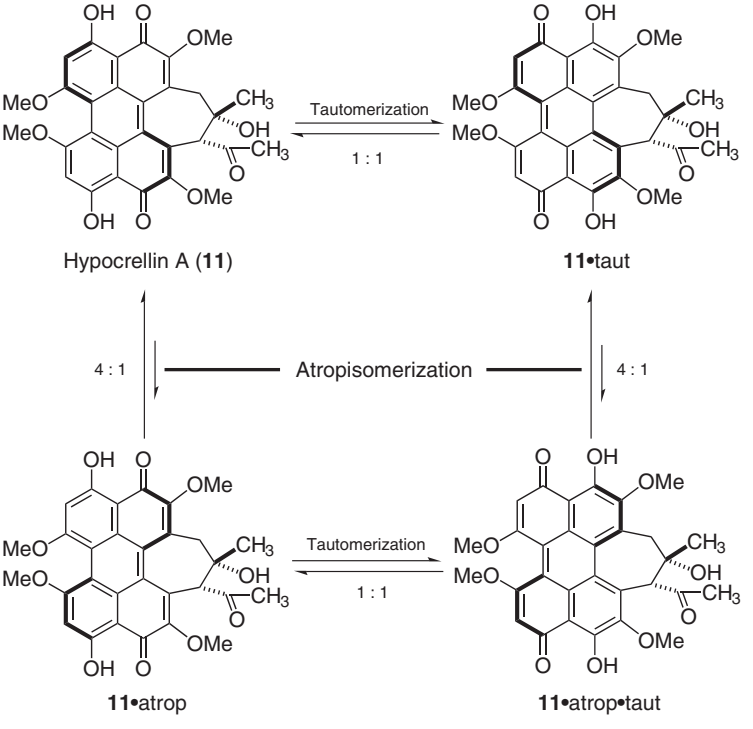

Figure 10.4 Equilibrating isomers of hypocrellin A.

The approach taken toward hypocrellin A focuses on generation of stable helical stereochemistry first, which would then direct the formation of the sp^3-hybridized stereocenters. However, formation of the seven-membered ring containing these stereocenters would dramatically lower the atropisomerization barrier essentially ablating the original helical stereochemistry. Thus, a "dynamic stereochemistry transfer" was envisioned. In turn, the required helical stereochemistry would be derived from an axial chiral structure using the enantioselective oxidative coupling pathway as described above. In contrast to other perylenequinone natural products, hypocrellin A exhibits the opposite helical stereochemistry (*P*). Thus, the opposite enantiomer of the copper catalyst was employed, namely the (*R,R*)-1,5-diaza-*cis*-decalin copper complex, under an oxygen atmosphere to afford **(*P*)-14** (Scheme 10.8). Suzuki–Miyaura cross-coupling, in turn, installed allyl groups at the C7,C7′ positions. Wacker oxidation converted the allyls to ketones, which were protected as ketals. Instead of using a conventional aromatic decarboxylation reaction that requires temperatures up to 180 °C and would isomerize the chiral axis, a palladium-assisted decarboxylation developed by Kozlowski group was used to remove the ester groups without atropisomerization. Subsequent debenzylation of **25** and MnO_2 oxidation provided the core pentacyclic system. Based on computational modeling, the *Z*-enolate system was predicted to access the final seven-membered ring equipped with the correct relative and absolute

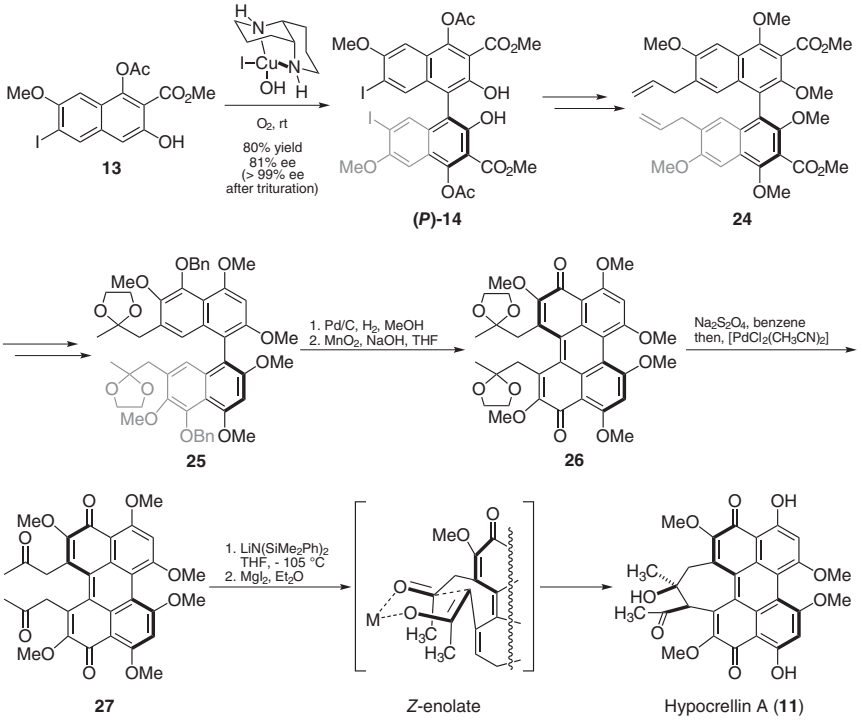

Scheme 10.8 Total synthesis of hypocrellin A (**11**).

stereochemistry. Indeed, an aldol reaction mediated by lithium disilazide did afford the desired natural product **11** as a major product [69, 72].

10.2.3 Bisoranjidiol

Myriad bisanthraquinone natural products have been found and isolated (Figure 10.5) [73, 74]. The bisanthraquinone dimers are known for their biological activities against bacteria, diabetes, depression, and more [75–78]. (*S*)-Bisoranjidiol (**30**) is differentiated from other bisanthraquinone natural products, by the lack of C4,C4′ substitution. In addition, it has methyl substituents at the C6, C6′ positions and no substituents at the C7, C7′ positions of distal ring. This unique axial chiral dimer acts as a photosensitizer by generating singlet oxygen in the presence of light [79].

In 2012, the Kozlowski group reported the first stereoselective total synthesis of (*S*)-bisoranjidiol (**30**) and its derivatives [80]. Direct oxidative coupling of the anthraquinone monomers proved intractable due to the high oxidation potential of these systems. As such a different retrosynthetic analysis of **30** was proposed where the additional aromatic ring would be prepared via a nonbiomimetic [4 + 2]-cycloaddition followed by aromatization (Scheme 10.9). Enantioselective oxidative coupling to form bisnaphthylene **32** with an axial chiral bond would require monomer **33** with C8-oxygenation that would allow subsequent oxidation to a bisnaphthoquinone.

After screening enantioselective oxidative coupling conditions with various monomers, the 8-benzyloxy-substituted monomer **34** was found to produce the axial chiral dimer **35** in good yield and enantioselectivity when a (*R*,*R*)-1,5-diaza-*cis*-decalin copper catalyst was employed (Scheme 10.10). A single trituration provided an enantiomerically pure **35** (>99% ee) and the following steps, including decarboxylation and debenzylation, provided 8,8′-dihydroxy biaryl compound **36**. Selective oxidation at C5,C5′ could be achieved by Co-salen complex catalyst under oxygen atmosphere without loss of enantiopurity. One of the most

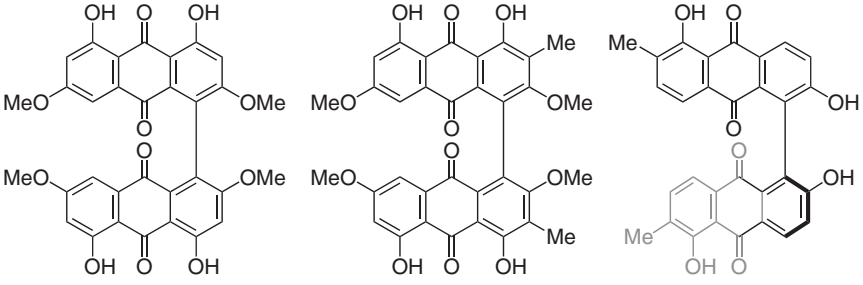

Figure 10.5 Representative bisanthraquinone natural products.

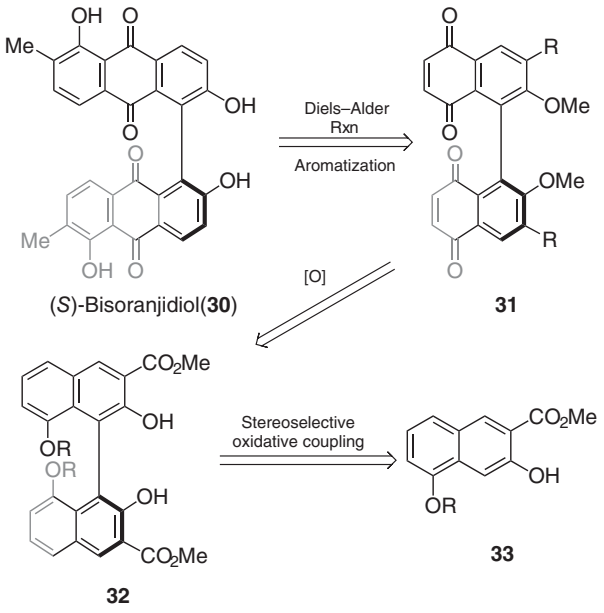

Scheme 10.9 Retrosynthesis of (*S*)-bisoranjidiol (**30**).

challenging steps of the synthesis was the regioselective Diels–Alder cycloaddition reaction. To control the regioselectivity, both Lewis acid-assisted cycloaddition and a halogen-directed approach were explored. Although good regioselectivity could be obtained from the Lewis acid route, decomposition and byproduct formation resulted in low yields. Selective halogen-directed cycloaddition reactions are known between vinyl ketene acetals and *para*-quinones [81–83]. With dibrominated compounds **38a**, [4 + 2]-cycloaddition with diene **39** afforded the desired "out–out" product **40** after aromatization over silica in moderate yield. Final demethylation provided the axial chiral (*S*)-bisoranjidiol successfully. An evaluation of atropisomeric stability of **30** showed that the enantiomeric excess of **30** eroded from >99% to 71% after 26 days corresponding to a half-life of 3.8 months in MeOH [84].

10.3 Vanadium-Catalyzed Asymmetric Oxidative Coupling to Construct a Chiral Axis

10.3.1 Viriditoxin

The natural product viriditoxin (**41**) possesses a core structure consisting of a 6,6′-binaphthopyran-2-one. This compound has garnered attention due to its pronounced ability to inhibit bacterial cell division by disrupting protein–membrane interactions and reducing membrane permeability [85, 86]. Notably, only

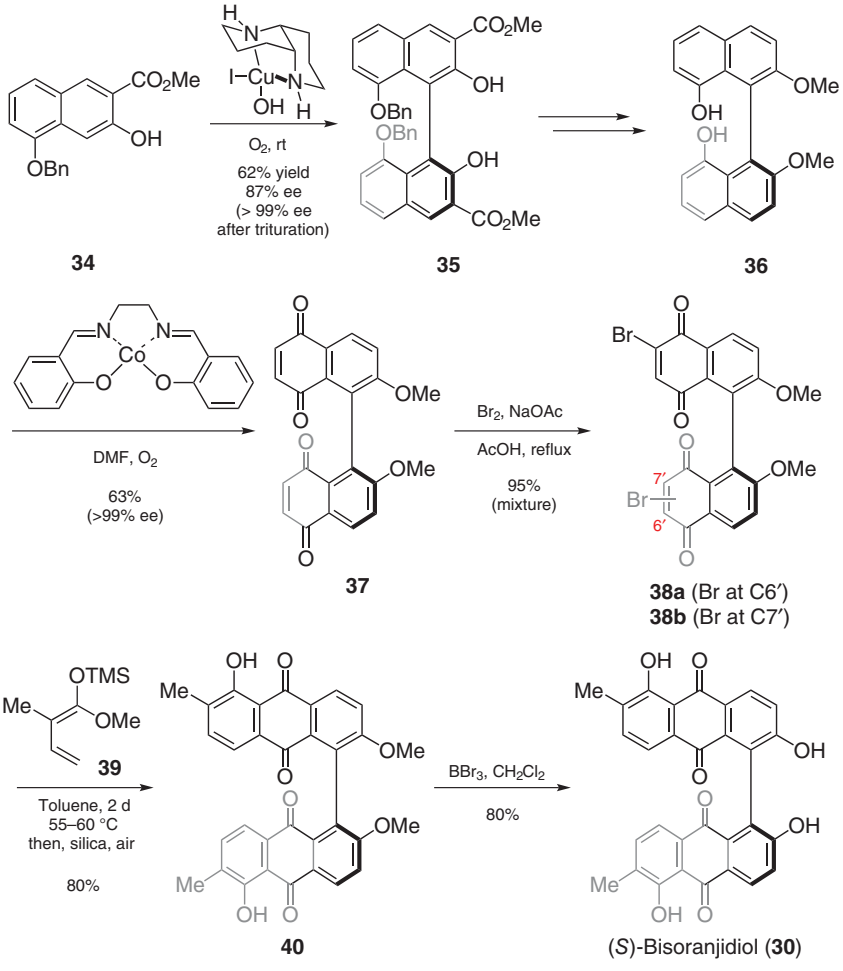

Scheme 10.10 Total synthesis of (*S*)-bisoranjidiol (**30**).

four structurally relevant natural products are known to feature the 6,6′-binaphthopyran-2-one motif (Figure 10.6).

In 2011, the Shaw group introduced the first synthetic approach to viriditoxin, utilizing a vanadium-catalyzed asymmetric biaryl ring-forming reaction [87]. The proposed retrosynthetic pathway involves the preparation of the target bis-naphthopyran compound through formation of the axial chiral bond by oxidative dimerization of monomer **45** (Scheme 10.11). The core tricyclic ring, including the central chirality at the C3 position, could be synthesized from poly-substituted aryl **46** and chiral pyranone **47** via a sequence of Michael addition and Dieckmann condensation reactions.

The stereoselective synthesis of viriditoxin (**41**) is outlined in Scheme 10.12a. Enantiomerically pure pyranone **49** was obtained from secondary alcohol **48** in four established steps [88, 89]. Employing a 1,4-conjugate addition poly-substituted

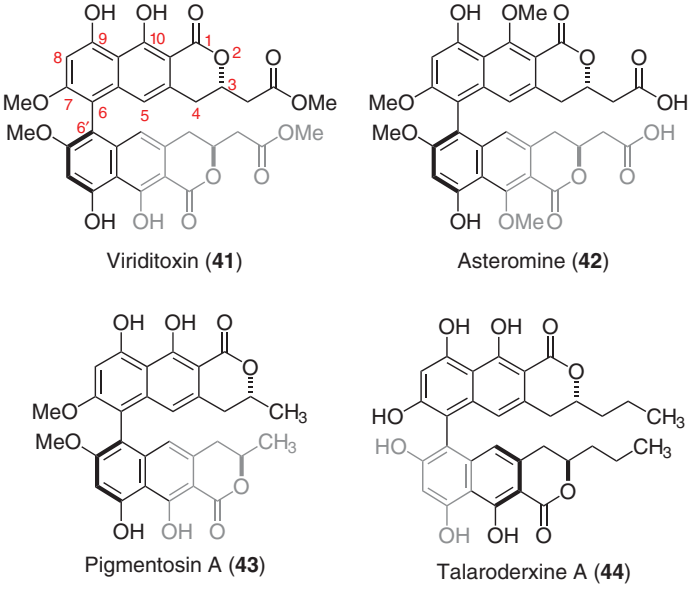

Figure 10.6 6,6′-Binaphthopyran-2-one natural products.

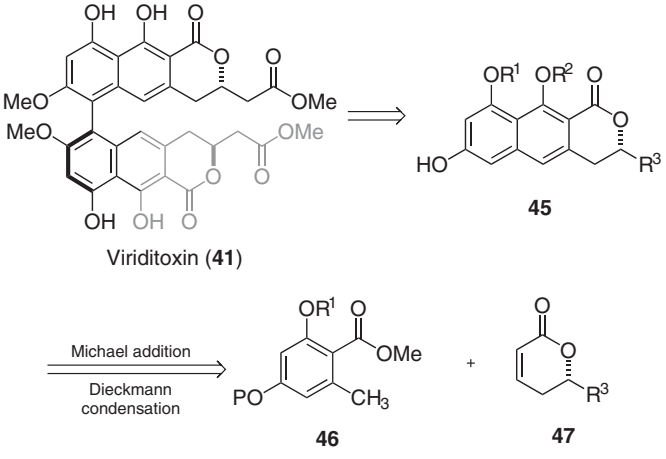

Scheme 10.11 Retrosynthesis of viriditoxin (**41**).

aryl **50** to pyranone **49** followed by a Dieckmann condensation protocol led to the formation of the viriditoxin core tricycle **51** with a good yield. Subsequent deprotection of the ethoxymethyl ether in the presence of propylene glycol paved the way for the vanadium-catalyzed oxidative coupling of **52**. Anticipating that the distal central chirality could guide the differentiation of the axial chiral bond via the less sterically hindered transition state **A**, favoring *M*-helicity dimer as the major product (Scheme 10.12b), Shaw and coworkers successfully achieved the desired **53a** in a 76 : 24 diastereomeric ratio (Scheme 10.12a). Consequently, the final

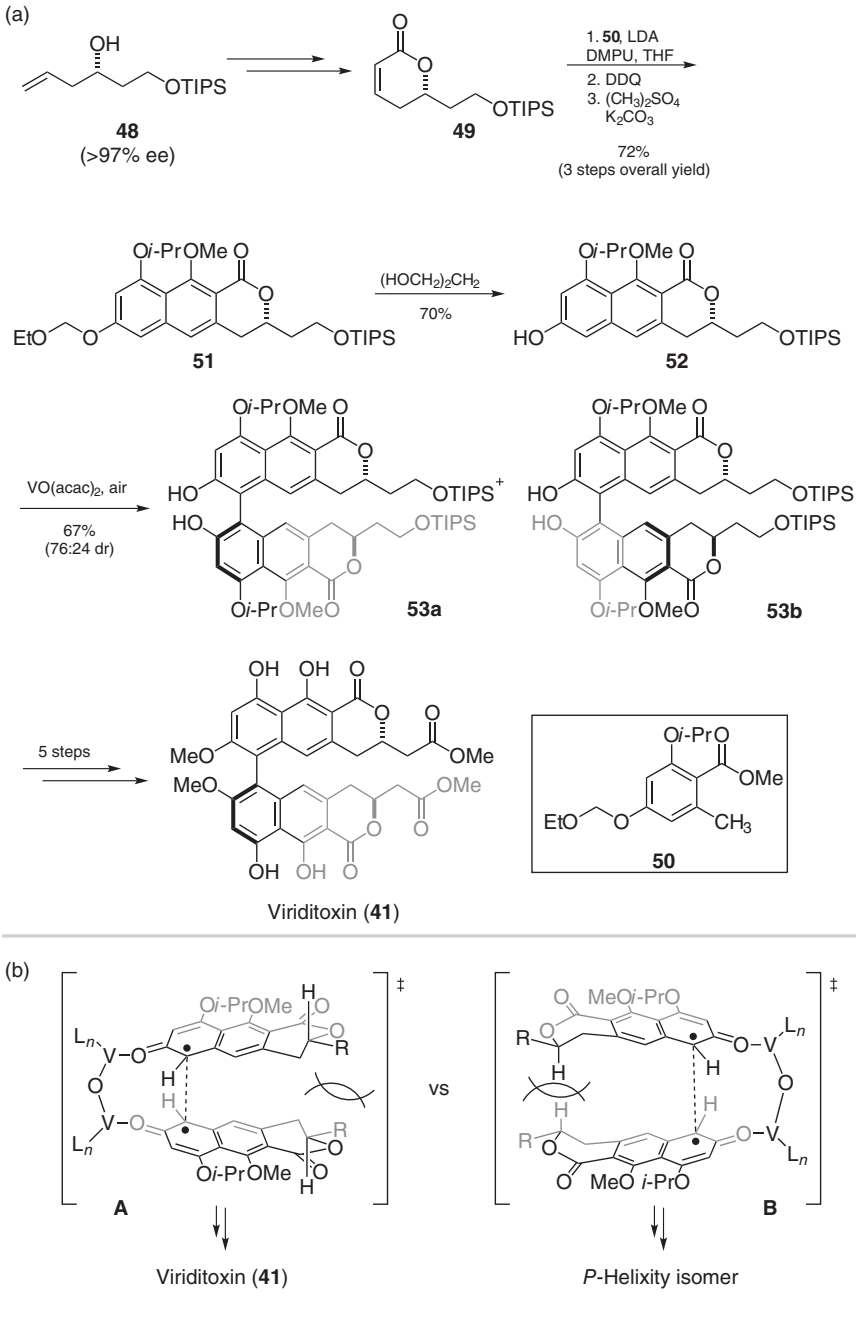

Scheme 10.12 (a) Stereoselective total synthesis of viriditoxin (**41**) and (b) substrate-controlled asymmetric induction.

Table 10.6 Diastereoselective oxidative coupling with bisvanadium catalysts.

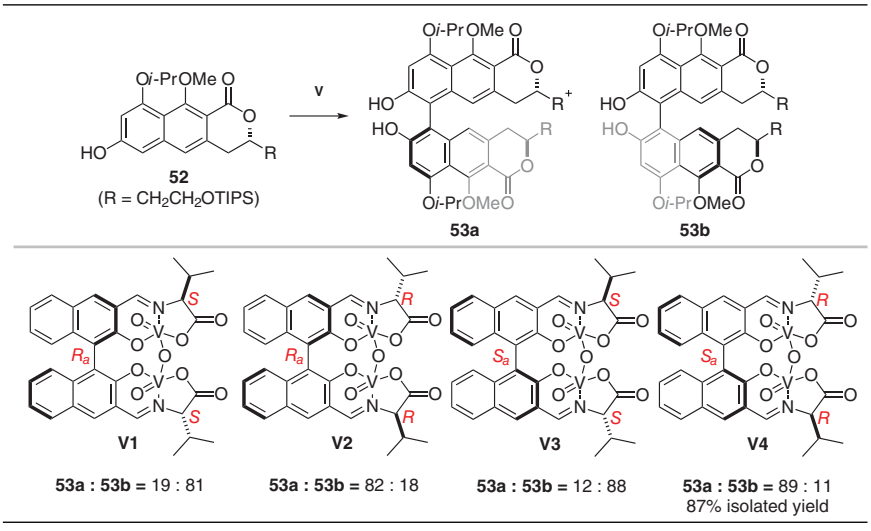

natural product **41** could be synthesized within five steps from **53a**. This observed diastereoselectivity marked one of the highest levels of stereoselection induced by a remote chiral center.

Further enhancements in diastereoselectivity were pursued using chiral bisvanadium catalysts, specifically the Gong-type catalysts (Table 10.6). Notably, the oxidative coupling with these catalysts revealed that the axial chiral information was controlled by amino acid portion of the catalyst. While (*S*)-configuration amino acids produced the predominant formation of the opposite axial chiral isomer **53b** (Table 10.6, **V1** and **V3**), the (*R*)-configured catalysts ensured the production of the desired axial chiral dimer **53a** with an improved stereoselectivity (Table 10.6, **V2** and **V4**) over the substrate with an achiral vanadium catalyst (see Scheme 10.12a). It is noteworthy that catalysts featuring axial (*S*)-configuration (**V3** and **V4**) exhibited slightly superior stereoselection compared to their counterparts (**V1** and **V2**).

In 2012, the Shaw group presented a second-generation synthesis of viriditoxin (**41**) [90]. They focus on devising more efficient synthetic pathways that are less toxic and amenable to scalability. For example, they replaced the use of a toxic allyl tin reagent to prepare compound **48** with epoxide-opening methods, which provided the same intermediate with higher yields in an environmentally friendly process [91, 92]. Furthermore, the protecting group was changed from triisopropylsilyl (TIPS) to *tert*-butyldiphenylsilyl (TBDPS). This modification not only led to improved overall yields but also enhanced diastereoselectivity (>95 : 5), while maintaining similar yields.

10.3.2 Sorazolon E2

In 2017, Sasai and co-workers unveiled a concise synthesis of (+)-sorazolon E2 [93], a hydroxycarbazole dimer that has antibacterial properties and cytotoxicity against fibroblast cell lines [94, 95]. The formation of sorazolon E2 (**54**) was achieved through an asymmetric vanadium-catalyzed oxidative coupling of sorazolon E (**55**), as depicted in Scheme 10.13. To create the highly substituted hydroxycarbazole, cyclohexanone **56** was utilized in a condensation and aromatization process with the corresponding aniline **57**.

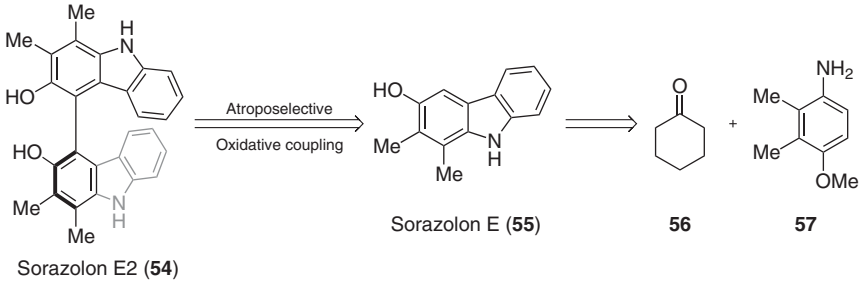

Scheme 10.13 Retrosynthetic analysis of (+)-sorazolon E2 (**54**).

The investigation of the monomeric hydroxycarbazole natural product **55** focused on a more efficient method toward its construction (Scheme 10.14). Despite multiple endeavors by several research group to synthesize sorazolon E (**55**) [96–101], prior approaches encountered notable challenges, including the reliance on toxic reagents such as $Hg(OAc)_2$ and $Tl(TFA)_3$, as well as the use of long synthetic pathways, up to eight steps. However, the Sasai group offered a novel solution by unveiling a concise two-step access to the highly substituted hydroxycarbazole using a one-pot protocol. Specifically, they developed a strategy involving condensation and aromatization processes in the presence of $Pd(OAc)_2$ and excess $Cu(OAc)_2$, resulting in a 60% yield of carbazole **58**. Upon demethylation, sorazolon E (**55**) was obtained with a high yield of 90%. Harnessing hydroxycarbazole **55**, the asymmetric oxidative coupling of hydroxycarbazole was evaluated using both monovanadium catalyst (**V5**) and bis-vanadium catalyst (**V6**). Despite similar levels of reactivity observed with both catalysts in producing the dimeric hydroxycarbazole, the asymmetric induction patterns revealed that only the dimeric vanadium catalyst (**V6**) exhibited promising levels of stereoselectivity. Notably, a single recrystallization provided highly enantiomerically pure sorazolon E2 (**54**) with 90% ee.

10.3.3 Chaetoglobin A

Chaetoglobin A (**62**), a naturally abundant azaphilone compound, features a chiral axis between the identical highly oxygenated bicyclic cores, along with quaternary chiral centers (Figure 10.7). Known for its inhibition of both colon

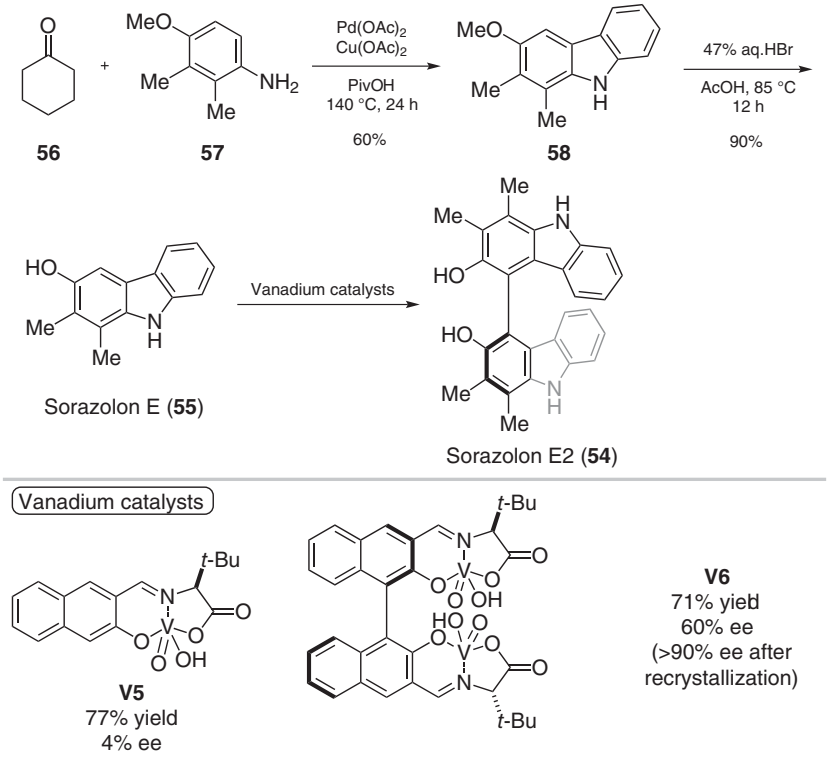

Scheme 10.14 Approaches to synthesize sorazolon E (**55**) and (+)-sorazolon E2 (**54**).

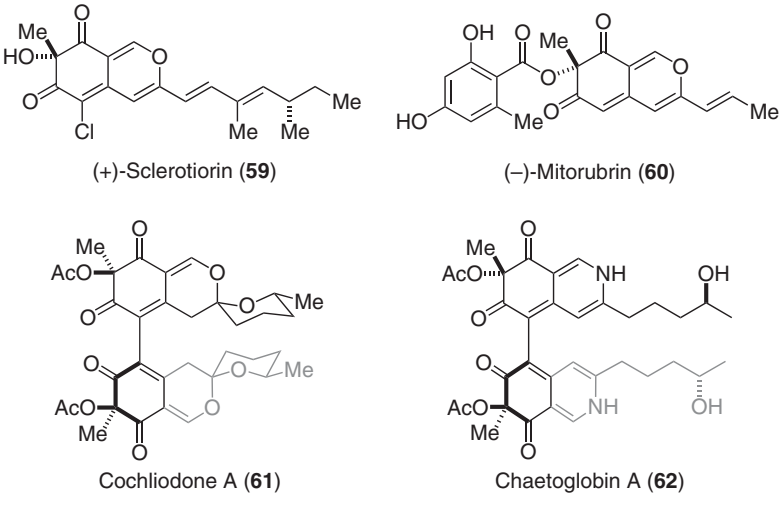

Figure 10.7 Azaphilone natural products.

cancer and breast cancer cell lines, the unique structural features of this compound have drawn significant attention [102]. Despite numerous reported azaphilone syntheses [103], the synthesis of dimeric azaphilones remained unexplored until 2018. The Kozlowski group undertook the total synthesis of azaphilone dimer, chaetoglobin A (**62**), employing a vanadium-catalyzed oxidative coupling method to introduce an axial chiral bond [104].

The retrosynthetic route to chaetoglobin A (**62**) involved the transformation of bis-formylated **63** through oxidative dearomatization and subsequent amination reactions (Scheme 10.15). The formation of dimeric compound **63** would stem from the asymmetric oxidative coupling of phenol **64**, followed by Vilsmeier–Haack formylation. The coupling of iodoaryl **65** with terminal alkyne **66** via a Sonogashira coupling reaction would provide monomer **64**.

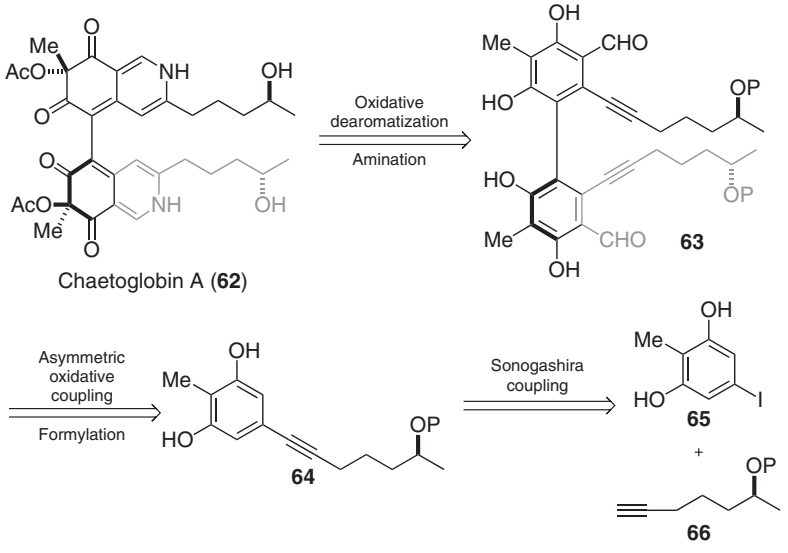

Scheme 10.15 Retrosynthetic analysis of chaetoglobin A (**62**).

The initial task was to identify the optimal phenol for introducing the axial chiral bond through oxidative coupling. The Kozlowski group found that the monomeric vanadium catalyst **V7** successfully facilitated the production of axial chiral bonds between resorcinols, providing good yields and selectivity [60, 61]. Subsequently, under optimal conditions, various oxidative coupling candidates were assessed for asymmetric phenol coupling (Table 10.7). Halogen-substituted compounds **67** and **68**, unfortunately, suffered from both low reactivity and poor enantioselectivity. In contrast, phenol **69**, incorporating a long-chain structure with an internal alkyne, generated axial chiral bisphenol with good yield and enantioselectivity.

The Sonogashira coupling partners **65** and **66** were synthesized in four steps from commercial sources [105–108]. Monomer **71** was obtained with quantitative yield

Table 10.7 Vanadium-catalyzed oxidative coupling of phenols.

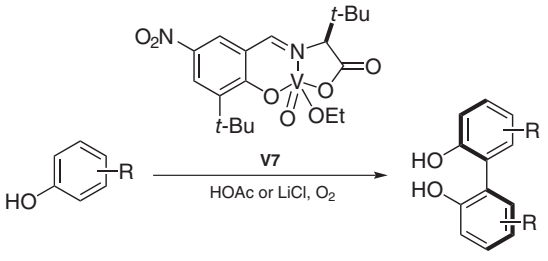

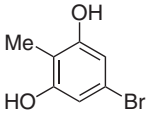

67
24% yield
20% ee

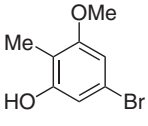

68
12% conversion
47% ee

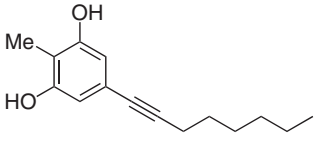

69
66% yield
89% ee

via a Sonogashira coupling reaction (Scheme 10.16). The diastereoselective oxidative phenol coupling, controlled by the catalyst, yielded the chiral axis with superior selectivity, exceeding a >15 : 1 dr, along with good yields. Notably, the addition of either HOAc or LiCl was found to enhance the selectivity, boosting the dr from 4 : 1 to >15 : 1. This enhancement was attributed to increased activation of the vanadium catalyst and a bridging effect between vanadium centers, which was thermodynamically favored by 7.5 kcal/mol, as supported by calculations [61]. Sequential Vilsmeier–Haack formylation, a modified oxidative dearomatization developed by the Porco group [109, 110], and acetylation led to the formation of the highly oxygenated bicyclic **73**. Due to the stability of the dimeric compound **73**, achieving selective deacetylation was a challenge. Among various hydrolysis conditions, an excess of $Ti(O\textit{i}\text{-}Pr)_4$ proved effective in generating the product with good yield and reproducibility. The final amination reaction provided the target natural product **62** in 96% yield.

10.3.4 Gonytolide A

Chromanone natural products, isolated from the fungus *Gonytrichum* sp., have been recognized as immune regulators (Figure 10.8) [111, 112]. These compounds influence responses to conditions like infectious diseases and cancer [113, 114]. Within the realm of chromanones, a distinct dimeric type prevails: the *para-para* coupled axial chiral chromanone. Notably, the synthesis of one such compound, gonytolide A (**74**), was unveiled via substrate-controlled oxidative coupling method by the Porco group in 2018 [115].

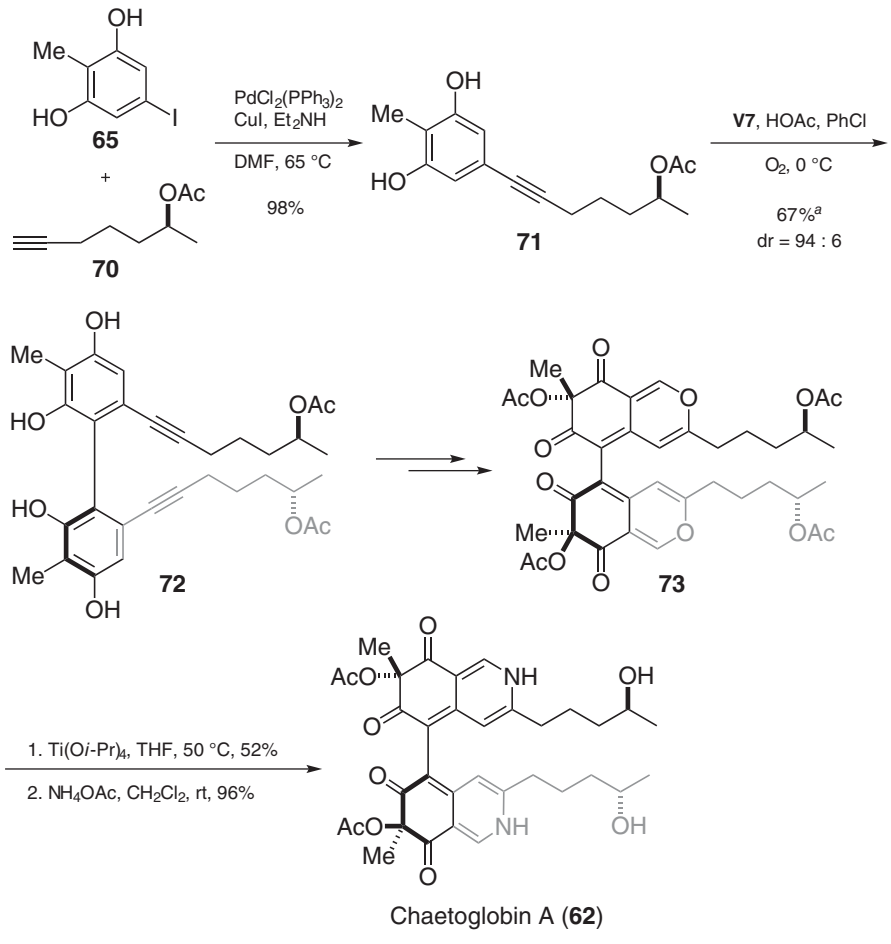

[a]Isolated yield based on recovery of substrate

Scheme 10.16 Total synthesis of chaetoglobin A (**62**).

Retrosynthetically, the oxidative coupling of **78** serves to introduce a chiral axis at the *para*-position relative to the phenol, the sole reactive site available (Scheme 10.17). To derive diastereomerically pure monomer **78**, two paths are feasible. One involves the dynamic kinetic resolution during asymmetric bromination of racemic gonytolide C (**76**), while the other entails an asymmetric conjugated reduction followed by bromination of diastereomerically pure **76**. The synthesis of monomeric chromanone natural product **76** can be prepared by conjugate addition between **79** and furan **80**.

The initial task for the synthesis was to refine the vinylogous addition reactions, a process previously developed by the same group in 2011 [116]. Previous studies had yielded a mixture of two diastereomers. After comprehensive investigation into the process, the mechanism outlined in Scheme 10.18 was proposed. The presence of silyl triflate activates chromone **79** to form benzopyrylium salt **81**. The combination

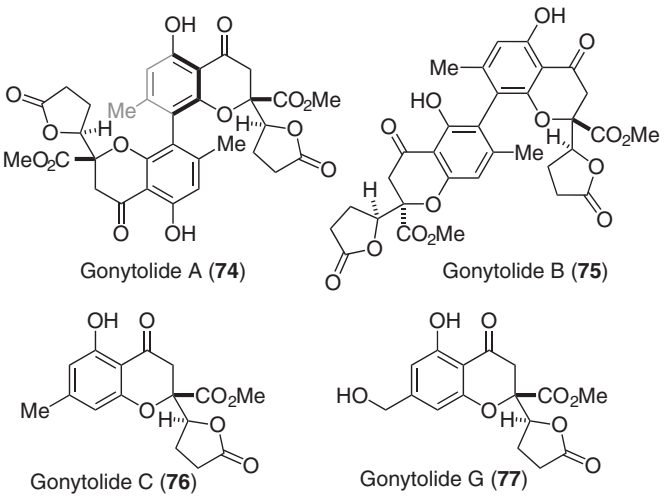

Figure 10.8 Monomeric and dimeric chromanones.

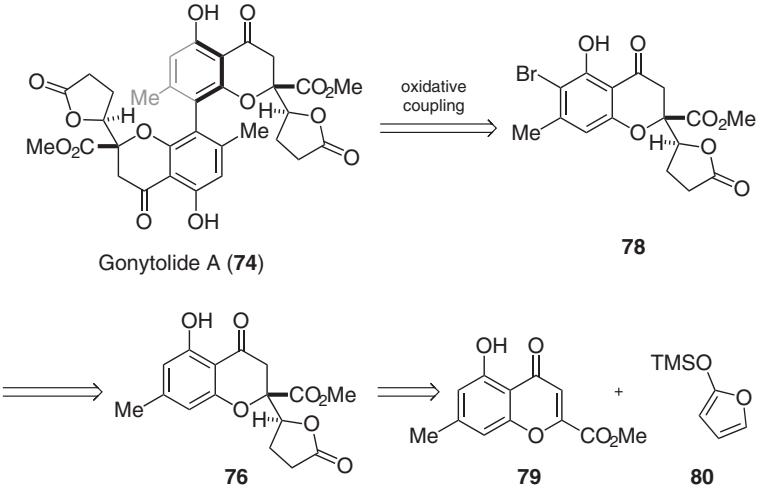

Scheme 10.17 Retrosynthesis of gonytolide A (**74**).

between benzopyrylium **81** and 2-siloxyfuran **80** generates two diastereomers. The diastereomeric ratio was determined by the reaction conditions, favoring kinetic product **82a** at lower temperatures. Subsequent desilylation and conjugate reduction gives the corresponding product **84**. On the other hand, elevated reaction temperatures promote the formation of thermodynamic product **82b**, resulting in the preparation of gonytolide C (**76**). Following rigorous screening of conditions, the desired **76** was predominantly obtained with a 3 : 1 diastereomeric ratio at 0 °C in CH_2Cl_2.

In pursuit of a diastereomerically pure monomer for the oxidative coupling, the first step involved testing asymmetric bromination using various known conditions

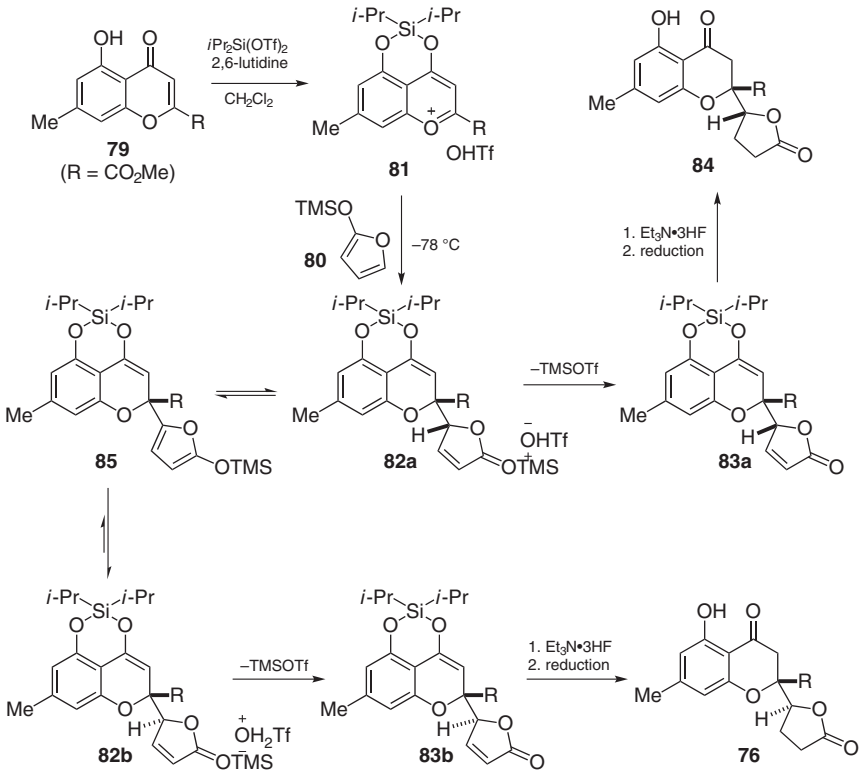

Scheme 10.18 Proposed mechanism of vinylogous addition to form diastereomers.

[26, 117–121]. Unfortunately, these attempts were unsuccessful in producing the desired brominated product. Instead, they resulted in the enantiomer, as well as a regioisomer from bromination at the *para*-position, leading to a mixture of dibrominated compounds. Consequently, Porco and coworkers opted to revise their initial strategy and pursue a diastereomerically pure monomer through asymmetric conjugate reduction of **85** (Scheme 10.19). Taking advantage of a well-established kinetic resolution by asymmetric reduction [122, 123], diastereomerically pure (+)-gonytolide C (**76**) was obtained with high stereoselectivity. Further recrystallization yielded **(+)-76** with a 94% enantiomeric excess, while bromination provided the corresponding *ortho*-brominated **(+)-86** without erosion of the enantiomeric excess. With the *ortho*-blocked monomer **(+)-86**, the oxidative coupling reaction was conducted with VOF_3 as a catalyst. Relative to numerous known oxidative coupling conditions, including those using Fe, Cr, Cu, Mn, Mo, V catalysts/reagents or electrochemical methods, it was found that VOF_3 under acidic media gave the most promising outcomes. With the optimized oxidative conditions, the substrate-controlled oxidative coupling of **(+)-86** provided a mixture of two atropoisomers, (+)-gonytolide A (**74**) and (+)-*atrop*-gonytolide A (***atrop*-74**). A noteworthy observation from their work was the pivotal role played by bromine. Not only did it block another active site for oxidative coupling but

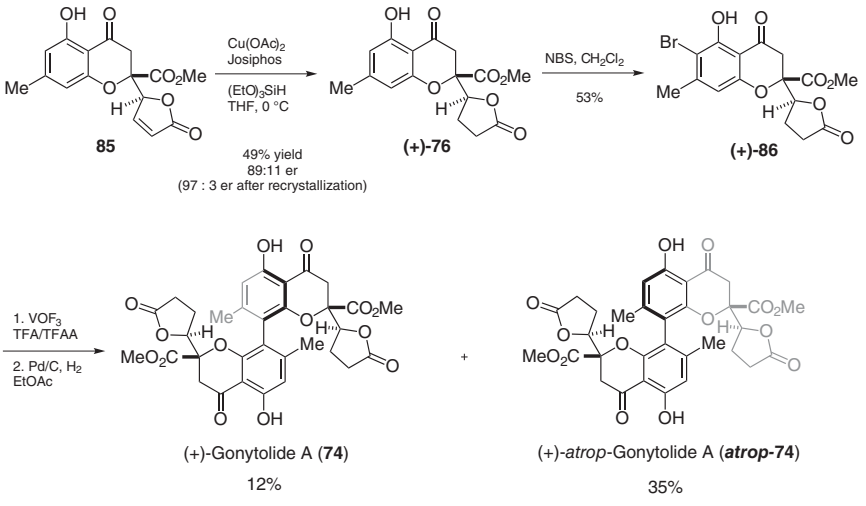

Scheme 10.19 End game of gonytolide A (**74**) synthesis.

it also demonstrated a stabilizing effect on radical species during the oxidative coupling reaction.

10.4 Enzymatic Strategies to Synthesize Natural Products *via* Atroposelective Coupling

10.4.1 Kotanin

While a plethora of chemical transformations enabling atroposelective coupling have been developed, the realm of biocatalysts capable of regio- and stereoselective coupling for constructing axial chiral bonds is nascent. Among these, the cytochrome P450 enzyme, renowned for its role in biosynthesizing several isoquinoline alkaloids [124], has emerged as a notable candidate for effectively establishing a chiral axis between biaryl scaffolds. Recent work by the Narayan group highlighted the capabilities of the P450 enzyme. It not only facilitated the generation of native oxidative dimeric biaryl products in a site-selective and atroposelective manner but also produced non-native cross-coupled biaryl coumarins by tuning the stoichiometry (Table 10.8) [55]. Notably, the presence of C4 or C5 substitutions did not hinder the reactivity of the enzyme. Although the efficiency of cross-coupled product formation was influenced by electronic factors, the enzyme generated a diverse array of cross-coupled products (Table 10.8).

In 2012, the Müller group disclosed a breakthrough involving the gene cluster *Aspergillus niger* FGSC A1180, capable of orchestrating the regio- and stereoselective biosynthesis of kotanin (**93**) (Figure 10.9) [125]. Their investigations revealed that the biosynthetic pathway leading to kotanin (**93**) was initiated from phenol **88d** rather than **91**, as illustrated in Scheme 10.20. The step involved in the methylation of dihydroxycoumarin **94** by O-methyltransferase KtnB, providing

Table 10.8 Selective scope of P450 enzyme-catalyzed oxidative coupling reaction.

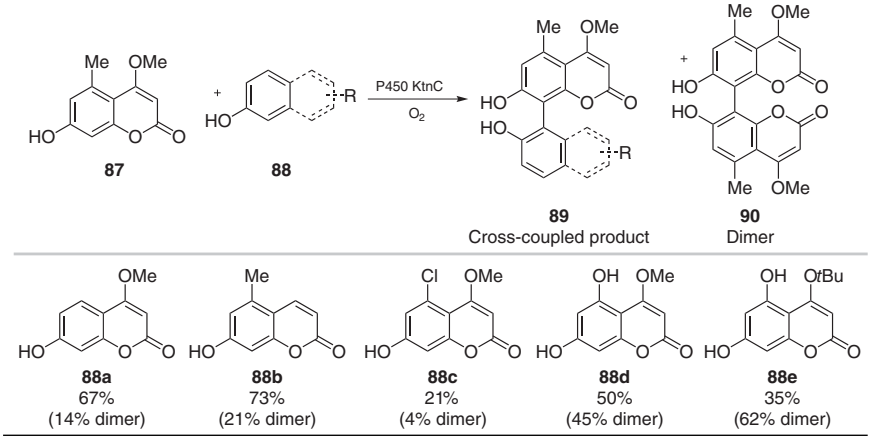

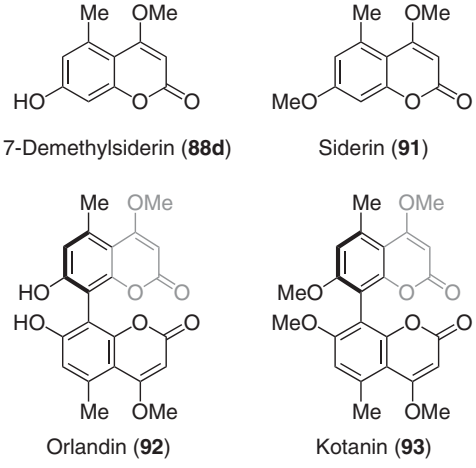

Figure 10.9 Coumarins and corresponding bicoumarin natural products.

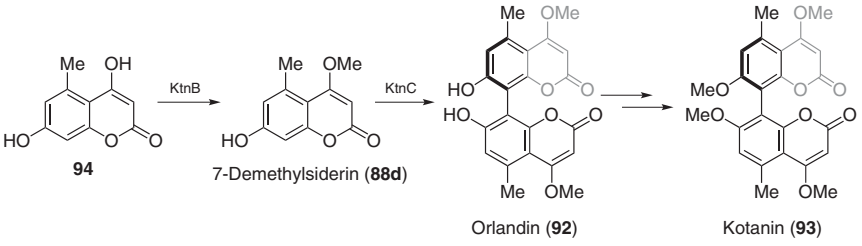

Scheme 10.20 Proposed biosynthetic pathway of kotanin (**93**).

7-demethylsiderin **(88d)**. Drawing upon their earlier findings, the presence of a methoxy group at C4 position was deemed essential for facilitating the oxidative coupling required for dimer formation [126]. The monooxygenase KtnC catalyzed the oxidative coupling of **88d**, yielding orlandin **(92)**, a hypothesis supported by docking experiments involving **88d** and the dimeric product **92**. Subsequent O-methylation events culminated in the formation of kotanin **93**.

10.4.2 Phlegmacins

Among the dihydroanthracenone dimers, the phlegmacins stand out as notable examples found in macromycetes (Figure 10.10) [127]. A captivating feature of phlegmacins is the presence of a chiral axis arising from an unsymmetrical coupling between the C7 and C10′ positions. Although there are a myriad of reported chemical oxidative coupling reactions, few are effective for achieving such regioselective unsymmetrical couplings.

In 2012, Lin and colleagues revealed the existence of a gene cluster comprising four proteins (*phl*A–D) responsible for the biosynthesis of phlegmacins, as determined through a bioinformatic analysis [128]. Notably, monomer **98** serves as a common biosynthetic precursor for the construction of anthraquinones such as emodin, cladofulvin, and skyrin (Scheme 10.21) [129–132]. Based on previous investigations, they postulated that the collaboration between PhlD and PhlA would furnish the trihydroanthraquinone **98** [129, 130, 132]. The oxidative coupling monomer **99** can be prepared by the methyltransferase AurJ. Utilizing a fasciclin domain-containing protein PhlB and a laccase PhlC facilitated the creation of unsymmetrical oxidative dimers, phlegmacin A1 (**94**) and B1 (**95**).

10.5 Conclusion

Asymmetric oxidative couplings allow access to a diverse array of axial chiral natural products. The evolution of atroposelective coupling methods, employing various strategies, has contributed to the synthesis of complex molecules.

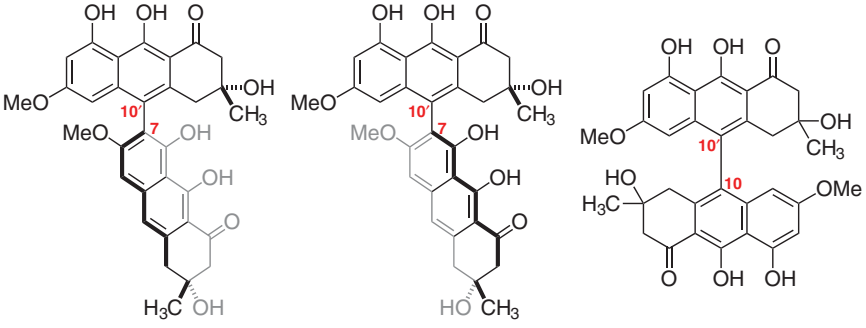

Figure 10.10 Representative bisdihydroanthracenone natural products.

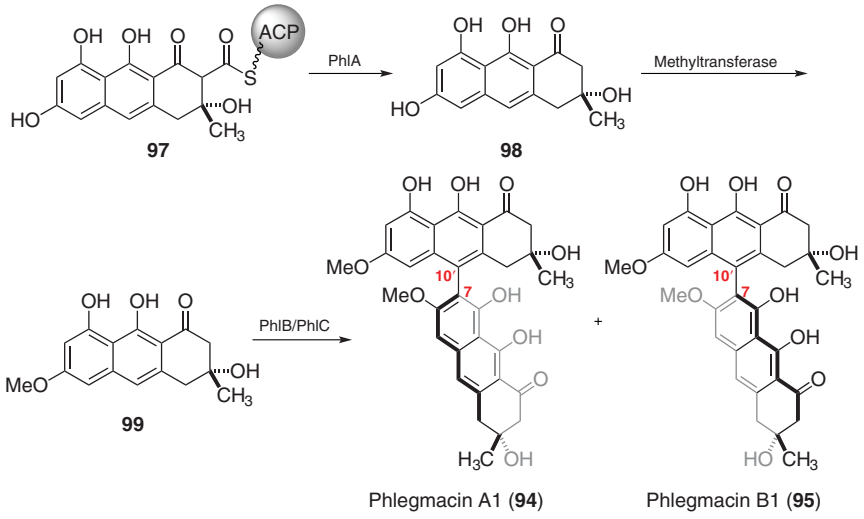

Scheme 10.21 Proposed biosynthetic pathway of phlegmacins.

Transition-metal-catalyzed asymmetric oxidative coupling reactions, combined with various oxidants, have demonstrated enhanced reactivity and selectivity. Among the diverse effective methods, specific attention has been given to copper- and vanadium-catalyzed methods in the synthesis of natural products. Notably, copper-mediated asymmetric oxidative couplings have utilized poly-substituted naphthols as coupling monomers [133]. In contrast, vanadium-catalyzed approaches have extended the utility beyond naphthol-type monomers to include monocyclic phenols for constructing axial chirality in natural product synthesis. The stereoselectivity of these processes arises from the interplay between asymmetric catalysts and any innate stereochemistry of substrates. Both catalysts and substrates can influence the stereochemical outcomes, leading to improved atroposelectivity. Enzymatic oxidative coupling strategies have emerged as an efficient means to construct axial chiral natural products, encompassing both symmetrical dimers and unsymmetrical coupling products, which is challenging to achieve through conventional chemical methods.

References

1 Kozlowski, M.C., Morgan, B.J., and Linton, E.C. (2009). Total synthesis of chiral biaryl natural products by asymmetric biaryl coupling. *Chem. Soc. Rev.* 38 (11): 3193–3207.

2 Bringmann, G., Gulder, T., Gulder, A.M.T., and Breuning, M. (2011). Atroposelective total synthesis of axially chiral biaryl natural products. *Chem. Rev.* 111 (2): 563–639.

3 Wang, N.-G., Zhou, L.-F., Guan, M.-H., and Lei, H.P. (1987). Effect of (−)- and (+)-gossypol on fertility in male rats. *J. Ethnopharmacol.* 20 (1): 21–24.

4 Band, V., Hoffer, A.P., Band, H. et al. (1989). Antiproliferative effect of gossypol and its optical isomers on human reproductive cancer cell lines. *Gynecol. Oncol.* 32 (3): 273–277.

5 Boyd, M.R., Hallock, Y.F., Cardellina, J.H. II, et al. (1994). Anti-HIV Michellamines from Ancistrocladus korupensis. *J. Med. Chem.* 37 (12): 1740–1745.

6 Francois, G., Timperman, G., Eling, W. et al. (1997). Naphthylisoquinoline alkaloids against malaria: evaluation of the curative potentials of dioncophylline C and dioncopeltine A against *Plasmodium berghei* in vivo. *Antimicrob. Agents Chemother.* 41 (11): 2533–2539.

7 Ponte-Cucre, A., Gulder, T., Wegehaupt, A. et al. (2009). Structure-activity relationship and studies on the molecular mechanism of leishmanicidal *N*,*C*-coupled arylisoquinolinium salts. *J. Med. Chem.* 52 (3): 626–636.

8 Lown, J.W. (1997). 1996 Hofmann-LaRoche award lecture photochemistry and photobiology of perylenequinones. *Can. J. Chem.* 75 (2): 99–119.

9 Chiarini, A., Whitfield, J.F., Pacchiana, R. et al. (2008). Photoexcited calphostin C selectively destroys nuclear lamin B1 in neoplastic human and rat cells – a novel mechanism of action of a photodynamic tumor therapy agent. *Biochim. Biophys. Acta* 1783 (9): 1642–1653.

10 Carmona, J.A., Rodriguez-Franco, C., Fernandez, R. et al. (2021). Atroposelective transformation of axially chiral (hetero)biaryls. From desymmetrization to modern resolution strategies. *Chem. Soc. Rev.* 50 (5): 2968–2983.

11 Cheng, J.K., Xiang, S.H., Li, S. et al. (2021). Recent advances in catalytic asymmetric construction of atropisomers. *Chem. Rev.* 121 (8): 4805–4902.

12 Yang, H., Sun, J., Gu, W., and Tang, W. (2020). Enantioselective cross-coupling for axially chiral tetra-ortho-substituted biaryls and asymmetric synthesis of gossypol. *J. Am. Chem. Soc.* 142 (17): 8036–8043.

13 Jia, Z.J., Merten, C., Gontla, R. et al. (2017). General enantioselective C-H activation with efficiently tunable cyclopentadienyl ligands. *Angew. Chem. Int. Ed.* 56 (9): 2429–2434.

14 Jang, Y.S., Wozniak, L., Pedroni, J., and Cramer, N. (2018). Access to P- and axially chiral biaryl phosphine oxides by enantioselective Cp(x) Ir(III)-catalyzed C-H arylations. *Angew. Chem. Int. Ed.* 57 (39): 12901–12905.

15 Newton, C.G., Braconi, E., Kuziola, J. et al. (2018). Axially chiral dibenzazepinones by a palladium(0)-catalyzed atropo-enantioselective C-H arylation. *Angew. Chem. Int. Ed.* 57 (34): 11040–11044.

16 Yan, S., Xia, W., Li, S. et al. (2020). Michael reaction inspired atroposelective construction of axially chiral biaryls. *J. Am. Chem. Soc.* 142 (16): 7322–7327.

17 Lipshutz, B.H., Kayser, F., and Liu, Z.-P. (1994). Asymmetric synthesis of biaryls by intramolecular oxidative couplings of cyanocuprate intermediates. *Angew. Chem. Int. Ed.* 33 (18): 1842–1844.

18 Meyers, A.I., Meier, A., and Rawson, D.J. (1992). A highly stereoselective synthesis of axially chiral biaryls. Application to the synthesis of a potential chiral catalyst. *Tetrahedron Lett.* 33 (7): 853–856.

19 Meyers, A.I. (1998). Chiral oxazolines – their legacy as key players in the renaissance of asymmetric synthesis. *J. Heterocyclic Chem.* 35 (5): 991–1002.

20 Meyers, A.I., Nelson, T.D., Moorlag, H. et al. (2004). Chiral oxazoline route to enantiomerically pure biphenyls: magnesio and copper mediated asymmetric hetero- and homo-coupling reactions. *Tetrahedron* 60 (20): 4459–4473.

21 Degnan, A.P. and Meyers, A.I. (1999). Total syntheses of (−)-herbertenediol, (−) Mastigophorene A, and (−)-Mastigophorene B. Combined utility of chiral bicyclic lactams and chiral aryl oxazolines. *J. Am. Chem. Soc.* 121 (12): 2762–2769.

22 Meyers, A.I. and Willemsen, J.J. (1998). An oxazoline based approach to (*S*)-gossypol. *Tetrahedron* 54 (35): 10493–10511.

23 Hayashi, T., Niizuma, S., Kamikawa, T. et al. (1995). Catalytic asymmetric synthesis of axially chiral biaryls by palladium-catalyzed enantioposition-selective cross-coupling. *J. Am. Chem. Soc.* 117 (35): 9101–9102.

24 Lu, S., Poh, S.B., Rong, Z.Q., and Zhao, Y. (2019). NHC-catalyzed atroposelective acylation of phenols: access to enantiopure NOBIN analogs by desymmetrization. *Org. Lett.* 21 (15): 6169–6172.

25 Munday, E.S., Grove, M.A., Feoktistova, T. et al. (2020). Isothiourea-catalyzed atroposelective acylation of biaryl phenols via sequential desymmetrization/kinetic resolution. *Angew. Chem. Int. Ed.* 59 (20): 7897–7905.

26 Mori, K., Ichikawa, Y., Kobayashi, M. et al. (2013). Enantioselective synthesis of multisubstituted biaryl skeleton by chiral phosphoric acid catalyzed desymmetrization/kinetic resolution sequence. *J. Am. Chem. Soc.* 135 (10): 3964–3970.

27 Zheng, J., Cui, W.J., Zheng, C., and You, S.L. (2016). Synthesis and application of chiral spiro Cp ligands in rhodium-catalyzed asymmetric oxidative coupling of biaryl compounds with alkenes. *J. Am. Chem. Soc.* 138 (16): 5242–5245.

28 Yao, Q.J., Zhang, S., Zhan, B.B., and Shi, B.-F. (2017). Atroposelective synthesis of axially chiral biaryls by palladium-catalyzed asymmetric C-H olefination enabled by a transient chiral auxiliary. *Angew. Chem. Int. Ed.* 56 (23): 6617–6621.

29 Wang, Q., Cai, Z.J., Liu, C.X. et al. (2019). Rhodium-catalyzed atroposelective C-H arylation: efficient synthesis of axially chiral heterobiaryls. *J. Am. Chem. Soc.* 141 (24): 9504–9510.

30 Romero-Arenas, A., Hornillos, V., Iglesias-Siguenza, J. et al. (2020). Ir-catalyzed atroposelective desymmetrization of heterobiaryls: hydroarylation of vinyl ethers and bicycloalkenes. *J. Am. Chem. Soc.* 142 (5): 2628–2639.

31 Shimada, T., Cho, Y.-H., and Hayashi, T. (2002). Nickel-catalyzed asymmetric Grignard cross-coupling of dinaphthothiophene giving axially chiral 1,1′-binaphthyls. *J. Am. Chem. Soc.* 124 (45): 13396–13397.

32 Zhao, K., Duan, L., Xu, S. et al. (2018). Enhanced reactivity by torsional strain of cyclic diaryliodonium in Cu-catalyzed enantioselective ring-opening reaction. *Chem* 4 (3): 599–612.

33 Li, Q., Zhang, M., Zhan, S. et al. (2019). Copper-catalyzed enantioselective ring-opening of cyclic diaryliodoniums and O-alkylhydroxylamines. *Org. Lett.* 21 (16): 6374–6377.

34 Zhu, K., Xu, K., Fang, Q. et al. (2019). Enantioselective synthesis of axially chiral biaryls via Cu-catalyzed acyloxylation of cyclic diaryliodonium salts. *ACS Catal.* 9 (6): 4951–4957.

35 Kina, A., Miki, H., Cho, Y.-H., and Hayashi, T. (2004). Palladium-catalyzed Heck and carbonylation reactions of a dinaphthaleneiodonium salt forming functionalized 2-iodo-1,1′-binaphthyls. *Adv. Synth. Catal.* 346 (13–15): 1728–1732.

36 Bringmann, G., Price Mortimer, A.J., Keller, P.A. et al. (2005). Atroposelective synthesis of axially chiral biaryl compounds. *Angew. Chem. Int. Ed.* 44 (34): 5384–5427.

37 Bringmann, G. and Hartung, T. (1992). First atropo-enantioselective ring opening of achiral biaryls containing lactone bridges with chiral hydride-transfer reagents derived from borane. *Angew. Chem. Int. Ed.* 31 (6): 761–762.

38 Bringmann, G. and Menche, D. (2001). First, atropo-enantioselective total synthesis of the axially chiral phenylanthraquinone natural products knipholone and 6′-O-methylknipholone. *Angew. Chem. Int. Ed.* 40 (9): 1687–1690.

39 Kim, K.H., Lee, D.-W., Lee, Y.-S. et al. (2004). Enantioselective oxidative coupling of methyl 3-hydroxy-2-naphthoate using mono-*N*-alkylated octahydrobinaphthyl-2,2′-diamine ligand. *Tetrahedron* 60 (41): 9037–9042.

40 Alamsetti, S.K., Poonguzhali, E., Ganapathy, D., and Sekar, G. (2013). Enantioselective oxidative coupling of 2-naphthol derivatives by copper-(*R*)-1,1′-binaphthyl-2,2′-diamine-TEMPO catalyst. *Adv. Synth. Catal.* 355 (14–15): 2803–2808.

41 Nakajima, M., Miyoshi, I., Kanayama, K. et al. (1999). Enantioselective synthesis of binaphthol derivatives by oxidative coupling of naphthol derivatives catalyzed by chiral diamine.copper complexes. *J. Org. Chem.* 64 (7): 2264–2271.

42 Li, X., Hewgley, J.B., Mulrooney, C.A. et al. (2001). Enantioselective oxidative biaryl coupling reactions catalyzed by 1,5-diazadecalin metal complexes: efficient formation of chiral functionalized BINOL derivatives. *Org. Lett.* 3: 1137–1140.

43 Tian, J.M., Wang, A.F., Yang, J.S. et al. (2019). Copper-complex-catalyzed asymmetric aerobic oxidative cross-coupling of 2-naphthols: enantioselective synthesis of 3,3′-substituted C(1)-symmetric BINOLs. *Angew. Chem. Int. Ed.* 58 (32): 11023–11027.

44 Nakajima, M., Kanayama, K., Miyoshi, I., and Hashimoto, S.-I. (1995). Catalytic asymmetric synthesis of binaphthol derivatives by aerobic oxidative coupling of 3-hydroxy-2-naphthoates with chiral diamine-copper complex. *Tetrahedron Lett.* 36 (52): 9519–9520.

45 Noji, M., Nakajima, M., and Koga, K. (1994). A new catalytic system for aerobic oxidative coupling of 2-naphthol derivatives by the use of CuCI-amine complex: a practical synthesis of binaphthol derivatives. *Tetrahedron Lett.* 35: 7983–7984.

46 Egami, H. and Katsuki, T. (2009). Iron-catalyzed asymmetric aerobic oxidation: oxidative coupling of 2-naphthols. *J. Am. Chem. Soc.* 131 (17): 6082–6083.

47 Egami, H., Matsumoto, K., Oguma, T. et al. (2010). Enantioenriched synthesis of C_1-symmetric BINOLs: iron-catalyzed cross-coupling of 2-naphthols and some mechanistic insight. *J. Am. Chem. Soc.* 132 (39): 13633–13635.

48 Narute, S., Parnes, R., Toste, F.D., and Pappo, D. (2016). Enantioselective oxidative homocoupling and cross-coupling of 2-naphthols catalyzed by chiral iron phosphate complexes. *J. Am. Chem. Soc.* 138 (50): 16553–16560.

49 Luo, Z., Liu, Q., Gong, L. et al. (2002). Novel achiral biphenol-derived diastereomeric oxovanadium(IV) complexes for highly enantioselective oxidative coupling of 2-naphthols. *Angew. Chem. Int. Ed.* 41 (23): 4532–4535.

50 Guo, Q.-X., Wu, Z.-J., Luo, Z.-B. et al. (2007). Highly enantioselective oxidative couplings of 2-naphthols catalyzed by chiral bimetallic oxovanadium complexes with either oxygen or air as oxidant. *J. Am. Chem. Soc.* 129 (45): 13927–13938.

51 Barhate, N.B. and Chen, C.-T. (2002). Catalytic asymmetric oxidative couplings of 2-naphthols by tridentate *N*-ketopinidene-based vanadyl dicarboxylates. *Org. Lett.* 4 (15): 2529–2532.

52 Chu, C.-Y. and Uang, B.J. (2003). Catalytic enantioselective coupling of 2-naphthols by new chiral oxovanadium complexes bearing a self accelerating functional group. *Tetrahedron: Asymmetry* 14 (1): 53–55.

53 Somei, H., Asano, Y., Yoshida, T. et al. (2004). Dual activation in a homolytic coupling reaction promoted by an enantioselective dinuclear vanadium(IV) catalyst. *Tetrahedron Lett.* 45 (9): 1841–1844.

54 Takizawa, S., Katayama, T., and Sasai, H. (2008). Dinuclear chiral vanadium catalysts for oxidative coupling of 2-naphthols via a dual activation mechanism. *Chem. Commun.* 35: 4113–4122.

55 Zetzsche, L.E., Yazarians, J.A., Chakrabarty, S. et al. (2022). Biocatalytic oxidative cross-coupling reactions for biaryl bond formation. *Nature* 603 (7899): 79–85.

56 Takemoto, M., Suzuki, Y., and Tanaka, K. (2002). Enantioselective oxidative coupling of 2-naphthol derivatives catalyzed by Camellia sinensis cell culture. *Tetrahedron Lett.* 43 (47): 8499–8501.

57 Irie, R., Masutani, K., and Katsuki, T. (2000). Asymmetric aerobic oxidative coupling of 2-naphthol derivatives catalyzed by photo-activated chiral (NO)Ru(II)-salen complex. *Synlett* 2000 (10): 1433–1436.

58 Chen, Y.H., Cheng, D.J., Zhang, J. et al. (2015). Atroposelective synthesis of axially chiral biaryldiols via organocatalytic arylation of 2-naphthols. *J. Am. Chem. Soc.* 137 (48): 15062–15065.

59 Wang, J.Z., Zhou, J., Xu, C. et al. (2016). Symmetry in cascade chirality-transfer processes: a catalytic atroposelective direct arylation approach to BINOL derivatives. *J. Am. Chem. Soc.* 138 (16): 5202–5205.

60 Kang, H., Lee, Y.E., Reddy, P.V.G. et al. (2017). Asymmetric oxidative coupling of phenols and hydroxycarbazoles. *Org. Lett.* 19 (20): 5505–5508.

61 Kang, H., Herling, M.R., Niederer, K.A. et al. (2018). Enantioselective vanadium-catalyzed oxidative coupling: development and mechanistic insights. *J. Org. Chem.* 83 (23): 14362–14384.

62 Koyama, K., Ominato, K., Natori, S. et al. (1988). Cytotoxicity and antitumor activities of fungal bis(naphtho-γ-pyrone)derivatives. *J. Pharmacobiodyn.* 11 (9): 630–635.

63 Boutibonnes, P., Auffray, Y., Malherbe, C. et al. (1984). Proprietes antibacteriennes et genotoxiques de 33 mycotoxines. *Mycopathologia* 87: 43–49.

64 DiVirgilio, E.S., Dugan, E.C., Mulrooney, C.A., and Kozlowski, M.C. (2007). Asymmetric total synthesis of Nigerone. *Org. Lett.* 9 (3): 385–388.

65 Kozlowski, M.C., Dugan, E.C., DiVirgilio, E.S. et al. (2007). Asymmetric total synthesis of Nigerone and ent-Nigerone: enantioselective oxidative biaryl coupling of highly hindered naphthols. *Adv. Synth. Catal.* 349 (4-5): 583–594.

66 Gorst-Allman, C.P., Stern, P.S., and Rabie, C.J. (1980). Structural elucidation of the nigerones, four new naphthopyrones from cultures of *Aspergillus niger*. *J. Chem. Soc. Perkin Trans.* 1 (1980): 2474–2479.

67 Diwu, Z., Zimmermann, J., Meyer, T., and William Lawn, J. (1994). Design, synthesis and investigation of mechanisms of action of novel protein kinase C inhibitors: perylenequinonoid pigments. *Biochem. Pharmacol.* 47 (2): 373–385.

68 Morgan, B.J., Dey, S., Johnson, S.W., and Kozlowski, M.C. (2009). Design, synthesis, and investigation of protein kinase C inhibitors: total syntheses of (+)-calphostin D, (+)-phleichrome, cercosporin, and new photoactive perylenequinones. *J. Am. Chem. Soc.* 131 (26): 9413–9425.

69 O'Brien, E.M., Morgan, B.J., and Kozlowski, M.C. (2008). Dynamic stereochemistry transfer in a transannular aldol reaction: total synthesis of hypocrellin A. *Angew. Chem. Int. Ed.* 47 (36): 6877–6880.

70 Morgan, B.J., Mulrooney, C.A., and Kozlowski, M.C. (2010). Perylenequinone natural products: evolution of the total synthesis of cercosporin. *J. Org. Chem.* 75 (1): 44–56.

71 Morgan, B.J., Mulrooney, C.A., O'Brien, E.M., and Kozlowski, M.C. (2010). Perylenequinone natural products: total syntheses of the diastereomers (+)-phleichrome and (+)-calphostin D by assembly of centrochiral and axial chiral fragments. *J. Org. Chem.* 75 (1): 30–43.

72 O'Brien, E.M., Morgan, B.J., Mulrooney, C.A. et al. (2010). Perylenequinone natural products: total synthesis of hypocrellin A. *J. Org. Chem.* 75 (1): 57–68.

73 Thomson, R.H. (1987). *Naturally Occurring Quinones III: Recent Advances*, 3e. London; New York: Chapman and Hall.

74 Montoya, S.C.N., Agnese, A.M., and Cabrera, J.L. (2006). Anthraquinone derivatives from *Heterophyllaea pustulata*. *J. Nat. Prod.* 69 (5): 801–803.

75 Wirz, A., Simmen, U., Heilmann, J. et al. (2000). Bisanthraquinone glycosides of *Hypericum perforatum* with binding inhibition to CRH-1 receptors. *Phytochemistry* 55 (8): 941–947.

76 Parker, J.C., McPherson, R.K., Andrews, K.M. et al. (2000). Effects of skyrin, a receptor-selective glucagon antagonist, in rat and human hepatocytes. *Diabetes* 49 (12): 2079–2086.

77 Lin, L.-C., Chou, C.-J., and Kuo, Y.-C. (2001). Cytotoxic principles from *Ventilago leiocarpa*. *J. Nat. Prod.* 64 (5): 674–676.

78 Comini, L.R., Núñez Montoya, S.C., Paez, P.L. et al. (2011). Antibacterial activity of anthraquinone derivatives from *Heterophyllaea pustulata* (Rubiaceae). *J. Photochem. Photobiol. B Biol.* 102 (2): 108–114.

79 Comini, L.R., Núñez Montoya, S.C., Sarmiento, M. et al. (2007). Characterizing some photophysical, photochemical and photobiological properties of photosensitizing anthraquinones. *J. Photochem. Photobiol. A Chem.* 188 (2-3): 185–191.

80 Podlesny, E.E. and Kozlowski, M.C. (2012). Enantioselective total synthesis of (*S*)-bisoranjidiol, an axially chiral bisanthraquinone. *Org. Lett.* 14 (6): 1408–1411.

81 Danishefsky, S.J., Uang, B.J., and Quallich, G. (1985). Total synthesis of vineomycinone-B2 methyl-ester. *J. Am. Chem. Soc.* 107 (5): 1285–1293.

82 Cameron, D.W. and Coller, D.R. (1999). Regioselective synthesis of O-methyl derivatives of the trihydroxy anthraquinones morindone and nataloe-emodin. *Aust. J. Chem.* 52 (10): 941–948.

83 Tietze, L.F., Singidi, R.R., Gericke, K.M. et al. (2007). Isolation, enantioselective total synthesis and structure determination of the anthrapyran metabolite SS 43405-e. *Eur. J. Org. Chem.* 2007 (35): 5875–5878.

84 Podlesny, E.E. and Kozlowski, M.C. (2013). Divergent approach to the bisanthraquinone natural products: total synthesis of (*S*)-bisoranjidiol and derivatives from binaphtho-para-quinones. *J. Org. Chem.* 78 (2): 466–476.

85 Callaway, E. (2008). Cell biology: bacteria's new bones. *Nature* 451 (7175): 124–126.

86 Lock, R.L. and Harry, E.J. (2008). Cell-division inhibitors: new insights for future antibiotics. *Nat. Rev. Drug Discov.* 7 (4): 324–338.

87 Park, Y.S., Grove, C.I., Gonzalez-Lopez, M. et al. (2011). Synthesis of (−)-viriditoxin: a 6,6′-binaphthopyran-2-one that targets the bacterial cell division protein FtsZ. *Angew. Chem. Int. Ed.* 50 (16): 3730–3733.

88 Keck, G.E. and Krishnamurthy, D. (1998). Catalytic asymmetric allylation reactions: (*S*)-1-(phenylmethoxy)-4-penten-2-ol. *Org. Synth.* 75: 12.

89 Keck, G.E., Li, X.Y., and Knutson, C.E. (1999). A versatile preparation of alpha,beta-unsaturated lactones from homoallylic alcohols. *Org. Lett.* 1 (3): 411–413.

90 Grove, C.I., Fettinger, J.C., and Shaw, J.T. (2012). Second-generation synthesis of (−)-viriditoxin. *Synthesis* 2012 (3): 362–371.

91 Shen, R.C., Inoue, T., Forgac, M., and Porco, J.A. (2005). Synthesis of photoactivatable acyclic analogues of the lobatamides. *J. Org. Chem.* 70 (9): 3686–3692.

92 Murata, T., Sano, M., Takamura, H. et al. (2009). Synthesis and structural revision of symbiodinolide C23–C34 fragment. *J. Org. Chem.* 74 (13): 4797–4803.

93 Sako, M., Ichinose, K., Takizawa, S., and Sasai, H. (2017). Short syntheses of 4-deoxycarbazomycin B, sorazolon E, and (+)-sorazolon E2. *Chem. Asian J.* 12 (12): 1305–1308.

94 Karwehl, S., Jansen, R., Huch, V., and Stadler, M. (2016). Sorazolons, carbazole alkaloids from *Sorangium cellulosum* strain soce375. *J. Nat. Prod.* 79 (2): 369–375.

95 Herrmann, J., Abou Fayad, A., and Muller, R. (2017). Natural products from myxobacteria: novel metabolites and bioactivities. *Nat. Prod. Rep.* 34 (2): 135–160.

96 Knölker, H.-J., Bauermeister, M., Bläser, D. et al. (1989). Highly selective oxidations of $Fe(CO)_3$-cyclohexadiene complexes: synthesis of 4b,8a-dihydrocarbazol-3-ones and the first total synthesis of carbazomycin A. *Angew. Chem. Int. Ed.* 28 (2): 223–225.

97 Moody, C.J. and Shah, P. (1989). Synthesis of the carbazole alkaloids carbazomycin A and B and hyellazole. *J. Chem. Soc. Perkin Trans.* 1 (2): 376–377.

98 Moody, C.J. and Shah, P. (1989). Diels–Alder reactivity of pyrano[3,4-*b*]indol-3-ones. Part 4. Synthesis of the carbazole alkaloids carbazomycin A and B and hyellazole. *J. Chem. Soc. Perkin Trans.* 1 (12): 2463–2471.

99 Knolker, H.J., Bauermeister, M., Pannek, J.B. et al. (1993). Transition metal-diene complexes in organic-synthesis – Part 13. Highly chemoselective and stereoselective oxidations of tricarbonyliron-cyclohexadiene complexes – synthesis of 4-deoxycarbazomycin B. *Tetrahedron* 49 (4): 841–862.

100 Knolker, H.J., Bauermeister, M., Pannek, J.B., and Wolpert, M. (1995). Transition metal-diene complexes in organic synthesis. Part 22. The iron-mediated quinone imine cyclization: a general route to 3-hydroxycarbazoles. *Synthesis* 1995 (4): 397–408.

101 Markad, S.B. and Argade, N.P. (2014). Diversity oriented convergent access for collective total synthesis of bioactive multifunctional carbazole alkaloids: synthesis of carbazomycin A, carbazomycin B, hyellazole, chlorohyellazole, and clausenaline D. *Org. Lett.* 16 (20): 5470–5473.

102 Ge, H.M., Zhang, W.Y., Ding, G. et al. (2008). Chaetoglobins A and B, two unusual alkaloids from endophytic *Chaetomium globosum* culture. *Chem. Commun.* 45: 5978–5980.

103 Gao, J.M., Yang, S.X., and Qin, J.C. (2013). Azaphilones: chemistry and biology. *Chem. Rev.* 113 (7): 4755–4811.

104 Kang, H., Torruellas, C., Liu, J.C., and Kozlowski, M.C. (2018). Total synthesis of chaetoglobin A via catalytic, atroposelective oxidative phenol coupling. *Org. Lett.* 20 (18): 5554–5558.

105 Klapars, A. and Buchwald, S.L. (2002). Copper-catalyzed halogen exchange in aryl halides: an aromatic Finkelstein reaction. *J. Am. Chem. Soc.* 124 (50): 14844–14845.

106 Murphy, J.M., Liao, X., and Hartwig, J.F. (2007). Meta halogenation of 1,3-disubstituted arenes via iridium-catalyzed arene borylation. *J. Am. Chem. Soc.* 129 (50): 15434–15435.

107 Wu, Y. and Gao, J. (2008). Total synthesis of (+)-brefeldin A. *Org. Lett.* 10 (8): 1533–1536.

108 Partridge, B.M. and Hartwig, J.F. (2013). Sterically controlled iodination of arenes via iridium-catalyzed C-H borylation. *Org. Lett.* 15 (1): 140–143.

109 Zhu, J.L., Germain, A.R., and Porco, J.A. (2004). Synthesis of azaphilones and related molecules by employing cycloisomerization of o-alkynylbenzaldehydes. *Angewandte Chemie-International Edition* 43 (10): 1239–1243.

110 Feng, X., Wang, H.Q., Yang, B., and Fan, R. (2014). One-pot synthesis of highly substituted 4-acetonylindoles via sequential dearomatization and silver-catalyzed domino reaction. *Org. Lett.* 16 (13): 3600–3603.

111 Kikuchi, H., Isobe, M., Sekiya, M. et al. (2011). Structures of the dimeric and monomeric chromanones, gonytolides A-C, isolated from the fungus *Gonytrichum sp*. and their promoting activities of innate immune responses. *Org. Lett.* 13 (17): 4624–4627.

112 Kikuchi, H., Isobe, M., Kurata, S. et al. (2012). New dimeric and monomeric chromanones, gonytolides D-G, isolated from the fungus *Gonytrichum sp*. *Tetrahedron* 68 (31): 6218–6223.

113 Yajima, M., Takada, M., Takahashi, N. et al. (2003). A newly established in vitro culture using transgenic Drosophila reveals functional coupling between the phospholipase A2-generated fatty acid cascade and lipopolysaccharide-dependent activation of the immune deficiency (IMD) pathway in insect immunity. *Biochem. J.* 371 (1): 205–210.

114 Sekiya, M., Ueda, K., Fujita, T. et al. (2006). Establishment of ex vivo systems to identify compounds acting on innate immune responses and to determine their target molecules using transgenic Drosophila. *Life Sci.* 80 (2): 113–119.

115 Wu, X., Iwata, T., Scharf, A. et al. (2018). Asymmetric synthesis of gonytolide A: strategic use of an aryl halide blocking group for oxidative coupling. *J. Am. Chem. Soc.* 140 (18): 5969–5975.

116 Qin, T., Johnson, R.P., and Porco, J.A. Jr., (2011). Vinylogous addition of siloxyfurans to benzopyryliums: a concise approach to the tetrahydroxanthone natural products. *J. Am. Chem. Soc.* 133 (6): 1714–1717.

117 Barrett, K.T. and Miller, S.J. (2013). Enantioselective synthesis of atropisomeric benzamides through peptide-catalyzed bromination. *J. Am. Chem. Soc.* 135 (8): 2963–2966.

118 Hu, D.X., Shibuya, G.M., and Burns, N.Z. (2013). Catalytic enantioselective dibromination of allylic alcohols. *J. Am. Chem. Soc.* 135 (35): 12960–12963.

119 Bucher, C., Deans, R.M., and Burns, N.Z. (2015). Highly selective synthesis of halomon, plocamenone, and isoplocamenone. *J. Am. Chem. Soc.* 137 (40): 12784–12787.

120 Diener, M.E., Metrano, A.J., Kusano, S., and Miller, S.J. (2015). Enantioselective synthesis of 3-arylquinazolin-4(3*H*)-ones via peptide-catalyzed atroposelective bromination. *J. Am. Chem. Soc.* 137 (38): 12369–12377.

121 Samanta, R.C. and Yamamoto, H. (2017). Catalytic asymmetric bromocyclization of polyenes. *J. Am. Chem. Soc.* 139 (4): 1460–1463.

122 Hughes, G., Kimura, M., and Buchwald, S.L. (2003). Catalytic enantioselective conjugate reduction of lactones and lactams. *J. Am. Chem. Soc.* 125 (37): 11253–11258.

123 Lipshutz, B.H., Servesko, J.M., and Taft, B.R. (2004). Asymmetric 1,4-hydrosilylations of alpha,beta-unsaturated esters. *J. Am. Chem. Soc.* 126 (27): 8352–8353.

124 Zenk, M.H., Gerardy, R., and Stadler, R. (1989). Phenol oxidative coupling of benzylisoquinoline alkaloids is catalyzed by regio- and stereo-selective

cytochrome P-450 linked plant enzymes – salutaridine and berbamunine. *J. Chem. Soc. Chem. Commun.* 22: 1725–1727.

125 Gil Girol, C., Fisch, K.M., Heinekamp, T. et al. (2012). Regio- and stereoselective oxidative phenol coupling in *Aspergillus niger*. *Angew. Chem. Int. Ed.* 51 (39): 9788–9791.

126 Huttel, W. and Muller, M. (2007). Regio- and stereoselective intermolecular oxidative phenol coupling in kotanin biosynthesis by *Aspergillus niger*. *Chembiochem* 8 (5): 521–529.

127 Muller, M., Lamottke, K., Steglich, W. et al. (2004). Biosynthesis and stereochemistry of phlegmacin-type fungal pigments. *Eur. J. Org. Chem.* 2004 (23): 4850–4855.

128 Zhao, Q., Zhuang, Z., Liu, T. et al. (2022). Unsymmetrically regioselective homodimerization depends on the subcellular colocalization of laccase/fasciclin protein in the biosynthesis of phlegmacins. *ACS Chem. Biol.* 17 (4): 791–796.

129 Awakawa, T., Yokota, K., Funa, N. et al. (2009). Physically discrete beta-lactamase-type thioesterase catalyzes product release in atrochrysone synthesis by iterative type I polyketide synthase. *Chem. Biol.* 16 (6): 613–623.

130 Griffiths, S., Mesarich, C.H., Saccomanno, B. et al. (2016). Elucidation of cladofulvin biosynthesis reveals a cytochrome P450 monooxygenase required for anthraquinone dimerization. *Proc. Natl. Acad. Sci.* 113 (25): 6851–6856.

131 Szwalbe, A.J., Williams, K., Song, Z.S. et al. (2019). Characterisation of the biosynthetic pathway to agnestins A and B reveals the reductive route to chrysophanol in fungi. *Chem. Sci.* 10 (1): 233–238.

132 Han, Y.B., Bai, W., Ding, C.X. et al. (2021). Intertwined biosynthesis of skyrin and rugulosin A underlies the formation of cage-structured bisanthraquinones. *J. Am. Chem. Soc.* 143 (35): 14218–14226.

133 Efforts continue to develop catalysts with new capabilities for asymmetric oxidative couplings: Gao, J., Wang, P., Shen, A. et al. (2024). Axially chiral copper catalyst for asymmetric synthesis of valuable diversely substituted BINOLs. *ACS Catal.* 14 (8): 5621–5629.

11

Atropisomerism in Drug Discovery and Development

Khaled M. Darwish[1], Asmaa S. A. Yassen[2], Ebtehal M. Husseiny[3], Mohammed I. A. Hamed[4], and Mohamed A. Helal[1,5]

[1] *Suez Canal University, Faculty of Pharmacy, Medicinal Chemistry Department, KM 4.5 Ring road, Ismailia 41522, Egypt*
[2] *Suez Canal University, Faculty of Pharmacy, Pharmaceutical Organic Chemistry Department, KM 4.5 Ring road, Ismailia 41522, Egypt*
[3] *Al-Azhar University, Faculty of Pharmacy (Girls), Pharmaceutical Organic Chemistry Department, Nasr City, Cairo 11754, Egypt*
[4] *Fayoum University, Faculty of Pharmacy, Department of Organic and Medicinal Chemistry, Fayoum 63514, Egypt*
[5] *University of Science and Technology, Biomedical Sciences Program, Zewail City of Science and Technology, Ahmed Zewail Road, October Gardens, Giza 12578, Egypt*

11.1 Introduction

Atropisomerism is considered a kind of dynamic axial chirality resulting from an extremely restricted single-bond rotation that usually occurs between two or more atoms with sp^2 hybridization [1]. Such rotation around a chiral axis can lead to the formation of racemic mixtures in a simple manner with no need to break and make a chemical bond [2]. Atropisomers are conformers that can be separated from each other as they have the ability for slow interconversion offering a half-life of racemization of more than one thousand seconds [3]. Atropisomers have a high enough rotational barrier to make it possible to separate the various conformers [1]. It is worth mentioning that atropisomers can exert diverse biological activity, selectivity, toxicity, pharmacodynamics, and pharmacokinetic features [4]. Reducing the number of attainable stereoisomers around chiral axes led to enhanced pharmacological activity, selectivity, safety, and physicochemical and pharmacokinetic criteria [5].

11.2 Configuration Assignment of Atropisomeric Drugs

Advances in separation and analytical techniques, as well as increasing awareness of the occurrence of atropisomerism, have helped medicinal chemists to better analyze and handle the accompanying challenges and successfully progress atropisomeric

Atropisomerism in Asymmetric Organic Synthesis: Challenges and Applications, First Edition.
Edited by Shinobu Takizawa and Mohamed S. H. Salem.

drug molecules. There are several methods available to obtain the pure atropisomers of a drug candidate. The scale at which drug candidates are manufactured determines which method is best. On milligram to multigram scale, chromatography of an atropisomeric mixture is the most used method for isolation. Atropisomers can be separated using chiral stationary phase (CSP) by high-performance liquid chromatography (HPLC), or supercritical fluid chromatography (SFC), which uses a micron chiral column and is more efficient and environmentally friendly [6–8]. For a multikilogram supply of the drug candidates, alternative methods are used to obtain pure atropisomers to avoid costly, time-demanding chromatography. Two possible strategies to obtain the pure atropisomers on larger multikilogram scales are (i) resolution by crystallization of diastereomeric salts [9] or (ii) asymmetric synthesis of the desired atropisomer. There are different techniques used to determine the free energy barrier of atropisomers interconversion including, for example, density functional theory (DFT) [10], variable temperature NMR (VT-NMR) [11], and HPLC [7]. Additionally, the definite atropisomeric configuration was detected utilizing single-crystal X-ray diffraction [12, 13]. If racemic mixtures cannot be separated through these techniques or isomerization occurs quickly either *in vitro* and/or *in vivo* as in the case of ibuprofen and thalidomide, the drug was developed as a racemic mixture. Although, the effectiveness, safety, and pharmacodynamics of both atropisomers should be accurately estimated.

11.3 Classification of Atropisomeric Drugs According to the Rotational Energy Barrier

LaPlante classified atropisomeric compounds into three categories (Figure 11.1) according to the rotational energy barrier required for racemization to occur

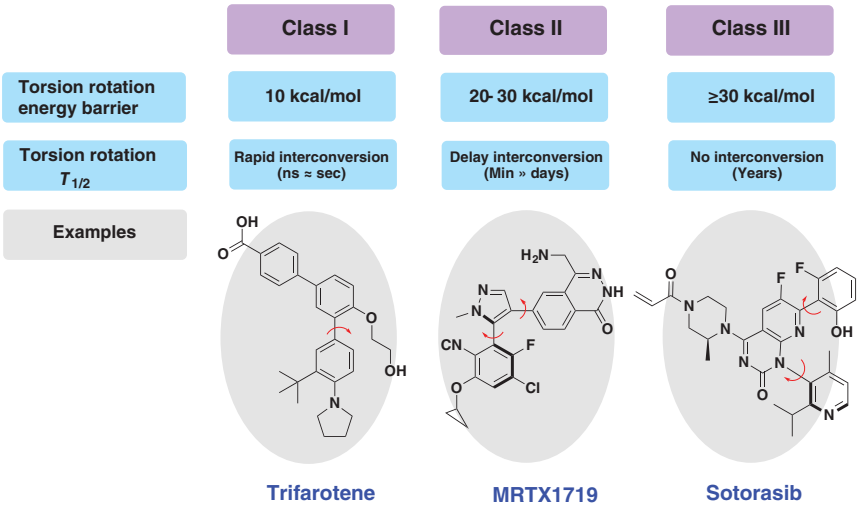

Figure 11.1 LaPlante's classification of atropisomeric compounds based on torsional rotation energy barrier and rotation half-lives.

(ΔE rotation) and the half-life of racemization at physiological temperature [14, 15]. Class I atropisomerism involves compounds that have low ΔE rotation (10 Kcal/mol). These compounds quickly interconvert at room temperature ($t_{1/2} < 60$ seconds) and cannot be differentiated as a single enantiomer. Class II atropisomerism includes molecules presenting modest interconversion energy (ΔE rotation = 20–30 Kcal/mol) and moderate stability ($t_{1/2}$ = 60 seconds–4.5 years). Class III atropisomerism contains stable isomers with a high rotational energy barrier (ΔE rotation is ≥30 Kcal/mol) and slowly interconvertible atropisomers ($t_{1/2} > 4.5$ years). The development of class III atropisomers as single isomers after atroposelective synthesis or separation using one of the numerous chiral purification procedures is ideal [16]. The greater energy barriers for rotation in classes II and III atropisomerism enable the separation of a single atropisomer [5]. Class II atropisomers demand further consideration owing to the complications resulting from modest interconversion. Noticeably, interconversion can happen during biological estimation, analytical differentiation, and drug storage, giving rise to challenges in drug discovery and evolution. Hence, atropisomerism must be identified early in order to be evaluated and treated, specifically in the case of moderate interconversion rates [17].

11.4 Analysis of Atropisomeric Drugs Across the Pharmaceutical Market

Atropisomerism, in terms of modern drug design and development, has been increasingly appealing to both the academia and pharmaceutical industry across the past decades. Generally, drug action depends on binding of the bioactive molecule into its protein target in a specific manner allowing the formation of the appropriate chemical interactions. Therefore, the impact of axial chirality is expected and should be carefully planned early enough in the drug design process. It is well established that the activity toward a particular target is dependent on one atropisomer, with a little contribution from the other. "Locking" the molecule in the bioactive atropisomeric form achieves not only a superior activity but also a better selectivity toward the biological target of interest [16]. Of course, this effect is restricted to "class III atropisomer," while the rapidly interconverting class I atropisomers are considered achiral and do not exhibit this differential binding effect [3]. Four FDA-approved drugs are recognized as class III stable atropisomers; Lesinurad (urate transporter inhibitor as antigout agent) [18], Telenzepine (selective M1 receptor blocker as antipeptic ulcer) [19], Colchicine (anti-inflammatory/gout agent) [20], and Sotorasib ($KRAS^{G12C}$ covalent inhibitor against non-small cell lung cancer (NSCLC)) [21]. These drugs are either marketed as racemate (Lesinurad and Telenzepine) and singular diastereoisomer (Colchicine) or even separated as single atropisomer (Sotorasib). Several other small molecules were identified within the literature [22–28] and clinical trials [29–33] possessing one or more class I atropisomeric axes, while in some cases being endorsed with symmetrical "pro-atropisomeric" axis. Within the 2010–2018 FDA-approved realm, Gustafson et al. illustrated that nearly 30% of marketed small molecules incorporate

class I atropisomeric axis within their chemical structure [16]. Further analysis of the 2019–2022 FDA-approved drugs depicted 26% of drugs possessing any of the LaPlante's atropisomerism stability classes, while 6% harbor at least one pro-atropisomeric axis [3].

The vast majority of FDA-approved, literature, and clinical trial small molecules are with class I atropisomeric axis across their biaryl/heterobiaryl scaffolds, while smaller portions endorse atropisomerism along other chemical synthons such as diaryl ethers/amines, benz/arylamide, and anilines (Figures 11.2–11.5). Prevalence of aromatic-based atropisomersim could be rationalized by the rise of applying aryl/heterocyclic functionalities for positive contributions within the drug's pharmacokinetic (ADMETox) and dynamics (hydrophobic target binding) properties across the drug development processes [1, 34]. This aryl-associated preferentiality can be extended with the employment of several synthetic pathways throughout the early drug discovery stages including; catalytic cross-couplings as well as nucleophilic and electrophilic aromatic substitutions [35, 36]. All these described chemical reactions are commonly employed on aromatic functionalities, which are capable of producing biaryl/heterobiaryls atropisomeric axis [37–39]. The advent of obtaining singular atropisomer and the challenges encountered during the process of drug discovery have been the main focus of the scientific research. In the following section, an overview of the utilization of the atropisomerism phenomena in drug discovery is provided together with examples from the recent literature and FDA-approved drugs. The compounds in discussion will be classified according to their chemical classes into biaryls/heterobiaryls, diaryl ethers or amines, benzamides, and macrocycles.

11.4.1 Biaryls and Heterobiaryls

In fact, biaryls and heterobiaryls are the most abundant class of atropisomers, with numerous examples in recent medicinal chemistry research and few as FDA-approved drugs. The focus of this part will be given on FDA-approved drugs which include, to date, four atropisomers belonging to this structural class [3]. A prominent example of a marketed drug that was found to exist as a mixture of stable atropisomers is Lesinurad, a hURAT1 inhibitor approved for the treatment of gout (Figure 11.6). It was demonstrated that the (S^a)-atropisomer is 3X more potent as a hURAT1 inhibitor. In addition to the difference in receptor affinity, it was interesting to notice that the atropisomers of Lesinurad exhibited significantly different pharmacokinetic properties. This observation highlights the need for careful consideration of atropisomerism during early drug design not only for optimizing the activity but also for obtaining acceptable pharmacokinetic profile [40]. Another interesting example is Sotorasib, which is the first ever FDA-approved drug that inhibits KRAS, a cancer target that has been termed "undruggable." This drug is approved for treatment of NSCLC with $KRAS^{G12C}$ mutation. It was proved that the (*M*)-atropisomer, which positioned the ortho substituent in the H95/Y96/Q99 hydrophobic pocket, is 10-fold more potent than the (*P*)-atropisomer. It is also worth noticing that Sotorasib is the first FDA-approved drug to be designed and

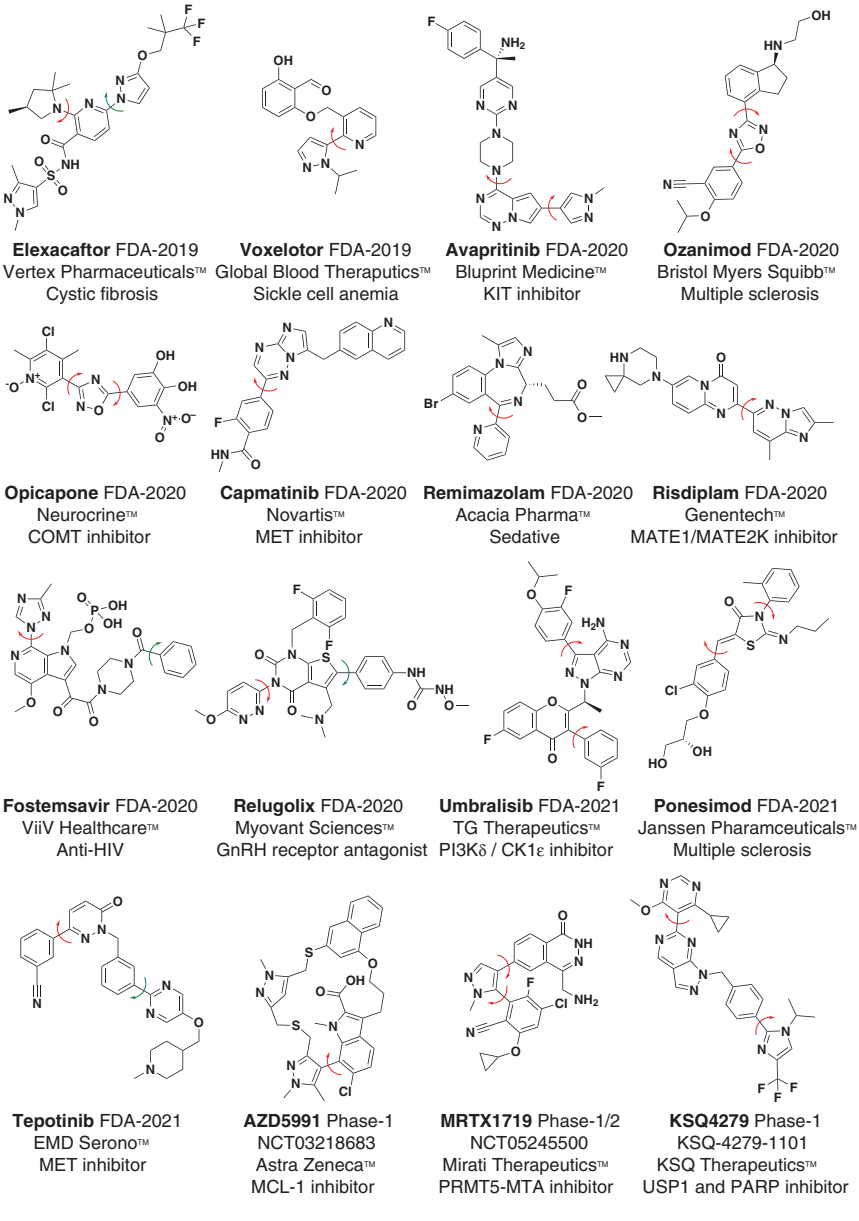

Figure 11.2 Examples of FDA-approved drugs and clinical trial candidates sorted based on the common biaryl/biheterocyclic chirality axis. Potential atropisomeric axes (red) and pro-atropisomeric ones (green) are represented as curved arrows.

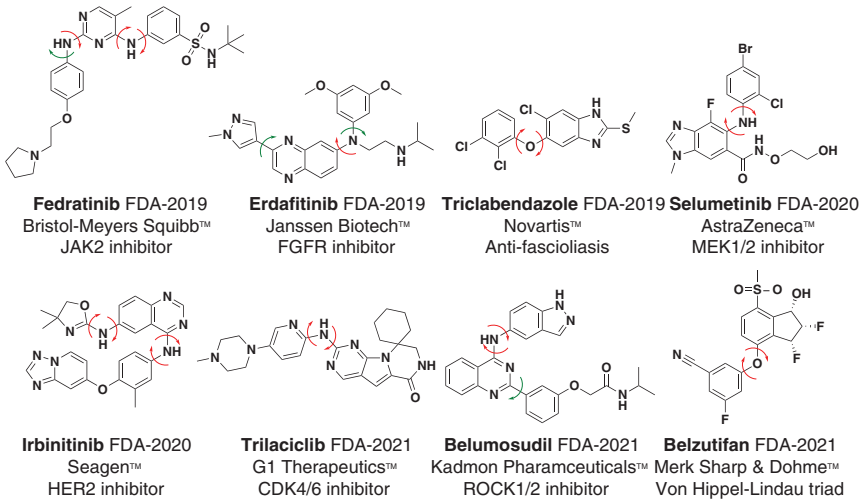

Figure 11.3 Examples of FDA-approved drugs sorted based on the common biaryl ether/amine chirality axis. Potential atropisomeric axes (red) and pro-atropisomeric ones (green) are represented as curved arrows.

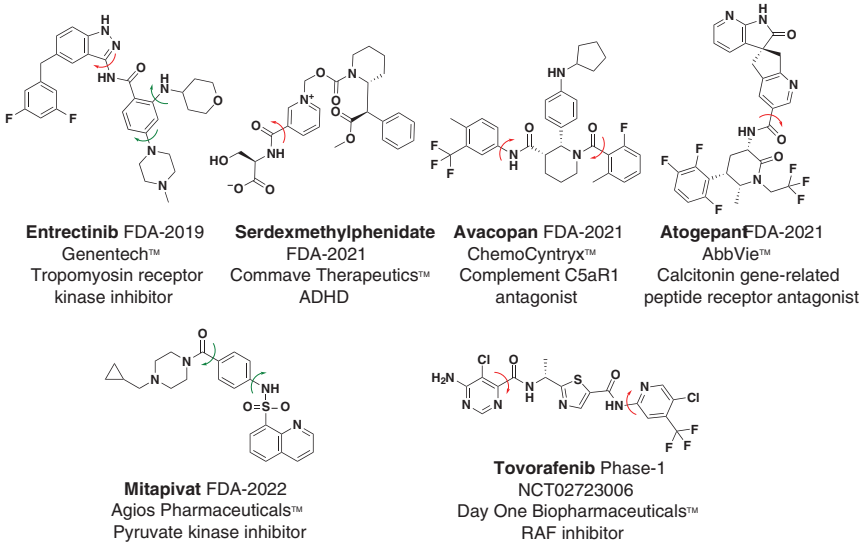

Figure 11.4 Examples of FDA-approved drugs and clinical trial candidates sorted based on the common benzamide/arylamide chirality axis. Potential atropisomeric axes (red) and pro-atropisomeric ones (green) are represented as curved arrows.

produced as a configurationally stable atropisomer [41]. Another two older but widely used drugs are Vancomycin B and Colchicine. The first is a glycopeptide antibiotic medication, approved in 1988, for treatment of a number of bacterial infections. The drug has three atropismorism axes due to the rotational restriction of certain bonds, and isomer present in the drug is the thermodynamically more stable one. Finally, Colchicine, a cytotoxic drug inhibiting microtubule polymerization,

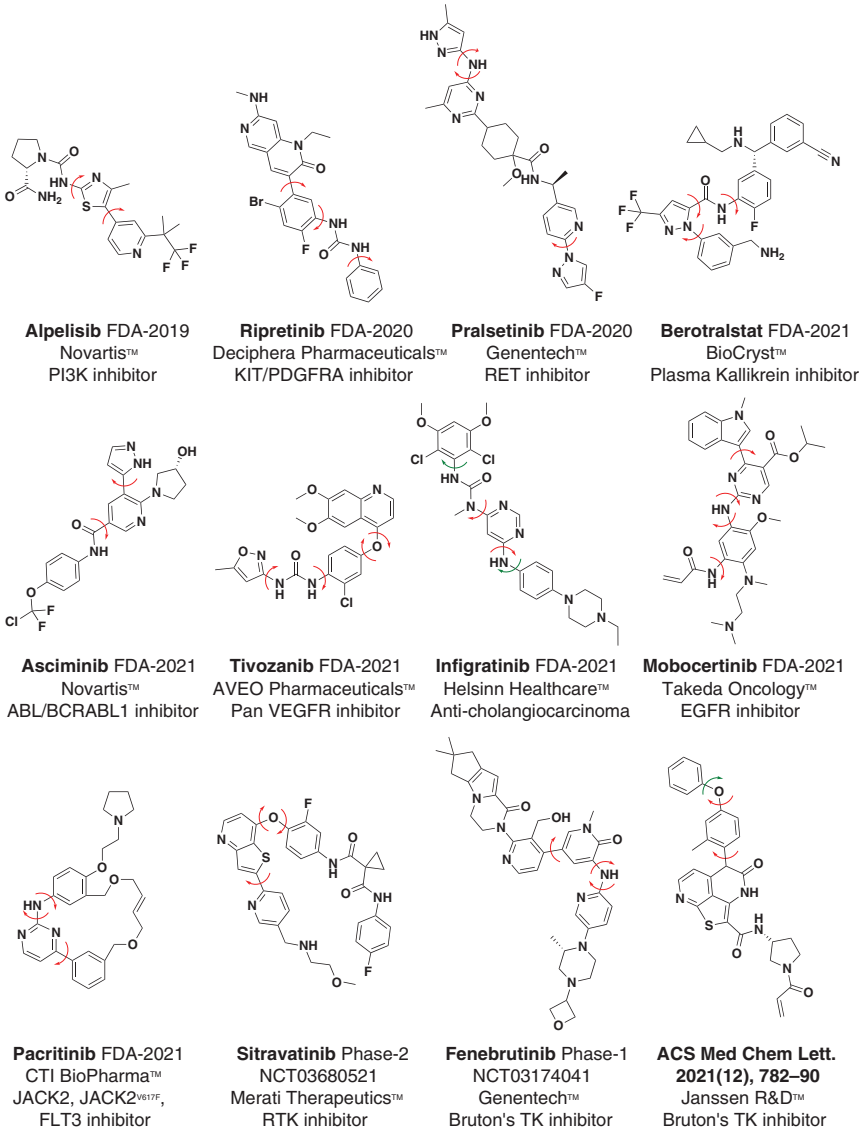

Figure 11.5 Examples of FDA-approved drugs, clinical trial candidates, and literature-reported small molecules sorted based on the common mixed chirality axis. Potential atropisomeric axes (red) and pro-atropisomeric ones (green) are represented as curved arrows.

is also a classic example of atropisomerism. The phenomenon here is due to a restricted rotation of its phenyl ring which is fused to a seven-membered ring. This constraint is augmented by a point chirality of the acetamide group at the seventh position, making the (R^a,7*S*)-colchicine indefinitely atropisomerically stable. This isomer is 40-fold more cytotoxic than its enantiomer. It is worth noting that the (R^a,7*R*)-Colchicine, the unnatural enantiomer, is devoid of tubulin binding activity due to the loss of the appropriate torsion angles between ring A and ring C [41].

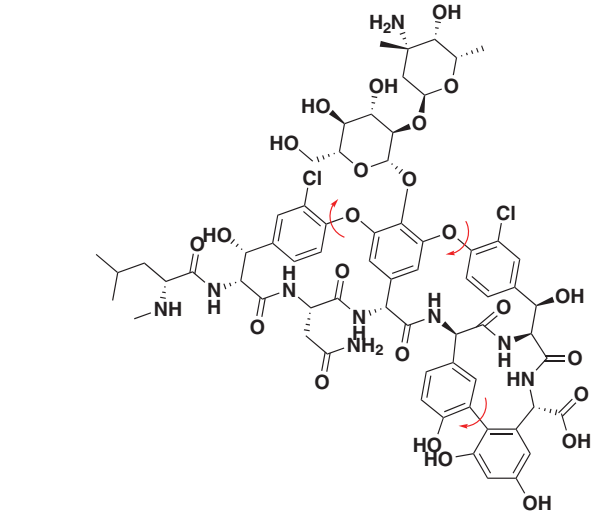

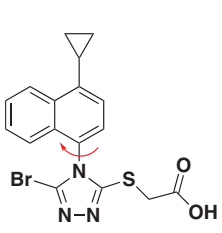

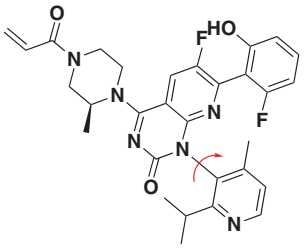

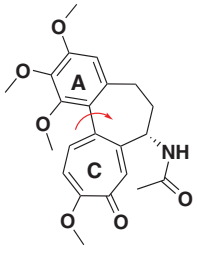

Figure 11.6 Examples of FDA-approved biaryls and heterobiaryls derivatives. Atropisomeric axes are represented as red arrows.

11.4.2 Diaryl Ethers

Contrary to the typical examples of biaryl and heterobiaryl atropisomers, the axial chirality of diary ether is frequently overlooked. Despite having relatively low stereochemical stabilities compared to biaryls, many of the reported diaryl ethers are known to have barriers to racemization >117 kJ/mol (28 kcal/mol) [42]. In 1958, Dahlgard and Brewster postulated that diaryl ethers might exist as stable atropisomers. In 2006, Betson and Clayden studied a series of potential atropisomers of the type tri- and tetra-substituted diaryl ethers and concluded that tropisomerism in these compounds depends mainly on the substitution pattern rather than the total number of substituents. They have also demonstrated that "diaryl ethers in which both rings are unsymmetrically substituted may exhibit atropisomerism, as long as at least one of the substituents is as large as a tert-butyl group". This rule could also be applied for diaryl ethers with only three *ortho* substituents [43]. As mentioned above, Vancomycin is a classic example of diaryl ether-stable atropisomers. Another

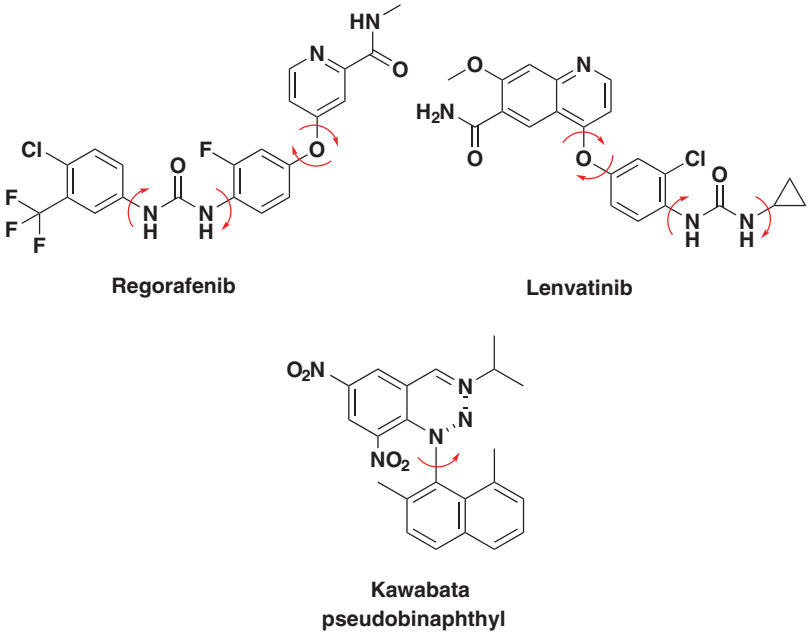

Figure 11.7 Examples of FDA-approved diaryl ethers and the diaryl amine derivatives reported by Kawabata and co-workers.

two FDA-approved drugs showing this kind of stereochemistry are Regorafenib and Lenvatinib (Figure 11.7); nevertheless, they belong to class I (rapidly interconverting atropismers). The first drug is a multikinase inhibitor targeting angiogenic the oncogenic receptor tyrosine kinase (RTK) for treatment of metastatic colorectal cancer. While Lenvatinib is an inhibitor of VEGFR1, VEGFR2, and VEGFR3 kinases used for the treatment of thyroid cancer and Ephrin families. The crystal structure of VEGFR2 in complex with Lenvatinib shows that the drug binds with both axes of the diaryl ether in the (S^a)-atropisomeric conformation, suggesting the potential for enhancing the activity and selectivity toward VEGFR2 via restricting the rotation of this diaryl ether. This strategy has been explored for other kinase inhibitors but has yet to be applied to Lenvatinib [44].

11.4.3 Diaryl Amines

Other nonclassical atropisomeric scaffold used frequently in drug development is the diaryl amine. Similar to the diaryl ethers, atropisomerism in diaryl amines was usually overlooked during the drug design process, and relatively little is known about the determinants of axial chirality in this class of compound. Despite the large number of diaryl amines in medicinal chemistry literature, examples of stable diaryl amine atropisomers have remained rare due to the nature of the C–N axes which allow for lower-energy racemization via their simultaneous rotation. The first diaryl amine with stable axial chirality was reported by Kawabata et al. in 2009 [45].

They have created novel atropisomeric binaphthyl scaffolds that are stable at room temperature due to the inner N—H—N H-bond (Figure 11.7). These binaphthyl surrogates could represent a different class of chiral proton donors since the proton in the N—H—NH-bond is situated in an asymmetric milieu. Diaryl amines are frequently used scaffolds for drug design with multiple examples of kinase inhibitors such as the FDA-approved Vandetanib, Bosutinib, and Afatinib, which exist as rapidly interconverting atropisomers. Despite the unstable axial chirality noticed with these molecules, their crystal structures in complex with RET, ABL, and EGFR kinases, respectively, show (S^a, S^a)-atropisomeric conformations. Again, this observation suggests the potential for further controlling the conformations of the diaryl amines via introducing bulky substituents or employing an N—H—N H-bonding motif [46–48]. As of July 2022, a search of the PDB revealed over 1600 diaryl amine small-molecule/protein complexes. Among them, more than 100 ligands, including FDA-approved drugs Bosutinib, Imatinib, and mefenamic acid, had diarylamines that were found to bind their targets with one planar axis and the other in an almost orthogonal atropisomeric orientation.

11.4.4 Benzamides

Due to the rigidity of the amide bond, the most studied non-biaryl atropisomers are either benzamide derivatives or anilides. As expected, the barriers to racemization of the benzamide scaffold depend mainly on the nature of the substituents at the *ortho* position, which should be bulky enough to achieve the required stereochemical stability. This could be exemplified with 2,6-disubstituted benzamides or 2-substituted 1-naphthamides. Surprisingly, the nature of the substituents at nitrogen has a relatively minor impact on the half-life of benzamide racemization [49]. There are numerous examples of atropisomeric amides in the medicinal chemistry literature with the majority being of the rapidly interconverting class I. One interesting example is the Indomethacin analog reported by Takahashi and Natsugari (Figure 11.8). Contrary to Indomethacin, this compound was selective for COX1

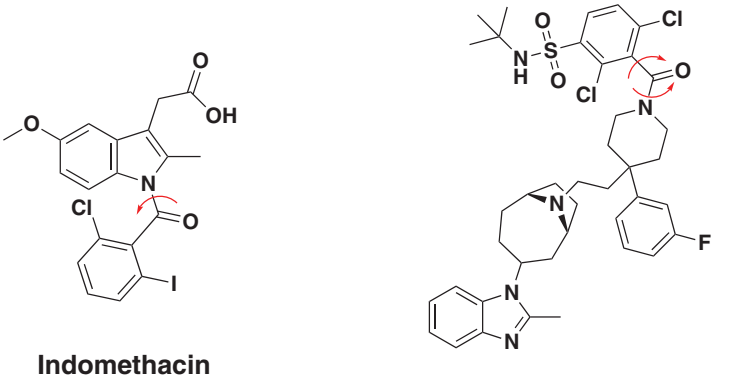

Figure 11.8 Examples of benzamides showing atropisomerism.

and the activity is largely affected by the (R^a) isomer [50]. Another well-studied example is the recently approved CCR5 antagonist GSK214096 developed by GSK (Figure 11.8). The dichloro substituents *ortho* to the atropisomeric axis directly affect the barrier to rotation of this compound. It was demonstrated by Kasmierski and co-workers that this compound exists as four isolable atropisomers, and the CCR5 affinity corresponds to two of these isomers only. The CCR5 receptor is a G-protein coupled receptor (GPCR) expressed on the surface of white blood cells that is involved in the immune system as it acts as a receptor for chemokines. It is also a coreceptor for the human immunodeficiency virus (HIV). This means that HIV needs to bind to the CCR5 receptor in order to enter a cell [51].

11.4.5 Macrocycles

Macrocycles are frequently encountered in nature and, to a lesser extent, in drug discovery. Due to the nature of their relatively rigid structures, it is more feasible to achieve atropisomeric stability compared to diaryl ether and diaryl amines, at least with energy barriers belonging to class II. However, with few exceptions, most medicinal chemists usually opt to eliminate atropisomerism during the lead optimization process to avoid problems of stereoselective synthesis, purification, and characterization of these isomers. In 2016, Fanard and co-workers cyclized a reported focal adhesion kinase (FAK) inhibitor to increase its affinity toward proline-rich tyrosine kinase 2 (PyK2). They have obtained a macrocycle with improved activity but with two rapidly interconverting atropisomers due to the differential orientation of the pyridine ring above and below the macrocycle plane (Figure 11.9). The crystal structure of PyK2 revealed that only one isomer is active. The researchers failed to introduce sufficient structural modifications, by installing bulky groups on the sulfonamide or the benzylic amine, to stabilize one of the atropisomers. Finally, they had to modify the macrocyclic structure to avoid atropisomerism altogether [52]. In a similar case, scientists from BMS reported a 16-membered macrocycle molecule as a Factor VIIa Inhibitor (Figure 11.9). This compound was found to exist as a 2 : 1 mixture of chromatographically separable atropisomers with one of the isomers being 25-fold more active, and racemization occurring upon heating at 100 °C in DMSO for two days. Crystal structure of the complex showed that the ethyl group of the active atropisomers forms a critical hydrophobic interaction with the enzyme S2 pocket which is not feasible with the other isomer. Again, the team eventually decided to eliminate this asymmetric factor by replacing this problematic ethyl moiety with two methyl groups on both sides of the phenyl ring to ensure the accomplishment of the required interaction with the S2 pocket [53].

A success story of stabilizing the most active atropisomer and introducing it to the clinic can be demonstrated by the development of the anaplastic lymphoma kinase (ALK) inhibitor Lorlatinib lead compound by Pfizer (Figure 11.9). This 12-membered macrocycle was designed to reduce the number of rotatable bonds, allow better shielding of polar surface area, and improve binding through its restricted conformation. All of these design elements led to better central nervous

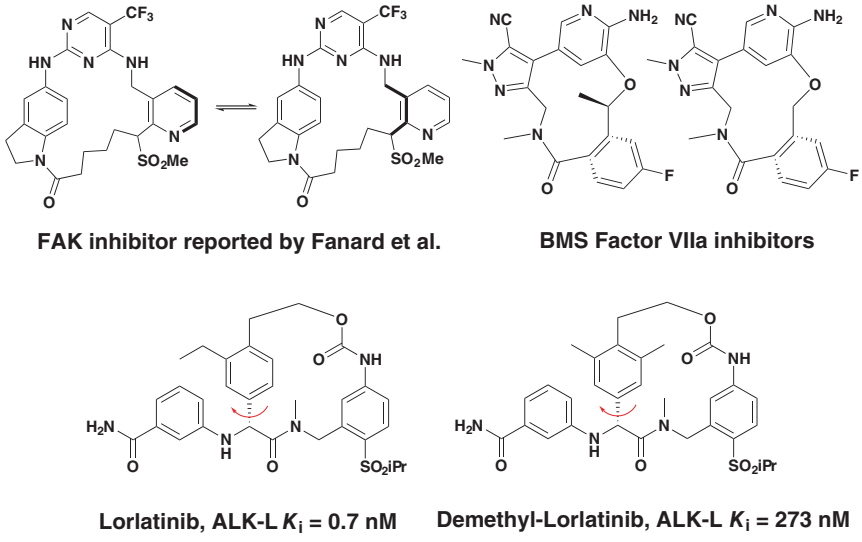

Figure 11.9 Examples of macrocycles showing variable degrees of atropisomerism.

system (CNS) permeability. It was found that the desmethyl analog exists as a pair of isolable atropisomers, showing an energy of activation for interconversion of 24.6 kcal/mol and a $t_{1/2}$ of approximately six hours at 37 °C. On the other hand, desmethyl derivative exists as a single atropisomer and showed no racemization after 24 hours at 65 °C. It was noticed that the presence of the chiral methyl group on the benzylic carbon stabilizes the desired conformation by providing a calculated ground state energy difference of 8.5 kcal/mol driving the equilibrium completely to the bioactive conformation [54].

11.5 Introducing Atroisomerism to Modulate Selectivity

Class I or rapidly interconverting atropisomers are usually treated by medicinal chemists as achiral compounds. However, at any given moment, it was found that only one atropisomer binds to its biological target. The other isomer has little or no contribution to the binding. This reduces the overall affinity of the molecule and could also lead to undesirable off-target effects. Therefore, rigidification or constraining a class I atropisomer into a stable class III analog is expected to improve its affinity as well as selectivity. One prominent example is Sotorasib, which is the first FDA-approved drug to be designed and produced as a configurationally stable atropisomer, as discussed earlier. Currently, this approach has gained a lot of interest in early drug discovery, and more examples will be provided in the next section.

Another example is the optimization of Lamellarin N, which is a hexacyclic pyrrole alkaloid originally isolated from marine invertebrates and shows promising anticancer activity due to its ability to inhibit various kinases (Figure 11.10). Unfortunately, this lack of selectivity could lead to off-target-associated toxicity.

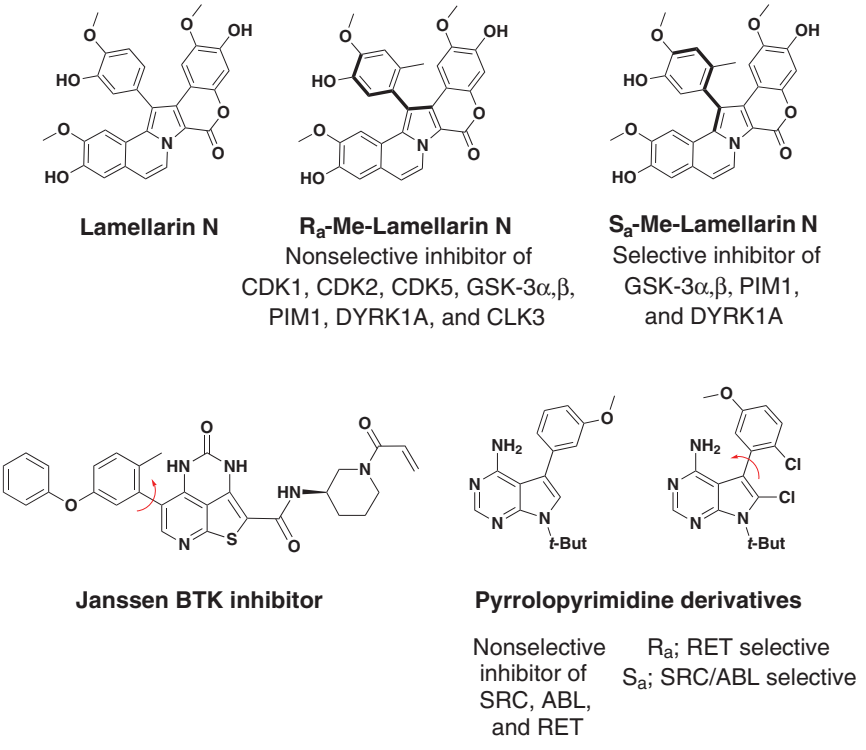

Figure 11.10 Examples of successful employment of atropisomerism to modulate selectivity.

Iwao and co-workers introduced a methyl group on the 16-position of Lamellarin N generating two stable atropisomers, referred to here as (R^a)-Me-Lamellarin and (S^a)-Me-Lamellarin. The researchers have evaluated the inhibitory activity of both isomers on eight protein kinases implicated in cancer and neurodegenerative diseases (CDK1/cyclin B, CDK2/cyclin A, CDK5/p25, GSK-3α/β, PIM1, DYRK1A, CLK3, and CK1). Interestingly, Enantiomer (R^a)-Me-Lamellarin N remained nonselective similar to the parent compound. Whereas the other isomer (S^a)-Me-Lamellarin N showed selective inhibition of GSK-3α/β, PIM1, and DYRK1A [55]. In 2021, Janssen reported a potent and selective covalent inhibitor of Bruton's tyrosine kinase (BTK) based on triazaacenaphthylene-2-carboxamid (Figure 11.10). Introduction of an *ortho*-methyl substituent on the lead compound phenyl ring produced a mixture of atropisomers that are chirally stable at ambient temperature. The atropisomers were chromatographically resolved and characterized. Interestingly, the (S^a) isomer displayed approximately 30-fold higher potency and 20-fold better cellular activity relative to the (R^a) counterpart. This was the basis for the design of the most active orally bioavailable compound of this series, which was later taken to preclinical development [24].

In an important study, Toenjes and Gustafson showed that different members of related enzymes with conserved active sites, such as kinases, can prefer specific

atropisomers of the same ligand and used this phenomenon to modulate inhibitor affinity and selectivity. In their study, they started with a nonselective pyrrolopyrimidine (PPY) inhibitor of SRC, RET, and ABL kinases and generated two stable atropisomers by installing a chlorine atom on the *ortho* position of its 3-phenyl moiety (Figure 11.10). The atropisomers were isolated, characterized, and evaluated for their ability to inhibit the aforementioned enzymes. The authors demonstrated that the (R^a) isomer was selective for RET, while the (S^a) retained the affinity for SRC and ABL kinases. They have also used molecular modeling to provide a plausible explanation and recommended the extension of this strategy to optimize the selectivity of other kinase inhibitors [16].

Constraining a rotatable bond into a singular atropisomer was shown beneficial in developing AZD-5991 (AstraZeneca) the selective pro-apoptotic protein, MCL-1, antagonist with improved pharmacodynamic profile [30]. Analogous to all pro-apoptotic proteins of the BCL-1 family, the binding site of MCL-1 is considered undruggable, being shallow, long, and with a dominant hydrophobic nature [56]. A class-I atropisomeric indole acid lead compound was initially developed showing significant MCL-1 potency and selectivity profile (MCL-1 $IC_{50} = 0.042\,\mu M$). Crystallized complex between MCL-1 and this lead compound depicted a U-shaped conformation at the target binding site (Figure 11.11). Notably, both side terminal scaffolds (naphthyl-3-carbon and pyrazole-methyl group) were only 3.6 Å distance apart via the rotation virtue around its atropisomeric axis. Entropically advantageous structure optimization was considered by constraining the molecule within a macrocycle using a nonpolar linker to avoid desolvation penalties at the MCL-1 hydrophobic pocket [56]. AZD-5991 was then developed with restrained bond rotation around its atropisomeric axis through the macrocyclization strategy and the indole ring steric substitution (*N*-methyl and C6-Cl). Notably, co-crystallized

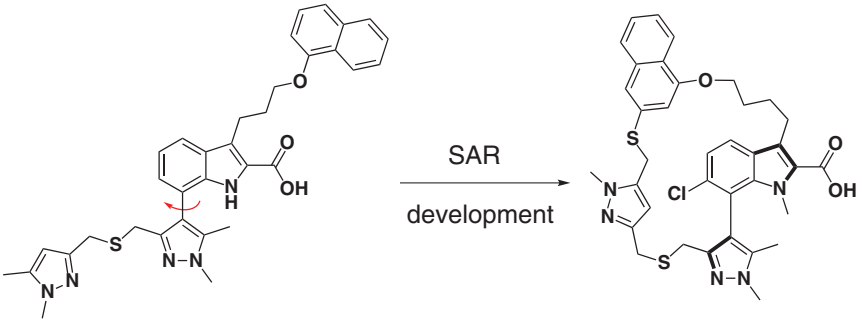

Figure 11.11 Evolution of singular atropisomeric development of specific MCL-1 inhibitors and their co-crystallized complexes with MCL-1 at the undruggable hydrophobic protein–protein interface (PDB: 6fs1 for lead compound; PDB: 6fs0 for AZD-5991).

complex of AZD-5991 with MCL-1 showed predominant binding for its atropisomeric (R_a) in accordance with its improved inhibition potency as compared to its other congruent (MCL-1 IC_{50} (R_a) = 0.17–0.7 nM; (S_a) = 0.98–6.3 nM) [30].

11.6 Challenges for Atropisomerism within Drug Discovery

Similar to geometrical isomerism and chirality within drug design and development, atropisomerism offers several advantages by introducing a pure atropisomeric form of the drug. As discussed earlier, singular atropisomer would offer safer profiles, higher/selective bioactivity, and thus lower administration doses as well as reduced off-target activities over racemates [57]. The ability of atropisomers to display widely different physiochemical and pharmacokinetic (absorption, distribution, metabolism, distribution) properties can be exploited to improve pharmacodynamic profiles and binding kinetics. In special cases, pure atropisomer would permit patent protection against generic drug competitors since manufacturers could exclusively market these atropisomeric pharmaceuticals following patent loss [58]. Despite these offered advantages, the development of pure atropisomers is considered challenging owing to interconversion, purification, analysis/detection, and discovery/process difficulties.

A singular atropisomer could be accessible through modern synthetic pathways, which are usually implemented for many axial bioactive natural metabolites with optical purity. Nevertheless, the cost of such approaches is still high [57]. Another approach is through symmetrizing the hindered rotation bond as an approach to avoid class-II atropisomer formation. The orally bioavailable SCH 351125 was developed by Schering-Plough company for treatment of HIV infections through targeting the human C-C chemokine receptor type-IV (CCR-5) for inhibition (Figure 11.12)

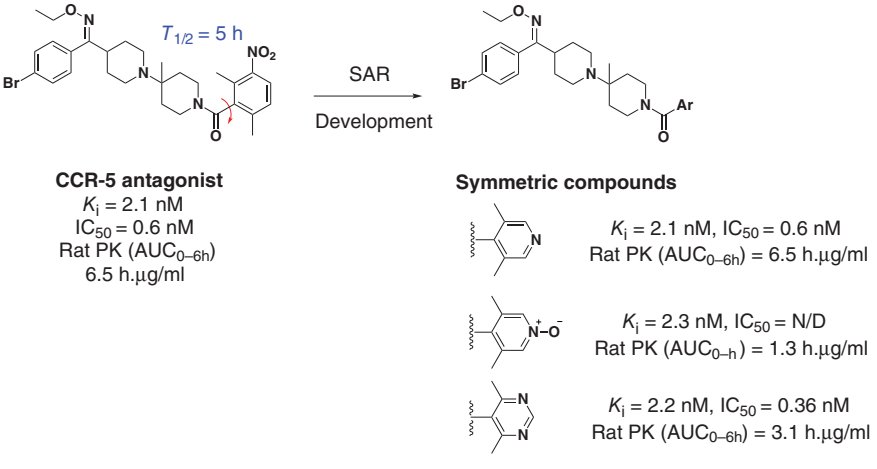

Figure 11.12 Concept of symmetrizing the hindered rotation bond to avoid class-II atropisomers.

[59]. Symmetrizing SCH 351125 was reported through shifting substitutions on the atropisomeric benzoyl moiety accompanied by even complete scaffold hopping [60, 61]. The symmetrizing approach developed potent antagonists of CCR5 biotarget with comparable efficacies in terms of binding affinity and viral entry relative to SCH 351125, yet with relatively lower pharmacokinetic profiles [60].

The full potential of the atropisomerism applications in drug design could be realized by developing novel analytical and separation approaches that would be explored for the isolation, separation, and characterization of atropisomers. In the successful example of the FDA-approved Sotorasib, chiral separation with the (+)-2,3-dibenzoyl-*D*-tartrate salt of the racemic dione intermediate was beneficial for preparing the more active (*M*)-atropisomer following a few steps (Figure 11.13) [62]. Novel polar organic chiral separation performed on immobilized amylose-based CSP was introduced by Radhakrishnanand et al. for the atropisomer isolation of the nonsteroidal mineralocorticoid receptor antagonist, Esaxerenone, achieving a resolution range of more than 0.30 [33].

It is worth noting that the rapid interconversion of class I atropisomers could hamper the sole application of several analytical and isolation techniques. Thus, prior encumbrance about a hindered bond for generating separable atropisomers of slower interconversion (i.e. "atroisomeric switch" into extended half-lives) can be considered beneficial before the application of chiral separation techniques [17]. Designing atropisomers with hindered bond rotations was found successful in developing the noncovalent BTK inhibitor in the clinical trial, BMS-986142. This compound is a stable atropisomer locked at two atropisomeric (class II and III) axes easily isolated through SFC chiral separation (Figure 11.14) [29]. Another example

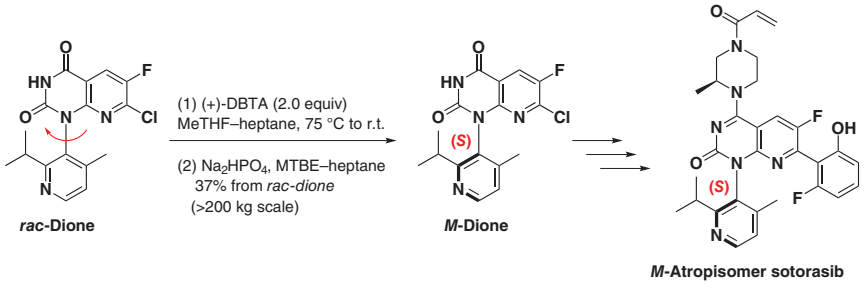

Figure 11.13 Concept of singular atropisomeric development of Sotorasib.

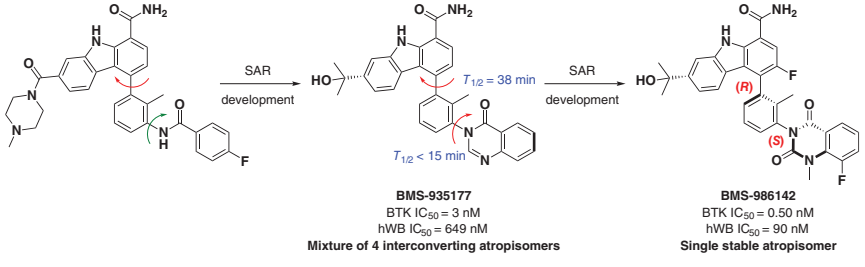

Figure 11.14 Evolution of singular atropisomeric development of BMS-986142.

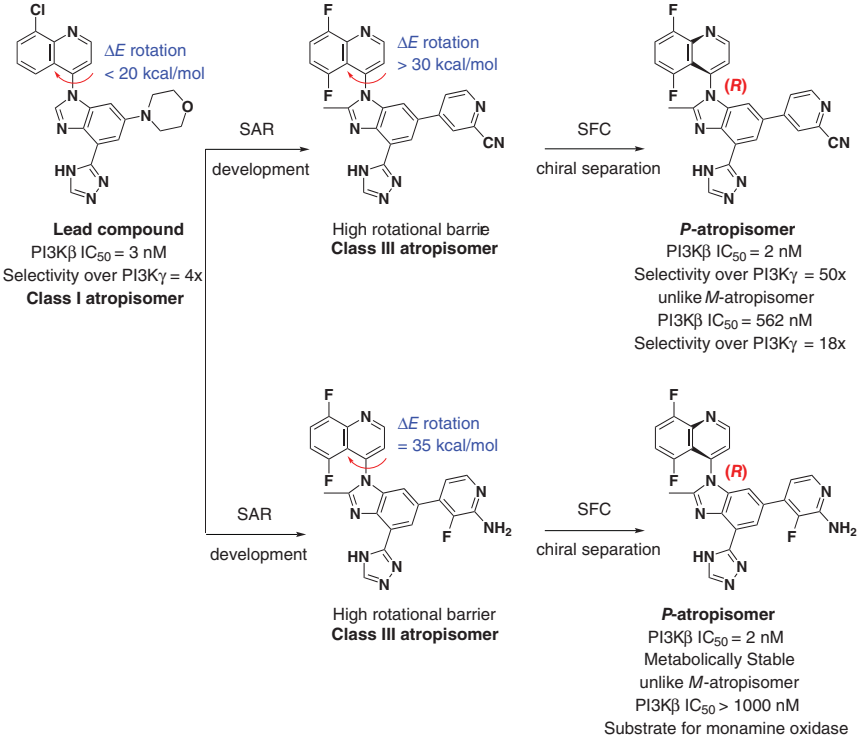

Figure 11.15 Evolution of singular atropisomeric development of selective PI3Kβ inhibitor.

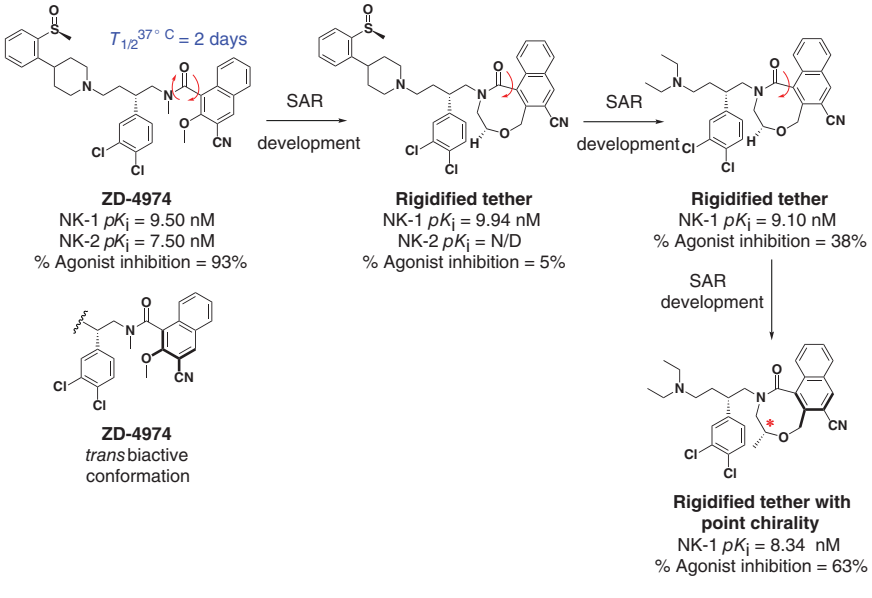

Figure 11.16 Evolution of singular atropisomeric development of selective NK-1 inhibitors.

of atropisomeric switch was also adopted by Gilead Sciences for the preparation of their selective PI3Kβ inhibitor following the development of a series of atropisomeric analogs [22, 23]. Utilizing bulkier sterically hindered scaffolds permitted atropisomeric switch from class I atroisomeric racemate to class III atropisomer easily separated via SFC chiral separation (Figure 11.15). Another approach for introducing rotation-hindered bond was applied to further refine the selective neurokinin-I (NK-1) receptor antagonist, ZD-4974, developed by AsteraZeneca [63]. This small molecule antagonist depicted inherited geared rotations around its aromatic amide bond resembling those of atropisomer class II ($t_{1/2} = 2$ days) (Figure 11.16). Constraining the system through introducing a rigidifying tether was found beneficial to restrict the rotating bond while maintaining the antagonistic affinity of NK-1 receptor [64]. Further stability was achieved through point chirality introduction on the ring to further dampen the aromatic carbonyl rotation stabilizing the molecule into its bioactive *trans*-conformation with regained significant % agonist inhibition.

11.7 Conclusion

The phenomenon of hindered rotation around a single bond or atropisomerism could greatly impact the drug affinity, selectivity, and pharmacokinetics. However, this type of chirality has long been overlooked during the rational design of drug candidates. It was noticed that considerable attention is usually paid to geometric and point chirality, while the effect of substitution on systems with relatively restricted bond rotation is frequently neglected. As discussed in this chapter, only four FDA-approved drugs are recognized as class III stable atropisomers, namely, Lesinurad, Telenzepine, Colchicine, and Sotorasib, with the latter being the only drug that is deliberately designed as a stable atropisomer. On the other hand, there is a wealth of FDA-approved drugs, about 30%, classified as class I atropisomers and could be transformed into stable class III isomers via simple modifications. A few other examples of pure atropisomers are currently being developed as kinase inhibitors and GPCR ligands. The challenges facing the synthesis, purification, and characterization of atropisomers could be the reason behind the low interest in the exploitation of axial chirality to modulate biological activities. Nevertheless, we believe that the potential benefits of employing atropisomers justify the cost of considering this type of chirality in the early stages of drug development.

References

1 Glunz, P.W. (2018). Recent encounters with atropisomerism in drug discovery. *Bioorg. Med. Chem. Lett.* 28 (2): 53–60.
2 Wang, Y.-B., Xiang, S.-H., and Tan, B. (2021). Application in drugs and materials. In: *Axially Chiral Compounds* (ed. B. Tan), 297–315. Wiley.

3 Basilaia, M., Chen, M.H., Secka, J. et al. (2022). Atropisomerism in the pharmaceutically relevant realm. *Acc. Chem. Res.* 55 (20): 2904–2919.

4 Agranat, I., Caner, H., and Caldwell, J. (2002). Putting chirality to work: the strategy of chiral switches. *Nat. Rev. Drug Discov.* 1 (10): 753–768.

5 Perreault, S., Chandrasekhar, J., and Patel, L. (2022). Atropisomerism in drug discovery: a medicinal chemistry perspective inspired by atropisomeric Class I PI3K inhibitors. *Acc. Chem. Res.* 55 (18): 2581–2593.

6 Yip, S.H., Wu, D.-R., Li, P. et al. (2019). Separation of Bruton's tyrosine kinase inhibitor atropisomers by supercritical fluid chromatography. *J. Chromatogr. A* 1586: 106–115.

7 He, B.L., Kleinsorge, N.G., Zhang, L. et al. (2020). Advancing stereoisomeric separation of an atropisomeric Bruton's tyrosine kinase inhibitor by using sub-2 μm immobilized polysaccharide-based chiral columns in supercritical fluid chromatography. *J. Chromatogr. A* 1626: 461320.

8 D'Acquarica, I., Gasparrini, F., Pierini, M. et al. (2006). Dynamic HPLC on chiral stationary phases: a powerful tool for the investigation of stereomutation processes. *J. Sep. Sci.* 29 (10): 1508–1516.

9 Pellissier, H. (2003). Dynamic kinetic resolution. *Tetrahedron* 59: 8291–8327.

10 Madarász, Á., Berta, D., and Paton, R.S. (2016). Development of a true transition state force field from quantum mechanical calculations. *J. Chem. Theory Comput.* 12 (4): 1833–1844.

11 Casarini, D., Lunazzi, L., and Mazzanti, A. (2010). Recent advances in stereodynamics and conformational analysis by dynamic NMR and theoretical calculations. *Eur. J. Org. Chem.* 2010 (11): 2035–2056.

12 Pescitelli, G. (2022). ECD exciton chirality method today: a modern tool for determining absolute configurations. *Chirality* 34 (2): 333–363.

13 Yang, Y.D., Yang, B.B., and Li, L. (2022). A nonneglectable stereochemical factor in drug development: atropisomerism. *Chirality* 34 (10): 1355–1370.

14 LaPlante, S.R., Edwards, P.J., Fader, L.D. et al. (2011). Revealing atropisomer axial chirality in drug discovery. *ChemMedChem* 6 (3): 505–513.

15 Laplante, S.R., Fader, L.D., Fandrick, K.R. et al. (2011). Assessing atropisomer axial chirality in drug discovery and development. *J. Med. Chem.* 54 (20): 7005–7022.

16 Toenjes, S.T. and Gustafson, J.L. (2018). Atropisomerism in medicinal chemistry: challenges and opportunities. *Future Med. Chem.* 10 (4): 409–422.

17 Clayden, J., Moran, W.J., Edwards, P.J. et al. (2009). The challenge of atropisomerism in drug discovery. *Angew. Chem. Int. Ed. Eng.* 48 (35): 6398–6401.

18 Wang, J., Zeng, W., Li, S. et al. (2017). Discovery and assessment of atropisomers of (±)-Lesinurad. *ACS Med. Chem. Lett.* 8 (3): 299–303.

19 Eveleigh, P., Hulme, E.C., Schudt, C. et al. (1989). The existence of stable enantiomers of telenzepine and their stereoselective interaction with muscarinic receptor subtypes. *Mol. Pharmacol.* 35 (4): 477–483.

20 Berg, U., Deinum, J., Lincoln, P. et al. (1991). Stereochemistry of colchicinoids. Enantiomeric stability and binding to tubulin of desacetamidocolchicine and desacetamidoisocolchicine. *Bioorg. Chem.* 19 (1): 53–65.

21 Lanman, B.A., Allen, J.R., Allen, J.G. et al. (2020). Discovery of a covalent inhibitor of KRAS(G12C) (AMG 510) for the treatment of solid tumors. *J. Med. Chem.* 63 (1): 52–65.

22 Chandrasekhar, J., Dick, R., Van Veldhuizen, J. et al. (2018). Atropisomerism by design: discovery of a selective and stable phosphoinositide 3-kinase (PI3K) β inhibitor. *J. Med. Chem.* 61 (15): 6858–6868.

23 Perreault, S., Arjmand, F., Chandrasekhar, J. et al. (2020). Discovery of an atropisomeric PI3Kβ selective inhibitor through optimization of the Hinge binding motif. *ACS Med. Chem. Lett.* 11 (6): 1236–1243.

24 Tichenor, M.S., Wiener, J.J.M., Rao, N.L. et al. (2021). Discovery of a potent and selective covalent inhibitor of Bruton's Tyrosine kinase with oral anti-inflammatory activity. *ACS Med. Chem. Lett.* 12 (5): 782–790.

25 Hoegenauer, K., Kallen, J., Jiménez-Núñez, E. et al. (2019). Structure-based and property-driven optimization of N-aryl imidazoles toward potent and selective oral RORγt inhibitors. *J. Med. Chem.* 62 (23): 10816–10832.

26 Kettle, J.G., Bagal, S.K., Bickerton, S. et al. (2020). Structure-based design and pharmacokinetic optimization of covalent allosteric inhibitors of the mutant GTPase KRASG12C. *J. Med. Chem.* 63 (9): 4468–4483.

27 Szlávik, Z., Ondi, L., Csékei, M. et al. (2019). Structure-guided discovery of a selective Mcl-1 inhibitor with cellular activity. *J. Med. Chem.* 62 (15): 6913–6924.

28 Rohde, J.M., Karavadhi, S., Pragani, R. et al. (2021). Discovery and optimization of 2H-1λ2-pyridin-2-one inhibitors of mutant isocitrate dehydrogenase 1 for the treatment of cancer. *J. Med. Chem.* 64 (8): 4913–4946.

29 Watterson, S.H., De Lucca, G.V., Shi, Q. et al. (2016). Discovery of 6-fluoro-5-(*R*)-(3-(*S*)-(8-fluoro-1-methyl-2,4-dioxo-1,2-dihydroquinazolin-3(4H)-yl)-2-methylphenyl)-2-(*S*)-(2-hydroxypropan-2-yl)-2,3,4,9-tetrahydro-1H-carbazole-8-carboxamide (BMS-986142): a reversible inhibitor of Bruton's tyrosine kinase (BTK) conformationally constrained by two locked atropisomers. *J. Med. Chem.* 59 (19): 9173–9200.

30 Tron, A.E., Belmonte, M.A., Adam, A. et al. (2018). Discovery of Mcl-1-specific inhibitor AZD5991 and preclinical activity in multiple myeloma and acute myeloid leukemia. *Nat. Commun.* 9 (1): 5341.

31 Smith, C.R., Aranda, R., Bobinski, T.P. et al. (2022). Fragment-based discovery of MRTX1719, a synthetic lethal inhibitor of the PRMT5·MTA complex for the treatment of MTAP-deleted cancers. *J. Med. Chem.* 65 (3): 1749–1766.

32 Satoh, F., Ito, S., Itoh, H. et al. (2021). Efficacy and safety of esaxerenone (CS-3150), a newly available nonsteroidal mineralocorticoid receptor blocker, in hypertensive patients with primary aldosteronism. *Hypertens. Res.* 44 (4): 464–472.

33 Radhakrishnanand, P., Rayala, V.V.S.P.K., Trivedi, K. et al. (2022). Development of polar organic mode chromatographic method by polysaccharide-based immobilized chiral selector and validation for the determination of the enantiopurity of novel mineralocorticoid receptor antagonist atropisomer–esaxerenone. *Chromatographia* 85 (7): 553–562.

34 Smyth, J.E., Butler, N.M., and Keller, P.A. (2015). A twist of nature – the significance of atropisomers in biological systems. *Nat. Prod. Rep.* 32 (11): 1562–1583.

35 Brown, D.G. and Boström, J. (2016). Analysis of past and present synthetic methodologies on medicinal chemistry: where have all the new reactions gone? *J. Med. Chem.* 59 (10): 4443–4458.

36 Bringmann, G., Price Mortimer, A.J., Keller, P.A. et al. (2005). Atroposelective synthesis of axially chiral biaryl compounds. *Angew. Chem. Int. Ed.* 44 (34): 5384–5427.

37 Gustafson, J.L., Lim, D., and Miller, S.J. (2010). Dynamic kinetic resolution of biaryl atropisomers via peptide-catalyzed asymmetric bromination. *Science* 328 (5983): 1251–1255.

38 Mori, K., Ichikawa, Y., Kobayashi, M. et al. (2013). Enantioselective synthesis of multisubstituted biaryl skeleton by chiral phosphoric acid catalyzed desymmetrization/kinetic resolution sequence. *J. Am. Chem. Soc.* 135 (10): 3964–3970.

39 Diener, M.E., Metrano, A.J., Kusano, S. et al. (2015). Enantioselective synthesis of 3-Arylquinazolin-4(3H)-ones via peptide-catalyzed atroposelective bromination. *J. Am. Chem. Soc.* 137 (38): 12369–12377.

40 Zhang,J., Dong, Y., Gao, S. et al. (2022). Design, synthesis and activity evaluation of novel lesinurad analogues containing thienopyrimidinone or pyridine substructure as human urate transporter 1 inhibitors. *Eur. J. Med. Chem.* 244: 114816.

41 Lanman,B.A., Parsons, A.T., and Zech, S.G. (2022). Addressing atropisomerism in the development of Sotorasib, a covalent inhibitor of KRAS G12C: structural, analytical, and synthetic considerations. *Acc. Chem. Res.* 55 (20): 2892–2903.

42 Bracegirdle, A., Clayden, J., and Lai, L.W. (2008). Asymmetric synthesis of biaryl atropisomers by dynamic resolution on condensation of biaryl aldehydes with (−)-ephedrine or a proline-derived diamine. *Beilstein J. Org. Chem.* 4: 47.

43 Betson, M.S., Clayden, J., Worrall, C.P. et al. (2006). Three groups good, four groups bad? Atropisomerism in ortho-substituted diaryl ethers. *Angew. Chem. Int. Ed. Eng.* 45 (35): 5803–5807.

44 Okamoto,K., Ikemori-Kawada, M., Jestel, A. et al. (2015). Distinct binding mode of multikinase inhibitor lenvatinib revealed by biochemical characterization. *ACS Med. Chem. Lett.* 6 (1): 89–94.

45 Kawabata,T., Jiang, C., Hayashi, K. et al. (2009). Axially chiral binaphthyl surrogates with an inner N–H–N hydrogen bond. *J. Am. Chem. Soc.* 131 (1): 54–55.

46 Knowles, P.P., Murray-Rust, J., Kjaer, S. et al. (2006). Structure and chemical inhibition of the RET tyrosine kinase domain. *J. Biol. Chem.* 281 (44): 33577–33587.

47 Yin, X.J., Xu, G.H., Sun, X. et al. (2010). Synthesis of bosutinib from 3-methoxy-4-hydroxybenzoic acid. *Molecules* 15 (6): 4261, 4261–4266, 4266.

48 Solca, F., Dahl, G., Zoephel, A. et al. (2012). Target binding properties and cellular activity of afatinib (BIBW 2992), an irreversible ErbB family blocker. *J. Pharmacol. Exp. Ther.* 343 (2): 342–350.

49 Clayden, J. (2004). Atropisomers and near-atropisomers: achieving stereoselectivity by exploiting the conformational preferences of aromatic amides. *Chem. Commun. (Camb.)* 2: 127–135.

50 Takahashi, H., Wakamatsu, S., Tabata, H. et al. (2011). Atropisomerism observed in indometacin derivatives. *Org. Lett.* 13 (4): 760–763.

51 Kazmierski, W.M., Danehower, S., Duan, M. et al. (2014). Biological and structural characterization of rotamers of C-C chemokine receptor type 5 (CCR5) inhibitor GSK214096. *ACS Med. Chem. Lett.* 5 (12): 1296–1299.

52 Farand, J., Mai, N., Chandrasekhar, J. et al. (2016). Selectivity switch between FAK and Pyk2: macrocyclization of FAK inhibitors improves Pyk2 potency. *Bioorg. Med. Chem. Lett.* 26 (24): 5926–5930.

53 Priestley, E.S., Cheney, D.L., DeLucca, I. et al. (2015). Structure-based design of macrocyclic coagulation factor VIIa inhibitors. *J. Med. Chem.* 58 (15): 6225–6236.

54 Elleraas, J., Ewanicki, J., Johnson, T.W. et al. (2016). Conformational studies and atropisomerism kinetics of the ALK clinical candidate lorlatinib (PF-06463922) and desmethyl congeners. *Angew. Chem. Int. Ed. Eng.* 55 (11): 3590–3595.

55 Baunbaek, D., Trinkler, N., Ferandin, Y. et al. (2008). Anticancer alkaloid lamellarins inhibit protein kinases. *Mar. Drugs* 6 (4): 514–527.

56 Verdine, G.L. and Walensky, L.D. (2007). The challenge of drugging undruggable targets in cancer: lessons learned from targeting BCL-2 family members. *Clin. Cancer Res.* 13 (24): 7264–7270.

57 Wang, Z., Meng, L., Liu, X. et al. (2022). Recent progress toward developing axial chirality bioactive compounds. *Eur. J. Med. Chem.* 243: 114700.

58 Bogaerts, J., Aerts, R., Vermeyen, T. et al. (2021). Tackling stereochemistry in drug molecules with vibrational optical activity. *Pharmaceuticals* 14 (9).

59 Palani, A., Shapiro, S., Clader, J.W. et al. (2001). Discovery of 4-[(*Z*)- (4-bromophenyl)-(ethoxyimino)methyl]-1′-[(2,4-dimethyl-3-pyridinyl)carbonyl]-4′-methyl-1,4′-bipiperidine *N*-oxide (SCH 351125): an orally bioavailable human CCR5 antagonist for the treatment of HIV infection. *J. Med. Chem.* 44 (21): 3339–3342.

60 Palani, A., Shapiro, S., Clader, J.W. et al. (2003). Oximino-piperidino-piperidinebased CCR5 antagonists. Part 2: synthesis, SAR and biological evaluation of symmetrical heteroaryl carboxamides. *Bioorg. Med. Chem. Lett.* 13 (4): 709–712.

61 McCombie, S.W., Tagat, J.R., Vice, S.F. et al. (2003). Piperazine-based CCR5 antagonists as HIV-1 inhibitors. III: synthesis, antiviral and pharmacokinetic profiles of symmetrical heteroaryl carboxamides. *Bioorg. Med. Chem. Lett.* 13 (3): 567–571.

62 Kocienski, P. (2021). Synthesis of Sotorasib. *Synfacts* 17 (10): 1071.

63 Albert, J.S., Aharony, D., Andisik, D. et al. (2002). Design, synthesis, and SAR of tachykinin antagonists: modulation of balance in NK(1)/NK(2) receptor antagonist activity. *J. Med. Chem.* 45 (18): 3972–3983.

64 Ohnmacht, C.J., Albert, J.S., Bernstein, P.R. et al. (2004). Naphtho[2,1-b][1,5] and [1,2-f][1,4]oxazocines as selective NK1 antagonists. *Bioorg. Med. Chem.* 12 (10): 2653–2669.

Index

Atropisomerism in Asymmetric Organic Synthesis: Challenges and Applications, First Edition.
Edited by Shinobu Takizawa and Mohamed S. H. Salem.

C